Continuum

LIFELONG LEARNING IN NEUROLOGY®

FEBRUARY 2023 VOL 29 NO 1

Neuroimaging

EDITOR-IN-CHIEF: J. NEIL E. JONES JR, MD, FAAN
GUEST EDITOR: JOSHUA P. KLEIN, MD, PHD, FAAN, FAEN, FAAN

Continuum
LIFELONG LEARNING IN NEUROLOGY®

AMERICAN ACADEMY OF NEUROLOGY

FEBRUARY 2023
VOL. 29 NO. 1

Neuroimaging

Guest Editor: Joshua P. Klein, MD, PhD, FANA, FASN, FAAN

14 Editor's Preface
Editor-in-Chief: Lyell K. Jones Jr, MD, FAAN

REVIEW ARTICLES

16 The Right Imaging Protocol for the Right Patient
Nandor K. Pinter, MD

27 Safety Considerations in MRI and CT
Robert E. Watson, MD, PhD; Lifeng Yu, PhD

54 Imaging of Central Nervous System Ischemia
Julie G. Shulman, MD; Mohamad Abdalkader, MD

73 Imaging of Central Nervous System Hemorrhage
Ryan Hakimi, DO, MS, NVS, RPNI, CPB, FNCS, FCCM

104 Neuroimaging in Adults and Children With Epilepsy
Erasmo A. Passaro, MD

156 Imaging of Skull Base Tumors
Wenya Linda Bi, MD, PhD

171 Imaging of Brain Tumors
Justin T. Jordan, MD, MPH, FAAN; Elizabeth R. Gerstner, MD

194 Imaging in Movement Disorders
Baijayanta Maiti, MD, PhD; Joel S. Perlmutter, MD

219 Neuroimaging in Dementia
Shannon L. Risacher, PhD; Liana G. Apostolova, MD, MS, FAAN

255 Imaging of Central Nervous System Autoimmune, Paraneoplastic, and Neuro-rheumatologic Disorders
Lama Abdel Wahed, MD; Tracey A. Cho, MD, FAAN

DENOTES *CONTINUUM* AUDIO INTERVIEW

DENOTES VIDEO CONTENT

Copyright © American Academy of Neurology. Unauthorized reproduction of this article is prohibited.

292 **Imaging of Central Nervous System Demyelinating Disorders**
Jan-Mendelt Tillema, MD

324 **Diagnostic Ultrasonography in Neurology**
Elsa Azevedo, MD, PhD

SELF-ASSESSMENT AND CME

4 **Learning Objectives and Core Competencies**

365 **Instructions for Completing Postreading Self-Assessment and CME Test and Tally Sheet**

367 **Postreading Self-Assessment and CME Test**

381 **Postreading Self-Assessment and CME Test—Preferred Responses**

393 **Index**

List of Abbreviations (Back Cover)

Copyright © American Academy of Neurology. Unauthorized reproduction of this article is prohibited.

CONTRIBUTORS[a]

Joshua P. Klein, MD, PhD, FANA, FASN, FAAN,
Guest Editor
Vice Chair, Clinical Affairs, and Chief, Division of Hospital Neurology, Department of Neurology, Brigham and Women's Hospital; Associate Professor of Neurology and Radiology, Harvard Medical School, Boston, Massachusetts

Relationship Disclosure: Dr Klein has received personal compensation in the range of $5000 to $9999 for serving as an editor, associate editor, or editorial advisory board member for Oakstone Publishing and in the range of $10,000 to $49,999 for serving as an editor, associate editor, or editorial advisory board member for AudioDigest, McGraw Hill, and SAGE Publications. Dr Klein has received publishing royalties in the range of $10,000 to $49,000 from a publication relating to health care. Dr Klein has received personal compensation in the range of $100,000 to $499,999 for serving as an expert witness for various law firms.

Unlabeled Use of Products/Investigational Use Disclosure: Dr Klein reports no disclosure.

Mohamad Abdalkader, MD
Assistant Professor of Radiology, Boston Medical Center, Boston University School of Medicine, Boston, Massachusetts

Relationship Disclosure: Dr Abdalkader reports no disclosure.

Unlabeled Use of Products/Investigational Use Disclosure: Dr Abdalkader reports no disclosure.

Lama Abdel Wahed, MD
Clinical Assistant Professor of Neurology, University of Iowa Carver College of Medicine; Associate Residency Program Director, Associate Clerkship Director, University of Iowa Healthcare, Iowa City, Iowa

Relationship Disclosure: Dr Abdel Wahed has received personal compensation in the range of $0 to $499 for serving as a resident honorary speaker with the Iowa Neurological Association and as an author for MedLink, LLC.

Unlabeled Use of Products/Investigational Use Disclosure: Dr Abdel Wahed discusses the unlabeled use of corticosteroids for the treatment of autoimmune neurologic diseases that have no US Food and Drug Administration–approved medications.

[a] All relevant financial relationships have been mitigated.

Copyright © American Academy of Neurology. Unauthorized reproduction of this article is prohibited.

Liana G. Apostolova, MD, MS, FAAN
Indiana University Distinguished Professor, Barbara and Peer Baekgaard Professor in Alzheimer's Disease Research, Indiana University School of Medicine, Indianapolis, Indiana

Relationship Disclosure: Dr Apostolova has received personal compensation in the range of $500 to $4999 for serving as a consultant for Florida Health, General Electric Company, Lilly, the National Institutes of Health (NIH), and NIH Biobank; on a data safety monitoring board for IQVIA Inc; and on advisory boards for Eisai Co, Ltd, F. Hoffman-La Roche Ltd, Genentech, Inc, and TwoLabs, LLC. Dr Apostolova has received personal compensation in the range of $5000 to $9999 for serving on an advisory board for Biogen and in the range of $10,000 to $49,999 for serving as an editor-in-chief for the Alzheimer's Association. An immediate family member of Dr Apostolova has stock in Cassava Sciences, Inc, Golden Seeds, and Semiring. The institution of Dr Apostolova has received research support from the Alzheimer's Association, Avid Radiopharmaceuticals, F. Hoffman-La Roche Ltd, Life Molecular Imaging, and the National Institute on Aging.

Unlabeled Use of Products/Investigational Use Disclosure: Dr Apostolova reports no disclosure.

Elsa Azevedo, MD, PhD
Department of Neurology, Centro Hospitalar Universitário de São João; Department of Clinical Neurosciences and Mental Health, Faculty of Medicine of University of Porto, Porto, Portugal

Relationship Disclosure: Dr Azevedo reports no disclosure.

Unlabeled Use of Products/Investigational Use Disclosure: Dr Azevedo reports no disclosure.

Wenya Linda Bi, MD, PhD
Assistant Professor of Neurosurgery, Harvard Medical School, Brigham and Women's Hospital, Boston, Massachusetts

Relationship Disclosure: Dr Bi reports no disclosure.

Unlabeled Use of Products/Investigational Use Disclosure: Dr Bi reports no disclosure.

Tracey A. Cho, MD, FAAN
Clinical Professor of Neurology, University of Iowa Carver College of Medicine; Director, Neuroimmunology Division, University of Iowa Healthcare, Iowa City, Iowa

Relationship Disclosure: Dr Cho has received personal compensation in the range of $500 to $4999 for serving as a consultant for Horizon Therapeutics plc and on a data safety monitoring board for the National Institutes of Health and has received publishing royalties from a publication relating to health care. The institution of an immediate family member of Dr Cho has received research support from the National Institutes of Health.

Unlabeled Use of Products/Investigational Use Disclosure: Dr Cho discusses the unlabeled use of corticosteroids for the treatment of autoimmune neurologic diseases that have no US Food and Drug Administration–approved medications.

Copyright © American Academy of Neurology. Unauthorized reproduction of this article is prohibited.

CONTRIBUTORS[a] (CONTINUED)

Elizabeth R. Gerstner, MD
Associate Professor of Neurology, Harvard Medical School; Associate Neurologist, Massachusetts General Hospital, Boston, Massachusetts

Relationship Disclosure: Dr Gerstner has received personal compensation in the range of $500 to $4999 for serving on a data safety monitoring board for Midatech Pharma PLC and in the range of $50,000 to $99,999 for serving as an officer or member of the board of directors for the Gerstner Family Foundation. The institution of Dr Gerstner has received research support from the National Cancer Institute.

Unlabeled Use of Products/Investigational Use Disclosure: Dr Gerstner discusses the unlabeled/investigational use of mitogen-associated protein kinase (MAPK) pathway with MAP-ERK kinase (MEK) inhibitors for the treatment of MAP kinase-altered tumors and various MRI and positron emission tomography (PET) techniques not approved for the imaging of brain tumors.

Ryan Hakimi, DO, MS, NVS, RPNI, CPB, FNCS, FCCM
Director, Neuro ICU and Transcranial Doppler Ultrasound Services, Prisma Health-Upstate; Professor, Department of Medicine (Neurology Division), University of South Carolina School of Medicine-Greenville, Greenville, South Carolina

Relationship Disclosure: Dr Hakimi has received personal compensation in the range of $0 to $499 for serving as a delegate in the American Medical Association House of Delegates for the American Society of Neuroimaging and in the range of $500 to $4999 for serving as the immediate past president for the South Carolina Osteopathic Medical Society and as a medical reviewer for the Office of Disciplinary Counsel in the South Carolina Department of Labor, Licensing and Regulation and has received publishing royalties from Osler, Hoskin & Harcourt LLP. Dr Hakimi has a noncompensated relationship as an annual meeting course committee member with the Neurocritical Care Society that is relevant to AAN interests or activities.

Unlabeled Use of Products/Investigational Use Disclosure: Dr Hakimi reports no disclosure.

[a] All relevant financial relationships have been mitigated.

Copyright © American Academy of Neurology. Unauthorized reproduction of this article is prohibited.

Justin T. Jordan, MD, MPH, FAAN
Clinical Director, Stephen E. and Catherine Pappas Center for Neuro-Oncology at Massachusetts General Hospital; Director, Family Center for Neurofibromatosis Massachusetts General Hospital; Assistant Professor of Neurology, Harvard Medical School, Boston, Massachusetts

Relationship Disclosure: Dr Jordan has received personal compensation in the range of $0 to $499 for serving as a consultant for Atheneum Partners, EM Partners, GLG Pharma, and Guidepoint Global, LLC; in the range of $500 to $4999 for serving as a consultant for Creative Educational Concepts, LLC, and Texas Health Resources; and in the range of $5000 to $9999 for serving as a consultant for Children's Tumor Foundation, Navio Theragnostics, Inc, and Recursion and on a scientific advisory board for Recursion. Dr Jordan has stock in The Doctor Lounge and Navio Theragnostics, Inc, has received publishing royalties from Elsevier, and has noncompensated relationships as a board member with ABA Academy, Neurofibromatosis Northeast, Neurofibromatosis Network, and the United Council for Neurologic Subspecialties that is relevant to AAN interests or activities. The institution of Dr Jordan has received research support from The Burke Foundation, the Department of Defense, and the National Institutes of Health.

Unlabeled Use of Products/Investigational Use Disclosure: Dr Jordan discusses the unlabeled/investigational use of mitogen-associated protein kinase (MAPK) pathway with MAP-ERK kinase (MEK) inhibitors for the treatment of MAP kinase-altered tumors and various MRI and positron emission tomography (PET) techniques not approved for the imaging of brain tumors.

Baijayanta Maiti, MD, PhD
Assistant Professor of Neurology, Washington University in St. Louis School of Medicine, St. Louis, Missouri

Relationship Disclosure: The institution of Dr Maiti has received research support from the National Center for Advancing Translational Sciences and the National Institute of Neurological Disorders and Stroke of the National Institutes of Health.

Unlabeled Use of Products/Investigational Use Disclosure: Dr Maiti reports no disclosure.

Erasmo A. Passaro, MD
Professor of Neurology, University of South Florida, Tampa; Director, Epilepsy Program, Bayfront Health; Medical Director, Epilepsy Surgery, Johns Hopkins All Children's Hospital; St Petersburg, Florida

Relationship Disclosure: Dr Passaro has received personal compensation in the range of $0 to $499 for serving on a speakers bureau and as a consultant for Neurelis, Inc; in the range of $500 to $4999 for serving on speakers bureaus and as a consultant for Eisai Co, Ltd, and Sunovion Pharmaceuticals, Inc; and in the range of $5000 to $9999 for serving on speakers bureaus and as a consultant for SK Life Science, Inc, and UCB, Inc.

Unlabeled Use of Products/Investigational Use Disclosure: Dr Passaro reports no disclosure.

Copyright © American Academy of Neurology. Unauthorized reproduction of this article is prohibited.

CONTRIBUTORS[a] (CONTINUED)

Joel S. Perlmutter, MD
Elliot Stein Family Professor Neurology; Head of Movement Disorders; Professor of Radiology, Neuroscience, Physical Therapy, Occupational Therapy, Washington University in St. Louis School of Medicine, St. Louis, Missouri

Relationship Disclosure: Dr Perlmutter has received personal compensation in the range of $0 to $499 for serving as an officer or member of the Board of Directors for the Parkinson Study Group, and in the range of $500 to $4999 for serving as an officer or member of the Board of Directors for the CHDI Foundation, as an expert witness for Wood, Cooper and Peterson, LLC, and Simmons and Simmons LLP, as a lecturer for Boston University, as an external advisor for Stanford University, and as a visiting professor with Beth Israel Hospital and the University of Pennsylvania. The institution of Dr Perlmutter has received research support from the American Parkinson Disease Association, the Barnes-Jewish Hospital Foundation, the CHDI Foundation, the Huntington Disease Society of America, The Michael J Fox Foundation, the National Institutes of Health, the University of California San Diego, and the University of Western Toronto.

Unlabeled Use of Products/Investigational Use Disclosure: Dr Perlmutter reports no disclosure.

Nandor K. Pinter, MD
Director, Neuroimaging Research, Dent Neurologic Institute, Amherst; Research Associate Professor, Department of Neurosurgery, Jacobs School of Medicine and Biomedical Sciences, University at Buffalo, Buffalo, New York; University of Amsterdam Medical Center, VUmc, Department of Radiology, Amsterdam, The Netherlands

Relationship Disclosure: Dr Pinter has received personal compensation in the range of $5000 to $10,000 for serving as a consultant for Koninklijke Philips N.V. and in the range of $10,000 to $49,000 for serving as a consultant for NeuroNetPro. The institution of Dr Pinter has received research support from the Dent Family Foundation and Koninklijke Philips N.V.

Unlabeled Use of Products/Investigational Use Disclosure: Dr Pinter reports no disclosure.

Shannon L. Risacher, PhD
Associate Professor of Radiology and Imaging Sciences; Neuroimaging Core Leader, Indiana Alzheimer's Disease Research Center, Indiana University School of Medicine, Indianapolis, Indiana

Relationship Disclosure: Dr Risacher has received research support from the Alzheimer's Association, New Vision Award, and the National Institute on Aging (K01 AG049050, R01 AG061788, P30 AG010133, and P30 AG072976).

Unlabeled Use of Products/Investigational Use Disclosure: Dr Risacher reports no disclosure.

[a] All relevant financial relationships have been mitigated.

Copyright © American Academy of Neurology. Unauthorized reproduction of this article is prohibited.

Julie G. Shulman, MD
Assistant Professor of Neurology, Boston Medical Center, Boston University School of Medicine, Boston, Massachusetts

Relationship Disclosure: Dr Shulman has received research support from the BU Spivack Neuroscience Pilot Award.

Unlabeled Use of Products/Investigational Use Disclosure: Dr Shulman reports no disclosure.

Jan-Mendelt Tillema, MD
Assistant Professor of Neurology, Mayo Clinic, Rochester, Minnesota

Relationship Disclosure: Dr Tillema reports no disclosure.

Unlabeled Use of Products/Investigational Use Disclosure: Dr Tillema reports no disclosure.

Robert E. Watson, MD, PhD
Professor of Radiology, Department of Radiology, Mayo Clinic, Rochester, Minnesota

Relationship Disclosure: Dr Watson has a noncompensated relationship as a Chair with the American Board of Magnetic Resonance Safety that is relevant to American Academy of Neurology interests or activities.

Unlabeled Use of Products/Investigational Use Disclosure: Dr Watson reports no disclosure.

Lifeng Yu, PhD
Professor of Medical Physics, Mayo Clinic, Rochester, Minnesota

Relationship Disclosure: Dr Yu reports no disclosure.

Unlabeled Use of Products/Investigational Use Disclosure: Dr Yu reports no disclosure.

Copyright © American Academy of Neurology. Unauthorized reproduction of this article is prohibited.

CONTRIBUTORS[a] (CONTINUED)

Self-Assessment and CME Test Writers

Nuri Jacoby, MD
Associate Professor of Clinical Neurology, SUNY Downstate Health Sciences University; Attending Neurologist, Maimonides Medical Center, Brooklyn, New York

Relationship Disclosure: Dr Jacoby has received personal compensation in the range of $500 to $4999 for serving as a multiple-choice question writer for *Continuum* with the American Academy of Neurology and on a scientific advisory or data safety monitoring board for Alexion Pharmaceuticals, Inc and in the range of $5000 to $9999 for serving as an expert witness. The institution of Dr Jacoby has received research support from the American Board of Psychiatry and Neurology.

Unlabeled Use of Products/Investigational Use Disclosure: Dr Jacoby reports no disclosure.

Allison L. Weathers, MD, FAAN
Associate Chief Medical Information Officer, Cleveland Clinic; Assistant Professor, Cleveland Clinic Lerner College of Medicine, Cleveland, Ohio

Relationship Disclosure: Dr Weathers has a noncompensated relationship as chair of the adult neurosciences specialty steering board for Epic and as co-chair of the neurology leadership council for Cerner Corporation and has received personal compensation in the range of $0 to $499 for serving as a consultant for Dent Neurologic Institute and in the range of $500 to $4999 for serving as an associate editor and as a CME question writer and presenter with the American Academy of Neurology.

Unlabeled Use of Products/Investigational Use Disclosure: Dr Weathers reports no disclosure.

[a] All relevant financial relationships have been mitigated.

Copyright © American Academy of Neurology. Unauthorized reproduction of this article is prohibited.

Copyright © American Academy of Neurology. Unauthorized reproduction of this article is prohibited.

EDITOR'S PREFACE

Looking Inward, Moving Forward

"The eyes aren't windows to the soul, they're windows to the brain. The optic discs are the only part of the brain you can see without a drill." I heard this comment from a senior neurologist when I was in training, and it has stuck with me, partly because it is pithy and partly because it is wrong. Advanced neuroimaging has given us windows into nervous system structure and function that still seem like a marvel to me despite how frequently we use it in clinical practice.

This issue of *Continuum* offers a view into all things neuroimaging, including spectacular images and expert descriptions of how imaging findings can help us better take care of our patients. It is also my first issue of *Continuum* as editor-in-chief, and while this issue has been in development for many months, this is an opportunity for me to offer a window into the future of this wonderful journal.

Continuum has been with me as a clinician ever since those formative years in neurology training. Since then, as an educator, I have found it to be an indispensable tool to introduce our expansive specialty to neurology trainees. *Continuum* was launched 30 years ago with a focus on CME, and in that interval, it has evolved into a widely respected review journal that meets the full career spectrum of education needs in neurology. It has become the de facto written curriculum of our specialty, and we have updated *Continuum*'s guiding statements to reflect that. The mission of *Continuum* is to help clinicians deliver the highest-quality neurologic care and demonstrate continued competency, and our vision is to be the essential education resource for neurologic clinicians.

As the audience for *Continuum* has grown in number and breadth, the journal has made its content available in new formats. With *Continuum* Audio and *Continuum* Read Aloud, listeners can enjoy the journal in new settings. Online access at ContinuumJournal.com complements the print version. The *Continuum* subscribership is increasingly global. During my tenure, I look forward to putting *Continuum* in as many hands as possible, introducing new topics and content that reflect the diversity of our specialty and patients, and making the experience of enjoying *Continuum* as seamless as possible. We will accomplish these goals with a brilliant editorial team, talented guest editors, and the most authoritative authors in our field.

I am so excited about the future of *Continuum*, and this Neuroimaging issue is a perfect encapsulation of the promise and progress in our field. It is impossible to overstate the stellar work of Dr Joshua P. Klein as guest editor of the issue; he has assembled a team of authors with rare dual expertise in imaging as well as their respective clinical domains. Dr Nandor K. Pinter kicks it off with a foundational overview of the approach to imaging in patients with neurologic disorders, followed by a definitive review of imaging safety by Drs Robert E. Watson and Lifeng Yu. The imaging features of all manner of cerebrovascular catastrophes are covered by Drs Julie G. Shulman and Mohamad Abdalkader (cerebral ischemia) and Dr Ryan Hakimi (central nervous system [CNS] hemorrhage). Dr Erasmo A. Passaro outlines the panorama of imaging tools available in patients with epilepsy. Separate articles provide expert presentations of existing and emerging tools to image brain tumors within (Drs Justin T. Jordan and Elizabeth R. Gerstner) and without (Dr Wenya Linda Bi)

Copyright © American Academy of Neurology. Unauthorized reproduction of this article is prohibited.

the CNS. Drs Baijayanta Maiti and Joel S. Perlmutter describe imaging modalities in patients with movement disorders, and Drs Shannon L. Risacher and Liana G. Apostolova complete the discussion of neurodegenerative disorders with their article on neuroimaging of patients with dementia. Imaging of patients with autoimmune and inflammatory disorders receives a complete treatment from Drs Lama Abdel Wahed and Tracey A. Cho, while Dr Jan-Mendelt Tillema details the specific imaging features of CNS demyelinating disease. Dr Elsa Azevedo closes out the reviews with a comprehensive overview of all things neurosonology. As always, after reading or listening to the content, subscribers can obtain CME and self-assessment credit with our post-test, written for the print issue by Drs Nuri Jacoby and Allison L. Weathers.

During my tenure I look forward to putting *Continuum* in as many hands as possible, introducing new topics and content that reflect the diversity of our specialty and patients, and making the experience of enjoying *Continuum* as seamless as possible.

I have learned much about *Continuum* in preparation for this role, and I am struck by the loyalty of our subscribers and deep affection our readers have for a journal that has become inseparable from our identity as a specialty. The journal's success is a monument to the visionary editorial leadership of Drs Elliot L. Mancall, Aaron E. Miller, and Steven L. Lewis. In particular, I am grateful for the words of advice Drs Miller and Lewis have shared with me and Dr Lewis's endless patience and generosity with my many questions about *Continuum*'s operations. I am grateful to the American Academy of Neurology, which has entrusted me with this role. Most of all, I am grateful to you, the reader, listener, and subscriber, without whom we would not have this treasured jewel of neurology.

—LYELL K. JONES JR, MD, FAAN
EDITOR-IN-CHIEF

© 2023 American Academy of Neurology.

Copyright © American Academy of Neurology. Unauthorized reproduction of this article is prohibited.

REVIEW ARTICLE

CONTINUUM AUDIO INTERVIEW AVAILABLE ONLINE

The Right Imaging Protocol for the Right Patient

By Nandor K. Pinter, MD

ABSTRACT

OBJECTIVE: **This article provides a high-level overview of the challenge of choosing the right imaging approach for an individual patient. It also presents a generalizable approach that can be applied to practice regardless of specific imaging technologies.**

ESSENTIAL POINTS: **This article constitutes an introduction to the in-depth, topic-focused analyses in the rest of this issue. It examines the broad principles that guide placing a patient on the right diagnostic trajectory, illustrated with real-life examples of current protocol recommendations and cases of advanced imaging techniques, as well as some thought experiments. Thinking about diagnostic imaging strictly in terms of imaging protocols is often inefficient because these protocols can be vague and have numerous variations. Broadly defined protocols may be sufficient, but their successful use often depends largely on the particular circumstances, with special emphasis on the relationship between neurologists and radiologists.**

CITE AS:
CONTINUUM (MINNEAP MINN) 2023;29(1, NEUROIMAGING): 16–26.

Address correspondence to Dr Nandor K. Pinter, 40 George Karl Blvd, Buffalo, NY 14221, npinter@dentinstitute.com.

RELATIONSHIP DISCLOSURE:
Dr Pinter has received personal compensation in the range of $5000 to $10,000 for serving as a consultant for Koninklijke Philips N.V. and in the range of $10,000 to $49,000 for serving as a consultant for NeuroNetPro. The institution of Dr Pinter has received research support from the Dent Family Foundation and Koninklijke Philips N.V.

UNLABELED USE OF PRODUCTS/INVESTIGATIONAL USE DISCLOSURE:
Dr Pinter reports no disclosure.

© 2023 American Academy of Neurology.

INTRODUCTION

The question of the best imaging techniques (in terms of modality, clinical value, and usefulness for differential diagnosis) for specific clinical indications and scenarios is widely discussed in the medical literature. Diagnostic imaging is an ever-changing field, and the articles in this issue of *Continuum* provide up-to-date detailed discussions about different strategies, technical considerations, clinical research data, advanced techniques, competing modalities, and best practices in the imaging of neurologic diseases.

The fact that each clinical area deserves its own review article, or sometimes an entire journal issue, testifies to the complexity of the topic. But how does one choose among the available technologies when treating an individual patient?

The American College of Radiology (ACR) Appropriateness Criteria are a list of evidence-based recommendations for imaging modalities and basic protocols to be used in the setting of specific diseases and typical clinical scenarios.[1] It is a heroic undertaking that rests on a vast library of literature. In the neurology section, brain studies described include "CT head without IV contrast," "MRI head without IV contrast," "MRI head without and with IV contrast," and "CT head without and with IV contrast." Also listed are CT angiography (CTA) and MR angiography

Copyright © American Academy of Neurology. Unauthorized reproduction of this article is prohibited.

(MRA), Doppler ultrasonography, and CT or MR perfusion for some cerebrovascular indications. However, there are no ACR recommendations for when and how to use specific protocols of these broadly described imaging studies, which is exactly what neurologists and radiologists are concerned with. For example, the 2021 Magnetic Resonance Imaging in Multiple Sclerosis (MAGNIMS) position statement specifies the imaging protocol for diagnosing and monitoring multiple sclerosis and recommends the use of three-dimensional fluid-attenuated inversion recovery (FLAIR)[2] (FIGURE 1-1[3]). The harmonized neuroimaging of epilepsy structural sequences (HARNESS) epilepsy protocol recommendation of the International League Against Epilepsy Neuroimaging Task Force includes a two-dimensional T2-weighted sequence with high in-plane resolution (specifically, 0.4 mm × 0.4 mm) acquired perpendicular to the hippocampal long axis for optimal evaluation of the internal structure of the hippocampus (FIGURE 1-2).[4] Gradient recalled echo (GRE) imaging or susceptibility-weighted imaging (SWI) can visualize microhemorrhages in cerebral amyloid angiopathy.[5] All of these applications use a customized version of a conventional sequence but fall under the category "head MRI." In addition, there are nonconventional MRI techniques that can be clinically helpful in the right settings. Examples include four-dimensional MRA in the evaluation of vascular malformations such as arteriovenous fistulas[6] (FIGURE 1-3), tractography to identify the location of the facial nerve in relation to a vestibular schwannoma,[7] arterial spin labeling to assess epileptogenic foci,[8] quantification of intracranial flow with two-dimensional phase-contrast MRI,[9] or vessel wall imaging for the evaluation of intracranial vascular pathology,[10] to name a few. Each of these can be the right imaging technique for a patient with a particular clinical indication and

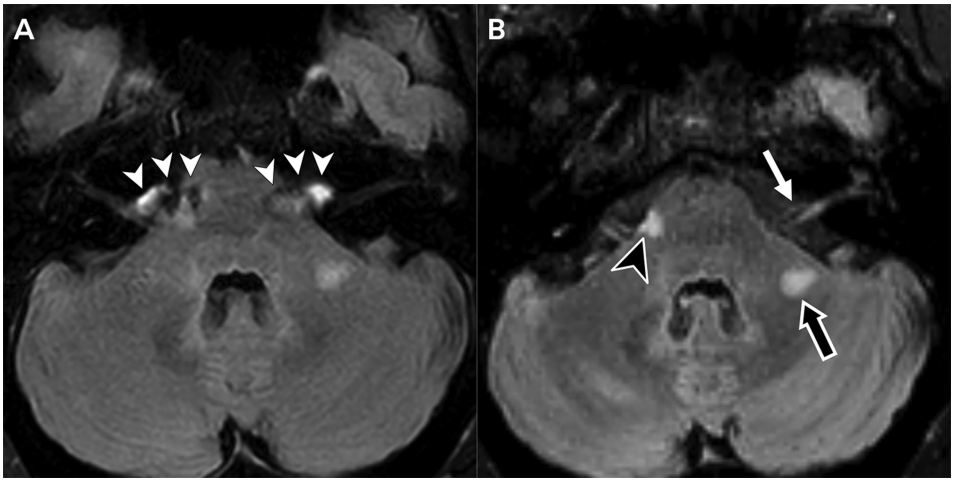

FIGURE 1-1

Axial two-dimensional fluid-attenuated inversion recovery (FLAIR) (*A*) versus three-dimensional FLAIR (*B*) MRI. On two-dimensional FLAIR, prominent CSF pulsation artifacts are seen in the cerebellopontine angles *(A, white arrowheads)*, obscuring a demyelinating lesion in the right lateral aspect of the pons, which becomes visible on three-dimensional FLAIR *(B, black arrowhead)*. With three-dimensional acquisition the fluid attenuation in cerebellopontine cisterns is homogeneous, allowing sharp visualization of not only the pons but the seventh and eighth cranial nerves *(B, white arrow)*. A second lesion is seen in the middle cerebellar peduncle on the left, which is also more conspicuous on the three-dimensional image *(B, black arrow)*.

Reprinted with permission from Pinter NK, Fritz JV, Neurol Clin.[3] © 2019 Elsevier Inc.

Copyright © American Academy of Neurology. Unauthorized reproduction of this article is prohibited.

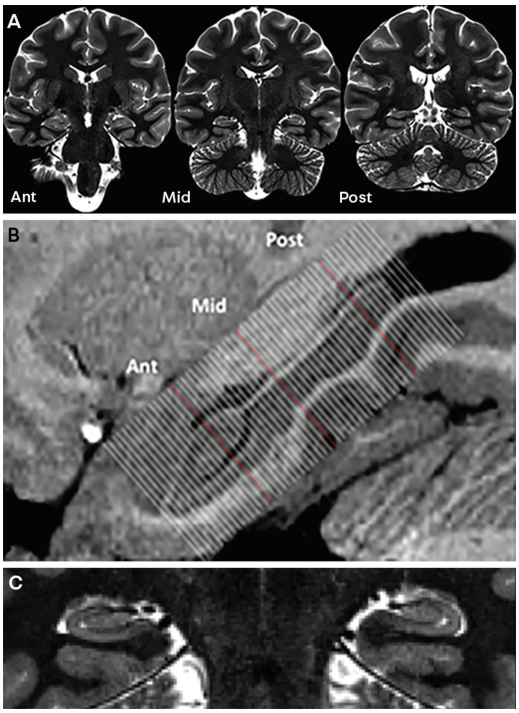

FIGURE 1-2

Harmonized neuroimaging of epilepsy structural sequences two-dimensional MRI (HARNESS-MRI) protocol at 3T. *A*, Coronal T2-weighted images at submillimeter in-plane resolution cover the entire extent of the temporal lobes and hippocampi. Representative cuts at the level of the hippocampal head (Ant), body (Mid), and tail (Post) are shown. *B*, Slices are acquired perpendicular to the long axis of the hippocampus, as shown in the sagittal view, to optimize the evaluation of the hippocampal internal structure. *C*, The magnified panel shows the densely myelinated molecular layer of the cornu ammonis (CA) and dentate gyrus fused across the hippocampal sulcus appearing as a dark ribbon, which allows for differentiation of these structures.

Reprinted with permission from Bernasconi A, et al. Epilepsia.[4] © 2019 International League Against Epilepsy.

can greatly increase diagnostic sensitivity and specificity compared with routine imaging protocols.

IMAGING PROTOCOLS ARE HELPFUL BUT NOT UNIVERSAL

In clinical radiology, there are no universal rules (ie, laws that are always true, irrespective of the circumstances) for choosing technology. Imaging protocols are general approaches, which hold in a narrow range of familiar circumstances, but for which exceptions almost always exist. This should not come as a surprise, as we know that medical knowledge, technology, and therefore rules change over time and, in medicine, circumstances (ie, context) mean everything. What are these circumstances? Not only clinical features such as symptoms and clinical history or urgency but also conditions that define the clinical care in a broader sense. These include access to imaging equipment, imaging staff members' experience with nonconventional imaging techniques, quality of routine brain MRI protocols ("Is a high-resolution scan already included?"), financial costs, reimbursement, time costs ("Is the scan time feasible?"), and even the level of communication between the radiologist and neurologist.

Luckily, the rules work fairly well, in part because they are being continuously improved, but they fail as universal laws for two reasons (this is also why the task of crafting a list of "how to do good imaging in every scenario" is impossible). First, the number of exceptions to rules is virtually infinite. As stated earlier, "MRI head without and with IV contrast" can come in many variants: older and newer technologies, combinations of different sequences, different flavors of the same sequences, and promising techniques in clinical research, resulting in virtually endless combinations of solutions to the same problem. Second, for most neurologic diseases no special sequences or protocols exist, because the

Copyright © American Academy of Neurology. Unauthorized reproduction of this article is prohibited.

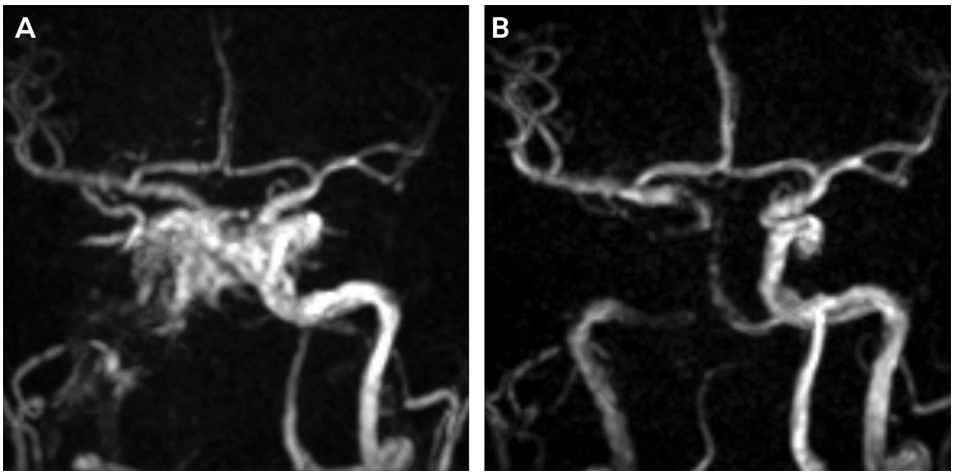

FIGURE 1-3
Carotid-cavernous fistula visualized with four-dimensional triggered angiography non–contrast-enhanced (TRANCE) imaging, which is a time-resolved three-dimensional MR angiography sequence based on arterial spin labeling technique (ie, no gadolinium was used). *A,* Initial status with early filling of the cavernous sinus from the right internal carotid artery. *B,* Posttreatment status, without the abnormal filling from the right internal carotid artery, and with normal filling of the circle of Willis branches.

KEY POINT

- The American College of Radiology Appropriateness Criteria provide a good starting point for finding the right imaging modality. The American College of Radiology does not prescribe disease-specific protocols.

information carried in CT or MRI images is mostly nonspecific and only a few product sequences or applications provide additional (physiologic) information that is proven to work in practice and has clinical evidence. Real disease-specific imaging requires specific pathologic features as targets (ie, biomarkers). For brain tumor, a contrast-enhanced MRI study, possibly with perfusion imaging, is an appropriate study to order today. In the near future, however, chemical exchange saturation transfer techniques, especially amide proton transfer, may become essential parts of tumor protocols (and therefore the "right" imaging studies to choose) if evidence shows that they improve outcomes by detecting histologic type, predicting tumor progression, or distinguishing radiation necrosis from recurrence better than current techniques (FIGURE 1-4[3]).[11-13] Similarly, high-resolution SWI in multiple sclerosis to detect the central vein sign is only optional according to the current MAGNIMS guidelines, but it may be recommended as standard in a future iteration.

Therefore, any specific technical recommendation today may be obsolete tomorrow, and this means that what makes imaging "right" is not the memorization and blind execution of a rigid set of rules but rather the knowledge that the rules are approximations and that one's understanding of circumstances (ie, broad clinical context) must be used to modify them. In more abstract terms, one employs an error-correcting mechanism before the error (the right study not being done) occurred. To fulfill this crucial role, neurologists must be familiar with the characteristics of imaging modalities (their reach, their limits, and how they complement each other) and must have expert clinical knowledge of the given case to direct the radiologist's thinking about the technical specifics (consider again the resolution of the T2-weighted image in the HARNESS protocol[3]). The success of imaging depends largely on communication between the neurologist, who knows the clinical history, and the radiologist, who has the most up-to-date technical

Copyright © American Academy of Neurology. Unauthorized reproduction of this article is prohibited.

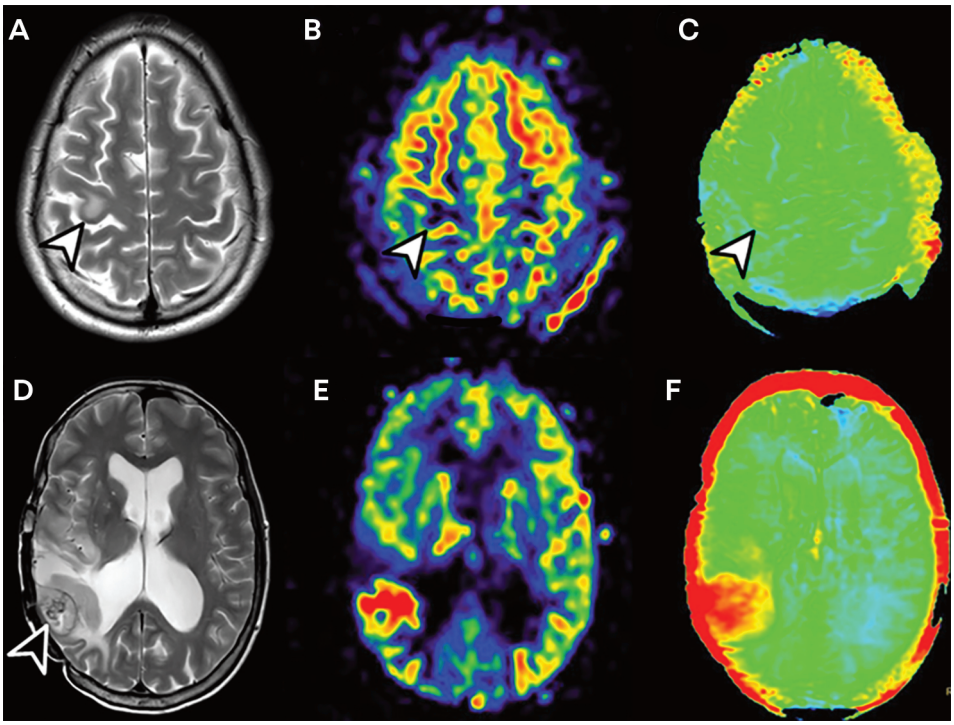

FIGURE 1-4

Two examples of brain tumor imaging using physiologic scans. T2-weighted (*A, D*), arterial spin labeling (*B, E*), and amide proton transfer (*C, F*) images are shown. The *top row* shows a case of low-grade glioma in the right precentral gyrus *(A, B, C, white arrowheads)*, with homogeneous high T2 signal, without increased cerebral blood flow on arterial spin labeling and without abnormal signal increase on amide proton transfer. The *bottom row* shows a case of recurrent glioblastoma with heterogeneous structure on T2-weighted imaging *(D, black arrowhead)* with markedly elevated cerebral blood flow and high signal on amide proton transfer.

Reprinted with permission from Pinter NK, Fritz JV. Neurol Clin.[3] © 2019 Elsevier Inc.

knowledge; the former guides the latter, and the case-specific optimal solution ("right imaging") is born out of this collaboration.

In sum, imaging protocols are not generally applicable laws but rather rules that change with time and may be overruled depending on the circumstances. With this understanding, some basic principles are helpful in getting closer to the right imaging for the right patient.

Relationship Between the Neurologist and the Radiologist

Problems surrounding neuroimaging planning and interpretation are common and can be prevented by maintaining active communication with the radiology team. Such communication is a natural and effective way to improve the quality of care and reduce frustration on both sides. Neurologists often complain, legitimately, that imaging studies do not address the most pressing clinical question, reports are too vague, or a study was not targeted to the area of interest. Establishing an engaging and trusting collegial relationship is therefore not just good but essential for successful care. Communication is key for two main reasons: (1) the default imaging approach may need to be changed based on relevant clinical data, and (2) communication can facilitate focused examinations and reporting.

Copyright © American Academy of Neurology. Unauthorized reproduction of this article is prohibited.

Providing the Necessary Clinical Information

In order to deliver good imaging results, the radiologist needs to be aware of the circumstances. Of course, the main practical reason to build the relationship with the radiology team is that imaging studies come in many forms and, with a few exceptions, no standard rules for disease-specific imaging or protocols equally apply to each scenario. Although radiologists design protocols, some cases do not fit into them and require direct input from the radiologist. In two different imaging suites, a routine brain MRI protocol could mean using significantly different variants of the same scan types, or even different sequences. Although it is not always necessary to discuss a case in advance, the radiology department always needs relevant clinical information and targeted questions from the neurologist to set up the right examination and use the right techniques. Perhaps an additional reconstruction must be done to highlight an anatomic area of interest, the contrast injection must be timed in a specific way, or a special sequence can be obtained. The importance of providing good clinical history and (when possible) targeted questions to help the radiologist's job cannot be overstated.

Choosing the Right Modality

As a general rule, one must always strive for the best diagnostic approach and quality with the means accessible, while following appropriate safety guidelines. When the goal is to evaluate bony structure, visualize calcification, or create a high-resolution map of a vascular structure, modalities that use an x-ray source will usually be the most informative—typically, CT or digital subtraction angiography. CT is also the method of choice in brain and spine imaging when time is of the essence and a quick definitive answer is needed, such as when ruling out hemorrhage in acute stroke care, when MRI would provide the most information but is not feasible for safety reasons or because of patient intolerance, or when not practical for reasons such as the presence of metal artifacts or a lack of access to an MRI scanner. Plain radiography can be helpful and sufficient in initial imaging of the postoperative spine to evaluate the position of prosthetics and hardware.[14] With ionizing studies, one should always follow the principle of "as low as reasonably achievable": refer the patient for studies that use ionizing radiation only if absolutely necessary, and make "every reasonable effort to maintain exposures to ionizing radiation as far below the dose limits as practical."[15] This is especially true in pediatric cases. Ultrasonography has a role mainly in vascular studies, primarily in the Doppler duplex of carotid arteries and transcranial Doppler, and in some neuromuscular settings. For everything else, there is MRI.

MRI Safety Considerations

An MR-unsafe implant simplifies the decision of ordering CT versus MRI. When the implant is MR-safe or MR-conditional, the specific information (ie, type of implant, product name, and ideally the safety card) should be sent along with the referral. Because the imaging team's primary concern is safety, the absence of this information at the MRI appointment can block the workflow; the study may have to be rescheduled or even canceled. Thus, providing MRI safety information with the referral is a courtesy that goes a long way with the radiology team. For more information, refer to the article "Safety Considerations in MRI and CT" by Robert E. Watson, MD, PhD, and Lifeng Yu, PhD,[16] in this issue of *Continuum*.

KEY POINTS

- Imaging protocols are not generally applicable laws but rather rules that may be adapted to the circumstances.
- Communication is key for two main reasons: (1) the default imaging approach may need to be changed based on relevant clinical data, and (2) communication can facilitate focused examinations and reporting.
- Even if MRI would be the method of choice, in urgent cases CT may be preferred.
- One should always follow the "as low as reasonably achievable" principle with studies that use ionizing radiation.
- Providing MRI safety information for patients with implants improves safety.

Copyright © American Academy of Neurology. Unauthorized reproduction of this article is prohibited.

Role of Contrast Agents

CT or MRI contrast agents can add valuable diagnostic information in many cases, such as brain tumors or inflammatory diseases. However, contrast agents do not automatically make a scan more informative, and clinical gain versus safety risks should always be considered.

For example, for nonspecific indications such as dizziness or headache, the contrast injection may have additional value, but often the nonenhanced study is enough. This principle is reflected in the ACR criteria.[1] It can be challenging to decide whether a contrast agent should be used; again, the clinical scenario and the presumed diagnosis have great significance in this decision. It should also be taken into account that gadolinium-based contrast agents create deposits in normal tissue and may have long-term safety implications (although, to date, no neurologic clinical relevance has been demonstrated).[17-19]

WHAT IS AN IMAGING PROTOCOL, AND WHY IS MORE THAN ONE NECESSARY IN THE FIRST PLACE?

If we had one imaging modality that was diagnostic for every condition, every tissue type, and every stage of any disease, there would be no need for multiple different imaging technologies. Consider MRI: T1- and T2-weighted, FLAIR, diffusion-weighted, susceptibility-weighted, perfusion, and other sequences would be redundant because one universal scan would be perfectly informative with respect to tissue contrast, water diffusion, perfusion, hemorrhage, iron, and other features. Disease-specific imaging protocols are mostly born out of necessity and refer to a distinct way of manipulating conventional image acquisition or reconstruction in order to produce specific views that highlight the pathologic features of the disease. Real disease-specific imaging operates with biomarkers.

We need these different sequences because they all provide some but not all tissue information, and they complement each other. Fundamentally, that is the reason for using multiple scan types and imaging protocols that are customized to different diseases. Therefore, developing disease-specific imaging protocols is a necessity that arises from the nonuniversality of state-of-the-art techniques, and the value of such protocols holds only until a more universal technology replaces them. Take, for example, the three-dimensional FLAIR sequence and its applications. For multiple sclerosis, the previous MAGNIMS recommendations were to use axial and sagittal FLAIR scans (to achieve the best possible visualization of the corpus callosum), whereas the 2021 recommendation prefers three-dimensional FLAIR imaging.[2] The old guidelines reflected the then-current state of the technology, with the FLAIR sequence available only in two-dimensional versions on most clinical scanners with a slice thickness of 3 mm to 5 mm, which did not allow multiplanar reconstructions; thus the acquisition plane did matter. As three-dimensional FLAIR acquisition emerges, this rule becomes obsolete, with the possibility of acquiring isotropic high-resolution scans that can be reformatted in any arbitrary plane. A single acquisition provides traditional axial views, sagittal views in multiple sclerosis, or coronal views of the temporal lobes in epilepsy. A standard MRI protocol with three-dimensional T1-weighted and FLAIR sequences thus becomes sufficient for the majority of indications. It can be reasoned against the three-dimensional approach that multiplanar data acquisition has value itself because it helps in clarifying certain signal abnormalities. This idea is worth considering, but the

Copyright © American Academy of Neurology. Unauthorized reproduction of this article is prohibited.

overall principle still holds; with the evolution of technology, applications become more universal, which renders previous specific applications (rules that hold only in a narrow range of familiar circumstances) decreasingly necessary. Another example is a dedicated orbit protocol that includes a fat-suppressed T1-weighted sequence with high in-plane resolution. Again, deploying a high-resolution full-brain three-dimensional T1-weighted scan with embedded fat suppression allows us to abandon the dedicated orbit scan.[3] Of course, for the three-dimensional FLAIR sequence, in both multiple sclerosis and epilepsy the disease specificity of the protocol meant a certain way of sampling and visualizing existing data and not the generation of a fundamentally new type of data. Adding qualitatively novel data would be a different challenge. For example, perfusion MRI could be part of routine brain imaging if the specific technology met certain criteria, such as being highly reproducible, quantifiable, clinically validated in different diseases, and fast to acquire.

TOWARD UNIVERSALITY IN IMAGING—A THOUGHT EXPERIMENT

If a theoretical universal MRI scan would also be good for high-resolution visualization of osseous tissue, with geometric fidelity that matches that of CT, then it could become an alternative for bone imaging. And if the scan time were no more than 1 or 2 minutes, then it would automatically become the method of choice for almost every indication where CT was the primary application before, with the exception of cases with MRI incompatibility. But if the technology were developed on a low-field-strength MRI system with none of the safety issues of the current clinical systems, that would render CT scanning potentially unnecessary (spectral CT[20] is ignored for the sake of the argument). Furthermore, if this system were also lightweight, portable, and inexpensive, it would have the potential to become so abundant in the world that it could be commonplace to get a quick brain scan even without the patient seeing a neurologist first. This may not be as futuristic as it sounds: it is easy to imagine that current research and development efforts in the areas of MRI of bone,[21,22] synthetic MRI,[23-25] and portable ultra-low-field MRI scanners[26-28] will be combined in one technology. Evolution of technology changes best practices dramatically, in neurology and medicine as a whole.

Imaging technologies advance, causing clinical protocols to change. A powerful future technology could rewrite prevailing practices regarding what is considered "right" imaging or even eliminate the question entirely. This will depend on many factors, an important one being the inertia of the medical industry and clinical practices.

CREATING DISEASE-SPECIFIC IMAGING PROTOCOLS

As previously discussed, many opportunities exist to develop imaging protocols that are "right" for a disease or a certain clinical question. Imaging technologies, especially MRI, offer ample room for creativity, which can, unfortunately, work against us; it is easy to go down the rabbit hole of protocol optimization because there are simply too many parameters to vary. Thus, before engaging in this task, one should review the plan according to practical criteria, such as concrete goals, realistic clinical gain, technical specifics, time constraints, and labor, as proficiency in the acquisition and interpretation of new techniques takes time (FIGURE 1-5). Preparation that involves a literature review and phased discussion with imaging personnel (ie, radiologists and technologists) will maximize

KEY POINTS

- Contrast agents do not automatically make a scan more informative, and clinical gain versus safety risks should always be considered.
- Disease-specific imaging protocols are mostly born out of necessity and refer to a distinct way of manipulating conventional image acquisition or reconstruction in order to produce specific views that highlight pathologic features of the disease. Real disease-specific imaging operates with biomarkers.
- Imaging technologies advance, causing clinical protocols to change. A powerful future technology could rewrite prevailing practices regarding what is considered "right" imaging, or even eliminate the question entirely. This will depend on many factors, an important one being the inertia of the medical industry and practices.

Copyright © American Academy of Neurology. Unauthorized reproduction of this article is prohibited.

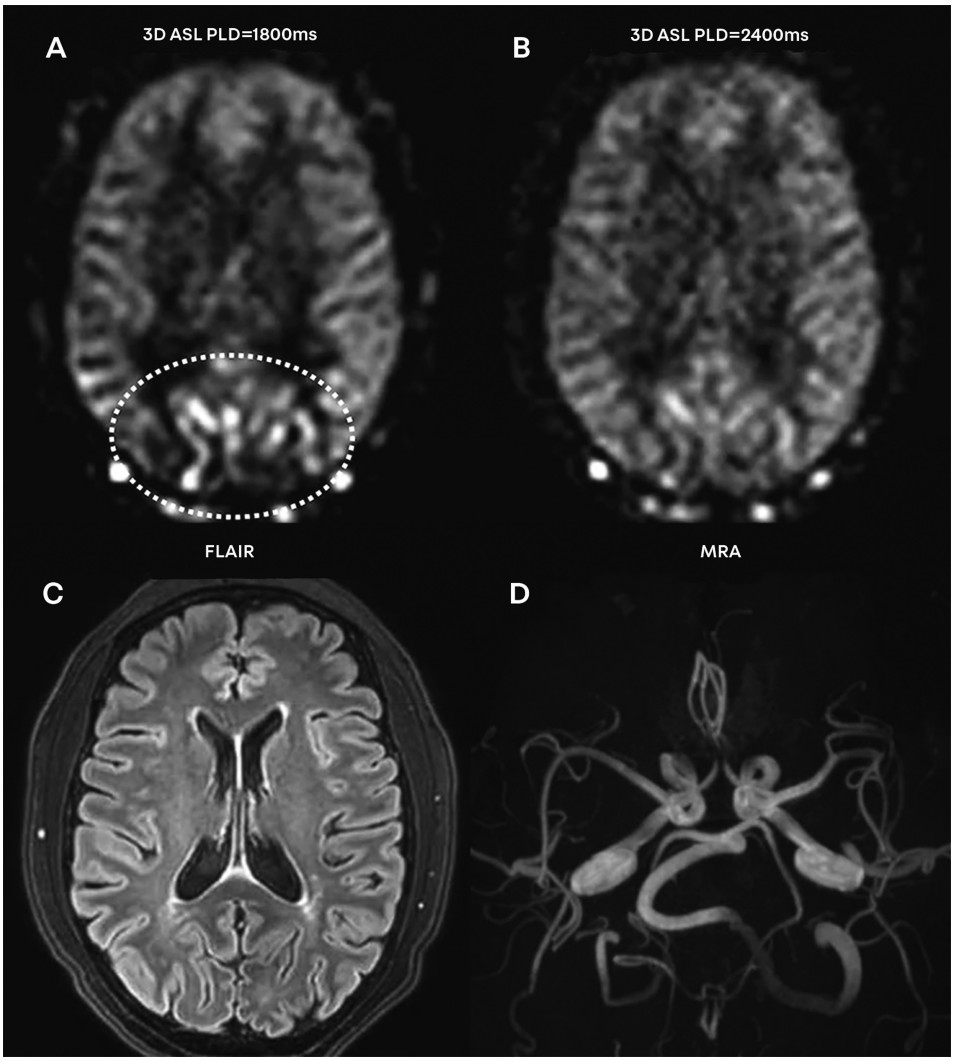

FIGURE 1-5

Effect of of timing on arterial spin labeling. *A, B,* Two consecutive arterial spin labeling (ASL) scans with different postlabeling delay values. With shorter postlabeling delay (PLD) (*A*), alternating areas of high and low signal are seen in the posterior territories *(dashed oval)*. This is known as arterial transit artifact, and it is caused by the longer arrival time (slower flow) in the vertebrobasilar system compared with internal carotid artery branches. The applied 1800 ms was not long enough for the labeled blood to reach the posterior capillaries and parenchyma; it still resides in the macrovascular compartment. This manifests as high signal in the posterior cerebral artery branches and concurrent low signal in the parenchyma, which can be misinterpreted as hypoperfusion. However, with longer postlabeling delay (*B*), the labeled blood has reached the tissue, demonstrated by the more evenly distributed signal. This is consistent with maintained perfusion. In other words, the shorter postlabeling delay is optimized to the arrival time of the anterior circulation and is suboptimal for the posterior circulation. Fluid-attenuated inversion recovery (FLAIR) MRI (*C*) and time-of-flight MR angiography (MRA) (*D*) show no evidence of acute ischemia and normal vascular status.

Copyright © American Academy of Neurology. Unauthorized reproduction of this article is prohibited.

success. For example, building a protocol for intracranial vessel wall imaging can start with gathering published indications and technical parameters. We will learn that vessel wall imaging has been applied in intracranial aneurysms, intracranial atherosclerotic disease, vasculitis, moyamoya disease, and reversible cerebral vasoconstriction syndrome.[10] The typical technique is a two-dimensional or three-dimensional T1-weighted or T2-weighted sequence, with high resolution (0.4 mm to 0.7 mm in-plane), before and after contrast administration. It is also recommended to use flow compensation to create "black blood" images. With this information, and based on disease prevalence, one can estimate how many patients could potentially benefit from vessel wall imaging and how challenging building the protocol will be. It is easier to replicate a sequence on the same scanner that it was developed on and more difficult if it must be created from scratch on a different platform: one must consider a two-dimensional versus three-dimensional approach, the scan time of high-resolution sequences, and image contrast parameters, including flow compensation. If the goal is to have more than one kind of image contrast, this will be done for every additional sequence. The first version of the scan can be tested on a small number of patients or volunteers to assess general image quality and reproducibility. Often the first version is improved upon in an attempt to increase the signal-to-noise ratio, resolution, or speed. Once this iterative process of sequence building and testing is complete and the final version is ready to deploy, we can start planning for the optimal use of the new protocol. Vessel wall scans can be up to 8 to 10 minutes long, adding significant time to the examination. A T1-weighted scan before and after contrast injection can add 16 to 20 minutes, forcing the clinical team to carefully consider which patients are the "right" candidates. As stated before, interdisciplinary teamwork is needed to achieve clinical success.

MRI protocol optimization is the process of creating a disease-specific protocol via iterative customization of imaging sequences. It can provide significant added value, but the process can be lengthy and resource-intensive. The optimization must be driven by clinical outcome and achieved through a systematic approach.

KEY POINT

● ***MRI protocol optimization*** **is the process of creating a disease-specific protocol via iterative customization of imaging sequences. It can provide significant added value, but the process can be lengthy and resource-intensive. The optimization must be driven by clinical outcome and achieved through a systematic approach.**

CONCLUSION

Imaging can be performed in myriad ways, and broadly described protocols are often insufficient to obtain a study that is focused on key details. The right imaging approach for the individual patient is the one that considers both general recommendations and case-specific circumstances (eg, targeted questions), thus providing efficient decision support. An outcome-oriented collaboration between neurologists and radiologists is essential to maximize diagnostic success.

REFERENCES

1 American College of Radiology. ACR Appropriateness Criteria. Accessed July 14, 2022. acr.org/Clinical-Resources/ACR-Appropriateness-Criteria

2 Wattjes MP, Ciccarelli O, Reich DS, et al. 2021 MAGNIMS–CMSC–NAIMS consensus recommendations on the use of MRI in patients with multiple sclerosis. Lancet Neurol 2021;20(8):653-670. doi:10.1016/S1474-4422(21)00095-8

Copyright © American Academy of Neurology. Unauthorized reproduction of this article is prohibited.

3 Pinter NK, Fritz JV. Neuroimaging for the neurologist: clinical MRI and future trends. Neurol Clin 2020;38(1):1-35. doi:10.1016/j.ncl.2019.08.002

4 Bernasconi A, Cendes F, Theodore WH, et al. Recommendations for the use of structural magnetic resonance imaging in the care of patients with epilepsy: a consensus report from the International League Against Epilepsy Neuroimaging Task Force. Epilepsia 2019;60(6):1054-1068. doi:10.1111/epi.15612

5 Greenberg SM, Charidimou A. Diagnosis of cerebral amyloid angiopathy: evolution of the Boston criteria. Stroke 2018;49(2):491-497. doi:10.1161/STROKEAHA.117.016990

6 Dissaux B, Eugène F, Ognard J, et al. Assessment of 4D MR angiography at 3T compared with DSA for the follow-up of embolized brain dural arteriovenous fistula: a dual-center study. AJNR Am J Neuroradiol 2021;42(2):340-346. doi:10.3174/ajnr.A6903

7 Connor SEJ. Imaging of the vestibular schwannoma: diagnosis, monitoring, and treatment planning. Neuroimaging Clin N Am 2021;31(4):451-471. doi:10.1016/j.nic.2021.05.006

8 Haller S, Zaharchuk G, Thomas DL, et al. Arterial spin labeling perfusion of the brain: emerging clinical applications. Radiology 2016;281(2):337-356. doi:10.1148/radiol.2016150789

9 Amin-Hanjani S, Du X, Zhao M, et al. Use of quantitative magnetic resonance angiography to stratify stroke risk in symptomatic vertebrobasilar disease. Stroke 2005;36(6):1140-1145. doi:10.1161/01.STR.0000166195.63276.7c

10 Vranic JE, Hartman JB, Mossa-Basha M. High-resolution magnetic resonance vessel wall imaging for the evaluation of intracranial vascular pathology. Neuroimaging Clin N Am 2021;31(2):223-233. doi:10.1016/j.nic.2021.01.005

11 Jia X, Lai C, Ma X. [Progress in clinical research of amide proton transfer imaging]. Zhongguo Yi Liao Qi Xie Za Zhi 2020;44(2):185-188. doi:10.3969/j.issn.1671-7104.2020.02.018

12 Kamimura K, Nakajo M, Yoneyama T, et al. Amide proton transfer imaging of tumors: theory, clinical applications, pitfalls, and future directions. Jpn J Radiol 2019;37(2):109-116. doi:10.1007/s11604-018-0787-3

13 Nichelli L, Casagranda S. Current emerging MRI tools for radionecrosis and pseudoprogression diagnosis. Curr Opin Oncol 2021;33(6):597-607. doi:10.1097/CCO.0000000000000793

14 Corona-Cedillo R, Saavedra-Navarrete MT, Espinoza-Garcia JJ, et al. Imaging assessment of the postoperative spine: an updated pictorial review of selected complications. Biomed Res Int 2021;2021:9940001. doi:10.1155/2021/9940001

15 United States Nuclear Regulatory Commission. USNRC web site. Accessed July 14, 2022. nrc.gov/reading-rm/basic-ref/glossary/alara.html

16 Watson RE, Yu L. Safety considerations in MRI and CT. Continuum (Minneap Minn) 2023;29(1, Neuroimaging):27-52.

17 Pinter NK, Klein JP, Mechtler LL. Potential safety issues related to the use of gadolinium-based contrast agents. Continuum (Minneap Minn) 2016;22(5, Neuroimaging):1678-1684. doi:10.1212/CON.0000000000000378

18 Mallio CA, Rovira À, Parizel PM, Quattrocchi CC. Exposure to gadolinium and neurotoxicity: current status of preclinical and clinical studies. Neuroradiology 2020;62(8):925-934. doi:10.1007/s00234-020-02434-8

19 Smith TE, Steven A, Bagert BA. Gadolinium deposition in neurology clinical practice. Ochsner J 2019;19(1):17-25. doi:10.31486/toj.18.0111

20 Willemink MJ, Persson M, Pourmorteza A, Pelc NJ, Fleischmann D. Photon-counting CT: technical principles and clinical prospects. Radiology 2018;289(2):293-312. doi:10.1148/radiol.2018172656

21 Johnson B, Alizai H, Dempsey M. Fast field echo resembling a CT using restricted echo-spacing (FRACTURE): a novel MRI technique with superior bone contrast. Skeletal Radiol 2020;50. doi:10.1007/s00256-020-03659-7

22 Chong LR, Lee K, Sim FY. 3D MRI with CT-like bone contrast - an overview of current approaches and practical clinical implementation. Eur J Radiol 2021;143:109915. doi:10.1016/j.ejrad.2021.109915

23 Ryu KH, Baek HJ, Skare S, et al. Clinical experience of 1-minute brain MRI using a multicontrast EPI sequence in a different scan environment. AJNR Am J Neuroradiol 2020;41(3):424-429. doi:10.3174/ajnr.A6427

24 Delgado AF, Kits A, Bystam J, et al. Diagnostic performance of a new multicontrast one-minute full brain exam (EPIMix) in neuroradiology: a prospective study. J Magn Reson Imaging 2019;50(6):1824-1833. doi:10.1002/jmri.26742

25 Ha JY, Baek HJ, Ryu KH, et al. One-minute ultrafast brain MRI with full basic sequences: can it be a promising way forward for pediatric neuroimaging? AJR Am J Roentgenol 2020;215(1):198-205. doi:10.2214/AJR.19.22378

26 Deoni SCL, Medeiros P, Deoni AT, et al. Development of a mobile low-field MRI scanner. Sci Rep 2022;12(1):5690. doi:10.1038/s41598-022-09760-2

27 O'Reilly T, Teeuwisse WM, de Gans D, Koolstra K, Webb AG. In vivo 3D brain and extremity MRI at 50 mT using a permanent magnet Halbach array. Magn Reson Med 2021;85(1):495-505. doi:10.1002/mrm.28396

28 Yuen MM, Prabhat AM, Mazurek MH, et al. Portable, low-field magnetic resonance imaging enables highly accessible and dynamic bedside evaluation of ischemic stroke. Sci Adv 2022;8(16):eabm3952. doi:10.1126/sciadv.abm3952

Copyright © American Academy of Neurology. Unauthorized reproduction of this article is prohibited.

Safety Considerations in MRI and CT

By Robert E. Watson, MD, PhD; Lifeng Yu, PhD

REVIEW ARTICLE

CONTINUUM AUDIO INTERVIEW AVAILABLE ONLINE

ABSTRACT

OBJECTIVE: **MRI and CT are indispensable imaging modalities for the evaluation of patients with neurologic disease, and each is particularly well suited to address specific clinical questions. Although both of these imaging modalities have excellent safety profiles in clinical use as a result of concerted and dedicated efforts, each has potential physical and procedural risks that the practitioner should be aware of, which are described in this article.**

LATEST DEVELOPMENTS: **Recent advancements have been made in understanding and reducing safety risks with MR and CT. The magnetic fields in MRI create risks for dangerous projectile accidents, radiofrequency burns, and deleterious interactions with implanted devices, and serious patient injuries and deaths have occurred. Ionizing radiation in CT may be associated with shorter-term deterministic effects on biological tissues at extremely high doses and longer-term stochastic effects related to mutagenesis and carcinogenesis at low doses. The cancer risk of radiation exposure in diagnostic CT is considered extremely low, and the benefit of an appropriately indicated CT examination far outweighs the potential risk. Continuing major efforts are centered on improving image quality and the diagnostic power of CT while concurrently keeping radiation doses as low as reasonably achievable.**

ESSENTIAL POINTS: **An understanding of these MRI and CT safety issues that are central to contemporary radiology practice is essential for the safe and effective treatment of patients with neurologic disease.**

INTRODUCTION

MRI and CT are essential imaging modalities for screening, diagnosis, treatment planning, and postprocedure follow-up of patients with neurologic disease. Since its introduction into the clinical realm in the early 1980s, MRI has distinguished itself as the primary imaging modality for neuroimaging of the brain, spine, and head and neck because of its superb distinction of soft tissue contrast. Although MRI is not based on x-rays and thus is not affected by radiation-related concerns, the unique fields underlying MRI present significant risks relating to projectiles, burns, and specific conditions needed for safe scanning of implanted devices. Unfortunately, deaths and serious injuries involving patients and health care staff members have occurred during MRI procedures.

CITE AS:
CONTINUUM (MINNEAP MINN) 2023;29(1, NEUROIMAGING): 27–53.

Address correspondence to Dr Robert E. Watson, Department of Radiology, Mayo Clinic, 200 First St SW, Rochester, MN 55905, Watson.robert16@mayo.edu.

RELATIONSHIP DISCLOSURE:
Dr Watson has a noncompensated relationship as a Chair with the American Board of Magnetic Resonance Safety that is relevant to American Academy of Neurology interests or activities. Dr Yu reports no disclosure.

UNLABELED USE OF PRODUCTS/INVESTIGATIONAL USE DISCLOSURE:
Drs Watson and Yu report no disclosures.

© 2023 American Academy of Neurology.

Copyright © American Academy of Neurology. Unauthorized reproduction of this article is prohibited.

The number of CT examinations performed has increased exponentially because of its fast volume coverage speed (up to 75 cm/s) and high spatial resolution (up to approximately 150 μm). It is estimated that more than 70 million CT examinations are performed annually in the United States.[1] However, CT is also associated with safety concerns that must be recognized, including radiation exposure, equipment malfunction, issues related to CT personnel and operators, and effects on electronic medical devices.

Increased safety events related to MRI and CT can be anticipated because of constantly growing patient numbers and throughput, with increasingly complex systems and vast amounts of information, together with the increasing number of patients with implanted devices. Such safety events can be minimized by improving education and rigorously abiding by well-designed policies and procedures. As will be made clear, clinicians referring patients for MRI and CT can also play an important role in maximizing patient safety in this challenging environment.

MRI SAFETY CONSIDERATIONS

The magnetic fields in MRI create significant risks for dangerous projectile accidents, radiofrequency burns, and deleterious interactions with implanted devices, which may lead to serious patient injury or death.

MRI Fields and Creation of an MRI

MRIs are essentially depictions of protons within different body tissues.[2] Randomly oriented protons align with the powerful main magnetic field (B_o) created by a helium-cooled superconducting magnet, typically 1.5T, 3T, or (now cleared by the US Food and Drug Administration [FDA]) 7T. A radiofrequency coil, typically located within the wall of the magnet (**FIGURE 2-1**), emits radiofrequency energy pulses, which change the orientation of the proton alignment and cause the protons to resonate, or spin in phase with one another. When this time-varying radiofrequency magnetic field (B_1) is turned off, the protons "relax" and begin to realign with the main magnetic field; as they do so, they give off their own radiofrequency signal (which is the basis of T1 signal). Also, as the radiofrequency pulse is turned off, the resonance with which the protons were spinning in phase with each other is lost (dephasing). The speed of dephasing is related to T2 signal, with greater T2 signal associated with slower dephasing. For example, protons in fat realign quickly when the radiofrequency pulse is turned off, leading to their characteristic T1 hyperintensity. Protons in water molecules dephase slowly, leading to the characteristic T2 hyperintensity in high-water-content tissues, cysts, and CSF. Finally, another set of radiofrequency coils producing "gradient" magnetic fields, also known as the time-varying gradient magnetic field (dB/dt), permits the MRI to "spatially encode" the radiofrequency signals such that through mathematical processing, the characteristic radiofrequency signals that are being received by the MRI can be placed in the proper anatomic location.

Safety Risks of the Different Components of MRI

The three different magnetic fields involved in creation of MR images are each associated with defined safety risks.[3,4]

The main magnetic field (B_o) is associated with risks related to its ability to produce translation and torque on ferromagnetic objects that come into

Copyright © American Academy of Neurology. Unauthorized reproduction of this article is prohibited.

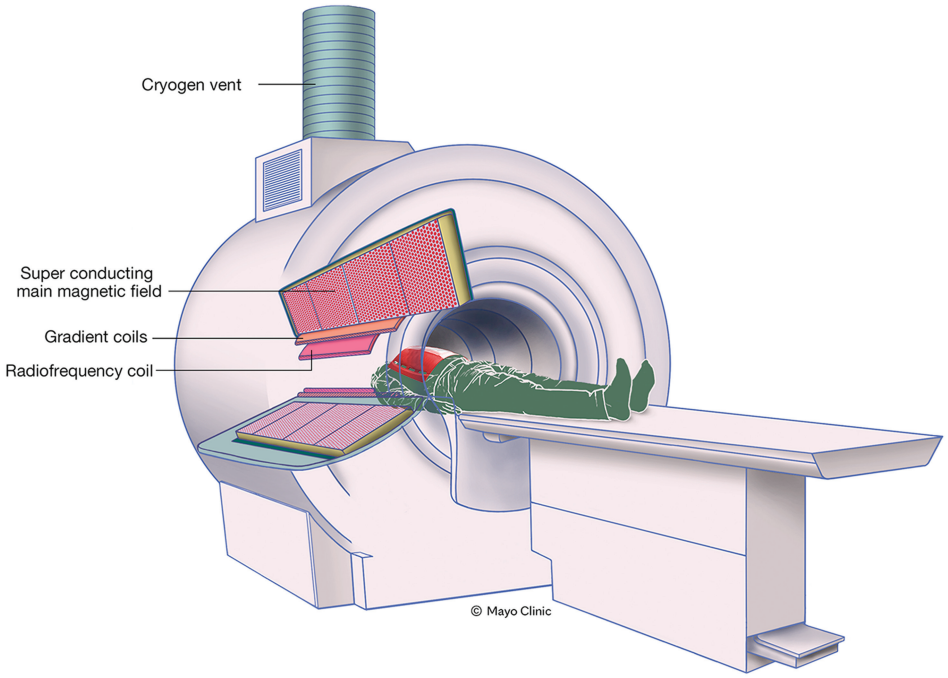

FIGURE 2-1

Schematic diagram of typical superconducting MR scanner. Closest to the bore wall adjacent to the patient are the radiofrequency coils; unsafe physical proximity to these can cause patient heating and burns. Peripheral to those are gradient coils underlying the B_1 field; rapid current changes in these produce the characteristic loud noises in MRI. Also, these fields can underlie peripheral nerve stimulation. The outermost ring is associated with the main magnetic field, B_0, creating the strong magnetic translational and torque forces in MRI. All three fields can interact with implanted and on-planted medical devices.

Reprinted with permission of the Mayo Foundation for Medical Education and Research. © Mayo Clinic.

KEY POINT

- **The three different magnetic fields involved in the creation of MRIs are each associated with defined safety risks.**

proximity. Deaths and serious injuries have resulted from these types of projectile incidents. The B_o field can also interact with implanted devices, such as older MR-unsafe ferromagnetic aneurysm clips, which can also cause deaths and serious injuries.

The time-varying radiofrequency magnetic field (B_1) is associated with risks of heating and burns and potentially dangerous heating of components of implanted devices, particularly leads in neurostimulators and cardiac devices.

The time-varying gradient magnetic field (dB/dt) is associated with risks of patient peripheral nerve stimulation and pain, interaction with implanted devices, and the characteristic loud noise in MRI.

Cryogens, typically liquid helium, are used for cooling the superconducting magnet wire coils. "Quenching" the magnet entails allowing the liquid helium to "boil off," resulting in the superconducting magnet's quickly losing its magnetic (B_o) qualities. Quenching usually occurs intentionally (as in an emergency, as described in the section titled "MRI Safety Labeling" later in this article) but can occur spontaneously and unexpectedly. As the liquid helium converts to the gaseous state, its volume increases by 760-fold; therefore, well-maintained reliable exhaust pathways to the outside external environment must be ensured. Typically, approximately 1800 L of liquid helium bathe the wires creating the superconduction. If the venting system fails, this volume of gaseous helium

Copyright © American Academy of Neurology. Unauthorized reproduction of this article is prohibited.

(1.37 million liters), explosively released into a relatively small MRI magnet room, can lead to serious injury or death as oxygen is quickly displaced. For this reason, it is taught that if a person is in a magnet room during a quench with a venting failure, they should drop to the floor as rapidly as possible to be near oxygen-containing air that is displaced downward by the less dense helium that first floods the upper regions of the room.

Overview of MRI Safety Events and Accidents

The MRI room is one of the most dangerous environments in the hospital. Root-cause analyses of MRI-related serious injuries, deaths, and near misses have revealed that in the vast majority of cases the problems have been related not to the MRI equipment itself but to human error and related shortcomings in systems and procedures. To continually improve MRI safety, it is essential that sites have reliable safety event reporting systems to investigate incidents. With this approach, necessary processes and procedures can be built in and appropriate education and training of staff can be conducted.

Minimum MRI Safety Knowledge

Three core points about MRI safety should be widely recognized by everyone in the health care setting:

1. **The magnet is always "on." A contemporary superconducting magnet and its powerful main magnetic field (B_0) are always active, regardless of whether a patient is being scanned or not. It is not "off" when no patient is in the scanner. Thus, entering the magnet room with a patient in a ferromagnetic wheelchair between MRI sessions could result in the wheelchair becoming a potentially deadly projectile, perhaps pinning the patient or staff member against the magnet with extraordinary force.**
2. **Only trained MRI personnel should enter the magnet room in a patient emergency (eg, cardiopulmonary arrest). The patient will be removed from the magnet and brought outside the magnet room for treatment and resuscitation. Ferromagnetic objects, including defibrillators, could become dangerous projectiles if a code team enters the magnet room.**
3. **To the extent possible, accurate information about a patient's implanted devices should be provided to the MRI team with the MRI order. Patients are frequently unaware of what is implanted in them, or they may have cognitive difficulties that prevent them from providing an accurate history. This situation can result in a patient with a potentially unsafe implanted device being scanned, with a possible consequence of death or serious injury.**

MRI Safety Zones

The *ACR Manual on MR Safety* from the American College of Radiology[4] (ACR) recommends a four-zone delineation of spaces related to MRI in an effort to prevent serious accidents (**FIGURE 2-2**).

The magnet itself, with its potential for serious ferromagnetic attraction–related projectile events, is situated in zone IV. Entrance to zone IV is restricted to highly trained MRI personnel, and any non-MRI personnel and patients gaining access to zone IV are under the direct supervision of these MRI personnel. The door to zone IV is opened only for monitored patient and personnel crossing and at other times is closed or protected by a safety strap, a plastic chain, or another physical barrier to prevent unauthorized individuals (who may be carrying lethal ferromagnetic objects such as oxygen canisters) from gaining access. Individuals with implanted devices can also be at great risk

Copyright © American Academy of Neurology. Unauthorized reproduction of this article is prohibited.

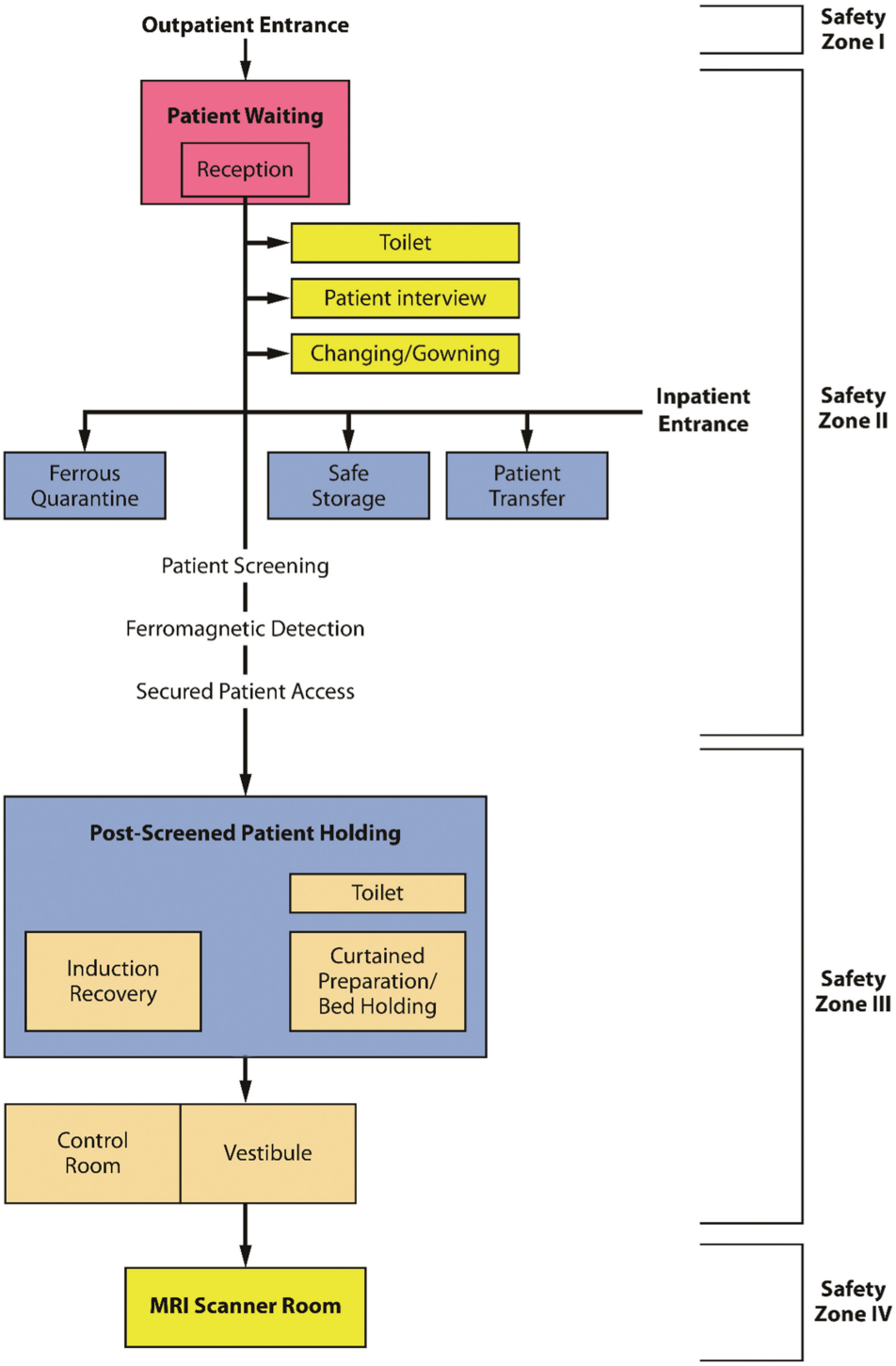

FIGURE 2-2

Depiction of the four-zone model of MRI safety. Transition from zone II into zone III is into the "controlled access area," through which entry is made into zone IV, the magnet room itself, which is the "projectile zone."

Reprinted with permission from the American College of Radiology, *ACR Manual on MR Safety*.[4] © 2020 American College of Radiology.

KEY POINTS

- The MRI room is one of the most dangerous environments in the hospital.
- The magnet is always "on." The tremendously powerful magnetic field creates a dangerous projectile risk in the MRI room regardless of whether a patient is being scanned or not.
- Only trained MRI personnel should enter the magnet room in a patient emergency (eg, cardiopulmonary arrest).
- Accurate information about a patient's implanted devices should be provided to the MRI team with the MRI order.
- Physical spaces related to MRI are defined by a four-zone model. Access to zone III (the technologist control area) and zone IV (the magnet room) is restricted.

Copyright © American Academy of Neurology. Unauthorized reproduction of this article is prohibited.

if they enter this zone, as the strong magnetic field can interact with these devices in unpredictable ways.

Zone III, the "controlled access area," typically houses the MRI technologist and MRI control panel. The doors to zone III are locked, with access granted only to properly trained MRI personnel. Access is often through keycard-activated lock mechanisms.

Zone II is the area outside zone III and is the typical location for patient changing areas, nursing assessment, and placement of IV lines for contrast administration.

Zone I is the surrounding public area, without MRI safety concerns.

MRI Safety Labeling

The standard MRI labeling terms *MR-safe*, *MR-conditional*, and *MR-unsafe* have been designated for use by the American Society for Testing Materials (ASTM) International in its standard "ASTM F2503-13: Standard Practice for Marking Medical Devices and Other Items for Safety in the Magnetic Resonance Environment (FIGURE 2-3).[5]

An *MR-safe* implant or device is safe in all MR environments. It contains no metallic, ferromagnetic, or conducting elements. An example would be a plastic catheter.

An *MR-conditional* implant or device is one for which, to be safe in the MR environment, strict conditions must be met. For example, certain neurostimulators can be safely scanned if the appropriate parameters for scanning are met, including the magnet field strength (1.5T, 3T), power of radiofrequency deposition (often measured in specific absorption rate), and time duration of scanning.

An *MR-unsafe* implant or device is unsafe in all MR environments. It could contain metallic, ferromagnetic, or conducting elements. MR-unsafe objects include ferromagnetic oxygen tanks, IV poles, and other pieces of equipment that could become dangerous projectiles. MR-unsafe implanted devices are those with metallic elements that are unsafe in all MR environments. Examples include certain neurostimulators with MR-unsafe pulse generators and lead systems ("active" implants in that they have an energy source) and certain older aneurysm clips that contain ferromagnetic metal (an example of a "passive" implant).

FIGURE 2-3

MRI safety symbols: MR-safe, green square; MR-conditional, yellow triangle; MR-unsafe, red circle.

Reprinted with permission from the American College of Radiology, ACR Manual on MR Safety.[4] © 2020 American College of Radiology.

Copyright © American Academy of Neurology. Unauthorized reproduction of this article is prohibited.

Use of the term *MR-compatible* is strongly discouraged, as it engenders confusion and uncertainty by not drawing a clear distinction between an MR-safe and an MR-conditional device.

Types of MRI Safety Events and Accidents

Specific types of MRI safety events and accidents include those involving dangerous projectiles, burns, and scanning of implanted devices. It is essential to have systems and procedures in place to prevent these categories of accidents and ensure safe practices for patients with implanted devices.

PROJECTILES. As stated previously, a variety of MRI safety events have led to deaths and serious injuries.[6,7] Many of these incidents involve objects that become projectiles, such as ferromagnetic oxygen tanks brought into zone IV magnet rooms. An example of this type of event occurred in 2001; a 6-year-old boy was killed while he was being scanned for follow-up of a resected brain tumor.[8] Two additional deaths from ferromagnetic oxygen tanks occurred in 2018 and 2021 in India and South Korea, respectively. Many other items have also become dangerous projectiles (including gurneys, IV poles, scissors, and guns), becoming attached to the magnet with great force, in some cases leading to injury. If an individual is pinned to the magnet by a ferromagnetic object, the magnet can be quenched by releasing the liquid helium cryogen that maintains the superconduction.

The magnetic fields around the opening of an MRI bore are not uniform; rather, there is a steep gradient in the forces as the magnet is approached.[2,9] Thus, an unsuspecting individual could be carrying a ferrous object into the magnet room and sense no pull on the object until they are within a critical proximity, when the object would be forcefully pulled from their grip without warning or any opportunity to counter the attractive force.

The main magnetic field can also interact with ferromagnetic implanted devices. Some models of older MR-unsafe intracranial aneurysm clips contained substantial amounts of ferromagnetic metal. Patient deaths have resulted when an unknown or improperly documented aneurysm clip was exposed to the strong magnetic forces during MRI, highlighting the necessity of accurately documenting the make and model of the clip before permitting the patient to undergo MRI. Since the 1990s, manufacturers have adapted the alloys in clips so that they are not ferromagnetic, and they have MR-conditional labeling.

BURNS. Heating and burns related to the radiofrequency field are the most common type of MRI safety event reported to the FDA's Manufacturer and User Facility Device Experience data repository.[10] Apposition of a patient's skin to the MR scanner's inner bore wall surface can cause a near-field radiofrequency burn. Therefore, insulating pads must be placed between the patient and the bore wall to prevent burns. During MRI performed under general anesthesia, severe burns can result if a pad slips out of its proper insulating position, and great care must be taken while advancing an anesthetized patient into the bore to prevent this. This issue can be especially problematic with very large or obese patients.

Burns can also occur in body areas with small amounts of skin-to-skin contact. Radiofrequency fields can induce electrical currents within the body; thus, in small areas of skin-to-skin contact, current can flow across a high-resistance contact zone, leading to heating and significant burns. For this reason, insulating

KEY POINTS

- Implanted devices are designated as MR-safe, MR-conditional, or MR-unsafe.
- Well-designed MRI safety systems and procedures must be in place and rigorously followed to prevent serious safety events and accidents involving dangerous projectiles, burns, and unplanned scanning of implanted devices.
- The magnetic fields around the opening of an MRI bore are not uniform; rather, a steep gradient exists in the forces as the magnet is approached.
- Older intracranial aneurysm clips contained ferromagnetic metal, resulting in patient deaths during MRI.
- Heating and burns related to the radiofrequency field are the most common type of MRI safety events.

Copyright © American Academy of Neurology. Unauthorized reproduction of this article is prohibited.

pads are often placed to prevent thigh-to-thigh contact. Careful attention must also be paid to other anatomic sites where such contact may occur, such as between finger and thigh and, in obese patients, between overhanging abdominal panniculus and thigh.

Burns can also occur when MR-heated electrical leads and other items come into contact with the skin. A lead containing a metal conductor converts the deposited radiofrequency energy into electrical current capable of producing heat. Serious burns have resulted from electrical leads crossing over patients' bodies during MRI, and the anesthesia environment is especially at risk for this scenario given the need for monitoring devices with cables and the patient's inability to respond to a developing burn injury.

Certain foil-backed medication patches are at risk of heating during MRI and must be removed if they will be within the radiofrequency exposure zone.[4] The communication with the patient's care team must be clear if a medication patch is removed to ensure an adequate ongoing care plan and, when needed, timely replacement. Such communication is especially important in hospitalized patients with foil-backed clonidine patches, as failure to replace these can lead to a hypertensive crisis.

Increasingly, fabrics used for clothing are incorporating metallic fibers, primarily for their antimicrobial properties, which have been associated with patient burns.[11] For this reason, patients should be changed into MR-safe scrubs or gowns before undergoing MRI. Face masks that have been worn because of COVID-19 precautions have also been the source of burns, with some types including copper microwires and metallic nose bridge wires.

IMPLANTED DEVICES. Scanning a patient with an MR-unsafe device or with an MR-conditional device without abiding by the conditions for safe scanning can lead to serious patient injury or death. It is believed that at least 13 deaths have resulted from MRI in patients with unrecognized implanted cardiac devices and pacemakers.[12] A patient with an unknown deep brain stimulator experienced a debilitating thalamic burn and hemorrhage when a long lead associated with an abdominal-implanted pulse generator heated during a contraindicated scan of the lumbar spine (**FIGURE 2-4**).[13] These cases illustrate the absolute necessity of knowing about the presence of implanted devices in patients undergoing MRI.

Intrathecal pumps can pose a hazard in MRI; indeed, they are the type of device associated with the greatest number of patient deaths in recent years.[12,14] Intrathecal pumps typically infuse morphine or its derivatives for pain control in conditions such as failed back surgery syndrome, and baclofen and its derivatives have been used for treatment of spasticity. Potential problems with infusion pumps in MRI have been the subject of an FDA advisory[14] because of some important inherent safety issues. Some types of infusion pumps simply stop during MRI, no longer infusing the medication. When the patient is removed from MRI, the great majority will restart and resume infusing. A small number, however, do not restart; if this situation is not identified, it could put the patient at risk for unintentional opiate withdrawal, as illustrated in **CASE 2-1**. If baclofen infusion is suddenly blocked, a baclofen withdrawal syndrome can ensue, with associated multisystem organ failure and a mortality risk of up to 20%.[15] Another manufacturer's infusion pump is labeled as MR-conditional, with the condition for safe scanning being that all the medication within the pump must be removed

Copyright © American Academy of Neurology. Unauthorized reproduction of this article is prohibited.

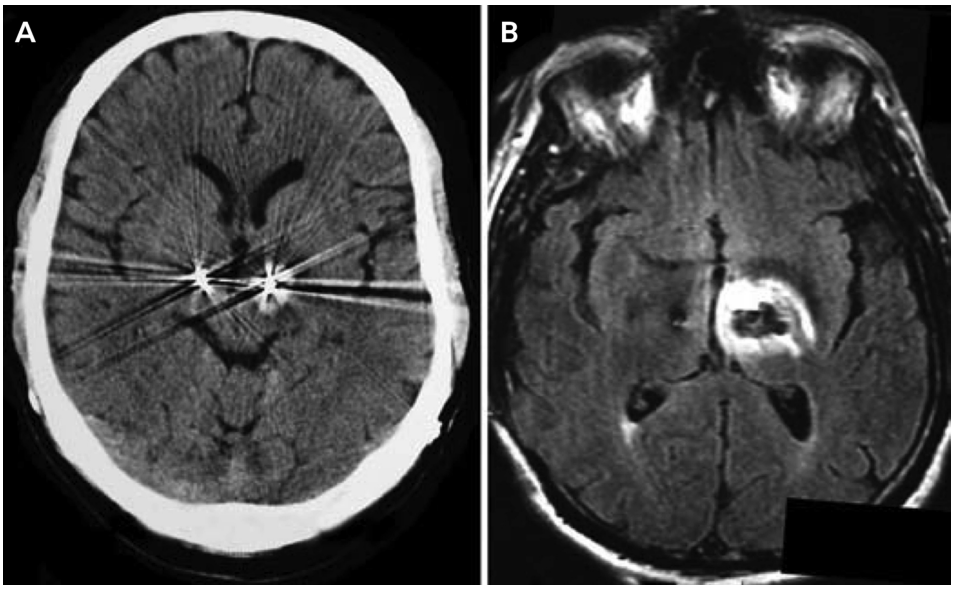

FIGURE 2-4

MRI-related radiofrequency burn and hemorrhage centered on the left thalamus, seen in axial CT (*A*) and T2-weighted fluid-attenuated inversion recovery (FLAIR) MR image (*B*) that resulted from off-label scanning of the lumbar spine in a patient with a deep brain stimulator system. The left pulse generator was implanted in the abdomen, and its associated relatively long lead received excessive radiofrequency energy and heated, leading to the injury. The right-sided pulse generator was implanted in the infraclavicular region and was not as affected by the radiofrequency energy from the lumbar spine MRI.

Reprinted with permission from Henderson JM, et al, Neurosurgery.[13] © 2005 Wolters Kluwer Health, Inc.

KEY POINTS

- **Foil-backed medication patches can cause burns during MRI.**
- **Scanning a patient with an MR-unsafe device or with an MR-conditional device without abiding by the conditions for safe scanning can lead to serious patient injury or death.**
- **Intrathecal pumps are the type of device associated with the greatest number of patient deaths during MRI in recent years.**
- **Patients with pacemakers and defibrillators can increasingly be safely scanned if important safety measures are strictly adhered to.**

before scanning. During MRI the pump contents can be spontaneously released in bulk, with possibly lethal consequences. This scenario illustrates the necessity of accurately identifying the make and model of an implanted device before exposing the patient to the MRI environment.

MR-CONDITIONAL AND MR-UNSAFE CARDIAC IMPLANTED ELECTRONIC DEVICES. In the past, scanning patients with MR-unsafe cardiac implanted electronic devices, such as pacemakers and defibrillators, was entirely contraindicated. Older devices included reed switches (electronic connectors activated by magnets), and these were clearly problematic in the strong magnetic field within the MRI environment. Other MRI fields, including the radiofrequency and gradient fields, had the ability to heat cardiac leads and adversely affect device programming. As it is estimated that 50% to 75% of patients with a cardiac implanted electronic device will at some point need to undergo MRI, device manufacturers have increasingly engineered MR-conditional cardiac implanted electronic devices so that safe scanning can be achieved if certain conditions are met.

Many devices now have MR-conditional labeling for safe scanning at 1.5T and 3T. A cardiac implanted electronic device system comprises both the implanted pulse generator and its associated leads. For the cardiac implanted electronic device system to be MR-conditional, the entire system of the implanted pulse generator and its leads must be individually MR-conditional; if an associated lead is not specifically labeled as MR-conditional, the entire system is considered non–MR-conditional, and technically MR-unsafe.

Copyright © American Academy of Neurology. Unauthorized reproduction of this article is prohibited.

Coincidentally, other more contemporary cardiac implanted electronic devices with newer engineering, although not specifically labeled as MR-conditional (and technically MR-unsafe), can now increasingly be safely scanned provided that, as endorsed by the Heart Rhythm Society and the American College of Radiology, an institutional protocol is followed with a responsible radiologist and cardiologist managing the practice, the MRI is medically necessary, no fractured or abandoned leads are permitted, the cardiac implanted electronic device is evaluated immediately before and after MRI and appropriate personnel are available to program the cardiac implanted electronic device, ECG and pulse oximetry are monitored throughout the procedure, a defibrillator with external pacing capabilities is available (outside zone IV), and advanced cardiac life support–certified personnel are in

CASE 2-1

A 35-year-old woman with a history of traumatic brain injury and spinal cord injuries presented to the emergency department for treatment of seizures that were speculated to be posttraumatic in etiology. No prior imaging or significant outside medical records were available. Physical examination demonstrated cognitive deficits and diffuse spasticity. The examination also revealed a device implanted in her lower back region, but no reliable information about it was available to the team. On the order for brain MRI with seizure protocol, the box was checked indicating "no known implanted devices."

When the patient arrived for MRI, she was presented with the usual written MRI safety screening form. She checked "no" for each device listed on the form and then underwent the requested head MRI without IV contrast. The imaging was reassuring and the patient improved enough to go home, but the following day, the patient was admitted to the emergency department with marked agitation and confusion, significant fever, worsening seizures, and increased spasticity.

The patient's medical records from an outside institution then arrived, revealing the presence of an intrathecal pump for baclofen delivery. The patient's symptoms were consistent with the onset of a serious baclofen withdrawal syndrome, which can be fatal.

The intrathecal pump had stalled in the high magnetic field during MRI and did not spontaneously restart upon removal from the field. The MRI had been performed without knowledge of the presence of the pump, and no post-MRI pump assessment had been performed. The patient's traumatic brain injury–associated cognitive impairment had prevented accurate completion of the MRI safety screening form, which did not reveal the presence of the intrathecal pump.

COMMENT

Implanted devices are increasingly MR-conditional, and patients can be scanned safely with these devices if proper precautions are taken. However, unrecognized devices or failure to follow proper guidelines for scanning in patients with implanted devices can lead to serious injury or death.

Copyright © American Academy of Neurology. Unauthorized reproduction of this article is prohibited.

attendance during the examination and until the device is reprogrammed after the examination.[4,16] Since 2018, the Centers for Medicare & Medicaid Services has permitted reimbursement for MRI performed in patients with non–MR-conditional (technically MR-unsafe) cardiac implanted electronic device systems.

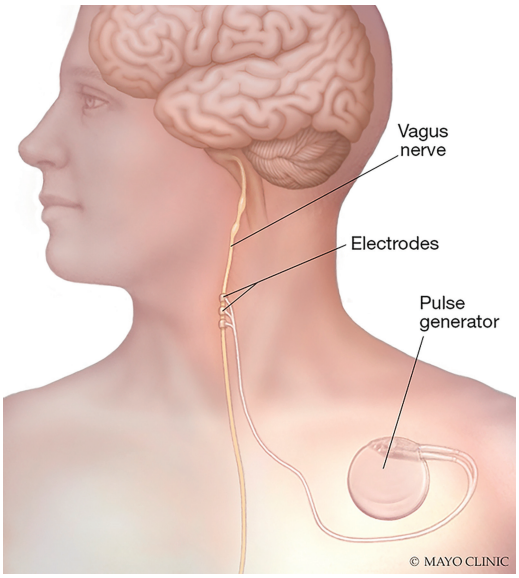

FIGURE 2-5

Vagus nerve stimulation system. The system consists of a pulse generator, typically implanted in the infraclavicular region. Leads are tunneled subcutaneously cephalad and then with deeper dissection, and positive and negative helical electrodes are attached to the left vagus nerve, inferior to the cardiac branches.

Reprinted with permission of the Mayo Foundation for Medical Education and Research. © Mayo Clinic.

VAGUS NERVE STIMULATORS. Vagus nerve stimulation (VNS) systems consist of an implanted pulse generator typically implanted in the left infraclavicular region with a lead that attaches to the left vagus nerve in the neck (FIGURE 2-5).[17,18] VNS is used primarily for seizure control in difficult-to-control epilepsy and for depression. As with MRI of all implanted devices, it is critical to know the precise make and model of the system that will undergo scanning, as the considerations are important regarding the allowable radiofrequency coils and body regions that can be scanned safely as defined by the MRI conditions for safe scanning. Radiofrequency coil selection is one of the most important MRI safety decisions made when planning scans in a patient with an implanted device. Transmit/receive coils keep the radiofrequency energy in a "local" region, for example, locally around the head for brain MRI; other transmit/receive coils are designed for wrist and ankle scanning. For brain MRI in a patient with an older VNS device, a transmit/receive coil permits obtaining the MRI safely because very little radiofrequency energy is deposited on the VNS device or its leads attached to the vagus nerve. No transmit/receive coils exist for scanning of other common locations, such as the lumbar spine. Newer-generation VNS devices are engineered to allow increasing deposition of radiofrequency energy safely, permitting use of the MRI's main body coil for radiofrequency transmission, allowing other body areas to be scanned, such as the lumbar spine. In addition, using receive-only head coils with body coil radiofrequency transmission substantially improves image quality, which is important for some head MRI examinations such as epilepsy protocols and metastatic disease evaluations.

Some newer VNS devices permit scanning with body coil transmit thereby allowing scanning of many other body parts, including the lumbar spine. Older systems not permitting body coil transmit are restricted to scans limited to use of local transmit/receive coils.

Copyright © American Academy of Neurology. Unauthorized reproduction of this article is prohibited.

When VNS therapy is not clinically effective, the implanted pulse generator is frequently removed. Detaching the leads from the vagus nerve at their attachment point runs the risk of damaging the nerve, with the potential for clinically significant complications. For this reason, the lead is often just left in place in case a future need to retry VNS therapy occurs. In this situation, a retained lead has a risk of unsafe heating during MRI and significant radiofrequency cannot be deposited over the lead because of this risk; thus, permissible scans are typically limited to those of the head, extremities, and other regions with transmit/receive coils. If the retained lead is snipped, with no more than 2 cm remaining attached to the nerve, more widespread radiofrequency deposition with use of the body transmit coil is permitted.

Other neurostimulation systems are becoming increasingly commonly used, including deep brain stimulation for Parkinson disease, tremor, and some psychiatric conditions; spinal cord stimulation for pain control and spasticity; sacral neuromodulation for bowel and bladder control and pain control; hypoglossal nerve stimulation for obstructive sleep apnea; and cochlear implants for conductive hearing loss. For all these active implanted electronic devices, accurate information about the precise make and model of the device system, including implanted pulse generator and leads, is mandatory to determine whether MRI is possible (ie, the system is MR-conditional and not MR-unsafe) and, if so, to clearly define the MRI parameters that will permit safe scanning. Ordering providers can assist in this effort by reminding patients of the importance of bringing any vendor-provided information about their implanted devices so that precise make and model can be identified. Facilitating accurate entry of make and model information into the electronic medical record is another important way to prevent device-related MRI safety events.[19]

Ferromagnetic Detection Systems

Significant recent incremental gains in MRI safety have resulted from the increasing use of devices specifically capable of identifying ferromagnetic metal that can pose a risk in MRI. Ferromagnetic detection systems detect the presence of ferromagnetic metal (and will not alert to nonferromagnetic metal). Ferromagnetic detection systems may be used both for patient screening and to help ensure safety in the MRI environment when approaching the magnet at the threshold of zone IV.

When used for patient screening, ferromagnetic detection systems can help prevent the inadvertent introduction of a dangerous ferromagnetic object with projectile risk that could be, for example, concealed under a patient's MR-safe scrubs or gown before MRI. In addition, ferromagnetic detection systems are increasingly useful in detecting external on-planted medical devices such as continuous glucose monitors and insulin pumps. An insulin pump that is inadvertently exposed to MRI is at serious risk of damage to its circuitry such that it could deliver insulin in an unreliable manner, with potential for dangerous hyperglycemia or hypoglycemia. Because multiple deaths have occurred as a result of scanning patients with cardiac implanted electronic device systems that were unrecognized and thus without proper scanning precautions, a study was performed to test the ability of ferromagnetic detection systems to detect cardiac implanted electronic devices, which indicated that cardiac implanted electronic devices could be reliably detected.[20]

Copyright © American Academy of Neurology. Unauthorized reproduction of this article is prohibited.

Ferromagnetic detection systems can also be used in the MRI environment to monitor personnel and patients as they approach the zone IV doorway and alert to the presence of dangerous ferromagnetic items (such as a ferrous oxygen canister that led to the death of the 6-year-old boy mentioned earlier in this article) that could pose a serious projectile risk if they came into proximity to the magnet.

Foreign Objects and Shrapnel

In clinical practice, it is relatively common to encounter patients with prior injuries involving retained metallic foreign objects such as shrapnel, bullets, and similar materials. Any injury to the eye involving metal, especially one for which the patient sought medical attention, must be carefully investigated, as cases of blindness caused by displacement of intraocular ferrous metal during MRI have occurred. Radiography and CT can be used to screen patients who may have retained intraorbital metal.

Relatively small metallic foreign bodies such as shrapnel and bullets can often be scanned, even if they are ferromagnetic, as long as they are not located near or within a vital structure. Over time, foreign objects become scarred in with surrounding dense connective tissue and are therefore not at risk of displacement. However, if a ferromagnetic object of substantial size is present in the spinal canal, brain, lungs, or another vital organ, it would probably be a contraindication to scanning because of the risk of displacement. A small metallic object not exceeding 2 cm, either ferromagnetic or nonferromagnetic, is not at risk of significant heating in typical high-field-strength (1.5T and 3T) MRI.[21]

Metallic foreign bodies and some implanted devices can degrade image quality by imparting susceptibility artifacts and potentially obscuring important information in adjacent tissues and structures. Particularly if the retained object is ferromagnetic, the amount of imparted artifact can be substantial. MRI methods may be used to minimize such metal-associated artifact and maximize diagnostic information.[22]

Auditory Considerations

MRI is associated with loud noise. Hearing protection is important, as Lorentz forces associated with gradient coils and the main magnetic field can produce sound pressures that substantially exceed 99 A-weighted decibels (dB[A]), which is the limit set by the FDA for significant risk. Hearing protection is typically in the form of earplugs, earmuffs, or both.[4]

Gadolinium-Based Contrast Agents

Gadolinium-based contrast agents administered with MRI provide clinically essential additional information to neuroradiology examinations by demonstrating regions of contrast enhancement, characterized by increased T1 relaxivity or hyperintensity, that frequently reflects underlying pathology. Such pathology is often associated with blood-brain or blood–spinal cord barrier breakdown, as in the case of enhancing neoplastic, demyelinating, infectious, or inflammatory processes. The overall safety profile of gadolinium-based contrast agents is extremely favorable, with an estimated number of doses administered worldwide exceeding 450 million since regulatory approval in 1988.[23] Gadolinium is a rare earth metal that in free form is cytotoxic; gadolinium-based contrast

KEY POINTS

- **An insulin pump exposed to MRI is likely unreliable and could lead to serious hyperglycemia or hypoglycemia.**
- **Displacement of an intraocular ferromagnetic foreign body during MRI can lead to blindness.**

Copyright © American Academy of Neurology. Unauthorized reproduction of this article is prohibited.

agents bind gadolinium in a chelate form, and it is primarily renally cleared from the body. It has been recognized for some time that following administration, some gadolinium is retained in tissues such as bone and liver. In 2014, Kanda and colleagues[24] observed increasing T1 hyperintensity in the globus pallidus, cerebellar dentate nucleus, and other brain structures in patients who had received repeated doses of gadolinium-based contrast agents. These brain regions are associated with calcium accumulation, and gadolinium's similarity to calcium may underlie the retention phenomenon, but the causative mechanism has not yet been established. The use of newer macrocyclic gadolinium-based contrast agents results in less retention than that of linear agents. To date, no deleterious clinical effects have been documented resulting from gadolinium retention, but continued study of this issue is important.

Nephrogenic systemic fibrosis is an extremely rare but serious condition associated with excess collagen deposition following gadolinium-based contrast agent administration. Nephrogenic systemic fibrosis is postulated to be associated with dechelation of relatively unstable gadolinium-based contrast agents, resulting in the liberation of free gadolinium that activates fibrocytes and macrophages. To date, approximately 613 cases have been reported, and these patients had clinically significant renal impairment. With new clinical guidelines for patients with renal disease and development of newer, more stable gadolinium-based contrast agents, nephrogenic systemic fibrosis has become largely preventable.[23]

Pregnancy

A cautious approach to scanning pregnant patients was the rule in the early clinical MRI era, as it was uncertain whether deleterious effects on the fetus would occur related to MRI-associated static magnetic field (B_o) and radiofrequency field (B_1) effects, as well as acoustic injury related to gradient field (dB/dt) loud noises.

Although some animal studies have suggested teratogenic effects in amphibian embryos and fish eggs exposed to ultrahigh magnetic fields (in excess of 9T) for long periods, retrospective human studies of children who were exposed to MRI while in utero have shown no evidence of harmful outcomes, including fetal death, neoplasms, congenital abnormalities, and hearing or vision loss.[25-27] The possibility of substantial deleterious tissue heating associated with radiofrequency deposition is mitigated by International Electrochemical Commission limits to scanning in normal mode (2 W/kg) when scanning pregnant patients. The *ACR Manual on MR Safety*[4] concludes that scanning pregnant patients at up to 3T in normal mode can be considered safe, although the decision to scan may be affected by local institutional policies.

Gadolinium-based contrast agents are secreted into the amniotic fluid in primates and likely accumulate in the fetus.[29] Previous studies suggesting some potential deleterious effects of fetal gadolinium-based contrast exposure exist.[25] As a result, both the *ACR Manual on MR Safety*[4] and *ACR Manual on Contrast Media*[29] recommend that gadolinium-based contrast be administered with caution to pregnant, or possibly pregnant, patients. In situations in which gadolinium-based contrast agents are being considered for use in a pregnant patient, the referring clinician and radiologist should confer and determine whether the gadolinium-based contrast agent is necessary to provide clinically important information (eg, tumor progression in the setting of a high-grade

Copyright © American Academy of Neurology. Unauthorized reproduction of this article is prohibited.

glioma) and that it is not prudent to defer gadolinium-based contrast agent administration until after the patient is no longer pregnant. Following this, an informed consent discussion should be held with the patient.

Lactation

Gadolinium-based contrast agents have an approximately 2-hour half-life in plasma and are typically essentially cleared from the bloodstream in 24 hours. Gadolinium-based contrast agents are excreted into breast milk, but this represents only a very small percentage of an intravascular dose, less than 0.04%. Only about 1% of orally ingested gadolinium-based contrast agents is absorbed from the gastrointestinal tract. Therefore, less than 0.0004% of the intravascular gadolinium-based contrast agent dose administered to the mother would be absorbed by the infant, markedly less than the dose permissible for intravascular administration in an infant. The *ACR Manual on Contrast Media*[29] concludes that it should be safe for the mother to continue breastfeeding after gadolinium-based contrast agent administration. Discussion with the mother before IV gadolinium-based contrast agent administration is valuable to provide an option to express and discard breast milk for the 24 hours after the administration if desired. Also, in anticipation of the contrast-enhanced examination, a breast pump can be used to obtain a quantity of milk for use over the post-MRI interval.

CT SAFETY CONSIDERATIONS

CT examinations are associated with safety concerns that must be recognized, including radiation exposure, equipment malfunction, issues related to CT personnel and operators, and effect on electronic medical devices.

Radiation Exposure

CT examinations involve the use of x-ray radiation exposure to create cross-sectional images. Following are some of the major considerations with regard to the risks of radiation exposure in CT.

HOW IS RADIATION DOSE IN CT QUANTIFIED? Before discussing safety considerations regarding radiation exposure, it is important to understand why radiation exposure is needed to generate CT images and how to quantify radiation dose in CT. CT images are created using a mathematical process, "reconstruction," based on the detected signals from thousands of x-ray projections. A CT image (typically in Hounsfield units) represents a map of x-ray linear attenuation coefficients in the body. The higher the radiation exposure of the patient, the higher the detected signal and the better the image quality that can be generated for diagnosis. The radiation dose used in a CT scan can be reduced, which may sacrifice image quality and can lead to misdiagnosis.

Radiation dose in CT is commonly quantified in terms of scanner radiation output, patient absorbed dose, and effective dose. It is important to differentiate these three radiation dose metrics.

Scanner radiation output can be specified or adjusted on the scanner console before a CT scan is initiated. A common metric used to quantify scanner radiation output is volume CT dose index ($CTDI_{vol}$; SI unit, mGy), which describes the radiation output in terms of radiation dose measured at two standardized acrylic phantoms, one at 16 cm in diameter to mimic the head size and the other at 32 cm to mimic the body size.[30] $CTDI_{vol}$ and a few other

KEY POINTS

- **No deleterious clinical effects of gadolinium retention have yet been identified, although continued study of this issue is important.**
- **Radiation dose in CT is commonly quantified in terms of scanner radiation output, patient absorbed dose, and effective dose.**

Copyright © American Academy of Neurology. Unauthorized reproduction of this article is prohibited.

TABLE 2-1

Typical Effective Dose Values for Common Diagnostic Imaging Examinations and Annual Background Radiation per Individual in the United States[a]

Imaging examination	Effective dose, mSv
CT	
Head CT[36]	1-2
Chest CT[36]	5-7
Abdomen CT[36]	5-7
Abdomen and pelvis CT[36]	8-14
Coronary CT angiography[36]	5-15
Coronary calcium CT[36]	1-3
Lung cancer screening CT[37]	1.5
Neck and cervical spine CT[40]	4-6
Brain perfusion CT[41]	3-7
Radiographic/fluoroscopic imaging	
Extremity (eg, hand and foot) x-ray[38]	<0.001
Dental x-ray[43]	<0.01
Bone densitometry (dual energy x-ray absorptiometry)[38]	0.001
Chest radiograph[36]	0.1-0.2
Mammogram[36]	0.3-0.6
Lumbar spine radiograph[36]	0.5-1.5
Barium enema examination[36]	3-6
Coronary angiogram (diagnostic)[36]	5-10
Nuclear medicine[36]	
Lung scan	2-3
Bone scan	3-5
Heart scan–sestamibi	13-16
Heart scan–thallium	35-40
Ubiquitous background (per individual in US population)[45]	3.11

[a] Modified from Yu L, et al, Imaging Med.[30] © 2009 Future Medicine Ltd.

Copyright © American Academy of Neurology. Unauthorized reproduction of this article is prohibited.

related quantities (eg, dose length product) are widely used to describe or optimize the scanner radiation output of scanning protocols in CT examinations.

It should be noted that $CTDI_{vol}$ does not directly quantify patient dose.[31] Instead, patient absorbed dose is the radiation dose absorbed by the patient, which is typically quantified using organ dose (ie, average absorbed dose at each organ). Organ dose can be calculated or estimated based on the $CTDI_{vol}$ and other scanner- and patient-related information. The process of estimating organ dose of a patient from a CT scan is tedious. For convenience, the size-specific dose estimate was introduced to approximate the average absorbed dose for a given patient size (represented by water-equivalent diameter), which can be readily converted from $CTDI_{vol}$ by a multiplication factor that is dependent on the size.[32]

Effective dose is a quantity calculated by summing the organ dose of each major organ after multiplying it by a weighting factor.[33] The weighting factor of each organ is proportional to the relative biological risk of that organ, which was determined on the basis of a large number of epidemiologic studies of radiation-induced biological damage and recommended by the International Commission on Radiological Protection.[34] Effective dose (typically in millisieverts, or mSv) is a derived quantity representing a "whole-body equivalent" dose.[33] Risk of radiation exposure to part of the body is converted to a "whole-body equivalent" such that the health detriment in different examinations (of different body parts) and different imaging modalities can be compared against each other. The concept of effective dose was introduced mainly for the purpose of risk management. It is based on a mathematically defined reference human body model, which is not age- or sex-specific.[37] TABLE 2-1[35-41] provides some typical effective dose values from common CT examinations and x-ray examinations. For convenience, effective dose in CT for a given examination type may be approximately estimated by multiplying the dose length product by an age-specific conversion factor.[42]

RISKS OF RADIATION EXPOSURE IN CT. Two types of biological effects occur from radiation exposure in CT. One is the deterministic effect (tissue reaction), and the other is the stochastic effect (cancer induction and hereditary effect).

The deterministic effect occurs when the radiation dose is higher than a certain threshold, which is typically two to three orders of magnitude higher than that in a single diagnostic CT examination. The skin dose threshold for transient erythema from a single acute exposure is approximately 2 Gy; temporary epilation (hair loss), 3 to 6 Gy; prolonged erythema and permanent partial epilation, 5 to 10 Gy; significant skin damage such as permanent epilation and moist desquamation, 10 Gy and above.[43] Although these thresholds are much higher than the radiation dose in a typical diagnostic CT examination, interventional CT might be an exception. CT has been increasingly used to provide image guidance in many interventional procedures, such as ablation, aspiration, biopsy, and drainage. Radiation dose in these procedures varies substantially, depending on patient size and complexity of the procedure. Radiation doses in most of these procedures are still low, but for very complicated procedures that involve prolonged CT guidance, patient skin dose in some examinations was reported to exceed the threshold of skin deterministic effects. Appropriate patient follow-up is needed when this occurs. The lens of the

KEY POINT

- **Two types of biological effects from radiation exposure in CT occur. One is the deterministic effect (tissue reaction), and the other is the stochastic effect (cancer induction and hereditary effect).**

Copyright © American Academy of Neurology. Unauthorized reproduction of this article is prohibited.

eye is especially sensitive to radiation exposure. Based on recent epidemiologic studies, it is believed that the threshold for cataract development may be on the order of 0.5 Gy.[44] Therefore, a much more conservative occupational dose limit for the lens of the eye was recommended by the International Commission on Radiologic Protection (20 mSv/y averaged over 5 years, with no single year exceeding 50 mSv) and the National Council on Radiation Protection and Measurements (50 mGy/y).[45]

Because deterministic effects rarely occur in diagnostic CT examinations except for some prolonged CT-guided interventional procedures, the risk of radiation exposure in CT refers mostly to stochastic effect. *Stochastic* means that the probability of cancer induction increases with radiation dose rather than severity of the disease. At low levels of radiation, considerable uncertainty exists regarding the risk of cancer induction.[46] A report by the National Academy of Sciences stated that at doses of 100 mSv or less, "statistical limitations make it difficult to evaluate cancer risk in humans."[46] Large epidemiologic studies involving lifetime follow-up of a huge population are required to quantify the increased risk of low radiation doses. For example, for a typical abdominal CT examination (10 mSv to 20 mSv) to show a statistically significant increase of cancer mortality, the required sample size that would need lifetime follow-up is approximately 1 million people. It is unlikely that the cancer risk in humans can be accurately and precisely quantified at doses much lower than 10 mSv.[42] Despite the controversies regarding increased cancer risk at low doses,[48,49] a "linear no-threshold" model was still recommended, mainly for the purpose of radiation protection (a preference to overprotect rather than underprotect).[46] With this model, no matter how low the radiation dose level, it is assumed to confer an increased cancer risk. Based on the linear no-threshold model and epidemiologic studies on survivors of the atomic bomb and nuclear workers, the average lifetime attributable risk of incidence and mortality for all cancers are estimated to be 0.1% and 0.05%, respectively, per 10 mSv of radiation exposure.[46] It should be emphasized that, even with these hypothetical and potentially overly aggressive risk estimates, they are much lower than the incidence and mortality rate of naturally occurring cancers, which are approximately 42% and 21%, respectively.[46]

Over the past 2 decades, many articles have been published in which the linear no-threshold model was used to predict the rate of cancer mortality due to CT examinations. The authors of one of these articles multiplied the risk factor from the linear no-threshold model and the large number of CT examinations performed to conclude that about 1.5% to 2.0% of all cancers in the United States may be attributable to the radiation exposure in CT.[50] As a result of publication of these alarming articles, some patients and doctors declined to use CT even if it was the most appropriate imaging tool available for diagnosis of the suspected disease. Because of the potential detrimental effects of these alarming articles on public health, many professional organizations recommended against quantitative estimation of cancer risk for individual patients receiving doses below 100 mSv.[51,52] The American Association of Physicists in Medicine (AAPM) issued the following position statement: "Given the lack of scientific consensus about potential risks from low doses of radiation, predictions of hypothetical cancer incidence and mortality from the use of diagnostic imaging are highly speculative. The AAPM and other radiation protection organizations specifically discourage these predictions of

Copyright © American Academy of Neurology. Unauthorized reproduction of this article is prohibited.

hypothetical harm. Such predictions . . . may lead some patients to fear or refuse safe and appropriate medical imaging, to the detriment of the patient."[51] Thus, it is generally believed that quantitative estimation of cancer risk for an individual patient receiving a radiation dose of less than 100 mSv during CT does not bring clinical value to the patient.

RADIATION DOSE MANAGEMENT IN CT. Although the cancer risk at low radiation doses is small and potentially negligible, it is likely nonzero. To maximize the benefit-to-risk ratio, it is still best practice to use the lowest possible radiation dose at each CT examination while generating images with sufficient diagnostic quality. Two basic principles must be followed for managing radiation dose in CT: justification and optimization.

First, every CT examination must be clinically justified. Referring physicians and radiologists should work together to prescribe the most appropriate imaging examination for each patient so that the clinical questions can be correctly answered. During this process, it is recommended that accumulated radiation dose in prior imaging examinations not become the basis for deciding whether the next CT examination should or should not be performed.[53] Instead, the decision must be based only on the analysis of potential benefit and the current clinical indication. Cumulative dose estimates do not have clinical relevance in making such decisions.[54]

Second, an "as low as reasonably achievable" (ALARA) radiation dose should be prescribed for each clinically justified CT examination while maintaining adequate image quality. For the ALARA principle, two perspectives need to be considered. The first perspective is to appropriately define the target image quality for each specific diagnostic task, not requiring higher image quality than necessary. For example, CT evaluation of ventricular size for pediatric patients with CSF shunts does not require a high image quality, and therefore the radiation dose can be reduced substantially (up to 90%) compared with a routine brain examination.[55] In contrast, brain CT involves the detection and characterization of low-contrast disease, which requires a relatively lower noise level and thus a higher dose. **FIGURE 2-6** shows images from a pediatric head examination at the routine radiation dose and a few simulated lower dose levels. Although the ventricular size can be evaluated at 10% of the routine radiation dose, subtle intracranial hemorrhage may be poorly identified at the lower radiation dose. The diagnostic reference level, typically as a percentile point on an observed dose distribution in patient examinations using a standardized dose metric, such as $CTDI_{vol}$, indirectly defines the target image quality. Diagnostic reference levels have been established by the ACR for adult head and abdomen CT and pediatric head and abdomen CT for the purpose of CT accreditation.[56] Users should investigate the potential for dose reduction when their dose levels are above the diagnostic reference level. Diagnostic reference levels have also been proposed for a variety of other CT examinations.[40] The second perspective of the ALARA principle is to minimize radiation dose to achieve a predefined target image quality for a given examination. This can be accomplished by optimizing CT systems, scanning techniques, and reconstruction methods, as briefly summarized below.

RADIATION DOSE–REDUCTION TECHNIQUES. Commonly used radiation dose–reduction techniques include automatic tube current modulation,

KEY POINTS

- **Deterministic effects rarely occur in diagnostic CT examinations except for some prolonged CT-guided interventional procedures. The risk of radiation exposure in CT refers mostly to stochastic effect.**
- **At low levels of radiation, considerable uncertainty exists regarding the risk of cancer induction. It was stated in a report by the National Academy of Sciences that at doses of 100 mSv or less, "statistical limitations make it difficult to evaluate cancer risk in humans."**
- **It is generally believed that quantitative estimation of cancer risk for an individual patient receiving a radiation dose of less than 100 mSv during CT does not bring clinical value to the patient.**
- **To maximize the benefit-to-risk ratio, it is still best practice to use the lowest possible radiation dose at each CT examination while generating images with sufficient diagnostic quality. Two basic principles must be followed for managing radiation dose in CT: justification and optimization.**
- **Commonly used radiation dose–reduction techniques include automatic tube current modulation, automatic tube potential selection, iterative reconstruction, and deep learning–based noise reduction.**

Copyright © American Academy of Neurology. Unauthorized reproduction of this article is prohibited.

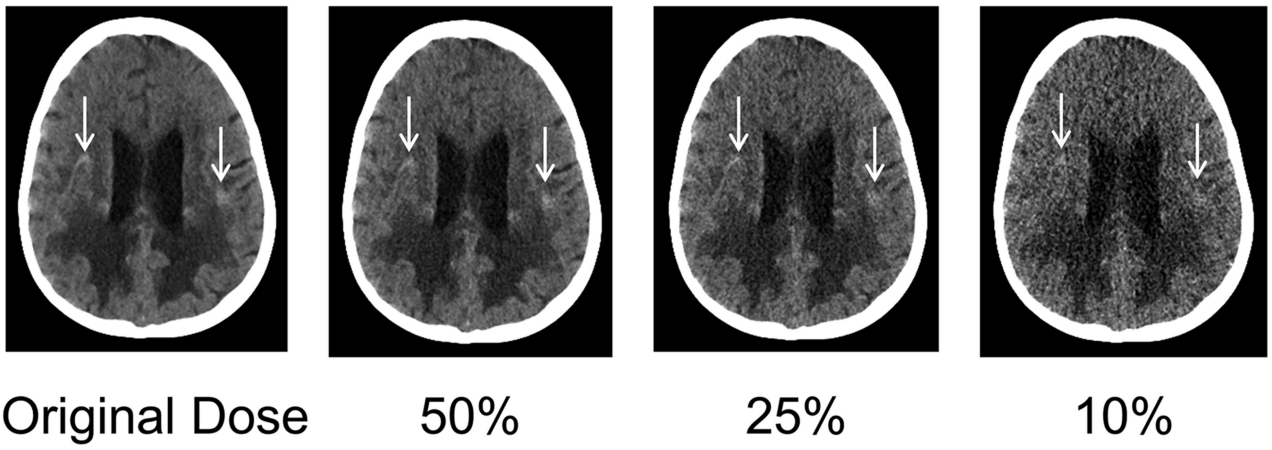

FIGURE 2-6

Images from a pediatric head CT in a patient with intracranial hemorrhage at the original routine radiation dose and a few simulated lower dose levels: 50%, 25%, and 10% of the routine dose. Subtle intracranial hemorrhage (*arrows*) can be identified with high confidence at the original dose but poorly at lower radiation doses. Ventricular size can be evaluated even at 10% of the routine radiation dose.

Reprinted with permission from Gabriel S, et al, AJNR Am J Neuroradiol.[55] © 2014 American Society of Neuroradiology.

automatic tube potential selection, iterative reconstruction, and deep learning–based noise reduction.

Automatic tube current modulation is one of the most effective radiation dose–reduction techniques.[57] It automatically adjusts the tube current, which is proportional to the x-ray intensity and radiation exposure, based on the patient attenuation level and a predetermined image quality index, increasing the tube current for larger patients or along projection directions with higher attenuations and decreasing the tube current for smaller patients or along projection directions with lower attenuations.

Automatic tube potential selection automatically selects the most dose-efficient tube potential for a given patient size and diagnostic task.[58] Low tube potential (in kilovoltage) can increase the iodine contrast enhancement but may increase image noise, especially for bigger patients. High tube potential may decrease image noise, but the iodine contrast may be enhanced poorly. The optimal tube potential depends on both patient size and diagnostic task, which can be automatically determined by software before the CT scan. Radiation dose can be reduced by up to 50% by using automatic tube potential selection techniques.

Iterative reconstruction and various deep learning–based noise-reduction methods have become popular choices to improve image quality, facilitating radiation dose reduction while maintaining the same target image quality.[59] However, some vendors of these noise-reduction techniques exaggerated the potential of radiation dose reduction. For example, one of the CT vendors automatically built in an approximately 70% radiation dose reduction when the iterative reconstruction was turned on in their default CT protocols. It turned out that some low-contrast lesions may be missed with such an aggressive radiation dose reduction.[60] This has been one of the major safety concerns during the process of deployment of these dose-reduction techniques. Careful and accurate image quality evaluation is key to ensuring

Copyright © American Academy of Neurology. Unauthorized reproduction of this article is prohibited.

that diagnostic performance is not sacrificed. Many rigorous studies have demonstrated that iterative reconstruction can reduce radiation dose by only 20% to 30% for examinations involving low-contrast lesion detection and characterization.[59] Deep learning–based noise reduction is promising in preserving natural noise textures.[61] However, the appropriate amount of radiation dose reduction allowed by these techniques remains to be investigated.

In addition, many components of CT systems, including x-ray source, collimators, prefiltration and bowtie filters, and x-ray detectors, can be optimized to improve radiation dose performance. With the introduction of photon-counting-detector CT in clinical practice, radiation dose efficiency can be further improved as a result of small detector pixels without septae, improved photon weighting factor, and reduced electronic noise.[62]

Successful and safe implementation of these dose-reduction techniques requires a team effort involving many parties, including referring physicians, radiologists, clinical physicists, technologists, CT manufacturers, and some of the regulatory bodies.

KEY POINT

- CT operators are required to receive appropriate training on scanner operation, radiation exposure, and emergency procedures.

Equipment Malfunction

CT equipment malfunction is another factor that may be relevant to patient safety. One type of CT equipment malfunction is caused by a system defect or incorrect calibration. This type of malfunction may generate artifacts in images. Some of these artifacts are easily recognizable, but some may mimic disease and lead to misdiagnosis. An example is provided in CASE 2-2.

Another type of system malfunction relevant to patient safety is related to mechanical aspects of the system. The CT gantry typically weighs 2 to 3 tons and rotates as fast as 4 to 5 revolutions per second. All components of the system need to be secured appropriately during the initial installation and after each service or repair. Any blockage during the gantry rotation could cause severe damage to the scanner and serious patient injuries.

Issues Related to CT Personnel and Operators

For CT personnel and operators who stay inside the room during a CT scan, such as during a CT-guided procedure or when providing help to the patient for contrast injection or positioning, appropriate protection is required to minimize radiation exposure. Reducing time in the room during radiation, increasing distance from the radiation source, and always wearing appropriate personal protective shielding devices are the guiding principles to minimize personnel radiation exposure. Radiation badges also need to be worn to monitor cumulative radiation exposure on a regular basis.

In addition, CT operators are required to receive appropriate training on scanner operation, radiation exposure, and emergency procedures. In 2009, more than 200 patients at one hospital received radiation doses of 3 Gy to 4 Gy to the head during their brain perfusion examinations, or more than 8 times the anticipated dose.[64] Some patients experienced reddened skin and hair loss after the examination. An FDA investigation showed that the cause was an error made by the hospital staff when they tried to reconfigure the scanning protocol to improve image quality. Knowledge of radiation and scanning protocols can help prevent this type of incident. Appropriate scanner operation is also important to ensure that patient safety is not jeopardized, especially for some special scanning

Copyright © American Academy of Neurology. Unauthorized reproduction of this article is prohibited.

modes. For example, CT is useful for evaluating serious issues in children who are receiving extracorporeal membrane oxygenation (ECMO), but extreme care must be taken during patient transportation and CT scanning to not disconnect the ECMO cannulas and other life-supporting lines, which could result in life-threatening accidents.[65] Fast helical scanning is helpful to reduce motion artifacts; however, it requires extra table excursion beyond the scan range. Close attention must be paid to prevent tension or disconnection of the ECMO

CASE 2-2

A 37-year-old woman underwent imaging for headache, and her CT showed artifacts in the brain mimicking hypodense white matter that raised serious concerns of cerebral edema (FIGURE 2-7A).[63] The patient was immediately transferred by ambulance to another facility, where a repeat head CT was performed, which was normal. It turned out that the initial diagnosis made at the original site was caused by artifacts generated by air bubbles that accidentally entered the x-ray tube cooling system. The artifacts were very subtle and intermittent. Retrospective review of daily quality control images (acquired on water phantom) identified those subtle artifacts only on a couple of testings and only when the images were displayed in a narrow window width (40 Hounsfield units) (FIGURE 2-7B).[63]

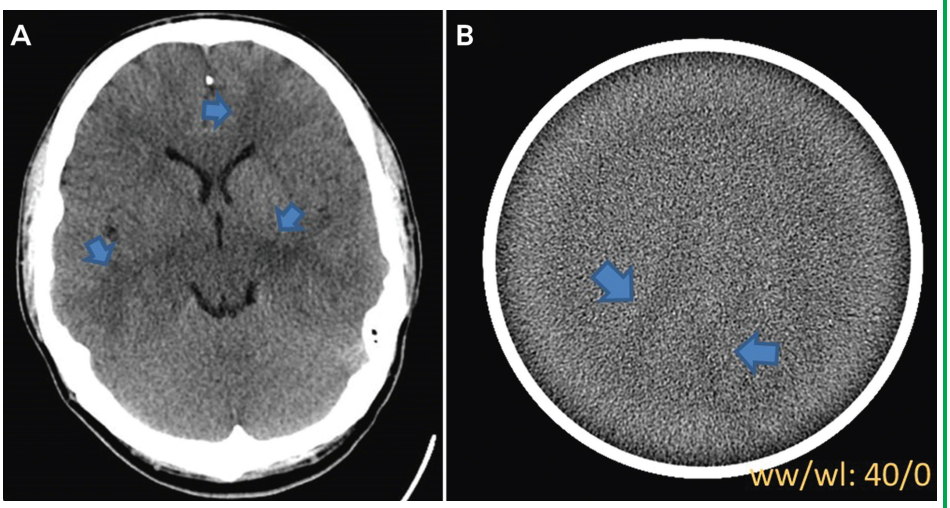

FIGURE 2-7
Subtle artifacts in a head CT resulting in misdiagnosis during the initial examination of the patient in CASE 2-2. *A,* Air bubbles in the x-ray tube cooling system caused artifacts mimicking hypodensity in cerebral white matter (*arrows*). *B,* The intermittent and subtle artifacts (*arrows*) were captured only during a morning quality control test using a narrow display window width (ww) of 40 Hounsfield units.
wl = window level.
Reprinted with permission from Long Z, et al, Med Phys.[63] © 2016 American Association of Physicists in Medicine.

COMMENT

This example demonstrates the importance of careful review of daily quality control images, which may capture system malfunction before it becomes a patient safety concern.

Copyright © American Academy of Neurology. Unauthorized reproduction of this article is prohibited.

cannulas during the scan. FIGURE 2-8 illustrates the extra CT table travel distance during the scan. CT operators must be aware of these safety concerns and receive appropriate training on these special types of patient scans.

Effects on Electronic Medical Devices

Implantable or external electronic medical devices are increasingly used, which must be taken into account for patients receiving CT examinations. Over the years, the FDA has received a small number of reports of adverse events that were believed to be associated with CT scanning of electronic devices.[66] A research study on implantable cardiac rhythm management devices (including pacemakers and cardioverter-defibrillators) indicated that ionizing radiation from CT scans directly over the devices can cause transient interruptions in device function (oversensing) at typical dose levels.[67] Partial electrical reset safety features were activated in two models at maximum doses but not at typical dose levels, and no devices were permanently damaged. A subsequent study on the impact of CT scans on a pegfilgrastim on-body injector at a much higher radiation dose than in routine scans found no sign of device error during or after the scans.[68] Based on available evidence over many years, the FDA determined that, even with the small number of reports of adverse effects received, little evidence existed that CT exposure was the cause of those events. The FDA concluded that the probability of an adverse event occurring as a result of exposing implantable or wearable electronic medical devices to radiation during a CT scan was extremely low and that the clinical benefit of a medically indicated CT examination greatly outweighed the potential risk.[66] Therefore,

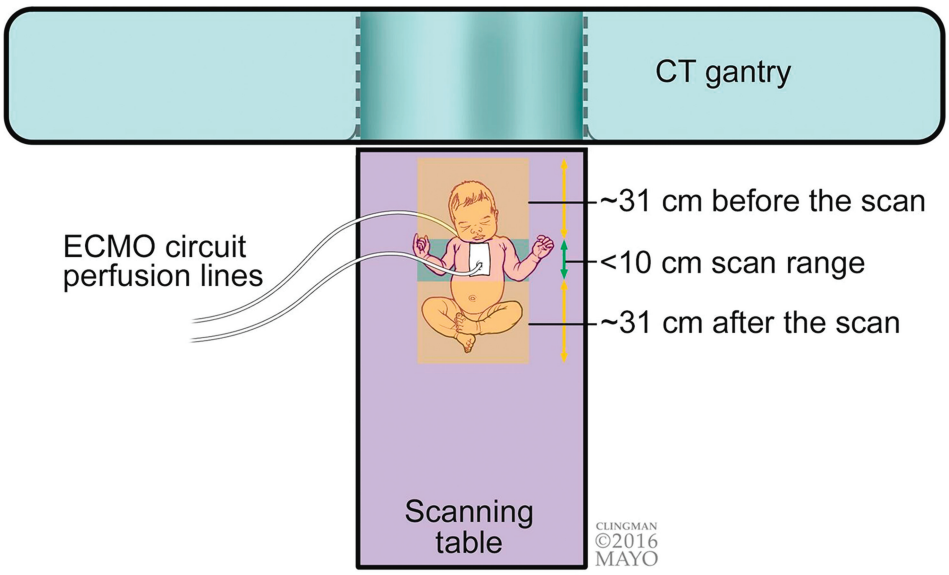

FIGURE 2-8

An illustration of table excursion that can be much greater than the actual scan range, which may generate substantial tension on the extracorporeal membrane oxygenation (ECMO) tubing during the scan that could result in disconnection of the cannulas and a catastrophic accident. The large amount of table excursion beyond the actual scan range is typically required when the pitch of a helical scan is high. Computed tomography (CT) operators must be aware of these safety concerns and receive appropriate training on these special types of patient scans.

Reprinted with permission of the Mayo Foundation for Medical Education and Research. © 2016 Mayo Clinic.

Copyright © American Academy of Neurology. Unauthorized reproduction of this article is prohibited.

KEY POINT

● The presence of implanted electronic devices should not preclude a clinically justified CT scan. However, to reduce the potential risk of interference between electronic devices and CT radiation, some precautions are needed.

the presence of these electronic devices should not preclude a clinically justified CT scan. However, to reduce the potential risk of interference between electronic devices and CT radiation, it is necessary to take some precautions. Following are some general recommendations:

- If possible, try to move the device outside the scan field of view or avoid direct radiation exposure over the device.
- If the device cannot be safely moved, determine if it can be safely and temporarily turned off during the CT scan; turn the device back on after the scan and verify that it functions properly.
- If the device must be scanned within the scan range and cannot be safely turned off, try to minimize the radiation exposure (while still generating sufficient diagnostic quality) and avoid the types of examination that may involve repeated scans over the device for an extended time, such as CT perfusion, dynamic CT, and CT fluoroscopy. Carefully monitor the device and the patient during and after the scan.

Detailed recommendations for patients, physicians ordering CT scans, radiologists, and technologists for specific electronic devices, including insulin pumps, cardiac implanted electronic devices, and neurostimulators, are available on the FDA website.[66]

CONCLUSION

With increased understanding of MRI safety issues and challenges, referring clinicians and staff members can greatly enhance MRI safety efforts. Conversely, lack of knowledge and failure to follow sound policies and procedures can result in serious patient or staff injury or death. Dangerous projectile events can result from bringing a ferromagnetic object into close proximity to the MR scanner. Because magnetic fields are invisible and imperceptible, it is often not recognized that the magnet is "always on." In any situation requiring urgent resuscitation, the patient must be brought out of the magnet room to prevent serious projectile accidents. Burns are the most common injury in MRI and can result from contact with the inner magnet bore; preventive measures include using insulating pads that prevent patient contact with the bore and eliminating skin-skin contact points, which can be problematic in obese patients. Implanted devices are becoming exceedingly common; some are MR-unsafe and others are MR-conditional, meaning that with the appropriate scanning parameters (eg, field strength of the magnet, radiofrequency deposition, specified imaging coils) patients with these devices can be safely scanned. Use of the term *MRI-compatible* is discouraged because of the lack of clarity regarding any special conditions needed for safe scanning. Referring providers can help reduce the chances of patient harm during MRI by accurately and precisely documenting the make and model of implanted devices in the medical record and working with a facility's MRI safety team.

In the CT environment, many factors must be considered to ensure patient and personnel safety, including radiation exposure, system malfunction, needs of CT personnel and operators, and electronic medical devices. Justification and optimization are the two guiding principles to manage radiation dose in CT. The appropriate use of various dose-reduction strategies is critical to accomplish the

Copyright © American Academy of Neurology. Unauthorized reproduction of this article is prohibited.

goal of ALARA, to not overdose but also to not underdose, which may result in errors in patient diagnosis, an important additional consideration regarding patient safety.

REFERENCES

1 Bioinformatics. 2020 CT benchmark report. IMV Medical Information Division. Accessed July 14, 2022. imvinfo.com/product/2020-ct-benchmark-report/

2 Stafford RJ. The physics of magnetic resonance imaging safety. Magn Reson Imaging Clin N Am 2020;28(4):517-536. doi:10.1016/j.mric.2020.08.002

3 Rogg J. Key elements of clinical magnetic resonance imaging safety: it takes a village. Magn Reson Imaging Clin N Am 2020;28(4):471-479. doi:10.1016/j.mric.2020.07.001

4 American College of Radiology. ACR manual on MR safety. Accessed May 18, 2022. acr.org/-/media/ACR/Files/Radiology-Safety/MR-Safety/Manual-on-MR-Safety.pdf

5 ASTM. ASTM F2503-13: standard practice for marking medical devices and other items for safety in the magnetic resonance environment. Accessed July 14, 2022. astm.org/f2503-13.html

6 Tsai LL, Grant AK, Mortele KJ, Kung JW, Smith MP. A practical guide to MR imaging safety: what radiologists need to know. RadioGraphics 2015;35(6):1722-1737. doi:10.1148/rg.2015150108

7 Cross NM, Hoff MN, Kanal KM. Avoiding MRI-related accidents: a practical approach to implementing MR safety. J Am Coll Radiol 2018;15(12):1738-1744. doi:10.1016/j.jacr.2018.06.022

8 Gilk T, Latino RJ. MRI Safety 10 years later. Accessed July 14, 2022. psqh.com/analysis/mri-safety-10-years-later/

9 Mittendorff L, Young A, Sim J. A narrative review of current and emerging MRI safety issues: what every MRI technologist (radiographer) needs to know. J Med Radiat Sci 2022;69(2):250-260. doi:10.1002/jmrs.546

10 Delfino JG, Krainak DM, Flescher SA, Miller DL. MRI-related FDA adverse event reports: a 10-yr review. Med Phys 2019;46(12):5562-5571. doi:10.1002/mp.13768

11 Pietryga JA, Fonder MA, Rogg JM, North DL, Bercovitch LG. Invisible metallic microfiber in clothing presents unrecognized MRI risk for cutaneous burn. AJNR Am J Neuroradiol 2013;34(5):E47-E50. doi:10.3174/ajnr.A2827

12 McRobbie DW. Essentials of MRI safety. 1st ed. Wiley-Blackwell; 2020.

13 Henderson JM, Tkach J, Phillips M, et al. Permanent neurological deficit related to magnetic resonance imaging in a patient with implanted deep brain stimulation electrodes for Parkinson's disease: case report. Neurosurgery 2005;57(5):E1063. doi:10.1227/01.neu.0000180810.16964.3e

14 Safety concerns with implantable infusion pumps in the magnetic resonance (MR) environment: FDA safety communication. Accessed July 15, 2022. wayback.archive-it.org/7993/20201224130324/https://www.fda.gov/medical-devices/safety-communications/safety-concerns-implantable-infusion-pumps-magnetic-resonance-mr-environment-fda-safety

15 Mohammed I, Hussain A. Intrathecal baclofen withdrawal syndrome- a life-threatening complication of baclofen pump: a case report. BMC Clin Pharmacol 2004;4:6. doi:10.1186/1472-6904-4-6

16 Yang E, Nazarian S, Halperin H. Performing MRI in patients with conventional (non-MR-conditional) cardiac devices. In: Shellock F, Crues J, editors. MRI Bioefects, Safety, and Patient Management. 2nd ed. Playa Del Rey; 2022.

17 Watson RE, Edmonson HA. MR safety: active implanted electronic devices. Magn Reson Imaging Clin N Am 2020;28(4):549-558. doi:10.1016/j.mric.2020.08.001

18 Lundstrom B, Lin C, Starnes D. Safety and management of implanted epilepsy devices for imaging and surgery. Mayo Clin Proc 2022;97(11):2123-2138. doi:10.1016/j.mayocp.2022.06.012

19 Watson RE, Cradick CM, Epps S, Mauck WD, Luetmer PH. Implementing an electronic health record medical device module-a critical patient safety enhancement. J Am Coll Radiol 2016;13(6):705-708. doi:10.1016/j.jacr.2015.10.009

20 Watson RE, Walsh SM, Felmlee JP, Friedman PA, Keene MN. Augmenting MRI safety screening processes: reliable identification of cardiac implantable electronic devices by a ferromagnetic detector system. J Magn Reson Imaging 2019;49(7):e297-e299. doi:10.1002/jmri.26277

21 US Food and Drug Administration. Testing and labeling medical devices for safety in the magnetic resonance (MR) environment. Guidance for industry and food and drug administration staff. Accessed November 17. fda.gov/regulatory-information/search-fda-guidance-documents/testing-and-labeling-medical-devices-safety-magnetic-resonance-mr-environment

Copyright © American Academy of Neurology. Unauthorized reproduction of this article is prohibited.

22 Edmonson HA, Carlson ML, Patton AC, Watson RE. MR imaging and cochlear implants with retained internal magnets: reducing artifacts near highly inhomogeneous magnetic fields. Radiographics 2018;38(1):94-106. doi:10.1148/rg.2018170135

23 McDonald JS, McDonald RJ. MR imaging safety considerations of gadolinium-based contrast agents: gadolinium retention and nephrogenic systemic fibrosis. Magn Reson Imaging Clin N Am 2020;28(4):497-507. doi:10.1016/j.mric.2020.06.001

24 Kanda T, Fukusato T, Matsuda M, et al. Gadolinium-based contrast agent accumulates in the brain even in subjects without severe renal dysfunction: evaluation of autopsy brain specimens with inductively coupled plasma mass spectroscopy. Radiology 2015;276(1):228-232. doi:10.1148/radiol.2015142690

25 Ray JG, Vermeulen MJ, Bharatha A, Montanera WJ, Park AL. Association between MRI exposure during pregnancy and fetal and childhood outcomes. JAMA 2016;316(9):952-961. doi:10.1001/jama.2016.12126

26 Chartier Al, Bouvier MJ, McPherson DR, et al. The safety of maternal and fetal MRI at 3T. AJR Am J Roentgenol 2019;213(5):1170-1173. doi:10.2214/AJR.19.21400

27 Little JT, Bookwalter CA. Magnetic resonance safety: pregnancy and lactation. Magn Reson Imaging Clin N Am 2020;28(4):509-516. doi:10.1016/j.mric.2020.06.002

28 Oh KY, Roberts VH, Schabel MC, et al. Gadolinium chelate contrast material in pregnancy: fetal biodistribution in the nonhuman primate. Radiology 2015;276(1):110-118. doi:10.1148/radiol.15141488

29 American College of Radiology. ACR manual on contrast media (2022). Accessed December 12, 2022. acr.org/-/media/acr/files/clinical-resources/contrast_media.pdf

30 International Electrotechnical Commission. Medical electrical equipment. Part 2-44: particular requirements for the safety of x-ray equipment for computed tomography. Accessed November 17, 2022. webstore.iec.ch/publication/24442

31 McCollough CH, Leng S, Yu L, et al. CT dose index and patient dose: they are not the same thing. Radiology 2011;259(2):311-316. doi:10.1148/radiol.11101800

32 American Association of Physicists in Medicine. AAPM Report No. 204. Size-specific dose estimates (SSDE) in pediatric and adult body CT examinations. Accessed November 17, 2022. aapm.org/pubs/reports/rpt_204.pdf

33 McCollough CH, Schueler BA. Calculation of effective dose. Med Phys 2000;27(5):828-837. doi:10.1118/1.598948

34 The 2007 recommendations of the International Commission on Radiological Protection. ICRP publication 103. Ann ICRP 2007;37(2-4):1-332. doi:10.1016/j.icrp.2007.10.003

35 Yu L, Liu X, Leng S, et al. Radiation dose reduction in computed tomography: techniques and future perspective. Imaging Med 2009;1(1):65-84. doi:10.2217/iim.09.5

36 American Association of Physicists in Medicine. AAPM Task Group 23 of the Diagnostic Imaging Council CT Committee. AAPM Report No. 96: the measurement, reporting, and management of radiation dose in CT. Accessed November 17, 2022. aapm.org/pubs/reports/rpt_96.pdf

37 National Lung Screening Trial Research Team. The National Lung Screening Trial: overview and study design. Radiology 2011;258(1):243-253. doi:10.1148/radiol.10091808

38 American College of Radiology. Radiation Dose reference chart of radiology (ACR). Accessed July 14, 2022. acr.org/Clinical-Resources/Radiology-Safety/Radiation-Safety

39 National Council on Radiation Protection and Measurements. NCRP Report No. 160: Ionizing Radiation Exposure of the Population of the United States. Accessed July 14, 2022. ncrponline.org/publications/reports/ncrp-report-160-2/

40 Kanal KM, Butler PF, Sengupta D, et al. U.S. diagnostic reference levels and achievable doses for 10 adult CT examinations. Radiology 2017;284(1):120-133. doi:10.1148/radiol.2017161911

41 Yu L, Leng S, Philips L, Berghart D, McCollough C. Dose considerations in perfusion CT. In: Bammer R, ed. MR & CT perfusion imaging: clinical applications and theoretical principles. Lippincott Williams & Wilkins; 2014:23-32.

42 Romanyukha A, Folio L, Lamart S, Simon SL, Lee C. Body size-specific effective dose conversion coefficients for CT scans. Rad Protect Dosimetry 2016;172(4):428-437. doi:10.1093/rpd/ncv511

43 Bushberg JT, Seibert JA, Leidholdt EM Jr, Boone JM. The essential physics of medical imaging. 3rd ed. Wolters Kluwer Health/Lippincott Williams & Wilkins; 2011.

44 International Commission on Radiological Protection. ICRP statement on tissue reactions. Accessed July 14, 2022. icrp.org/page.asp?id=123

45 National Council on Radiation Protection (NCRP). National Council on Radiation Protection and Measurements. Guidance on radiation dose limits for the lens of the eye. Accessed July 14, 2022. ncrponline.org/shop/commentaries/commentary-no-26-guidance-on-radiation-dose-limits-for-the-lens-of-the-eye-2016/

Copyright © American Academy of Neurology. Unauthorized reproduction of this article is prohibited.

46 National Academy of Sciences. Biologic effects of ionizing radiation (BEIR) Report VII. Health risks from exposure to low levels of ionizing radiation. Accessed November 17, 2022. nap.nationalacademies.org/catalog/11340/health-risks-from-exposure-to-low-levels-of-ionizing-radiation

47 Brenner DJ, Doll R, Goodhead DT, et al. Cancer risks attributable to low doses of ionizing radiation: assessing what we really know. Proc Natl Acad Sci U S A 2003;100(24):13761-13766. doi:10.1073/pnas.2235592100

48 Little MP, Wakeford R, Tawn EJ, Bouffler SD, Berrington de Gonzalez A. Risks associated with low doses and low dose rates of ionizing radiation: why linearity may be (almost) the best we can do. Radiology 2009;251(1):6-12. doi:10.1148/radiol.2511081686

49 Tubiana M, Feinendegen LE, Yang C, Kaminski JM. The linear no-threshold relationship is inconsistent with radiation biologic and experimental data. Radiology 2009;251(1):13-22. doi:10.1148/radiol.2511080671

50 Brenner DJ, Hall EJ. Computed tomography–an increasing source of radiation exposure. N Engl J Med 2007;357(22):2277-2284. doi:10.1056/NEJMra072149

51 American Association of Physicists in Medicine. AAPM Position Statement on Radiation Risks From Medical Imaging Procedures. Accessed July 14, 2022. aapm.org/org/policies/details.asp?id=2548#13

52 The Health Physics Society. Radiation risk in perspective. Position statement of The Health Physics Society. Accessed May 15, 2022. hps.org/documents/radiationrisk.pdf

53 American Association of Physicists in Medicine. AAPM/ACR/HPS Joint Statement on Proper Use of Radiation Dose Metric Tracking for Patients Undergoing Medical Imaging Exams. Accessed July 14, 2022. aapm.org/org/policies/details.asp?id=1533

54 Durand DJ, Dixon RL, Morin RL. Utilization strategies for cumulative dose estimates: a review and rational assessment. J Am Coll Radiol 2012;9(7):480-485. doi:10.1016/j.jacr.2012.03.003

55 Gabriel S, Eckel LJ, DeLone DR, et al. Pilot study of radiation dose reduction for pediatric head CT in evaluation of ventricular size. AJNR Am J Neuroradiol 2014;35(12):2237-2242. doi:10.3174/ajnr.A4056

56 American College of Radiology. CT accreditation quality control manual. Accessed November 17, 2022. acr.org/-/media/ACR/Files/Clinical-Resources/QC-Manuals/CT_QCManual.pdf

57 McCollough CH, Bruesewitz MR, Kofler JM. CT dose reduction and dose management tools: overview of available options. RadioGraphics 2006;26(2):503-512. doi:10.1148/rg.262055138

58 Yu L, Li H, Fletcher JG, McCollough CH. Automatic selection of tube potential for radiation dose reduction in CT: a general strategy. Med Phys 2010;37(1):234-243. doi:10.1118/1.3264614

59 Mileto A, Guimaraes LS, McCollough CH, Fletcher JG, Yu L. State of the art in abdominal CT: the limits of iterative reconstruction algorithms. Radiology 2019;293(3):491-503. doi:10.1148/radiol.2019191422

60 Favazza CP, Ferrero A, Yu L, et al. Use of a channelized Hotelling observer to assess CT image quality and optimize dose reduction for iteratively reconstructed images. J Med Imaging (Bellingham) 2017;4(3):031213. doi:10.1117/1.JMI.4.3.031213

61 Solomon J, Lyu P, Marin D, Samei E. Noise and spatial resolution properties of a commercially available deep learning-based CT reconstruction algorithm. Medical Physics 2020;47(9):3961-3971. doi:10.1002/mp.14319

62 Rajendran K, Petersilka M, Henning A, et al. First clinical photon-counting detector CT system: technical evaluation. Radiology 2022;303(1):130-138. doi:10.1148/radiol.212579

63 Long Z, Bruesewitz MR, Sheedy EN, et al. Technical note: display window setting: an important factor for detecting subtle but clinically relevant artifacts in daily CT quality control. Med Phys 2016;43(12):6413. doi:10.1118/1.4966698

64 Gould P. Radiation overdose in 200 patients leads to FDA safety notice. BMJ 2009;339:b4217. doi:10.1136/bmj.b4217

65 Hull NC, Schooler GR, Binkovitz LA, et al. Chest computed tomography angiography in children on extracorporeal membrane oxygenation (ECMO). Pediatr Radiol 2018;48(7):1021-1030. doi:10.1007/s00247-017-4034-3

66 US Food and Drug Administration. Interference between CT and electronic medical devices. Accessed July 14, 2022. fda.gov/radiation-emitting-products/electromagnetic-compatibility-emc/interference-between-ct-and-electronic-medical-devices

67 McCollough CH, Zhang J, Primak AN, Clement WJ, Buysman JR. Effects of CT Irradiation on implantable cardiac rhythm management devices. Radiology 2007;243(3):766-774. doi:10.1148/radiol.2433060993

68 Long Z, Kurup AN, Jensen NM, et al. Initial testing of pegfilgrastim (Neulasta Onpro) on-body injector in multiple radiological imaging environments. J Appl Clin Med Phys 2021;22(1):343-349. doi:10.1002/acm2.13156

Copyright © American Academy of Neurology. Unauthorized reproduction of this article is prohibited.

REVIEW ARTICLE

CONTINUUM AUDIO INTERVIEW AVAILABLE ONLINE

Imaging of Central Nervous System Ischemia

By Julie G. Shulman, MD; Mohamad Abdalkader, MD

ABSTRACT

OBJECTIVE: **This article describes imaging modalities used in the evaluation of patients presenting with symptoms of acute ischemic stroke.**

LATEST DEVELOPMENTS: **The year 2015 marked the beginning of a new era in acute stroke care with the widespread adoption of mechanical thrombectomy. Subsequent randomized controlled trials in 2017 and 2018 brought the stroke community even further into this new territory with the expansion of the eligibility window for thrombectomy using imaging-based patient selection, which led to an increase in the use of perfusion imaging. Now, after several years of routine use, the debate is ongoing as to when this additional imaging is truly required and when it results in unnecessary delays in time-sensitive stroke care. At this time, more than ever, a robust understanding of neuroimaging techniques, applications, and interpretation is essential for the practicing neurologist.**

ESSENTIAL POINTS: **CT-based imaging is the first step in most centers for the evaluation of patients presenting with symptoms of acute stroke because of its wide availability, speed, and safety. Noncontrast head CT alone is sufficient for IV thrombolysis decision making. CT angiography is very sensitive for the detection of large-vessel occlusion and can be used reliably to make this determination. Advanced imaging including multiphase CT angiography, CT perfusion, MRI, and MR perfusion can provide additional information useful for therapeutic decision making in specific clinical scenarios. In all cases, it is essential that neuroimaging be performed and interpreted rapidly to allow for timely reperfusion therapy.**

CITE AS:
CONTINUUM (MINNEAP MINN) 2023;29(1, NEUROIMAGING): 54–72.

Address correspondence to Dr Julie G. Shulman, Boston Medical Center, 85 E Concord St, Ste 1127, Boston, MA 02118, Julie.Shulman@bmc.org.

RELATIONSHIP DISCLOSURE:
Dr Shulman has received research support from the BU Spivack Neuroscience Pilot Award. Dr Abdalkader reports no disclosure.

UNLABELED USE OF PRODUCTS/INVESTIGATIONAL USE DISCLOSURE:
Drs Shulman and Abdalkader report no disclosures.

© 2023 American Academy of Neurology.

INTRODUCTION

Rapid neuroimaging is essential to acute stroke management. Multiple imaging modalities are available for use in this setting depending on the resources and systems of care established at an individual institution. In all cases, imaging must be performed as quickly as possible to allow for efficient administration of acute therapies, including IV thrombolysis (ie, with tissue plasminogen activator [tPA]) and mechanical thrombectomy. This article reviews the imaging modalities commonly used for the evaluation of ischemic stroke.

Copyright © American Academy of Neurology. Unauthorized reproduction of this article is prohibited.

NONCONTRAST CT

Noncontrast CT of the head is the most common initial imaging modality used in the evaluation of a patient presenting with acute stroke symptoms. It is widely available and fast and has a high sensitivity for detecting intracerebral hemorrhage. Exclusion of intracerebral hemorrhage is a critical step in evaluating a patient's candidacy for IV tPA, and a noncontrast CT alone is sufficient to make this determination. In geographic areas that utilize mobile stroke units (ambulances equipped with a CT scanner and specialized personnel), IV tPA can be administered before hospital arrival after performance and interpretation of a noncontrast head CT.[1] In addition to ruling out hemorrhage, CT can provide important information about ischemia.

Early Ischemic Changes

Early ischemic changes evident on noncontrast CT include three classic radiographic findings: obscuration of the lentiform nucleus, loss of the gray-white matter differentiation in the insula (insular ribbon sign), and effacement of the cortical sulci (cortical ribbon sign).[2] An example of these findings can be seen in FIGURE 3-1. When CT is performed within 6 hours of stroke onset, these changes can be seen in approximately 60% of cases.[3]

KEY POINT

- Early ischemic changes evident on noncontrast CT include obscuration of the lentiform nucleus, loss of the gray-white boundary in the insula (insular ribbon sign), and effacement of the cortical sulci (cortical ribbon sign).

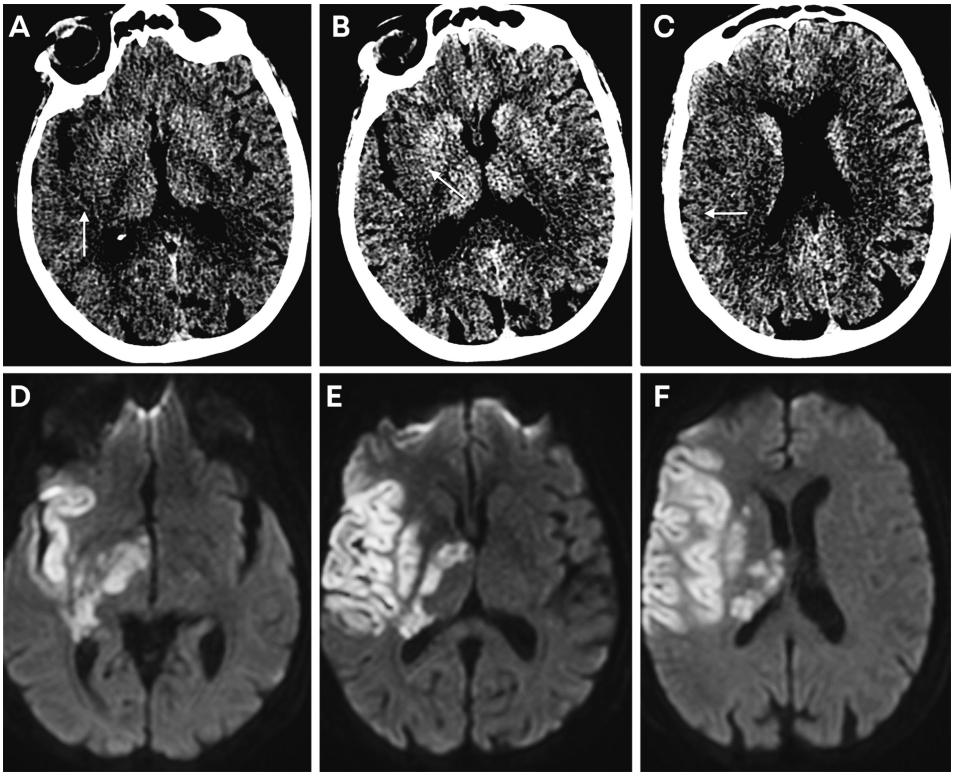

FIGURE 3-1

Early ischemic changes evident on noncontrast head CT. *A-C*, Axial noncontrast CT showing early ischemic changes. Obscuration and loss of the gray-white boundary in the right insular cortex (insular ribbon sign) (*A, arrow*), obscuration of the right lentiform nucleus (*B, arrow*), and effacement of the right cortical sulci (cortical ribbon sign) (*C, arrow*). *D-F*, Axial diffusion-weighted imaging sequences from MRI performed 2 days later, confirming that the hypodense areas seen on the initial noncontrast CT represented ischemia.

Copyright © American Academy of Neurology. Unauthorized reproduction of this article is prohibited.

Although early ischemic changes are helpful in determining the presence and extent of ischemia[4] and have been shown to correlate with an increased risk of poor functional outcome,[5] they should not be used to exclude patients from IV tPA in the standard treatment window of less than 3 hours from last known well time. In a study of 624 patients, early ischemic changes were not independently associated with risk of adverse outcomes after treatment with IV tPA, and the patients who were treated with IV tPA did better regardless of whether or not early ischemic changes were present.[6]

Alberta Stroke Programme Early CT Score

In contrast to IV tPA decision making, evaluation of early ischemic changes can be an important tool in determining a patient's candidacy for mechanical thrombectomy. In this scenario, the Alberta Stroke Programme Early CT Score (ASPECTS) is commonly used. ASPECTS is a standardized quantitative 10-point grading system intended for use in acute, anterior-circulation ischemic stroke.[7] The ASPECTS value is calculated by assessment of axial slices of noncontrast CT at two standardized levels—the ganglionic level (the level of the thalamus and basal ganglia) and the supraganglionic level (above the caudate head). At these two levels, 10 regions are identified and evaluated for evidence of early ischemic changes. These regions are illustrated in FIGURE 3-2. If early ischemic changes are present, a score of 0 is assigned to that region. If early ischemic changes are absent, a score of 1 is assigned. These individual region scores are then summed to determine the total ASPECTS value. The maximum score of 10 indicates no evidence of early ischemic changes. Although the original ASPECTS value is calculated on noncontrast CT with 10-mm slice thickness,[7] recent studies have suggested improved accuracy when the ASPECTS value is calculated on either

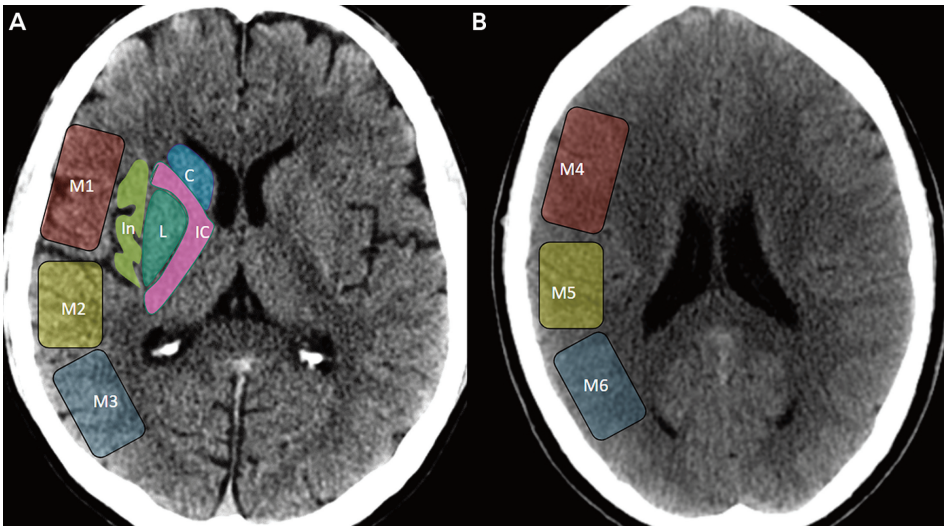

FIGURE 3-2

Axial noncontrast CT images showing the 10 specific regions to assess when calculating an Alberta Stroke Programme Early CT Score (ASPECTS). *A,* Ganglionic-level image showing caudate nucleus (C), internal capsule (IC), lentiform nucleus (L), insular ribbon (In), anterior middle cerebral artery (MCA) cortex (M1), lateral MCA cortex (M2), and posterior MCA cortex (M3). *B,* Supraganglionic-level image showing anterior MCA cortex (M4), lateral MCA cortex (M5), and posterior MCA cortex (M6).

Copyright © American Academy of Neurology. Unauthorized reproduction of this article is prohibited.

the CT angiography (CTA) source images[8] or the contrast-enhanced CT images obtained during a CT perfusion study.[9]

Of the five landmark randomized controlled trials published in 2015 that demonstrated the benefit of endovascular therapy for large-vessel occlusion stroke, four used neuroimaging to exclude patients with evidence of a large ischemic core in an effort to optimize both efficacy and safety of revascularization.[10-14] Of those four, three used ASPECTS to determine this, with a required score of 6 to 7 or greater for randomization. As a result of these trials, the American Heart Association/American Stroke Association (AHA/ASA) guidelines recommend proceeding with mechanical thrombectomy for patients with large-vessel occlusion and an ASPECTS value of 6 or greater who present within 6 hours of last known well time, without additional advanced imaging.[15] Additional imaging in this clinical scenario may lead to the unnecessary exclusion of patients who may otherwise benefit from treatment. The appropriateness of mechanical thrombectomy for patients with low ASPECTS values (less than or equal to 5) is uncertain and is a topic of ongoing investigation.[16-18] An example of patient selection for thrombectomy using noncontrast CT and CTA is shown in **CASE 3-1**.

In the delayed-window thrombectomy trials,[19,20] which included patients presenting at 6 to 24 hours from last known well time, CT perfusion or MRI was used to determine the ischemic core. However, all patients randomly assigned in both studies had noncontrast CT–based ASPECTS values of 7 or greater. Although the AHA/ASA guidelines recommend adherence to the trials' inclusion criteria (including use of advanced imaging) when selecting patients for thrombectomy beyond 6 hours from last known well time,[15] some institutions use noncontrast CT and the ASPECTS value alone to select patients for endovascular therapy in the delayed window. This practice is often a result of the resources and systems of care established at a given institution. It has been both supported[21] and refuted[22] by recent literature.

Posterior-Circulation Alberta Stroke Programme Early CT Score

A limitation of ASPECTS is that it is designed for use only in anterior-circulation ischemia. As a result, a novel ASPECTS tool intended for use in the posterior circulation has been developed.[23] This score, known as posterior-circulation ASPECTS (pc-ASPECTS), is a quantitative 10-point grading system for use in suspected vertebrobasilar ischemia. Although it can be calculated from noncontrast CT, beam-hardening artifact in the posterior fossa can be limiting, and accuracy is improved when the calculation is based on CTA source images. In this score, eight distinct brain regions are identified: right and left thalamus, right and left cerebellum, right and left occipital lobes, midbrain, and pons. For early ischemic changes evident in the midbrain or pons, two points are deducted from the total score. Each of the other six regions accounts for one point. These regions and their point values are shown in **FIGURE 3-4**. As with the traditional ASPECTS value, a score of 10 indicates a lack of early ischemic changes. The pc-ASPECTS value has been shown to improve the detection of ischemia and predict functional outcome.[24] However, given the less widespread use of pc-ASPECTS and the very high morbidity and mortality of basilar artery occlusion, most centers do not use a specific pc-ASPECTS threshold when selecting patients for mechanical thrombectomy.

KEY POINTS

- **The Alberta Stroke Programme Early CT Score (ASPECTS) is a quantitative assessment of early ischemic changes calculated by visual inspection of 10 specific neuroanatomic regions on noncontrast CT. The maximum score of 10 indicates no evidence of early ischemia.**
- **The American Heart Association/American Stroke Association guidelines recommend proceeding with mechanical thrombectomy for patients with large-vessel occlusion stroke and an Alberta Stroke Programme Early CT Score (ASPECTS) of 6 or greater who present within 6 hours of last known well time, without additional advanced imaging.**
- **The posterior-circulation Alberta Stroke Programme Early CT Score (ASPECTS) is a 10-point scale that assesses eight brain regions supplied by the vertebrobasilar system for evidence of early ischemic changes. It has been shown to improve detection of ischemia and predict functional outcome.**

Copyright © American Academy of Neurology. Unauthorized reproduction of this article is prohibited.

CASE 3-1

A 62-year-old man with atrial fibrillation not receiving anticoagulation therapy presented after being found on the floor by his family. He was seen by family members in his usual state of health 1 hour previously. He had an initial National Institutes of Health (NIH) Stroke Scale score of 20, with examination notable for left gaze deviation, right visual field loss, right hemiparesis, and aphasia. Initial noncontrast CT was notable for a hyperdense left middle cerebral artery sign (FIGURE 3-3). The Alberta Stroke Programme Early CT Score was determined to be 10. IV tissue plasminogen activator was administered in the CT scanner. While the infusion was running, CT angiography (CTA) was performed and was notable for a left M1 segment occlusion. He was taken for emergent mechanical thrombectomy, which resulted in Thrombolysis in Cerebral Infarction scale grade 3 reperfusion. After stabilization, he was discharged to an acute care rehabilitation facility with an NIH Stroke Scale score of 8.

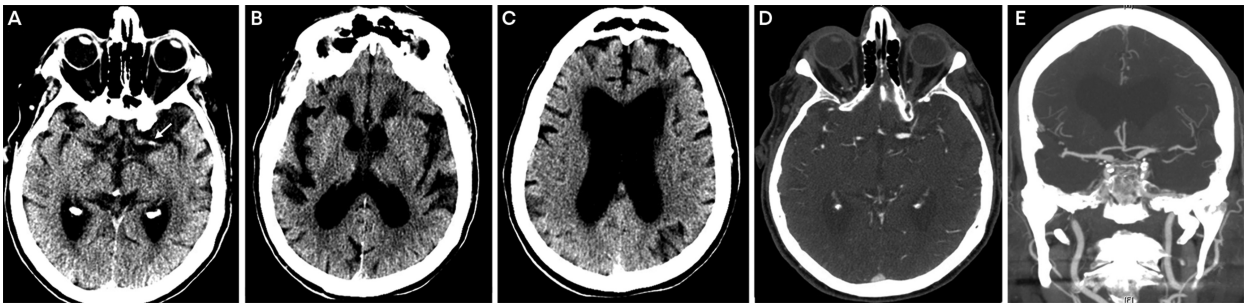

FIGURE 3-3

Imaging of the patient in CASE 3-1. The initial axial noncontrast CT (*A*) demonstrates a hyperdense left middle cerebral artery sign. The patient's left gaze deviation can also be seen on this image. The Alberta Stroke Programme Early CT Score (ASPECTS) was 10, as determined by visual assessment of the ganglionic (*B*) and supraganglionic (*C*) levels of the same initial axial noncontrast head CT. Axial source images (*D*) and coronal maximal intensity projections (*E*) from the CT angiogram reveal a left M1 segment middle cerebral artery occlusion.

COMMENT

This case demonstrates patient selection for thrombectomy using noncontrast CT and CTA in the early window. This practice is supported by the American Heart Association/American Stroke Association guidelines, which recommend proceeding with mechanical thrombectomy for patients with large-vessel occlusion and an Alberta Stroke Programme Early CT Score of 6 or greater who present within 6 hours of last known well time, without additional advanced imaging.

Copyright © American Academy of Neurology. Unauthorized reproduction of this article is prohibited.

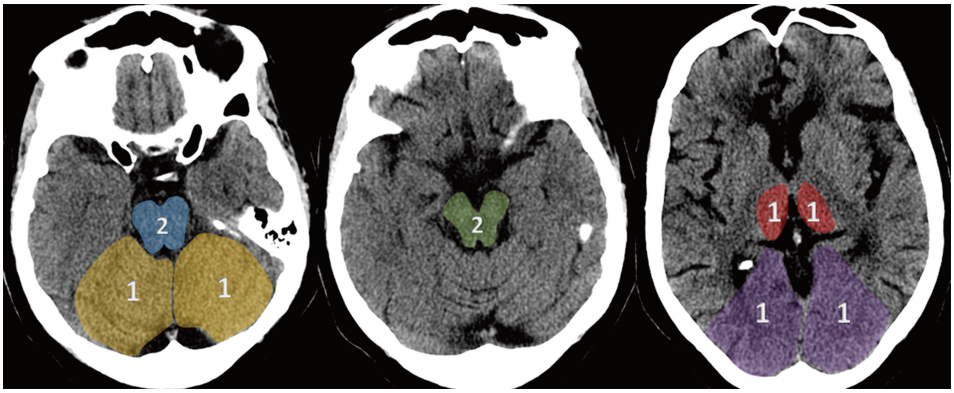

FIGURE 3-4
Axial noncontrast CT showing the eight distinct brain regions evaluated for evidence of early ischemic changes to derive the posterior-circulation Alberta Stroke Programme Early CT Score (pc-ASPECTS). The superimposed numbers indicate the point values assigned to each region. Specifically, the midbrain and pons each account for two points in the scoring system, whereas the bilateral cerebellar hemispheres, bilateral thalami, and bilateral occipital lobes account for one point each.

KEY POINT

- The hyperdense vessel sign can be seen on noncontrast CT and is highly specific for large-vessel occlusion.

Hyperdense Vessel Sign

Unilateral hyperdensity of a proximal large vessel can be seen on noncontrast CT when a thrombus is present within the lumen.[25] This is most commonly seen in the proximal middle cerebral artery (MCA), with a reported frequency of 30% to 40% of MCA infarctions, and is highly specific for MCA occlusion.[26] Similar findings can be seen with more distal MCA occlusions and in the basilar artery. Examples of hyperdense vessel signs are shown in FIGURE 3-5. Identification of a hyperdense vessel on noncontrast CT should result in the patient's being treated as if a large-vessel occlusion were present until proven otherwise.

CT ANGIOGRAPHY

CTA is a result of carefully timed CT imaging obtained after administration of an IV bolus of iodinated contrast. To accommodate a high flow rate and optimize

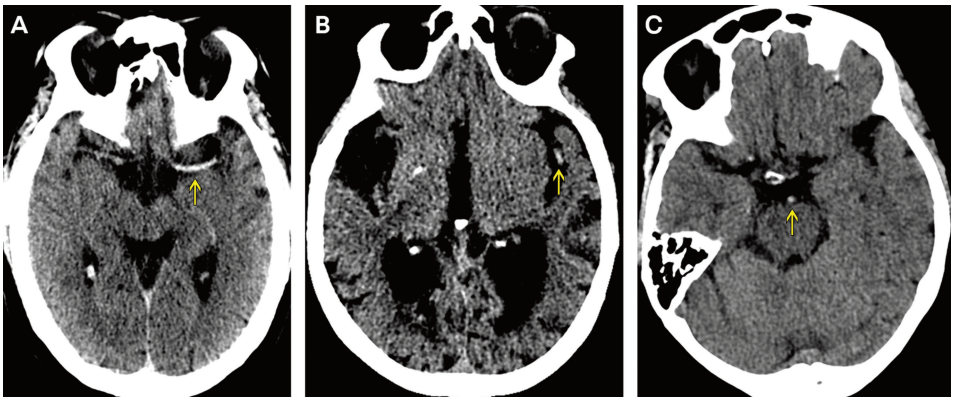

FIGURE 3-5
Examples of hyperdense vessel signs on noncontrast CT images. *A,* Long thrombus in the left M1 segment appearing as a hyperdense vessel (*arrow*). *B,* Hyperdense left M2 branch in the Sylvian fissure (*arrow*). *C,* Hyperdense basilar artery (*arrow*). In each of these cases, the patient was confirmed to have a large-vessel occlusion by CT angiography, digital subtraction angiography, or both.

Copyright © American Academy of Neurology. Unauthorized reproduction of this article is prohibited.

KEY POINTS

- It is recommended to proceed with CT angiography before measuring a serum creatinine level in patients eligible for mechanical thrombectomy without known renal impairment to avoid unnecessary delays in reperfusion.
- CT angiography is extremely accurate for detecting large-vessel occlusion, with sensitivity and specificity of approximately 98%.
- Multiphase CT angiography can be used to obtain a more robust assessment of a patient's collateral circulation. Quality of collateral flow has been shown to correlate with rate of infarct growth and predict prognosis in some studies.

timing, the contrast should be administered through a 20-gauge or larger IV catheter in the right antecubital fossa.[27] In rare cases, administration of iodinated contrast can cause contrast-induced nephropathy. However, the risk of acquiring contrast-induced nephropathy from a CTA is exceedingly low, especially in patients without a history of renal impairment.[28,29] Awaiting laboratory studies to assess renal function can delay mechanical thrombectomy, which is associated with worse functional outcomes.[30] Thus, it is recommended to proceed with CTA before measuring the serum creatinine level in patients eligible for mechanical thrombectomy without known renal impairment.[15] Rarely, a patient is truly unable to safely undergo CTA because of documented severe allergy to iodine contrast. In that circumstance, immediate MR angiography (MRA) or a direct to digital subtraction angiography (DSA) pathway is reasonable if there is a strong clinical suspicion of large-vessel occlusion.

Identification of Large-Vessel Occlusion

The images obtained by CTA capture the contrast in the lumen of the extracranial and intracranial vasculature and can be combined to create two-dimensional maximal-intensity projections and three-dimensional reconstructions. With this technique, an intraluminal thrombus will appear as a lack of contrast opacification in a given vessel segment, creating a filling defect. CTA is extremely accurate for detecting large-vessel occlusion, with sensitivity of 98.4% and specificity of 98.1%.[31] The interoperator reliability is high, with a Pearson correlation coefficient of 0.951 measured in one study.[32] As a result of its availability, efficiency, and accuracy, it has become the standard noninvasive test for identifying large-vessel occlusion.

Multiphase CT Angiography

In addition to identification of large-vessel occlusion, CTA can also be used to assess a patient's collateral circulation. Traditionally timed CTA images underestimate collateral quality, as intraarterial contrast has not yet arrived in these collateral circulations at the time of image acquisition because of slower flow. To compensate for this, multiphase CTA images can be obtained. With this technique, two additional sets of images are acquired after the arterial time point: one at the peak venous phase and one at the late venous phase.[33] When considered together, these three sets of images obtained at three different time points allow for a more robust assessment of collateral circulation. Multiple different scoring systems are used to assign numeric values to a collateral circulation seen by multiphase CTA, typically on a 4- or 5-point scale. However, practically speaking, these scores are often dichotomized into either "good" or "poor" collaterals. Poor collateral scores have been shown in some studies to predict a poor prognosis.[34] Multiphase CTA was used in the ESCAPE (Endovascular Treatment for Small Core and Anterior Circulation Proximal Occlusion) trial to aid in selection of patients for mechanical thrombectomy and, in that context, demonstrated good interrater reliability.[11] Examples of "good" and "poor" collateral circulations are shown in FIGURE 3-6 and FIGURE 3-7.

CT PERFUSION

Like multiphase CTA, CT perfusion (CTP) imaging is performed by acquiring multiple scans over time following IV administration of iodinated contrast. The number of scans required and the resultant radiation exposure is higher for CTP

Copyright © American Academy of Neurology. Unauthorized reproduction of this article is prohibited.

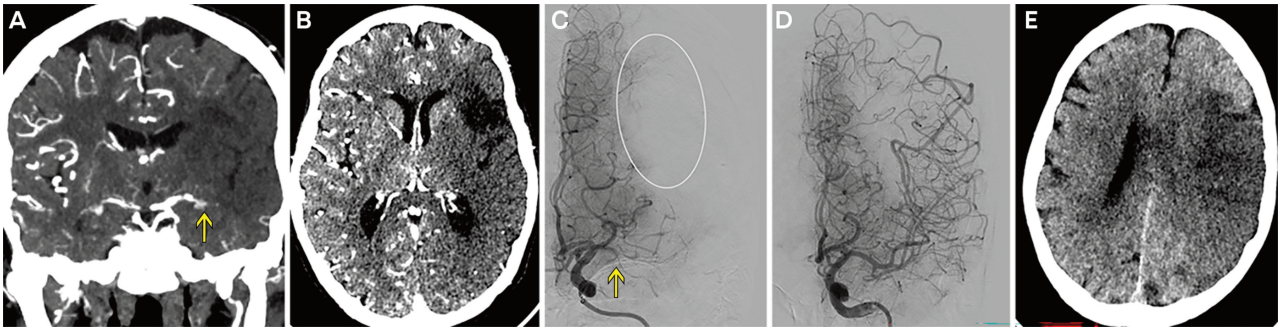

FIGURE 3-6

Images from a 74-year-old woman who presented with sudden, witnessed onset of right-sided weakness and aphasia 1 hour before arrival at the hospital. Her initial National Institutes of Health Stroke Scale score was 19. Initial coronal (*A*) and axial (*B*) CT angiograms demonstrating a left M1 occlusion *(A, arrow)* with very poor collateral flow. Initial digital subtraction angiogram confirms the occlusion (*C*, arrow) and poor collaterals (*C, oval*). Subsequent digital subtraction angiogram following mechanical thrombectomy demonstrates Thrombolysis in Cerebral Infarction scale grade 3 recanalization (complete reperfusion) that was achieved after two passes (*D*). *E,* Follow-up axial noncontrast head CT showing large left middle cerebral artery infarct despite timely reperfusion.

compared with multiphase CTA.[35] The series of images follows the contrast material as it arrives in the arteries, perfuses brain tissue, and washes out through the venous system. With this information, the scanner then determines estimates of cerebral blood flow, cerebral blood volume, and mean transit time. Cerebral blood flow is the amount of blood that travels through a given brain region over time, measured as milliliters per 100 g per minute. Cerebral blood volume is the total volume of blood in a brain region, measured as milliliters per 100 g. Mean transit time is the average time it takes the blood to travel through a given brain region, measured in seconds.[36] Taken together, these three measures can be used to determine whether a given brain region is normally perfused, ischemic, or infarcted, as shown in **TABLE 3-1**.

Rate of infarct growth is variable among individuals and is strongly dependent on the presence of collateral circulation.[37] In areas with poor collaterals, lack of

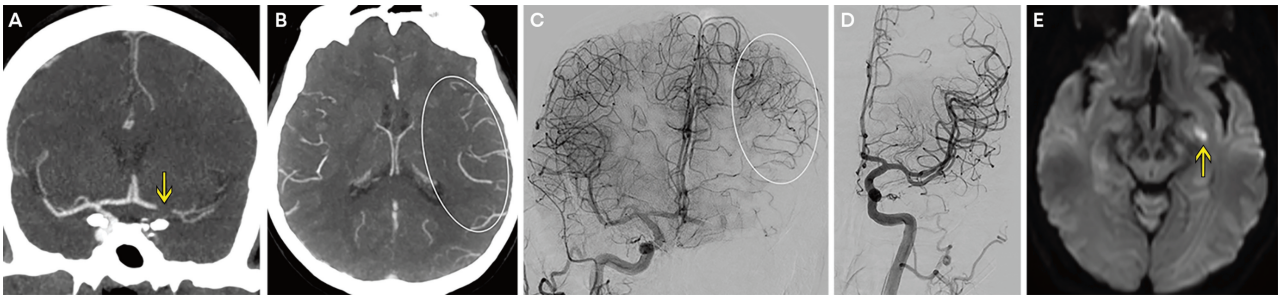

FIGURE 3-7

Images from a 66-year-old man who presented with sudden onset of right-sided weakness and aphasia 3 hours before arrival. His initial National Institutes of Health Stroke Scale score was 12. Initial coronal (*A*) and axial (*B*) CT angiogram demonstrating a left internal carotid artery terminus occlusion *(A, arrow)* with good collaterals and retrograde filling of the left middle cerebral artery territory *(B, oval)*. Initial digital subtraction angiogram confirms the occlusion and robust collaterals (*C, oval*). Subsequent digital subtraction angiogram after mechanical thrombectomy demonstrates Thrombolysis in Cerebral Infarction scale grade 3 recanalization (complete reperfusion) after one pass (*D*). *E,* Follow-up diffusion-weighted imaging MRI revealed only a very small resultant infarct *(arrow)*.

Copyright © American Academy of Neurology. Unauthorized reproduction of this article is prohibited.

blood flow results in irreversible metabolic and cellular failure leading to tissue infarction (infarct core). In areas with good collaterals, the tissue will be dysfunctional but not irreversibly infarcted (ischemic penumbra).[37] Postprocessing of CTP images creates maps that approximate the size and location of the infarct core and the ischemic penumbra, as shown in FIGURE 3-8. When interpreting these maps, the reader is looking to identify either a mismatch between the size of the core infarct and the size of the ischemic penumbra or a mismatch between the patient's clinical examination and the size and location of the core infarct.

Identification of a mismatch suggests reversibility of ischemia with timely reperfusion and therefore has been used to select patients for mechanical thrombectomy beyond 6 hours from stroke onset.[19,20] Using perfusion imaging in this way results in a patient-specific "tissue clock," as opposed to a standardized time window of eligibility for all patients. This approach of individualized patient selection for delayed mechanical thrombectomy using perfusion imaging is supported by the AHA/ASA guidelines.[15]

Although perfusion imaging can be helpful when performed and interpreted correctly, current perfusion techniques have many pitfalls and are affected by both conceptual issues and measurement errors that can result in overestimation of the core infarct.[38] There is debate as to the need for perfusion imaging in the selection of patients with acute ischemic stroke.[39] Several trials on the endovascular treatment of stroke due to large-vessel occlusion did not use perfusion imaging for patient selection in the early time window and showed large treatment benefit in this population.[40] In a recent multicenter observational cohort of 1530 patients, there was no difference in outcomes based on modality of imaging selection between CT and CT perfusion imaging.[41]

MRI

CT-based studies remain the primary imaging modalities for initial evaluation of most patients worldwide presenting with symptoms of acute stroke.[42] However, MRI offers some advantages over CT in the evaluation of these patients, and its use as a primary modality has increased in the United States over the past 2 decades.[43] MRI is more sensitive and specific than CT for the detection of acute ischemia and is better at identifying stroke mimics, including infectious, inflammatory, tumoral, and traumatic conditions.[44,45]

Diffusion-Weighted Imaging

Using diffusion-weighted imaging (DWI), MRI can identify cerebral ischemia as early as a few minutes after the stroke onset.[46] The sensitivity of MRI to detect

TABLE 3-1 **Parameters of Perfusion Imaging Used to Differentiate Normal, Ischemic, and Infarcted Brain Regions**

	Cerebral blood flow	Cerebral blood volume	Mean transit time
Normal tissue	Symmetric to contralateral side	Symmetric to contralateral side	Symmetric to contralateral side
Ischemic penumbra	Mildly decreased	Normal or mildly increased	Mildly increased
Infarct core	Markedly decreased	Mildly decreased	Markedly increased

Copyright © American Academy of Neurology. Unauthorized reproduction of this article is prohibited.

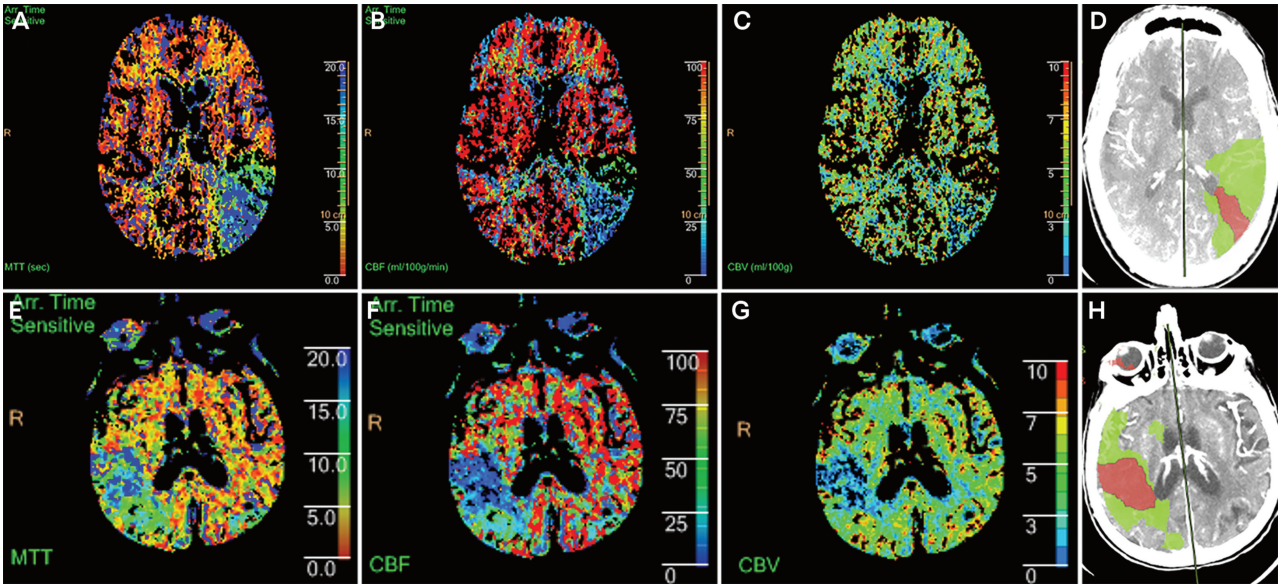

FIGURE 3-8

CT perfusion imaging in acute ischemic stroke. *A-D,* Images from a single CT perfusion study. An abnormality is seen in the left parietal lobe with prolonged mean transit time *(A, blue area)* and decreased cerebral blood flow *(B, blue area)*. Cerebral blood volume is decreased centrally but preserved in the periphery of the lesion (*C*). This pattern is consistent with an area of core infarction surrounded by ischemic penumbra. The perfusion map illustrates the infarcted tissue (*D*, *red area*) with a large area of potentially salvageable tissue (*D*, *green area*) with timely reperfusion. *E-H,* Images from a CT perfusion study of a different patient. An abnormality in the right hemisphere demonstrates prolonged mean transit time (*E, blue area*) and decreased cerebral blood flow (*F, blue area*). Most of this area also has decreased cerebral blood volume (*G, blue area*). The perfusion map shows a large core infarct (*H*, *red area*) with a relatively small surrounding ischemic penumbra (*green area*).

ischemic lesions is about 92% when performed at the time of symptom presentation, much higher than that of CT. This sensitivity can increase up to 97.5% if perfusion imaging is included.[47] DWI is also more accurate than noncontrast CT in determining the core infarct, which usually represents the irreversibly infarcted tissue.[48] Determining the core infarct is of critical importance in the assessment of potential risk and benefit of reperfusion treatment, especially for those with unknown time of stroke onset or those presenting beyond 6 hours from symptom onset.[19]

Acute ischemic lesions typically demonstrate a high signal intensity on DWI, which results from the alteration of the brownian movement of water protons due to cytotoxic edema in the early phases of acute ischemic stroke. DWI images should always be interpreted in conjunction with the apparent diffusion coefficient (ADC), a quantitative measure of the water protons' diffusion. In true restricted diffusion seen in acute ischemic stroke, the region of increased DWI signal will demonstrate low signal intensity on the ADC sequence (DWI is bright, ADC is dark). An example of this is shown in FIGURE 3-9. In contrast, when a high signal on DWI is associated with high signal intensity on ADC imaging (DWI is bright, ADC is bright), it is T2 shine-through. T2 shine-through occurs when there is increased water content in tissue (as in vasogenic edema or cystic lesions) and is not consistent with acute ischemia. In ischemic lesions, the decreased signal intensity on ADC appears earlier than the increased signal intensity on

Copyright © American Academy of Neurology. Unauthorized reproduction of this article is prohibited.

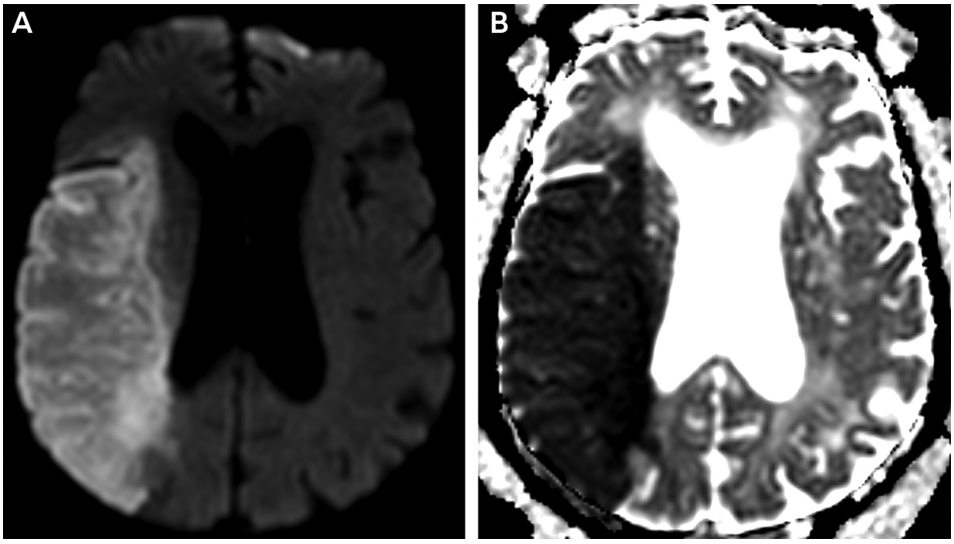

FIGURE 3-9
Imaging markers of acute ischemic stroke on MRI. *A*, Diffusion-weighted imaging (DWI) with high signal intensity in the region of the right middle cerebral artery. *B*, This same region also has low signal intensity on the apparent diffusion coefficient (ADC) sequence. The result is an imaging pattern that is "bright" on DWI and "dark" on ADC, consistent with true restricted diffusion.

DWI and therefore is more sensitive in detecting stroke.[49] The decreased signal intensity on ADC imaging usually persists for 1 week after stroke onset. Therefore, a dark ADC map means that the stroke is less than 1 week old.[49] A pseudonormalization of the ADC map from low to high signal intensity occurs 1 to 2 weeks after stroke onset.[49]

Although DWI is considered the most sensitive sequence to detect ischemic lesions, a small percentage (6.8%) of patients with true acute ischemic stroke have a negative DWI scan.[50] DWI-negative stroke is most frequently seen in patients with small, posterior-circulation, or hyperacute strokes.[50] It is important to be aware of the possibility of DWI-negative stroke and not exclude patients from reperfusion therapies or other stroke workup based on a negative DWI scan. The possibility of false-negative DWI decreases considerably after 3 hours. Repeat DWI is recommended in patients for whom stroke is strongly clinically suspected and with initial negative DWI that was performed within 2 hours of symptom onset.[51] In addition, if there is clinical suspicion of posterior fossa ischemia and negative initial DWI, repeat MRI with coronal DWI acquisition through the posterior fossa is recommended to increase sensitivity.[51,52]

T2-Weighted and Fluid-Attenuated Inversion Recovery Sequences

Another MRI finding in ischemic stroke is increased signal intensity on T2-weighted and fluid-attenuated inversion recovery (FLAIR) sequences. Although increased DWI signal intensity appears within the first few hours of stroke because of cytotoxic edema, increased signal intensity on the T2-weighted and FLAIR sequences is delayed and results from the increased concentration of water in the interstitial spaces (interstitial edema). Previous studies have indicated that FLAIR does not show signal changes within the first 4.5 hours.[53,54] This mismatch between DWI and FLAIR sequences (positive

Copyright © American Academy of Neurology. Unauthorized reproduction of this article is prohibited.

DWI, negative FLAIR) has been used to estimate the stroke onset and therefore select patients who may benefit from IV tPA. This is particularly useful in patients who awake with neurologic deficits or patients with unknown last known well times.[53,55] Specifically, patients with acute ischemic stroke of unknown onset who received IV tPA based on a DWI-FLAIR mismatch had significantly better functional outcomes than those who did not receive IV tPA in this setting.[53] An example of this MRI-based tPA decision making is shown in CASE 3-2.

Additional markers of ischemia on FLAIR sequences include loss of the gray-white matter differentiation with gyral swelling and sulcal effacement. Pseudonormalization of signal intensity on T2-weighted images, known as "fogging," may occur 1 to 4 weeks after stroke, with a peak around 2 to 3 weeks. Fogging occurs as a result of infiltration of the infarcted tissue by inflammatory cells.[49] The FLAIR sequence is also useful in detecting subarachnoid hemorrhage, a contraindication to thrombolytic therapy.[56]

Susceptibility-Weighted Sequences

Susceptibility-weighted or gradient recalled echo (GRE) sequences are routinely used in MRI of patients with acute stroke. These sequences are very sensitive for detecting blood products that may not be detected on other MRI sequences or even by CT. Blood products and other ferromagnetic compounds (eg, minerals, calcifications) cause distortion of the local magnetic field, resulting in loss of the MRI signal (hypointensity) with an area of blooming.[57] With the use of these sequences, MRI is as accurate as CT for the detection of hyperacute hemorrhage.[58] In addition, MRI may be more accurate than CT for the detection of hemosiderin deposits of chronic intracerebral hemorrhage, which are usually undetected by CT.[58] This ability to detect hemorrhage with high sensitivity is important for centers using rapid MRI as first-line neuroimaging in patients presenting with symptoms of acute stroke.

Vessel and Clot Imaging

On T2-weighted sequences, patent arteries with normally flowing blood usually appear dark, a finding known as a "flow void." Therefore, lack of flow due to a vessel occlusion or thrombosis, slow flow due to stenosis, or retrograde collateral flow manifests as a lack of the normal flow void and results in increased signal intensity of the involved vessels on T2-weighted sequences. This arterial hyperintensity, best seen on FLAIR images, is called the "hyperintense vessel sign" and may be the only sign of early infarction.[56] Additionally, acute intraarterial thrombus produces susceptibility artifact and blooming on GRE or susceptibility-weighted images and is strongly suggestive of large-vessel occlusion, akin to the hyperdense vessel sign on noncontrast CT. These MRI findings of acute infarction are shown in FIGURE 3-11.

The hyperdense vessel sign on noncontrast CT and the susceptibility artifact or "blooming sign" on MRI reflect the high red blood cell content of the occlusive thrombus. Absence of this sign in a patient with large-vessel occlusion may indicate a fibrin-predominant thrombus. This differentiation has clinical implications, as fibrin-rich thrombi represent a potential target for pharmacologic fibrinolysis, whereas red blood cell–rich thrombi may have a better response to stent retriever versus contact aspiration during endovascular treatment.[59,60]

KEY POINTS

- CT perfusion uses three parameters to assess a given brain region: cerebral blood flow, cerebral blood volume, and mean transit time. Postprocessing software creates maps based on these measures to approximate the size and location of the infarct core and the ischemic penumbra.
- MRI is more sensitive and specific than CT for the identification of acute stroke and can detect ischemia as early as a few minutes after stroke onset.
- In true restricted diffusion seen in acute ischemic stroke, a region of increased diffusion-weighted imaging signal correlates with a region of low signal intensity on the apparent diffusion coefficient image.
- Diffusion-weighted imaging–negative stroke is rare and most frequently seen in patients with small, posterior-circulation, or hyperacute strokes. Repeat diffusion-weighted imaging is recommended if there is a strong clinical suspicion of ischemia.
- Diffusion-weighted imaging positivity appears within the first few minutes after stroke onset, whereas fluid-attenuated inversion recovery (FLAIR) signal changes take longer to develop. This mismatch has been used to estimate stroke onset and select patients for thrombolysis.

Copyright © American Academy of Neurology. Unauthorized reproduction of this article is prohibited.

CASE 3-2

A 67-year-old man with a medical history of hypertension, hyperlipidemia, diabetes, and prior strokes presented with right-sided weakness and slurred speech. He was in his usual state of health when he went to sleep the previous night at 10:00 PM, and he noticed these symptoms when he awoke in the morning at 8:00 AM. The initial National Institutes of Health Stroke Scale score was 8. He had an immediate noncontrast CT that showed neither acute hemorrhage nor territorial infarction and a CTA that demonstrated patent intracerebral vessels. Subsequent MRI revealed a small area of restricted diffusion in the left corona radiata without an associated T2/fluid-attenuated inversion recovery (FLAIR) signal abnormality (FIGURE 3-10). As a result, IV tissue plasminogen activator was administered, and he was admitted to the neurocritical care unit for post–tissue plasminogen activator monitoring.

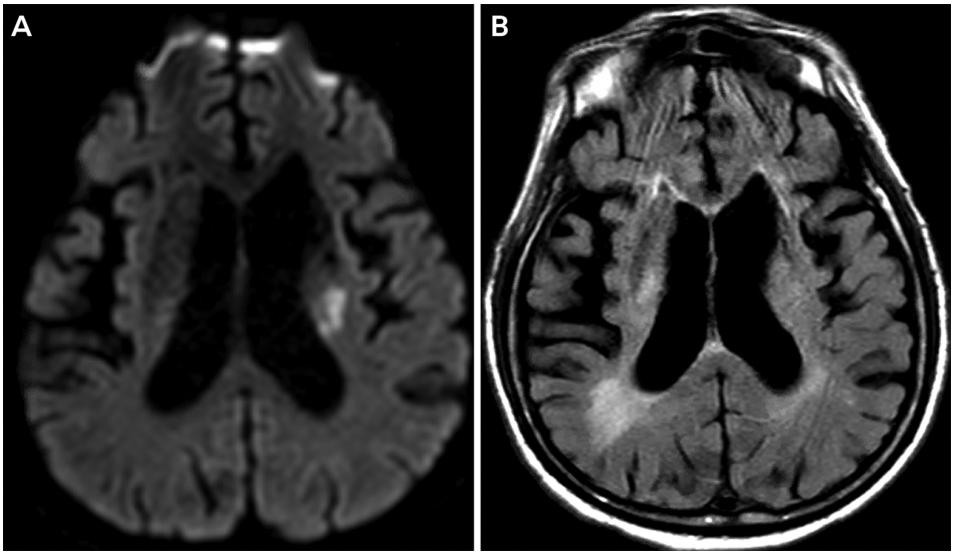

FIGURE 3-10
Imaging of the patient in CASE 3-2. Axial MRI images show a small area of restricted diffusion in the left corona radiata (*A*) without an associated fluid-attenuated inversion recovery (FLAIR) signal abnormality (*B*).

COMMENT

This case is an example of MRI-based decision making for acute stroke with unknown last known well time. The diffusion-weighted imaging–FLAIR mismatch described is consistent with infarction less than 4.5 hours old and can therefore be used to approximate the time of stroke onset. This approach is supported by the WAKE-UP (Efficacy and Safety of MRI-based Thrombolysis in Wake-up Stroke) study and the American Heart Association/American Stroke Association guidelines.

Copyright © American Academy of Neurology. Unauthorized reproduction of this article is prohibited.

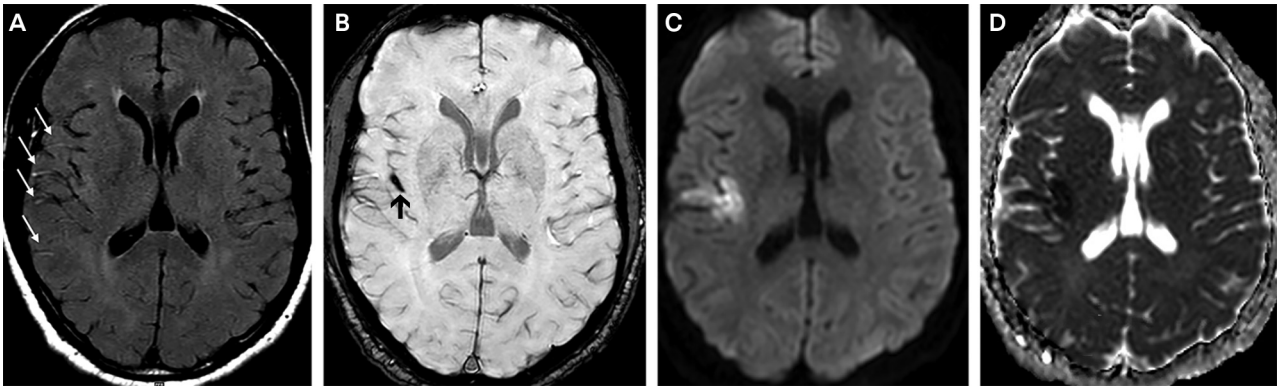

FIGURE 3-11

Axial MRI findings in acute ischemic stroke. *A*, Hyperintense vessel signs (*arrows*) are seen on a fluid-attenuated inversion recovery (FLAIR) sequence as a result of slow or retrograde flow. *B*, The susceptibility or "blooming sign" (*arrow*) is seen on a susceptibility-weighted sequence as a result of high red blood cell content in an acute occlusive thrombus in an M2 branch of the right middle cerebral artery. Diffusion-weighted imaging (DWI) sequence (*C*) shows high signal intensity while the apparent diffusion coefficient (ADC) sequence (*D*) demonstrates low signal intensity, a pattern consistent with acute ischemic stroke.

MR Angiography

MRA is an essential component of the acute stroke MRI protocol. It helps in determining the location and extent of vascular lesions of the head and neck such as acute occlusion, atherosclerotic disease, dissection, or fibromuscular dysplasia. One disadvantage of noncontrast MRA is the difficulty in distinguishing between stenosis and acute occlusion, as slow or turbulent flow can result in intravoxel phase dispersion, which leads to signal loss and subsequent overestimation of arterial stenosis that may appear as an occlusion on MRA.[61]

MR Perfusion Imaging

Analogous to CT perfusion, MR perfusion imaging uses serial consecutive imaging after contrast injection to quantify blood flow and the blood volume through the brain parenchyma. As previously mentioned, the area of restricted diffusion on DWI represents the core infarct. Therefore, the mismatch between the perfusion and diffusion abnormality represents the potentially salvageable ischemic tissue at risk for infarction.[62]

Limitations of MRI in Acute Stroke

Despite the advantages of MRI for evaluating patients with acute stroke, it has several limitations compared with CT. MRI scanners are more expensive and less widely available than CT scanners. In addition, MRI has more contraindications and requires screening patients for ferromagnetic objects that pose safety concerns in the MRI environment. MRI takes longer to perform than CT because of the multiple sequences required. Moreover, MRI may not be feasible in patients with a diminished level of consciousness, vomiting, agitation, hemodynamic compromise, or hypoxia.[63]

On a more technical level, a caveat of DWI in estimating the core infarct is the possibility of DWI reversibility. DWI reversibility refers to partial or complete reversal of the initial DWI signal abnormality when compared with follow-up DWI or FLAIR imaging. Given this finding, it is possible that DWI may

Copyright © American Academy of Neurology. Unauthorized reproduction of this article is prohibited.

overestimate the nonreversible ischemic core in the early hours of stroke.[64] Partial DWI reversibility has been reported to occur in 26.5% of cases in DWI-based studies.[65] Total DWI reversibility is rare and is estimated to occur in about 0.8% of cases.[64]

DIGITAL SUBTRACTION ANGIOGRAPHY

DSA remains the gold standard modality to evaluate most cerebrovascular diseases. It can accurately determine the type and location of vascular lesions as well as the flow characteristics and collateral circulation in the setting of vascular occlusion or stenosis.

In patients with acute ischemic stroke, DSA is used to confirm and treat stroke due to large-vessel occlusion. After endovascular treatment of a large-vessel occlusion, the degree of resultant reperfusion is radiographically assessed. The modified Thrombolysis in Cerebral Infarction (mTICI) scale is the most commonly used scoring system to describe the degree of reperfusion achieved and has value in predicting outcomes.[66,67] A detailed description and examples of each mTICI score are shown in FIGURE 3-12.[68] An mTICI score of 2b, 2c, or 3 is considered adequate reperfusion and a successful thrombectomy.

DSA is also useful as an aid to determine the etiology of a large-vessel occlusion, which can be due to thromboembolism or intracranial atherosclerotic disease.[69] Knowing the occlusion type is important, as large-vessel occlusion due to intracranial atherosclerotic disease requires specific endovascular modalities to achieve successful recanalization[70] as well as appropriate secondary stroke prevention. Findings suggestive of large-vessel occlusion due to intracranial atherosclerotic disease include residual stenosis after thrombectomy, truncal-type occlusion (an arterial occlusion found at the middle of an artery with visible distal major branches and bifurcation site beyond occlusion), robust collateral circulation, and microcatheter first-pass effect (blood flow through the occlusion after the withdrawal of the microcatheter).[71] DSA also provides

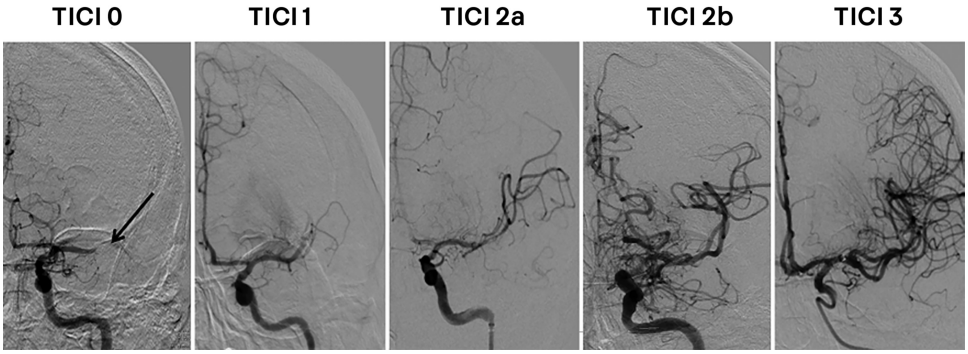

FIGURE 3-12

Modified Thrombolysis in Cerebral Infarction (mTICI) scoring system in relation to a left M1 occlusion. A score of TICI 0 indicates no reperfusion beyond the site of occlusion (*arrow*). TICI 1 indicates recanalization beyond the initial occlusion, but with minimal reperfusion of the distal territories. TICI 2a corresponds to recanalization with less than 50% reperfusion of the distal territories. TICI 2b reflects greater than 50% reperfusion of the distal territories. A score of TICI 2c (*not shown*) is sometimes used when near complete reperfusion except for a small number of distal cortical vessels occurs. A score of TICI 3 indicates complete total reperfusion of the entire territory distal to the occlusion.

Reprinted from Mokin M, et al, Neurosurg Focus.[68] © 2014 American Association of Neurological Surgeons.

Copyright © American Academy of Neurology. Unauthorized reproduction of this article is prohibited.

valuable information about the collateral circulation that is important to maintain perfusion downstream from arterial occlusions and determine the pace of infarct evolution.[72] In tandem occlusions or in the setting of a nonopacified carotid artery on CTA, DSA can accurately distinguish true cervical internal carotid artery occlusion from pseudo-occlusion secondary to distal thrombosis that impedes ascending blood flow.[73]

CONCLUSION

There are multiple acceptable imaging approaches when evaluating a patient with symptoms of acute ischemic stroke. Given its wide availability, speed, and safety, CT-based imaging is the first step in the vast majority of centers. Noncontrast head CT alone is sufficient for IV thrombolysis decision making in the appropriate clinical context. CTA is extremely sensitive for detection of large-vessel occlusion and is a critical step for patients presenting with clinical symptoms consistent with this syndrome. Advanced imaging including multiphase CTA, CTP, MRI, or MR perfusion can provide additional information useful for therapeutic decision making in specific clinical scenarios described above. In all cases, it is paramount that neuroimaging be performed and accurately interpreted as quickly as possible to allow for timely reperfusion therapy for all who are eligible.

KEY POINTS

- **Acute intraarterial thrombus produces susceptibility artifact and blooming on gradient recalled echo or susceptibility-weighted MRI. This finding is similar to the "hyperdense vessel sign" seen on noncontrast CT and is strongly suggestive of large-vessel occlusion.**
- **The modified Thrombolysis in Cerebral Infarction scale is used to describe the degree of reperfusion achieved after mechanical thrombectomy. A score of 2b, 2c, or 3 is considered successful reperfusion.**

REFERENCES

1 Grotta JC, Yamal JM, Parker SA, et al. Prospective, Multicenter, Controlled Trial of Mobile Stroke Units. N Engl J Med 2021;385(11): 971-981. doi:10.1056/NEJMoa2103879

2 Demchuk AM, Hill MD, Barber PA, et al. Importance of early ischemic computed tomography changes using ASPECTS in NINDS rtPA Stroke Study. Stroke 2005;36(10):2110-2115. doi:10.1161/01.STR.0000181116.15426.58

3 Wardlaw JM, Mielke O. Early signs of brain infarction at CT: observer reliability and outcome after thrombolytic treatment–systematic review. Radiology 2005;235(2):444-453. doi:10.1148/radiol.2352040262

4 Marks MP, Holmgren EB, Fox AJ, et al. Evaluation of early computed tomographic findings in acute ischemic stroke. Stroke 1999;30(2):389-392. doi:10.1161/01.str.30.2.389

5 Hill MD, Buchan AM. Canadian Alteplase for Stroke Effectiveness Study (CASES) Investigators. Thrombolysis for acute ischemic stroke: results of the Canadian Alteplase for Stroke Effectiveness Study. CMAJ 2005;172(10): 1307-1312. doi:10.1503/cmaj.1041561

6 Patel SC, Levine SR, Tilley BC, et al. Lack of clinical significance of early ischemic changes on computed tomography in acute stroke. JAMA 2001;286(22):2830-2838. doi:10.1001/jama.286.22.2830

7 Barber PA, Demchuk AM, Zhang J, Buchan AM. Validity and reliability of a quantitative computed tomography score in predicting outcome of hyperacute stroke before thrombolytic therapy. ASPECTS Study Group Alberta Stroke Programme Early CT Score 2000;355(9216):1670-1674. doi:10.1016/s0140-6736(00)02237-6

8 Coutts SB, Lev MH, Eliasziw M, et al. ASPECTS on CTA source images versus unenhanced CT: added value in predicting final infarct extent and clinical outcome. Stroke 2004;35(11):2472-2476. doi:10.1161/01.STR.0000145330.14928.2a

9 Parsons MW, Pepper EM, Chan V, et al. Perfusion computed tomography: prediction of final infarct extent and stroke outcome. Ann Neurol 2005;58(5):672-679. doi:10.1002/ana.20638

10 Berkhemer OA, Fransen PSS, Beumer D, et al. A randomized trial of intraarterial treatment for acute ischemic stroke. N Engl J Med 2015;372(1): 11-20. doi:10.1056/NEJMoa1411587

11 Goyal M, Demchuk AM, Menon BK, et al. Randomized assessment of rapid endovascular treatment of ischemic stroke. N Engl J Med 2015; 372(11):1019-1030. doi:10.1056/NEJMoa1414905

12 Jovin TG, Chamorro A, Cobo E, et al. Thrombectomy within 8 hours after symptom onset in ischemic stroke. N Engl J Med 2015; 372(24):2296-2306. doi:10.1056/NEJMoa1503780

Copyright © American Academy of Neurology. Unauthorized reproduction of this article is prohibited.

13 Saver JL, Goyal M, Bonafe A, et al. Stent-retriever thrombectomy after intravenous t-PA vs. t-PA alone in stroke. N Engl J Med 2015;372(24): 2285-2295. doi:10.1056/NEJMoa1415061

14 Campbell BCV, Mitchell PJ, Kleinig TJ, et al. Endovascular therapy for ischemic stroke with perfusion-imaging selection. N Engl J Med 2015; 372(11):1009-1018. doi:10.1056/NEJMoa1414792

15 Powers WJ, Rabinstein AA, Ackerson T, et al. Guidelines for the Early Management of Patients With Acute Ischemic Stroke. In: Update to the 2018 Guidelines for the Early Management of Acute Ischemic Stroke: A Guideline for Healthcare Professionals From the American Heart Association/American Stroke Association. Stroke 2019;50(12):e344-e418. doi:10.1161/STR.0000000000000211

16 Yoshimura S, Sakai N, Yamagami H, et al. Endovascular Therapy for Acute Stroke with a Large Ischemic Region. N Engl J Med 2022; 386(14):1303-1313. doi:10.1056/NEJMoa2118191

17 Kaesmacher J, Chaloulos-Iakovidis P, Panos L, et al. Mechanical Thrombectomy in Ischemic Stroke Patients With Alberta Stroke Program Early Computed Tomography Score 0-5. Stroke 2019;50(4):880-888. doi:10.1161/STROKEAHA.118.023465

18 Turc G, Bhogal P, Fischer U, et al. European Stroke Organisation (ESO) - European Society for Minimally Invasive Neurological Therapy (ESMINT) Guidelines on Mechanical Thrombectomy in Acute Ischaemic StrokeEndorsed by Stroke Alliance for Europe (SAFE). Eur Stroke J 2019;4(1):6-12. doi:10.1177/2396987319832140

19 Nogueira RG, Jadhav AP, Haussen DC, et al. Thrombectomy 6 to 24 hours after stroke with a mismatch between deficit and infarct. N Engl J Med 2018;378(1):11-21. doi:10.1056/NEJMoa1706442

20 Albers GW, Marks MP, Kemp S, et al. Thrombectomy for stroke at 6 to 16 hours with selection by perfusion imaging. N Engl J Med 2018;378(8):708-718. doi:10.1056/NEJMoa1713973

21 Nannoni S, Ricciardi F, Strambo D, et al. Correlation between ASPECTS and core volume on CT perfusion: impact of time since stroke onset and presence of large-vessel occlusion. AJNR Am J Neuroradiol 2021;42(3):422-428. doi:10.3174/ajnr.A6959

22 Haussen DC, Dehkharghani S, Rangaraju S, et al. Automated CT perfusion ischemic core volume and noncontrast CT ASPECTS (Alberta Stroke Program Early CT Score): correlation and clinical outcome prediction in large vessel stroke. Stroke 2016;47(9):2318-2322. doi:10.1161/STROKEAHA.116.014117

23 Puetz V, Sylaja PN, Coutts SB, et al. Extent of hypoattenuation on CT angiography source images predicts functional outcome in patients with basilar artery occlusion. Stroke 2008;39(9): 2485-2490. doi:10.1161/STROKEAHA.107.511162

24 Puetz V, Khomenko A, Hill MD, et al. Extent of hypoattenuation on CT angiography source images in basilar artery occlusion: prognostic value in the Basilar Artery International Cooperation Study. Stroke 2011;42(12):3454-3459. doi:10.1161/STROKEAHA.111.622175

25 Schuierer G, Huk W. The unilateral hyperdense middle cerebral artery: an early CT-sign of embolism or thrombosis. Neuroradiology 1988; 30(2):120-122. doi:10.1007/BF00395612

26 Leys D, Pruvo JP, Godefroy O, Rondepierre P, Leclerc X. Prevalence and significance of hyperdense middle cerebral artery in acute stroke. Stroke 1992;23(3):317-324. doi:10.1161/01.str.23.3.317

27 Raman SS. ACR-NASCI-SIR-SPR Practice Parameter for the Performance and Interpretation of Body Computed Tomography Angiography (CTA). Internet Published online 2021. acr.org/-/media/acr/files/practice-parameters/body-cta.pdf

28 Krol AL, Dzialowski I, Roy J, et al. Incidence of radiocontrast nephropathy in patients undergoing acute stroke computed tomography angiography. Stroke 2007;38(8):2364-2366. doi:10.1161/STROKEAHA.107.482778

29 Lima FO, Lev MH, Levy RA, et al. Functional contrast-enhanced CT for evaluation of acute ischemic stroke does not increase the risk of contrast-induced nephropathy. AJNR Am J Neuroradiol 2010;31(5):817-821. doi:10.3174/ajnr.A1927

30 Saver JL, Goyal M, Lugt A, et al. Time to treatment with endovascular thrombectomy and outcomes from ischemic stroke: a meta-analysis. JAMA 2016;316(12):1279-1288. doi:10.1001/jama.2016.13647

31 Lev MH, Farkas J, Rodriguez VR, et al. CT angiography in the rapid triage of patients with hyperacute stroke to intraarterial thrombolysis: accuracy in the detection of large vessel thrombus. J Comput Assist Tomogr 2001;25(4): 520-528. doi:10.1097/00004728-200107000-00003

32 Bash S, Villablanca JP, Jahan R, et al. Intracranial vascular stenosis and occlusive disease: evaluation with CT angiography, MR angiography, and digital subtraction angiography. AJNR Am J Neuroradiol 2005;26(5):1012-1021.

33 Dundamadappa S, Iyer K, Agrawal A, Choi DJ. Multiphase CT angiography: a useful technique in acute stroke imaging-collaterals and beyond. AJNR Am J Neuroradiol 2021;42(2):221-227. doi:10.3174/ajnr.A6889

34 García-Tornel A, Carvalho V, Boned S, et al. Improving the evaluation of collateral circulation by multiphase computed tomography angiography in acute stroke patients treated with endovascular reperfusion therapies. Interv Neurol 2016;5(3-4):209-217. doi:10.1159/000448525

Copyright © American Academy of Neurology. Unauthorized reproduction of this article is prohibited.

35 Menon BK, d'Esterre CD, Qazi EM, et al. Multiphase CT angiography: a new tool for the imaging triage of patients with acute ischemic stroke. Radiology 2015;275(2):510-520. doi:10.1148/radiol.15142256

36 Allmendinger AM, Tang ER, Lui YW, Spektor V. Imaging of stroke: part 1, perfusion CT—overview of imaging technique, interpretation pearls, and common pitfalls. AJR Am J Roentgenol 2012; 198(1):52-62. doi:10.2214/AJR.10.7255

37 Vagal A, Aviv R, Sucharew H, et al. Collateral clock is more important than time clock for tissue fate. Stroke 2018;49(9):2102-2107. doi:10.1161/STROKEAHA.118.021484

38 Goyal M, Menon BK, Derdeyn CP. Perfusion imaging in acute ischemic stroke: let us improve the science before changing clinical practice. Radiology 2013;266(1):16-21. doi:10.1148/radiol.12112134

39 Nogueira RG, Haussen DC, Liebeskind D, et al. Stroke imaging selection modality and endovascular therapy outcomes in the early and extended time windows. Stroke 2021;52(2): 491-497. doi:10.1161/STROKEAHA.120.031685

40 Campbell BCV, Majoie CBLM, Albers GW, et al. Penumbral imaging and functional outcome in patients with anterior circulation ischaemic stroke treated with endovascular thrombectomy versus medical therapy: a meta-analysis of individual patient-level data. Lancet Neurol 2019; 18(1):46-55. doi:10.1016/S1474-4422(18)30314-4

41 Nguyen TN, Abdalkader M, Nagel S, et al. Noncontrast computed tomography vs computed tomography perfusion or magnetic resonance imaging selection in late presentation of stroke with large-vessel occlusion. JAMA Neurol 2022;79(1):22-31. doi:10.1001/jamaneurol.2021.4082

42 Potter CA, Vagal AS, Goyal M, Nunez DB, Leslie-Mazwi TM, Lev MH. CT for treatment selection in acute ischemic stroke: a code stroke primer. RadioGraphics 2019;39(6):1717-1738. doi:10.1148/rg.2019190142

43 Burke JF, Kerber KA, Iwashyna TJ, Morgenstern LB. Wide variation and rising utilization of stroke magnetic resonance imaging: data from 11 states. Ann Neurol 2012;71(2):179-185. doi:10.1002/ana.22698

44 Abdalkader M, Xie J, Cervantes-Arslanian A, Takahashi C, Mian AZ. Imaging of intracranial infections. Semin Neurol 2019;39(3):322-333. doi:10.1055/s-0039-1693161

45 Sung EK, Farris C, Abdalkader M, Mian A. Acute neurologic syndromes beyond stroke: the role of emergent mr imaging. Neuroimaging Clin N Am 2018;28(3):375-395. doi:10.1016/j.nic.2018.03.012

46 Matsumoto K, Lo EH, Pierce AR, Wei H, Garrido L, Kowall NW. Role of vasogenic edema and tissue cavitation in ischemic evolution on diffusion-weighted imaging: comparison with multiparameter MR and immunohistochemistry. AJNR Am J Neuroradiol 1995;16(5):1107-1115.

47 Simonsen CZ, Madsen MH, Schmitz ML, Mikkelsen IK, Fisher M, Andersen G. Sensitivity of diffusion- and perfusion-weighted imaging for diagnosing acute ischemic stroke is 97.5%. Stroke 2015;46(1):98-101. doi:10.1161/STROKEAHA.114.007107

48 Campbell BC, Purushotham A, Christensen S, et al. The infarct core is well represented by the acute diffusion lesion: sustained reversal is infrequent. J Cereb Blood Flow Metab 2012;32(1): 50-56. doi:10.1038/jcbfm.2011.102

49 Allen LM, Hasso AN, Handwerker J, Farid H. Sequence-specific MR imaging findings that are useful in dating ischemic stroke. Radiographics 2012;32(5):1297-1299. doi:10.1148/rg.325115760

50 Edlow BL, Hurwitz S, Edlow JA. Diagnosis of DWI-negative acute ischemic stroke: a meta-analysis. Neurology 2017;89(3):256-262. doi:10.1212/WNL.0000000000004120

51 Shono K, Satomi J, Tada Y, et al. Optimal timing of diffusion-weighted imaging to avoid false-negative findings in patients with transient ischemic attack. Stroke 2017;48(7):1990-1992. doi:10.1161/STROKEAHA.117.014576

52 Felfeli P, Wenz H, Al-Zghloul M, Groden C, Förster A. Combination of standard axial and thin-section coronal diffusion-weighted imaging facilitates the diagnosis of brainstem infarction. Brain Behav 2017;7(4):e00666. doi:10.1002/brb3.666

53 Thomalla G, Simonsen CZ, Boutitie F, et al. MRI-guided thrombolysis for stroke with unknown time of onset. N Engl J Med 2018;379(7):611-622. doi:10.1056/NEJMoa1804355

54 Cho AH, Sohn SI, Han MK, et al. Safety and efficacy of MRI-based thrombolysis in unclear-onset stroke. A preliminary report. Cerebrovasc Dis 2008;25(6):572-579. doi:10.1159/000132204

55 Emeriau S, Serre I, Toubas O, Pombourcq F, Oppenheim C, Pierot L. Can diffusion-weighted imaging-fluid-attenuated inversion recovery mismatch (positive diffusion-weighted imaging/negative fluid-attenuated inversion recovery) at 3 Tesla identify patients with stroke at <4.5 hours? Stroke 2013;44(6):1647-1651. doi:10.1161/STROKEAHA.113.001001

56 Makkat S, Vandevenne JE, Verswijvel G, et al. Signs of acute stroke seen on fluid-attenuated inversion recovery MR imaging. AJR Am J Roentgenol 2002;179(1):237-243. doi:10.2214/ajr.179.1.1790237

57 Halefoglu AM, Yousem DM. Susceptibility weighted imaging: clinical applications and future directions. World J Radiol 2018;10(4):30-45. doi:10.4329/wjr.v10.i4.30

58 Kidwell CS, Chalela JA, Saver JL, et al. Comparison of MRI and CT for detection of acute intracerebral hemorrhage. JAMA 2004; 292(15):1823-1830. doi:10.1001/jama.292.15.1823

Copyright © American Academy of Neurology. Unauthorized reproduction of this article is prohibited.

59 Liebeskind DS, Sanossian N, Yong WH, et al. CT and MRI early vessel signs reflect clot composition in acute stroke. Stroke 2011;42(5): 1237-1243. doi:10.1161/STROKEAHA.110.605576

60 Mohammaden MH, Haussen DC, Camara C, et al. Hyperdense vessel sign as a potential guide for the choice of stent retriever versus contact aspiration as first-line thrombectomy strategy. J Neurointerv Surg 2021;13(7):599-604. doi:10.1136/neurintsurg-2020-016005

61 Anderson CM, Saloner D, Lee RE, et al. Assessment of carotid artery stenosis by MR angiography: comparison with x-ray angiography and color-coded Doppler ultrasound. AJNR Am J Neuroradiol 1992;13(3):1005-1008.

62 Petrella JR, Provenzale JM. MR perfusion imaging of the brain: techniques and applications. AJR Am J Roentgenol 2000;175(1):207-219. doi:10.2214/ajr.175.1.1750207

63 Singer OC, Sitzer M, du Mesnil de Rochemont R, Neumann-Haefelin T. Practical limitations of acute stroke MRI due to patient-related problems. Neurology 2004;62(10):1848-1849. doi:10.1212/01.wnl.0000125320.53244.fa

64 Nagaraja N. Diffusion weighted imaging in acute ischemic stroke: a review of its interpretation pitfalls and advanced diffusion imaging application. J Neurol Sci 2021;425(117435). doi:10.1016/j.jns.2021.117435

65 Kranz PG, Eastwood JD. Does diffusion-weighted imaging represent the ischemic core? An evidence-based systematic review. AJNR Am J Neuroradiol 2009;30(6):1206-1212. doi:10.3174/ajnr.A1547

66 Yoo AJ, Simonsen CZ, Prabhakaran S, et al. Refining angiographic biomarkers of revascularization: improving outcome prediction after intra-arterial therapy. Stroke 2013;44(9): 2509-2512. doi:10.1161/STROKEAHA.113.001990

67 Marks MP, Lansberg MG, Mlynash M, et al. Correlation of AOL recanalization, TIMI reperfusion and TICI reperfusion with infarct growth and clinical outcome. J Neurointerv Surg 2014;6(10):724-728. doi:10.1136/neurintsurg-2013-010973

68 Mokin M, Khalessi A, Mocco J, et al. Endovascular treatment of acute ischemic stroke: the end or just the beginning? Neurosurgical focus 2014; 36(1). doi:10.3171/2013.10.FOCUS13374

69 Baek JH, Kim BM. Angiographical identification of intracranial, atherosclerosis-related, large vessel occlusion in endovascular treatment. Front Neurol 2019;10(298). doi:10.3389/fneur.2019.00298

70 Yi TY, Chen WH, Wu YM, et al. Special endovascular treatment for acute large artery occlusion resulting from atherosclerotic disease. World Neurosurg 2017;103:65-72. doi:10.1016/j.wneu.2017.03.108

71 Li H, Liu P, Liu P, et al. Current knowledge of large vascular occlusion due to intracranial atherosclerosis: focusing on early diagnosis. Chin Neurosurg J 2020;6(32). doi:10.1186/s41016-020-00213-1

72 Liebeskind DS, Cotsonis GA, Saver JL, et al. Collateral circulation in symptomatic intracranial atherosclerosis. J Cereb Blood Flow Metab 2011; 31(5):1293-1301. doi:10.1038/jcbfm.2010.224

73 Diouf A, Fahed R, Gaha M, et al. Cervical internal carotid occlusion versus pseudo-occlusion at CT angiography in the context of acute stroke: an accuracy, interobserver, and intraobserver agreement study. Radiology 2018;286(3): 1008-1015. doi:10.1148/radiol.2017170681

Copyright © American Academy of Neurology. Unauthorized reproduction of this article is prohibited.

Imaging of Central Nervous System Hemorrhage

By Ryan Hakimi, DO, MS, NVS, RPNI, CPB, FNCS, FCCM

REVIEW ARTICLE

CONTINUUM AUDIO INTERVIEW AVAILABLE ONLINE

ABSTRACT

OBJECTIVE: **This article aims to familiarize the reader with the various types of nontraumatic central nervous system (CNS) hemorrhage and the various neuroimaging modalities used to help diagnose and manage them.**

LATEST DEVELOPMENTS: **According to the 2019 Global Burden of Diseases, Injuries, and Risk Factors Study, intraparenchymal hemorrhage accounts for 28% of the global stroke burden. In the United States, hemorrhagic stroke makes up 13% of all strokes. The incidence of intraparenchymal hemorrhage increases substantially with age; thus, despite improvements in blood pressure control through various public health measures, the incidence is not decreasing as the population ages. In fact, in the most recent longitudinal study of aging, autopsy findings showed intraparenchymal hemorrhage and cerebral amyloid angiopathy in 30% to 35% of patients.**

ESSENTIAL POINTS: **Rapid identification of CNS hemorrhage, which includes intraparenchymal hemorrhage, intraventricular hemorrhage, and subarachnoid hemorrhage, requires either head CT or brain MRI. Once hemorrhage is identified on the screening neuroimaging study, the pattern of blood in conjunction with the history and physical examination can guide subsequent neuroimaging, laboratory, and ancillary tests as part of the etiologic assessment. After determination of the cause, the chief aims of the treatment regimen are reducing hemorrhage expansion and preventing subsequent complications such as cytotoxic cerebral edema, brain compression, and obstructive hydrocephalus. In addition, nontraumatic spinal cord hemorrhage will also be briefly discussed.**

INTRODUCTION

This article reviews nontraumatic sources of hemorrhage noted on neuroimaging studies. For the purposes of this review, central nervous system (CNS) hemorrhage includes both intracranial hemorrhage and spinal hemorrhage. *Intracranial hemorrhage* is subdivided into spontaneous intraparenchymal hemorrhage, aneurysmal subarachnoid hemorrhage (SAH), and intraventricular hemorrhage (IVH). Traumatic causes of CNS hemorrhage are outside the scope of this article. The initial evaluation of a patient with an acute or subacute neurologic change

CITE AS:
CONTINUUM (MINNEAP MINN) 2023;29(1, NEUROIMAGING): 73–103.

Address correspondence to Dr Ryan Hakimi, 200 Patewood Dr, Ste B350, Greenville, SC 29615, Ryan.Hakimi@prismahealth.org.

RELATIONSHIP DISCLOSURE:
Dr Hakimi has received personal compensation in the range of $0 to $499 for serving as a delegate in the American Medical Association House of Delegates for the American Society of Neuroimaging and in the range of $500 to $4999 for serving as the immediate past president for the South Carolina Osteopathic Medical Society and as a medical reviewer for the Office of Disciplinary Counsel in the South Carolina Department of Labor, Licensing and Regulation and has received publishing royalties from Osler, Hoskin & Harcourt LLP.
Dr Hakimi has a noncompensated relationship as an annual meeting course committee member with the Neurocritical Care Society that is relevant to AAN interests or activities.

UNLABELED USE OF PRODUCTS/INVESTIGATIONAL USE DISCLOSURE:
Dr Hakimi reports no disclosure.

© 2023 American Academy of Neurology.

Copyright © American Academy of Neurology. Unauthorized reproduction of this article is prohibited.

usually begins with a noncontrast head CT or brain MRI. Common clinical presentations include new onset severe headache, focal neurologic findings, depressed level of consciousness, or combinations of all three. This initial screening test can determine whether hemorrhage is a contributor to the change in the patient's neurologic status. Although in the United States only 13% of strokes are hemorrhagic, neuroimaging is the only practical method of making this diagnosis.[1] Once hemorrhage is identified on the screening neuroimaging study, the pattern of blood in conjunction with the history and physical examination can guide subsequent neuroimaging, laboratory, and ancillary tests as part of the etiologic assessment. After determination of the cause, the chief aims of the treatment regimen are reducing hemorrhage expansion and preventing subsequent complications such as cytotoxic cerebral edema, brain compression, and obstructive hydrocephalus.

NEUROIMAGING TO IDENTIFY CNS HEMORRHAGE

The incidence of intracranial hemorrhage is increasing globally, primarily because of an increasing prevalence of hypertension; a secondary cause is the increasing use of antiplatelet agents and anticoagulants.[2] Noncontrast head CT is typically the first screening modality used in cases of acute neurologic change. This modality is available at nearly all acute care hospitals and because of its short scanning time is feasible in unstable patients, those with claustrophobia, and those with implanted hardware.

Acute hemorrhage appears hyperdense on noncontrast head CT. Over time, however (typically in about 1 week), this hyperdensity decreases, and the lesion becomes isodense with the brain parenchyma, ultimately leading to encephalomalacia and a hypodense cavity. Not only does noncontrast head CT identify the location of the lesion, but it also allows for the identification of IVH (if present) and demonstrates the extent of cerebral edema and brain compression, which is important for communication among care teams and ultimately affects treatment and prognosis. Communication about CNS hemorrhage noted on head CT should include the type, location, acuity (acute or chronic), volume of the lesion, presence or absence of IVH, and extent of cerebral edema and brain compression.

Limitations of Head CT With CNS Hemorrhage

It is important to understand the limitations of head CT and CT angiography (CTA) in the imaging of CNS hemorrhage. First, beam-hardening artifact limits the ability to identify hemorrhage in the posterior fossa because of x-ray scatter as the beam of radiation traverses the thick petrous and occipital bones. In addition, what makes an acute hemorrhage hyperdense on head CT is the iron within the hemoglobin molecule. Therefore, if a patient is anemic, the presence of CNS hemorrhage may be overlooked. Furthermore, in cases in which the patient's hemoglobin is elevated, such as with polycythemia or hemoconcentration due to dehydration, the patient's vasculature can appear hyperdense, limiting the ability to identify a hemorrhage adjacent to the vessels.

Limitations of Head CT Angiography With CNS Hemorrhage

Head CTA may be performed in the setting of intracranial hemorrhage to identify potentially causative vascular lesions. Head CTA requires an IV injection of iodinated contrast. One must exclude prior IV iodinated contrast reactions,

Copyright © American Academy of Neurology. Unauthorized reproduction of this article is prohibited.

especially anaphylaxis, by reviewing the electronic medical record and querying the patient to ensure patient safety. In addition, individuals who have an iodine food allergy are at an increased risk for an adverse reaction to IV iodinated contrast. A 20-gauge or larger IV line in the forearm or more proximally is necessary. Moreover, ensuring that the contrast bolus is properly timed requires some understanding of the patient's cardiac function to ensure that the images are captured at the appropriate time. Finally, although it occurs infrequently, iodinated IV contrast places patients at risk for acute kidney injury, especially those who have an elevated serum creatinine level at baseline.[3] This risk can be mitigated by contemporaneous IV fluid hydration. In patients who are dependent on dialysis, it is important to determine whether they are oliguric or anuric at baseline. Oliguric dialysis-dependent patients have some intrinsic renal function, which may be permanently lost with the administration of IV iodinated contrast, leading to anuric dialysis dependence. In this group, one could consider forgoing the head CTA when the pretest probability of an underlying vascular lesion is low based on the pattern of blood and instead repeat the noncontrast head CT 3 to 6 hours after the index study. However, patients who have anuric renal failure lack any intrinsic renal function and therefore are not subject to any further renal dysfunction as a result of exposure to IV iodinated contrast. Therefore, the only additional caution needed in patients with anuric renal failure is in the coordination of care to ensure that the patient's dialysis schedule will not be interrupted and to determine whether they need to be converted from hemodialysis to continuous renal replacement therapy.

Use and Limitations of Brain MRI in CNS Hemorrhage

Compared with head CT, brain MRI has greater sensitivity for the detection of CNS hemorrhage, as it distinguishes between acute and chronic hemorrhages, the latter of which are noted as hypointensities on two-dimensional gradient recalled echo (GRE) T2*-weighted imaging and susceptibility-weighted imaging ([SWI] or three-dimensional GRE imaging).[4,5] TABLE 4-1 summarizes the evolution of hemorrhage appearance on CT and MRI.[6] In addition, brain MRI can identify concomitant ischemic stroke, which may be relevant in cases of hemorrhagic transformation of an acute ischemic stroke. Moreover, brain MRI is superior to CT in imaging of the posterior fossa contents, as it is not subject to artifacts such as beam hardening that can obscure visualization of those structures.

The primary limitations of brain MRI center on logistic limitations and patient-specific characteristics. Logistic limitations include higher cost and the inability to obtain the scan in a timely fashion. Patient-specific limitations include large body habitus, the presence of MR-unsafe or MR-conditional devices or ferromagnetic foreign objects, claustrophobia, the duration of the procedure in patients with critical illness who may develop hemodynamic instability, and the inability to lie flat and still for the duration of the procedure without respiratory compromise, as motion degrades image quality.

Digital Subtraction Angiography

Conventional cerebral angiography or digital subtraction angiography (DSA) is the gold standard in the investigation of SAH due to a suspected underlying vascular lesion. It involves placing a vascular sheath introducer in the femoral artery or, less often, in the radial or brachial artery. Then, a catheter is advanced to the artery of interest while the patient undergoes imaging with continuous

KEY POINTS

- Intracranial hemorrhage may be subdivided into spontaneous intraparenchymal hemorrhage, aneurysmal subarachnoid hemorrhage, and intraventricular hemorrhage.
- The pattern of hemorrhage in conjunction with the history and physical examination can guide subsequent neuroimaging, laboratory, and ancillary tests as part of the etiologic assessment.
- Communication about central nervous system hemorrhage noted on head CT should include the type, location, acuity (acute or chronic), volume of the lesion, presence or absence of intraventricular hemorrhage, and extent of cerebral edema and brain compression.
- Compared with head CT, brain MRI has greater sensitivity for the detection of central nervous system hemorrhage, as it identifies both acute and chronic hemorrhages, which are noted as hypointensities on two-dimensional gradient recalled echo (GRE) T2*-weighted imaging and susceptibility-weighted imaging (SWI), or three-dimensional GRE imaging.

Copyright © American Academy of Neurology. Unauthorized reproduction of this article is prohibited.

fluoroscopy. Contrast is then injected into the catheter while images are obtained using time-controlled x-rays. The images are then subtracted from a precontrast image, revealing only the vascular imaging, hence the term *digital subtraction angiography*.

This modality offers 99% sensitivity and specificity in identifying underlying vascular lesions in cases of CNS hemorrhage. However, because of its invasive nature, the procedure comes with a risk of complications including vessel dissection, vessel perforation, contrast allergic reaction, contrast-induced nephropathy, and sheath site hematoma, which occur in 1% to 2% of patients while also exposing the patient to radiation.[7] Due to these risks, CTA and MR angiography have largely replaced DSA as screening tests for vascular causes of CNS hemorrhage.[8] DSA is usually only available at tertiary and quaternary care centers.

Transcranial Doppler Ultrasonography and Transcranial Color-Coded Duplex

Transcranial Doppler ultrasonography (TCD) allows for the noninvasive assessment of cerebral hemodynamics, detection of cerebral artery vasospasm, and noninvasive monitoring of the treatment effects of therapies for vasospasm and cytotoxic cerebral edema.[9] Unlike other imaging modalities, TCD is portable and can be brought to the patient's bedside for rapid assessment. Moreover, it can be performed in austere environments. TCD displays spectral waveforms that correlate the depth, direction, and intensity of the cerebral blood flow through the intracranial vasculature. The instrument measures the peak systolic

TABLE 4-1 **Appearance of Intracerebral Hemorrhage on Noncontrast CT and MRI by Stages[a]**

Stage	Phase of blood	Noncontrast CT	T1-weighted MRI	T2-weighted MRI	T2*-weighted MRI
Hyperacute	Oxyhemoglobin	Smooth, hyperdense	Hypointense or isointense	Hyperintense	Marked hypointensity
Acute (12-48 hours)	Deoxyhemoglobin	Hyperdense with fluid levels	Isointensity or slight hypointensity with thin hyperintense rim in the periphery	Hypointense with hyperintense perilesional rim	Marked hypointensity
Early subacute (72 hours)	Methemoglobin intracellular	Hypodense region of edema with mass effect	Hyperintensity	Hypointensity	Hypointensity
Late subacute (3-20 days)	Methemoglobin extracellular	Less prominent with ringlike profile	Hyperintensity	Hyperintensity	Hypointensity
Chronic (9 weeks)	Hemosiderin and ferritin	Isodense or modest confined hypodensity	Hypointensity	Hypointensity	Hyperintense or isointense core surrounded by hypointense rim

CT = computed tomography; MRI = magnetic resonance imaging.
[a] Reprinted with permission from Macellari F, et al, Stroke.[6] © 2014 American Heart Association, Inc.

Copyright © American Academy of Neurology. Unauthorized reproduction of this article is prohibited.

velocity and end-diastolic velocities of blood flow in the large intracranial vessels, allowing for calculation of the mean flow velocity, which has the highest correlation with vasospasm in patients with aneurysmal SAH. In addition, it allows for the calculation of the pulsatility index, defined as peak systolic velocity minus end-diastolic velocity divided by mean flow velocity.

Detection of vasospasm is essential when treating patients with aneurysmal SAH, as vasospasm leading to delayed cerebral ischemia is a leading cause of death and disability in these patients. TCD can predict symptomatic vasospasm and has high sensitivity, specificity, and positive and negative predictive values.[10-14] The American Heart Association (AHA)/American Stroke Association (ASA), the American Academy of Neurology (AAN), and the Neurocritical Care Society all endorse the use of TCD in the care of patients with aneurysmal SAH. The use of TCD for such patients carries a Class IIA/Level B evidence designation from the AHA/ASA. The AAN and Neurocritical Care Society have designated the use of TCD in aneurysmal SAH as moderate-quality evidence/strong recommendation.

In a meta-analysis of 2870 patients, Kumar and colleagues[15] pooled 17 studies and reviewed the use of TCD for aneurysmal SAH. They reported TCD evidence of vasospasm to be highly predictive of delayed cerebral ischemia, with a sensitivity of 90%, specificity of 71%, positive predictive value of 57%, and negative predictive value of 92%. It is important to note that the aim of TCD is to capitalize on its high sensitivity and high negative predictive value to screen patients with aneurysmal SAH for vasospasm before the emergence of clinical manifestations, allowing for additional confirmatory diagnostic studies or therapies to be undertaken.[16,17]

Moreover, serial TCD examinations allow one to monitor the treatment effects of therapies for vasospasm, such as induced hypertension or intraarterial calcium channel antagonists. In addition, serial trending of the pulsatility index values can serve as a surrogate for monitoring the effects of intracranial pressure mitigation strategies such as hyperosmolar therapy or adjustment of the patient's external ventricular drain settings.[18] Perhaps most important of all is the fact that TCD informs the clinician of when to de-escalate therapies because of its high sensitivity in detecting vasospasm, thereby reducing morbidity associated with unnecessary induced hypertension or unnecessary neurointerventional procedures.

Transcranial color-coded duplex differs from TCD in that it adds a structural imaging component to the study. Transcranial color-coded duplex usually involves the purchase of an add-on package to the standard ultrasound cart used for peripheral vascular imaging or body ultrasound. Thus, the machines are much less portable and substantially more expensive than standard TCD. However, because of the ability to see the vessels of interest, it takes less technical skill and experience to use transcranial color-coded duplex compared with TCD. The structural imaging does, however, allow for serial monitoring of intraparenchymal hematomas or subdural hematomas, which is not possible with TCD.

From a practical standpoint, in the United States, The Joint Commission and Det Norske Veritas Healthcare require the availability of TCD at all comprehensive stroke centers.[19,20] However, the use of the modality, frequency of assessments, credentials of performing technologists, and credentials of the interpreting physicians are not prescribed, adding to the heterogeneity of

KEY POINTS

- **Digital subtraction angiography offers 99% sensitivity and specificity in identifying underlying vascular lesions in cases of central nervous system hemorrhage.**
- **Transcranial Doppler ultrasonography can predict symptomatic vasospasm and has high sensitivity, specificity, and positive and negative predictive values.**

Copyright © American Academy of Neurology. Unauthorized reproduction of this article is prohibited.

experiences by treating providers and limiting its benefits. To ensure optimal diagnostic assessment and treatment decisions using TCD, the 13 sponsoring organizations of the Intersocietal Accreditation Commission Standards and Guidelines, which include the AAN, recommend that every TCD laboratory in the United States be accredited by the Intersocietal Accreditation Commission, every TCD technologist be certified in TCD by holding the neurovascular specialist credential from the American Society of Neuroimaging or equivalent, and every interpreting physician be certified in TCD by being a registered physician in neurovascular interpretation by the American Society of Neuroimaging or equivalent.[9,21]

Standard Treatment After Identification of CNS Hemorrhage

Certain treatments are applicable to all types of CNS hemorrhage. As with any neurologic emergency, management begins with addressing the airway, breathing, and circulation. Thereafter, the first intervention usually involves the treatment of hypertension using short-acting, titratable calcium channel antagonists. Second is the correction of an anticoagulant-induced coagulopathy if present. The final step is the implementation of procedures, when applicable, that are targeted at mitigating the extent of the brain injury.

Guidance for Additional Neuroimaging

The pattern of blood noted on the initial brain imaging study often guides subsequent neuroimaging. In the case of intraparenchymal hemorrhage, repeat head CT may be needed to reassess the extent of cerebral edema and brain compression. In addition, head CTA with or without venography is recommended in patients without hypertension who are younger than 70 years old and present with a lobar intraparenchymal hemorrhage, as one in seven to one in four patients will have an underlying vascular etiology.[22] A similar investigation should be undertaken in patients with a deep or posterior fossa intraparenchymal hemorrhage who are 45 to 70 years old or in patients younger than 45 years old without a history of hypertension who present with an intraparenchymal hemorrhage in any location of the brain.[22,23] In select patients in the aforementioned cohorts who have marginal renal function, DSA may be considered in place of head CTA when searching for an underlying vascular lesion, as DSA usually uses 7 mL to 10 mL of IV iodinated contrast per vessel, whereas head CTA uses 50 mL to 100 mL of IV iodinated contrast. In such patients with a spontaneous intraparenchymal hemorrhage without an underlying etiology in whom DSA is performed and found to be negative, repeat DSA in 3 to 6 months should be considered, as intraparenchymal hemorrhage secondary to a treatable underlying vascular lesion such as an aneurysm, arteriovenous malformation (AVM), or dural arteriovenous fistula can be seen in approximately 15% of cases.[22,24,25]

The presence of spontaneous SAH necessitates additional vascular neuroimaging beginning with head and neck CTA. In those who have an aneurysmal pattern of SAH, DSA and TCD should also be pursued, as identification of an aneurysmal cause changes the prognosis, with higher rates of delayed cerebral ischemia and obstructive hydrocephalus, while portending a poorer neurologic outcome.[26] In cases with concomitant intraparenchymal hemorrhage and IVH, serial head CT is used to evaluate for developing obstructive hydrocephalus. When IVH is noted in isolation, DSA and brain MRI are warranted.

Copyright © American Academy of Neurology. Unauthorized reproduction of this article is prohibited.

DISEASE-SPECIFIC IMAGING CONSIDERATIONS

Once CNS hemorrhage is identified on the initial neuroimaging study, the subsequent appropriate neuroimaging algorithm can vary by type of CNS hemorrhage. The various types of CNS hemorrhage and the associated neuroimaging studies as part of the etiologic assessment are described in the following sections.

Spontaneous Intraparenchymal Hemorrhage

Intraparenchymal hemorrhage is by far the most common type of intracranial hemorrhage.[27] Intraparenchymal hemorrhage can be divided into primary intraparenchymal hemorrhage and secondary intraparenchymal hemorrhage. Primary intraparenchymal hemorrhage is most commonly due to arteriosclerosis, which is synonymous with lipohyalinosis, defined as vascular wall thickening due to hyaline deposition. It is usually associated with hypertension, diabetes, and advanced age.[28] Years of uncontrolled hypertension with or without diabetes may lead to arterial rupture and leaking of blood into the parenchymal tissue.[27] Primary intraparenchymal hemorrhage most commonly affects the lenticulostriate branches off of the middle cerebral arteries, the thalamic perforators off of the posterior cerebral arteries or posterior communicating arteries, or the perforating arteries off of the basilar artery. Because of the variability in the location of these hemorrhages, as shown in FIGURE 4-1,[29,30] patients can present with a variety of neurologic findings.

CALCULATING HEMORRHAGE VOLUME. When describing hemorrhage size, it is best to calculate the hemorrhage volume as opposed to simply indicating the largest

KEY POINTS

- **Head CT angiography with or without venography is recommended in patients without hypertension who are less than 70 years old and present with a lobar intraparenchymal hemorrhage, as one in seven to one in four patients will have an underlying vascular etiology.**
- **When intraventricular hemorrhage is noted in isolation, digital subtraction angiography and brain MRI are warranted.**
- **Primary intraparenchymal hemorrhage is most commonly due to arteriosclerosis.**

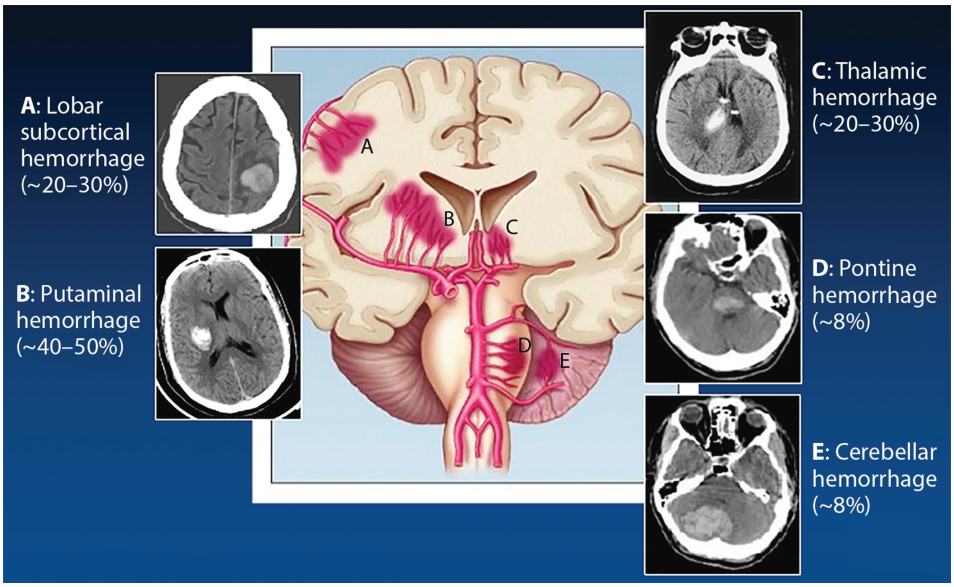

FIGURE 4-1

Common sites of spontaneous intraparenchymal hemorrhage secondary to chronic hypertension.

Reprinted with permission from Qureshi AI, et al, N Engl J Med. © 2001 Massachusetts Medical Society.[29] Complete image reprinted from Alberts M, Stroke Belt Consortium. © 2006 National Stroke Association.[30]

Copyright © American Academy of Neurology. Unauthorized reproduction of this article is prohibited.

dimensions. The hemorrhage volume is easily calculated using the ABC/2 method.[31] Given that most CT imaging is now stored on a picture archiving and communication system, one can begin by scrolling through the axial images and identifying the slice in which the hemorrhage size is maximal. Next, the diameter of the longest axis is measured (in centimeters) using the caliper function, and that distance is labeled A. Then, the diameter of the widest axis of the hemorrhage is marked such that it is perpendicular to line A, and this distance is measured (in centimeters) and labeled B. Finally, one scrolls through the images with special attention to the hemorrhagic lesion, measuring the vertical extent of the hemorrhage in centimeters (labeled C). To calculate the hemorrhage volume in milliliters, the product of A, B, and C is computed and divided by 2, as shown in FIGURE 4-2. However, the typical slice thickness of an axial head CT is 0.5 cm. Therefore, for simplicity, when standard 0.5-cm slice thickness has been confirmed, the volume of the CNS hemorrhage can be calculated by multiplying A, B, and C and dividing by 4. Thereafter, repeat head CT in conscious patients with static neurologic examinations can be performed 6 hours and 24 hours after the index scan to document the final hematoma volume.[28]

CASE 4-1 describes a typical presentation of a patient with intraparenchymal hemorrhage caused by a lobar hemorrhage.

CT ANGIOGRAPHY SPOT SIGN. One-third of patients with intraparenchymal hemorrhage will have hemorrhage expansion within 3 hours of the index scan. In fact, one study indicated that 26% of patients had hemorrhage expansion on repeat imaging within 1 hour of the index scan.[32] Performing head CTA immediately after the noncontrast head CT can allow for rapid identification of this high-risk cohort when the spot sign is noted.[33-37] The spot sign is the presence of contrast within the hemorrhage, which is usually more hyperdense than the

FIGURE 4-2
Calculating the intracranial hemorrhage volume (in milliliters).
Reprinted from Albert M, Stroke Belt Consortium.[30] © 2006 National Stroke Association.

Copyright © American Academy of Neurology. Unauthorized reproduction of this article is prohibited.

background hemorrhage and suggests active bleeding. This finding often precedes the patient's neurologic deterioration and thus will change the patient's disposition, frequently leading to the transfer of the patient to a comprehensive stroke center or planned admission to the neurocritical care unit as opposed to a stroke unit or an intermediate care unit. Furthermore, head CTA can identify underlying vascular lesions such as an AVM, which can change subsequent management. Lastly, obtaining the head CTA immediately after the noncontrast head CT, while the patient is still in the scanner, limits patient transport, which improves patient safety and prevents treatment delays.

CALCULATION OF THE INTRACEREBRAL HEMORRHAGE SCORE. Once an intraparenchymal hemorrhage is identified and its associated volume is calculated, it is best to calculate the Intracerebral Hemorrhage (ICH) Score, which is used as a standard communication tool for describing the patient's clinical condition as well as to document the patient's extent of illness for purposes of quality assurance and mortality risk stratification. The ICH Score, as shown in TABLE 4-2,[38] takes into account the patient's initial Glasgow Coma Scale score, the hematoma volume (in milliliters), the presence or absence of IVH, the presence or absence of infratentorial hemorrhage, and the patient's age. The calculated score of 0 to 6 correlates in part with the patient's 30-day mortality, although newer data have called into question the previously reported increasing risk of death with each integral increase in the ICH Score. The 2022 AHA/ASA guidelines for patients with intraparenchymal hemorrhage recommend that the ICH Score not be used in isolation as the basis for limiting life-sustaining measures.[28] The ICH Score is also used by regulatory bodies such as The Joint Commission and Det Norske Veritas Healthcare to track the care and outcomes of patients with intraparenchymal hemorrhage, necessitating its documentation within 6 hours of admission or before any neurosurgical intervention.[19,20] Pragmatically, compliance can be ensured by having a field in the admission order set within the electronic health record that mandates that the provider document the ICH Score within the admission orders before submitting them.

It is important to identify potential secondary causes of intraparenchymal hemorrhage. Cerebral amyloid angiopathy (CAA) is the most common secondary cause of intraparenchymal hemorrhage. CAA is caused by β-amyloid deposition in the capillary and arteriolar walls of the leptomeninges as well as the cerebral and cerebellar cortices. These patients usually are older, have cognitive decline, may have apolipoprotein E genotypes containing the ε-4 or ε-2 alleles, and have distinct characteristics on neuroimaging studies.[28] Noncontrast head CT typically demonstrates acute cortico-subcortical hemorrhage located near the gray-white junction, as in CASE 4-2. Less commonly, patients will present with multiple simultaneous acute hemorrhage types (in the absence of trauma or coagulopathy) such as an acute intraparenchymal hemorrhage and subdural hematoma. However, brain MRI is most revealing, with cortical microhemorrhages and superficial siderosis noted on SWI or T2* sequences. Asymptomatic microhemorrhages of all types can be seen in more than 20% of individuals who are older than 60 years when using T2* sequences.[39,40]

Statistically, brainstem, subcortical gray matter, and cerebellar hemorrhages are less likely to be attributable to CAA[41] and were absent on

KEY POINTS

- Hemorrhage volume is calculated using the ABC/2 method.
- When using 0.5-cm slice thickness, the volume of the central nervous system hemorrhage is calculated by multiplying A, B, and C and dividing by 4.
- One-third of patients with intraparenchymal hemorrhage will have hemorrhage expansion within 3 hours of the index scan.
- Head CT angiography immediately after the noncontrast head CT can allow for quick identification of patients at high risk for rapid hemorrhage expansion when the spot sign is noted.
- The ICH Score is a standard communication tool for describing the patient's clinical condition and is used to document the patient's extent of illness for purposes of quality assurance and mortality risk stratification.
- The 2022 American Heart Association/American Stroke Association guidelines recommend that the ICH Score not be used in isolation as the basis for limiting life-sustaining measures.
- Cerebral amyloid angiopathy is the most common secondary cause of intraparenchymal hemorrhage.
- For diagnosing cerebral amyloid angiopathy, brain MRI is most revealing, with cortical microhemorrhages and superficial siderosis noted on SWI or T2* sequences.

Copyright © American Academy of Neurology. Unauthorized reproduction of this article is prohibited.

the patient's MRI in CASE 4-2. The Boston and modified Boston criteria, shown in TABLE 4-3,[42,43] have been validated using an MRI genetic correlation in individuals carrying CAA-specific, fully penetrant amyloid precursor protein mutations.[40,44,45]

Accurate diagnosis of CAA is particularly important. Often, risk-benefit assessments need to be undertaken when considering single or dual antiplatelet use or the need for anticoagulant use, because these individuals

CASE 4-1

A 58-year-old woman with uncontrolled hypertension and morbid obesity presented to the hospital after having a witnessed seizure characterized by right upper extremity tonic followed by clonic movements lasting 10 seconds. Thereafter, the patient was encephalopathic with right hemiparesis. The patient was noted to have a systolic blood pressure exceeding 220 mm Hg. Head CT revealed a large acute intraparenchymal hemorrhage centered in the posterior left frontal lobe with resultant brain compression and rightward subfalcine herniation (FIGURE 4-3A). Head CT angiography did not demonstrate an underlying vascular lesion or spot sign (FIGURE 4-3B). Because of the lobar nature of the hemorrhage, a brain MRI was performed, which did not show any other hemorrhages but did show intraventricular hemorrhage in the left greater than right lateral ventricle without hydrocephalus (FIGURES 4-3C and 4-3D). She was started on levetiracetam 750 mg 2 times a day for the prevention of subsequent seizures. Her hypertension was treated with IV nicardipine, with a transition over the course of several days to five oral antihypertensive medications. She was discharged to an inpatient rehabilitation hospital with a short course of levetiracetam with a plan for outpatient neurologic reassessment.

COMMENT

This case demonstrates the thorough neuroimaging evaluation needed when patients with hypertension present with an atypical hemorrhage pattern to ensure that the proper diagnosis is made and the appropriate treatment initiated.

Copyright © American Academy of Neurology. Unauthorized reproduction of this article is prohibited.

also have an increased risk for ischemic stroke.[46] Thus, appropriate neuroimaging investigation and diagnosis are critical in making treatment decisions in patients who may have CAA. One must also consider that the risk of recurrent hemorrhage is higher in patients with CNS hemorrhage with underlying CAA (7.39% per year) than in those with CNS hemorrhage due to non-CAA related causes (1.1% per year).[47] Sympathomimetics and underlying vascular abnormalities such as cavernous malformations, AVMs,

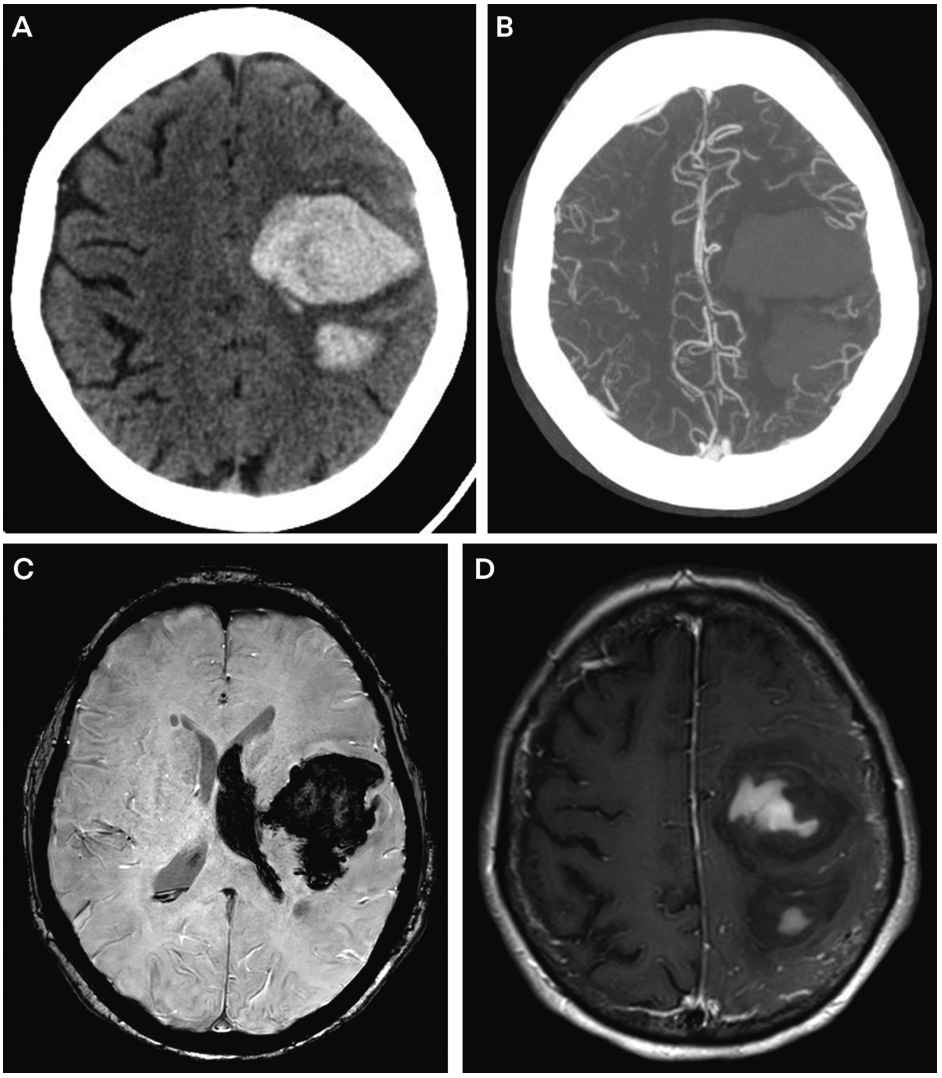

FIGURE 4-3

Imaging of the patient in CASE 4-1. *A,* Axial noncontrast head CT showing acute multilobulated lobar intraparenchymal hemorrhage with resultant brain compression. *B,* Axial head CT angiogram demonstrating absence of an underlying vascular lesion or spot sign. *C,* Axial susceptibility-weighted brain MRI demonstrating intraventricular extension of lobar intraparenchymal hemorrhage with absence of other microhemorrhages, supporting the diagnosis of a primary intracerebral hemorrhage. *D,* Axial contrast-enhanced T1-weighted brain MRI demonstrating acute to early subacute intraparenchymal hemorrhage with absence of an underlying structural lesion.

Copyright © American Academy of Neurology. Unauthorized reproduction of this article is prohibited.

cerebral artery aneurysms, fistulas (eg, carotid-cavernous and dural arteriovenous), and cerebral venous sinus thromboses are other secondary causes of intraparenchymal hemorrhage.

In one single-center observational study of 239 patients with intraparenchymal hemorrhage admitted to a neurointensive care unit where all patients had repeat head CT at 6, 24, and 48 hours, it was noted that 35% of patients required emergent neurosurgical interventions. Of those who required emergent neurosurgical interventions after admission, 54% of interventions were based on clinical examination changes, whereas 46% were triggered by neuroimaging findings on serial imaging.[48] Close neurologic monitoring in the neurocritical care unit is sufficient to guide subsequent medical decision-making, and routine repeat CT in the absence of any clinical change or concern is not considered necessary beyond 24 hours.

Certain other characteristics noted on head CT portend a higher risk of hemorrhage expansion. These include a heterogeneous hematoma density as

TABLE 4-2

Determination of the Intracerebral Hemorrhage Score[a]

Component	ICH score
Glasgow Coma Scale	
3-4	2
5-12	1
13-15	0
ICH volume (mL)	
≥30	1
<30	0
Intraventricular hemorrhage	
Yes	1
No	0
Infratentorial origin[b]	
Yes	1
No	0
Age, years	
≥80	1
<80	0
Total ICH Score	0-6

ICH = intracerebral hemorrhage.

[a] Reprinted with permission from Hemphill JC III, et al, Stroke.[38] © 2001 American Heart Association, Inc.

[b] Includes all interior cerebral areas below the undersurface of the temporal and occipital lobes extending to the upper cervical cord; includes the cerebellum.

Copyright © American Academy of Neurology. Unauthorized reproduction of this article is prohibited.

CASE 4-2

A 77-year-old woman with depression, obesity, and hyperlipidemia was brought to the hospital by emergency medical personnel after she was found on the floor at home by neighbors. The patient was noted to be awake but confused. Noncontrast head CT demonstrated an acute left frontal intraparenchymal hemorrhage with intraventricular extension and subfalcine herniation due to cerebral edema (FIGURE 4-4A). The patient was not hypertensive and was not taking any antithrombotic drugs. Head CT angiography did not reveal a spot sign (FIGURE 4-4B). Brain MRI was obtained, which revealed multifocal microhemorrhages without any evidence of brainstem or cerebellar hemorrhages, consistent with CAA (FIGURE 4-4C). The patient was ultimately discharged to the inpatient rehabilitation hospital.

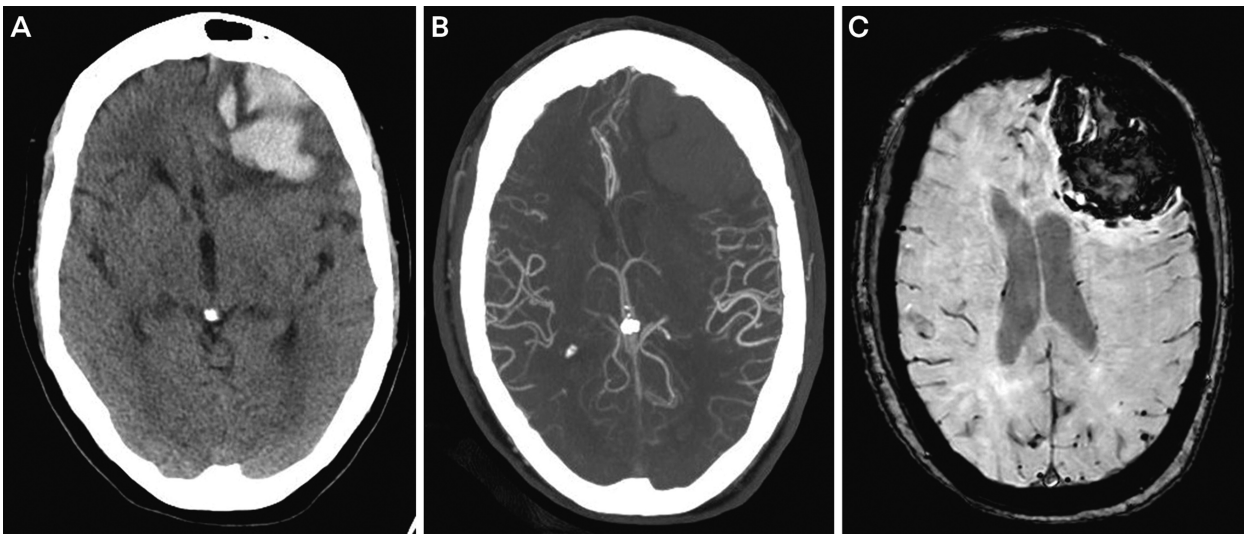

FIGURE 4-4
Imaging of the patient in CASE 4-2. *A,* Axial noncontrast head CT showing acute lobar intraparenchymal hemorrhage with resultant brain compression. *B,* Axial head CT angiogram showing intraparenchymal hemorrhage with absence of an underlying vascular lesion or spot sign. *C,* Axial susceptibility-weighted brain MRI demonstrating lobar intraparenchymal hemorrhage with microhemorrhages in the left greater than right parietooccipital lobe supporting the diagnosis of cerebral amyloid angiopathy.

COMMENT

Both the patient in this case and the patient in CASE 4-1 presented with a lobar hemorrhage. However, the ultimate diagnosis was different despite similar findings on initial diagnostic studies. Advanced neuroimaging was needed in both cases to ensure the proper diagnosis, which also affects the counseling of the patient (regarding hypertension management in CASE 4-1 and cognitive impairment in this case). It should be noted that although both patients presented with a spontaneous intraparenchymal hemorrhage, the patient in this case was not hypertensive at the time of presentation. When this is noted, the clinician should consider that arteriosclerosis, although statistically the most common cause of acute spontaneous intraparenchymal hemorrhage, is unlikely to be the cause.

Copyright © American Academy of Neurology. Unauthorized reproduction of this article is prohibited.

TABLE 4-3 **Boston and Modified Boston Criteria for Diagnosis of Cerebral Amyloid Angiopathy in Patients With Intracerebral Hemorrhage[a,b]**

	Classic Boston criteria	Modified Boston criteria
Definite CAA	Full postmortem examination demonstrating: Lobar, cortical, or cortico-subcortical hemorrhage[c] Severe CAA with vasculopathy Absence of other diagnostic lesion[d]	No modification compared with the classic Boston criteria
Probable CAA with supporting pathology	Clinical data and pathologic tissue (evacuated hematoma or cortical biopsy) demonstrating: Lobar, cortical, or cortico-subcortical hemorrhage[c] Some degree of CAA in specimen Absence of other diagnostic lesion[d]	No modification compared with the classic Boston criteria
Probable CAA	Clinical data and MRI or CT demonstrating: Multiple hemorrhages[c] restricted to lobar, cortical, or cortico-subcortical regions (cerebellar hemorrhage allowed) Age ≥55 years Absence of other cause of hemorrhage[d]	Clinical data and MRI or CT demonstrating: Multiple hemorrhages[c] restricted to lobar, cortical, or cortico-subcortical regions (cerebellar hemorrhage allowed) OR Single lobar, cortical, or cortico-subcortical hemorrhage and focal[e] or disseminated[f] superficial siderosis Age ≥55 years Absence of other cause of hemorrhage or superficial siderosis[d]
Possible CAA	Clinical data and MRI or CT demonstrating: Single lobar, cortical, or cortico-subcortical hemorrhage[c] Age ≥55 years Absence of other cause of hemorrhage[d]	Clinical data and MRI or CT demonstrating: Single lobar, cortical, or cortico-subcortical hemorrhage[c] and focal[e] or disseminated[f] superficial siderosis Age ≥55 years Absence of other cause of hemorrhage or superficial siderosis[d]

CAA = cerebral amyloid angiopathy; CT = computed tomography; MRI = magnetic resonance imaging.

[a] Adapted from Linn J, et al, Neurology. [42] © 2010 American Academy of Neurology.

[b] Reprinted with permission from Domingues R, et al, Neurol Clin.[43] © 2015 Elsevier Inc.

[c] The term *hemorrhage* referred, in the pathologic validation, to lobar intracerebral hemorrhage (ICH). However, some authors suggest that multiple lobar cerebral microbleeds, without lobar ICH, may be considered as probable cerebral amyloid angiopathy.

[d] Other causes of ICH that question the diagnosis of cerebral amyloid angiopathy are excessive warfarin dose (international normalized ratio [INR] higher than 3.0; INR 3.0 or lower or other nonspecific laboratory abnormalities are permitted for diagnosis of possible cerebral amyloid angiopathy), antecedent of head trauma or ischemic stroke, hemorrhagic transformation of an ischemic stroke, arteriovenous malformation, central nervous system tumor or vasculitis, blood dyscrasia, or coagulopathy.

[e] Siderosis restricted to three or fewer sulci.

[f] Siderosis affecting at least four sulci.

Copyright © American Academy of Neurology. Unauthorized reproduction of this article is prohibited.

well as irregularities at the perimeter of the hematoma border, sometimes referred to as a fluid level, a black hole, or a swirl, among other descriptors (FIGURE 4-5 [35]).[49]

Subarachnoid Hemorrhage

Nontraumatic SAH is most often due to a ruptured cerebral artery aneurysm. Other etiologies include AVM, fistulas, intracranial dissection, cerebral

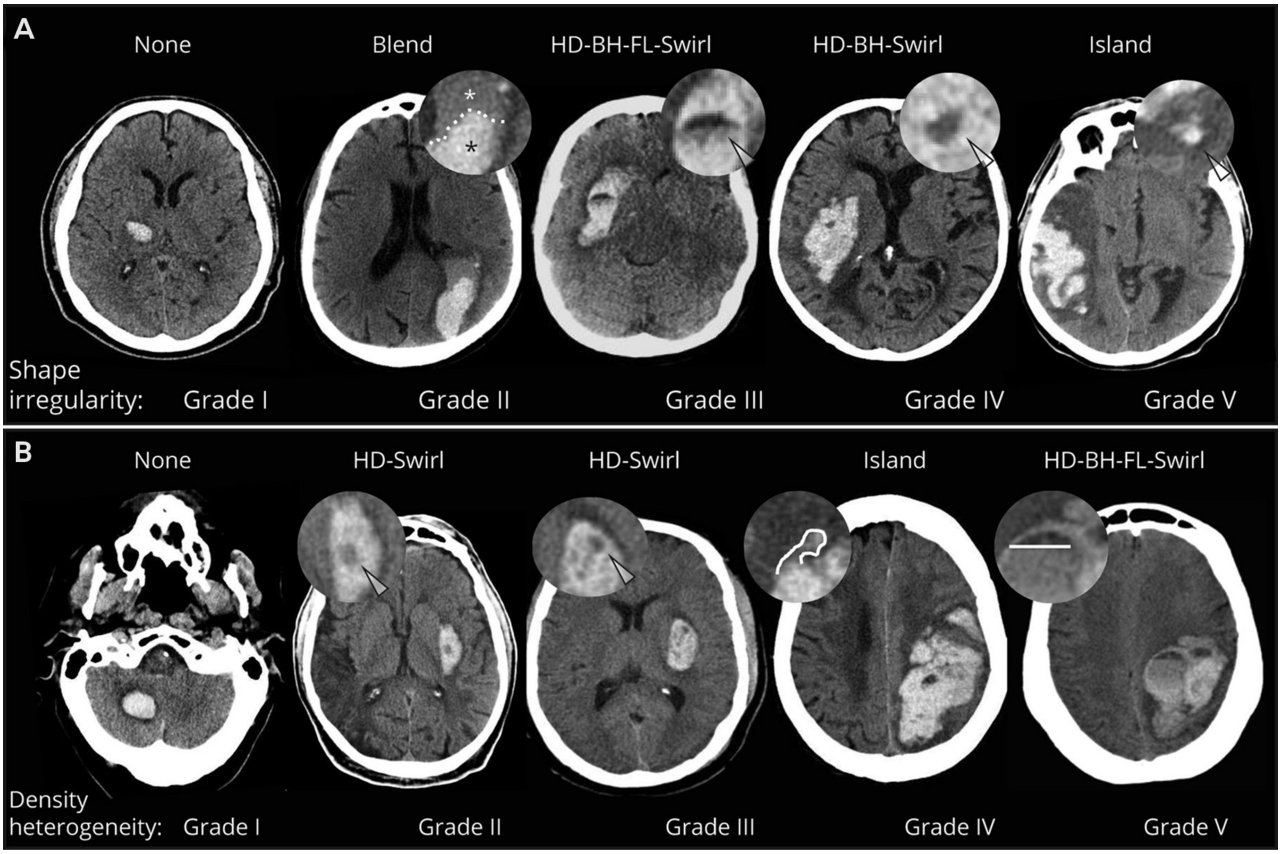

FIGURE 4-5

Definitions and illustrative examples of noncontrast CT markers of features predicting intraparenchymal hemorrhage expansion. *A*, Increasing shape irregularity. *B*, Increasing density heterogeneity. Detection of all noncontrast CT markers is based on visual inspection except black hole sign and blend sign that require additional density measures in Hounsfield units (HU). Irregular shape: ≥2 focal hematoma margin irregularities, in contact or disconnected from the hematoma edge. Island sign: ≥3 scattered small hematomas all separate from the main intracerebral hemorrhage (ICH) or ≥ 4 small hematomas, some or all of which may be connected with the ICH. Heterogeneous density: ≥3 foci of hypoattenuation, compared with the density of the main ICH. Swirl sign: area of hypoattenuation or isoattenuation (compared with brain parenchyma), connected or not with structures surrounding the ICH. Hypodensity (HD): any hypodense area encapsulated in the hemorrhage with any shape, size, and density. Fluid level (FL): hypoattenuating area (hypodense to the brain) above and hyperattenuating area (hyperdense to the brain) below a clear straight line of separation. Black hole sign (BH): hypodense region with a density difference > 28 HU compared with the surrounding ICH and not connected with structures outside the ICH. Blend sign: hypoattenuating area next to a hyperattenuating area of the ICH. Clear, sharp distinction and density difference > 18 HU between these 2 areas.

Reprinted with permission from Morotti A, et al, Neurology.[35] © 2020 American Academy of Neurology.

Copyright © American Academy of Neurology. Unauthorized reproduction of this article is prohibited.

venous sinus thrombosis, reversible cerebral vasoconstriction syndrome, vasculitis, use of antithrombotic or sympathomimetic drugs, and to a lesser degree uncontrolled hypertension. Neuroimaging findings guide the treatment, timing of treatment, and prognostication of these patients. For example, given that approximately 25% of patients with a nontraumatic SAH present with more than one cerebral artery aneurysm, it is important to conduct a thorough diagnostic assessment to confirm or refute that the patient has only one aneurysm. This is usually accomplished with head CTA followed by DSA. If more than one aneurysm is identified, it is important to determine which one is symptomatic so that acute treatment can be provided for it while treatment of the asymptomatic aneurysms may be deferred.

As with intraparenchymal hemorrhage that uses the ICH Score for communication and quality metrics, the clinical neurologic examination and the extent of hemorrhage in patients with SAH are communicated and documented using the Hunt and Hess scale and the modified Fisher scale, respectively, as shown in TABLE 4-4[50] and TABLE 4-5.[51] It is important to note that The Joint Commission and Det Norske Veritas Healthcare both require documentation of the Hunt and Hess scale before any neurosurgical intervention, and thus placing it as a mandatory field in the admission orders within the electronic medical record is one way to ensure compliance.[19,20]

In addition, patients can present with localized SAH from a minor head injury and then have an incidental finding of a cerebral artery aneurysm. The location of the aneurysm and its proximity to the SAH—together with details of the nature of the head injury, location of scalp and soft tissue swelling (if present), history, and physical examination—can allow one to differentiate between the aneurysm as the etiology of the SAH versus an incidental finding. This was the situation in CASE 4-3, in which the patient presented with intraparenchymal hemorrhage and SAH after a low-speed motor vehicle collision.

TABLE 4-4 Hunt and Hess Scale for Subarachnoid Hemorrhage[a]

Grade	Characteristics	Mortality rate, %
0	Unruptured aneurysm without symptoms	0
1	Asymptomatic or minimal headache and slight nuchal rigidity	1
1a	No acute meningeal or brain reaction but with fixed neurologic deficit	1
2	Moderate to severe headache, nuchal rigidity, no neurologic deficit other than cranial nerve palsy	5
3	Drowsy, confused, or mild focal deficit	19
4	Stupor, moderate to severe hemiparesis, possible early decerebrate rigidity, and vegetative disturbances	42
5	Deep coma, decerebrate rigidity, moribund	77

[a] Reprinted with permission from Hacein-Bey L and Provenzale J, AJR Am J Roentgenol.[50] © 2011 American Roentgen Ray Society.

Copyright © American Academy of Neurology. Unauthorized reproduction of this article is prohibited.

Cervical spine AVMs and spinal dural arteriovenous fistulas represent uncommon causes of SAH noted on head CT. CASE 4-4 describes a patient with a spinal dural arteriovenous fistula and his clinical course.

NEUROIMAGING IN CT-NEGATIVE SUSPECTED SUBARACHNOID HEMORRHAGE. Occasionally patients will present with a thunderclap headache or "worst headache of life" but head CT is normal and head CTA reveals no structural vascular abnormality. Advances in SWI sequences now provide a useful adjunct in ruling out SAH in patients whose clinical history is consistent with an aneurysmal SAH but whose head CT and head and neck CTA are normal. Obtaining a brain MRI in such patients can help exclude a sentinel SAH, reducing the need for unnecessary admission and DSA.

Isolated Intraventricular Hemorrhage

Isolated IVH is generally uncommon.[52] Sometimes reviewing images in multiple planes (eg, sagittal, coronal) identifies a subtle parenchymal component of a hemorrhage, in which case the IVH is not isolated and is due to intraventricular extension. Intraventricular extension of an intraparenchymal hemorrhage, on the other hand, is very common. In fact, it has been shown that among patients with intraparenchymal hemorrhage, delayed IVH can occur in up 21% of patients without any initial IVH on the index scan and is a predictor of poor neurologic outcome.[52-54] A truly isolated IVH warrants additional advanced neuroimaging, including brain MRI with gadolinium, to exclude a choroid plexus tumor or another underlying structural mass lesion. If the MRI is unrevealing, DSA is needed to exclude an intraventricular vascular lesion such as a choroidal artery aneurysm or AVM.[55] In general, brain MRI has a higher sensitivity for identifying a small IVH compared with head CT.[56] Among nonstructural etiologies of isolated IVH, anticoagulation and sympathomimetic drug use are the most common.

Modified Fisher Scale for Subarachnoid Hemorrhage[a] TABLE 4-5

Grade	Criteria	Patients, %	Frequency, % (n)	
			Delayed cerebral ischemia	Infarction
0	No subarachnoid hemorrhage (SAH) or intraventricular hemorrhage (IVH)	5	0 (0/15)	0 (0/15)
1	Minimal/thin SAH, no IVH in both lateral ventricles	30	12 (10/83)	6 (5/83)
2	Minimal/thin SAH, with IVH in both lateral ventricles	5	21 (3/14)	14 (2/14)
3	Thick SAH,[b] no IVH in both lateral ventricles	43	19 (22/117)	12 (14/117)
4	Thick SAH,[b] with IVH in both lateral ventricles	17	40 (19/47)	28 (13/47)
All patients		100	20 (54/276)	12 (34/276)

[a] Reprinted with permission from Claassen J, et al, Stroke.[51] © 2001 American Heart Association.
[b] Completely filling ≥1 cistern or fissure.

Copyright © American Academy of Neurology. Unauthorized reproduction of this article is prohibited.

CASE 4-3

A 45-year-old man without any known comorbidities was brought to the hospital by emergency medical personnel after being involved in a low-speed motor vehicle collision that resulted in essentially no damage to his vehicle. Upon arrival at the emergency department, the patient was noted to have airway obstruction, and he was intubated and taken for immediate imaging as part of a trauma assessment. All imaging was unremarkable except the head and neck CT angiography, which demonstrated an acute left frontal intraparenchymal hemorrhage, subarachnoid hemorrhage, and a large left paraophthalmic artery aneurysm (FIGURES 4-6A and 4-6B). The patient had external ventricular drainage placed for obstructive hydrocephalus and was taken for digital subtraction angiography with successful coil embolization (FIGURES 4-6C and 4-6D). His clinical course was complicated by persistent encephalopathy attributable to cerebral artery vasospasm noted on transcranial Doppler ultrasonography. The patient underwent induced hypertension without improvement. After 3 days of induced hypertension and persistent vasospasm on transcranial Doppler ultrasonography, a head CT angiogram was obtained (FIGURE 4-6E) and the patient was taken for intraarterial calcium channel antagonist therapy, which resulted in clinical improvement and successful extubation.

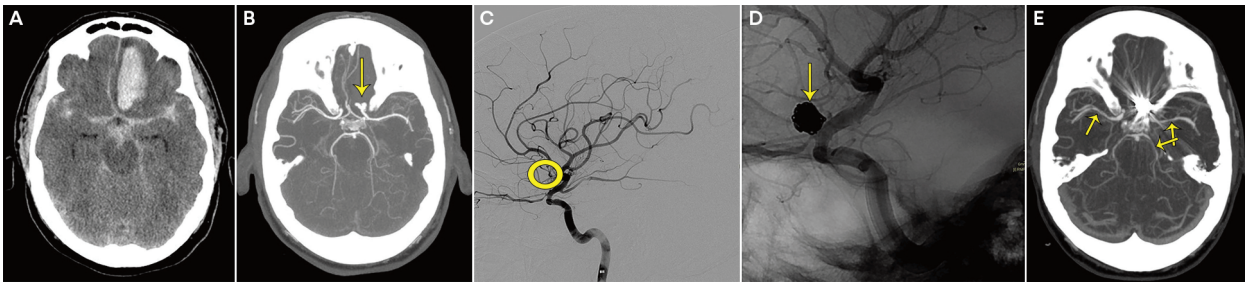

FIGURE 4-6
Imaging of the patient in CASE 4-3. *A,* Axial noncontrast head CT showing acute left frontal intraparenchymal hemorrhage and subarachnoid hemorrhage. *B,* Axial head CT angiogram demonstrating multilobulated calcific left paraophthalmic artery aneurysm (*arrow*). *C,* Digital subtraction angiogram demonstrating coil embolization of the left paraophthalmic artery aneurysm (*oval*). *D,* Close-up image of digital subtraction angiogram demonstrating coil embolization of the left paraophthalmic artery aneurysm (*arrow*). *E,* Axial head CT angiogram confirming transcranial Doppler ultrasonography findings of cerebral artery vasospasm involving the bilateral middle cerebral arteries and left posterior cerebral artery (*arrows*).

COMMENT

This case exemplifies the need to differentiate between traumatic and nontraumatic causes of central nervous system hemorrhage, as acute central nervous system hemorrhage can lead to trauma. The clinical management of a patient with an aneurysmal subarachnoid hemorrhage with an associated intraparenchymal hemorrhage is completely different from that of a patient with the same hemorrhage pattern that is due to head trauma, reinforcing the need for thorough neuroimaging investigation to determine which came first, the hemorrhage or the trauma.

Copyright © American Academy of Neurology. Unauthorized reproduction of this article is prohibited.

The CLEAR III (Clot Lysis Evaluation of Accelerated Resolution of Intraventricular Hemorrhage) trial addressed the treatment of IVH with external ventricular drainage (EVD) and fibrinolysis in patients with intraparenchymal hemorrhage and IVH. It did not address patients with a large amount of isolated IVH who are at high risk for obstructive hydrocephalus but whose overall good neurologic examination results do not justify the risk of EVD placement.[57] In this situation, limited case reports suggest the safety and feasibility of performing serial lumbar punctures to reduce the intraventricular blood burden to minimize the biochemical toxicity of blood constituents (hemoglobin, iron, and thrombin) while minimizing the procedural risk to the patient and avoiding EVD placement.[58,59]

Hemorrhage Secondary to Cerebral Venous Thrombosis

Cerebral venous thrombosis is an all-encompassing descriptive term that includes thrombosis of the sinuses and the cortical veins of the brain. Venous sinus thrombosis refers to thrombosis of the large draining sinuses of the brain such as the transverse sinus, sigmoid sinus, superior sagittal sinus, straight sinus, and their components. In contrast, cortical vein thrombosis refers to the cerebral venous thrombosis of a vein. These thromboses can present with an element of surrounding SAH because of leakage of blood, at times masquerading as SAH or a hemorrhagic tumor. Diagnosing a patient with cerebral venous thrombosis can be challenging considering that headache is the most common reason for outpatient neurologic evaluation and many patients with cerebral venous thrombosis have a long-standing history of primary headache disorders with prior unremarkable imaging, reducing the likelihood of repeat neuroimaging until the patient develops other neurologic signs and symptoms.

It is important to note that there is substantially greater variability in the size, caliber, and appearance of intracranial venous segments compared with the arterial segments when performing side-to-side comparison in a given individual, as shown in FIGURE 4-8, with asymmetry of the transverse sinuses. Therefore, asymmetry between one transverse sinus and its contralateral sinus may be quite normal for a given individual and not signify disease. Furthermore, local venous compression, such as in the case of adjacent cerebral edema from an acute ischemic stroke or an adjacent intraparenchymal hemorrhage, as shown in FIGURE 4-9, may lead to a decrease in vessel caliber and the incorrect conclusion of suspected thrombosis. Asymmetry in venous sinuses is common, and identification of asymmetry between one transverse sinus and its contralateral sinus may be quite normal for a given individual and not signify disease.

Neuroimaging of cerebral venous thrombosis is most frequently done with brain MRI and MR venography (MRV). Although MRV with gadolinium is preferred, time-of-flight MRV without gadolinium remains a viable option for patients with oliguric renal failure and end-stage renal disease on dialysis. However, CT venography can also be used. Although continuous fluoroscopy allows for capture of the venous phase of DSA, DSA is not the optimal study for making the diagnosis of cerebral venous thrombosis. Once the diagnosis is made, the standard treatment involves therapeutic anticoagulation even in the presence of adjacent intraparenchymal hemorrhage, with the exception of cases involving immune thrombotic thrombocytopenia, including heparin-induced thrombocytopenia and thrombosis with thrombocytopenia syndrome.[60,61] Moreover, an etiologic assessment is undertaken, which may lead to the

KEY POINTS

- The risk of recurrent hemorrhage is higher in patients with central nervous system hemorrhage with underlying cerebral amyloid angiopathy (7.39% per year) than in those with central nervous system hemorrhage due to other causes (1.1% per year).
- Besides a ruptured aneurysm, other etiologies of subarachnoid hemorrhage include arteriovenous malformation, fistula, intracranial dissection, cerebral venous sinus thrombosis, reversible cerebral vasoconstriction syndrome, vasculitis, use of antithrombotic or sympathomimetic drugs, and to a lesser degree uncontrolled hypertension.
- The clinical neurologic examination and the extent of hemorrhage in patients with subarachnoid hemorrhage are communicated and documented using the Hunt and Hess scale and the modified Fisher scale, respectively.
- Advances in SWI sequences now provide a useful adjunct in ruling out subarachnoid hemorrhage in patients whose clinical history is consistent with an aneurysmal subarachnoid hemorrhage but whose head CT and head and neck CT angiography are normal.

Copyright © American Academy of Neurology. Unauthorized reproduction of this article is prohibited.

CASE 4-4

A 67-year-old man with hypertension and ongoing tobacco abuse presented to a referring hospital with an acute-onset severe occipital headache, characterized as pain rating 10 out of 10 radiating down his neck, accompanied by nausea and emesis. Head CT revealed a large acute subarachnoid hemorrhage in the posterior fossa (FIGURE 4-7A). Head CT angiography demonstrated abnormal vessels along the margin of the medulla and upper cervical spinal cord consistent with a dural arteriovenous fistula (FIGURES 4-7B, 4-7C, 4-7D, and 4-7E). The patient underwent digital subtraction angiography and embolization of the dural arteriovenous fistula (FIGURES 4-7F and 4-7G). His clinical course was complicated by a partial cervical spinal cord infarction (FIGURE 4-7H). He was monitored with daily transcranial Doppler ultrasonography, which did not reveal any vasospasm. The patient was transferred to the inpatient rehabilitation hospital, from which he was discharged home. His outpatient head CT 3 months after his ictus revealed mild atrophy in the region of the previous subarachnoid hemorrhage (FIGURE 4-7I).

COMMENT

The most common structural vascular cause of acute subarachnoid hemorrhage is a ruptured cerebral artery aneurysm. As demonstrated in this case, however, other structural vascular lesions can also be the cause and should be considered.

Copyright © American Academy of Neurology. Unauthorized reproduction of this article is prohibited.

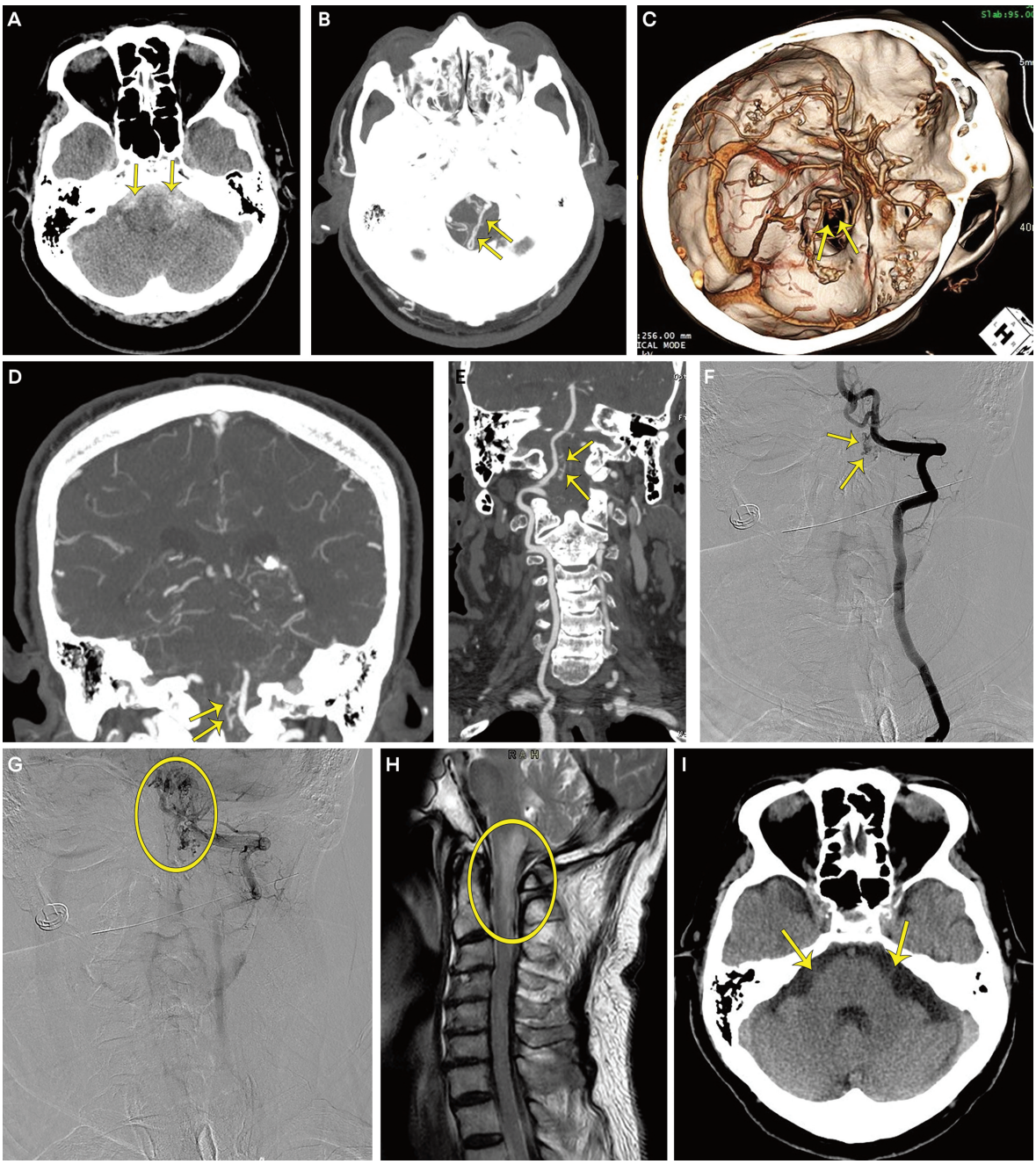

FIGURE 4-7

Imaging of the patient in CASE 4-4. *A,* Axial noncontrast head CT demonstrating acute subarachnoid hemorrhage in the prepontine cistern (*arrows*). *B,* Axial head CT angiogram (CTA) demonstrating abnormal vessels along the margin of the medulla and upper cervical spinal cord consistent with a dural arteriovenous fistula (*arrows*). *C,* Reconstructed axial head CTA with overhead view allowing for visualization of the dural arteriovenous fistula in the foramen magnum (*arrows*). Coronal head CTA (*D*), three-dimensional reconstructed coronal neck CTA (*E*), and arterial phase of digital subtraction angiography with left vertebral artery injection (*F*) all demonstrating abnormal vessels along the margin of the medulla and upper cervical spinal cord consistent with a dural arteriovenous fistula (*D, E, F, arrows*). *G,* Capillary phase of digital subtraction angiography with left vertebral artery injection demonstrating the extensive number of abnormal vessels associated with the dural arteriovenous fistula (*oval*). *H,* Short tau inversion recovery (STIR) sequence of sagittal cervical spine MRI demonstrating intramedullary edema consistent with acute spinal cord infarction involving primarily the posterior spinal cord (*oval*). *I,* Axial noncontrast head CT 3 months after acute subarachnoid hemorrhage with mild atrophy in the region (pons, bilateral cerebellar hemispheres, and bilateral anterior temporal lobes) (*arrows*).

Copyright © American Academy of Neurology. Unauthorized reproduction of this article is prohibited.

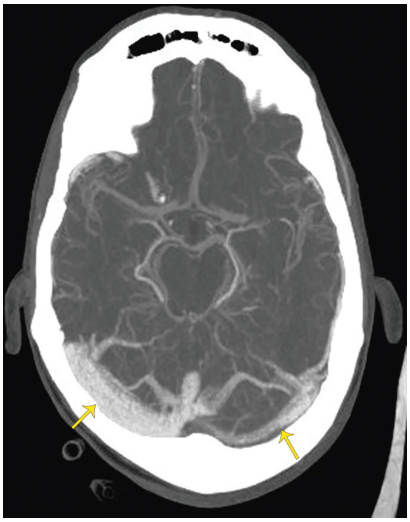

FIGURE 4-8
Axial head CT angiogram showing normal asymmetry of transverse sinuses (*arrows*).

discovery of a genetic thrombophilic disorder or antiphospholipid antibody syndrome.[62] Additional potential contributors include pregnancy, the early postpartum state, and cancer-associated hypercoagulability. In some instances, the clot burden is so large that venous embolectomy can be pursued as an adjunctive treatment, but to date, the largest clinical trial of venous embolectomy versus anticoagulation with heparin was stopped early, as a variety of endovascular techniques were used, which were thought to limit the ability to draw meaningful conclusions.[63]

Hemorrhagic Transformation of Acute Ischemic Stroke

With improving care provided by stroke, neuroendovascular, and neurocritical care teams, the risk of symptomatic hemorrhagic transformation of an ischemic stroke is declining and currently stands at approximately 1% to 3%.[64] This condition is defined as an increase in the National Institutes of Health Stroke Scale score of 4 or more points in the first 36 hours of stroke onset that is attributable to the hemorrhagic transformation. Risk factors include advanced age, greater stroke severity as measured by the National Institutes of Health Stroke Scale, hypertension, hyperglycemia, poor collaterals, early infarction on brain imaging, use of antithrombotic drugs, and reperfusion therapy.[51] When several of these risk factors are combined, the patient has a much higher risk of hemorrhagic transformation of an ischemic stroke, as seen in CASE 4-5.

Intraparenchymal Hemorrhage Secondary to Anticoagulation and Sympathomimetic Drugs

During the past decade, the number of Medicare beneficiaries receiving oral anticoagulation therapies has doubled to more than 5 million.[65] Thus, the prevalence of anticoagulant-associated intraparenchymal hemorrhage has also increased. However, this is a diagnosis of exclusion, and the presence of a concomitant underlying vascular or structural abnormality must always be

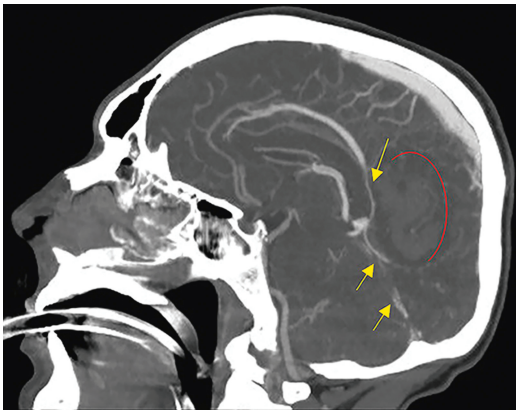

FIGURE 4-9
Head CT angiogram showing local compression of the inferior sagittal sinus and straight sinus (*yellow arrows*) by an intraparenchymal hemorrhage (*red arc*).

Copyright © American Academy of Neurology. Unauthorized reproduction of this article is prohibited.

excluded. Once anticoagulant-associated intraparenchymal hemorrhage is identified, rapid reversal with appropriate reversal agents is paramount, as this condition is associated with larger hematoma volumes, greater hematoma expansion, and greater morbidity and mortality.[66-68]

Sympathomimetic drugs can also produce a variety of hemorrhage patterns. Therefore, a similar thorough etiologic assessment with advanced neuroimaging must be pursued to exclude an underlying vascular or structural abnormality in individuals who test positive for sympathomimetic drugs.

It is important to note that anticoagulation and sympathomimetic drug use often pose the greatest challenge in cases of CNS hemorrhage and an underlying vascular abnormality, as they do not cause a uniform pattern of hemorrhage and can present with intraparenchymal hemorrhage, SAH, or IVH, among other hemorrhage patterns.

Intraparenchymal Hemorrhage Secondary to Septic Emboli

Intraparenchymal hemorrhage secondary to septic emboli is an uncommon condition and is most frequently seen in immunocompromised individuals, patients with prosthetic heart valves, and IV drug users. CASE 4-6 describes a man with a long-standing history of IV drug use who presented with intraparenchymal hemorrhage.

Nontraumatic Spinal Cord Hemorrhage

Nontraumatic spinal cord hemorrhage is a rare finding most often attributable to an underlying vascular abnormality such as an arteriovenous malformation or cavernous malformation. Other causes include the use of anticoagulants, coagulopathies (eg, von Willebrand disease, factor VII, VIII, or IX deficiency), primary spinal cord malignancies (eg, ependymoma, fibrillary astrocytomas and primary melanoma of the CNS), metastasis (eg, lung, breast, and renal cell carcinoma), and complications of radiotherapy.[69,70] Patients with nontraumatic spinal cord hemorrhage can present with acute, subacute, or chronic back pain with or without radicular symptoms.[70] Initial imaging usually begins with MRI with gadolinium of the related part of the spine. T2 imaging sequence usually demonstrates serpiginous flow voids representing dilated epidural vessels. If a spinal arteriovenous malformation is identified, digital spinal angiography is used to characterize and subsequently treat the lesion.[70]

Future Directions

Studies are needed to determine whether the use of mobile CT scanners such as those in mobile stroke units will lead to better outcomes in patients with an intracranial hemorrhage due to earlier detection versus strategies aimed at minimizing on-scene time.

CONCLUSION

Identification of CNS hemorrhage begins with neuroimaging. Once the type of hemorrhage is identified, the combination of the history, physical examination, laboratory studies, and pattern of hemorrhage guides subsequent neuroimaging as part of the etiologic assessment. After the etiology is

KEY POINTS

- Isolated intraventricular hemorrhage warrants additional advanced neuroimaging, including brain MRI with gadolinium, to exclude a choroid plexus tumor or another underlying structural mass lesion. If the MRI is unrevealing, digital subtraction angiography is needed to exclude an intraventricular vascular lesion such as a choroidal artery aneurysm or arteriovenous malformation.
- Asymmetry in venous sinuses is common, and identification of asymmetry between one transverse sinus and its contralateral sinus may be quite normal for a given individual and not signify disease.
- With improving care provided by stroke, neuroendovascular, and neurocritical care teams, the risk of symptomatic hemorrhagic transformation of an ischemic stroke is declining and currently stands at approximately 1% to 3%.
- Intracerebral hemorrhage secondary to septic emboli is overall an uncommon condition and is most frequently seen in immunocompromised individuals, patients with prosthetic heart valves, and IV drug users.

Copyright © American Academy of Neurology. Unauthorized reproduction of this article is prohibited.

CASE 4-5

A 57-year-old woman with hypertension developed acute left hemiparesis and was brought to the hospital by emergency medical personnel. Initial examination revealed a National Institutes of Health Stroke Scale score of 15, and she was given IV tissue plasminogen activator (tPA) after a head CT that revealed only mild hypodensity in the right middle cerebral artery distribution primarily involving the right basal ganglia (FIGURE 4-10A). The patient then underwent head and neck CT angiography with perfusion, which revealed a right M1 thrombosis and a perfusion mismatch of 268 mL (FIGURES 4-10B and 4-10C). She underwent mechanical thrombectomy, which resulted in Thrombolysis in Cerebral Infarction scale grade 3 flow. After the procedure, the patient lost consciousness and was sent for a head CT, which revealed hemorrhagic transformation of her acute ischemic stroke (FIGURE 4-10D). It was later determined that the patient had been receiving dual antiplatelet therapy.

COMMENT

This case exemplifies the risks associated with IV thrombolytics and mechanical thrombectomy, namely, hemorrhagic transformation of an acute ischemic stroke. The hemorrhage is generally in the same location as the ischemic stroke. Concomitant dual antiplatelet therapy can increase this risk but is not a contraindication.

Copyright © American Academy of Neurology. Unauthorized reproduction of this article is prohibited.

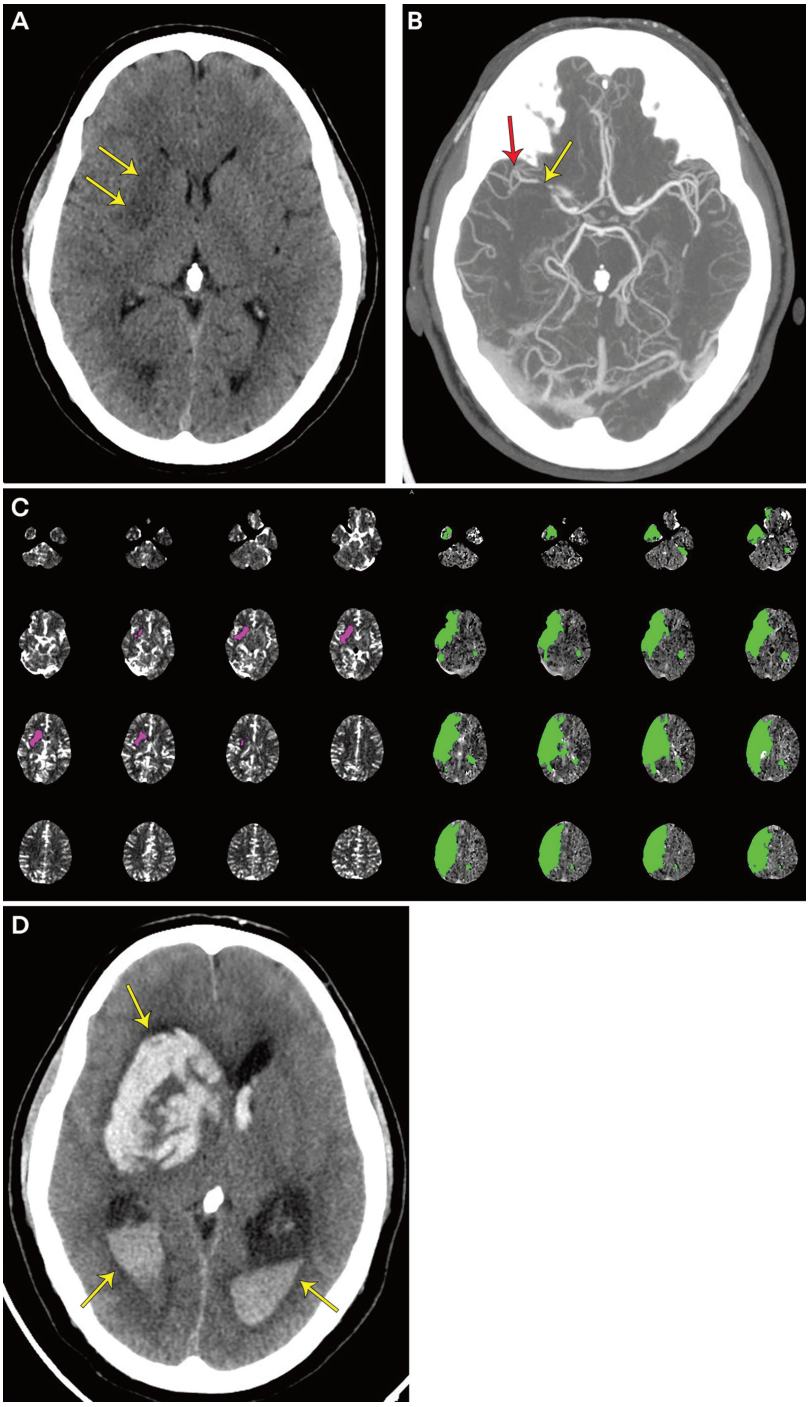

FIGURE 4-10

Imaging of the patient in CASE 4-5. *A,* Axial noncontrast head CT demonstrating acute ischemic changes of the right basal ganglia (*yellow arrows*). *B,* Axial head CT angiogram demonstrating acute right M1 occlusion (*yellow arrow*) with distal reconstitution of flow (*red arrow*). *C,* CT perfusion image demonstrating a small ischemic core in the region of the right basal ganglia (*shaded magenta*) and an extremely large penumbra encompassing nearly the entire right middle cerebral artery distribution (*shaded green*). *D,* Axial noncontrast head CT showing hemorrhagic transformation of the right middle cerebral artery ischemic stroke centered at the right basal ganglia with intraventricular extension, obstructive hydrocephalus, and brain compression (*yellow arrows*).

Copyright © American Academy of Neurology. Unauthorized reproduction of this article is prohibited.

CASE 4-6

A 36-year-old man with current IV use of methamphetamine and heroin, depression, and hepatitis C presented to the hospital after being discovered unresponsive. Head CT revealed multifocal intracranial hemorrhages in the left frontal lobe, left parietal lobe, and left cerebellum (FIGURES 4-10A, 4-10B, and 4-10C). Given that the patient was also febrile, blood cultures were obtained, which were positive for methicillin-sensitive *Staphylococcus aureus*. The patient was started on IV antibiotics. Transthoracic and transesophageal echocardiograms confirmed the diagnosis of aortic valve endocarditis. Head CT angiography excluded the presence of mycotic aneurysms. Brain MRI confirmed multifocal septic emboli with associated intraparenchymal hemorrhage (FIGURES 4-11D, 4-11E, and 4-11F). The patient's clinical course was complicated by acute respiratory failure with hypoxemia necessitating mechanical ventilation, tracheostomy, and percutaneous endoscopic gastrostomy tube placement. After a prolonged hospitalization, the patient underwent successful aortic valve replacement and was discharged to a skilled nursing facility.

COMMENT

This case demonstrates the importance of obtaining temperature in patients with stroke. Multifocal ischemic infarcts with or without concomitant hemorrhage in a febrile patient should prompt an infectious evaluation including blood cultures and prompt initiation of IV antibiotics for suspected bacterial endocarditis.

Copyright © American Academy of Neurology. Unauthorized reproduction of this article is prohibited.

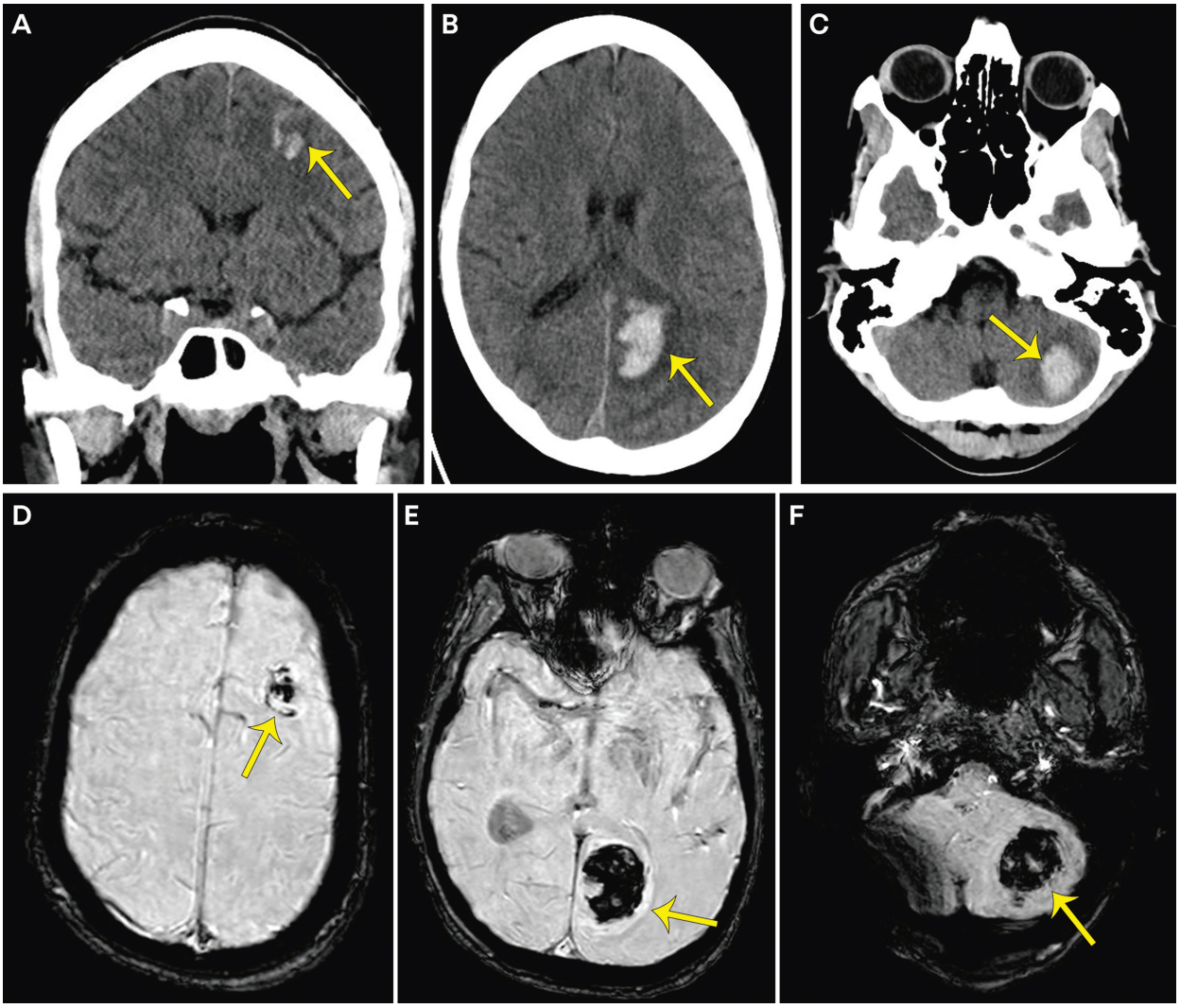

FIGURE 4-11

Imaging of the patient in CASE 4-6. *A,* Coronal noncontrast head CT showing hemorrhagic transformation of the left frontal lobe middle cerebral artery ischemic infarction (*arrow*). *B,* Axial noncontrast head CT showing hemorrhagic transformation of the left parietal lobe posterior cerebral artery ischemic infarction (*arrow*). *C,* Axial noncontrast head CT showing hemorrhagic transformation of the cerebellar ischemic infarction (*arrow*). *D,* Axial susceptibility-weighted brain MRI demonstrating left frontal intraparenchymal hemorrhage (*arrow*). *E,* Axial susceptibility-weighted brain MRI demonstrating left parietal intraparenchymal hemorrhage (*arrow*). *F,* Axial susceptibility-weighted brain MRI demonstrating left cerebellar intraparenchymal hemorrhage (*arrow*).

Copyright © American Academy of Neurology. Unauthorized reproduction of this article is prohibited.

determined, goal-directed therapy is aimed at reducing hemorrhage expansion, preventing complications, and managing cytotoxic cerebral edema, brain compression, and obstructive hydrocephalus.

REFERENCES

1 American Stroke Association. Hemorrhagic strokes (bleeds). Accessed July 19, 2022. stroke.org/en/about-stroke/types-of-stroke/hemorrhagic-strokes-bleeds

2 GBD 2019 Stroke Collaborators. Global, regional, and national burden of stroke and its risk factors, 1990-2019: a systematic analysis for the Global Burden of Disease Study 2019. Lancet Neurol 2021;20(10):795-820. doi:10.1016/S1474-4422(21)00252-0

3 Oleinik A, Romero JM, Schwab K, et al. CT angiography for intracerebral hemorrhage does not increase risk of acute nephropathy. Stroke 2009;40(7):2393-2397. doi:10.1161/STROKEAHA.108.546127

4 Fiebach JB, Schellinger PD, Gass A, et al. Stroke magnetic resonance imaging is accurate in hyperacute intracerebral hemorrhage: a multicenter study on the validity of stroke imaging. Stroke 2004;35(2):502-506. doi:10.1161/01.STR.0000114203.75678.88

5 Kidwell CS, Chalela JA, Saver JL, et al. Comparison of MRI and CT for detection of acute intracerebral hemorrhage. JAMA 2004;292(15):1823-1830. doi:10.1001/jama.292.15.1823

6 Macellari F, Paciaroni M, Agnelli G, et al. Neuroimaging in intracerebral hemorrhage. Stroke 2014;45(3):903-908. doi:10.1161/STROKEAHA.113.003701

7 Russell EJ, Hetts SW, Bello JA. ACR-ASNR-SIR-SNIS practice parameter for the performance of diagnostic cervicocerebral catheter angiography in adults. 2016. Accessed January 3, 2023. acr.org/-/media/ACR/Files/Practice-Parameters/CervicoCerebralCathAngio. pdf

8 Zaidat OO, Lazzaro M, McGinley E, et al. Demand-supply of neurointerventionalists for endovascular ischemic stroke therapy. Neurology 2012;79(13 Suppl 1):S35-41. doi:10.1212/WNL.0b013e31826957ef

9 Hakimi R, Alexandrov AV, Garami Z. Neuro-ultrasonography. Neurol Clin 2020;38(1):215-229. doi:10.1016/j.ncl.2019.09.006

10 Grosset DG, Straiton J, du Trevou M, Bullock R. Prediction of symptomatic vasospasm after subarachnoid hemorrhage by rapidly increasing transcranial Doppler velocity and cerebral blood flow changes. Stroke 1992;23(5):674-679. doi:10.1161/01.str.23.5.674

11 Kassell NF, Haley EC, Apperson-Hansen C, Alves WM. Randomized, double-blind, vehicle-controlled trial of tirilazad mesylate in patients with aneurysmal subarachnoid hemorrhage: a cooperative study in Europe, Australia, and New Zealand. J Neurosurg 1996;84(2):221-228. doi:10.3171/jns.1996.84.2.0221

12 Lysakowski C, Walder B, Costanza MC, Tramèr MR. Transcranial Doppler versus angiography in patients with vasospasm due to a ruptured cerebral aneurysm: a systematic review. Stroke 2001;32(10):2292-2298. doi:10.1161/hs1001.097108

13 Macdonald RL, Kassell NF, Mayer S, et al. Clazosentan to overcome neurological ischemia and infarction occurring after subarachnoid hemorrhage (CONSCIOUS-1): randomized, double-blind, placebo-controlled phase 2 dose-finding trial. Stroke 2008;39(11):3015-3021. doi:10.1161/STROKEAHA.108.519942

14 Neil-Dwyer G, Mee E, Dorrance D, Lowe D. Early intervention with nimodipine in subarachnoid haemorrhage. Eur Heart J 1987;8 Suppl K:41-47. doi:10.1093/eurheartj/8.suppl_k.41

15 Kumar G, Shahripour RB, Harrigan MR. Vasospasm on transcranial Doppler is predictive of delayed cerebral ischemia in aneurysmal subarachnoid hemorrhage: a systematic review and meta-analysis. J Neurosurg 2016;124(5):1257-1264. doi:10.3171/2015.4.JNS15428

16 Babikian VL, Feldmann E, Wechsler LR, et al. Transcranial Doppler ultrasonography: year 2000 update. J Neuroimaging 2000;10(2):101-115. doi:10.1111/jon2000102101

17 Sloan MA, Alexandrov AV, Tegeler CH, et al. Assessment: transcranial Doppler ultrasonography: report of the Therapeutics and Technology Assessment Subcommittee of the American Academy of Neurology. Neurology 2004;62(9):1468-1481. doi:10.1212/wnl.62.9.1468

18 Rajajee V, Fletcher JJ, Pandey AS, et al. Low pulsatility index on transcranial Doppler predicts symptomatic large-vessel vasospasm after aneurysmal subarachnoid hemorrhage. Neurosurgery 2012;70(5):1195-1206; discussion 1206. doi:10.1227/NEU.0b013e3182417dca

19 Specifications Manual for Joint Commission National Quality Measures (v2018A). CSTK-03. Accessed July 19, 2022. manual.jointcommission.org/releases/TJC2018A/MIF0288.html

20 Det Norske Veritas. Comprehensive stroke certification program requirements. Accessed November 16, 2022. dnv.us/Default

Copyright © American Academy of Neurology. Unauthorized reproduction of this article is prohibited.

21 Intersocietal Accreditation Commission. IAC standards and guidelines for vascular testing accreditation (2021). Accessed November 17, 2022.intersocietal.org/programs/vascular-testing/standards/

22 van Asch CJJ, Velthuis BK, Rinkel GJE, et al. Diagnostic yield and accuracy of CT angiography, MR angiography, and digital subtraction angiography for detection of macrovascular causes of intracerebral haemorrhage: prospective, multicentre cohort study. BMJ 2015; 351:h5762. doi:10.1136/bmj.h5762

23 Hilkens NA, van Asch CJJ, Werring DJ, et al. Predicting the presence of macrovascular causes in non-traumatic intracerebral haemorrhage: the DIAGRAM prediction score. J Neurol Neurosurg Psychiatry 2018;89(7): 674-679. doi:10.1136/jnnp-2017-317262

24 Hino A, Fujimoto M, Yamaki T, Iwamoto Y, Katsumori T. Value of repeat angiography in patients with spontaneous subcortical hemorrhage. Stroke 1998;29(12):2517-2521. doi:10.1161/01.str.29.12.2517

25 Biswas S, Chandran A, Radon M, et al. Accuracy of four-dimensional CT angiography in detection and characterisation of arteriovenous malformations and dural arteriovenous fistulas. Neuroradiol J 2015;28(4):376-384. doi: 10.1177/1971400915604526

26 Nesvick CL, Oushy S, Rinaldo L, Wijdicks EF, Lanzino G, Rabinstein AA. Clinical complications and outcomes of angiographically negative subarachnoid hemorrhage. Neurology 2019; 92(20):e2385-e2394. doi:10.1212/WNL.0000000000007501

27 Sacco RL, Kasner SE, Broderick JP, et al. An updated definition of stroke for the 21st century: a statement for healthcare professionals from the American Heart Association/American Stroke Association. Stroke 2013;44(7):2064-2089. doi:10.1161/STR.0b013e318296aeca

28 Greenberg SM, Ziai WC, Cordonnier C, et al. 2022 Guideline for the management of patients with spontaneous intracerebral hemorrhage: a guideline from the American Heart Association/American Stroke Association. Stroke 2022;53(7): e282-e361. doi:10.1161/STR.0000000000000407

29 Qureshi AI, Tuhrim S, Broderick JP, et al. Spontaneous intracerebral hemorrhage. N Engl J Med 2001;344(19):1450-1460. doi:10.1056/NEJM200105103441907

30 Alberts M. ICH diagnosis and management. Presented at: 11th Annual Stroke Belt Consortium Meeting; 2006.

31 Kothari RU, Brott T, Broderick JP, et al. The ABCs of measuring intracerebral hemorrhage volumes. Stroke 1996;27(8):1304-1305. doi:10.1161/01.str.27.8.1304

32 Brott T, Broderick J, Kothari R, et al. Early hemorrhage growth in patients with intracerebral hemorrhage. Stroke 1997;28(1):1-5. doi:10.1161/01.str.28.1.1

33 Demchuk AM, Dowlatshahi D, Rodriguez-Luna D, et al. Prediction of haematoma growth and outcome in patients with intracerebral haemorrhage using the CT-angiography spot sign (PREDICT): a prospective observational study. Lancet Neurol 2012;11(4):307-314. doi:10.1016/S1474-4422(12)70038-8

34 Dowlatshahi D, Brouwers HB, Demchuk AM, et al. Predicting intracerebral hemorrhage growth with the spot sign: the effect of onset-to-scan time. Stroke 2016;47(3):695-700. doi:10.1161/STROKEAHA.115.012012

35 Morotti A, Arba F, Boulouis G, Charidimou A. Noncontrast CT markers of intracerebral hemorrhage expansion and poor outcome: A meta-analysis. Neurology 2020;95(14):632-643. doi:10.1212/WNL.0000000000010660

36 Phan TG, Krishnadas N, Lai VWY, et al. Meta-Analysis of accuracy of the spot sign for predicting hematoma growth and clinical outcomes. Stroke 2019;50(8):2030-2036. doi:10.1161/STROKEAHA.118.024347

37 Xu X, Zhang J, Yang K, et al. Accuracy of spot sign in predicting hematoma expansion and clinical outcome: a meta-analysis. Medicine (Baltimore) 2018;97(34):e11945. doi:10.1097/MD.0000000000011945

38 Hemphill JC, Bonovich DC, Besmertis L, Manley GT, Johnston SC. The ICH score: a simple, reliable grading scale for intracerebral hemorrhage. Stroke 2001;32(4):891-897. doi:10.1161/01.str.32.4.891

39 Graff-Radford J, Botha H, Rabinstein AA, et al. Cerebral microbleeds: prevalence and relationship to amyloid burden. Neurology 2019; 92(3):e253-e262. doi:10.1212/WNL.0000000000006780

40 Vernooij MW, van der Lugt A, Ikram MA, et al. Prevalence and risk factors of cerebral microbleeds: the Rotterdam Scan Study. Neurology 2008;70(14):1208-1214. doi:10.1212/01.wnl.0000307750.41970.d9

41 Charidimou A, Gang Q, Werring DJ. Sporadic cerebral amyloid angiopathy revisited: recent insights into pathophysiology and clinical spectrum. J Neurol Neurosurg Psychiatry 2012; 83(2):124-137. doi:10.1136/jnnp-2011-301308

42 Linn J, Halpin A, Demaerel P, et al. Prevalence of superficial siderosis in patients with cerebral amyloid angiopathy. Neurology 2010;74(17): 1346-1350. doi:10.1212/WNL.0b013e3181dad605

43 Domingues R, Rossi C, Cordonnier C. Diagnostic Evaluation for nontraumatic intracerebral hemorrhage. Neurol Clin 2015;33(2):315-328. doi: 10.1016/j.ncl.2014.12.001

44 Greenberg SM, Charidimou A. Diagnosis of cerebral amyloid angiopathy: evolution of the boston criteria. Stroke 2018;49(2):491-497. doi:10.1161/STROKEAHA.117.016990

Copyright © American Academy of Neurology. Unauthorized reproduction of this article is prohibited.

45 Sanchez-Caro JM, de Lorenzo Martínez de Ubago I, de Celis Ruiz E, et al. Transient focal neurological events in cerebral amyloid angiopathy and the long-term risk of intracerebral hemorrhage and death: a systematic review and meta-analysis. JAMA Neurol 2022;79(1):38-47. doi:10.1001/jamaneurol.2021.3989

46 Du H, Wilson D, Ambler G, et al. Small vessel disease and ischemic stroke risk during anticoagulation for atrial fibrillation after cerebral ischemia. Stroke 2021;52(1):91-99. doi:10.1161/STROKEAHA.120.029474

47 Charidimou A, Imaizumi T, Moulin S, et al. Brain hemorrhage recurrence, small vessel disease type, and cerebral microbleeds: a meta-analysis. Neurology 2017;89(8):820-829. doi:10.1212/WNL.0000000000004259

48 Maas MB, Rosenberg NF, Kosteva AR, et al. Surveillance neuroimaging and neurologic examinations affect care for intracerebral hemorrhage. Neurology 2013;81(2):107-112. doi:10.1212/WNL.0b013e31829a33e4

49 Morotti A, Boulouis G, Dowlatshahi D, et al. Standards for detecting, interpreting, and reporting noncontrast computed tomographic markers of intracerebral hemorrhage expansion. Ann Neurol 2019;86(4):480-492. doi:10.1002/ana.25563

50 Hacein-Bey L, Provenzale JM. Current imaging assessment and treatment of intracranial aneurysms. AJR Am J Roentgenol 2011;196(1):32-44. doi:10.2214/AJR.10.5329

51 Claassen J, Bernardini GL, Kreiter K, et al. Effect of cisternal and ventricular blood on risk of delayed cerebral ischemia after subarachnoid hemorrhage: the Fisher scale revisited. Stroke 2001;32(9):2012-2020. doi:10.1161/hs0901.095677

52 Li Q, Li R, Zhao LB, et al. Intraventricular hemorrhage growth: definition, prevalence and association with hematoma expansion and prognosis. Neurocrit Care 2020;33(3):732-739. doi:10.1007/s12028-020-00958-8

53 Maas MB, Nemeth AJ, Rosenberg NF, et al. Delayed intraventricular hemorrhage is common and worsens outcomes in intracerebral hemorrhage. Neurology 2013;80(14):1295-1299. doi:10.1212/WNL.0b013e31828ab2a7

54 Yogendrakumar V, Ramsay T, Fergusson D, et al. New and expanding ventricular hemorrhage predicts poor outcome in acute intracerebral hemorrhage. Neurology 2019;93(9):e879-e888. doi:10.1212/WNL.0000000000008007

55 Hilkens NA, van Asch CJ, Rinkel GJ, Klijn CJ. Yield of angiographic examinations in isolated intraventricular hemorrhage: a case series and systematic review of the literature. Eur Stroke J 2016;1(4):288-293. doi:10.1177/2396987316666589

56 Romanova AL, Nemeth AJ, Berman MD, et al. Magnetic resonance imaging versus computed tomography for identification and quantification of intraventricular hemorrhage. J Stroke Cerebrovasc Dis 2014;23(8):2036-2040. doi:10.1016/j.jstrokecerebrovasdis.2014.03.005

57 Ziai WC, Tuhrim S, Lane K, et al. A multicenter, randomized, double-blinded, placebo-controlled phase III study of Clot Lysis Evaluation of Accelerated Resolution of Intraventricular Hemorrhage (CLEAR III). Int J Stroke 2014;9(4):536-542. doi:10.1111/ijs.12097

58 Wilkinson DA, Pandey AS, Thompson BG, Keep RF, Hua Y, Xi G. Injury mechanisms in acute intracerebral hemorrhage. Neuropharmacol 2018;134(Pt B):240-248. doi:10.1016/j.neuropharm.2017.09.033

59 Pahlavanzadeh M, Hakimi R. Lumbar puncture as a treatment for IVH in patients with a good neurological examination. J Neuroimaging 2018;28(2):229. doi:10.1111/jon.12507

60 Einhäupl KM, Villringer A, Meister W, et al. Heparin treatment in sinus venous thrombosis. Lancet 1991;338(8767):597-600. doi:10.1016/0140-6736(91)90607-q

61 Scully M, Singh D, Lown R, et al. Pathologic antibodies to platelet factor 4 after ChAdOx1 nCoV-19 vaccination. N Engl J Med 2021;384(23):2202-2211. doi:10.1056/NEJMoa2105385

62 Ferro JM, Canhão P, Stam J, et al. Prognosis of cerebral vein and dural sinus thrombosis: results of the International Study on Cerebral Vein and Dural Sinus Thrombosis (ISCVT). Stroke 2004;35(3):664-670. doi:10.1161/01.STR.0000117571.76197.26

63 Coutinho JM, Zuurbier SM, Bousser MG, et al. Effect of endovascular treatment with medical management vs standard care on severe cerebral venous thrombosis: the TO-ACT randomized clinical trial. JAMA Neurol 2020;77(8):966-973. doi:10.1001/jamaneurol.2020.1022

64 Spronk E, Sykes G, Falcione S, et al. Hemorrhagic Transformation in ischemic stroke and the role of inflammation. Front Neurol 2021;12:661955. doi:10.3389/fneur.2021.661955

65 Troy A, Anderson TS. National trends in use of and spending on oral anticoagulants among US Medicare beneficiaries from 2011 to 2019. JAMA Health Forum 2021;2(7):e211693. doi:10.1001/jamahealthforum.2021.1693

66 Flaherty ML, Haverbusch M, Sekar P, et al. Location and outcome of anticoagulant-associated intracerebral hemorrhage. Neurocrit Care 2006;5(3):197-201. doi:10.1385/NCC:5:3:197

67 Flibotte JJ, Hagan N, O'Donnell J, Greenberg SM, Rosand J. Warfarin, hematoma expansion, and outcome of intracerebral hemorrhage. Neurology 2004;63(6):1059-1064. doi:10.1212/01.wnl.0000138428.40673.83

Copyright © American Academy of Neurology. Unauthorized reproduction of this article is prohibited.

68 Seiffge D, Goeldlin M, Tatlisumak T, et al. Meta-analysis of haematoma volume, haematoma expansion and mortality in intracerebral haemorrhage associated with oral anticoagulant use. J Neurol 2019;266:3126-3135. doi:10.1007/s00415-019-09536-1

69 Shaban A, Moritani T, Al Kasab S, et al. Spinal cord hemorrhage. J Stroke Cerebrovasc Dis 2018;27(6):1435-1446. doi:10.1016/j.jstrokecerebrovasdis.2018.02.014

70 Feng Wang H, Ming Wang D. Exclusively epidural spinal arteriovenous malformation: a short review. Neuropsychiatry 2017;07(06):1000295. doi:10.4172/Neuropsychiatry.1000295

Copyright © American Academy of Neurology. Unauthorized reproduction of this article is prohibited.

REVIEW ARTICLE

CONTINUUM AUDIO INTERVIEW AVAILABLE ONLINE

Neuroimaging in Adults and Children With Epilepsy

By Erasmo A. Passaro, MD

ABSTRACT

OBJECTIVE: **This article discusses the fundamental importance of optimal epilepsy imaging using the International League Against Epilepsy–endorsed Harmonized Neuroimaging of Epilepsy Structural Sequences (HARNESS) protocol and the use of multimodality imaging in the evaluation of patients with drug-resistant epilepsy. It outlines a methodical approach to evaluating these images, particularly in the context of clinical information.**

LATEST DEVELOPMENTS: **Epilepsy imaging is rapidly evolving, and a high-resolution epilepsy protocol MRI is essential in evaluating newly diagnosed, chronic, and drug-resistant epilepsy. The article reviews the spectrum of relevant MRI findings in epilepsy and their clinical significance. Integrating multimodality imaging is a powerful tool in the presurgical evaluation of epilepsy, particularly in "MRI-negative" cases. For example, correlation of clinical phenomenology, video-EEG with positron emission tomography (PET), ictal subtraction single-photon emission computerized tomography (SPECT), magnetoencephalography (MEG), functional MRI, and advanced neuroimaging such as MRI texture analysis and voxel-based morphometry enhances the identification of subtle cortical lesions such as focal cortical dysplasias to optimize epilepsy localization and selection of optimal surgical candidates.**

ESSENTIAL POINTS: **The neurologist has a unique role in understanding the clinical history and seizure phenomenology, which are the cornerstones of neuroanatomic localization. When integrated with advanced neuroimaging, the clinical context has a profound impact on identifying subtle MRI lesions or finding the "epileptogenic" lesion when multiple lesions are present. Patients with an identified lesion on MRI have a 2.5-fold improved chance of achieving seizure freedom with epilepsy surgery compared with those without a lesion.**

This clinical–radiographic integration is essential to accurate classification, localization, determination of long-term prognosis for seizure control, and identification of candidates for epilepsy surgery to reduce seizure burden or attain seizure freedom.

CITE AS:
CONTINUUM (MINNEAP MINN) 2023;29(1, NEUROIMAGING): 104–155.

Address correspondence to Dr Erasmo A. Passaro, 1607 Dr. Martin Luther King Jr St N, St Petersburg, FL 33704-4203, erasmo.passaro@verizon.net.

RELATIONSHIP DISCLOSURE:
Dr Passaro has received personal compensation in the range of $0 to $499 for serving on a speakers bureau and as a consultant for Neurelis, Inc; in the range of $500 to $4999 for serving on speakers bureaus and as a consultant for Eisai Co, Ltd, and Sunovion Pharmaceuticals, Inc; and in the range of $5000 to $9999 for serving on speakers bureaus and as a consultant for SK Life Science, Inc, and UCB, Inc.

UNLABELED USE OF PRODUCTS/INVESTIGATIONAL USE DISCLOSURE:
Dr Passaro reports no disclosure.

© 2023 American Academy of Neurology.

Copyright © American Academy of Neurology. Unauthorized reproduction of this article is prohibited.

INTRODUCTION

An epileptic seizure is a transient occurrence of signs or symptoms due to abnormal excessive or synchronous neuronal activity in the brain.[1] The lifetime risk of a single unprovoked seizure is approximately 10%,[1] and the lifetime risk for having epilepsy in one's lifetime is 1 in 26.[2]

The International League Against Epilepsy (ILAE) definition of epilepsy is as follows[3,4]:

- **The patient has at least two unprovoked seizures occurring more than 24 hours apart.**
- **The patient has a single unprovoked seizure. Upon review of clinical data (which may include EEG and imaging data), the physician estimates that the likelihood of further seizures over 10 years is (at least) 60% or greater.[5,6]**
- **The diagnosis of an epilepsy syndrome.**

The diagnosis of an epilepsy syndrome by an EEG and clinical symptoms or clinically relevant symptomatic etiology on MRI of the brain is essential. According to the World Health Organization (WHO), epilepsy is the fourth most common neurologic disorder after stroke, Alzheimer's dementia, and migraine.[7] Epilepsy is estimated to affect more than 65 million people worldwide.[8] One percent of the United States population, approximately 3.4 million people, have active epilepsy.[9]

Each year, 150,000 new cases of epilepsy are diagnosed.[10] Estimates for the annual economic burden of epilepsy in the United States range from $9.6 billion to $12.4 billion per year.[7,11]

Neuroimaging plays a fundamental role in the clinical evaluation of epileptic seizures and epilepsy. This article does not address neuroimaging for the evaluation of acute and emergent evaluation of seizures; refer to the April 2022 *Continuum* issue on epilepsy for coverage of that topic.[12]

This article reviews the spectrum of MRI findings in epilepsy, how to approach the interpretation of an epilepsy protocol MRI, and what comprises an optimal study. The reader will learn the clinical use of epilepsy neuroimaging to classify seizures and epilepsy, determine long-term prognosis, and select patients with drug-resistant epilepsy for presurgical epilepsy evaluations. The article also reviews the importance of integrating clinical information in evaluating epilepsy neuroimaging studies.

TABLE 5-1 outlines the clinical uses of neuroimaging in the evaluation of epilepsy in terms of classification, long-term prognosis, and evaluation of drug-resistant epilepsy.

KEY POINT

- **MRI is essential to classify epilepsy as focal or generalized and guides treatment decisions.**

INTEGRATION AND CORRELATION OF FUNCTIONAL CLINICAL AND ANATOMIC IMAGING FOR LOCALIZATION

Correlation of clinical history including the epileptic aura and behavioral sequence of seizure phenomenology, particularly the earliest features, with knowledge of functional neuroanatomy and epilepsy protocol imaging is critical in identifying the epileptogenic "lesion" on MRI.

The Role of Auras in Localization

Understanding the role of seizure phenomenology and epileptic auras in facilitating localization of focal cortical dysplasia is vital but a detailed discussion

Copyright © American Academy of Neurology. Unauthorized reproduction of this article is prohibited.

is beyond the scope of this article.[13,14] Often, via details of the history and seizure events, patients tell clinicians where to "look" on their MRI to find the lesion as illustrated by CASE 5-1.

For example, a clinician may miss a subtle bottom-of-the-sulcus dysplasia on the initial MRI review but subsequently identify the lesion after the clinical correlation of MRI with seizure phenomenology, particularly the epileptic aura. This correlation provides essential clues about the epileptogenic network.

The correlation of clinical phenomenology and integration of multimodality imaging and computer-based analysis programs is essential to identifying subtle lesions critical to localization and achieving seizure freedom through surgery.

Understanding Normal Cortical Sulcal Anatomy

The neurologist, particularly the epileptologist, must understand normal cortical sulcal anatomy to identify deviations from normal and precise clinical anatomic imaging correlation and localization. In this regard, the author refers the reader to the work of Naidich and Yousry[15] and Duvernoy.[16]

Optimal Imaging for Seizures and Epilepsy

The advent of high-resolution MRI in the early 1990s with a dedicated epilepsy protocol MRI significantly increased the frequency of identifying the causative pathologic substrate. MRI revolutionized the evaluation and management of epilepsy by improving epilepsy classification, determining etiology and long-term prognosis for remission, predicting response to antiseizure medications, identifying potential surgical candidates, and improving surgical seizure-free outcomes.[17]

TABLE 5-1 Clinical Uses of Neuroimaging in the Epilepsy Evaluation

- Acute and emergent evaluation of seizures (CT readily available and most helpful)[12]
- Determine the risk for seizure recurrence in a person with a single unprovoked seizure, which can help determine whether treatment with an antiseizure medication is appropriate
- Assist with the classification of epilepsy, in conjunction with EEG, as focal, multifocal, diffuse, or cryptogenic
- Determine the presence of a structural etiology for epilepsy and determine the long-term prognosis for seizure control
- Evaluate, select, or potentially exclude patients with drug-resistant epilepsy for possible epilepsy surgery
- In patients with drug-resistant epilepsy, particularly in those with epilepsy who are "MRI-negative," advanced multimodality imaging with fludeoxyglucose positron emission tomography (FDG-PET), ictal subtraction single-photon emission tomography coregistered to MRI (SISCOM), voxel-based morphometry (VBM), and other computer-automated detection techniques and magnetic source imaging are critical to identifying subtle focal cortical dysplasias
- Functional MRI and magnetoencephalography (MEG) for lateralization of language function and localization of hand sensorimotor function

CT = computed tomography; EEG = electroencephalogram; MRI = magnetic resonance imaging.

Copyright © American Academy of Neurology. Unauthorized reproduction of this article is prohibited.

The 1997 ILAE guidelines for neuroimaging in patients with epilepsy recommended a dedicated epilepsy protocol MRI for all patients with a new-onset seizure or newly diagnosed epilepsy in a nonemergent setting.[18] The updated 2019 ILAE guidelines reiterate this recommendation.[19]

In a prospective study of adults with new-onset epileptic seizures, MRI with an epilepsy protocol identified potentially epileptogenic lesions in 28%; the frequency was 53% in those with focal-onset seizures. The most common lesions were gliosis or encephalomalacia (49%), developmental abnormalities (15%), vascular lesions (15%), tumors (15%), and mesial temporal sclerosis (8%).[20] In a cross-sectional study of 495 patients in an epilepsy clinic, 51% had an abnormal scan (CT or MRI).[21] In those patients with chronic focal epilepsy who had a

CASE 5-1

A 17-year-old girl was evaluated in clinic for seizures that began at the age of 15, and a brain MRI was obtained (FIGURE 5-1). The seizures began with numbness in her left shoulder and the first three digits of her left hand. Her hand then started to tremble and jerk, and she tried to "squeeze it out." Her left hand then clenched into a fist, and her head turned to the left. She lost awareness once the left hand was in a fist. She said that with the first seizure her left eye forcefully twitched.

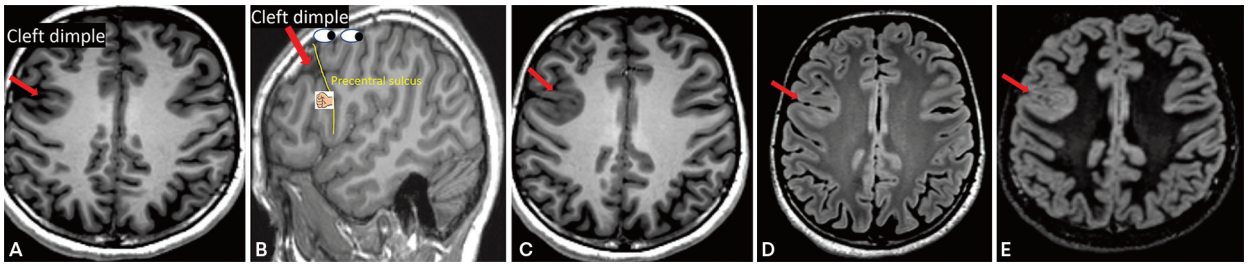

FIGURE 5-1
Imaging of the patient in CASE 5-1. Axial (*A*) and parasagittal (*B*) T1-weighted MRI shows a cleft dimple complex with a wide sulcus at the right precentral sulcus ventral to the superior frontal sulcus adjacent to the frontal eye fields (*B, eyes*) and hand region of the ventral premotor cortex (*B, fist*). Axial T1-weighted magnetization-prepared rapid gradient echo (MPRAGE) (*C*), axial three-dimensional fluid-attenuated inversion recovery (FLAIR) (*D*), and axial T2 double inversion recovery (DIR) (*E*) show gray matter thickening in the middle frontal gyrus (*C, D, E, arrows*).

COMMENT

Although the location of the lesion seems obvious, knowledge of normal sulcal anatomy helps identify the lesion because the wide sulcus is outside the range of normal. The seizure phenomenology helps with finding the lesion. For example, an eye-blinking seizure can occur near the frontal eye fields at the dorsal anterior precentral sulcus; left shoulder and hand numbness lateralizes to the right hemisphere. The left hand being in a fist before the loss of awareness suggests the hand grasp region at the ventral premotor cortex at the posterior ventral portion of the lesion (posterior inferior frontal gyrus adjacent to the precentral sulcus).

Copyright © American Academy of Neurology. Unauthorized reproduction of this article is prohibited.

standard MRI, an abnormality was found in 49%. In those who had an epilepsy protocol MRI, an abnormality was found in 72%.[21]

A landmark study showed that both an epilepsy protocol MRI and an interpretation by an expert neuroradiologist increased the yield of identifying a lesion from 39% to a striking 85%.[22] For example, standard MRI interpreted by nonexpert neuroradiologists identified 39% as abnormal, and the expert reports of the same MRI identified 50% as abnormal. Furthermore, epilepsy protocol MRI interpreted by an expert further improved the detection of a focal lesion in 85% of those with a prior "normal" standard MRI.[22]

Advances with phased-array head coils and 3T MRI have further optimized lesion detection. With an 8-channel phased-array head coil at 3T, 48% more lesions were identified than with a routine 1.5T MRI. In patients with prior epilepsy protocol 1.5T MRIs that were interpreted as normal, subsequent 3T phased-array MRI resulted in the detection of a new lesion in 65% of patients.[23] It is expected that, with newer 32- and 64-channel phased-array head coils, lesion conspicuity and detection will improve through a higher signal-to-noise ratio. Based on these compelling data, clinicians should follow the ILAE Neuroimaging Task Force 2019 guidelines for optimal imaging for all

TABLE 5-2 **Mandatory and Optional Sequences of the HARNESS MRI Protocol[a,b]**

Name	Primary MR image weighting	MR image acquisition	Advantages
Mandatory sequences			
Magnetization-prepared rapid gradient echo (MPRAGE), spoiled gradient echo (SPGR), or turbo field echo (TFE)	T1-weighted	3D	High-resolution images that can be reformatted to be viewed on coronal, axial, and sagittal planes; optimal visualization of brain anatomy and morphology
3D fluid attenuation inversion recovery (FLAIR)	T2-weighted	3D	3D high-resolution images that can be reformatted to any plane; CSF nulling enhances visibility of epileptic pathologies such as focal cortical dysplasia, hippocampal sclerosis, tubers, hamartomas, and glial scars
Coronal spin echo (acquisition plane perpendicular to the long axis of the hippocampus)	T2-weighted	2D	High in-plane resolution; optimal visualization of hippocampal internal structure on coronal cuts
Optional sequences			
Gadolinium-enhanced MRI	T1-weighted	3D	Best for assessing tumor-like lesions, vascular malformations, or infectious processes
Susceptibility-weighted imaging (SWI)	T2*-weighted	3D	Sensitive to iron deposits, blood products, and calcifications

2D = two-dimensional; 3D = three-dimensional; CSF = cerebrospinal fluid; HARNESS = Harmonized Neuroimaging of Epilepsy Structural Sequences; MRI = magnetic resonance imaging.

[a] Modified from Wang I, et al, Epileptic Disord.[24] © 2020 John Libbey Eurotext. Data from Bernasconi A, et al, Epilepsia.[19]

[b] International League Against Epilepsy Neuroimaging Task Force 2019 guidelines for optimal HARNESS MRI protocol are standard for all patients. Acquisition on 1.5T or 3T scanners is possible.[19]

Copyright © American Academy of Neurology. Unauthorized reproduction of this article is prohibited.

patients with epilepsy by using a Harmonized Neuroimaging of Epilepsy Structural Sequences (HARNESS) 3T MRI protocol (TABLE 5-2).[19,24] For optimized imaging, a 3T MRI is essential for patients who are considered candidates for epilepsy surgery. However, in settings where only a 1.5T MRI is available, the same protocol can be used, and image resolution optimized by using a phased-array head coil with a minimum of 8 channels.[19]

Many MRI findings are subtle, and the clinician must correlate their relevance to clinical history and clinical neurophysiology.[24,25]

Imaging of Patients With New-Onset Seizures and Newly Diagnosed and Established Epilepsy

A patient with a single seizure and a remote symptomatic cause (ie, a lesion) identified by MRI has a greater than 60% chance of having another seizure in 5 to 10 years leading to a diagnosis of epilepsy.[5,6,26]

Compared with patients whose cause of a seizure is unknown, the seizure recurrence rate increases twofold in those with a lesion on MRI, from 10% to 26% at 1 year and from 29% to 48% at 5 years.[5]

The American Academy of Neurology (AAN) 2021 practice advisory[27] on antiseizure medication states that, for adults who are seizure free for at least 2 years, the clinician and the patient or caregiver should have a discussion about the risks and benefits of antiseizure medication withdrawal. This discussion should include the risk that seizure recurrence is possibly higher in patients who had antiseizure medication withdrawal and, if seizures recur during or after withdrawal, patients have a small although significant chance they will no longer respond to medications.

In this regard, MRI findings provide information to guide decisions on whether an antiseizure medication should be started and whether a clinician should discontinue an antiseizure medication. In patients with chronic epilepsy who are seizure free for 2 or more years, prolonged remission of epilepsy off antiseizure medication is approximately 65%.[28] However, when an etiology is known, the chance for remission is less than 50%.[27]

Furthermore, specific pathologic substrates have an impact on the long-term prognosis for seizure control, such as hippocampal sclerosis, malformations of cortical development, and dual pathology (hippocampal sclerosis and malformations of cortical development), which portend poor long-term seizure control with antiseizure medications. One study found that patients with epilepsy with hippocampal sclerosis had an 11% chance of attaining sustained seizure control, and patients with dual pathology had a 3% chance of the same.[29] In this regard, optimal epilepsy protocol MRI can help determine seizure recurrence risk when considering antiseizure medication discontinuation and providing long-term prognostic information as illustrated by CASE 5-2 and CASE 5-3.

Imaging in Patients With Drug-Resistant Epilepsy

Approximately one-third of patients with focal epilepsy have drug-resistant epilepsy, defined as failing at least two first-line antiseizure medications. In 2000, Kwan and Brodie[31] found that 47% of patients with newly diagnosed epilepsy became seizure free (12 months of seizure remission) with the first antiseizure medication and only 14% with the second. Subsequent antiseizure medication trials achieved seizure freedom in only an additional 5% of patients. The same authors' follow-up to this study found that 32% of patients did not

KEY POINTS

- Clinical anatomic correlation of epileptic auras and seizure phenomenology can increase the yield of identifying a structural abnormality on MRI, particularly when the finding is subtle.
- In patients with new-onset seizures, epilepsy protocol MRI identifies a cause in 53% of cases.
- In patients with chronic focal epilepsy who had a standard MRI, an abnormality was found in 49%. In those who had an epilepsy protocol MRI, an abnormality was found in 72%.
- An epilepsy protocol MRI and an interpretation by an expert neuroradiologist increased the yield of identifying a lesion from 39% to a striking 85% in patients with drug-resistant epilepsy.
- By using an 8-channel phased-array head coil at 3T, 48% more lesions were identified than with a routine 1.5T MRI. In patients with prior epilepsy protocol, 1.5T MRI was interpreted as normal, and 3T phased-array MRI resulted in the detection of a new lesion in 65% of patients.
- The International League Against Epilepsy Neuroimaging Task Force 2019 guidelines for optimal imaging should be followed for all patients with epilepsy using a Harmonized Neuroimaging of Epilepsy Structural Sequences (HARNESS) 3T MRI protocol.

Copyright © American Academy of Neurology. Unauthorized reproduction of this article is prohibited.

achieve long-term seizure remission.[34] Intractable epilepsy is more common than generally believed and can be identified early. However, a delayed referral from epilepsy onset to epilepsy surgery of greater than 20 years results in increased morbidity and mortality and impaired cognitive, social, and educational development that is even more pronounced in children with epilepsy.[35,36]

In one study, greater than 10% of patients died within 2 years of developing medically intractable epilepsy. Fewer than 2% of patients who may have benefited from epilepsy surgery received it.[37]

Patients with an MRI-identified lesion have a better seizure-free outcome after epilepsy surgery. For example, a 64% seizure-free outcome has been seen postsurgically in patients with hippocampal sclerosis along with improved seizure-free outcome in extratemporal lobe epilepsies, particularly for those with glioneuronal tumors and focal cortical dysplasia type IIb (see the section Focal Cortical Dysplasia, CASE 5-4, and CASE 5-5).[38-43]

Furthermore, a 2020 retrospective, multicenter European cohort study of more than 9000 patients who had undergone epilepsy surgery found that patients with long-term-epilepsy–associated neuroepithelial tumors, vascular

CASE 5-2

A right-handed 38-year-old woman presented to clinic after she had a single bilateral tonic-clonic seizure that occurred while she was shopping. She suddenly "felt weird," which she could not elaborate on further. Her husband caught her when she fell to the ground. She sustained a tongue injury and was confused for a few minutes afterward. She had a brain CT that was normal. Brain MRI without epilepsy protocol showed nonspecific white matter changes in the left frontal lobe.

Her routine awake-sleep 30-minute EEG and long-term EEG without video were both normal. She reported anxiety and short-term memory loss since the seizure. In this clinical scenario, the clinician would decide whether starting an antiseizure medication is indicated. With a normal MRI, her chance for a recurrent seizure was estimated to be 11% at 1 year and 21% at 5 years.[30] An epilepsy protocol MRI performed to improve yield (FIGURE 5-2) showed a left prefrontal lesion consistent with a glioneuronal tumor such as a dysembryoplastic neuroepithelial tumor (DNET).

COMMENT

The MRI finding of a lesion known to cause epilepsy places the patient's 5-year risk of having a recurrent seizure at approximately 48%.[5,26] Therefore, treatment with an antiseizure medication is indicated. Lesions such as DNETs increase the risk for drug-resistant epilepsy.[31] Prefrontal lesions may cause focal nonmotor seizures that can go unrecognized for years.[32] The patient should be counseled about events or spells that are sudden, strange, stereotyped, and short (lasting seconds to 1 or 2 minutes) and consume her attention. Such events would be consistent with focal aware seizures.

Copyright © American Academy of Neurology. Unauthorized reproduction of this article is prohibited.

malformations, or hippocampal sclerosis attained seizure freedom rates 2 years after surgery ranging from 71% to 77%.[41] Finding a lesion on MRI improved surgical seizure-free success 2.5-fold.[42]

These data underscore the fundamental role of high-resolution epilepsy protocol MRI in finding a lesion and identifying potential candidates for epilepsy surgery early, thus providing an optimal chance of achieving seizure freedom. Early surgery prevents or reverses the morbidity of chronic drug-resistant epilepsy and reduces mortality for patients with drug-resistant epilepsy, which is 5- to 10-fold greater than the general population.[44]

Special Considerations in Children Younger Than Two Years Old

Children younger than the age of 2 years require a different MRI protocol because of the dynamic changes in myelination during this period (FIGURE 5-6[45]). In newborns and infants to 6 to 8 months old, cortical gray matter is hypointense on T2-weighted MRI and hyperintense on T1-weighted MRI. After 1 year of age, an early adult pattern appears, initially on T1-weighted MRI and later on T2-weighted MRI.[46] The cortex is delineated in the neonatal period and loses this delineation after the first few months of life such that dysplastic lesions seen

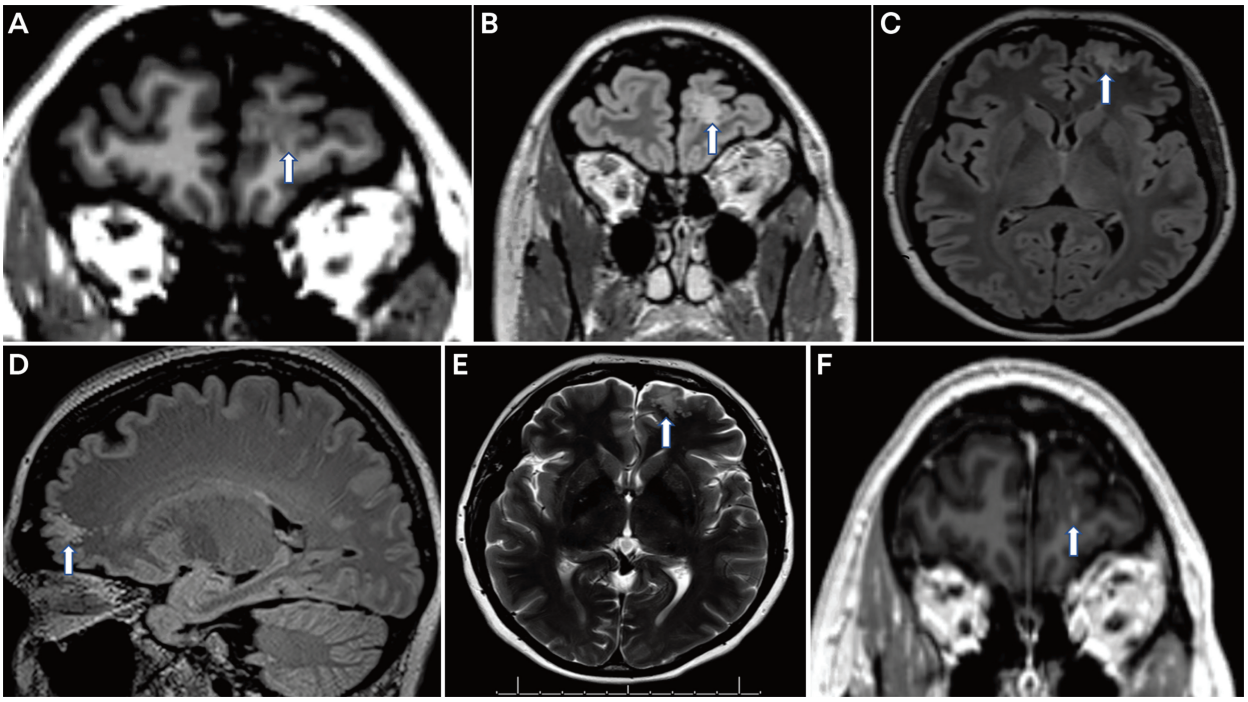

FIGURE 5-2

Imaging from the patient in CASE 5-2 showing left prefrontal cortex lesion with features of a glioneuronal tumor such as a dysembryoplastic neuroepithelial tumor (DNET). Coronal T1-weighted magnetization-prepared rapid gradient echo (MPRAGE) MRI (*A*) shows the lesion with isointensity medial to the superior frontal sulcus (*arrow*). Coronal (*B*) and axial (*C*) fluid-attenuated inversion recovery (FLAIR) MRI shows the hyperintense lesion with a "bubbly" appearance (*arrows*). Sagittal FLAIR (*D*) and the axial T2-weighted MRI (*E*) shows "bubbly" T2 hyperintensity (*arrow*), and coronal postcontrast T1-weighted (*F*, *arrow*) MRI shows faint patchy enhancement.

Copyright © American Academy of Neurology. Unauthorized reproduction of this article is prohibited.

CASE 5-3

A 40-year-old man had a history of a single bilateral tonic-clonic seizure and denied ever having had a prior seizure or episodes of loss of awareness. He asked, "Why do I need an antiseizure medication when I have had only one seizure?" At his initial visit, when asked about stereotyped sensations, he denied these. His imaging is shown in FIGURE 5-3. However, on his second visit, he reported spells that were sudden, short, strange, and the same every time. These spells, representing auras or focal seizures without loss of awareness, had been occurring 3 to 4 times a day. In retrospect, the auras had been occurring for years. He called it a conscious clarity; as he focused on something, "Things around [me] get shut out." He would get a guilt-ridden thought or feel bad about something or want to change something, which made him feel anxious. He could not tolerate levetiracetam because of side effects; he continued to have seizures despite taking lacosamide 400 mg/d, which was increased to 600 mg/d.

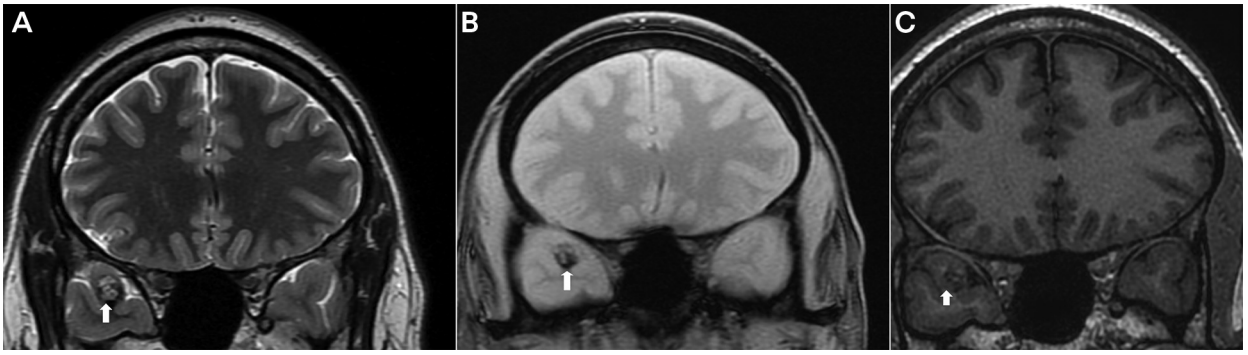

FIGURE 5-3
Imaging of the patient in CASE 5-2 showing a right temporal polar cortex cavernous malformation. *A*, Coronal T2-weighted MRI showing a circular lesion with central hyperintensity representing subacute hemorrhage (methemoglobin) and circumferential hypointensity that represents chronic hemorrhage (hemosiderin) (*arrow*). *B*, Coronal T2* gradient echo (GRE) image shows magnetic susceptibility changes with augmentation of hypointense signal due to the hemosiderin (*arrow*). *C*, Coronal T1-weighted MRI shows central T1 hyperintensity and circumferential T1 hypointensity (*arrow*).

COMMENT

Cerebral cavernous malformations present with epileptic seizure as their first symptom 40% to 70% of the time,[33] and 35% to 40% of these patients develop drug-resistant epilepsy. The MRI obtained a few days before this patient's clinic visit showed findings that were consistent with a cavernous malformation. After one antiseizure medication failed (not attaining 12 consecutive months of seizure freedom), the chance that the second antiseizure medication will control this patient's seizures is approximately 14%.[31,34] Patients with cavernous malformation are excellent surgical candidates with seizure-free rates of 65% to 70% if they do not attain seizure freedom after two antiseizure medications. Focal nonmotor seizures often are not diagnosed for years.[32]

Copyright © American Academy of Neurology. Unauthorized reproduction of this article is prohibited.

when the patient was a neonate are not visible. From infancy to 18 months, fluid-attenuated inversion recovery (FLAIR) MRI is less informative since the gray and white matter blend in because of reduced myelination and water content (FIGURE 5-6).[45-48] The epilepsy protocol MRI is different for each age group (younger than 1 year, 1 year to 2 years, and 2 years and older; TABLE 5-3).

Patients with epilepsy who are 2 years old and older with a prior normal MRI or drug-resistant epilepsy should have a follow-up epilepsy protocol MRI; the boundaries between the gray and white matter become more distinct because of myelination. As a result, focal cortical dysplasia and cortical tubers become evident at this age.[48] In general, contrast-enhanced T1-weighted images are unnecessary unless a neoplastic, vascular, demyelinating, or infectious process was previously seen.

Assessing Quality and Understanding the Information MRI Provides

An orderly and methodical approach to epilepsy protocol imaging is fundamental to optimal and accurate MRI interpretation. In this regard, making sure that the imaging is optimal and presented in the correct format and knowing what information each sequence provides are essential (FIGURE 5-7). Furthermore, one should know normal gyral and cortical anatomy, looking for symmetry and deviations from the normal cortical thickness and signal intensity and gyral thickness, depth, and morphology. In addition, one must be acutely aware of common sources of image misinterpretation that can affect the evaluation of the medial temporal structures and identification of subtle cortical dysplasias (TABLE 5-4).

MRI OF THE TEMPORAL LOBE

Lesions in the anteromedial temporal lobe are a common cause of focal seizures, and it is crucial to understand normal medial temporal anatomy and to be able to identify the causes of epilepsy in this region. Common epilepsy substrates in this region involve the temporal polar cortex, the amygdala, the hippocampus, the entorhinal cortex, and dual pathology that sometimes accompanies hippocampal sclerosis.

Hippocampal Sclerosis

Hippocampal sclerosis is characterized by neuronal loss and gliosis. It is seen in 36.4% of all epilepsy surgical specimens, 44.5% of those from adults and 15.0% from children.[49] When evaluating the medial temporal structures (hippocampus, amygdala, entorhinal cortex, and parahippocampal gyrus), one should assess the size, signal, and shape and be vigilant for dual pathology. High-resolution MRI is 80% to 90% sensitive for identifying hippocampal sclerosis by visual analysis (FIGURE 5-8).[50] Bilateral hippocampal atrophy has been observed in 10% to 20% of patients.[50]

FLAIR MRI identifies increased signal within the hippocampus in patients with hippocampal sclerosis; it is an ideal sequence for identifying signal changes within the hippocampus because gliotic changes have increased water content, appearing as increased signal (FIGURE 5-8).[19,50] The FLAIR sequence nulls the increased signal intensity of the CSF in the temporal horn of the lateral ventricle and the choroidal fissure that can dwarf the increased signal in the hippocampus on a conventional thin-slice T2-weighted fast spin echo image. One must also be aware that the baseline signal of the hippocampus on FLAIR MRI is greater than

KEY POINTS

- Many MRI findings are subtle, and the clinician must correlate their relevance to clinical history and clinical neurophysiology.
- In a patient with a single unprovoked seizure, an abnormal MRI showing pathology that causes epilepsy increases the risk for a recurrent seizure twofold and, according to the International League Against Epilepsy, the patient would be classified as having epilepsy even with a normal EEG and would warrant treatment with an antiseizure medication.
- In patients with chronic epilepsy who are seizure-free for 2 or more years, prolonged remission of epilepsy off antiseizure medication is approximately 65%. However, when an etiology is known, the chance for remission is less than 50%.
- MRI can show certain pathologic substrates that predict a poor prognosis for long-term seizure control, such as hippocampal sclerosis, malformations of cortical development, and cavernous malformations.
- In one study, greater than 10% of patients died within 2 years of developing medically intractable epilepsy. Fewer than 2% of patients who may have benefited from epilepsy surgery received it.
- Patients with long-term-epilepsy–associated neuroepithelial tumors, vascular malformation, or hippocampal sclerosis attained seizure freedom rates 2 years after surgery ranging from 71% to 77%.

Copyright © American Academy of Neurology. Unauthorized reproduction of this article is prohibited.

that of the cortex and can be mistakenly interpreted as bilateral hippocampal sclerosis. Therefore, thin-slice 2.0-mm, with no interslice gap, voxel size 0.4 mm × 0.4 mm × 2.0 mm, coronal oblique T2-weighted turbo fast spin echo images should be reviewed for confirmation (FIGURE 5-8D).[19,50]

Hippocampal atrophy and increased signal are not always seen together in the same patient. Some patients have increased T2 signal without accompanying atrophy.[50,51] The high T2 signal reflects gliosis rather than neuronal cell loss.[50,51]

Although most patients with temporal lobe epilepsy show marked hippocampal sclerosis on pathologic examination, 40% present with no significant cell loss and gliotic changes only.[51] In 2016, it was shown that hippocampal sclerosis presented with cell loss across all subfields, whereas in hippocampal gliosis, the changes were subtle and restricted to the CA4 subfield and the dentate gyrus.[50]

CASE 5-4

A 54-year-old woman with drug-resistant epilepsy since the age of 5 with periods of remission was referred for epilepsy surgery evaluation (FIGURE 5-4). When she had a feeling of a "tension-build-up" inside, her pupils became large, she giggled, and a few seconds later she slapped her lap with her right hand. She then rocked her torso and would sometimes turn prone. At the end of each event, she had a big sigh of relief and immediately returned to baseline.

COMMENT

Gelastic seizures usually involve a network of the ventral anterior cingulate. This patient's lesion was in the right inferior frontal gyrus (pars triangularis), which has short white matter connections to the ventral anterior cingulate.[13,14] Focal cortical dysplasia type IIb shows a deep sulcus with cortical thickening at the sulcal depth with a wisp of gray matter that extends into the white matter (transmantle sign).

Copyright © American Academy of Neurology. Unauthorized reproduction of this article is prohibited.

Secondary findings of hippocampal sclerosis can also be observed, such as (1) enlargement of the ipsilateral temporal horn of the lateral ventricle; (2) thinning of the ipsilateral fornix; (3) ipsilateral mamillary body atrophy; (4) loss of normal interdigitations of the hippocampal head; and (5) atrophy of the white matter between the hippocampus and the collateral sulcus (FIGURE 5-9).[52]

Hippocampal Shape and Position

Approximately 40% of patients with temporal lobe epilepsy present with hippocampal malrotation, a shape variant characterized by an abnormally round and vertically oriented hippocampus and a deep collateral sulcus (FIGURE 5-10).[53,54] This neurodevelopmental variant also occurs in people without temporal lobe epilepsy and does not usually have a clear pathologic significance.[54] Hippocampal shape and positional changes occur in 10% of healthy controls, 63% of patients

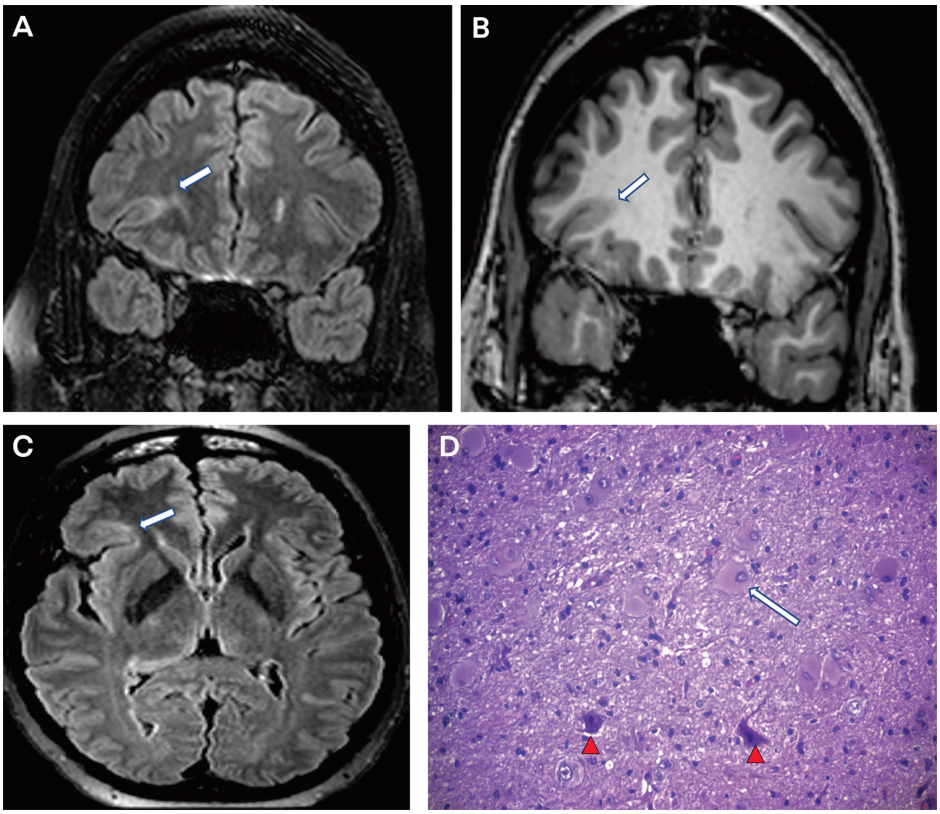

FIGURE 5-4

Imaging of the patient in CASE 5-4. *A*, Coronal three-dimensional fluid-attenuated recovery (FLAIR) MRI shows a right inferior frontal gyrus T2 hyperintensity at the bottom of the sulcus with a wisp of gray matter ("transmantle sign") (*arrow*). *B*, Coronal T1-weighted magnetization-prepared rapid gradient echo (MPRAGE) shows a right inferior frontal gyrus T1 gray matter isointense lesion at the bottom of the sulcus and transmantle sign (*arrow*).[43] *C*, Axial FLAIR image showing the same findings (*arrow*) as in panel *B*. *D*, Pathology shows a focal cortical dysplasia type IIb with large dysmorphic neurons (*red arrowheads*) and balloon cells with prominent eosinophilic cytoplasm (*white arrow*). Gelastic seizures usually involve a network of the ventral anterior cingulate. The patient's lesion is in the right inferior frontal gyrus (pars triangularis), which has short white matter connections to ventral anterior cingulate.[13,14]

Copyright © American Academy of Neurology. Unauthorized reproduction of this article is prohibited.

CASE 5-5

A 53-year-old woman had a history of seizures that began at age 11 with serial seizures that were diagnosed as psychogenic seizures. At age 52, still having several seizures a week, she was referred for epilepsy surgery evaluation (FIGURE 5-5). Her seizures were mostly nocturnal and began with a feeling of the ground "falling out" from under her; she would then tonically extend her right leg more than her left leg, appear startled, and hold onto things because of the sensation that she was falling.

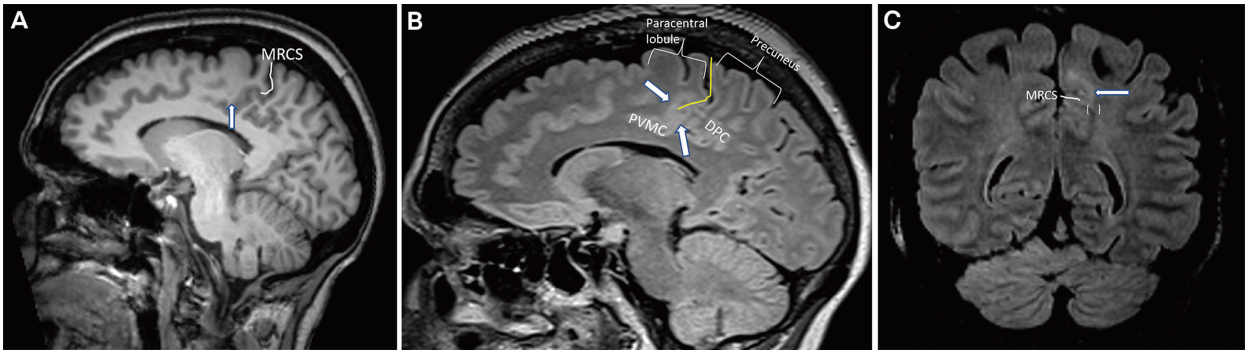

FIGURE 5-5

Imaging of the patient in CASE 5-5 showing cortical thickening of the dorsal posterior cingulate (DPC) adjacent to the ventral posterior paracentral lobule and ventral anterior precuneus. The patient had stereo-EEG and resective surgery and has been seizure-free for 3 years. Pathology showed focal cortical dysplasia type IIa. *A,* Sagittal T1-weighted MRI shows gray matter sulcal thickening at the inferior marginal ramus of the cingulate sulcus (MRCS) (*arrow*). *B*, Sagittal fluid-attenuated inversion recovery (FLAIR) image with hyperintensity at the MRCS (*yellow curved line*) at the posterior ventral motor cingulate (PVMC) and the dorsal posterior cingulate (DPC). The lesion is identified by the *arrows* and *red brackets*. *C*, Coronal fluid-attenuated inversion recovery (FLAIR) image at the periventral MRCS (*arrow* points to the lesion) with a wisp of gray matter at the bottom. The DPC is granular cortex and has vestibular function (giving the patient the feeling as though she is falling) and is adjacent to the PVMC (tonic leg extension).

COMMENT

The patient's initial seizures were not associated with loss of awareness and had unusual clinical features. However, the seizures were the same, sudden, and short every time, which is consistent with focal seizures. The feeling of the "ground falling out" indicates a vestibular network in the parietal region such as the posterior long gyrus of the insula, the inferior parietal lobule, the posterior precuneus of the medial parietal lobe, or the dorsal posterior cingulate gyrus. The bilateral leg extension suggests the medial parietal lobe and possibly the left hemisphere because the leg extension is primarily on the right. Correlating clinical phenomenology with MRI helps identify a lesion in the dorsal posterior cingulate gyrus dorsal to the posterior ventral motor cingulate. She had resective surgery at the age of 54 and remained seizure free with mild right leg weakness postoperatively.

Copyright © American Academy of Neurology. Unauthorized reproduction of this article is prohibited.

Normal cortex	Axial T2-weighted	Axial T1-weighted	Comments
Neonatal/early infantile period (from birth until 6-8 months of age)	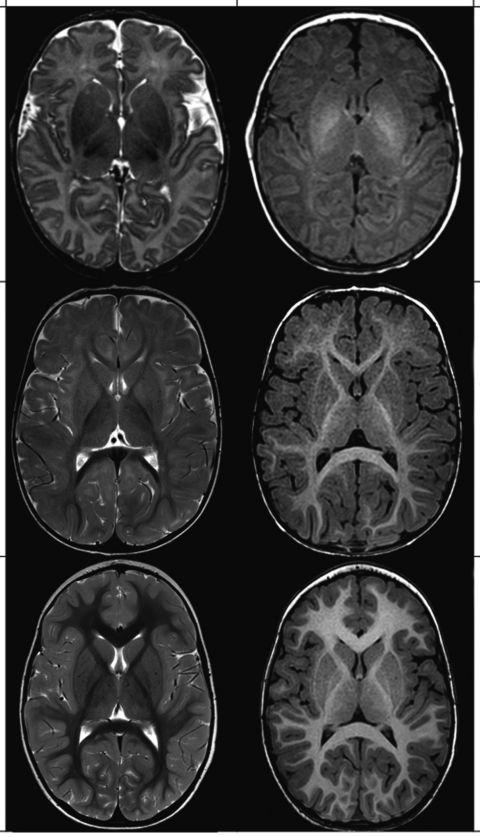		At birth, most white matter is unmyelinated and appears hypointense on T1-weighted imaging and hyperintense on T2-weighted imaging. Myelination generally proceeds from central to peripheral, from inferior to superior, and from posterior to anterior.
Infantile period (from 6-8 to 24 months of age)			Progression of myelination is more rapid on T1-weighted imaging (reaching adult contrast at 12 months) than on T2-weighted imaging (reaching maturity at approximately 24 months).
After myelination (after 24-36 months of age)			During the third year, myelination of subcortical white matter is accomplished; relative white-to-gray matter contrast does not significantly change thereafter.

FIGURE 5-6

Normal early developmental progression on brain MRI. This figure shows the normal evolution of T1-weighted and T2-weighted MRI cortical and white matter signal changes from birth to age 6 to 8 months, from the age of 6 to 8 months to 24 to 36 months, and after the age of 24 to 26 months when radiographic myelination is complete. At this stage, the MRI signal changes are similar to the mature adult pattern.

Reprinted with permission from Severino M, et al, Brain.[45] © 2020 The Authors.

with heterotopias, 41% with polymicrogyria, and 38% with cortical dysplasia.[54] These changes were also found in 43% of patients with hippocampal atrophy, and no relationship has been found between the side of hippocampal shape abnormality and the epileptogenic zone.[50,54]

Entorhinal Cortex Atrophy

Entorhinal cortex size can be evaluated by visual assessment. Entorhinal cortex atrophy is often seen concomitantly with hippocampal atrophy but can also be seen independently. It is characterized by thinning of the collateral white matter of the entorhinal cortex (FIGURE 5-11).[55]

Hippocampal Sclerosis and Dual Pathology

Hippocampal atrophy and a coexisting extrahippocampal macroscopic lesion on MRI, not encroaching on the hippocampal structure, defines dual pathology, with early reports finding that 15% to 20% of patients with hippocampal sclerosis have dual pathology.[56] The number is likely lower (5%) because earlier studies

KEY POINTS

- **Finding a lesion on MRI improves surgical seizure-free success 2.5-fold.**
- **Children younger than the age of 2 years require a different MRI protocol because of the dynamic changes in myelination during this period. From infancy to 18 months, fluid-attenuated inversion recovery (FLAIR) MRI is less informative since the gray and white matter blend in because of reduced myelination and water content.**
- **Hippocampal sclerosis is characterized by neuronal loss and gliosis and is seen in 36.4% of all epilepsy surgical specimens, 44.5% of those from adults and 15.0% from children.**
- **High-resolution MRI is 80% to 90% sensitive for identifying hippocampal sclerosis by visual analysis.**
- **Although most patients with temporal lobe epilepsy show marked hippocampal sclerosis on pathologic examination, 40% demonstrate no significant cell loss and gliotic changes only.**

Copyright © American Academy of Neurology. Unauthorized reproduction of this article is prohibited.

included patients with focal cortical dysplasia type I, classified differently as focal cortical dysplasia type III (see the section Focal Cortical Dysplasias).[57] Patients with vascular malformations, perinatal ischemic lesions, malformations of cortical development, glioneuronal tumors, and vascular malformations can have dual pathology.[56]

With vascular malformations, hippocampal sclerosis is more likely to be present if the lesion is close to the hippocampus and does not involve the hippocampus.[56] Focal cortical dysplasia type III with hippocampal sclerosis is not considered dual pathology.[58]

Temporal Polar Cortex

The temporal polar cortex anterior limit corresponds to the tip of the temporal lobe. Its posterior limit corresponds to the first coronal section that intersects the uncinate bundle at the limen insulae (the region that connects the anterior temporal white matter with the overlying insular white matter) (FIGURE 5-12).[59,60]

TABLE 5-3

Epilepsy Protocol MRI for Children Younger Than Two Years Old[a]

Epilepsy protocol MRI for neonates and infants younger than 1 year old

- Three-dimensional axial turbo fast spin echo T2-weighted images: slice thickness 2 mm, gap 0 mm, voxel size 0.4 mm × 0.4 mm × 2.0 mm
- Coronal turbo fast spin echo T2-weighted high-resolution coronal oblique sequence: maximum slice thickness of 2 mm, gap 0 mm, voxel size 0.4 mm × 0.4 mm × 2.0 mm
- Axial diffusion-weighted imaging (DWI)
- Gradient echo (GRE) or susceptibility-weighted imaging (SWI) can identify calcification or old hemorrhage (the field of view for the sequences should be adjusted based on size)

Epilepsy protocol MRI for children ages 1 year to 18 months

- Axial turbo fast spin echo T2-weighted images: slice thickness 2-3 mm, gap 0 mm, voxel size 0.4 mm × 0.4 mm × 2.0 mm
- Coronal turbo fast spin echo T2-weighted high-resolution coronal oblique sequence: maximum slice thickness of 2-3 mm, gap 0 mm, voxel size 0.4 mm × 0.4 mm × 2.0 mm
- Axial DWI
- T2*GRE or SWI to identify calcification or old hemorrhage (the field of view for the sequences should be adjusted based on head size)
- Three-dimensional volumetric T1-weighted magnetization-prepared rapid gradient echo (MPRAGE) or spoiled gradient echo (SPGR)-weighted sequence: 1-mm slice thickness, gap 0 mm, isotropic voxels 1.0 mm
- If MRI done before the age of 2 years is normal and seizures persist, the MRI should be repeated with the Harmonized Neuroimaging of Epilepsy Structural Sequences (HARNESS) epilepsy protocol MRI at 2 years and older because with myelination focal cortical dysplasias and tuberous sclerosis lesions can become more conspicuous

MRI = magnetic resonance imaging.

[a] Modified with permission from Martinez-Rios C, et al, J Magn Reason Imaging.[46] © 2016 John Wiley & Sons, Inc.

Copyright © American Academy of Neurology. Unauthorized reproduction of this article is prohibited.

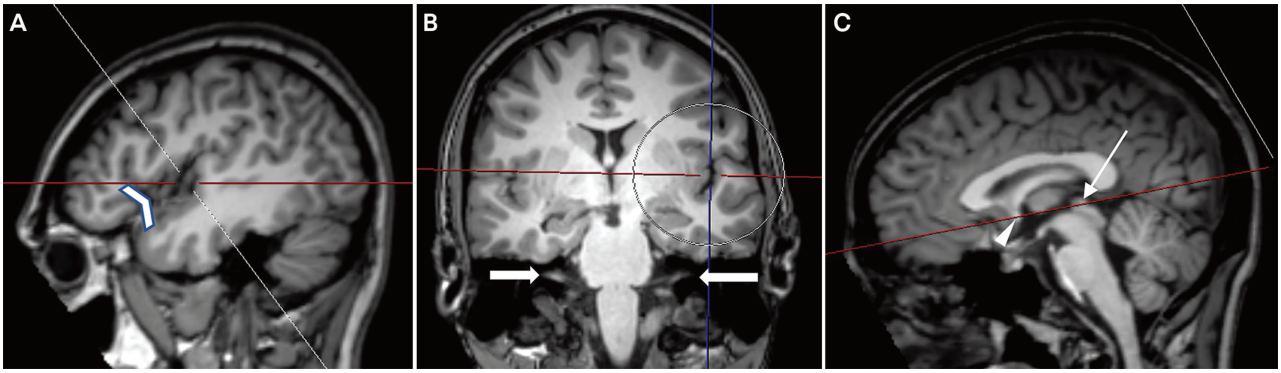

FIGURE 5-7

Optimal planes to view three-dimensional MRI epilepsy protocol images and to determine symmetry of MRI images. *A*, Sagittal T1-weighted MRI shows the coronal oblique plane where coronal images are sliced perpendicularly to the axis of the sylvian fissure (*arrowhead*) to optimally visualize medial temporal anatomy. *B*, Coronal T1-weighted MRI: the VII and VIII cranial nerve complexes (*arrows*) are symmetric, indicating that the head position is midline (this confirms that the head alignment is accurate and not tilted). *C*, Sagittal T1-weighted MRI shows the anterior commissure (*arrowhead*)-posterior commissure (*arrow*) line. The plane of the axial images should always be in this plane to see critical anatomic landmarks.

The frequency of temporal polar cortex abnormalities was found to range from 28% to 66% in patients with drug-resistant temporal lobe epilepsy, and the abnormalities are usually ipsilateral to the side of hippocampal sclerosis. In that series, 72% of patients with temporal lobe epilepsy had reduced temporal polar cortex volume, often accompanied by changes in the underlying white matter.[60]

FLAIR MRI shows temporal polar cortex blurring, and T1-weighted and T2-weighted MRI shows white matter changes with preserved cortical thickness and well-demarcated cortical-subcortical white matter transition on T1-weighted images in patients with drug-resistant temporal lobe epilepsy. Often temporal polar cortex atrophy accompanies these changes. Pathology shows a reduced number of myelinated axons (FIGURE 5-13).[61,62] These temporal polar cortex changes are seen in some patients with hippocampal sclerosis and in children

Common Sources of Error and Pitfalls in Epilepsy-protocol MRI Interpretation

TABLE 5-4

- Volume-averaging of slices through a sulcus may be mistaken for cortical thickening, particularly when the imaging planes and imaging reformats are in the incorrect plane or with a nonvolumetric scan; multiplanar reformatting of three-dimensional imaging in three planes is essential
- Abnormal amygdala or hippocampal enlargement is incorrectly interpreted as the contralateral side having atrophy
- Hippocampal sclerosis on fluid-attenuated inversion recovery (FLAIR) can be incorrectly interpreted because of thick image slices, a large interslice gap, and not confirming findings on thin-slice T2 turbo coronal fast spin echo
- When the head is misaligned in the scanner, hippocampal atrophy is incorrectly identified because the hippocampal head (typically larger) is compared with the contralateral hippocampal body (which is smaller)

Copyright © American Academy of Neurology. Unauthorized reproduction of this article is prohibited.

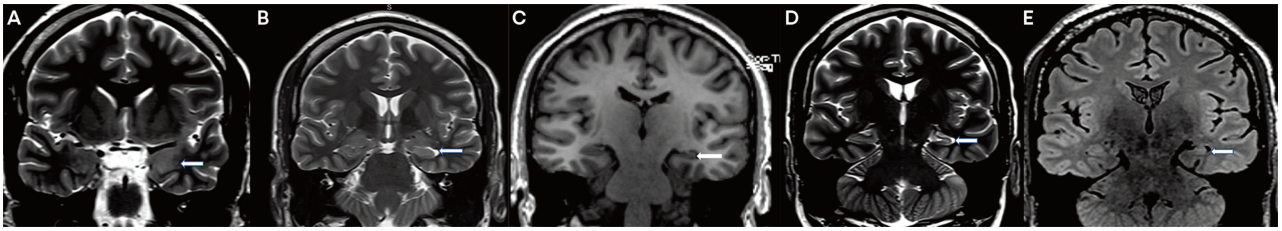

FIGURE 5-8

MRI of hippocampal sclerosis. *A*, Coronal T2-weighted MRI shows left amygdala hyperintensity, which is occasionally seen with hippocampal sclerosis (*arrow*). *B*, Coronal T2-weighted MRI shows loss of hippocampal head interdigitations. Note the ridges in the normal right hippocampus and the faint T2 hyperintensity in the hippocampal head (*arrow*). *C*, Coronal T1-weighted MRI shows atrophy (*arrow*) of the left hippocampus. *D*, Coronal T2-weighted MRI shows the T2 hyperintense left hippocampus (*arrow*). *E*, Coronal fluid-attenuated inversion recovery (FLAIR) MRI shows a hyperintense left hippocampus (*arrow*) corresponding to the coronal T2-weighted MRI in panel *D*.

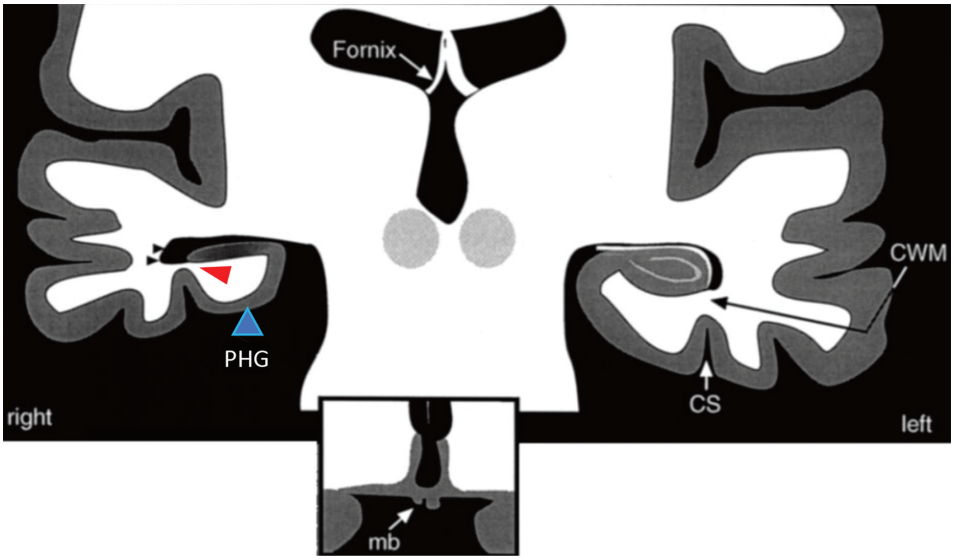

FIGURE 5-9

Schematic diagram of coronal T1-weighted magnetization-prepared rapid gradient echo (MPRAGE) showing typical signs of hippocampal sclerosis: (1) right hippocampal atrophy; (2) loss of internal hippocampal detail; (3) mildly reduced signal intensity; (4) T2 hyperintensity (*not shown*) on coronal fluid-attenuated inversion recovery (FLAIR) and coronal T2-weighted fast spin echo. Secondary findings include (1) collateral white matter thinning (*red arrowhead*); (2) thinning of the ipsilateral fornix; (3) enlargement of the ipsilateral temporal horn (*black arrowheads*); and (4) atrophy of the collateral white matter (CWM) (*red arrowhead*; the *black arrow* on left is normal CWM). *CS* indicates the collateral sulcus; the mamillary body (mb) atrophy is shown on the inset on a more anterior image. The parahippocampal gyrus (PHG) (*blue arrowhead*) is ventral to the hippocampus and medial to the collateral sulcus CS (*small white arrow*).

Modified with permission from Bronen R, AJNR Am J Neuoradiol.[52] © 1998 American Society of Neuroradiology.

Copyright © American Academy of Neurology. Unauthorized reproduction of this article is prohibited.

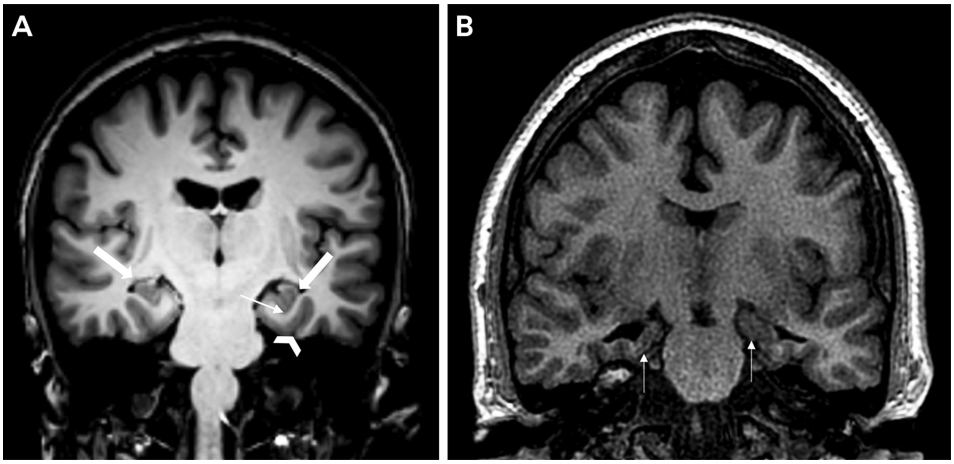

FIGURE 5-10
Hippocampal malrotation. *A*, Coronal oblique T1-weighted magnetization-prepared rapid gradient echo (MPRAGE) 3T image shows hippocampal malrotation in a person without epilepsy: vertically or obliquely oriented hippocampi (*thick arrows*), a deep collateral sulcus (*arrowhead*), and hippocampal indentation of collateral white matter (*thin arrow*). *B*, Coronal oblique T1-weighted MPRAGE 1.5T image shows hippocampal malrotation (*thin arrows*) in a highly functional patient with focal occipital seizures, bilateral occipital ulegyria (*not shown*), and dysgenesis of the splenium of corpus callosum (*not shown*).

KEY POINT

- The frequency of temporal polar cortex abnormalities was found to range from 28% to 66% in patients with drug-resistant temporal lobe epilepsy, usually ipsilateral to the side of hippocampal sclerosis.

with focal cortical dysplasias type I and type II without hippocampal sclerosis (see the section Focal Cortical Dysplasias).[63,64]

Although these temporal polar cortex changes on MRI can appear similar to focal cortical dysplasia type II, in temporal polar cortex blurring, the cortical-subcortical white matter transition is still well defined, and the other features of focal cortical dysplasia type II are absent (compare FIGURE 5-14 with FIGURE 5-15).[61,62] A more recent study evaluated temporal pole abnormalities in patients with focal cortical dysplasia and found focal cortical dysplasia type II (FIGURE 5-15) was more likely to be identified on MRI as isolated gray-white matter T1 blurring. In contrast, focal cortical dysplasia type I was associated with an MRI finding of gray-white matter blurring best seen on T2-weighted and FLAIR imaging with regionally decreased myelination.[63]

Furthermore, temporal polar cortex blurring is not caused by focal cortical dysplasia itself because focal cortical dysplasia

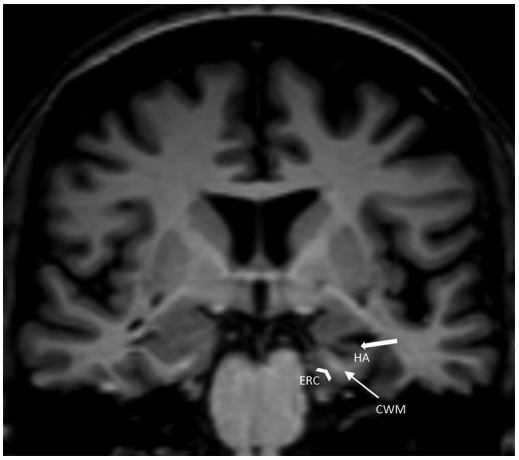

FIGURE 5-11
Entorhinal cortex atrophy. Coronal T1-weighted magnetization-prepared rapid gradient echo (MPRAGE) MRI in a patient with drug-resistant temporal lobe epilepsy shows left hippocampal head atrophy (HA) with T1 hypointense signal (*thick arrow*), accompanying left entorhinal cortex (ERC) atrophy (*arrowhead*), and thinning of the collateral white matter (CWM) (*thin arrow*). Compare this with the normal right ERC.

Copyright © American Academy of Neurology. Unauthorized reproduction of this article is prohibited.

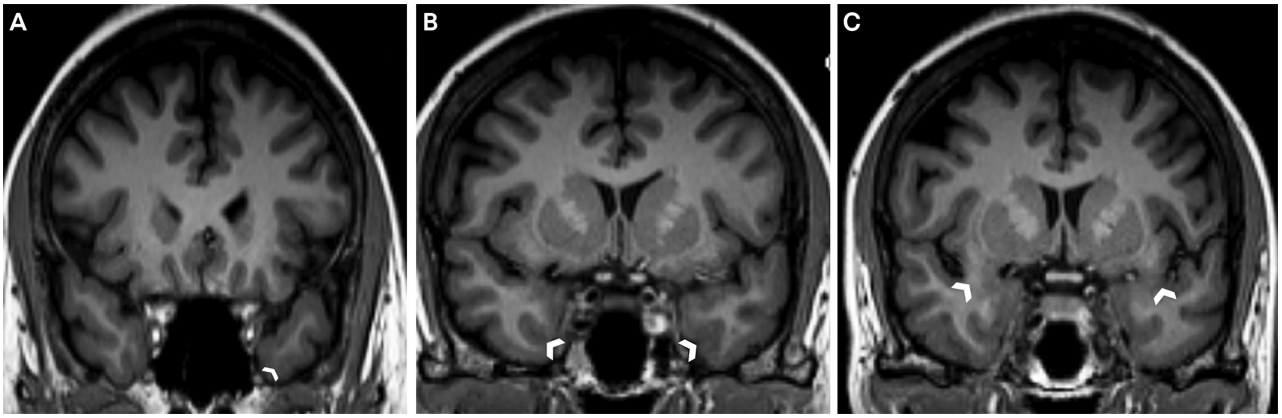

FIGURE 5-12

Temporal polar cortex landmarks shown in coronal MRI. The caudal boundary is the limen insulae and the perirhinal cortex; it is immediately rostral to the entorhinal cortex and the amygdala. *A*, Most anterior border of temporal polar cortex (*arrowhead*). *B*, Mid temporal polar cortex: perirhinal cortex and collateral sulcus (*arrowheads*). *C*, The appearance of limen insulae indicates the posterior margin of temporal polar cortex (*arrowheads*).

type I, temporal gliosis, and heterotopic neurons are frequently seen on histopathology equally in patients with hippocampal sclerosis with and without temporal polar cortex blurring. Therefore, seizures may cause this delayed myelination and arrest of white matter development before or near the age of 2 years.[61,62]

Interestingly, the temporal polar cortex undergoes slower myelination than other brain regions, particularly during the first 2 years of life, leading to potential vulnerability to insults to the temporal polar cortex during this period.[63]

Evaluating the temporal polar cortex is critical. It is the epileptogenic focus in some "MRI-negative temporal lobe epilepsy" cases. The temporal polar cortex is

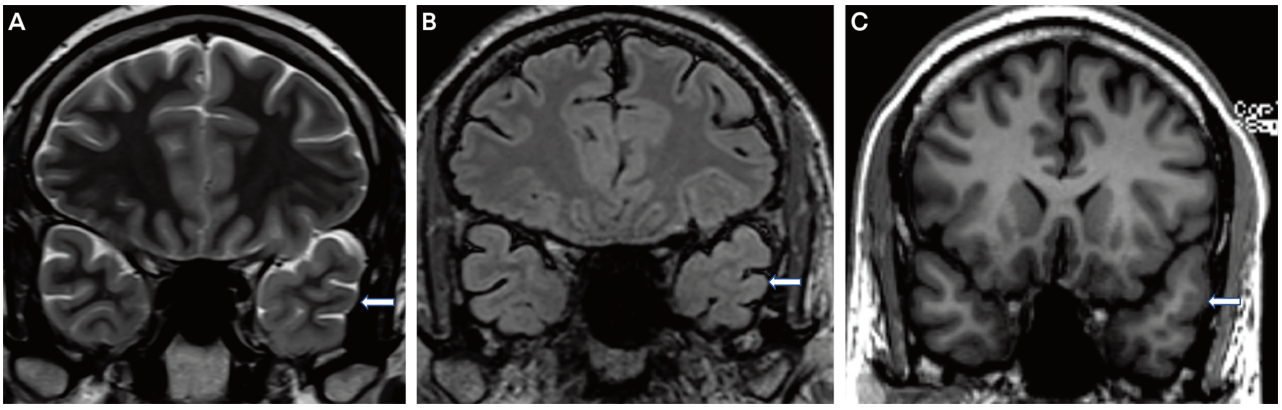

FIGURE 5-13

Left temporal pole blurring in a patient with hippocampal sclerosis and onset of seizures before the age of 2 years. On coronal T2-weighted (*A*) and fluid-attenuated inversion recovery (FLAIR) (*B*), the left temporal polar cortex white matter (*A, B, arrows*) is less well defined than the right. *C*, On coronal T1-weighted magnetization-prepared rapid gradient echo (MPRAGE), the gray-white matter boundary is distinct (*arrow*). In focal cortical dysplasia type II, however, the T1-weighted MRI would show cortical thickening and blurring of the gray-white matter junction (see FIGURE 5-14 and FIGURE 5-16).

Copyright © American Academy of Neurology. Unauthorized reproduction of this article is prohibited.

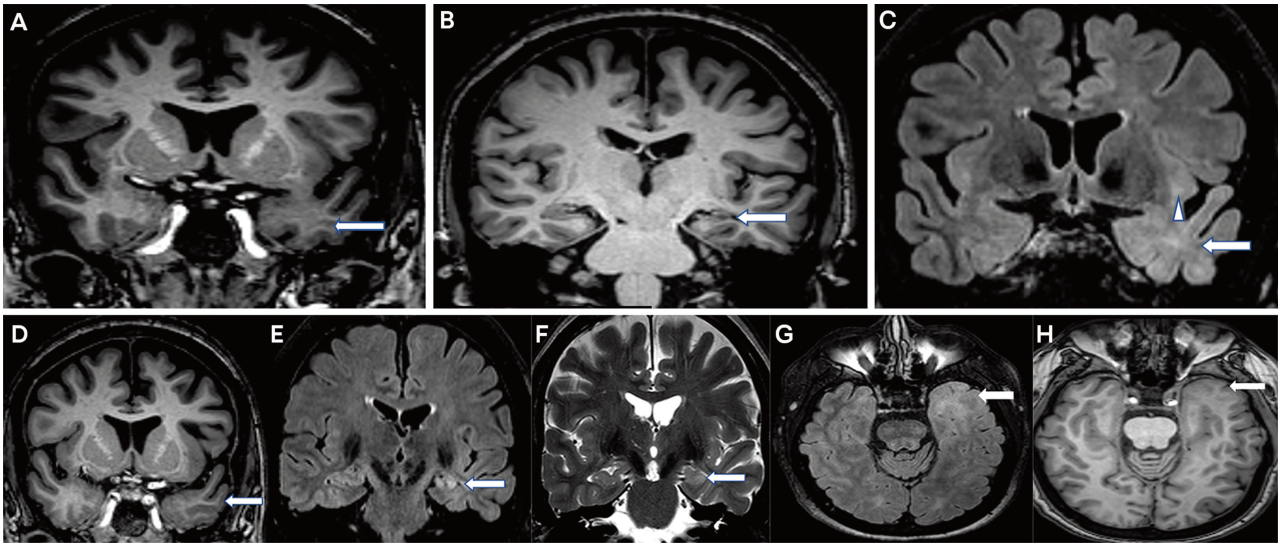

FIGURE 5-14

Temporal tip dysplasia accompanying left hippocampal sclerosis. *A*, Coronal T1-weighted magnetization-prepared rapid gradient echo (MPRAGE) shows grey matter isointense signal (*arrow*) in temporal polar cortex white matter. *B*, Coronal T1-weighted MPRAGE shows left hippocampal body atrophy with hypointense signal (*arrow*). *C*, Coronal three-dimensional fluid-attenuated inversion recovery (FLAIR) shows left temporal polar cortex atrophy (*arrow*) and blurring with indistinct gray-white matter boundary (*arrowhead*). *D*, Coronal T1-weighted MPRAGE shows left temporal polar cortex atrophy (*arrow*). *E*, Coronal FLAIR demonstrating T2-hyperintense signal (*arrow*) in the left hippocampus. *F*, Coronal T2-weighted fast spin echo also showing T2-hyperintense signal (*arrow*) in the left hippocampus. *G*, Axial FLAIR white matter hyperintense signal and gray-white matter blurring at the temporal pole (*arrow*). *H*, Axial T1-weighted MPRAGE with white matter blurring and indistinct gray-white matter boundary (*arrow*).

a critical hub that often presents with a typical automotor seizure phenomenology. However, the temporal polar cortex also produces hypermotor frontal seizure phenomenology or temporal-parietal-occipital EEG propagation patterns that confound localization.[64,65]

Amygdala

The amygdala should be evaluated for symmetry in size and signal intensity. The amygdala can be smaller in the setting of with hippocampal atrophy. Amygdalar atrophy accompanying hippocampal sclerosis is identified with volumetric analysis in 12% to 20% of patients with pathologically confirmed hippocampal sclerosis.[66,67]

The amygdala can also be abnormally enlarged, indicating amygdalar dysplasia, hamartoma, gliosis, or a low-grade neoplasm or developmental tumor.[68] In amygdalar enlargement, pathology findings include dysplasia with hypertrophic, clustered neurons, or astrocytic gliosis.[66,67]

Amygdala enlargement without hippocampal atrophy is often overlooked in "imaging-negative" temporal lobe epilepsy.[68] Amygdalar enlargement is best seen on three-dimensional coronal T1-weighted magnetization-prepared rapid gradient echo (MPRAGE) imaging and may not be associated with increased signal on FLAIR MRI. Accompanying enlargement of the uncus is best seen on axial T1-weighted MPRAGE and axial T2-weighted turbo fast spin echo along with blurring of the adjacent lateral entorhinal area.[66,67] Amygdalar enlargement can be accompanied by hippocampal head enlargement with or without

Copyright © American Academy of Neurology. Unauthorized reproduction of this article is prohibited.

KEY POINTS

- The amygdala can be abnormally enlarged in patients with epilepsy, indicating amygdalar dysplasia, hamartoma, gliosis, or a low-grade neoplasm or developmental tumor. In amygdalar enlargement, pathology findings include dysplasia with hypertrophic, clustered neurons or astrocytic gliosis.
- Malformations of cortical development are classified into three groups based on the main developmental stage affected, with consideration that alteration of early developmental events often affects later events.
- Malformations of cortical development account for the most common surgical pathologies in children and the third most common in adults undergoing epilepsy surgery, with focal cortical dysplasia representing almost 75% of all malformation of cortical development cases.

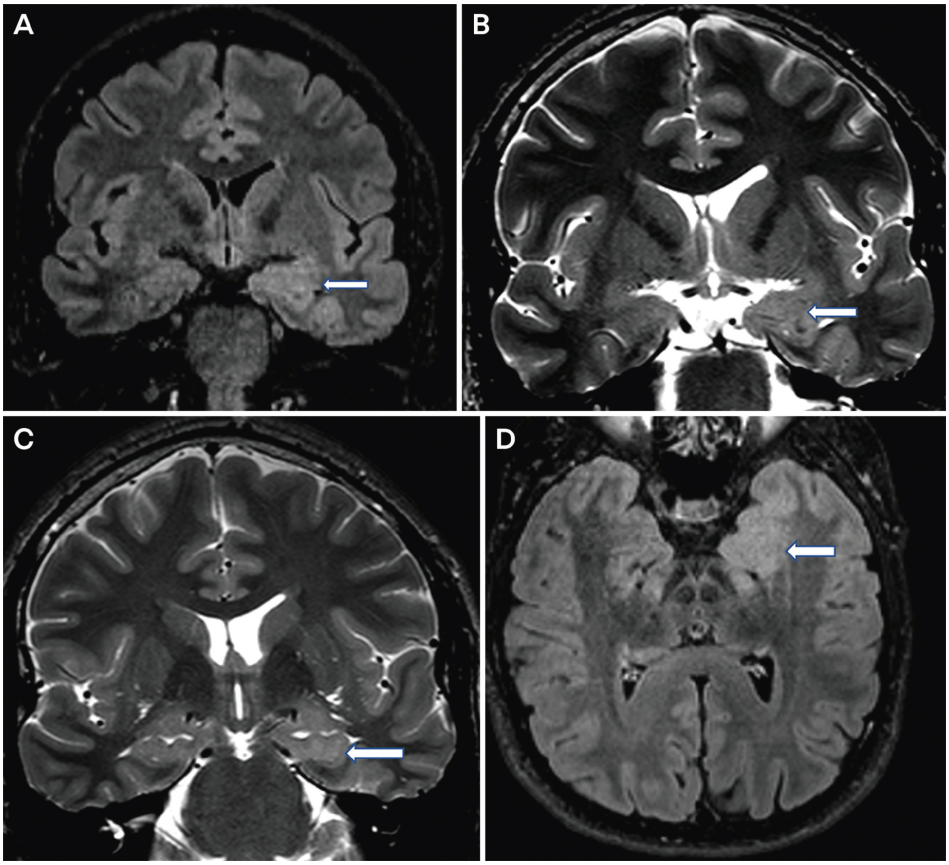

FIGURE 5-15
Amygdala and hippocampal enlargement. *A*, Coronal fluid-attenuated inversion recovery (FLAIR) shows the left amygdala is enlarged and T2 hyperintense (*arrow*). *B*, Coronal T2-weighted MRI also shows left amygdala T2 hyperintensity (*arrow*). *C*, The left hippocampal head shows T2 hyperintensity without atrophy and hippocampal head interdigitations (*arrow*). *D*, Axial FLAIR shows the left uncus and amygdala are enlarged (*arrow*). The temporal pole (*not shown*) is normal. The patient had epilepsy surgery at age 33 and has been seizure-free for 4 years.

accompanying T2 hyperintensity; in these cases, the uncal recess of the temporal horn, which separates the hippocampal head inferiorly and the cortical amygdala superiorly, is blurred (FIGURE 5-15).[66]

Distinguishing amygdalar enlargement from tumors such as low-grade glioma or a developmental tumor is essential. Usually, other features accompany tumors: (1) T1 hypointensity and cystic changes; (2) irregular margins; (3) extension into the white matter with blurring of the entorhinal cortex; and (4) nonconfluent variable T1 or T2 signal intensities, a peripheral hypointense nodule, and occasionally contrast enhancement. However, isolated amygdalar enlargement has confluent T1 isointense gray matter or confluent T2 hyperintensity on FLAIR and T2-weighted turbo fast spin echo as illustrated by CASE 5-6.[66,67]

MALFORMATIONS OF CORTICAL DEVELOPMENT

Malformations of cortical development result from disruption of three major stages of cortical development: cell proliferation and apoptosis, cell migration, and postmigration development. Malformations of cortical development are

Copyright © American Academy of Neurology. Unauthorized reproduction of this article is prohibited.

classified into these three main groups based on the main developmental stage in which it is first affected, with consideration that alteration of early developmental events often affects later events (TABLE 5-5).[69,70]

Based on the three stages, malformations of cortical developments are classified in TABLE 5-5. The first category consists of reduced proliferation of neurons (microcephaly, shown in FIGURE 5-17) and increased proliferation (hemimegalencephaly).

Malformations of cortical development account for the most common epilepsy surgery pathologies in children and are the third most common in adults, with focal cortical dysplasia representing almost 75% of all malformation of cortical development cases.[49]

In 2017, Blumcke and colleagues[49] examined resected brain specimens collected over 25 years from approximately 10,000 patients who underwent epilepsy surgery and reported hippocampal sclerosis as the most common histopathologic diagnosis among adults and focal cortical dysplasia as the most common diagnosis among children. Tumors (mainly ganglioglioma) were the second most common lesion in both groups. When evaluating malformations of

CASE 5-6

A 57-year-old man had drug-resistant epilepsy since the age of 36. He had undergone left anteromedial temporal resection at the age of 47 and had been seizure free since. The preoperative MRI performed with epilepsy protocol showed amygdalar, hippocampal, and medial temporal polar dysplasia (FIGURE 5-16).

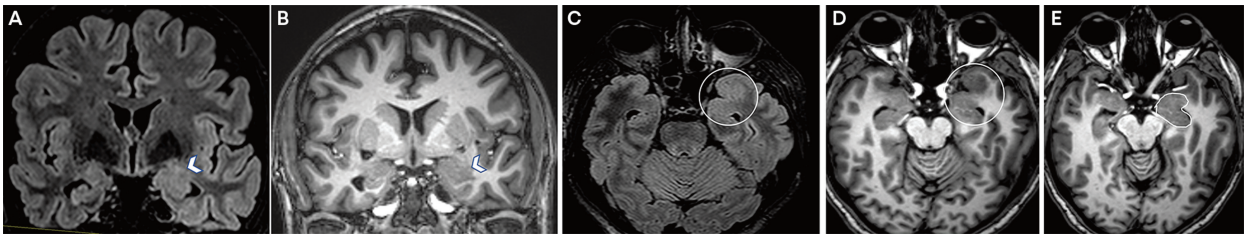

FIGURE 5-16
Amygdalar enlargement and temporal tip cortical dysplasia in the patient in CASE 5-6. *A*, Coronal T2-weighted fluid-attenuated inversion recovery (FLAIR) showing a T2-hyperintense amygdala with blurring of the uncal recess of the temporal horn. *B*, Coronal T1-weighted magnetization-prepared rapid gradient echo (MPRAGE) also shows an enlarged amygdala with an indistinct uncal recess of the temporal horn (*arrowheads* in panels *A* and *B*). Axial FLAIR (*C*) and T1-weighted (*D*) MRI show cortical thickening in the left medial temporal pole (*white outline* in panels *C* and *D*). *E*, Axial T1-weighted MRI shows the left amygdala and temporal uncus are enlarged (*white outline*). Pathology showed amygdalar, hippocampal, and temporal tip dysplasia.

COMMENT

Clinicians should always look beyond the hippocampus, such as in the temporal polar cortex and the amygdala, for abnormalities. Unilateral amygdalar enlargement can falsely appear as contralateral atrophy. Early epilepsy protocol MRI identified this patient as a surgical candidate, preventing further delay to surgical cure of his epilepsy.

Copyright © American Academy of Neurology. Unauthorized reproduction of this article is prohibited.

cortical development on MRI, one must carefully evaluate the cortical gyri and sulci for deviation from normal patterns.

Focal Cortical Dysplasias

Focal cortical dysplasia classified as type I (a through c) is characterized by abnormal neuron distribution that can occur in one of the following patterns: (1) columnar/radial (Ia); (2) laminar/tangential (Ib), or (3) both (Ic).[71] Focal cortical dysplasia type I is usually occult on imaging. However, lobar hypoplasia or atrophy, unusual sulcal patterns, and lack of subcortical myelination have been described for focal cortical dysplasia type I.[72,73]

Multimodality imaging with fludeoxyglucose positron emission tomography (FDG-PET) MRI fusion, subtraction ictal single-photon emission computerized tomography (SPECT) coregistered to MRI (SISCOM), or magnetoencephalography (MEG) can enhance the detection of focal cortical dysplasia type I.[74]

Focal cortical dysplasia type II has been described as a "bottom-of-sulcus dysplasia": focal cortical dysplasia with dysplastic features maximal at the sulcal

TABLE 5-5 **Classification of Malformations of Cortical Development[a]**

- **I Malformations due to abnormal neuronal and glial proliferation or apoptosis**
  - **A** Abnormalities of brain size (decreased proliferation or increased apoptosis, or increased proliferation or decreased apoptosis)
    - **1** Microcephaly with normal to thin cortex
    - **2** Microlissencephaly (extreme microcephaly with thick cortex)
    - **3** Microcephaly with extensive polymicrogyria
    - **4** Macrocephalies
  - **B** Abnormal proliferation (abnormal cell types)
    - **1** Non-neoplastic
      - **a** Cortical hamartomas of tuberous sclerosis
      - **b** Cortical dysplasia with balloon cells
      - **c** Hemimegalencephaly
    - **2** Neoplastic (associated with disordered cortex)
      - **a** Dysembryoplastic neuroepithelial tumor (DNET)
      - **b** Ganglioglioma
      - **c** Gangliocytoma
- **II Malformations due to abnormal neuronal migration**
  - **A** Lissencephaly or subcortical band heterotopia spectrum
  - **B** Cobblestone complex and congenital muscular dystrophy syndromes

CONTINUED ON PAGE 127

Copyright © American Academy of Neurology. Unauthorized reproduction of this article is prohibited.

depth, tapering to a relatively normal gyral crown as illustrated in CASE 5-4 and CASE 5-5 (FIGURE 5-4, FIGURE 5-5, and FIGURE 5-18).[2,3,43,70] Bottom-of-sulcus dysplasias are characterized by neuronal dyslamination and dysmorphology at the bottom of the sulcus with hypomyelination in the underlying white matter on pathology (focal cortical dysplasia type IIa without balloon cells and focal cortical dysplasia type IIb with balloon cells) (see TABLE 5-6 and TABLE 5-7[75] for focal cortical dysplasia classification).[43,70] A cleft dimple complex can also be a clue to identifying a focal cortical dysplasia. It is defined as the cortex buckling inward, away from the brain surface, with a prominent space between the cortex and leptomeninges (cleft and dimple) as illustrated by CASE 5-1 (FIGURE 5-1).[76]

Focal cortical dysplasia type IIa and type IIb are associated with germline mutations in the mammalian target of rapamycin (mTOR) pathway. These mutations include but are not limited to *DEPDC5*, *NPRL2*, and *NPRL3* mutations and, in some cases, can be associated with multiple cortical dysplasias, some of which are MRI occult.[77,78] Focal cortical dysplasias in patients who have undergone epilepsy surgery can have somatic mutations in the dysplastic tissue.[75,79]

CONTINUED FROM PAGE 126

- **C** Heterotopia
  - **1** Subependymal (periventricular)
  - **2** Subcortical (other than band heterotopia)
  - **3** Marginal glioneuronal

III Malformations due to abnormal cortical organization (including late neuronal migration)

- **A** Polymicrogyria and schizencephaly
  - **1** Bilateral polymicrogyria syndromes
  - **2** Schizencephaly (polymicrogyria with clefts)
  - **3** Polymicrogyria or schizencephaly as part of multiple congenital anomaly developmental delay
- **B** Cortical dysplasia without balloon cells
- **C** Microdysgenesis

IV Malformations of cortical development, not otherwise classified

- **A** Malformations secondary to inborn errors of metabolism
  - **1** Mitochondrial and pyruvate metabolic disorders
  - **2** Peroxisomal disorders
- **B** Other unclassified malformations
  - **1** Sublobar dysplasia
  - **2** Others

[a] Reprinted with permission from Colombo N, et al, Neuroradiology.[70] © 2012 Springer-Verlag.

Copyright © American Academy of Neurology. Unauthorized reproduction of this article is prohibited.

KEY POINTS

- Focal cortical dysplasia type II has been described as a "bottom-of-sulcus dysplasia" resulting from dysplastic features maximal at the sulcal depth, tapering to a relatively normal gyral crown.
- A cleft dimple complex can be a clue to identifying a focal cortical dysplasia. It is defined as the cortex buckling inward, away from the brain surface, with a prominent space between the cortex and leptomeninges (cleft and dimple).
- Focal cortical dysplasia type IIa and type IIb are associated with germline mutations in the mammalian target of rapamycin (mTOR) pathway. These mutations include but are not limited to *DEPDC5*, *NPRL2*, and *NPRL3* mutations and, in some cases, can be associated with multiple cortical dysplasias, some of which are MRI occult.
- Grey matter nodular heterotopia refers to a collection of neurons in an abnormal location such as the subcortical white matter and subependymal region or under normal-appearing cortex in a laminar pattern. On MRI, the lesions are gray matter isointense on both T1- and T2-weighted sequences.

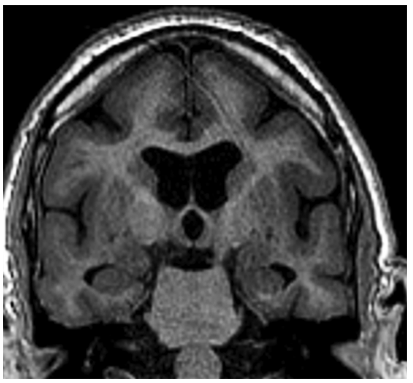

FIGURE 5-17
Microcephaly with a simplified gyral pattern. Note the broad gyri and the simplified pattern of the gyri and sulci on coronal T1-weighted MRI.

Focal cortical dysplasia type III is a focal cortical dysplasia type I with an additional lesion in the same lobe and is classified as follows: IIIa (with hippocampal sclerosis); IIIb (with tumor); IIIc (with vascular malformation); and IIId (lesion acquired early in life, eg, glial scar due to infectious or ischemic injury).[58]

Focal cortical dysplasia type II, however, when seen with hippocampal sclerosis, is referred to as *dual pathology* (as noted earlier) because the two lesions likely reflect distinct pathologic processes (TABLE 5-6 and TABLE 5-7).[58]

Hemimegalencephaly

Hemimegalencephaly is an abnormally large lobe, multiple lobes, or hemisphere

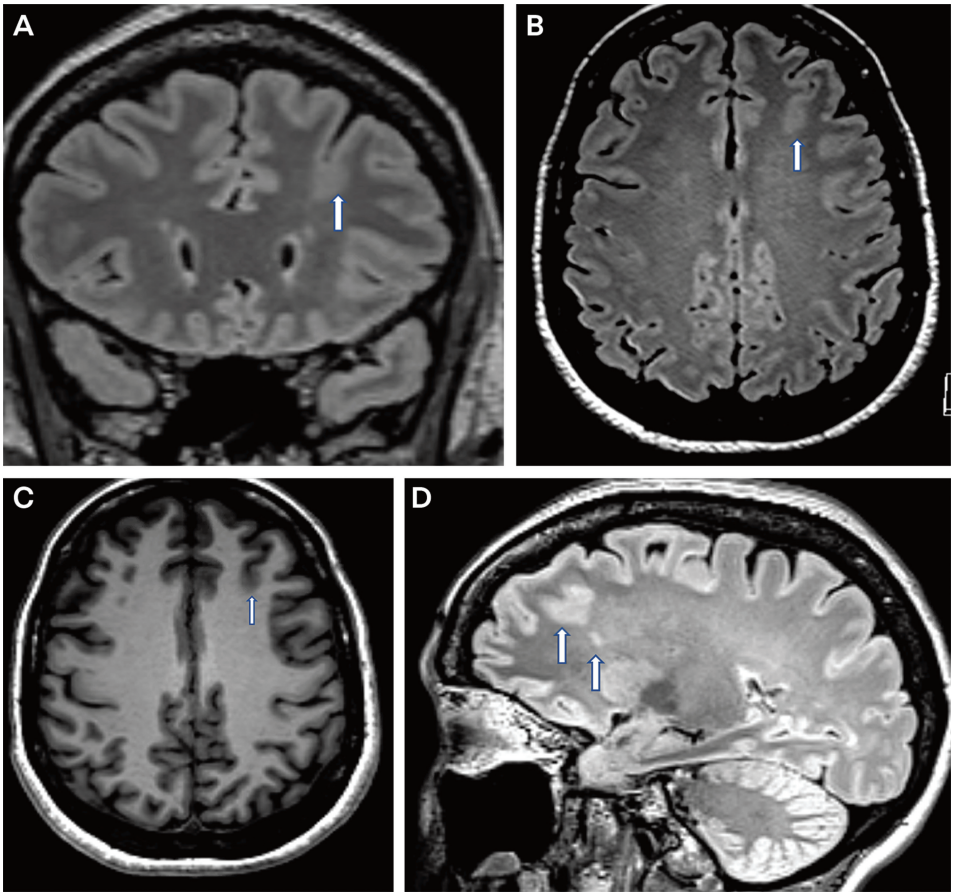

FIGURE 5-18
Focal cortical dysplasia type II at the left superior frontal sulcus. Coronal fluid-attenuated inversion recovery (FLAIR) (*A*), axial FLAIR (*B*), and axial T1-weighted magnetization-prepared rapid gradient echo (MPRAGE) (*C*), demonstrating dysplasia at the bottom of the sulcus (*A, B, C, arrows*). Sagittal FLAIR (*D*) demonstrating dysplasia (*upper arrow*) and transmantle sign (*lower arrow*).

Copyright © American Academy of Neurology. Unauthorized reproduction of this article is prohibited.

caused by marked dysplasia (FIGURE 5-19).[80] Imaging findings include large clumps of gray matter that extend from the pial surface to the ventricle. The white matter shows increased signal on T2-weighted images. The dysplastic hemisphere often shows ventricular enlargement.

Gray Matter Heterotopias

Gray matter nodular heterotopia refers to a collection of neurons in an abnormal location: (1) subcortical white matter; (2) subependymal region (periventricular); or (3) under the normal-appearing cortex in a laminar pattern (FIGURE 5-20 and FIGURE 5-21).[45,69,73,75]

The heterotopias can extend from the ventricle wall to the cortical surface (known as *transmantle heterotopia*).[69] On MRI, the lesions are gray matter isointense on both T1- and T2-weighted sequences.[45,69] They have been associated with mutations 22q11.2 and mutations in *FLNA*.[75]

Current Classification of Focal Cortical Dysplasia[a] TABLE 5-6

Type of focal cortical dysplasia	Histologic characteristics	MRI features
Ia	Abnormal radial cortical lamination	Mild hemispheric hypoplasia, areas with thin cortex, blurring of the gray-white matter junction, abnormally shaped sulci and sometimes deep sulci; MRI results are often negative and MRI cannot differentiate these subtypes
Ib	Abnormal tangential cortical lamination	
Ic	Abnormal radial and tangential cortical lamination	
IIa	Dysmorphic neurons without balloon cells	Gradient of morphologic changes: from dysplastic lesions that can be easily identified by conventional MRI techniques to minor structural abnormalities, including small areas of discrete cortical thickening or blurring of the gray-white matter interface that often go unrecognized; sometimes subtle hyperintense T2 signal in the subcortical and deep white matter
IIb	Dysmorphic neurons with balloon cells	Increased T2 or fluid-attenuated inversion recovery (FLAIR) signal in the subcortical white matter underneath the focal cortical dysplasia, transmantle sign (tapering of abnormal white matter signal from cortex to ventricle surface), blurring of the gray-white matter junction, increased cortical thickness, deep sulci, abnormal cortical gyration and sulcation
IIIa	Architectural abnormalities associated with hippocampal sclerosis	Variable combination of MRI features of focal cortical dysplasia described above and the associated lesion that is most frequently in the same lobe or region
IIIb	Architectural abnormalities adjacent to tumors	
IIIc	Architectural abnormalities adjacent to vascular malformation	
IIId	Architectural abnormalities adjacent to lesions acquired early in life (ie, trauma, ischemic injury, encephalitis)	

MRI = magnetic resonance imaging.
[a] Reprinted with permission from Blümcke I, et al, Epilepsia.[58] © 2011 International League Against Epilepsy.

Copyright © American Academy of Neurology. Unauthorized reproduction of this article is prohibited.

Subcortical band heterotopia's "double cortex" consists of gray matter that lines the subcortical white matter parallel to the adjacent neocortex. One also observes reduced sulcation (pachygyria) (FIGURE 5-22).[45] Subcortical band heterotopia is considered a lissencephaly spectrum disorder based on its etiology and genetics.[45]

Lissencephaly

Lissencephaly, or "smooth brain," is caused by impaired neuronal migration resulting in agyria with no cortical convolutions (FIGURE 5-22). MRI of lissencephaly shows a thick cerebral cortex associated with reduced gyration. When agyria has occurred, the most severe but rare phenotype, the brain has a figure-eight shape due to a complete absence of sulci and wide, vertically oriented sylvian fissures.[45,81]

More commonly, a few shallow sulci are seen, subdividing the cortex into broad, coarse gyri and leading to the appearance of pachygyria. Lissencephaly is often bilateral and symmetric,[45] and it is classified based on its severity, gyral malformation, cortical thickness, and presence of associated brain malformations.[81]

Polymicrogyria

Polymicrogyria consists of an excessive number of small gyri with shallow sulci. Polymicrogyria can be (1) focal and limited; (2) focal, unilateral, and extensive;

TABLE 5-7 **Proposed Amendments to Focal Cortical Dysplasia Classification Scheme[a]**

Focal cortical dysplasia type	Subtypes			
I	Ia: vertical microcolumns	Ib: abnormal layering	Ic: vertical and horizontal abnormalities	
II	IIa: dysmorphic neurons	IIb: dysmorphic neurons and balloon cells		
III	IIIa: cortical dyslamination associated with hippocampal sclerosis	IIIb: cortical dyslamination adjacent to brain tumor	IIIc: cortical dyslamination adjacent to vascular malformation	IIId: cortical dyslamination adjacent to lesion acquired during early life (eg stroke)
White matter lesions	Mild malformation of cortical development[b] with excessive heterotopic neurons	Mild malformation of cortical development with oligodendroglial hyperplasia in epilepsy		
No focal cortical dysplasia	When histopathologic findings are not compatible with focal cortical dysplasia type I, II, or III[c]			

[a] Reprinted with permission from Blümcke I, et al, Epilepsia.[75] © 2021 The Authors.
[b] Mild malformation of cortical development not associated with any other principal lesions, such as hippocampal sclerosis, brain tumor, or vascular malformation.[53-56]
[c] No focal cortical dysplasia: a descriptive report is recommended to highlight anatomic ambiguities (if applicable).

Copyright © American Academy of Neurology. Unauthorized reproduction of this article is prohibited.

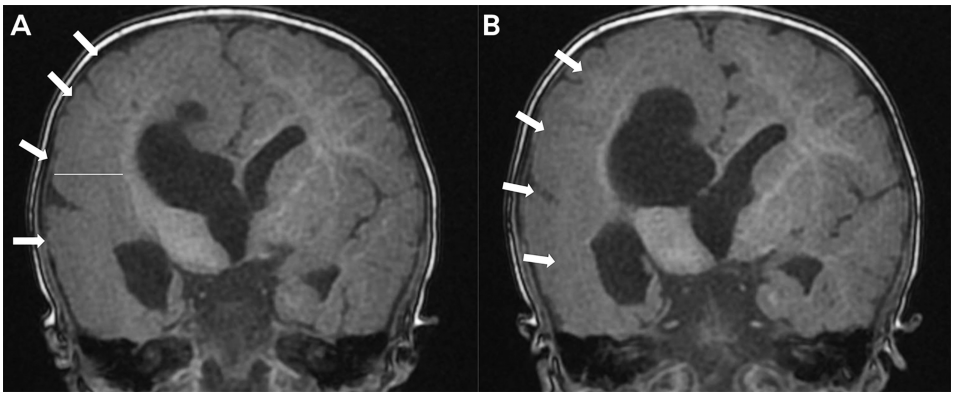

FIGURE 5-19
Hemimegalencephaly. A 12-month-old girl with drug-resistant epilepsy and right hemisphere hemimegalencephaly with diffusely thickened cortex and pachygyria. The white matter is not well defined in this study because myelination is not complete until the age of 24 months. Note the thickness of the gray matter (*white line*) of the right hemisphere and loss of normal sulcation (*arrows*) shown in coronal T1-weighted MRI.

KEY POINT

- Polymicrogyria consists of an excessive number of small gyri with shallow sulci. Polymicrogyria can be (1) focal and limited; (2) focal, unilateral, and extensive; (3) bilateral and symmetric; (4) bilateral and asymmetric; (5) multifocal; or (6) diffuse. MRI shows numerous small gyri with shallow sulci, and the cortical-subcortical junction is often irregular.

(3) bilateral and symmetric (FIGURE 5-23); (4) bilateral and asymmetric; (5) multifocal; or (6) diffuse.[45,69,73] MRI shows numerous small gyri with shallow sulci (FIGURE 5-23). The cortical-subcortical junction is often irregular.[73]

Cobblestone Malformation

On MRI, cobblestone malformations are characterized by reduced sulci on the cerebral surface, a mildly to moderately thickened cortex, and a jagged cortical–white matter border with frequent vertical (perpendicular to the cortical-white matter border) striations. This cortical malformation is usually bilateral and symmetric, often involving the entire brain or large areas of the cerebral hemispheres with an anterior (more frequently) or posterior predominance.[45,69,73] Overmigration of neurons creates "gaps" (holes) in the pia.

Schizencephaly

Schizencephaly consists of a CSF cleft extending from the subarachnoid space to the lateral ventricle.[45,69,73] Dysgyric cortex or polymicrogyria lines the cleft

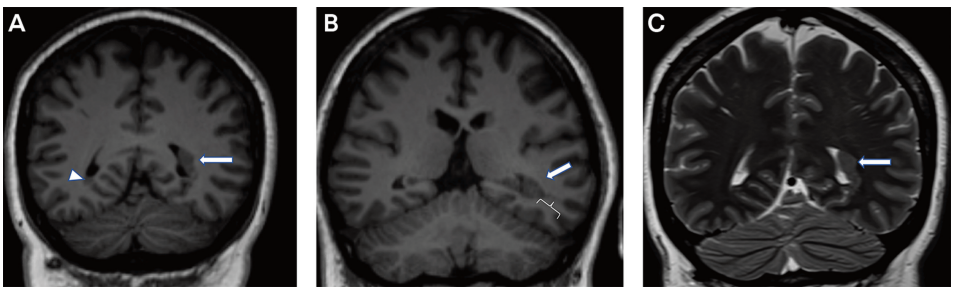

FIGURE 5-20
Periventricular and subcortical nodular heterotopia. *A*, Coronal T1-weighted MRI shows bilateral nodular heterotopia at the left (*arrow*) more than the right (*arrowhead*) occipital horns of the lateral ventricles that are isointense to gray matter. *B*, Nodular heterotopia (*arrow*) in the left temporal horn of the lateral ventricle on coronal T1-weighted MRI. Note the wisp of isointense gray matter extending to the cortical surface (*bracket*). *C*, Coronal T2-weighted MRI shows gray matter–isointense ventricular nodular heterotopia (*arrow*) in the left occipital trigone.

Copyright © American Academy of Neurology. Unauthorized reproduction of this article is prohibited.

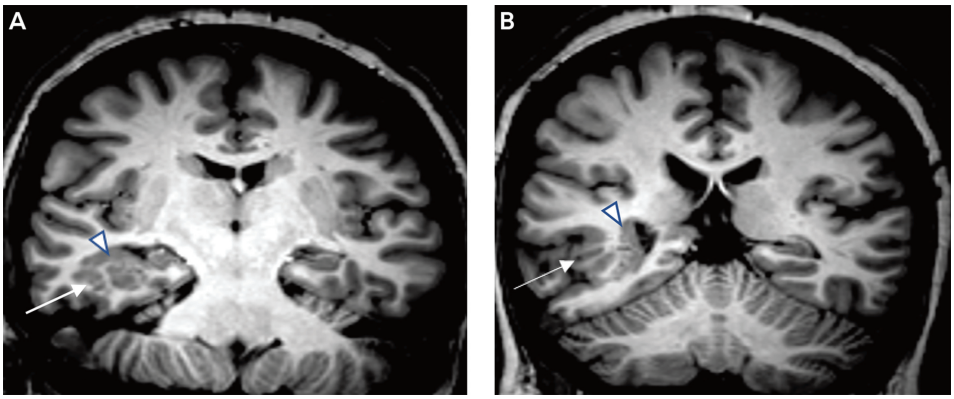

FIGURE 5-21
Heterotopias. Coronal T1-weighted magnetization-prepared rapid gradient echo (MPRAGE) MRI shows nodular heterotopias in the right temporal horn of the lateral ventricle (*A, arrowhead*) and nodular subcortical heterotopias (*A, arrow*) and nodular heterotopias at right posterior temporal horn of the lateral ventricle (B, arrowhead) and dysgyric cortex (*B, arrow*).

wall (FIGURE 5-23). The lips of the cleft can be closed (type 1) or open (type 2). The most common location is the posterior perisylvian cortex. Two-thirds of cases are unilateral, and one-third are bilateral.[45,69,73,75]

Dysgyria

Dysgyria is a recently introduced term referring to a nonspecific malformation in which the cortex is dysmorphic. The mechanisms of dysgenesis are not fully understood and, in some cases, are associated with tubulin mutations.[82] Imaging shows normal cortical thickness but an abnormal gyral pattern characterized by sulcal depth and orientation abnormalities, with a smooth cortical surface and radially oriented sulci, or narrow gyri separated by abnormally deep or shallow sulci (FIGURE 5-24).[45,83]

Mild Malformation of Cortical Development With Oligodendroglial Hyperplasia and Epilepsy

Mild malformation of cortical development with oligodendroglia hyperplasia and epilepsy is a newly described, rare histopathologic entity detected in resected brain tissue of patients with refractory epilepsies. MRI shows gyral and sulcal morphology changes, mild cortical thickening, slight T2 increased signal intensity in the subcortical white matter, mild cortical-subcortical blurring, and laminar T2 white matter hyperintensity at the corticomedullary junction (FIGURE 5-25).[84,85]

Histologically, mild malformations of cortical development with oligodendroglial hyperplasia and epilepsy are characterized by blurred gray-white matter boundaries with increased numbers of heterotopic neurons in the subcortical white matter and increased density of oligodendroglia.[82,85] Some cases are associated with *SLC35A2* mutations.[85]

LONG-TERM-EPILEPSY–ASSOCIATED TUMORS

In patients with intractable epilepsy treated with epilepsy surgery, neoplasms account for approximately 22% of cases, with long-term-epilepsy–associated tumors accounting for the majority and ganglioglioma the most common.[49,79,86,87] Their histologic appearance can be variable with dysplastic

Copyright © American Academy of Neurology. Unauthorized reproduction of this article is prohibited.

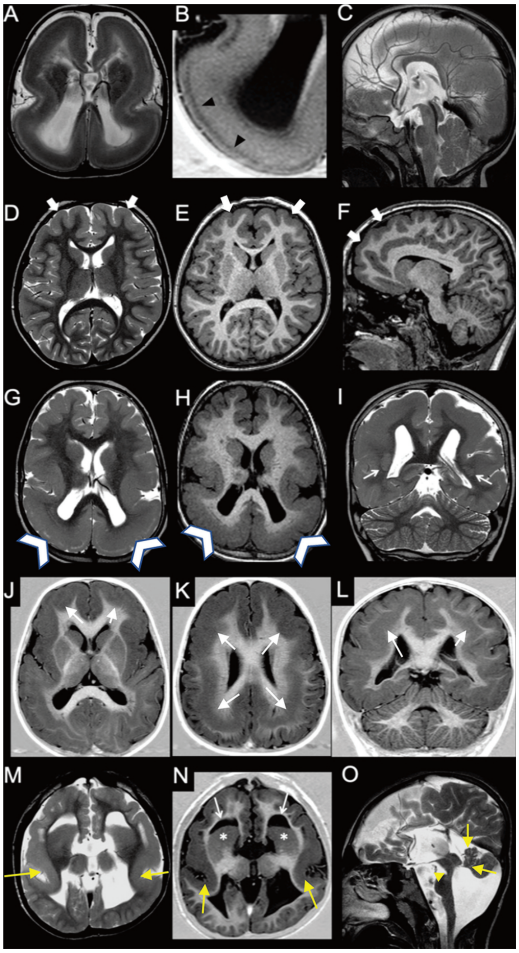

FIGURE 5-22
Imaging characteristics of lissencephaly. Axial T2-weighted MRI (*A*), magnification of axial T1-weighted MRI (*B*, *black arrowhead*, smooth cortex), and sagittal T2-weighted MRI (*C*) show lissencephaly with a *PAFAH1B1* mutation. Axial T2-weighted MRI (*D*), axial T1-weighted MRI (*E*), and sagittal T1-weighted MRI (*F*) from a patient with pachygyria of both frontal lobes with a simplified gyral pattern (*D*, *E*, *F*, *arrows*). Axial T2-weighted MRI (*G*), axial T1-weighted MRI (*H*), and coronal T2-weighted MRI (*I*) show posterior pachygyria with a lissencephaly appearance posteriorly in a patient with a *PAFAH1B1* mutation. Note the minimal to absent cortical sulci (*G*, *H*, *arrowheads*) and subcortical heterotopia (*I*, *arrows*). Axial T1-weighted MRI (*J*), axial T1-weighted MRI (*K*), and coronal T1-weighted MRI (*L*) from a patient with a bilateral subcortical band heterotopia with *DCX* mutation that appears as a "double cortex" (*J*, *K*, *L*, *arrows*). Axial T2-weighted (*M*) and T1-weighted (*N*) MRI shows bilateral perisylvian pachygyria (*M*, *N*, *yellow arrows*) due to a *TUBA4A* (tubulin) mutation. Sagittal T2-weighted MRI shows dysmorphic basal ganglia (*N*, *asterisks*), and frontal horns (*N*, *white arrows*) that seem to wrap around the caudate heads are typical of tubulinopathies. Associated vermian hypoplasia (*O*, *arrows*) with a dysmorphic brainstem (*O*, *arrowhead*) is also seen.
Reprinted with permission from Severino M, et al, Brain.[45] © 2020 Oxford University Press.

KEY POINTS

- **In patients with intractable epilepsy treated with epilepsy surgery, neoplasms account for approximately 22% of cases, with long-term-epilepsy–associated tumors accounting for the majority and ganglioglioma the most common.**
- **Long-term-epilepsy–associated tumors most commonly occur in the temporal lobe with a mean age of 16 years at seizure onset. They can be associated with focal cortical dysplasia type 1 with cortical disorganization in 80% of patients with long-term-epilepsy–associated tumors and type II cortical dysplasia in 11%.**

neurons and glial neoplasia and are classified as glioneuronal tumors by the World Health Organization (WHO). Long-term-epilepsy–associated tumors most commonly occur in the temporal lobe with a mean age of 16 years at seizure onset.[49,79,86] They can be associated with focal cortical dysplasia (type IIIb) with frequent cortical disorganization in 80% of patients, with long-term-epilepsy–associated tumors and focal cortical dysplasia type II in 11%.[88] Unlike infiltrating gliomas, they do not have *IDH1* mutations or 1p/19q deletions. However, oncofetal markers are frequently seen, such as CD34, and mutations in *BRAF* or mTOR signaling have also been identified. At times, these lesions are missed because often they do not enhance with contrast and are confused with alternative diagnoses, resulting in delayed referral for surgery up to 12 years.[86]

Glioneuronal Tumors

Glioneuronal tumors are commonly associated with epilepsy and are most often located in the temporal lobe, although not exclusively. They

Copyright © American Academy of Neurology. Unauthorized reproduction of this article is prohibited.

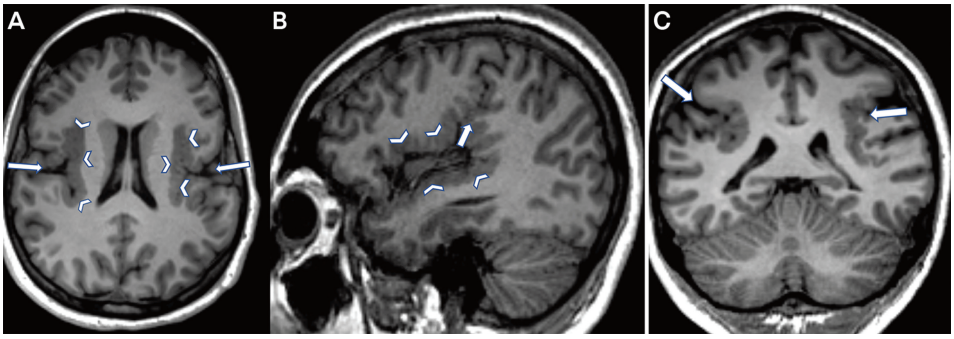

FIGURE 5-23
Axial (*A*), sagittal (*B*), and coronal (*C*) T1-weighted MRI shows bilateral closed-lip schizencephaly lined with polymicrogyria (*A, B, C, arrows*) accompanied by bilateral perisylvian insular polymicrogyria (*A, B, arrowheads*).

are most commonly seen in children and adults younger than the age of 30.[49,79,86]

GANGLIOGLIOMAS. Gangliogliomas are most commonly seen in the temporal lobe. The majority (80%) are found in children and young adults younger than the age of 30. More than 75% of gangliogliomas arise in the temporal lobe and 10% in the frontal lobe.[89] Gangliogliomas are usually located peripherally at the cortex with a mural nodule that often enhances and can diffusely infiltrate with ill-defined borders. Gangliogliomas are calcified 30% to 50% of the time. They are hypointense to isointense on T1-weighted imaging and hyperintense on FLAIR imaging, usually with no surrounding edema. Enhancement is variable from none to minimal to moderate. The typical pattern is a cystic lesion with an enhancing mural nodule (FIGURE 5-26). These lesions can be associated with cortical dysplasia, usually focal cortical dysplasia type IIIb.[79,83]

DYSEMBRYOPLASTIC NEUROEPITHELIAL TUMORS. Dysembryoplastic neuroepithelial tumors (DNETs) are benign low-grade, multicystic cortically based tumors and

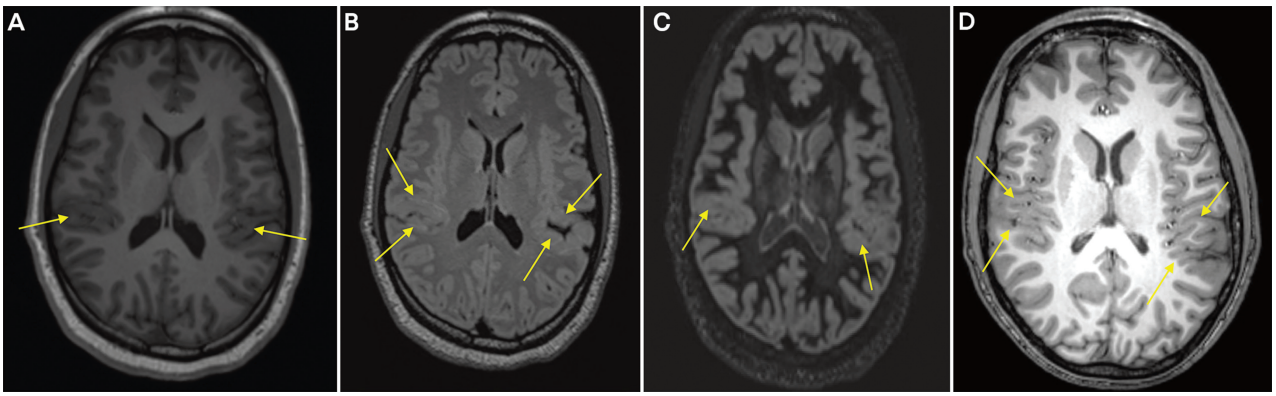

FIGURE 5-24
Dysgyria. Axial T1-weighted MRI (*A*), fluid-attenuated inversion recovery (FLAIR) (*B*), and T2-weighted double inversion recovery (*C*) show bilateral dysgyria (*arrows*) in a woman with epilepsy. *D*, Axial T1-weighted MRI from a different patient with drug-resistant epilepsy with myoclonic seizures and a *KCNMA1* mutation (*arrows*).

Copyright © American Academy of Neurology. Unauthorized reproduction of this article is prohibited.

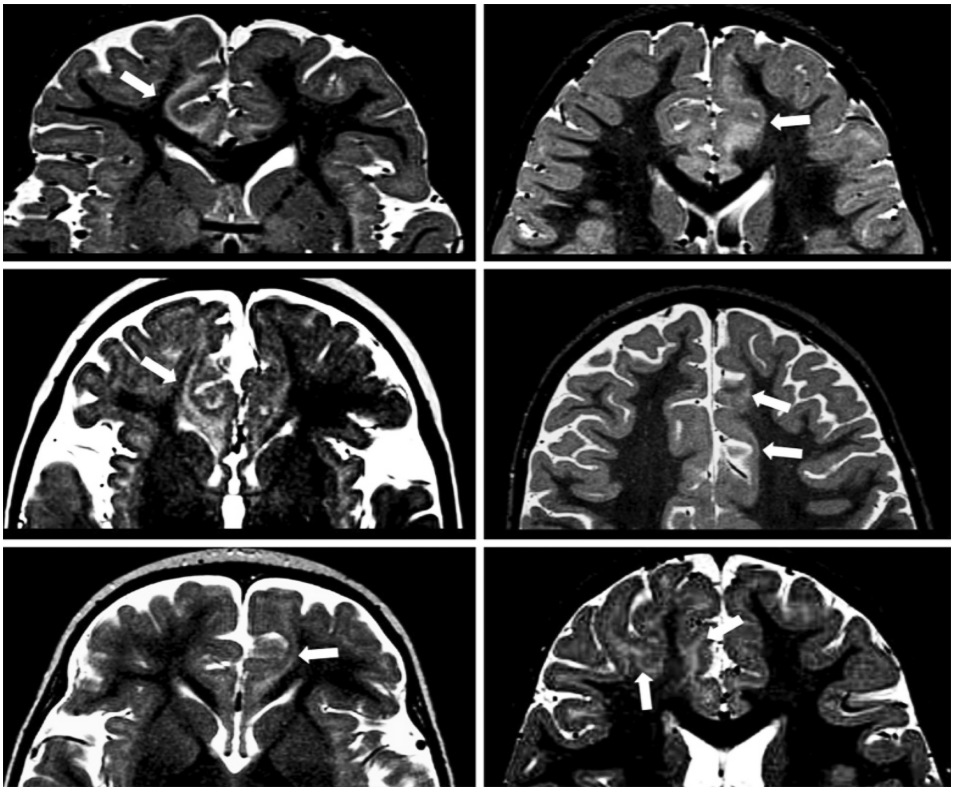

FIGURE 5-25

Mild malformation of cortical development with microglial hyperplasia and epilepsy. Axial T2-weighted MRI showing mild malformation of cortical development with microglial hyperplasia and epilepsy. This is often underrecognized. Note the laminar T2 hyperintensity at the corticomedullary junction (*arrows*).

Reprinted with permission from Hartlieb T, et al, Epilepsy Behav.[82] © 2019 Elsevier Inc.

are commonly associated with cortical dysplasia.[89] Between 45% and 50% are located in the temporal lobes, and one-third occur in the frontal lobes. They are mostly seen in children and young adults. MRI (both T1- and T2-weighted) shows a characteristic "pseudocystic" or "bubbly" appearance on MRI. FLAIR imaging reveals hyperintensity relative to the cortex, which is even more hyperintense at the tumor rim as illustrated in CASE 5-2 (FIGURE 5-2). Focal bony scalloping or calvarial remodeling is common. Peritumoral edema is usually absent. DNETs show minimal to no enhancement, and when they do enhance, they have a punctate or a mild nodular pattern. MRI can show a hypointense nodule at the neocortex on T1-weighted images (FIGURE 5-27). Cortical dysplasia occurs in 20% to 30% of these tumors; usually, focal cortical dysplasia type IIIb and type II are much less common.[79,88]

Pleomorphic Xanthoastrocytoma

Pleomorphic xanthoastrocytomas are superficial tumors involving the cortex adjacent to the leptomeninges with an enhancing mural nodule.[89] The solid portion of the pleomorphic xanthoastrocytoma is heterogeneously T1 hypointense or isointense to the cortex. The cystic portion of the pleomorphic xanthoastrocytoma is usually hyperintense relative to CSF on T2-weighted and FLAIR MRI. More than 90% of pleomorphic xanthoastrocytomas

Copyright © American Academy of Neurology. Unauthorized reproduction of this article is prohibited.

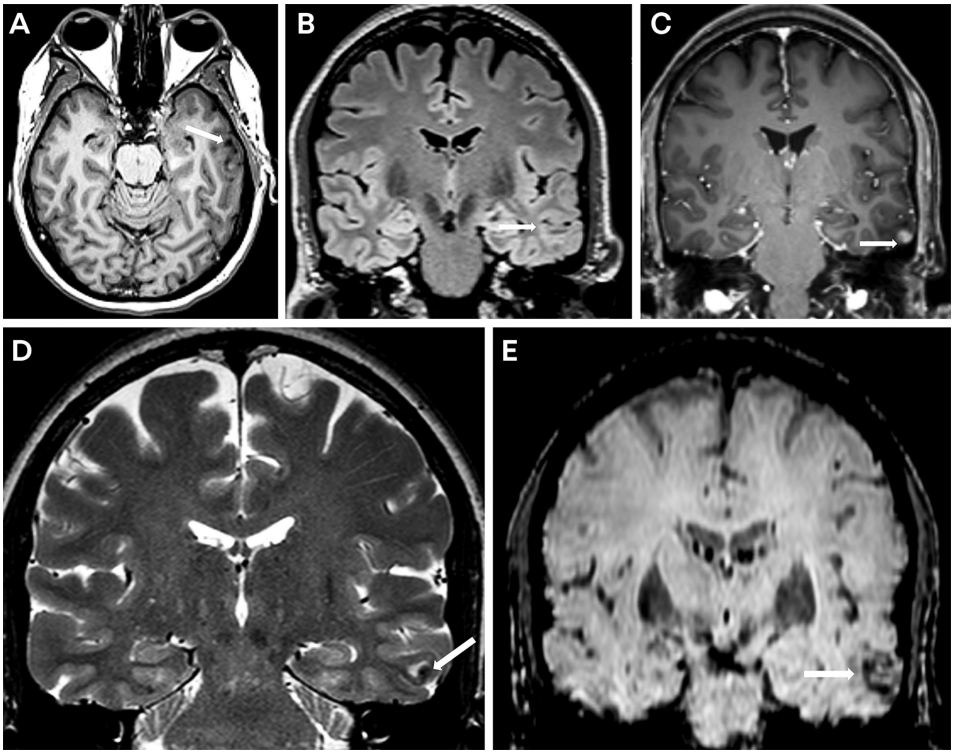

FIGURE 5-26

Left middle temporal gyrus ganglioglioma. *A*, Axial T1-weighted MRI shows a lesion at left superior temporal sulcus that is a hypointense cortical-based nodule with surrounding T1 isointensity similar to gray matter (*arrow*). *B*, Coronal fluid-attenuated inversion recovery (FLAIR) shows mild hyperintensity (*arrow*). *C*, Coronal postcontrast T1-weighted MRI shows an enhancing mural nodule (*arrow*). Coronal T2-weighted MRI (*D*) (*arrow*) shows T2 hypointensity suggestive of calcification, and this is confirmed on coronal susceptibility-weighted imaging (*E*) with magnetic susceptibility changes (*arrow*). Pathology (*not pictured*) showed a ganglioglioma.

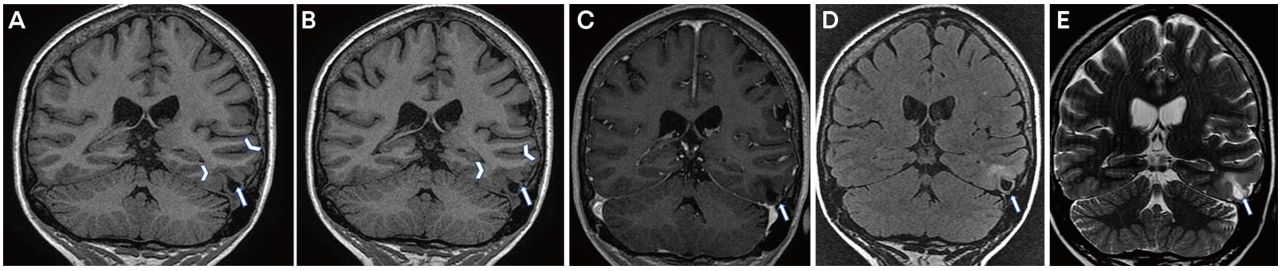

FIGURE 5-27

Dysembryoplastic neuroepithelial tumor (DNET). Coronal T1-weighted MRI shows a cortically based nodule (*A*, *B*, *arrows*) that is T1 hypointense, with surrounding T2 hyperintensity with no enhancement (*C, arrow*). A hypointense area is seen on fluid-attenuated inversion recovery (FLAIR) with mild protrusion (*D*, *E*, *arrows*) into the pia consistent with a glioneuronal tumor, such as a DNET. Pleomorphic xanthoastrocytomas often have a dural tail, and gangliogliomas have a mural nodule that enhances. Although DNETs can have a cystic "bubbly" appearance, this is not always seen. Note that cortical gray matter thickening at the margins of the tumor (*A* and *B*, *arrowheads*) suggests focal cortical dysplasia type II, which accompanies glioneuronal tumors in approximately 11% of cases. Most glioneuronal tumors show focal cortical dysplasia type I changes often not visible on MRI.

Copyright © American Academy of Neurology. Unauthorized reproduction of this article is prohibited.

abut the pia and can cause reactive thickening of the adjacent dura. Leptomeningeal involvement is characteristic of this tumor.[90] A dural tail sign is seen in 15% to 50% of cases (FIGURE 5-28). Local recurrence and malignant transformation can occur in 50% of cases of pleomorphic xanthoastrocytoma.[89]

Angiocentric Gliomas

Angiocentric gliomas are rare, slowly growing cerebral tumors that have been recognized by the WHO as a grade I tumor.[89] Angiocentric gliomas most often occur in children and young adults. Angiocentric gliomas have a cerebrocortical location, typically involving the frontoparietal and temporal lobes.[90]

MRI shows a well-circumscribed, solid, T2-hyperintense, and nonenhancing lesion often with subcortical white matter involvement. Angiocentric gliomas show a high signal on T1-weighted images and a stalk-like extension to the ventricle. Necrosis and calcification are rare. They are also associated with cortical dysplasia (type I).[89]

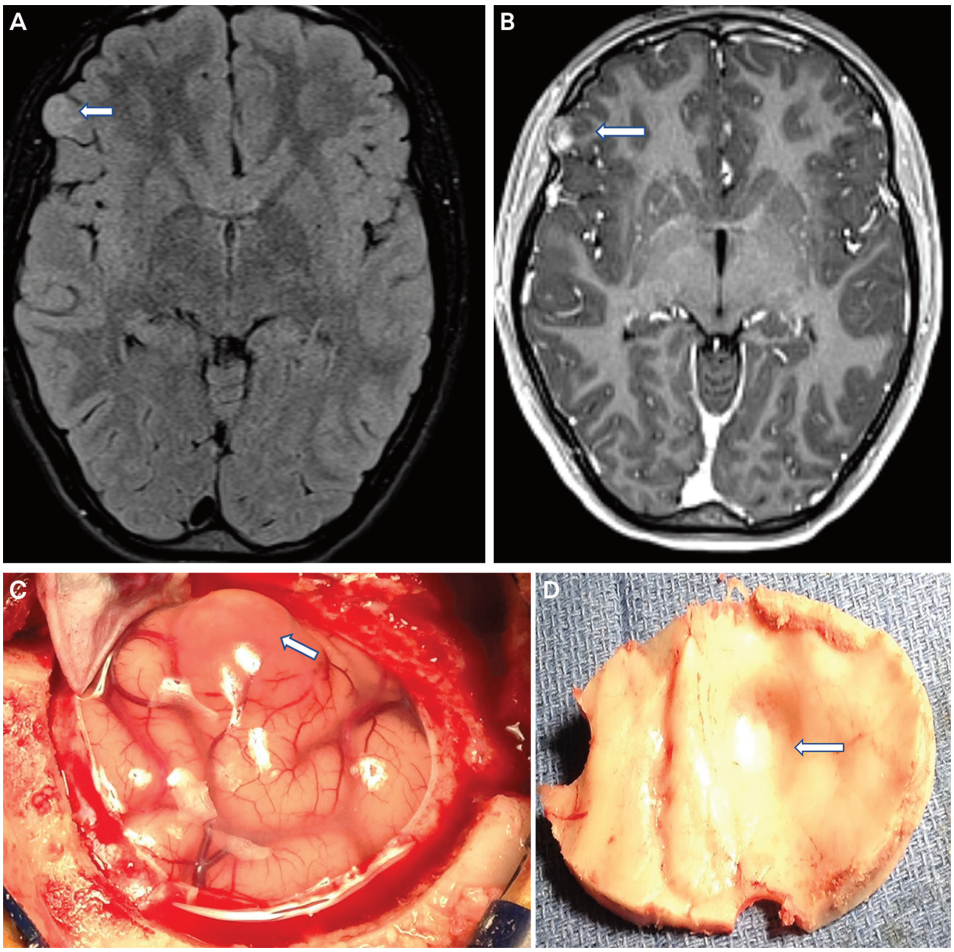

FIGURE 5-28

Pleomorphic xanthoastrocytoma. Axial 1.5T fluid-attenuated inversion recovery (FLAIR) MRI shows a cortically based T2-hyperintense lesion (*A*, arrow) that protrudes into the pia and a T1-hypointense to isointense lesion (*B*, *arrow*) with an enhancing mural nodule. At surgery, the tumor protrudes into the pia (*C*, *arrow*), and remodeling with scalloping of the calvarium can be seen (*D*, *arrow*).

Copyright © American Academy of Neurology. Unauthorized reproduction of this article is prohibited.

Other Neoplasms Associated With Epilepsy

The neoplasms described so far account for more than 70% of tumor-associated epilepsy.[49] Other neoplasms are associated with epilepsy, such as pilocytic astrocytomas (mostly in children), diffuse low-grade astrocytomas, and oligodendrogliomas and are all most commonly seen in the temporal lobe. Meningiomas, an extra-axial neoplasm, are also associated with epilepsy in middle-aged and older adults. For details of tumor imaging, refer to the article, "Imaging of Skull Base Tumors" by Wenya Linda Bi, MD, PhD,[91] in this issue of *Continuum*.

IMAGING FINDINGS ASSOCIATED WITH OTHER CAUSES OF EPILEPSY

So far, imaging findings in temporal lobe epilepsy, malformations of cortical development, and long-term-epilepsy–associated tumors have been addressed. This section addresses other important MRI findings in epilepsy including hamartomas, chronic encephalitis, infections, vascular malformations, encephaloceles, and neurocutaneous syndromes. Acute autoimmune-associated seizures are not addressed in this article; refer to the April 2022 *Continuum* issue on epilepsy for additional information.[92]

Hypothalamic Hamartomas

Hypothalamic hamartomas are rare, occurring in 1 in 200,000 children. They are typically located between the infundibular stalk anteriorly and the mamillary bodies posteriorly (FIGURE 5-29). They are T1 hypointense and T2 hyperintense on MRI.[93] They can be sessile or pedunculated. Most hypothalamic hamartomas manifest in patients between the ages of 1 and 3 years and clinically present as gelastic seizures in one-third of cases, although other seizure types occur. Of patients with hypothalamic hamartomas, 75% have precocious puberty.[83,93]

Rasmussen Encephalitis

Rasmussen encephalitis is a rare progressive chronic encephalitis with severe drug-resistant epilepsy, progressive hemiparesis, and cognitive decline. The MRI features evolve throughout the disease. Initially, the MRI can be normal and gradually evolve to FLAIR hyperintensity in both the cortex and subcortical white matter. These MRI changes will eventually involve the entire hemisphere, culminating in unilateral progressive cortical and basal ganglia atrophy (FIGURES 5-30A, 5-30B, and 5-30C).[94] A limited focal form can also occur (FIGURES 5-30D and 5-30E).

Temporal Lobe Encephaloceles

Temporal lobe encephaloceles are herniations of the temporal lobe and meninges through the dura and the skull (FIGURE 5-31). The temporal lobe encephaloceles associated with drug-resistant epilepsy are typically located at the anterior inferior medial temporal lobe (temporal pole) in the middle cranial fossa, most commonly along the greater wing of the sphenoid bone.[95,96] The optimal MRI sequence to visualize temporal lobe encephaloceles is a thin-sliced T2-weighted turbo fast spin echo in the coronal, axial, and sagittal planes and a skull base CT (once the lesion has been identified on MRI). Temporal lobe encephaloceles account for 0.30% of patients with newly diagnosed epilepsy and 2.0% to 5.5% of patients with drug-resistant epilepsy. Ancillary imaging findings include an

Copyright © American Academy of Neurology. Unauthorized reproduction of this article is prohibited.

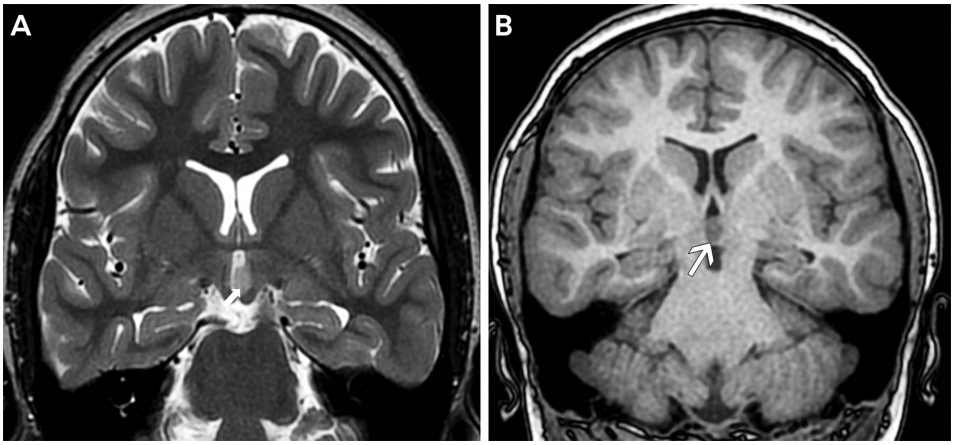

FIGURE 5-29
Hypothalamic hamartoma. Coronal T2-weighted (*A*) and T1-weighted (*B*) MRI showing a T2 gray matter–isointense (*A, arrow*) and T1 mildly hypointense lesion arising from the hypothalamus protruding into the third ventricle (*B, arrow*) in a 10-year-old girl with gelastic seizures.

KEY POINTS

- Hypothalamic hamartomas are rare, occurring in 1 in 200,000 children. They are typically located between the infundibular stalk anteriorly and the mamillary bodies posteriorly. They are T1 hypointense and T2 hyperintense on MRI. In one-third of cases, they present with gelastic seizures.

- Temporal lobe encephaloceles are herniations of the temporal lobe and meninges through the dura and the skull; they account for 0.30% of patients with newly diagnosed epilepsy and 2.0% to 5.5% of patients with drug-resistant epilepsy.

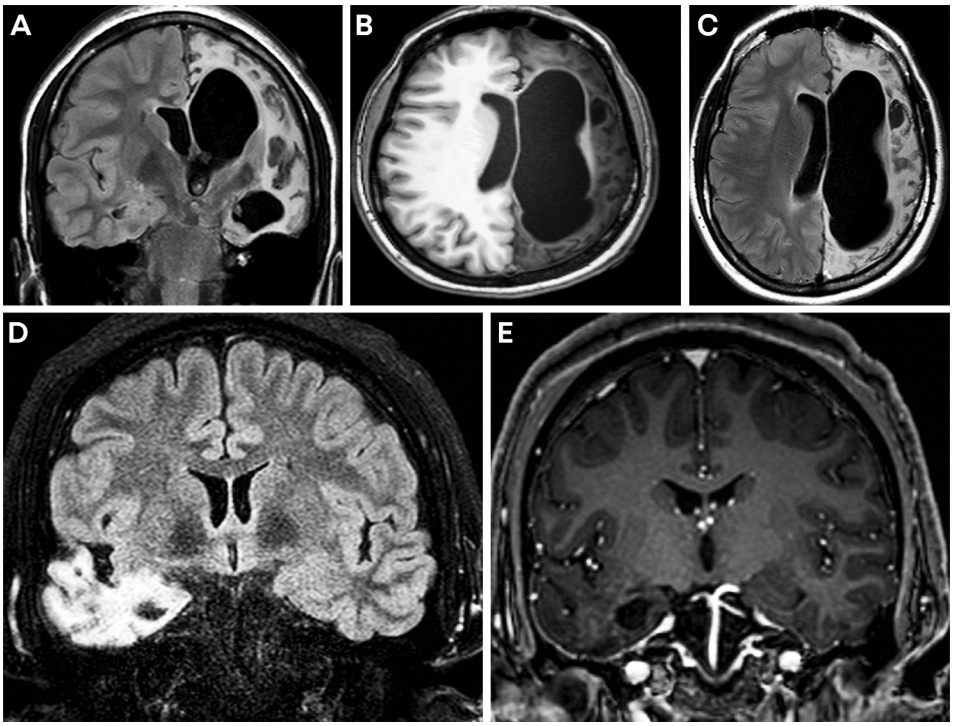

FIGURE 5-30
Rasmussen encephalitis. Coronal fluid-attenuated inversion recovery (FLAIR) image (*A*) shows typical hemispheric Rasmussen encephalitis with hemispheric atrophy and diffuse gliosis. Axial T1-weighted image (*B*) and axial FLAIR image (*C*) also show hemispheric atrophy, encephalomalacia, and gliosis. Focal Rasmussen encephalitis as shown in coronal FLAIR MRI (*D*). Focal "burned-out" Rasmussen encephalitis of the right temporal lobe is seen in a coronal postcontrast T1-weighted image (*E*) with gliosis and encephalomalacia that represents a focal burned-out form of Rasmussen encephalitis pathologically.

Copyright © American Academy of Neurology. Unauthorized reproduction of this article is prohibited.

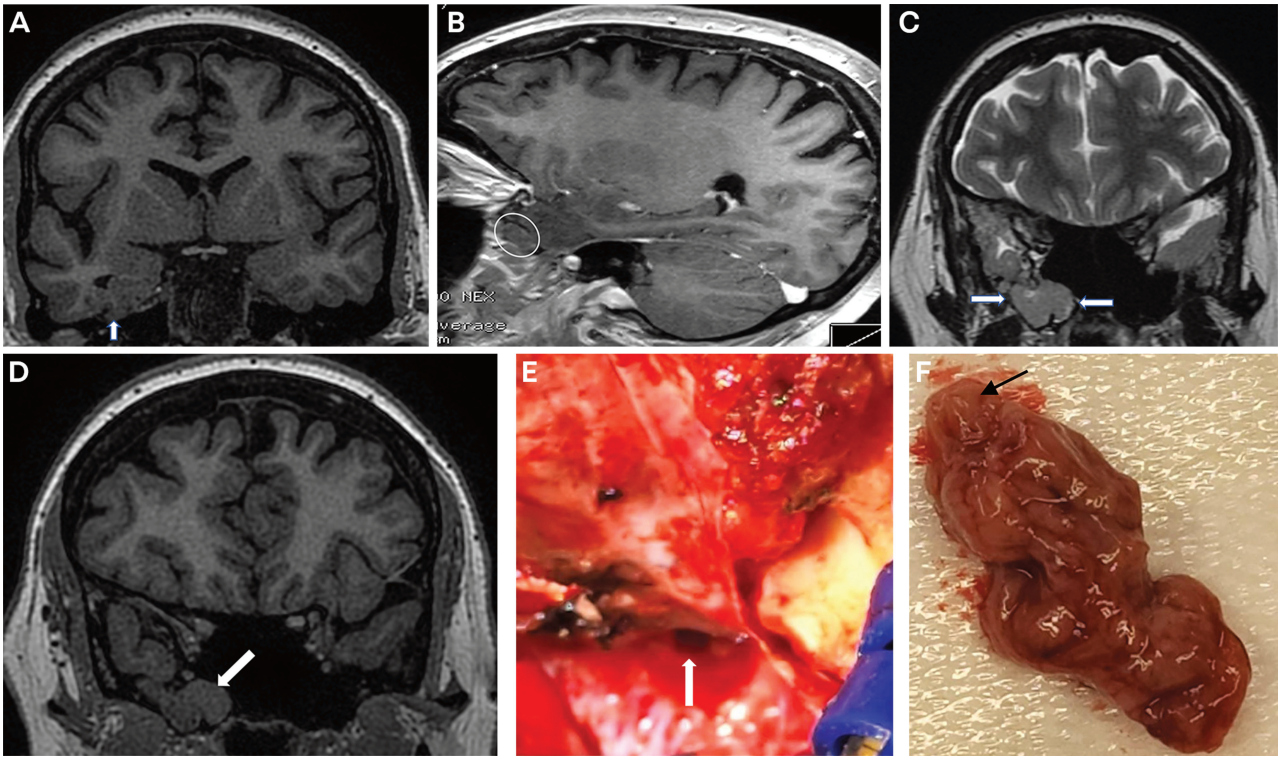

FIGURE 5-31

Encephalocele. *A*, Coronal T1-weighted MRI shows right entorhinal cortex herniation through the meninges (*arrow*). *B*, Sagittal T1-weighted MRI shows herniation of the right temporal pole into the middle cranial fossa (*outline*). Coronal T2-weighted (*C*) and T1-weighted (*D*) MRI shows herniation of the medial temporal polar cortex into the sphenoid sinus (*arrows*). The typical location of temporal encephaloceles associated with epilepsy is at the middle cranial fossa at the sphenoid wing. *E,* A cranial defect at surgery (*arrow*) through which the temporal polar cortex was herniated. *F*, The right temporal polar cortex, including the part that herniated through the middle cranial fossa (*arrow*).

empty sella syndrome, an enlarged Meckel cave, and a dilated optic nerve sheath; these indicate a possible prior history of intracranial hypertension. Of patients with temporal lobe encephaloceles and drug-resistant epilepsy, 67% to 75% have ipsilateral temporal hypometabolism on functional FDG-PET imaging.[96]

Sometimes, temporal lobe encephaloceles can show temporoparietal EEG changes, or a hypermotor phenomenology suggests a frontal localization.[65] The hippocampus and amygdala are usually normal on MRI.

TUBEROUS SCLEROSIS. Tuberous sclerosis complex is a neurocutaneous syndrome with skin lesions (adenoma sebaceum, hypomelanotic macules or "ash leaf" spots, subungual fibromas, and subungual nodules) and cerebral, cardiac, pulmonary, and renal lesions.[97]

Approximately 50% of tuberous sclerosis complex cases are autosomal dominant involving the *TSC1* and *TSC2* genes. The other noninherited cases are caused by de novo somatic or mosaic germline mutations. The brain MRI findings include cortical tubers that are frequently multiple and best visualized on FLAIR imaging demonstrating a blurring of the gray-white matter junction and increased T2 signal intensity, similar to focal cortical dysplasia

Copyright © American Academy of Neurology. Unauthorized reproduction of this article is prohibited.

type II (FIGURE 5-32). Some tubers can show accompanying T1 hypointensity and are less conspicuous on T1-weighted sequences (FIGURE 5-32). Despite multiple cortical tubers, patients can have a single epilepsy localization. MRI can also show subependymal glial nodules and giant cell astrocytomas.[97]

STURGE-WEBER SYNDROME. Sturge-Weber syndrome is a rare, sporadic neurocutaneous syndrome characterized by vascular malformations involving the skin, brain, and occasionally the eyes.[98,99] Children typically present with the classic triad of (1) facial port-wine stain in a V2 distribution; (2) ipsilateral leptomeningeal angiomatosis; and (3) glaucoma or other vascular ophthalmic abnormalities.

A single somatic mutation, c.548G>A (p.R183Q) in the *GNAQ* gene, has been described as a major genetic factor in Sturge-Weber syndrome.[100] MRI shows leptomeningeal enhancement on the T1 postgadolinium sequence with accompanying enlargement of the choroid plexus (FIGURE 5-33). MRI demonstrates calcification as T2 hypointensity or susceptibility-weighted imaging (SWI) magnetic susceptibility changes. Focal or diffuse unilateral cortical atrophy and T2 hyperintensity in the white matter, likely reflecting chronic ischemia, are often seen. In some cases, histopathology shows an abnormal gyral pattern, indicating polymicrogyria, and concomitant cortical dysplasia.[98,99]

NEUROCYSTICERCOSIS. Neurocysticercosis is the infection of the central nervous system by the larval stage of the pork tapeworm *Taenia solium*.[101] This tapeworm is endemic in most low-income countries and is one of the most common infectious causes of seizures in the world.[101] The MRI imaging findings evolve

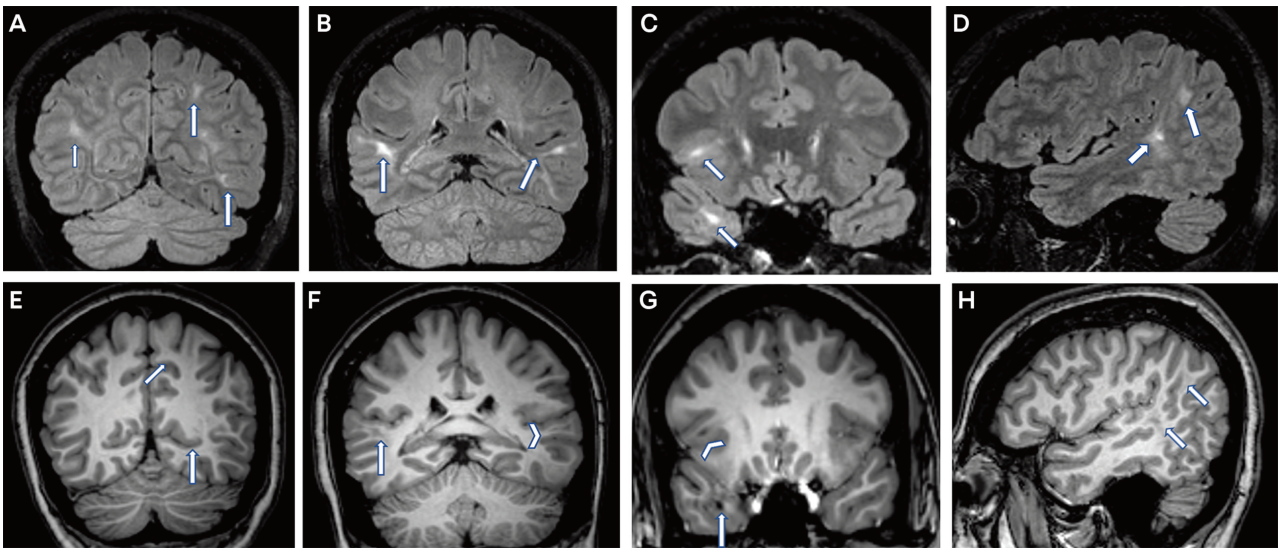

FIGURE 5-32
Cortical tubers in tuberous sclerosis. MRI shows multiple cortical tubers (*arrows*) best seen on fluid-attenuated inversion recovery (FLAIR) MRI (*top row*) in coronal (*A*, *B*, *C*) and sagittal (*D*) images. The cortical tubers are T2 hyperintense at the subcortical white matter of the gyrus and show cortical-subcortical white matter blurring that is less conspicuous on coronal T1-weighted magnetization-prepared rapid gradient echo (MPRAGE) (*bottom row*) with T1 subtle iso- and hypointensity (*arrows* and *arrowheads*) on coronal (*E*, *F*, and *G*) and sagittal (*H*) images. Many of the tubers would be easily missed without correlation with FLAIR MRI.

Copyright © American Academy of Neurology. Unauthorized reproduction of this article is prohibited.

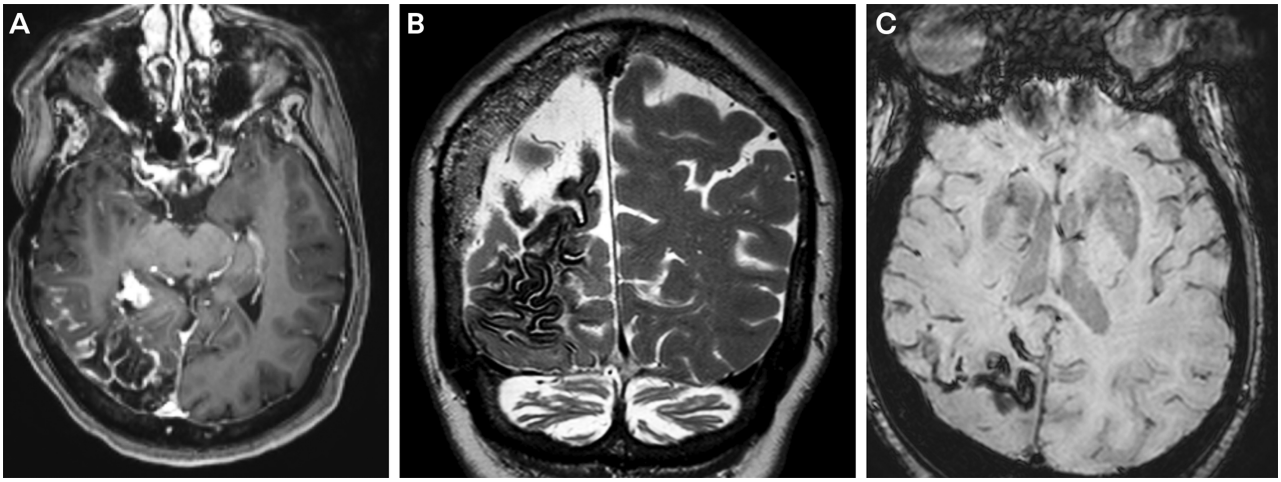

FIGURE 5-33
Sturge-Weber syndrome. *A*, Axial T1-weighted MRI with contrast shows leptomeningeal enhancement and globular enhancement and enlargement of the choroid plexus and occipital encephalomalacia. *B*, Coronal T2-weighted MRI shows gyral T2 hypointensity due to hemosiderin and parietal atrophy. *C*, Axial susceptibility-weighted imaging (SWI) shows gyral magnetic susceptibility changes due to hemosiderin.

from the early vesicular stage with a CSF signal intensity cyst that has a scolex, the headlike part of the tapeworm, that is T2 hyperintense and T1 hypointense and enhances with contrast, followed by the colloidal stage with a cyst that is mildly T1 hyperintense to CSF and T2 hyperintense and lacks a scolex; postcontrast images show a ring enhancement pattern and T2-weighted and FLAIR imaging shows adjacent edema and a rim of low signal intensity. In the granular nodular stage, MRI shows enhancement of the nodular lesion or a small ring-enhancing lesion. In the late granular nodular stage, the lesion is calcified on CT, and on MRI, the lesions are hypointense on T1-weighted and T2-weighted sequences, with faint ring enhancement (FIGURE 5-34).[101]

POSTTRAUMATIC, POSTINFECTIOUS, POSTSTROKE, AND PERINATAL ISCHEMIC LESIONS. Following trauma, infection (ie, viral encephalitis or brain abscess), or ischemic and hemorrhagic stroke, chronic lesions show encephalomalacia, laminar necrosis, and gliosis with cortical and subcortical white matter T2 hyperintensity. If the lesion communicates with the ventricle, it creates a porencephalic cyst (FIGURE 5-35). Perinatal ischemic lesions show a similar pattern.

At these border zone arterial distributions and posterior cortex, polymicrogyria or ulegyria are often seen. MRI shows reduced gyral depth with a "mushroom" appearance, cortical thinning, a smooth cortical-white matter junction, and gliosis of the underlying white matter (FIGURE 5-36).[101] SWI can show microhemorrhages in the lesion, particularly with posttraumatic or posthemorrhagic etiologies.[102]

Vascular Malformations Associated With Epilepsy

Vascular malformations constitute 5% of epileptogenic substrates in the general population of patients with epilepsy. Arteriovenous malformations and cavernous malformations are the most common vascular malformations causing seizures.[103] Arteriovenous malformations consist of a tangle of blood vessels

Copyright © American Academy of Neurology. Unauthorized reproduction of this article is prohibited.

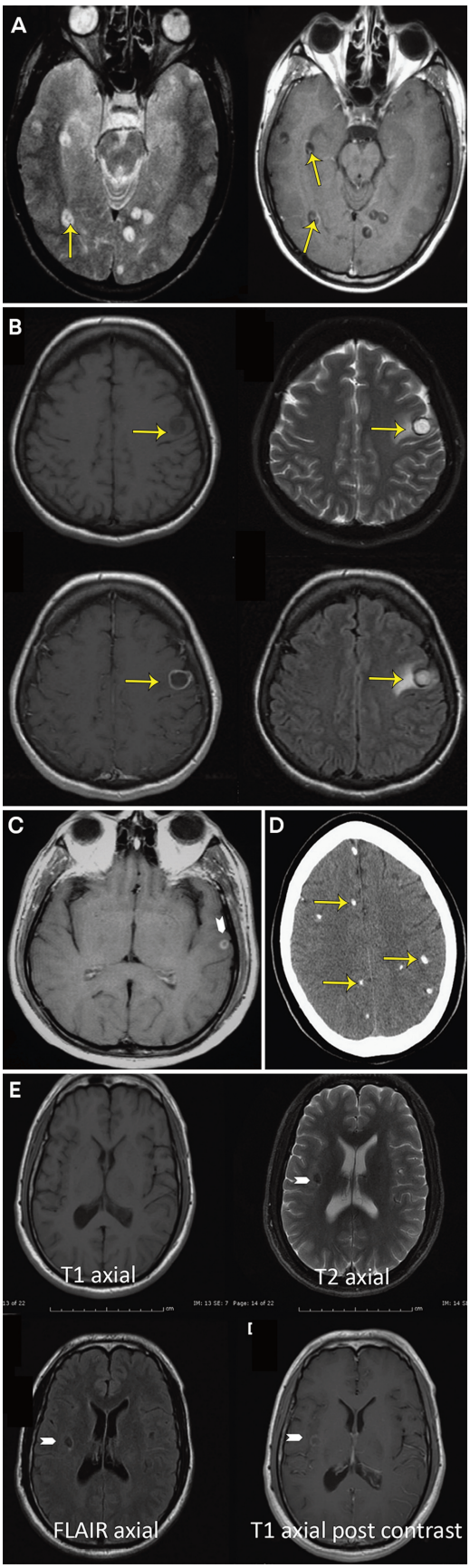

FIGURE 5-34

MRI findings of cysticercosis at various stages. *A*, Axial T2-weighted fast spin echo (FSE) (*left)* and axial T1-weighted MRI (*right*) show vesicular stage with T2 hyperintensity and T1 hypointensity with scolex in the center of the cyst (*arrows*). *B*, Axial T1-weighted MRI (*upper left*, without contrast; *lower left*, with contrast) and axial T2-weighted FSE (*upper right*) and axial FLAIR (*lower right*) show colloid vesicular stage with scolex no longer seen, ring enhancement, and fluid-filled cyst with a T2-hypointense rim and circumferential edema (*arrows*). *C*, Axial T1-weighted MRI with contrast shows the granular nodular stage with nodular enhancing cyst (*arrowhead*). *D*, Axial CT shows the nodular calcified stage (*arrows*). *E*, A nodular calcified stage fluid cyst (*arrowheads*) is shown with no edema and appears faint on axial T1-weighted MRI without contrast (*top left*), axial T1-weighted MRI with contrast (*lower right*), axial T2-weighted FSE (*upper right*), and fluid-attenuated inversion recovery (FLAIR) (*lower left*) MRI.

Modified with permission from Lerner A, et al, Neuroimaging Clin N Am.[100] © 2012 Elsevier Inc.

Copyright © American Academy of Neurology. Unauthorized reproduction of this article is prohibited.

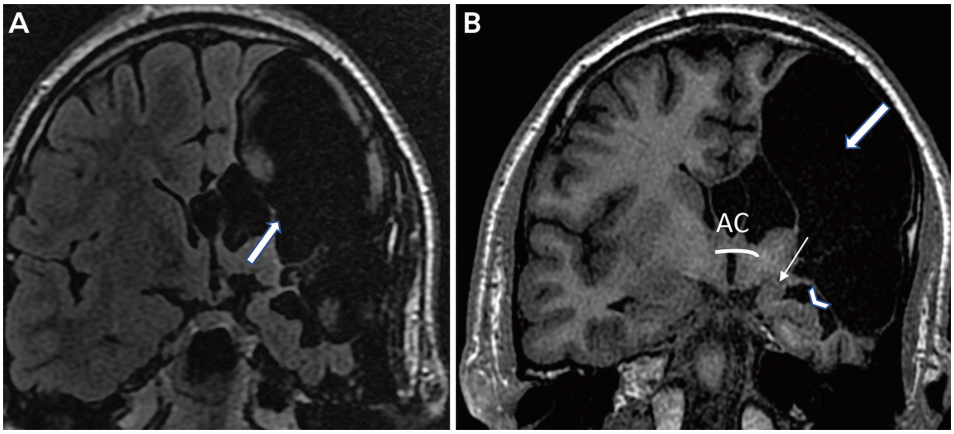

FIGURE 5-35
Left hemisphere porencephaly. Coronal fluid-attenuated inversion recovery (FLAIR) (*A*) and T1-weighted magnetization-prepared rapid gradient echo (MPRAGE) (*B*) MRI shows diffuse left hemispheric encephalomalacia that communicates with the ventricle creating a porencephalic cyst (*A*, *B*, *thick arrows*) and spares the medial basal temporal neocortex, parahippocampal gyrus, and hippocampal head. The frontal lobe (*not shown*) is largely preserved. Note that the residual medial amygdala (*B*, *thin arrow*) and hippocampal head inferiorly (*B*, *arrowhead*) still have connections to the anterior commissure (AC) (B, *curved line*).

lacking an intervening capillary network, leading to direct arteriovenous shunting of blood. Both T1- and T2-weighted images demonstrate serpiginous flow voids with areas of T2 prolongation in the adjacent brain.[103] The high-velocity flow masks gadolinium enhancement.

Cavernous malformations are composed of well-circumscribed vascular spaces with blood in varying stages of evolution as illustrated in CASE 5-3 (FIGURE 5-3).[33] A characteristic feature is the absence of intervening brain tissue. Most cavernous malformations are sporadic; however, 10% to 30% are familial.[33] An associated developmental venous anomaly is seen in 25% of patients with cavernous malformations; hemosiderin deposition results in magnetic susceptibility artifacts, which appear as areas of hypointensity on MRI. Therefore, images that are affected by magnetic susceptibility (ie, gradient recalled echo [GRE] or SWI sequences) are highly sensitive to identifying small cavernous malformations. Cavernous malformations demonstrate evidence of acute, subacute, and chronic internal bleeding. Subacute bleeding demonstrates

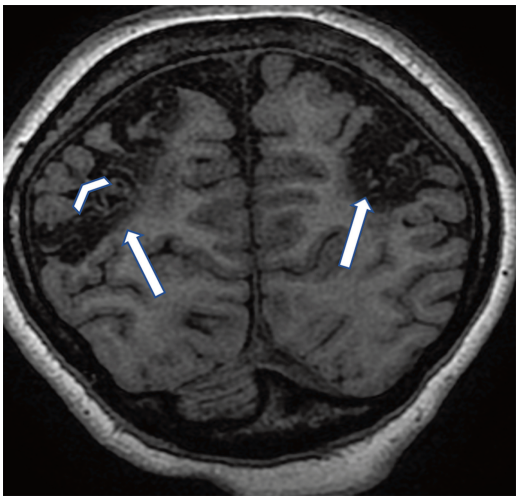

FIGURE 5-36
Ulegyria. Coronal T1-weighted MRI shows leukomalacia and encephalomalacia in an arterial border zone distribution (*arrows*) with ulegyria "mushroom-shaped gyri" (*arrowhead*).

Copyright © American Academy of Neurology. Unauthorized reproduction of this article is prohibited.

conversion of hemoglobin to methemoglobin, producing foci of central hyperintensity on T1-weighted images. The peripheral hemosiderin produces T2 shortening, causing a "black halo" surrounding the lesion (FIGURE 5-3).[33] SWI uses the paramagnetic properties of deoxygenated blood to visualize tissue vasculature. SWI helps detect microhemorrhages from remote trauma or cavernous malformations and identifies calcification.[102]

ADVANCED AND FUNCTIONAL IMAGING STUDIES IN THE EVALUATION OF PATIENTS WITH EPILEPSY

Functional imaging studies such as PET and subtraction ictal SPECT coregistered to MRI (SISCOM) are helpful in identifying subtle MRI lesions or mapping the epileptogenic network to optimize stereo-EEG planning. Magnetic source imaging maps interictal epileptic dipole sources. Integration and concordance of localization with these three modalities optimizes presurgical localization of the epileptogenic network for invasive EEG planning and improved surgical seizure-free outcome. Functional MRI and magnetic source imaging are used for functional mapping of language and sensorimotor function.

Positron Emission Tomography

PET is a nuclear medicine imaging modality that detects gamma rays released by a positron-emitting radioactive tracer. The most commonly used tracer for epilepsy neuroimaging is 2-deoxy-2-(^{18}F) FDG.[104] This tracer approximates brain metabolic processes and shows cerebral glucose hypometabolic regions, indicating epileptogenic regions and associated dysfunctional neuronal networks.

Statistical parametric mapping software objectively analyzes hypometabolic regions compared with a normal control group. A z-score is set such that three standard deviations from the mean show regions of hypometabolism.[105] In addition, coregistering PET to three-dimensional epilepsy protocol MRI optimizes the identification of subtle focal cortical dysplasias and helps localize the epileptogenic region (FIGURE 5-37).[106]

Single-Photon Emission Tomography

SPECT is a nuclear medicine imaging modality that uses gamma rays and allows the assessment of regional cerebral blood flow (FIGURE 5-38).[104,107] Cerebral blood flow increases during an epileptic seizure, and SPECT allows for mapping of the epileptic network of seizure initiation and network propagation. Either technetium 99m–hexamethylpropyleneamine oxime (^{99m}Tc-HMPAO) or ^{99m}Tc–ethyl cysteinate dimer (ECD) is stable for injection after preparation at 4 and 6 hours, respectively. For accurate assessment of ictal SPECT, an early injection time from clinical or EEG onset, whichever is sooner, is essential. SISCOM is a technique in which the interictal SPECT is subtracted from the ictal SPECT and then coregistered to MRI; this enhances the sensitivity, specificity, and interreader reliability of localizing epileptogenic regions and lesions.[107,108] A word of caution is that SPECT can show larger regions of cerebral hyperperfusion than the actual epileptogenic region, reflecting regions of seizure propagation rather than onset.

Functional MRI

Functional MRI (fMRI) acquisitions use the blood oxygen level–dependent (BOLD) effect to indirectly infer brain activity through task-related increases in

KEY POINTS

- Cavernous malformations are composed of well-circumscribed vascular spaces with blood in varying stages of evolution.
- Susceptibility-weighted imaging (SWI) capitalizes on the paramagnetic properties of deoxygenated blood. SWI helps detect microhemorrhages from remote trauma or cavernous malformations and identifies calcification.
- Coregistering positron emission tomography (PET) to three-dimensional epilepsy protocol MRI optimizes the identification of subtle focal cortical dysplasias or helps localize the epileptogenic region.
- Subtraction ictal single-photon emission computerized tomography (SPECT) coregistered to MRI (SISCOM) is a technique in which the interictal SPECT is subtracted from the ictal SPECT and then coregistered to MRI, which enhances the sensitivity, specificity, and interreader reliability of localizing epileptogenic regions and lesions.
- SPECT can show larger regions of cerebral hyperperfusion than the actual epileptogenic region, reflecting regions of seizure propagation rather than onset.
- Functional MRI (fMRI) acquisitions use the blood oxygen level-dependent (BOLD) effect to indirectly infer brain activity through task-related increases in cerebral blood flow via T2* acquisitions.

Copyright © American Academy of Neurology. Unauthorized reproduction of this article is prohibited.

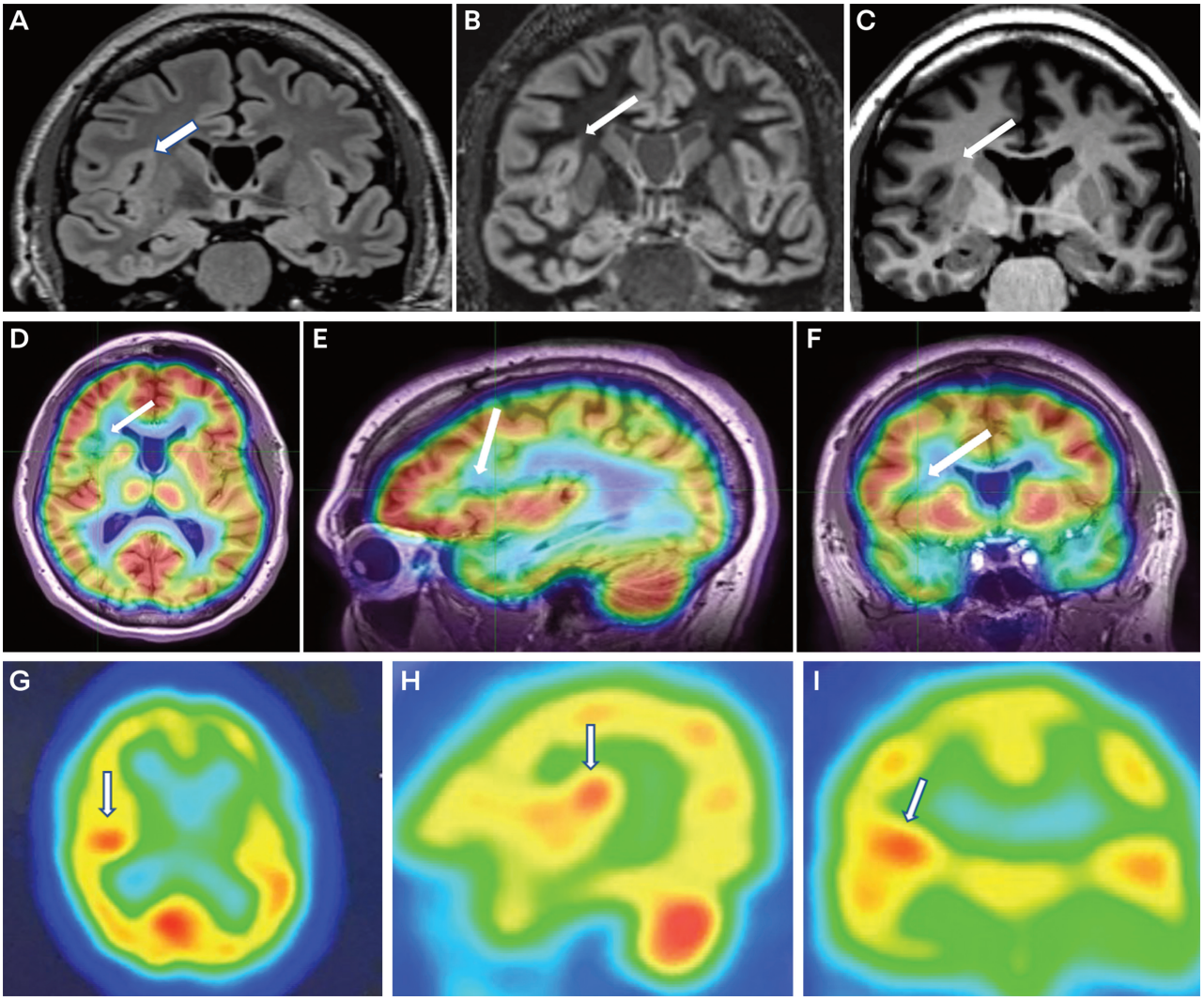

FIGURE 5-37

Multimodality imaging of subtle bottom of the sulcus type IIb cortical dysplasia. *A*, Coronal three-dimensional fluid-attenuated inversion recovery (FLAIR) MRI shows cortical thickening (*arrow*) in the right pars opercularis of the inferior frontal gyrus at the circular sulcus adjacent to the dorsal anterior insula. *B*, T2-weighted double inversion recovery shows that cortical thickening (*arrow*) at the right circular sulcus becomes more conspicuous on this sequence with the wisp of gray matter at the depth of the sulcus (transmantle sign). *C*, T1-weighted magnetization-prepared rapid gradient echo (MPRAGE) shows gray matter thickening (*arrow*) at the right circular sulcus of the frontal operculum with a faint wisp of grey matter extending into the white matter at the depth of the sulcus. Axial (*D*), sagittal (*E*), and coronal (*F*) three-dimensional MRI fused with fludeoxyglucose positron emission tomography (FDG-PET) shows reduced glucose metabolism at the cortical dysplasia (*D, E, F, arrows*). PET-MRI fusion enhances lesion conspicuity. Axial (*G*), sagittal (*H*), and coronal (*I*) ictal single photon emission tomography (SPECT) shows hyperperfusion (*arrows*) in this region.

Copyright © American Academy of Neurology. Unauthorized reproduction of this article is prohibited.

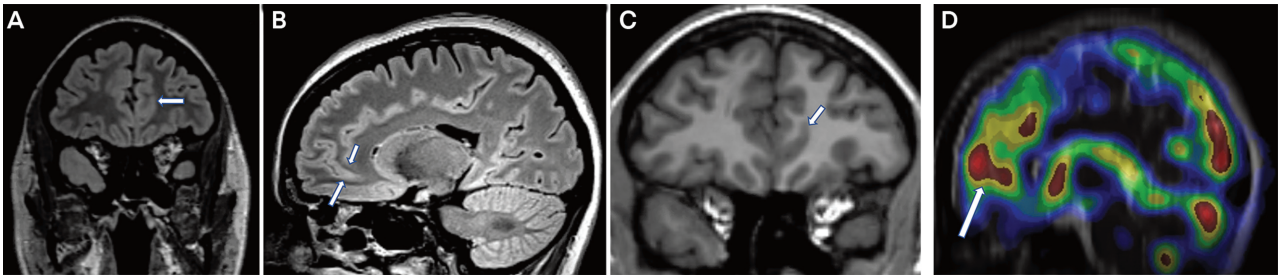

FIGURE 5-38

Left prefrontal cortex focal cortical dysplasia type II in a 44-year-old woman with chapeau gendarme (ictal frowning), which typically involves a network of the ventral anterior cingulate cortex. Note the cortical thickening and deep sulcus at the ventral medial prefrontal cortex and a wisp of gray matter extending to the ventral anterior cingulate gyrus as shown in coronal three-dimensional fluid-attenuated inversion recovery (FLAIR) (*A*, *arrow*), sagittal FLAIR (*B*, *arrows*), coronal T1-weighted magnetization-prepared rapid gradient echo (MPRAGE) (*C*, *arrow*), and sagittal subtraction ictal single-photon emission computerized tomography (SPECT) (*D*, *arrow*) views.

cerebral blood flow via T2* acquisitions.[109,110] These sequences are sensitive to changes in magnetic susceptibility due to blood oxygenation because oxygenated hemoglobin is diamagnetic whereas deoxygenated hemoglobin is paramagnetic. Local neural activity leads to increases in cerebral blood flow through neurovascular coupling. This results in a decrease of deoxygenated hemoglobin and an increase in local field homogeneity, and, therefore, a small increase in the T2* signal in regions with increased neural activity. Consequently, fMRI can be used to image brain activities in response to an external task. Changes in T2* in response to task conditions are usually very small (less than 10%).[111] Task-based fMRI is widely used in presurgical evaluation to determine language hemispheric dominance, often in planned temporal lobe resection in the dominant hemisphere.[110,112] The AAN practice guideline summary[112] advises that presurgical fMRI could be an adequate alternative to intracarotid amobarbital Wada memory testing for predicting verbal memory outcome (Level C).

Magnetoencephalography and Magnetic Source Imaging

MEG and magnetic source imaging is a direct electrophysiologic measurement of neural activity recording of the magnetic field outside the scalp on a millisecond basis. It is highly accurate in the localization of interictal epileptiform discharges and is more sensitive to tangential dipoles than radial dipoles recorded by scalp EEG. It uses 200 to 300 channels and has a wide bandwidth to identify spikes.[113] Furthermore, MEG dipoles are less likely to be distorted by the intervening scalp and calvarium. MEG can identify spike activity 3 to 10 times smaller than scalp EEG can. In one study, scalp interictal EEG and MEG co-identified spikes in 80%, 8% with no spikes on either EEG or MEG, and 20% MEG-identified spikes not seen on scalp EEG.[114] However, only those spikes seen on both EEG and MEG were most localizing. It is critical to analyze MEG dipole sources for the early phase of EEG spikes not seen on MEG and high-voltage slow waves on EEG because these can have localizing value.[113] Patients with a single tight cluster of dipoles have improved localization compared with patients with scattered dipoles.[113] The MEG is then coregistered to a three-dimensional epilepsy protocol MRI that shows the relationship of the

Copyright © American Academy of Neurology. Unauthorized reproduction of this article is prohibited.

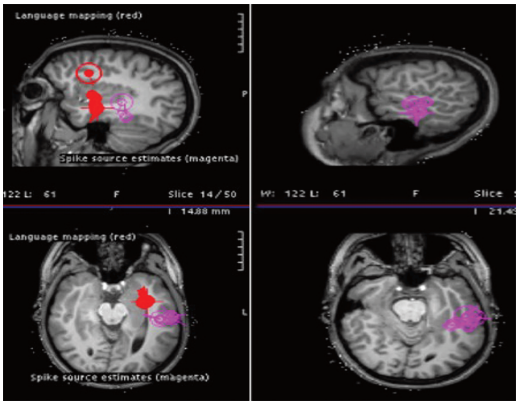

FIGURE 5-39
Magnetoencephalography. Dipole tight cluster (*purple markings*) at the superior temporal sulcus and receptive language area and anterior superior temporal sulcus (*red markings*) in a patient with MRI-negative epilepsy.

spike dipoles to the cortical anatomy (FIGURE 5-39). MEG can direct the clinician to identify subtle cortical dysplasia or guide intracranial electrode placement to optimize surgical localization, particularly in MRI-negative patients.[111,113] An ictal MEG can be highly localizing.[32] MEG can also localize primary motor and sensory, visual, and receptive language functions (FIGURE 5-39).[113]

Multimodality Imaging

Multimodality imaging is most useful in MRI-negative epilepsies, where the surgical seizure-free outcome can be 20% or less. It can optimize localization in conjunction with video-EEG and seizure phenomenology, guide intracranial EEG implantation, and, in some cases, identify a previously missed subtle focal cortical dysplasia. Clinicians should look for concordance between interictal FDG-PET coregistered to MRI, ictal subtraction SPECT, and MEG and clinical features and EEG data. In some cases, one imaging modality will provide valuable localizing information that another modality does not.

Each modality does have limitations as follows:

- **SPECT shows seizure propagation patterns that are affected by the latency of tracer injection.[107,108]**
- **FDG-PET shows a functional deficit zone that can be larger than the epileptogenic zone, but, in some cases, such patterns may have predictive value for a surgical seizure-free outcome.[104,108]**
- **MEG must be correlated to the patient's habitual interictal EEG patterns. Because MEG duration is typically 2 hours or less, sampling time limits the yield of identifying MEG dipoles, particularly those with infrequent spikes. Furthermore, optimal localization of a MEG source requires at least five or more spike clusters in the same sublobar region with a constant orientation.[113]**

Multimodality imaging must be correlated to early seizure phenomenology sequences and epileptic auras to inform the clinician about the epileptogenic network to ensure that imaging data are concordant and reconcile discordant data.

Advanced MRI Detection Techniques

Texture analysis using voxel-based modeling of gray-white matter blurring and gray matter intensity from three-dimensional T1-weighted MRI increases the identification of focal cortical dysplasia type II by 40% compared with visual analysis (FIGURE 5-40).[115] More recently, fully automated techniques have been developed by using three-dimensional T1-weighted and three-dimensional FLAIR MRI. In one study, these techniques identified focal

Copyright © American Academy of Neurology. Unauthorized reproduction of this article is prohibited.

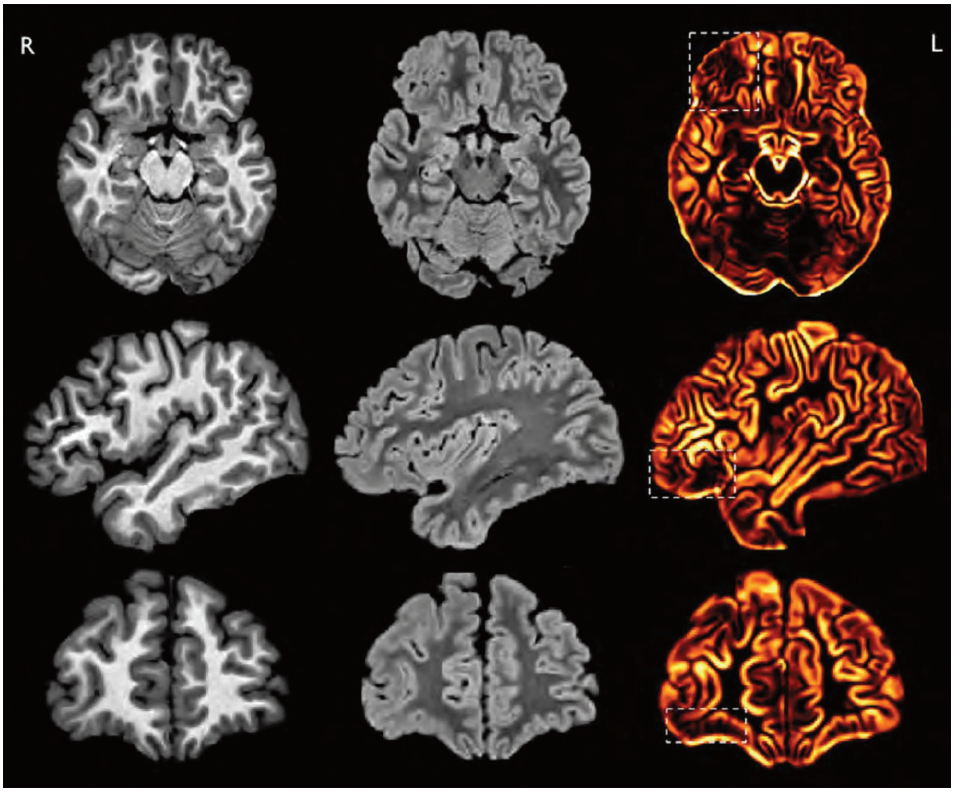

FIGURE 5-40

Texture analysis of "MRI-negative" focal cortical dysplasia. Axial (*top row*), sagittal (*middle row*), and coronal (*bottom row*) three-dimensional T1-weighted (*first column*) and fluid-attenuated inversion recovery (FLAIR) (*second column*) views in a patient with right frontal lobe epilepsy initially reported as "MRI-negative" are shown. The *third column* shows cuts of the three-dimensional gradient map obtained from the T1-weighted MRI, which calculates the rate of change of intensities, thereby modeling blurring at the interface between the gray and white matter. In regions of normal transition, the gradient is expected to be steep, thus appearing hyperintense. In regions of blurring, the gradient is expected to be less steep, thus appearing hypointense. In this case, a clear breakdown in the gradient is shown, with a hypointense region within the right orbitofrontal region (outlined by the *dashed rectangles*). The reinspection of the T1-weighted and T2-weighted images, informed by the texture map, reveals an extensive blurring in the same area initially overlooked by conventional radiologic examination.

Reprinted with permission from Bernasconi A, et al, Epilepsia.[19] © 2019 International League Against Epilepsy.

cortical dysplasia type II in greater than 70% of patients where visual analysis did not identify the lesion.[116] In addition, T2 relaxometry can be helpful to identify subtle hippocampal sclerosis, determine severity when hippocampal sclerosis is bilateral, or distinguish hippocampal signal changes from an artifact.[117]

HEALTH CARE DISPARITIES

People with epilepsy who have reduced health care literacy are more likely to have lower quality-of-life scores than those with health care literacy.[118] It has been shown that low health care literacy is widespread in the United States and costs between $106 billion and $238 billion annually or between 7.0% and 17% of personal health care expenditures.[119] The treatment gap, defined as the number of people who need treatment for epilepsy compared with those who receive it, is 10% in high-income countries and more than 75% in low-income

KEY POINTS

- Task-based fMRI is widely used in presurgical evaluation to determine language hemispheric dominance, often in planned temporal lobe resection in the dominant hemisphere.
- Magnetoencephalography and magnetic source imaging use direct electrophysiologic measurements of neural activity recording of the magnetic field outside the scalp on a millisecond basis. It is highly accurate in the localization of interictal epileptiform discharges and is more sensitive to tangential dipoles than radial dipoles recorded by scalp EEG.
- Patients with a single tight cluster of dipoles have improved localization compared with patients with scattered dipoles. The MEG coregistered to a three-dimensional epilepsy protocol MRI shows the relationship of the spike dipoles to the cortical anatomy.
- Magnetoencephalography can direct the clinician to identify subtle cortical dysplasia or guide intracranial electrode placement to optimize surgical localization, particularly in MRI-negative patients.

Copyright © American Academy of Neurology. Unauthorized reproduction of this article is prohibited.

countries.[120] In the United States, access to high-quality care, including video-EEG and epilepsy surgery, is reduced in underrepresented groups and those with lower incomes. One study that evaluated patients followed at different intervals between 1988 and 2003 showed that those with a lack of health insurance (Medicare, Medicaid, commercial, or other) were 85% less likely to have an anterior temporal lobe resection. African American race independently predicted a 50% lower chance of an anterior temporal lobe resection.[121]

Generally speaking, the cost to payers of an epilepsy protocol MRI is no different from a routine MRI, even though the scan time is longer. The use of IV gadolinium further increases the cost of a scan. Therefore, for some patients with epilepsy who have had a prior MRI with no lesion and the clinician has reviewed the images, they may not need gadolinium on a subsequent MRI. It can be inferred that these same patients may not have access to high-resolution epilepsy protocol MRI, which is correlated with access to video-EEG and eventual epilepsy surgery.

KEY POINTS

- **Multimodality imaging is most useful in MRI-negative epilepsies, where the surgical seizure-free outcome can be 20% or less. It can optimize localization in conjunction with video-EEG and seizure phenomenology, guide intracranial EEG implantation, and, in some cases, identify a previously missed subtle focal cortical dysplasia.**
- **Fludeoxyglucose positron emission tomography (FDG-PET) shows a functional deficit zone that can be larger than the epileptogenic zone, but in some cases such patterns may have predictive value for a surgical seizure-free outcome.**
- **Texture analysis using voxel-based modeling of gray-white matter blurring and gray matter intensity from three-dimensional T1-weighted MRI increases the identification of focal cortical dysplasia type II by 40% compared with visual analysis.**

CONCLUSION

This article discussed the fundamental role of neuroimaging in the evaluation and treatment of epilepsy to optimize clinical decision-making from diagnosis to treatment, in predicting drug-resistant epilepsy, and in the early identification of candidates for epilepsy surgery.

Clinical history and knowledge of anatomy are critical in evaluating patients. A neurologist must have fluency in interpreting neuroimaging, particularly MRI, when evaluating epilepsy.

Integrating clinical information is vital to identifying subtle findings with enormous clinical impact (ie, seizure freedom, reduced mortality, reduced cognitive and psychiatric morbidity). In the 21st century, clinicians can integrate this information with high-resolution MRI. In this regard, a thoughtful and methodical approach to interpreting epilepsy protocol MRI by using the ILAE-endorsed HARNESS protocol and multimodality imaging in patients with drug-resistant epilepsy is crucial.

Often, epilepsy is evaluated in a cross-sectional manner, but it must be seen as a longitudinal disease for which MRI plays a crucial role. As advances in genetics and neuroimaging techniques evolve, clinicians will be able to integrate genetics and imaging as surrogate markers for interictal dysfunction that will help in the understanding of the burden of epilepsy and how this extends beyond the seizures. Such advanced neuroimaging techniques will elucidate neural connectivity and functional network disturbances in newly diagnosed and chronic epilepsy and will optimize localization in drug-resistant epilepsy to improve surgical seizure-free outcome.[122]

REFERENCES

1 Fisher RS, van Emde Boas W, Blume W, et al. Epileptic seizures and epilepsy: definitions proposed by the International League Against Epilepsy (ILAE) and the International Bureau for Epilepsy (IBE). Epilepsia 2005;46(4):470-472. doi:10.1111/j.0013-9580.2005.66104.x

2 Hauser WA, Annegers JF, Rocca WA. Descriptive epidemiology of epilepsy: contributions of population-based studies from Rochester, Minnesota. Mayo Clin Proc 1996;71(6):576-586. doi:10.4065/71.6.576

Copyright © American Academy of Neurology. Unauthorized reproduction of this article is prohibited.

3 Hesdorffer DC, Logroscino G, Benn EK, et al. Estimating risk for developing epilepsy: a population-based study in Rochester, Minnesota. Neurology 2011;76(1):23-27. doi:10.1212/WNL.0b013e318204a36a

4 Fisher RS, et al. Operational classification of seizure types by the International League Against Epilepsy: Position Paper of the ILAE Commission for Classification and Terminology. Epilepsia 2017;58(4):522-530. doi:10.1111/epi.13670

5 Hauser WA, Rich SS, Annegers JF, Anderson VE. Seizure recurrence after a 1st unprovoked seizure: an extended follow-up. Neurology 1990; 40(8):1163-1170. doi:10.1212/wnl.40.8.1163

6 Hesdorffer DC, Benn EK, Cascino GD, Hauser WA. Is a first acute symptomatic seizure epilepsy? Mortality and risk for recurrent seizure. Epilepsia 2009;50(5):1102-1108. doi:10.1111/j.1528-1167.2008.01945.x

7 Yoon D, Frick KD, Carr DA, Austin JK. Economic impact of epilepsy in the United States. Epilepsia 2009;50(10):2186-2191. doi:10.1111/j.1528-1167.2009.02159.x

8 Ngugi AK, Bottomley C, Kleinschmidt I, Sander JW, Newton CR. Estimation of the burden of active and life-time epilepsy: a meta-analytic approach. Epilepsia 2010;51(5):883-890. doi:10.1111/j.1528-1167.2009.02481.x

9 Zack MM, Kobau R. National and state estimates of the numbers of adults and children with active epilepsy—United States, 2015. MMWR Morb Mortal Wkly Rep 2017;66:821–825. doi:10.15585/mmwr.mm6631a1.html

10 Hirtz D, Thurman DJ, Gwinn-Hardy K, et al. How common are the "common" neurologic disorders? Neurology 2007;68(5):326-337. doi:0.1212/01.wnl.0000252807.38124.a3

11 Begley CE, Famulari M, Annegers JF, et al. The cost of epilepsy in the United States: an estimate from population-based clinical and survey data. Epilepsia 2000;41(3):342-351. doi:10.1111/j.1528-1157.2000.tb00166.x

12 Wirrell E. Evaluation of first seizure and newly diagnosed epilepsy. Continuum (Minneap Minn) 2022;28(2, Epilepsy):230-260. doi:10.1212/CON.0000000000001074

13 Chauvel P, McGonigal A. Emergence of semiology in epileptic seizures. Epilepsy Behav 2014;38:94-103. doi:10.1016/j.yebeh.2013.12.003

14 McGonigal A. Semiology and epileptic networks. Neurosurg Clin N Am 2020;31(3):373-385. doi:10.1016/j.nec.2020.03.003

15 Naidich TP, Yousry TA. Functional Neuroanatomy. In: Stippich C, eds. Clinical functional MRI. Medical radiology (diagnostic imaging). Springer; 2007.

16 Duvernoy HM. The human brain: surface, blood supply, and three-dimensional anatomy. 2nd ed. Springer; 1991.

17 Vakharia VN, Duncan JS, Witt JA, et al. Getting the best outcomes from epilepsy surgery. Ann Neurol 2018;83(4):676-690. doi:10.1002/ana.25205

18 Guidelines for neuroimaging evaluation of patients with uncontrolled epilepsy considered for surgery. Commission on Neuroimaging of the International League Against Epilepsy. Epilepsia 1998;39(12):1375-1376. doi:10.1111/j.1528-1157.1998.tb01341.x

19 Bernasconi A, Cendes F, Theodore WH, et al. Recommendations for the use of structural magnetic resonance imaging in the care of patients with epilepsy: a consensus report from the International League Against Epilepsy Neuroimaging Task Force. Epilepsia 2019;60(6): 1054-1068. doi:10.1111/epi.15612

20 Hakami T, McIntosh A, Todaro M, et al. MRI-identified pathology in adults with new-onset seizures. Neurology 2013;81(10):920-927. doi:10.1212/WNL.0b013e3182a35193

21 Wieshmann UC. Clinical application of neuroimaging in epilepsy. J Neurol Neurosurg Psychiatry 2003;74(4):466-470. doi:10.1136/jnnp.74.4.466

22 Von Oertzen J, Urbach H, Jungbluth S, et al. Standard magnetic resonance imaging is inadequate for patients with refractory focal epilepsy. J Neurol Neurosurg Psychiatry 2002; 73(6):643-647. doi:10.1136/jnnp.73.6.643

23 Knake S, Triantafyllou C, Wald LL, et al. 3T phased array MRI improves the presurgical evaluation in focal epilepsies: a prospective study. Neurology 2005;65(7):1026-1031. doi:10.1212/01.wnl.0000179355.04481.3c

24 Wang I, Bernasconi A, Bernhardt B, et al. MRI essentials in epileptology: a review from the ILAE Imaging Taskforce. Epileptic Disord 2020;22(4): 421-437. doi:10.1684/epd.2020.1174

25 Federico P, Ng DW, Bernasconi A, et al. ILAE Neuroimaging Task Force highlight: review MRI scans with semiology in mind. Epileptic Disord 2020;22(5):683-687. doi:10.1684/epd.2020.1202

26 Berg AT, Shinnar S. The risk of seizure recurrence following a first unprovoked seizure: a quantitative review. Neurology 1991(7):965-972. doi:10.1212/wnl.41.7.965

27 Gloss D, Pargeon K, Pack A, et al; AAN Guideline Subcommittee. Antiseizure medication withdrawal in seizure-free patients: practice advisory update summary: report of the AAN Guideline Subcommittee. Neurology 20217; 97(23):1072-1081. doi:10.1212/WNL.0000000000012944

28 Berg AT, Shinnar S. Relapse following discontinuation of antiepileptic drugs: a meta-analysis. Neurology 1994;44(4):601-608. doi:10.1212/wnl.44.4.601

29 Semah F, Picot MC, Adam C, et al. Is the underlying cause of epilepsy a major prognostic factor for recurrence? Neurology 1998;51(5): 1256-62. doi:10.1212/wnl.51.5.1256

Copyright © American Academy of Neurology. Unauthorized reproduction of this article is prohibited.

30 Berg AT, Langfitt J, Shinnar S, et al. How long does it take for partial epilepsy to become intractable? Neurology 2003;60(2):186-190. doi:10.1212/01.wnl.0000031792.89992.ec

31 Kwan P, Brodie MJ. Early identification of refractory epilepsy. N Engl J Med 20003;342(5): 314-319. doi:10.1056/NEJM200002033420503

32 Iwasaki M, Pestana E, Burgess RC, et al. Detection of epileptiform activity by human interpreters: blinded comparison between electroencephalography and magnetoencephalography. Epilepsia 2005;46(1): 59-68. doi:10.1111/j.0013-9580.2005.21104.x

33 Benson JC, Chiu S, Flemming K, et al. MR characteristics of unruptured intracranial arteriovenous malformations associated with seizure as initial clinical presentation. J Neurointerv Surg 2020;12(2):186-191. doi:10.1136/neurintsurg-2019-015021

34 Brodie MJ, Barry SJ, Bamagous GA, Norrie JD, Kwan P. Patterns of treatment response in newly diagnosed epilepsy. Neurology 2012;78(20): 1548-1554. doi:10.1212/WNL.0b013e3182563b19

35 Strzelczyk A, Griebel C, Lux W, Rosenow F, Reese JP. The burden of severely drug-refractory epilepsy: a comparative longitudinal evaluation of mortality, morbidity, resource use, and cost using german health insurance data. Front Neurol 2017;8:712. doi:10.3389/fneur.2017.00712

36 Braun KPJ, Cross JH. Pediatric epilepsy surgery: the earlier the better. Expert Rev Neurother 2018; 18(4):261-263. doi:10.1080/14737175.2018.1455503

37 Burneo JG, Shariff SZ, Liu K, et al. Disparities in surgery among patients with intractable epilepsy in a universal health system. Neurology 2016;86(1): 72-78. doi:10.1212/WNL.0000000000002249

38 Bonini F, McGonigal A, Scavarda D, et al. Predictive factors of surgical outcome in frontal lobe epilepsy explored with stereoelectroencephalography. Neurosurgery 2018;83(2):217-225. doi:10.1093/neuros/nyx342

39 Englot DJ, Berger MS, Barbaro NM, Chang EF. Factors associated with seizure freedom in the surgical resection of glioneuronal tumors. Epilepsia 2012 Jan;53(1):51-7. doi:10.1111/j.1528-1167.2011.03269.x. Epub 2011 Sep 20. PMID: 21933181 Review.

40 Bell GS, de Tisi J, Gonzalez-Fraile JC, et al. Factors affecting seizure outcome after epilepsy surgery: an observational series. J Neurol Neurosurg Psychiatry 2017;88(11):933-940. doi:10.1136/jnnp-2017-316211

41 Lamberink HJ, Otte WM, Blümcke I, Braun KPJ; European Epilepsy Brain Bank writing group; study group; European Reference Network EpiCARE. Seizure outcome and use of antiepileptic drugs after epilepsy surgery according to histopathological diagnosis: a retrospective multicentre cohort study. Lancet Neurol 2020;19(9):748-757. doi:10.1016/S1474-4422(20)30220-9

42 Téllez-Zenteno JF, Hernández Ronquillo L, Moien-Afshari F, Wiebe S. Surgical outcomes in lesional and non-lesional epilepsy: a systematic review and meta-analysis. Epilepsy Res 2010; 89(2-3):310-318. doi:10.1016/j.eplepsyres.2010.02.007

43 Raybaud C, Widjaja E. Development and dysgenesis of the cerebral cortex: malformations of cortical development. Neuroimaging Clin N Am 2011;21(3):483-543. doi:10.1016/j.nic.2011.05.014

44 Sperling MR, Barshow S, Nei M, Asadi-Pooya AA. A reappraisal of mortality after epilepsy surgery. Neurology 2016;86(21):1938-44. doi:10.1212/WNL.0000000000002700

45 Severino M, Geraldo AF, Utz N, et al. Definitions and classification of malformations of cortical development: practical guidelines. Brain 2020; 143(10):2874-2894. doi:10.1093/brain/awaa174

46 Martinez-Rios C, McAndrews MP, Logan W, et al. MRI in the evaluation of localization-related epilepsy. J Magn Reson Imaging 2016;44(1):12-22. doi:10.1002/jmri.25269

47 Gaillard WD, Chiron C, Cross JH, et al; ILAE, Committee for Neuroimaging, Subcommittee for Pediatric Guidelines. Guidelines for imaging infants and children with recent-onset epilepsy. Epilepsia 2009;50(9):2147-2153. doi:10.1111/j.1528-1167.2009.02075.x

48 Sankar R, Curran JG, Kevill JW, et al. Microscopic cortical dysplasia in infantile spasms: evolution of white matter abnormalities. AJNR Am J Neuroradiol 1995;16(6):1265-1272.

49 Blumcke I, Spreafico R, Haaker G, et al; EEBB Consortium. Histopathological findings in brain tissue obtained during epilepsy surgery. N Engl J Med 2017;377(17):1648-1656. doi:10.1056/NEJMoa1703784

50 Bernhardt BC, Bernasconi A, Liu M, et al. The spectrum of structural and functional imaging abnormalities in temporal lobe epilepsy. Ann Neurol 2016;80(1):142-153. doi:10.1002/ana.24691

51 Briellmann RS, Kalnins RM, Berkovic SF, Jackson GD. Hippocampal pathology in refractory temporal lobe epilepsy: T2-weighted signal change reflects dentate gliosis. Neurology 2002; 58(2):265-271. doi:10.1212/wnl.58.2.265

52 Bronen R. MR of mesial temporal sclerosis: how much is enough? AJNR Am J Neuroradiol 1998; 19(1):15-18.

53 Tsai MH, Vaughan DN, Perchyonok Y, et al. Hippocampal malrotation is an anatomic variant and has no clinical significance in MRI-negative temporal lobe epilepsy. Epilepsia 2016;57(10): 1719-1728. doi:10.1111/epi.13505

54 Bernasconi N, Kinay D, Andermann F, Antel S, Bernasconi A. Analysis of shape and positioning of the hippocampal formation: an MRI study in patients with partial epilepsy and healthy controls. Brain 2005;128(Pt 10):2442-2452. doi:10.1093/brain/awh599

Copyright © American Academy of Neurology. Unauthorized reproduction of this article is prohibited.

55 Bernasconi N, Bernasconi A, Caramanos Z, et al. Entorhinal cortex atrophy in epilepsy patients exhibiting normal hippocampal volumes. Neurology 2001;56(10):1335-1339. doi:10.1212/wnl.56.10.1335

56 Cendes F, Cook MJ, Watson C, et al. Frequency and characteristics of dual pathology in patients with lesional epilepsy. Neurology 1995;45(11):2058-64. doi:10.1212/wnl.45.11.2058

57 Blümcke I, Spreafico R. Cause matters: a neuropathological challenge to human epilepsies. Brain Pathol 2012;22(3):347-349. doi:10.1111/j.1750-3639.2012.00584.x

58 Blümcke I, Thom M, Aronica E, et al. The clinicopathologic spectrum of focal cortical dysplasias: a consensus classification proposed by an ad hoc Task Force of the ILAE Diagnostic Methods Commission. Epilepsia 2011;52(1):158-174. doi:10.1111/j.1528-1167.2010.02777.x

59 Chabardès S, Kahane P, Minotti L, Hoffmann D, Benabid AL. Anatomy of the temporal pole region. Epileptic Disord 2002;4(Suppl 1):S9-S15.

60 Coste S, Ryvlin P, Hermier M, et al. Temporopolar changes in temporal lobe epilepsy: a quantitative MRI-based study. Neurology 2002;59(6):855-861. doi:10.1212/wnl.59.6.855

61 Garbelli R, Milesi G, Medici V, et al. Blurring in patients with temporal lobe epilepsy: clinical, high-field imaging and ultrastructural study. Brain 2012;135(Pt 8):2337-2349. doi:10.1093/brain/aws149

62 Bartolini L, Whitehead MT, Ho CY, et al. Temporal lobe epilepsy and focal cortical dysplasia in children: A tip to find the abnormality. Epilepsia 2017;58(1):113-122. doi:10.1111/epi.13615

63 Kinney HC, Brody BA, Kloman AS, Gilles FH. Sequence of central nervous system myelination in human infancy. II. Patterns of myelination in autopsied infants. J Neuropathol Exp Neurol 1988;47(3):217-234. doi:10.1097/00005072-198805000-00003

64 Clavijo Prado CA, Federico P, Bernasconi A, et al. Imaging characteristics of temporopolar blurring in the context of hippocampal sclerosis. Epileptic Disord 2022;24(1):1-8. doi:10.1684/epd.2021.1378

65 Fong MW, Sala-Padro J, Bartley M, et al. The varied semiology of seizures in the context of small anterior temporal encephaloceles. Epileptic Disord 2019;21(4):347-352. doi:10.1684/epd.2019.1081

66 Capizzano AA, Kawasaki H, Sainju RK, et al. Amygdala enlargement in mesial temporal lobe epilepsy: an alternative imaging presentation of limbic epilepsy. Neuroradiology 2019;61(2):119-127. doi:10.1007/s00234-018-2109-y

67 Beh SMJ, Cook MJ, D'Souza WJ. Isolated amygdala enlargement in temporal lobe epilepsy: a systematic review. Epilepsy Behav 2016;60:33-41. doi:10.1016/j.yebeh.2016.04.015

68 Muhlhofer W, Tan YL, Mueller SG, Knowlton R. MRI-negative temporal lobe epilepsy–what do we know? Epilepsia 2017;58(5):727-742. doi:10.1111/epi.13699

69 Barkovich AJ, Guerrini R, Kuzniecky RI, Jackson GD, Dobyns WB. A developmental and genetic classification for malformations of cortical development: update 2012. Brain 2012;135(Pt 5):1348-1369. doi:10.1093/brain/aws019

70 Colombo N, Tassi L, Deleo F, et al. Focal cortical dysplasia type IIa and IIb: MRI aspects in 118 cases proven by histopathology. Neuroradiology 2012;54(10):1065-1077. doi:10.1007/s00234-012-1049-1

71 Najm IM, Sarnat HB, Blümcke I. Review: The international consensus classification of Focal Cortical Dysplasia–a critical update 2018. Neuropathol Appl Neurobiol 2018;44(1):18-31. doi:10.1111/nan.12462

72 Krsek P, Maton B, Korman B, et al. Different features of histopathological subtypes of pediatric focal cortical dysplasia. Ann Neurol 2008;63(6):758-769.doi:10.1002/ana.21398

73 Barkovich AJ, Raybaud C. Pediatric malformations of the brain and skull. In: Barkovich AJ, Raybaud C, editors. Pediatric neuroimaging. Wolters Kluwer; 2019:405-632.

74 Jayalakshmi S, Nanda SK, Vooturi S, et al. Focal cortical dysplasia and refractory epilepsy: role of multimodality imaging and outcome of surgery. AJNR Am J Neuroradiol 2019;40(5):892-898. doi:10.3174/ajnr.A6041

75 Blümcke I, Coras R, Busch RM, Morita-Sherman M, et al. Toward a better definition of focal cortical dysplasia: an iterative histopathological and genetic agreement trial. Epilepsia 2021;62(6):1416-1428. doi:10.1111/epi.16899

76 Bronen RA, Spencer DD, Fulbright RK. Cerebrospinal fluid cleft with cortical dimple: MR imaging marker for focal cortical dysgenesis. Radiology 2000;214(3):657-663. doi:10.1148/radiology.214.3.r00mr40657

77 Iffland PH 2nd, Carson V, Bordey A, Crino PB. GATORopathies: the role of amino acid regulatory gene mutations in epilepsy and cortical malformations. Epilepsia 2019;60(11):2163-2173. doi:10.1111/epi.16370

78 Guerrini R, Dobyns WB. Malformations of cortical development: clinical features and genetic causes. Lancet Neurol 2014l;13(7):710-26. doi:10.1016/S1474-4422(14)70040-7

79 Palmini A, Paglioli E, Silva VD. Developmental tumors and adjacent cortical dysplasia: single or dual pathology? Epilepsia 2013;54(Suppl 9):18-24. doi:10.1111/epi.12438

80 Di Donato N, Chiari S, Mirzaa GM, et al. Lissencephaly: expanded imaging and clinical classification. Am J Med Genet A 2017;173(6):1473-1488. doi:10.1002/ajmg.a.38245

Copyright © American Academy of Neurology. Unauthorized reproduction of this article is prohibited.

81 Mutch CA, Poduri A, Sahin M, et al. Disorders of microtubule function in neurons: imaging correlates. AJNR Am J Neuroradiol 2016;37(3): 528-535. doi:10.3174/ajnr.A4552

82 Hartlieb T, Winkler P, Coras R, et al. Age-related MR characteristics in mild malformation of cortical development with oligodendroglial hyperplasia and epilepsy (MOGHE). Epilepsy Behav 2019;91:68-74. doi:10.1016/j.yebeh.2018.07.009

83 Freeman JL, Coleman LT, Wellard RM, et al. MR imaging and spectroscopic study of epileptogenic hypothalamic hamartomas: analysis of 72 cases. AJNR Am J Neuroradiol 2004;25(3):450-462. doi:10.3171/2013.3.FOCUS1355

84 Mendes Coelho VC, Morita-Sherman M, Yasuda CL, et al. Magnetic resonance imaging findings and clinical characteristics in mild malformation of cortical development with oligodendroglial hyperplasia and epilepsy in a predominantly adult cohort. Epilepsia 2021;62(6):1429-1441. doi:10.1111/epi.16907

85 Blumcke I, Aronica E, Urbach H, Alexopoulos A, Gonzalez-Martinez JA. A neuropathology-based approach to epilepsy surgery in brain tumors and proposal for a new terminology use for long-term epilepsy-associated brain tumors. Acta Neuropathol 2014;128(1):39-54. doi:10.1007/s00401-014-1288-9

86 Cossu M, Fuschillo D, Bramerio M, et al. Epilepsy surgery of focal cortical dysplasia-associated tumors. Epilepsia 2013;54(Suppl 9):115-122. doi:10.1111/epi.12455

87 Osborn AG, Hedlund GL. Osborn's brain. Imaging, pathology and anatomy. 2nd ed. Elsevier; 218.

88 Kasper BS, Kasper EM. New classification of epilepsy-related neoplasms: the clinical perspective. Epilepsy Behav 2017b;67:91-97. doi:10.1016/j.yebeh.2016.12.020

89 Cohen NT, Cross JH, Arzimanoglou A, et al. Hypothalamic hamartomas: evolving understanding and management. Hypothalamic Hamartoma Writing Group. Neurology 2021;97(18): 864-873. doi:10.1212/WNL.0000000000012773

90 Usui N, Mihara T, Baba K, et al. Posterior cortex epilepsy secondary to ulegyria: is it a surgically remediable syndrome? Epilepsia 2008;49(12): 1998-2007. doi:10.1111/j.1528-1167.2008.01697.x

91 Bi WY. Imaging of skull base tumors. Continuum (Minneap Minn) 2021;29(1, Neuroimaging): 156-170.

92 Gillinder L, Britton J. Autoimmune-associated seizures. Continuum (Minneap Minn) 2022; 28(2, Epilepsy):363-398. doi:10.1212/CON.0000000000001079

93 Granata T, Andermann F. Rasmussen encephalitis. Handb Clin Neurol 2013;111:511-519. doi:10.1016/B978-0-444-52891-9.00054-3

94 Campbell ZM, Hyer JM, Lauzon S, et al. Detection and characteristics of temporal encephaloceles in patients with refractory epilepsy. AJNR Am J Neuroradiol 2018;39(8):1468-1472. doi:10.3174/ajnr.A5704

95 Sandhu MRS, Mandel M, McGrath H, et al. Management of patients with medically intractable epilepsy and anterior temporal lobe encephaloceles. J Neurosurg 2021;136(3):709-716. doi:10.3171/2021.3.JNS21133

96 Hasbani DM, Crino PB. Tuberous sclerosis complex. Handb Clin Neurol 2018;148:813-822. doi:10.1016/B978-0-444-64076-5.00052-1

97 Maton B, Krsek P, Jayakar P, 10.3171/2021.3.JNS21133. Medically intractable epilepsy in Sturge-Weber syndrome is associated with cortical malformation: implications for surgical therapy. Epilepsia 2010;51(2):257-267. doi:10.1111/j.1528-1167.2009.02304.x

98 Pinto AL, Chen L, Friedman R, 10.3171/2021.3.JNS21133. Sturge-Weber Syndrome: Brain magnetic resonance imaging and neuropathology findings. Pediatr Neurol 2016;58: 25-30. doi:10.1016/j.pediatrneurol.2015.11.005

99 Nakashima M, Miyajima M, Sugano H, et al. The somatic GNAQ mutation c.548G>A (p.R183Q) is consistently found in Sturge-Weber syndrome. J Hum Genet 2014;59(12):691-693. doi:10.1038/jhg.2014.95

100 Lerner A, Shiroishi MS, Zee CS, Law M, Go JL. Imaging of neurocysticercosis. Neuroimaging Clin N Am 2012;22(4):659-676. doi:10.1016/j.nic.2012.05.004

101 Saini J, Kesavadas C, Thomas B, et al. Susceptibility weighted imaging in the diagnostic evaluation of patients with intractable epilepsy. Epilepsia 2009;50(6): 1462-1473. doi:10.1111/j.1528-1167.2008.01882.x

102 Jehi LE, Palmini A, Aryal U, Coras R, Paglioli E. Cerebral cavernous malformations in the setting of focal epilepsies: pathological findings, clinical characteristics, and surgical treatment principles. Acta Neuropathol 2014;128(1):55-65. doi:10.1007/s00401-014-1294-y

103 Duncan JS, Winston GP, Koepp MJ, Ourselin S. Brain imaging in the assessment for epilepsy surgery. Lancet Neurol 2016;15(4):420-433. doi:10.1016/S1474-4422(15)00383-X

104 Bacon EJ, Jin C, He D, et al. Epileptogenic zone localization in refractory epilepsy by FDG-PET: The Comparison of SPM and SPM-CAT with different parameter settings. Front Neurol 2021; 12:724680. doi:10.3389/fneur.2021.724680

105 Salamon N, Kung J, Shaw SJ, et al. FDG-PET/MRI coregistration improves detection of cortical dysplasia in patients with epilepsy. Neurology 2008;71(20):1594-601. doi:10.1212/01.wnl.0000334752.41807.2f

106 Von Oertzen TJ. PET and ictal SPECT can be helpful for localizing epileptic foci. Curr Opin Neurol 2018;31(2):184-191. doi:10.1097/WCO.0000000000000527

Copyright © American Academy of Neurology. Unauthorized reproduction of this article is prohibited.

107 Krsek P, Kudr M, Jahodova A, et al. Localizing value of ictal SPECT is comparable to MRI and EEG in children with focal cortical dysplasia. Epilepsia 2013;54(2):351-358. doi:10.1111/epi.12059

108 Logothetis NK. The underpinnings of the BOLD functional magnetic resonance imaging signal. J Neurosci 2003;23(10):3963-3971. doi:10.1523/JNEUROSCI.23-10-03963.2003

109 Htet NN, Pizarro R, Nair VA, et al. Comparison of language and memory lateralization by functional MRI and Wada test in epilepsy. Front Neurol Neurosci Res 2021;2:100009.

110 Agarwal S, Sair HI, Gujar S, Pillai JJ. Language mapping with fMRI: current standards and reproducibility. Top Magn Reson Imaging 2019;28(4):225-233. doi:10.1097/RMR.0000000000000216

111 Englot DJ, Nagarajan SS, Imber BS, Htet NN, Pizarro R, Nair VA, et al. Comparison of language and memory lateralization by functional MRI and Wada test in epilepsy. Epileptogenic zone localization using magnetoencephalography predicts seizure freedom in epilepsy surgery. Epilepsia 2015;56(6):949-958. doi:10.1111/epi.13002

112 Szaflarski JP, Gloss D, Binder JR, et al. Practice guideline summary: use of fMRI in the presurgical evaluation of patients with epilepsy: report of the Guideline Development, Dissemination, and Implementation Subcommittee of the American Academy of Neurology. Neurology 2017;88(4):395-402. doi:10.1212/WNL.0000000000003532

113 Burgess RC. MEG for greater sensitivity and more precise localization in epilepsy. Neuroimaging Clin N Am 2020;30(2):145-158. doi:10.1016/j.nic.2020.02.004

114 Alkawadri R, Burgess RC, Kakisaka Y, Mosher JC, Alexopoulos AV. Assessment of the utility of ictal magnetoencephalography in the localization of the epileptic seizure onset zone. JAMA Neurol 2018;75(10):1264-1272. doi:10.1001/jamaneurol.2018

115 Bernasconi A, Antel SB, Collins DL, et al. Texture analysis and morphological processing of magnetic resonance imaging assist detection of focal cortical dysplasia in extra-temporal partial epilepsy. Ann Neurol 2001;49(6):770-775.

116 Adler S, Wagstyl K, Gunny R, et al. Novel surface features for automated detection of focal cortical dysplasias in paediatric epilepsy. Neuroimage Clin 2016;14:18-27. doi:10.1016/j.nicl.2016.12.030

117 Vos SB, Winston GP, Goodkin O, et al. Hippocampal profiling: localized magnetic resonance imaging volumetry and T2 relaxometry for hippocampal sclerosis. Epilepsia 2020;61(2):297-309. doi:10.1111/epi.16416

118 Bautista RE, Glen ET, Shetty NK, Wludyka P. The association between health literacy and outcomes of care among epilepsy patients. Seizure 2009;18(6):400-4. doi:10.1016/j.seizure.2009.02.004

119 Vernon JA, Trujillo A, Rosenbaum S, DeBuono B. Low health literacy: Implications for national health policy. Washington, DC: Department of Health Policy, School of Public Health and Health Services. The George Washington University; 2007.

120 Dua T, de Boer HM, Prilipko LL, Saxena S. Epilepsy care in the world: results of an ILAE/IBE/WHO Global Campaign Against Epilepsy survey. Epilepsia 2006;47(7):1225-1231. doi:10.1111/j.1528-1167.2006.00595.x

121 McClelland S 3rd, Guo H, Okuyemi KS. Racial disparities in the surgical management of intractable temporal lobe epilepsy in the United States: a population-based analysis. Arch Neurol 2010;67(5):577-583. doi:10.1001/archneurol.2010.86

122 Bernasconi N, Wang I. Emerging trends in neuroimaging of epilepsy. Epilepsy Curr 2021;21(2):79-82. doi:10.1177/1535759721991161

Copyright © American Academy of Neurology. Unauthorized reproduction of this article is prohibited.

REVIEW ARTICLE

CONTINUUM AUDIO INTERVIEW AVAILABLE ONLINE

Imaging of Skull Base Tumors

By Wenya Linda Bi, MD, PhD

ABSTRACT

OBJECTIVE: **This article provides an overview of imaging modalities and findings associated with common skull base tumors including meningiomas and how to use imaging features to guide surveillance and treatment decision making.**

LATEST DEVELOPMENTS: **Ease of access to cranial imaging has led to a higher number of incidentally diagnosed skull base tumors, which merit careful consideration for management with observation or treatment. The point of origin of the tumor dictates the pattern of anatomic displacement and involvement by the tumor as it grows. Careful study of vascular encroachment on CT angiography, as well as the pattern and extent of bony invasion on CT, abets treatment planning. Quantitative analyses of imaging, such as with radiomics, may further elucidate phenotype-genotype associations in the future.**

ESSENTIAL POINTS: **Combinatorial application of CT and MRI analyses improves the diagnosis of skull base tumors, clarifies their point of origin, and dictates the extent of treatment needed.**

INTRODUCTION

Skull base tumors encompass a wide spectrum of intracranial pathologies that refer to either their origin outside of brain parenchyma or their anatomic location within the cranium. Collectively, these pathologies account for the majority of intracranial neoplasms and include meningioma, pituitary tumors, craniopharyngioma, schwannoma, chordoma, chondrosarcoma, and paraganglioma, among others.[1] Non-neoplastic entities that exert similar mass effect and insinuation around cranial nerves and vessels, such as epidermoid and dermoid cysts, are also commonly clustered with skull base tumors in the differential diagnosis. Additionally, pathologies from the closely adjacent orbit, head, and neck structures often involve the skull base and should be considered together from a differential diagnosis and management perspective.

Although most skull base tumors are considered benign, several pathologies exhibit malignant subtypes or may be locally destructive in their growth, causing premature morbidity and mortality. Distinguishing these more aggressive subtypes from their benign counterparts is the subject of extensive radiographic investigation using both conventional and advanced imaging modalities, because earlier intervention in these nonbenign entities may improve outcomes.

CITE AS:
CONTINUUM (MINNEAP MINN) 2023;29(1, NEUROIMAGING): 156-170.

Address correspondence to Dr Wenya Linda Bi, Department of Neurosurgery, Brigham and Women's Hospital, 75 Francis St, Boston, MA 02115, WBI@bwh.harvard.edu.

RELATIONSHIP DISCLOSURE:
Dr Bi Reports no disclosure.

UNLABELED USE OF PRODUCTS/INVESTIGATIONAL USE DISCLOSURE:
Dr Bi reports no disclosure.

© 2023 American Academy of Neurology.

Copyright © American Academy of Neurology. Unauthorized reproduction of this article is prohibited.

Conversely, the easy availability of cranial imaging in the contemporary era and its wide application for common symptoms such as headache and dizziness or after a fall have led to an increase in incidentally discovered tumors. Many of these tumors, such as small or calcified convexity meningiomas or pituitary microadenomas, may never cause harm. Judicious observation through serial imaging, therefore, is a critical component of the management of skull base tumors. General indications for treatment include (1) symptomatic mass effect, (2) a large tumor, (3) progressive growth over time, or (4) impending neurologic deficit that may be irreversible without intervention. Invocation of these indications, especially the last three, is subject to patient preference and clinician judgment. Given the extra-axial origin (ie, the cell of origin is outside of the brain parenchyma) of skull base tumors, they frequently exhibit symptoms through gradual growth over time and compression of eloquent neural or vascular

KEY POINTS

- Skull base tumors refer to both tumors whose cell of origin is outside of the brain parenchyma as well as tumors that are physically located in or near the base of the skull.
- Many skull base tumors, such as meningiomas or pituitary microadenomas, are incidentally diagnosed and may be safely observed as the initial strategy.

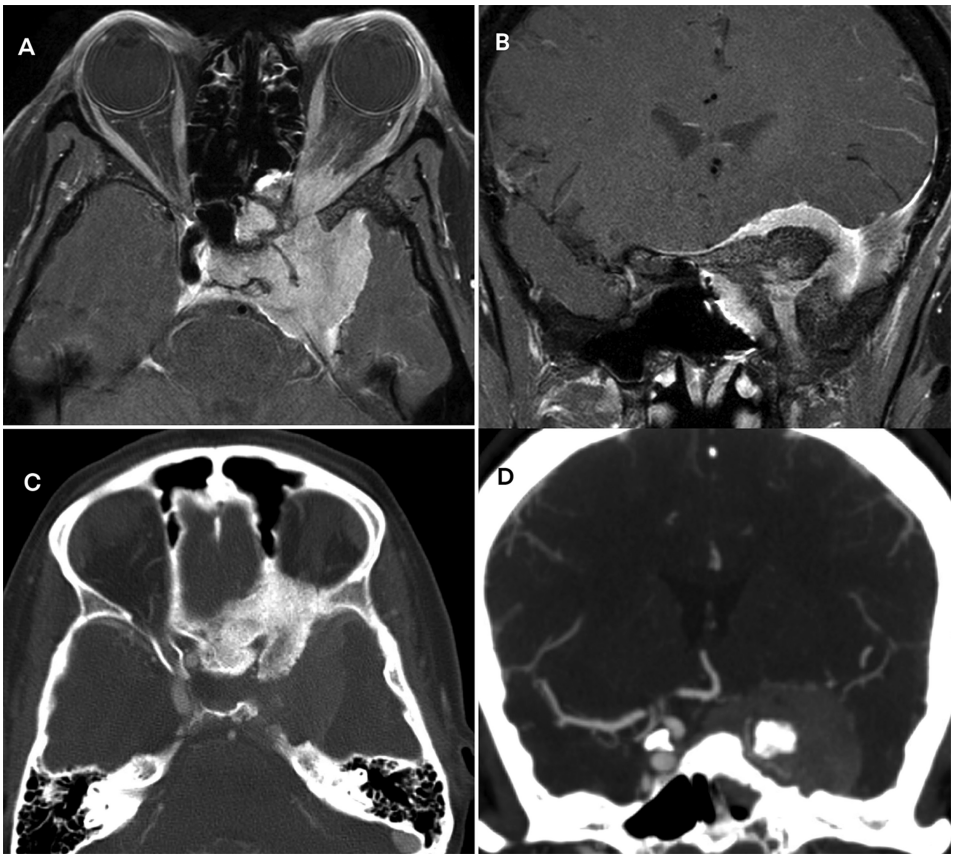

FIGURE 6-1

Spheno-clinoidal cavernous meningioma. A 45-year-old woman with gradual left eye visual loss, progressing to blindness, left proptosis, and periorbital pain was found to have a spheno-clinoidal cavernous meningioma. Axial (*A*) and coronal (*B*) postcontrast T1-weighted MRI shows an enhancing extra-axial tumor expanding the cavernous sinus, with extension along the orbital roof and sphenoid wing, completely encasing and narrowing the left internal carotid artery and growing through the hyperostostic-involved skull base, including the orbital roof and sphenoid wing. *C*, Axial CT further confirms marked hyperostosis of the left anterior clinoid process, medial sphenoid wing, and orbital roof. *D*, Coronal CT angiogram highlights the diminutive left internal carotid artery and proximal anterior and middle cerebral arteries, due to tumor encasement, with distal reconstitution of the left middle cerebral artery branches.

Copyright © American Academy of Neurology. Unauthorized reproduction of this article is prohibited.

structures, which may be reversed with alleviation of the symptomatic mass effect.

This article highlights general principles in the interpretation of imaging for skull base tumors and addresses specific considerations for common pathologies.

GENERAL PRINCIPLES

Contrast-enhanced MRI is the most common modality by which skull base tumors are diagnosed and followed over time. T2-weighted images, however, can distinguish the boundary between tumor and brain, track the relationship of cranial nerves with respect to skull base tumors, and serve as a surrogate for identifying key vascular supply.

More so than for intrinsic brain tumors, CT aids in the diagnosis and assessment of tumor extent for skull base tumors, which often exhibit characteristic bony invasion, lytic erosion, or intratumoral calcification. Failure to assess the extent of bony involvement, such as in meningioma, may lead to underappreciation of growth and change over time.

Skull base tumors also have a predilection for extracranial extension given their location. They may abut, compress, encase, or occlude adjacent vascular structures and nerves, leading to morbidity with observation or treatment. Yet

CASE 6-1

A 60-year-old woman presented with 1 year of progressive cognitive difficulties, followed by blurry vision affecting her left eye and persistent headaches. Neuro-ophthalmology evaluation confirmed a left compressive optic neuropathy with reduced acuity, a relative afferent pupillary defect, and significant depression of the visual field throughout the left eye. Imaging revealed a homogeneous enhancing extra-axial tumor centered on a hyperostotic left anterior clinoid process (FIGURE 6-2).

The patient underwent a left cranio-orbitozygomatic approach for total excision of the tumor and the involved anterior clinoid bone. Pathology confirmed a World Health Organization grade I meningioma. She recovered full vision and neurologic function.

COMMENT

This case exemplifies the hyperostotic bony change signaling the origin of meningiomas, vascular encasement by meningiomas with minimal ischemic risk, and good recovery after resection.

Copyright © American Academy of Neurology. Unauthorized reproduction of this article is prohibited.

because of their characteristic slow pace of growth, vascular encasement or even occlusion rarely leads to ischemia. Assessment of vascular patency, both arterial and venous, is important when considering the risk of intervention or continued observation.

The point of origin of skull base tumors dictates their pattern of growth and relationship with adjacent neurovascular structures and the brain. Although the absolute anatomic position may be distorted by a growing tumor, relative anatomic relationships tend to remain steadfast.

MENINGIOMAS

Meningiomas are the most common primary central nervous system tumor in adults (FIGURE 6-1). Approximately 85% of meningiomas are considered benign, or World Health Organization (WHO) grade I, 3% are considered malignant, or WHO grade III, and another 10% to 15% straddle an intermediate course of growth and are considered atypical, or WHO grade II.[2] Meningiomas are traditionally defined by histopathologic features, although the genetic and epigenetic makeup of these tumors is increasingly associated with their long-term outcome, often more robustly than the WHO grade alone.[3] Consistent with their putative origin from arachnoid cap cells, meningiomas are distributed

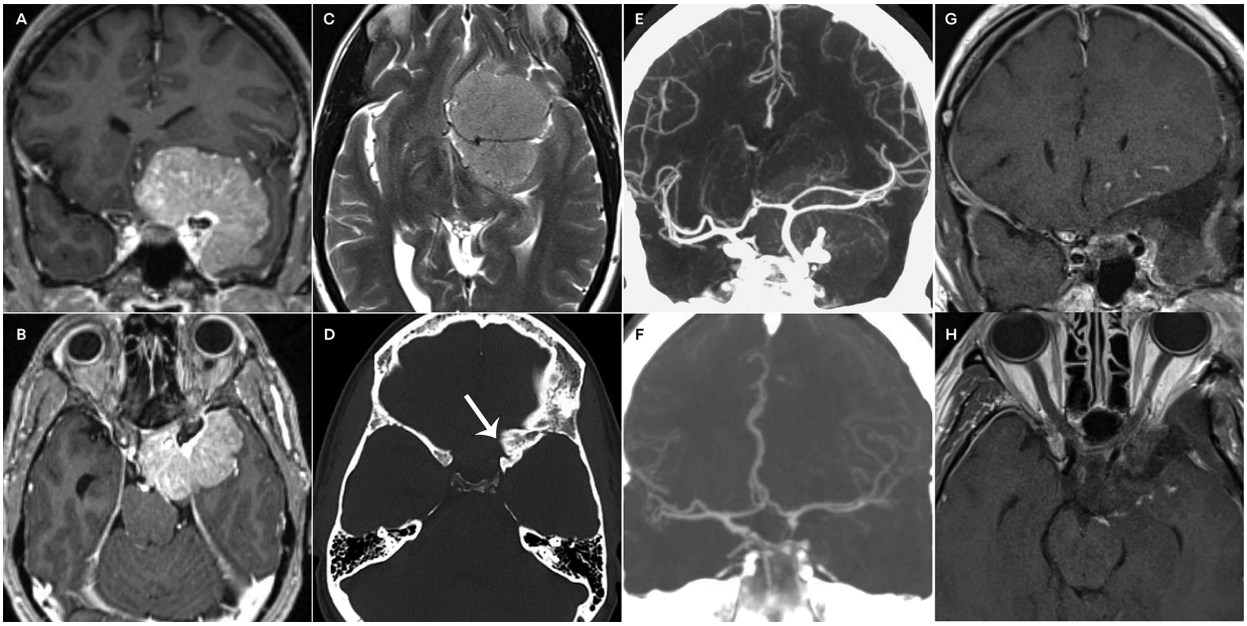

FIGURE 6-2

Clinoidal meningioma shown in the imaging of the patient in CASE 6-1. Gadolinium-enhanced T1-weighted MRI in the coronal (*A*) and axial (*B*) planes shows an avidly enhancing mass centered on the clinoid process. Axial T2-weighted MRI (*C*) highlights encasement of the left internal carotid bifurcation into the proximal anterior cerebral artery and middle cerebral artery. Axial CT scan in the bone window confirms hyperostosis of the left anterior clinoid process (*D*, *arrow*), further supporting the origin of the tumor. Coronal CT angiogram (*E*) shows full encasement of the left internal carotid artery and carotid bifurcation by the clinoidal meningioma, with normalization of the internal carotid artery and proximal anterior and middle cerebral arteries after tumor resection (*F*), confirmed on coronal (*G*) and axial (*H*) T1-weighted contrast-enhanced images.

Copyright © American Academy of Neurology. Unauthorized reproduction of this article is prohibited.

across the cranial vault, with three general location categories: the skull base (anterior, middle, and posterior fossa), the calvarium (frontal, parietal, temporal, occipital, and cerebellar convexities), and the dividing membrane between hemispheres (falcine, parasagittal, and tentorial origins). Intraventricular meningiomas are most often located in the atrium of the lateral ventricle, especially on the left.

Classically, meningiomas exhibit avid contrast enhancement on MRI, with an associated dural tail. They may be hypointense, isointense, or hyperintense on T2-weighted MRI, with more hyperintense signal often correlating with softer tumor texture, which is important in considering the ease, or lack thereof, during surgical resection. In patients who have a known meningioma and cannot tolerate gadolinium, thin-cut T2 sequences may be sufficient for tracking tumor growth, as is CT with contrast.

CT is helpful to determine the true extent of meningioma spread, given the frequent involvement of adjacent bone. Bony involvement exhibited by central calcification or hyperostosis often reflects more indolent growth whereas lytic

CASE 6-2

A 63-year-old woman with a history of breast cancer presented with 2 weeks of severe progressive ophthalmoparesis. Her visual acuity remained excellent on neuro-ophthalmology evaluation, despite near-complete oculomotor and abducens palsies.

Imaging revealed an extensive extra-axial enhancing tumor encasing the superior orbital fissure and accounting for the extraocular nerve compression with consequent ophthalmoparesis (FIGURE 6-3). She underwent a right cranio-orbitozygomatic approach for removal of the tumor encroaching on the periorbita and superior orbital fissure and removal of the lateral wall of the orbit, sphenoid wing, and roof of the optic canal to allow for wide decompression of the involved cranial nerves. Pathology revealed metastatic carcinoma consistent with a breast cancer primary. She regained complete normalization of extraocular movements within weeks after surgery, with preserved visual acuity, to allow for the safe delivery of adjuvant radiation to the resection bed.

COMMENT

This case illustrates nonmeningioma pathologies, such as breast metastasis, which can mimic extra-axial enhancing tumors with bony involvement.

Copyright © American Academy of Neurology. Unauthorized reproduction of this article is prohibited.

erosion of the bone is concerning for more aggressive growth, both of which may be easier to appreciate on CT than MRI. Meningiomas may grow through the skull and invade adjacent muscles or spread along the subgaleal space. This is most commonly seen in subsets of sphenoid wing meningiomas, where coronal plane images should be carefully inspected for tumor migration out of the foramen ovale or rotundum and into the infratemporal fossa or temporalis muscle, especially during serial imaging for monitoring.

Vascular imaging, such as through a dynamic CT angiogram or CT venogram, highlights the vascular supply of meningiomas and helps assess venous sinus patency or cortical venous rerouting for operative planning in patients who need treatment; this imaging also helps distinguish meningiomas from mimickers such as hemangiopericytoma, now known as *solitary fibrous tumor*.[4] Meningiomas may abut, compress, or encase neurovascular structures, depending on their point of origin (CASE 6-1). Slow compression or even complete occlusion of a venous sinus, such as the superior sagittal sinus by parasagittal meningiomas, is rarely associated with vascular infarct. Likewise,

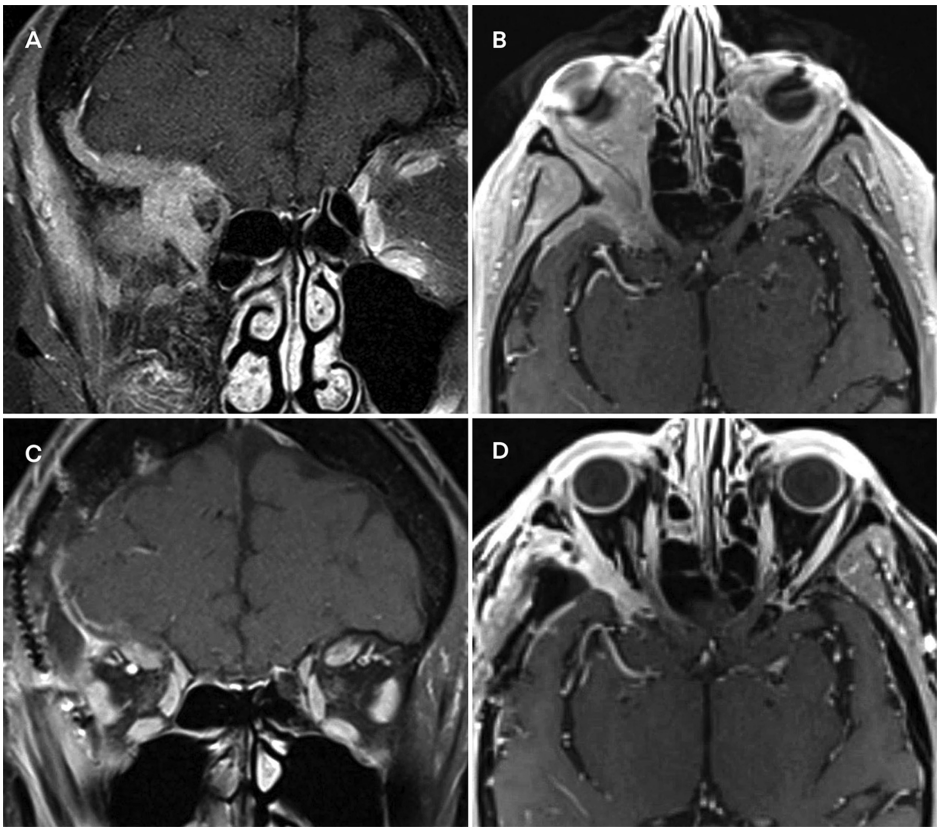

FIGURE 6-3

Extra-axial breast metastasis mimicking a right spheno-orbital meningioma, causing ophthalmoplegia in the patient in CASE 6-2. Coronal (*A*) and axial (*B*) contrast-enhanced MRI shows an extra-axial enhancing tumor involving the right sphenoid wing, with encasement of the superior orbital fissure, extending to the right orbital roof and temporal pole. Coronal (*C*) and axial (*D*) contrast-enhanced MRI after surgery shows decompression of the orbital apex with normalization of the extraocular muscles at their insertion.

Copyright © American Academy of Neurology. Unauthorized reproduction of this article is prohibited.

KEY POINTS

- The point of origin of skull base tumors dictates their relationship with adjacent nerves, vessels, and the brain because relative anatomic relationships are usually maintained even while absolute anatomic positions are distorted.
- Meningiomas frequently involve the adjacent bone, which should be specifically examined on surveillance imaging.
- Venous sinus occlusion through natural growth of a meningioma leads to rerouting of venous drainage from cortical veins at the anterior and posterior limits of the occluded sinus and does not result in venous infarction on its own.
- Enlarging benign meningiomas typically grow 1 to 2 mm per year; rates faster than this raise concern for more atypical behavior.
- A meningioma growth rate exceeding that of benign meningioma trajectories, irregular tumor shape, intratumoral heterogeneity including the presence of central necrosis or hemorrhage, a knobby or ill-defined pattern of tumor-brain interface, and potentially the extent of peritumoral edema all raise concern for more aggressive behavior.
- Falcine and parasagittal meningiomas are more likely to be higher grade whereas midline anterior skull base meningiomas tend to be benign.

constriction of the internal cerebral artery by an encasing meningioma is rarely associated with stroke.

Meningiomas account for approximately 30% of incidentally diagnosed neoplasms on brain MRI conducted for non-neurologic symptoms.[5,6] While some asymptomatic meningiomas continue to grow on surveillance imaging, some do not, especially those that are predominantly ossified. Enlarging, benign meningiomas typically grow 1 to 2 mm per year; rates faster than this raise concern for more atypical behavior. Radiographic features associated with more aggressive behavior include large tumor size, tumor growth rate exceeding that of benign meningioma trajectories, irregular tumor shape, intratumoral heterogeneity including the presence of central necrosis or hemorrhage, a knobby or ill-defined pattern of tumor-brain interface, and potentially the extent of peritumoral edema. Meningioma location also associates with a predilection for benign or more aggressive character, with tumors of the midline anterior skull base being almost exclusively benign, even if they can grow to a large size before detection, whereas falcine and parasagittal meningiomas are predisposed to being higher grade. Multiple closely adjacent enhancing pachymeningeal foci, like a studding of meningiomas, suggest meningiomatosis, which portends malignant behavior and potential for rapid growth.

Extra-axial mimics of meningioma include solitary fibrous tumors (formerly known as *hemangiopericytomas*), dural-based metastases (breast cancer being a common culprit), plasmacytomas, and sarcomas (CASE 6-2). Solitary fibrous tumors may be indistinguishable from meningioma on postcontrast T1-weighted MRI given their avid enhancement. They more frequently cause bony erosion, as opposed to hyperostosis, and rarely exhibit intratumoral calcification.[7] Importantly, high-grade solitary fibrous tumors are highly vascular, with prominent flow voids on T2-weighted MRI or a cast of vessels on CT angiogram or digital subtraction angiogram, which must be dealt with if planning a surgical intervention. Solitary fibrous tumors may metastasize outside of the central nervous system, which should be screened for in the setting of radiographic suspicion or pathologic confirmation. ^{68}Gallium-dodecanetetraacetic acid tyrosine-3-octreotate (DOTATATE) positron emission tomography (PET) for detection of somatostatin receptor expression, which is enriched in meningiomas, can sometimes help distinguish meningiomas from mimickers, although it is not highly specific.[8]

SCHWANNOMAS

Schwannomas are benign spindle cell neoplasms arising from Schwann cells, most classically described as from the Obersteiner-Redlick glial-Schwann cell junction. Within the cranium, schwannomas of the vestibular nerve, historically and colloquially termed *acoustic neuromas*, are the most common location, followed by schwannomas of the trigeminal and lower cranial nerves. Schwannomas of the motor cranial nerves, including the hypoglossal, facial, and oculomotor nerves, are fairly rare, and each harbors a distinct presentation.

Vestibular schwannomas may originate anywhere along the peripheral eighth cranial nerve, from the distal internal auditory canal to the cerebellopontine cistern, with its point of origin relative to the cisternal arachnoid dictating its relationship to the closely abutting cochlear nerve, facial nerve, brainstem, and their corresponding functions.[9] A subset of schwannomas do not appear to grow after detection; those that do grow increase by 1 to 1.5 mm per year on average, although not always linearly across long-term follow-up.[10] Absence of

Copyright © American Academy of Neurology. Unauthorized reproduction of this article is prohibited.

radiographic growth may still be associated with progressive hearing loss over time. Most schwannomas are solid in consistency and show homogeneous or heterogeneous enhancement on MRI, with the heterogeneity reflecting intratumoral cysts or microhemorrhages (FIGURE 6-4). Cystic sporadic schwannomas, and those associated with neurofibromatosis type 2 (NF2), tend to exhibit more rapid growth compared with solid sporadic schwannomas.

Management of these tumors is heavily influenced by the size at presentation and the presence of neurologic deficits. Large (greater than 3 cm) and giant (greater than 4 cm) schwannomas generally need treatment, with surgery being the most effective at alleviating symptomatic mass effect. Small- and medium-sized schwannomas may be observed or treated, which entails surgery or radiation, after a detailed discussion of quality of life, functional preservation, and risks of treatment considerations with a clinician experienced in skull base tumors. T2-weighted MRI is suitable for serial monitoring of known sporadic schwannomas to minimize long-term gadolinium exposure.[11]

In patients with NF2, multiple synchronous schwannomas and meningiomas of different grades and subtypes may present on imaging. Given the lifetime cumulative risk of new tumor development, observation of growing tumors is

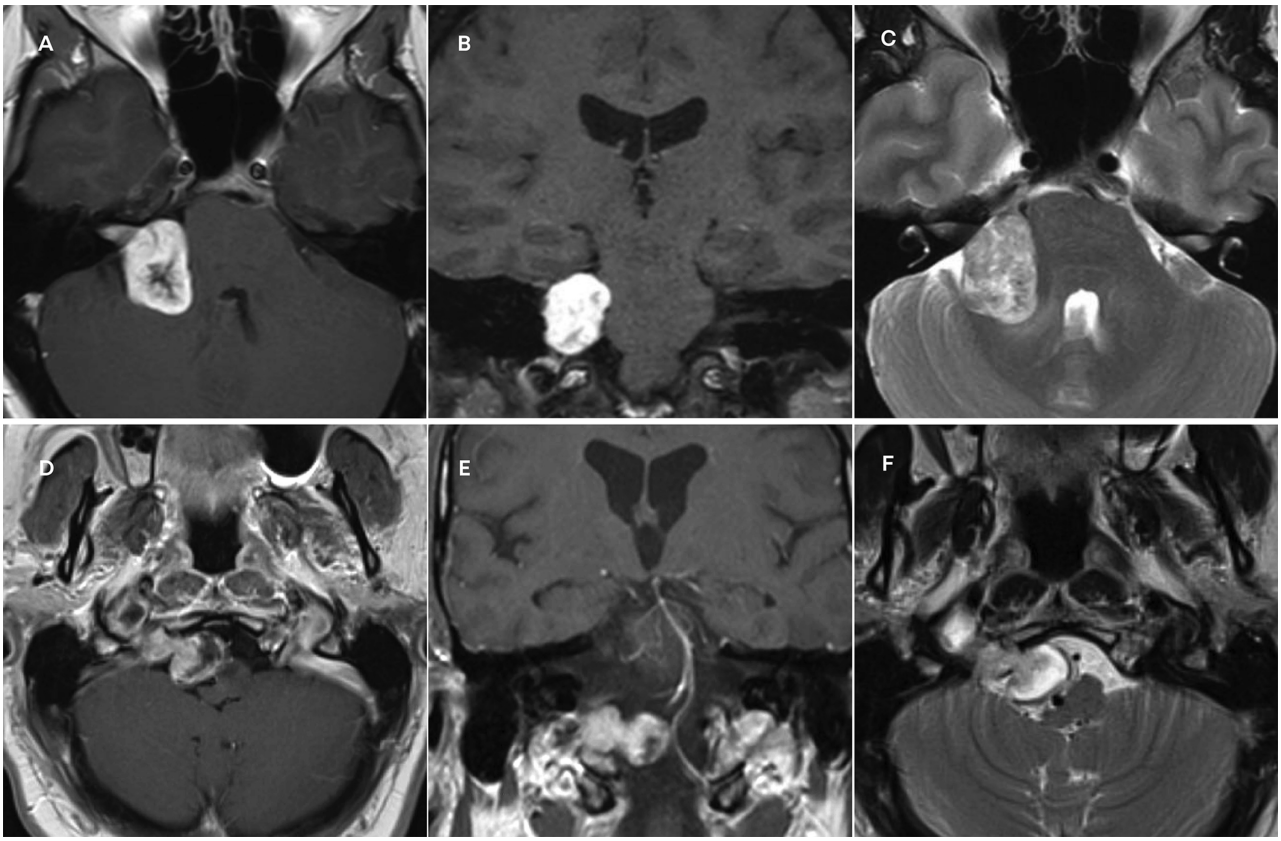

FIGURE 6-4

Schwannomas. Postcontrast T1-weighted axial (*A*) and coronal (*B*) postcontrast T1-weighted MRI of a right vestibular schwannoma demonstrating avid enhancement with a speckled appearance on T2-weighted images (*C*). Postcontrast T1-weighted axial (*D*) and coronal (*E*) postcontrast T1-weighted MRI of a right hypoglossal schwannoma demonstrating irregular enhancement with partially cystic and partially centrally necrotic features seen on the T2-weighted images (*F*).

Copyright © American Academy of Neurology. Unauthorized reproduction of this article is prohibited.

the general rule until symptomatic mass effect occurs. Discerning malignant from benign tumors in the setting of NF2 can also inform the order of tumor treatment in this setting.

PITUITARY TUMORS AND CRANIOPHARYNGIOMAS

The sellar and parasellar region contains a confluence of tissue types, each of which may give rise to a tumor (FIGURE 6-5[12]). The most common tumor within the sella is the pituitary adenoma, arising from the anterior pituitary gland (adenohypophysis) and comprising approximately 16% of all primary brain tumors.[13] Other less common lesions in the sellar and suprasellar region include craniopharyngioma, Rathke cleft cyst, arachnoid cyst, meningioma, metastasis, germ cell tumors, sarcoid and other inflammatory lesions, hypothalamic hamartomas or lymphocytic hypophysitis, and vascular pathologies.

The pituitary gland is fed by two major vascular supplies, reflective of its dual embryologic origin. The adenohypophysis and infundibulum are primarily supplied by the superior hypophysial artery and branches of the posterior communicating artery whereas the posterior neurohypophysis derives blood supply from the inferior hypophysial artery, with a robust portal network in between. This rich blood supply contributes to differential (faster) uptake of contrast by pituitary adenomas compared with the normal pituitary gland, as teased out by dynamic contrast MRI protocols.

Pituitary adenomas are classified based on size, direction, the extent of growth, hormonal status, and, more recently, expression of transcription factors. Tumors smaller than 1 cm in diameter are considered *microadenomas* whereas those 1 cm and larger are termed *macroadenomas*. Smaller tumors are diagnosed either incidentally or by perturbing the endocrinologic equilibrium through overproduction (hypersecretion) of a critical hormone. Serologic testing for

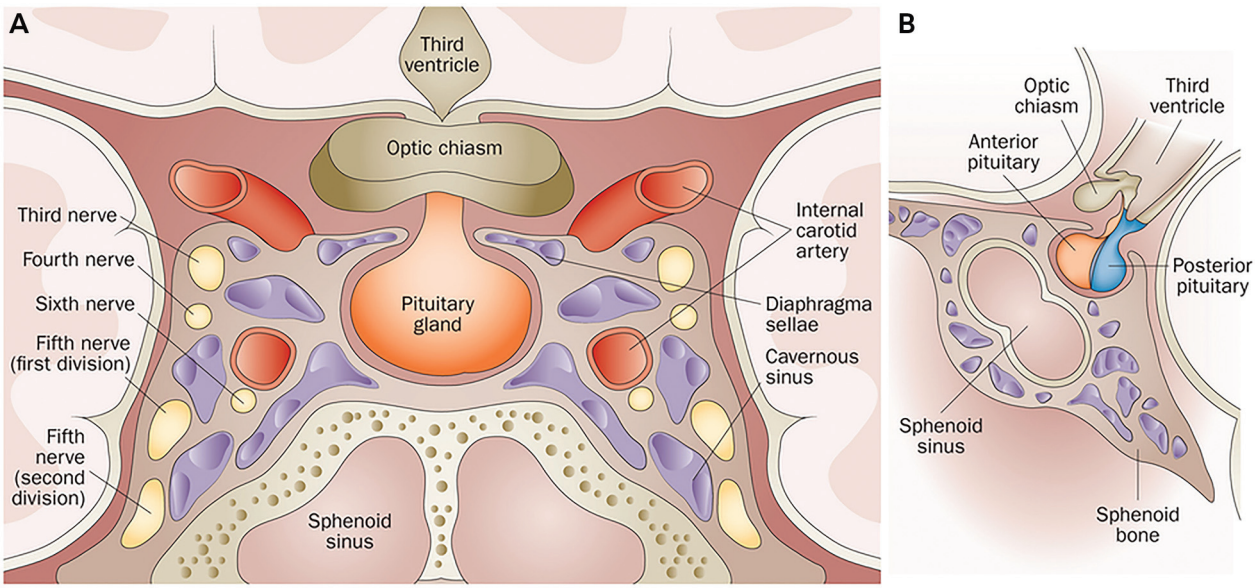

FIGURE 6-5

Normal anatomy of the sellar and parasellar regions surrounding the pituitary gland in the coronal (*A*) and sagittal (*B*) planes.

Reprinted with permission from Di Ieva A, et al, Nat Rev Endocrinol.[12] © 2014 Nature Publishing Group.

Copyright © American Academy of Neurology. Unauthorized reproduction of this article is prohibited.

adrenocorticotropic hormone (ACTH), cortisol, growth hormone, insulinlike growth factor 1, follicle-stimulating hormone, luteinizing hormone, thyroid-stimulating hormone (TSH), and prolactin is the most steadfast method of establishing a functional, or hormone-secreting, pituitary adenoma. Among these, a microadenoma leading to Cushing disease may be more capricious to establish serologically as well as radiographically if it is very small. Dynamic contrast protocols and 7T MRI protocols provide high resolution but may still not confirm the precise location of a microadenoma secreting ACTH. In these cases, inferior petrosal sinus sampling may help distinguish the diagnosis of Cushing disease from Cushing syndrome and the laterality of the tumor within the gland.

Macroadenomas manifest with visual alterations when tumors grow rostrally to compress the optic chiasm, causing visual field or acuity deficits, or laterally to compress the nerves of the cavernous sinus, causing diplopia or upper facial numbness. Both hypersecretion and underproduction of hormones due to compression of the normal pituitary gland by a large tumor can exert cumulative physiologic effects over time. Sudden infarction of a pituitary macroadenoma,

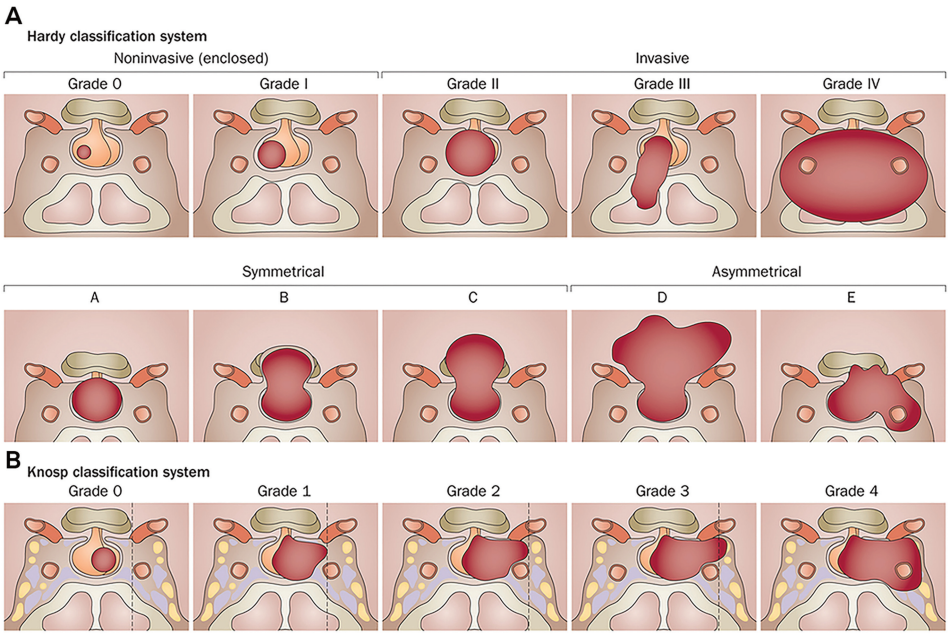

FIGURE 6-6

Hardy and Knosp classifications of pituitary macroadenoma growth. Hardy classification system: Grade 0; intact with normal contour; grade I, intact with bulging floor; grade II, intact, enlarged fossa; grade III, invasive with localized sellar destruction; grade IV, invasive with diffuse destruction. Suprasellar tumors can be symmetric, occupying the suprasellar cistern only (*A*), the recess of the third ventricle (*B*), or the whole anterior portion of the third ventricle (*C*); asymmetric and intracranial extradural (*D*); or extracranial extradural (*E*) occupying the cavernous sinus. Knosp classification system; Grade 0 is no cavernous sinus involvement; grade 1 indicates compression against the medial wall of the cavernous sinus restricted to a hypothetical line extending between the centers of the two segments of the internal carotid artery; grade 2 extends beyond this line without passing a line tangent to the lateral margins of the artery itself; grade 3 confers tumor extension laterally to the internal carotid artery within the cavernous sinus; grade 4 describes total encasement of the intracavernous portion of the carotid artery.

Reprinted with permission from Di Ieva A, et al, Nat Rev Endocrinol.[12] © 2014 Nature Publishing Group.

KEY POINTS

- Solitary fibrous tumors, formerly termed *hemangiopericytoma*, are a highly vascular mimic of meningiomas and may metastasize outside of the central nervous system.
- Schwannomas demonstrate variable growth rates, with cystic and neurofibromatosis type 2–associated tumors more likely to exhibit faster growth.
- Although contrast-enhanced T1-weighted MRI remains the most common modality to visualize schwannomas, T2-weighted MRI may be suitable for long-term surveillance of schwannoma growth.

Copyright © American Academy of Neurology. Unauthorized reproduction of this article is prohibited.

which can be either hemorrhagic (detectable as blood on CT or MRI) or ischemic, leads to pituitary tumor apoplexy. Pituitary (tumor) apoplexy is a clinical diagnosis manifesting with sudden onset headache, ophthalmoparesis, and potential visual loss, with or without accompanying hemorrhagic conversion on imaging.

Growth of pituitary adenomas beyond the boundary of the sella turcica is commonly described by the Knosp classification for lateral extension to the cavernous sinus and the Hardy classification, as modified by Wilson, for rostral-caudal extension (FIGURE 6-6).[14,15] Different adenoma subtypes exhibit predilections for specific trajectories of growth. For example, growth hormone macroadenomas more frequently grow caudally and involve the bony clivus.[16]

Consistent with the general skull base principle that the origin of the tumor dictates displacement of adjacent anatomic structures, inspection of the pituitary stalk in the sagittal plane may provide clues to the diagnosis of a sellar mass. Tumors of the posteriorly located neurohypophysis tend to deflect

CASE 6-3

A 36-year-old man presented with several months of blurry vision and increased thirst and was found to have a heterogeneously enhancing suprasellar mass with extension to the optic chiasm and left proximal optic nerve (FIGURE 6-7). The profound extent of T2-weighted hyperintense signal along the optic nerves and tracts was confounding for tumor involvement or edema. Visual field examination revealed an inferior temporal field deficit in his left eye. He underwent a right cranio-orbitozygomatic approach for gross total resection of the tumor. Pathology revealed a *BRAF*^{V600E}-mutant papillary craniopharyngioma. His vision recovered fully, but he continued to experience diabetes insipidus, as anticipated given the tumor origin from and involvement of the infundibulum.

COMMENT

This case illustrates the potential for optic nerve T2-hyperintense signal to reflect either edema or infiltrative tumor. With the complete recovery, in this case, it signified edema from a craniopharyngioma rather than an optic nerve tumor.

Copyright © American Academy of Neurology. Unauthorized reproduction of this article is prohibited.

the infundibulum forward, as do Rathke cleft cysts, which arise from the vestigial lumen of the Rathke pouch between the anterior and posterior pituitary lobes. Cystic lesions of the sellar and suprasellar compartments also include cystic pituitary adenoma, craniopharyngioma, or, less commonly, an arachnoid cyst.

Craniopharyngiomas fall into two types, adamantinomatous and papillary, with distinct histology, epidemiology, and genetic signatures. Craniopharyngiomas span the age spectrum, from children to adults, with a bimodal peak. Pediatric craniopharyngiomas are almost exclusively adamantinomatous whereas adult craniopharyngiomas can be either type. Adamantinomatous craniopharyngiomas classically exhibit cystic or a mixture of cystic and nodular appearance on MRI whereas papillary types are more often solid or mixed cystic-solid, although a predominantly cystic appearance does not exclude papillary craniopharyngioma (CASE 6-3). Intratumoral calcification, best detected on CT, may support the diagnosis of a craniopharyngioma over that of cystic pituitary adenoma or other cystic lesions.

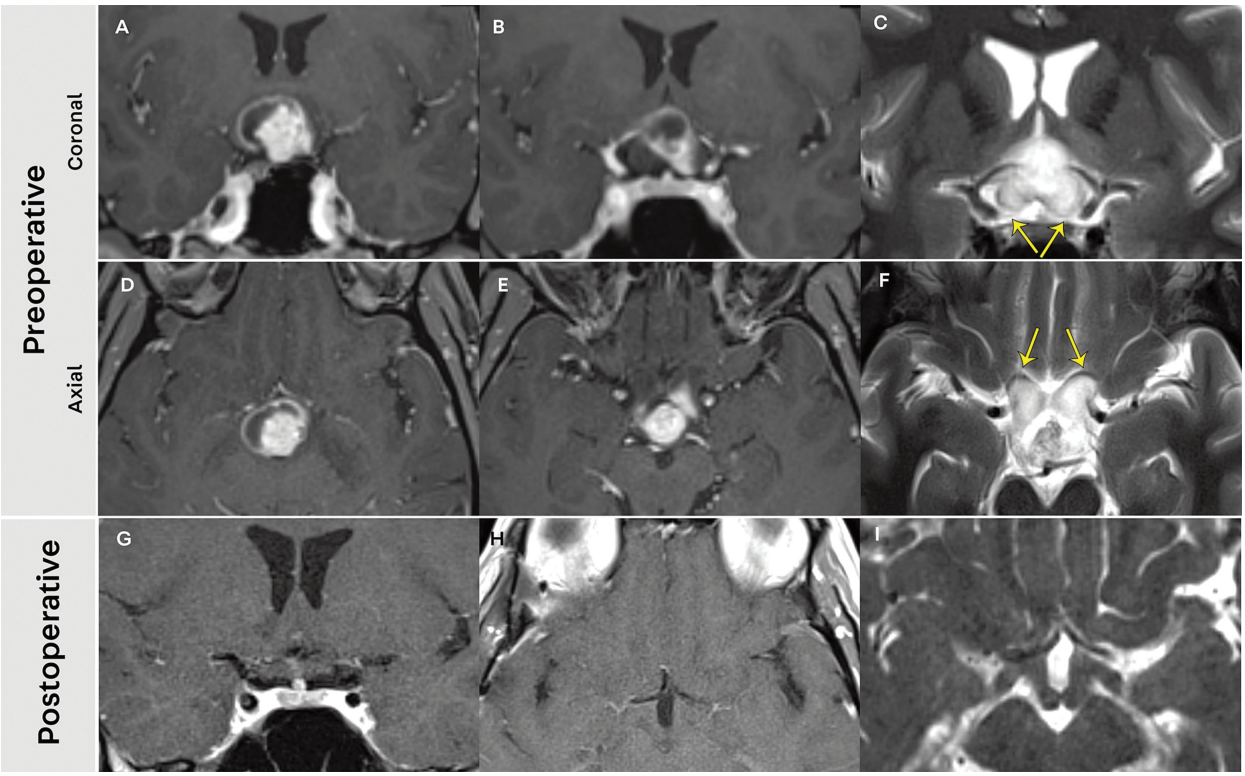

FIGURE 6-7

Papillary craniopharyngioma shown in the imaging of the patient in CASE 6-3. Coronal postcontrast T1-weighted (*A*, *B*) and T2-weighted (*C*) sequences, as well as axial postcontrast T1-weighted (*D*, *E*) and T2-weighted (*F*) sequences, highlighting a rim-enhancing cystic and nodular suprasellar mass with significant T2-hyperintense signal within bilateral proximal optic nerves. *Arrows* in panels *C* and *F* show the enlarged optic nerves. Postoperative coronal postcontrast T1-weighted (*G*), axial postcontrast T1-weighted (*H*), and axial T2-weighted (*I*) images showing gross total resection and resolution of edema within the bilateral optic nerves.

Copyright © American Academy of Neurology. Unauthorized reproduction of this article is prohibited.

Craniopharyngiomas arise anywhere along the infundibulum and may be primarily sellar, suprasellar, or even within the third ventricle. Given its involvement in the pituitary stalk, diabetes insipidus is a common symptom of craniopharyngiomas, either on presentation or after treatment.

Suspicion for a papillary craniopharyngioma in an adult based on imaging carries therapeutic implications since the discovery that 95% of papillary craniopharyngiomas possess a *BRAF*^{V600E} mutation and may be susceptible to targeted inhibition.[17,18] In comparison, adamantinomatous craniopharyngiomas are largely driven by alterations in the WNT signaling pathway, for which no effective pharmacologic therapies exist to date.

CHORDOMAS AND CHONDROSARCOMAS

The clivus and petroclival junction, just caudal to the sella, gives rise to chordomas and chondrosarcomas. Although these two pathologies are often linked together, they exhibit different degrees of local aggressiveness and response to treatment. Expression of the notochord transcription factor brachyury protein is pathognomonic for chordomas and absent in chondrosarcomas.

Chordomas arise from remnants of the primitive notochord and are, therefore, frequently midline in location. In comparison, chondrosarcomas are mesenchymal tumors arising from the petroclival junction and exhibit paramedian eccentric growth through the skull base. On MRI, both may appear hyperintense on T2-weighted images and hypointense or isointense on T1-weighted images. Chondrosarcomas, in contrast to chordomas, often exhibit pronounced calcification, which is best appreciated on CT. Depending on the trajectory of growth, involvement of the abducens nerve causing diplopia is a common symptom of these tumors, most often in either its cisternal segment or as it courses through the Dorello canal. Furthermore, the tumor may abut or encase the internal carotid artery along its course from the cervical segment to the petrous segment or beyond.

Surgical resection, with or without radiation, confers long-term disease control for benign chondrosarcomas. In comparison, chordomas are more likely to recur over time, especially if subtotal resection was achieved at initial diagnosis, and mandates lifelong surveillance.

OTHER SKULL BASE PATHOLOGIES

Diverse other pathologies pepper the skull base, each with unique imaging characteristics. A comprehensive discussion of each is beyond the scope of this review. Notable non-neoplastic extra-axial pathologies that frequently cluster with skull base tumors include epidermoid and dermoid cysts.

Epidermoid cysts are keratin collections lined by a thin layer of stratified squamous epithelium. They avidly restrict on diffusion-weighted MRI, are hyperintense to isointense on T2-weighted MRI, and are hypointense on T1-weighted images, with minimal contrast enhancement typically of the cyst wall. Dermoid cysts are inclusion bodies of ectodermal tissue entrapped during development. Hence, they may contain a mixture of squamous epithelium, sebaceous content, and hair (dermal) structures. Consistent with the contents of dermoid cysts, they often exhibit a more heterogeneous appearance on MRI, with fatty components being hyperintense on unenhanced T1-weighted MRI.

Copyright © American Academy of Neurology. Unauthorized reproduction of this article is prohibited.

TRENDS

Improved understanding of the natural history of skull base tumors and predictors for deleterious impact on quality of life has empowered clinicians to better guide patients with these diagnoses. Advanced imaging modalities, including on MRI and PET scans, hold additional promise to enhance diagnostic capabilities. Tailoring imaging protocols to the characteristics of the tumor, such as the use of T2-based surveillance imaging in long-term follow-up of vestibular schwannomas, can further diminish the risk to patients.

In parallel with hardware and software developments, advances in the fields of radiomics and artificial intelligence have highlighted a strong link between the phenotype (radiographic features) and genotype or biological character of tumors.[19,20] If further developed, radiomic analyses hold great promise as a democratizing force in brain and skull base tumor stratification because MRI or CT is far more accessible globally compared with genomic profiling platforms. Imaging characterization of cranial tumors, down to their molecular signatures, by MRI alone may disrupt our current clinical workflow of obtaining definitive pathology only through tissue sampling of the tumor. These techniques could broaden the management options on upfront detection of a tumor, as well as improve prognostication and tracking of tumor transformation over time.

CONCLUSION

Imaging has offered one of the greatest advances in our understanding of skull base pathologies over the past half century. Detailed review of CT and MRI often provides insights into the growth rate, benign or malignant nature, and specific diagnosis of skull base tumors. Ready access to imaging and the ease of prescribing imaging for myriad reasons heighten the need for careful understanding of indications for treatment because serial observation may be a safe and prudent alternative for many skull base pathologies. If treatment, especially surgery, becomes indicated, the soft tissue, bony, and vascular relationships of skull base tumors each contribute to the safe planning of surgery. Furthermore, the combination of these radiographic and anatomic factors allows for stratification in discussing the risks of intervention with patients. As future software advances couple with hardware advances, clinicians may be able to extract even greater biological information from imaging.

KEY POINTS

- **Rathke cleft cysts and neurohypophysial tumors push the pituitary stalk anteriorly, as best appreciated on sagittal imaging, because of their origin posterior to the adenohypophysis.**
- **Craniopharyngiomas in children are almost exclusively adamantinomatous whereas papillary craniopharyngiomas are found in adults, commonly with a *BRAF*^{V600E} mutation.**
- **Chondrosarcomas exhibit pronounced calcification in comparison to chordomas and are typically eccentric toward one side as opposed to midline.**
- **Epidermoid cysts are best characterized by their avid restricted diffusion on diffusion-weighted imaging sequences.**
- **Radiomic analyses of conventional tumor imaging may augment the prediction of biological signatures in the future.**

REFERENCES

1 Ostrom QT, Patil N, Cioffi G, Waite K, Kruchko C, Barnholtz-Sloan JS. CBTRUS statistical eport: primary brain and other central nervous system tumors diagnosed in the United States in 2013-2017. Neuro Oncol 2020;22(12 Suppl 2): iv1-iv96. doi:10.1093/neuonc/noaa200

2 Louis DN, Perry A, Wesseling P, et al. The 2021 WHO classification of tumors of the central nervous system: a summary. Neuro Oncol 2021; 23(8):1231-1251. doi:10.1093/neuonc/noab106

3 Driver J, Hoffman SE, Tavakol S, et al. A molecularly integrated grade for meningioma. Neuro Oncol 2022;24(5):796-808. doi:10.1093/neuonc/noab213

4 Bi WL, Brown PA, Abolfotoh M, et al. Utility of dynamic computed tomography angiography in the preoperative evaluation of skull base tumors. J Neurosurg 2015;123(1):1-8. doi:10.3171/2014.10.JNS141055

5 Morris Z, Whiteley WN, Longstreth WT, et al. Incidental findings on brain magnetic resonance imaging: systematic review and meta-analysis. BMJ 2009;339:b3016. doi:10.1136/bmj.b3016

Copyright © American Academy of Neurology. Unauthorized reproduction of this article is prohibited.

6 Islim AI, Mohan M, Moon RDC, et al. Incidental intracranial meningiomas: a systematic review and meta-analysis of prognostic factors and outcomes. J Neuro-Oncol 2019;142(2):211-221. doi:10.1007/s11060-019-03104-3

7 Chiechi MV, Smirniotopoulos JG, Mena H. Intracranial hemangiopericytomas: MR and CT features. AJNR Am J Neuroradiol 1996;17(7): 1365-1371.

8 Palmisciano P, Watanabe G, Conching A, et al. The role of [(68)Ga]Ga-DOTA-SSTR PET radiotracers in brain tumors: a systematic review of the literature and ongoing clinical trials. Cancers (Basel) 2022;14(12):2925. doi:10.3390/cancers14122925

9 Dunn IF, Bi WL, Erkmen K, et al. Medial acoustic neuromas: clinical and surgical implications. J Neurosurg 2014;120(5):1095-1104. doi:10.3171/2014.1.JNS131701

10 Marinelli JP, Schnurman Z, Killeen DE, et al. Long-term natural history and patterns of sporadic vestibular schwannoma growth: a multi-institutional volumetric analysis of 952 patients. Neuro Oncol 2022;24(8):1298-1306. doi:10.1093/neuonc/noab303

11 Dunn IF, Bi WL, Mukundan S, et al. Congress of neurological surgeons systematic review and evidence-based guidelines on the role of imaging in the diagnosis and management of patients with vestibular schwannomas. Neurosurgery 2018;82(2):E32-E34. doi:10.1093/neuros/nyx510

12 Di Ieva A, Rotondo F, Syro LV, et al. Aggressive pituitary adenomas–diagnosis and emerging treatments. Nat Rev Endocrinol 2014;10(7): 423–435. doi:10.1038/nrendo.2014.64

13 Gittleman H, Ostrom QT, Farah PD, et al. Descriptive epidemiology of pituitary tumors in the United States, 2004-2009. J Neurosurg 2014; 121(3):527-535. doi:10.3171/2014.5.JNS131819

14 Micko AS, Wohrer A, Wolfsberger S, Knosp E. Invasion of the cavernous sinus space in pituitary adenomas: endoscopic verification and its correlation with an MRI-based classification. J Neurosurg 2015;122(4):803-811. doi:10.3171/2014.12.JNS141083

15 Wilson CB. A decade of pituitary microsurgery. The Herbert Olivecrona lecture. J Neurosurg 1984;61(5):814-833. doi:10.3171/jns.1984.61.5.0814

16 Pangal DJ, Wishart D, Shiroishi MS, Ruzevick J, Carmichael JD, Zada G. Growth hormone secreting pituitary adenomas show distinct extrasellar extension patterns compared to nonfunctional pituitary adenomas. Pituitary 2022; 25(3):480-485. doi:10.1007/s11102-022-01217-z

17 Brastianos PK, Taylor-Weiner A, Manley PE, et al. Exome sequencing identifies BRAF mutations in papillary craniopharyngiomas. Nat Genet 2014; 46(2):161-165. doi:10.1038/ng.2868

18 Brastianos PK, Shankar GM, Gill CM, et al. Dramatic response of BRAF V600E mutant papillary craniopharyngioma to targeted therapy. J Natl Cancer Inst 2016;108(2). doi:10.1038/ng.2868

19 Coroller TP, Bi WL, Huynh E, et al. Radiographic prediction of meningioma grade by semantic and radiomic features. PloS One 2017;12(11):e0187908. doi:10.1371/journal.pone.0187908

20 Bi WL, Hosny A, Schabath MB, et al. Artificial intelligence in cancer imaging: clinical challenges and applications. CA Cancer J Clin 2019;69(2): 127-157. doi:10.3322/caac.21552

Copyright © American Academy of Neurology. Unauthorized reproduction of this article is prohibited.

Imaging of Brain Tumors

By Justin T. Jordan, MD, MPH, FAAN; Elizabeth R. Gerstner, MD

REVIEW ARTICLE

CONTINUUM AUDIO INTERVIEW AVAILABLE ONLINE

CITE AS:
CONTINUUM (MINNEAP MINN) 2023;29(1, NEUROIMAGING): 171–193.

Address correspondence to Dr Justin T. Jordan, 55 Fruit St, Yawkey 9E, Boston, MA 02114, JTJordan@mgh.harvard.edu.

RELATIONSHIP DISCLOSURE:
Dr Jordan has received personal compensation in the range of $0 to $499 for serving as a consultant for Atheneum Partners, EM Partners, GLG Pharma, and Guidepoint Global, LLC; in the range of $500 to $4999 for serving as a consultant for Creative Educational Concepts, LLC, and Texas Health Resources; and in the range of $5000 to $9999 for serving as a consultant for Children's Tumor Foundation, Navio Theragnostics, Inc, and Recursion and on a scientific advisory board for Recursion. Dr Jordan has stock in The Doctor Lounge and Navio Theragnostics, Inc, has received publishing royalties from Elsevier, and has noncompensated relationships as a board member with ABA Academy, Neurofibromatosis Northeast, Neurofibromatosis
Continued on page 193

UNLABELED USE OF PRODUCTS/INVESTIGATIONAL USE DISCLOSURE:
Drs Jordan and Gerstner discuss the unlabeled/investigational use of mitogen-associated protein kinase (MAPK) pathway with MAP-ERK kinase (MEK) inhibitors for the treatment of MAP kinase-altered tumors and various MRI and positron emission tomography (PET) techniques not approved for the imaging of brain tumors.

© 2023 American Academy of Neurology.

ABSTRACT

OBJECTIVE: **This article focuses on neuroimaging as an essential tool for diagnosing brain tumors and monitoring response to treatment.**

LATEST DEVELOPMENTS: **Neuroimaging is useful at all stages of brain tumor care. Technologic advances have improved the clinical diagnostic capability of neuroimaging as a vital complement to history, examination, and pathologic assessment. Presurgical evaluations are enriched by novel imaging techniques, through improved differential diagnosis and better surgical planning using functional MRI (fMRI) and diffusion tensor imaging. The common clinical challenge of differentiating tumor progression from treatment-related inflammatory change is aided by novel uses of perfusion imaging, susceptibility-weighted imaging (SWI), spectroscopy, and new positron emission tomography (PET) tracers.**

ESSENTIAL POINTS: **Using the most up-to-date imaging techniques will facilitate high-quality clinical practice in the care of patients with brain tumors.**

INTRODUCTION

More than 120 types of brain tumors are recognized by the World Health Organization (WHO) Classification of Tumors of the Central Nervous System. Symptoms are determined by tumor location and tend to develop quickly with malignant tumors and more insidiously with nonmalignant tumors. With the increasing availability of nervous system imaging for symptom evaluation, neurologists are often on the front lines of brain tumor identification. Thus, neurologists should be familiar with the neuroimaging findings associated with tumors to appropriately triage and refer patients. This article describes how specific imaging techniques may aid in characterizing intraaxial brain tumors (those arising from cells in the brain), as well as distinguishing tumor growth from treatment-associated imaging changes. Imaging of extraaxial tumors (those arising from nerves, meninges, or other structures outside the brain parenchyma) is addressed in a separate article; refer to "Imaging of Skull Base Tumors" by Wenya Linda Bi, MD, PhD,[1] in this issue of *Continuum*.

This year in the United States, approximately 25,000 primary malignant tumors and 62,000 nonmalignant tumors of the nervous system will be diagnosed, and approximately 17,000 people will die as a result of nervous system tumors.[2] Glioblastoma is the most commonly occurring malignant primary brain tumor in adults, and meningioma is the most common nonmalignant intracranial tumor.[2]

Copyright © American Academy of Neurology. Unauthorized reproduction of this article is prohibited.

Neuroimaging is crucial when a brain tumor is suspected. Anatomic MRI with a gadolinium-based contrast agent is the current standard in such cases. CT may be used in urgent evaluations or where MRI is not safe or feasible but is substantially less sensitive for tumor detection and less specific for tumor discrimination. TABLE 7-1[3] compares the utility of different diagnostic modalities and sequences for tumor imaging. Not all intraaxial mass lesions are tumors, however, and neurologists should keep in mind a broader differential diagnosis that may include abscess, stroke, or inflammatory lesions as well as tumor. Specific signal characteristics on neuroimaging may further refine the differential diagnosis, although neuroimaging alone is generally not sufficient to confirm a tumor diagnosis. Additional diagnostic evaluation requirements are generally determined based on neuroimaging results.

INITIAL IMAGING

Head CT or brain MRI is usually the first step in the evaluation of a patient who presents with neurologic symptoms suggestive of a mass lesion. Although MRI is more sensitive for identifying central nervous system (CNS) tumors, CT is typically faster, cheaper, and more widely available so is often the first screening test for a brain tumor. CT can also quickly exclude other possibilities such as ischemic stroke or intraparenchymal hemorrhage. However, contrast-enhanced MRI is the current gold standard for diagnosis and long-term management of CNS tumors.

MRI capitalizes on the magnetization properties of protons in the water molecules within tissue. A powerful magnetic field is applied to align the

TABLE 7-1 Tumor Imaging Modalities[a]

Imaging technique	Role in brain tumor imaging
CT	Mass effect, herniation, hydrocephalus, hemorrhage, calcifications
Precontrast and postcontrast T1-weighted imaging	Enhancement characteristics (eg, homogeneous, heterogeneous, rim), necrosis, extent of tumor that is enhancing
T2-weighted or fluid-attenuated inversion recovery (FLAIR)	Peritumoral edema, infiltrative or nonenhancing tumor
Diffusion-weighted imaging	Low apparent diffusion coefficient in hypercellular portions of tumor, postoperative devitalized tissue
Diffusion tensor imaging	Tractography for surgical planning
Susceptibility-weighted imaging (SWI)	Blood products, calcifications, microhemorrhages
Perfusion imaging	Tumor vascularity and permeability
Magnetic resonance spectroscopy	Metabolic profile for differentiating tumor from other pathologies, including oncometabolite 2-hydroxyglutarate measurement
Functional MRI (fMRI)	Preoperative functional mapping
Positron emission tomography (PET)	Increase uptake of amino acid tracers in active, higher-grade tumors

CT = computed tomography; MRI = magnetic resonance imaging.
[a] Modified with permission from Baig MA, et al, Continuum (Minneap Minn).[3] © 2016 American Academy of Neurology.

Copyright © American Academy of Neurology. Unauthorized reproduction of this article is prohibited.

normally randomly oriented protons into one plane.[4] This alignment is then perturbed by an externally applied radiofrequency pulse. After some tissue-specific time, the protons relax into their resting orientation and, in doing so, emit radiofrequency energy that is collected and processed through Fourier transformation to create a corresponding image. By varying the sequence of radiofrequency pulses applied, different imaging sequences are created that are sensitive to different aspects of molecular behavior within different tissue types. Thus, MRI provides excellent contrast between different CNS tissues such as gray matter, white matter, CSF, and pathologic tissue within a tumor.

MRI SEQUENCES

MRI provides excellent insight into brain pathology by allowing evaluation of the brain in multiple ways to expose different physiologic and anatomic changes.

T1-Weighted and T2-Weighted Sequences

T1-weighted, T2-weighted, and fluid-attenuated inversion recovery (FLAIR) sequences are the most common anatomic sequences used for brain tumor diagnosis and response assessment. Typically, brain tumors are hypointense on T1-weighted images and hyperintense on T2-weighted images, reflecting the increased water content in tumor and surrounding vasogenic edema. Notable exceptions include tumors that have calcification (eg, oligodendrogliomas) or old blood products or melanin. FLAIR is a type of T2-weighted pulse sequence that suppresses the signal from CSF and is most useful in assessing the extent of nonenhancing tumor, vasogenic edema, or gliosis. Imaging patterns for some of the most common intraaxial brain tumors are outlined in TABLE 7-2.[3]

Diffusion-Weighted Imaging

Diffusion-weighted imaging uses MR sequences sensitive to the intrinsic random (brownian) movement of water molecules. Reduced diffusivity, or increased anisotropy, refers to a limitation in the free movement of water molecules in tissue. Because tumors have increased cellularity relative to surrounding normal brain tissue, they tend to have more restricted diffusion; this can be quantitated by the apparent diffusion coefficient (ADC), which measures the diffusion of water molecules measured in square millimeters per second. In tumor imaging, ADC values are typically inversely correlated with cellularity: low ADC values imply increased cellularity and restricted diffusion, as seen in higher-grade tumors or lymphomas. However, the tumor microenvironment can be quite variable, with a mix of tumor cells, edema, and necrosis, making the ADC less specific for tumor grading. Recent studies have suggested that the ADC may help predict response to antiangiogenic treatment.[5,6]

Diffusion tensor imaging is an extension of diffusion-weighted imaging and allows for visualization of the direction of water motion, thus providing information on the orientation and anisotropy of white matter tracts in the brain. Knowing where the white matter tracts are in relation to a brain tumor has been helpful in surgical planning to reduce surgical morbidity.

Susceptibility-Weighted Imaging

Susceptibility-weighted imaging (SWI) is a sequence that is sensitive to paramagnetic and diamagnetic compounds that distort the local magnetic field. In the setting of a brain tumor, SWI is used to detect blood products or

KEY POINTS

- Approximately 25,000 primary malignant brain tumors are diagnosed each year in the United States.
- Glioblastoma is the most common malignant primary intracranial brain tumor in adults.
- Keeping a broad differential diagnosis is important for mass lesions, including abscesses, strokes, or inflammatory disease.
- Although CT may show acute changes such as stroke or hemorrhage, gadolinium-enhanced MRI is the preferred imaging modality for brain tumors.
- T1-weighted, T2-weighted, and fluid-attenuated inversion recovery (FLAIR) sequences are critical to diagnosing and treating patients with brain tumors.
- Diffusion-weighted imaging may be helpful to detect ischemic strokes, hypercellularity within tumors (especially lymphomas and high-grade gliomas), and perioperative devitalized tissues.

Copyright © American Academy of Neurology. Unauthorized reproduction of this article is prohibited.

TABLE 7-2 MRI Characteristics of Common Brain Tumors[a]

Type of brain tumor	MRI characteristics
Pilocytic astrocytoma	T1-weighted images: hypointense cystic component, isointense solid component T2-weighted images: hyperintense cystic component, hyperintense solid component Postgadolinium images: heterogeneous enhancement of solid component and wall of cystic component
Isocitrate dehydrogenase (*IDH*)–mutated astrocytoma	T1-weighted images: hypointense mass T2-weighted images: hyperintense mass, presence of surrounding hyperintense edema increases with grade; fluid-attenuated inversion recovery (FLAIR) imaging may be relatively hypointense (T2-FLAIR mismatch sign) Diffusion restriction: unlikely Postgadolinium images: likelihood and amount of heterogeneous enhancement increases with grade
***IDH*-mutated and 1p/19q-codeleted oligodendroglioma**	T1-weighted images: hypointense mass, may extend to include cortex T2-weighted images: heterogeneously hyperintense Postgadolinium images: enhancement unlikely in grade 2, may be heterogeneous in grade 3
***IDH* wild-type glioblastoma**	T1-weighted images: hypointense mass; hyperintense blood products may be present T2-weighted images: hyperintense mass with extensive surrounding hyperintense edema; may be hypointense centrally because of necrosis Diffusion restriction: infrequent Postgadolinium images: heterogeneous enhancement, often ringlike with central nonenhancing necrotic region
H3 K27–altered diffuse midline glioma	T1-weighted images: hypointense mass in brainstem or thalami or spinal cord T2-weighted images: hyperintense, heterogeneous Postgadolinium images: rim enhancement with central necrosis
Lymphoma of the central nervous system	T1-weighted images: hypointense to isointense mass, often multifocal; hyperintense blood products may be seen in immunocompromised patients T2-weighted images: hypointense to isointense, may have hyperintense surrounding edema Diffusion restriction: often present Postgadolinium images: for immunocompetent patients, homogeneous enhancement; for immunocompromised patients, rim enhancement with central necrosis
Central nervous system metastasis	T1-weighted images: isointense to hypointense (except mucinous lesions, which are hyperintense) T2-weighted images: heterogeneously hyperintense (except mucoepidermoid type, which are hypointense); usually surrounded by hyperintense edema Diffusion restriction: may be present, especially in very small lesions Postgadolinium images: enhancement usually rimlike

MRI = magnetic resonance imaging.
[a] Modified with permission from Baig MA, et al, Continuum (Minneap Minn).[3] © 2016 American Academy of Neurology.

Copyright © American Academy of Neurology. Unauthorized reproduction of this article is prohibited.

calcifications. The presence of a microhemorrhage within a brain tumor can be associated with higher-grade gliomas and can be seen following radiation therapy, potentially reflecting radiation vasculopathy.[7] Calcifications can be seen in lower-grade meningiomas or oligodendrogliomas, as these entities are more indolent in nature. Different MRI vendors have different names for these sequences, and there are differences in how the images are acquired, making comparisons across vendors challenging. For example, a gradient recalled echo (GRE) sequence provides similar information as an SWI sequence but is acquired at lower spatial resolution so it can be less sensitive to microhemorrhages.

Perfusion Imaging

Perfusion imaging is used to evaluate tumor vascularity and blood-brain barrier permeability. Both contrast-dependent approaches (eg, dynamic susceptibility contrast imaging) and non–contrast-dependent approaches (eg, arterial spin labeling) exist. In dynamic susceptibility contrast imaging, the most common approach, kinetic analysis of the passage of the contrast bolus through tissue enables calculation of several physiologic biomarkers, including cerebral blood volume (CBV), cerebral blood flow, and mean transit time. Cerebral blood volume is typically elevated in higher-grade tumors because of the increase in angiogenesis and correlates with tumor grade and response to therapy.[8,9] Perfusion imaging is increasingly being used clinically in the management of brain tumors, and recent consensus guidelines include recommendations on how best to perform it in an effort to standardize this technique (FIGURE 7-1).[10]

MR Spectroscopy

MR spectroscopy is used to measure metabolites in the brain. Tumors have a characteristic appearance with an increase in the choline peak, a decrease in the *N*-acetylaspartate (NAA) peak, increased choline-to-creatine ratio, and, in high-grade glioma, a lactate peak. MR spectroscopy has been used to help with tumor diagnosis, for example, to distinguish tumors from other pathologic processes and to track tumor response to treatment. A new MR spectroscopy technique has been developed that can measure the oncometabolite 2-hydroxyglutarate (2HG), which is present in isocitrate dehydrogenase (*IDH*)–mutated gliomas.[11] With this approach, a tool that potentially reflects tumor burden more accurately than just contrast dye leakage on postcontrast sequences is available. Studies have suggested that 2HG can be used as a marker of tumor response to treatment.[12,13] Measuring 2HG with MR spectroscopy is still a research technique but holds great promise for improving our ability to diagnose tumors (particularly if in a surgically inaccessible location) and for interpretation of tumor response to treatment (FIGURE 7-2).

Functional MRI

Functional MRI (fMRI) is a technique that reflects brain metabolic activity by measuring blood oxygenation changes within blood vessels in the brain. Increased brain activity leads to increased blood flow and oxygen extraction from the blood, resulting in an increase in deoxyhemoglobin. Because deoxyhemoglobin is paramagnetic, a change occurs in the blood oxygen level-dependent (BOLD) contrast signal, thus highlighting active areas of the brain depending on the task the patient is performing. fMRI is primarily used by neurosurgeons preoperatively to help them plan a maximal safe surgical

KEY POINTS

- Susceptibility-weighted imaging is helpful to identify calcifications in low-grade tumors or hemorrhage in typically higher-grade tumors.
- Perfusion imaging may help visualize vascularity and help distinguish between low- and high-grade tumors, as well as between tumor growth and inflammatory changes.
- MR spectroscopy that measures 2-hydroxyglutarate may aid in diagnosing an isocitrate dehydrogenase (*IDH*)-mutated tumor and may improve monitoring of treatment response.

Copyright © American Academy of Neurology. Unauthorized reproduction of this article is prohibited.

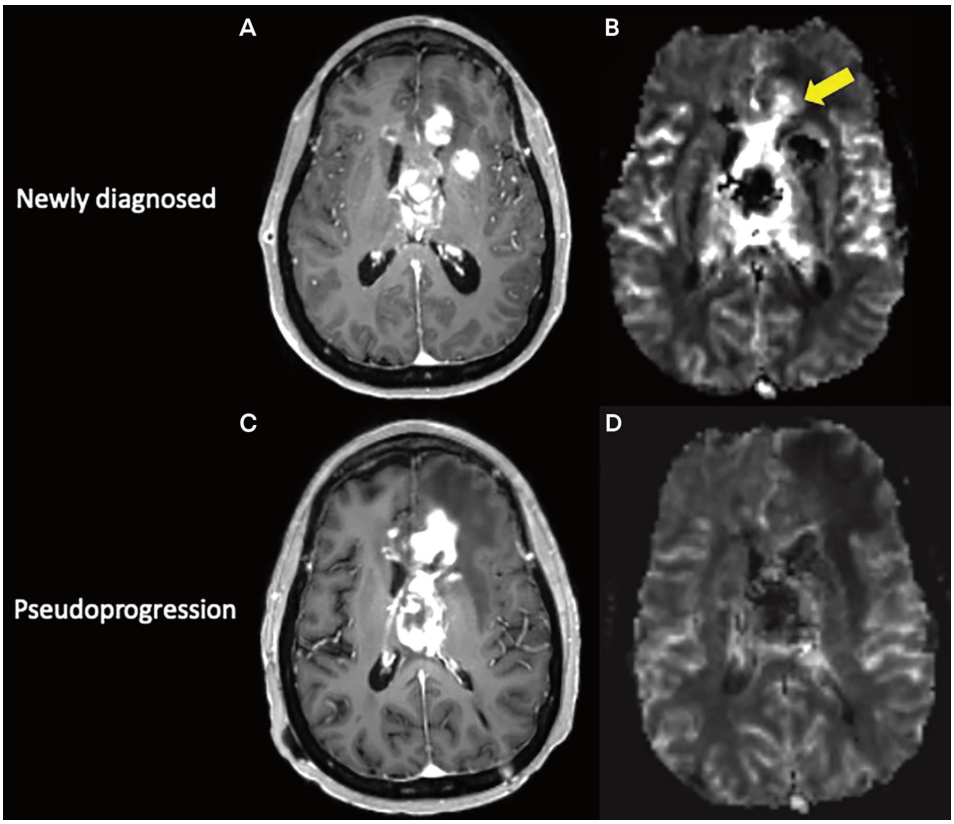

FIGURE 7-1
Isocitrate dehydrogenase (*IDH*) wild-type glioblastoma. *A,* Axial postcontrast T1-weighted MRI of a newly diagnosed tumor shows heterogeneous enhancement. *B,* Perfusion imaging shows elevated cerebral blood volume in the left frontal tumor (*arrow*). *C,* Axial postcontrast T1-weighted MRI 2 months after chemoradiotherapy shows evidence of pseudoprogression by increased enhancement in the left frontal tumor. *D,* Perfusion imaging shows no increase in cerebral blood volume.

resection. fMRI helps identify eloquent parts of the brain, such as cortical areas important in speech and white matter tracts important in motor function.

NEW IMAGING APPROACHES

Although MRI has been the backbone of brain tumor diagnosis and monitoring response to treatment, there is increasing interest in using positron emission tomography (PET) to monitor tumor response. Because of high physiologic glucose metabolism within the normal brain, ^{18}F-fludeoxyglucose has poor diagnostic accuracy for gliomas and therefore has a limited role. Alternatively, amino acid PET tracers (eg, 3,4-dihydroxy-6-^{18}F-fluoro-L-phenylalanine, fluoroethyl-L-tyrosine, or ^{18}F-fluciclovine) are being explored because of low background noise in normal brain tissue. The uptake of amino acid tracers into the tumor cells is mediated via the L-amino acid transporter system, which is overexpressed in neoplastic cells but not in non-neoplastic cells, making amino acid tracers more tumor-specific. These tracers are still under clinical development in the United States but are more widely used in Europe. Indeed, the Response Assessment in Neuro-Oncology (RANO) working group and the European Association for Neuro-Oncology have recommended incorporating

Copyright © American Academy of Neurology. Unauthorized reproduction of this article is prohibited.

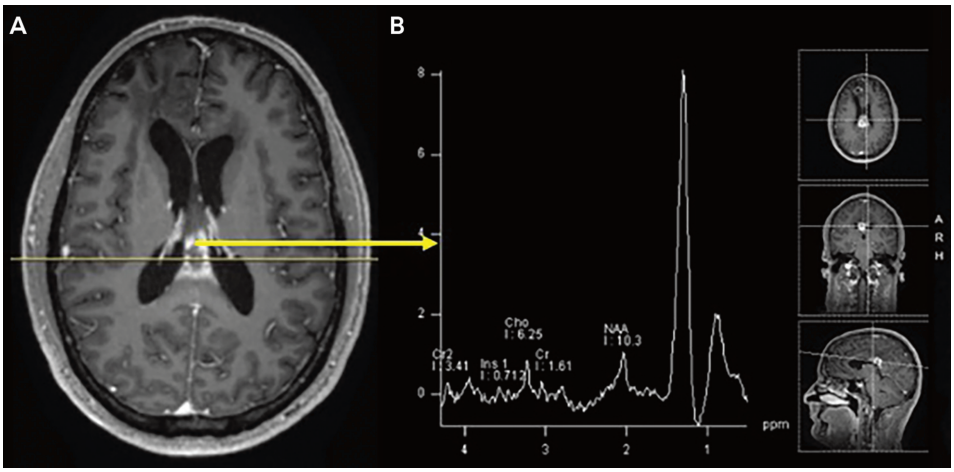

FIGURE 7-2

Isocitrate dehydrogenase (*IDH*) wild-type glioblastoma with pseudoprogression following chemoradiotherapy. *A,* Axial postcontrast T1-weighted MRI demonstrates heterogeneous enhancement in the corpus callosum that developed 8 weeks after chemoradiotherapy. *B,* Single-voxel (*arrow*) MR spectroscopy without an elevated choline, creatine, or *N*-acetylaspartate (NAA) peak, supporting a diagnosis of pseudoprogression.

Figure courtesy of Eva Ratai, PhD.

KEY POINTS

- **Functional MRI is useful for determining the anatomic location of brain activity for various tasks such as speaking or motor function and may help surgical planning.**
- **Amino acid positron emission tomography (PET) tracers may aid in distinguishing tumor growth from inflammatory changes.**

amino acid PET scans into the management of brain tumors to aid in the diagnosis and monitoring of tumor response.[14]

Other approaches on the horizon that are intended to explore physiologic changes in brain tumors include chemical exchange-dependent saturation transfer imaging, which can measure tumor pH, and hyperpolarized carbon-13 MRI, which can measure dynamic changes in different cellular metabolic pathways. Lastly, deep-learning algorithms and radiomics are increasingly pervasive in medical imaging. In the setting of brain tumors, deep-learning algorithms and radiomics have been explored in the noninvasive differentiation of tumor types, predicting tumor mutation status, tumor segmentation, and assessing treatment response.[15-18] These techniques have been challenging to deploy universally, however, because of methodologic errors, small data sets, and lack of external validation cohorts.

COMMON CLINICAL CONUNDRUMS

Despite the increasing sophistication of MRI, several clinical conundrums remain in which MRI may be misleading or not definitive.

True Tumor Progression Versus Treatment-Related Changes

Differentiating true tumor progression from treatment-related changes, both of which may present with an increase in contrast enhancement, can be challenging on routine anatomic MRI sequences. This clinical conundrum can occur early after radiation treatment with or without chemotherapy (pseudoprogression), months to years later (radiation necrosis), or after immunotherapy. Studies have suggested that elevated cerebral blood volume on perfusion imaging, increased uptake on amino acid PET, low ADC, or the classic MR spectroscopy spectrum of elevated choline, a decrease in NAA, and an increased choline-to-creatine ratio favor progressive tumor.[19] Unfortunately, no single imaging technique is perfect in differentiating tumor progression from treatment-related changes. Part of the

Copyright © American Academy of Neurology. Unauthorized reproduction of this article is prohibited.

challenge has been establishing ground truth to validate an imaging biomarker. In particular, with pseudoprogression or inflammatory change following immunotherapy, pathologic examination can show a heterogeneous mix of tumor cells and treatment-related changes and is subject to sampling error, that is, what is evaluated under the microscope may not be representative of any tissue left behind.

Although this conundrum is classically associated with postcontrast images, it also extends to nonenhancing tumors that are seen best on T2-weighted and FLAIR images. With nonenhancing tumors treated with radiation, there can be a slow progression of FLAIR hyperintensity that reflects gliosis and scarring from radiation that is hard to distinguish from slow, infiltrative tumor growth. Often, active surveillance is employed at the onset of such changes, using the pace of growth or morphologic changes (eg, with a more masslike, expansile appearance) to determine the likelihood of true tumor growth. In *IDH*-mutated gliomas, 2HG MR spectroscopy holds particular promise to help distinguish tumor growth versus gliosis, as tumor growth would be associated with elevated 2HG. However, MR spectroscopy can fail when 2HG concentrations are very low, as may occur in tumors with low cellularity.

Pseudoresponse

Another clinical conundrum occurs in the setting of antiangiogenic therapy, such as bevacizumab. Bevacizumab targets vascular endothelial growth factor (VEGF) on the tumor blood vessels, thereby closing the blood-brain barrier and decreasing contrast leakage into the tumor region. This reduction in enhancing disease is known as pseudoresponse and is often accompanied by an initial reduction in FLAIR hyperintensity related to restricted extravasation of fluid and inflammatory cells (CASE 7-1). However, active tumors still need a rich blood supply, and when angiogenesis is blocked, the tumors may ultimately co-opt native brain blood vessels with an intact blood-brain barrier, resulting in a later increase in nonenhancing tumor burden with more masslike expansile FLAIR hyperintensity but relatively less contrast enhancement.

MONITORING TUMOR RESPONSE TO TREATMENT

The RANO criteria are the most commonly used criteria to monitor tumor response to treatment (TABLE 7-3). The criteria were created by expert consensus primarily for the standardization of clinical trial outcomes, and different criteria exist for most tumor types (eg, RANO criteria for high-grade glioma, low-grade glioma, meningiomas, brain metastases, and leptomeningeal disease).[20-22]

TUMOR-SPECIFIC IMAGING CHARACTERISTICS

More than 120 recognized nervous system tumor types exist, and neurologists will certainly encounter some of the most common of these in routine clinical practice. Understanding imaging characteristics of these tumors may aid in triage for subspecialty consultation, diagnostic considerations, and monitoring for treatment response. The tumor types that are most likely to be seen in routine clinical practice are reviewed below.

Pilocytic Astrocytoma

Pilocytic astrocytoma (WHO grade 1) is a nonmalignant tumor arising from glial cells, primarily in the pediatric population (median age, 11 years).[2] These tumors

Copyright © American Academy of Neurology. Unauthorized reproduction of this article is prohibited.

are well demarcated, are most frequently located in the posterior fossa, and often cause positional headache or ataxia. The classic histologic finding of Rosenthal fibers remains a diagnostic hallmark of these tumors, and more recently a *KIAA1549-BRAF* gene fusion has been identified in approximately 70% of pilocytic astrocytomas as well.[23] Pilocytic astrocytomas may be curable with complete resection alone, although unresectable or progressive tumors may require additional treatments such as radiotherapy or chemotherapy; emerging evidence suggests a role for targeting the mitogen-associated protein kinase pathway with MAP-ERK kinase (MEK) inhibitors.[24]

On imaging, pilocytic astrocytomas are generally well-circumscribed cystic lesions with a heterogeneously enhancing mural nodule. The contents of the cyst are usually isointense to CSF signal on all sequences, except in the case of very proteinaceous cystic contents, in which case the signal may be hyperintense to CSF on certain sequences. Additional differential considerations for cystic tumors are listed in TABLE 7-4.[3]

A notable subgroup of pilocytic astrocytomas arise in the optic pathway, and these are found in roughly 15% of patients with neurofibromatosis type 1 (NF1). These are almost exclusively diagnosed in children, and consensus recommendations exist for ophthalmologic screening of patients with NF1 during early childhood as a preferred screening strategy.[25] Imaging may show FLAIR hyperintensity with expansion or tortuosity of optic nerves, chiasm, optic tracts, or even the hypothalamus. Contrast enhancement is variable, often patchy or absent. Any such finding in a patient with NF1 should prompt consideration of an optic pathway glioma. Importantly, in many patients, NF1-associated optic pathway gliomas may remain static or even decrease in size spontaneously. Diagnostic tissue sampling is generally not required, and treatment is indicated only for symptomatic tumors.

Subependymal Giant Cell Astrocytoma

Subependymal giant cell astrocytomas (SEGAs) are histologically benign tumors found almost exclusively in patients with tuberous sclerosis complex, occurring in 5% to 20% of these patients. These tumors are well demarcated and generally found in the periventricular space, although they may extend into the intraventricular space and even cause obstructive hydrocephalus. The foramen of Monro is the classic location for SEGA development.

The differentiation between non-neoplastic subependymal nodules and SEGAs can be difficult on imaging. A size cutoff of 1 cm or larger has been posed as more likely to reflect SEGA than a subependymal nodule. CT may show an intraventricular mass that is isodense or slightly hypodense to gray matter, often with internal calcification. MRI may show an enhancing mass that is hyperintense on T2-weighted images and has calcified components.

Although intervention is not warranted for all SEGAs, surgical intervention may be necessary for obstructive hydrocephalus, and mammalian/mechanistic target of rapamycin (mTOR) inhibitors such as everolimus may be used to stabilize or even shrink tumors in many patients.

Grade 2 to 4 *IDH*–Mutated Astrocytoma

It is now understood that *IDH1* and *IDH2* mutations are the molecular drivers of most gliomas referred to historically as "low grade," which are generally less aggressive than *IDH* wild-type tumors (historically called "high grade"). These

KEY POINTS

- Pseudoprogression in high-grade gliomas is often associated with increased contrast enhancement and hyperintensity on T2-weighted and FLAIR images and is caused by inflammatory change.
- Distinguishing tumor progression from inflammatory change is a frequent challenge, and a thorough evaluation may incorporate perfusion MRI, amino acid positron emission tomography, or MR spectroscopy.
- Lower-grade tumors may exhibit inflammatory radiation change through slow progression of hyperintensity on FLAIR images.
- Drugs targeting vascular endothelial growth factor (VEGF) such as bevacizumab may reduce enhancement and hyperintensity on FLAIR images temporarily for high-grade gliomas, a phenomenon known as pseudoresponse.
- Based on expert consensus, the Response Assessment in Neuro-Oncology criteria provide a standardized framework for monitoring brain tumor treatment response.
- Despite their nonmalignant behavior, pilocytic astrocytomas present as heterogeneously enhancing nodules with adjacent cystic structures.
- Subependymal giant cell astrocytomas are a classic feature of tuberous sclerosis complex and are generally found near the foramen of Monro.

Copyright © American Academy of Neurology. Unauthorized reproduction of this article is prohibited.

CASE 7-1

A 55-year-old right-handed man presented with increasing headaches and confusion for 2 months' duration. MRI of the brain, with and without contrast, revealed a right temporal rim-enhancing mass with surrounding fluid-attenuated inversion recovery (FLAIR) hyperintensity (FIGURE 7-3).

An open biopsy was performed, and pathologic evaluation confirmed isocitrate dehydrogenase (*IDH*) wild-type glioblastoma. The patient was treated with radiation and both concurrent and adjuvant temozolomide. Following completion of this therapy, the patient had an increase in heterogeneous enhancement and surrounding FLAIR hyperintensity, as well as clinical decline. Bevacizumab therapy was initiated, and follow-up MRI showed reduced contrast enhancement and reduced vasogenic edema, consistent with pseudoresponse to vascular endothelial growth factor (VEGF)–directed therapy. The patient also had clinical benefit at this time.

COMMENT

This case exemplifies the pattern of heterogeneous enhancement and marked surrounding T2 or FLAIR hyperintensity that is classically seen with glioblastoma, as well as the reversal of these findings with the use of bevacizumab (pseudoresponse).

Copyright © American Academy of Neurology. Unauthorized reproduction of this article is prohibited.

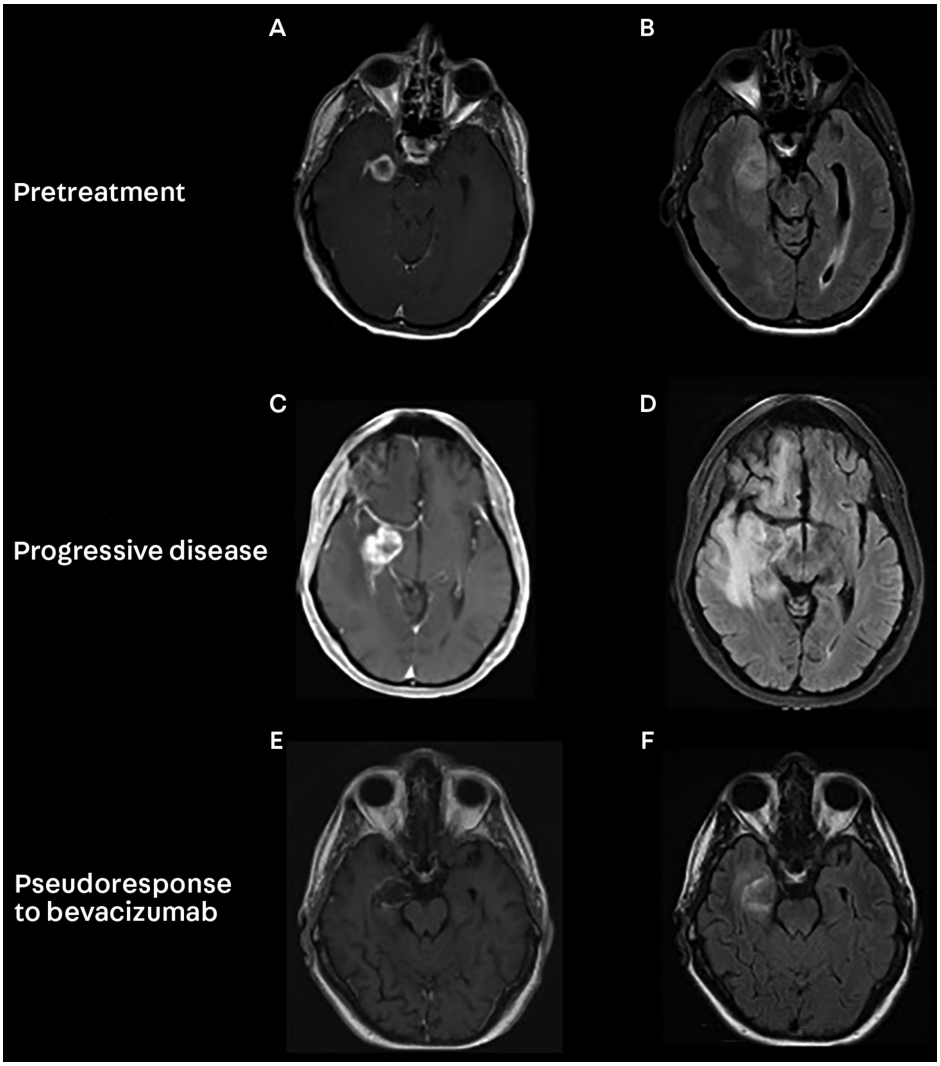

FIGURE 7-3

Imaging of the patient in CASE 7-1 with isocitrate dehydrogenase (*IDH*) wild-type glioblastoma. Before treatment, axial postcontrast T1-weighted MRI (*A*) shows a rim-enhancing right temporal lesion, and fluid-attenuated inversion recovery (FLAIR) (*B*) shows surrounding vasogenic edema. Six months after completion of standard radiation therapy and chemotherapy, axial postcontrast T1-weighted MRI (*C*) shows increased heterogeneous enhancement, and FLAIR image (*D*) shows marked increase in surrounding vasogenic edema. After initiation of bevacizumab, axial postcontrast T1-weighted MRI (*E*) shows reduced enhancement, and FLAIR image (*F*) shows reduced hyperintensity, consistent with pseudoresponse to vascular endothelial growth factor (VEGF)–directed therapy.

Copyright © American Academy of Neurology. Unauthorized reproduction of this article is prohibited.

IDH-mutated tumors are more common in younger adults, and median overall survival for *IDH*-mutated grade 2 astrocytoma is generally more than 10 years, compared with 5 to 10 years for grade 3 tumors and about 3 years for grade 4 tumors.[26]

CT of these tumors generally identifies a diffuse hypodensity with mass effect but with infrequent enhancement, especially in lower grades. MRI may show a lesion that is hypointense on T1-weighted images and hyperintense on T2-weighted images, often with expansion of underlying parenchyma. A T2-FLAIR mismatch sign may be present, with T2 hyperintensity but relative hypointensity on FLAIR imaging thought to stem from spatial differences in the cellularity and microenvironment of these tumors (FIGURE 7-4).[27,28] Gadolinium enhancement is infrequent in grade 2 tumors but increasingly common in grade 3 and 4 tumors, with the possible appearance of central necrosis and increasing vasogenic edema in higher grades as well. As noted previously, MR spectroscopy may be able to detect 2HG, the oncometabolite derived from *IDH* mutations, and may aid in diagnosis or treatment monitoring.

Grade 2 to 3 *IDH*–Mutated and 1p/19q-Codeleted Oligodendroglioma

Oligodendrogliomas are molecularly defined as having both an *IDH* mutation and codeletion of chromosome arms 1p and 19q. The average age at diagnosis is in the fifth decade of life, and seizures are the presenting symptom in two-thirds of patients.[29] Approximately 60% of oligodendrogliomas have a frontal lobe location.[30] Studies of prognosis for oligodendrogliomas are confounded by the inclusion of other tumor types, including *IDH* wild-type tumors, which is a byproduct of the rapidly evolving understanding of glioma biology and molecularly driven tumor distinctions. Using retrospective molecular stratification of prior data, oligodendrogliomas are generally considered to have a favorable response to radiation therapy and chemotherapy, with overall patient survival of more than 10 years.[27]

CT of oligodendrogliomas generally shows a diffuse, hypodense lesion involving both the cortex and subcortical white matter. Calcifications are commonly seen but are not diagnostic. MRI reveals a mass that is hypointense on T1-weighted images and hyperintense on T2-weighted images with contrast enhancement in a small minority of grade 2 oligodendrogliomas but in greater

TABLE 7-3 **Response Assessment in Neuro-oncology Criteria[a]**

	Complete response	Partial response	Stable disease	Progressive disease
Contrast enhancement	No enhancement	≥50% decrease	<50% decrease to <25% increase	≥25% increase
FLAIR	Stable or decrease	Stable or decrease	Stable or decrease	Stable or increase
New lesion	No	No	No	Present
Corticosteroid dose	None	Stable or decrease	Stable or decrease	Not applicable
Clinical status	Stable or improved	Stable or improved	Stable or improved	Worsened

FLAIR = fluid-attenuated inversion recovery.
[a] Patient must meet all criteria to be categorized as having complete or partial response or having stable or progressive disease.

Copyright © American Academy of Neurology. Unauthorized reproduction of this article is prohibited.

than 70% of grade 3 oligodendrogliomas.[31] MR spectroscopy may identify elevated 2HG (FIGURE 7-5).

IDH Wild-Type Glioblastoma

The most recent iteration of the WHO classification of tumors of the CNS specifies that the term *glioblastoma* can be applied only to *IDH* wild-type tumors (ie, this term can no longer be applied to astrocytic tumors with *IDH* mutations). Glioblastomas may affect adults at any age but are more common in older adults, and the time from symptom onset to diagnosis is less than 3 months in most patients.[32] Treatment includes a combination of surgical resection, radiation therapy, and chemotherapy. Prognosis is better with younger age, better performance status, greater extent of resection, and presence of *MGMT* promoter methylation. Median overall survival for WHO grade 4 *IDH* wild-type glioblastoma is about 8 months (15 to 18 months with radiation therapy and chemotherapy), and the 5-year survival rate is 6.8% in the United States.[2]

Imaging of *IDH* wild-type glioblastoma generally reveals a supratentorial space–occupying mass with prominent surrounding edema. Satellite lesions may be present, as well as evidence of diffuse spread along white matter tracts, sometimes causing bilateral involvement. On MRI, these tumors are generally hypointense on T1-weighted images and hyperintense on T2-weighted images and demonstrate heterogeneous enhancement that is sometimes in the pattern of irregular rim enhancement with evidence of central necrosis (CASE 7-1). Intratumoral blood products are not uncommon, affecting SWI as well as potentially causing foci of intrinsic T1 hyperintensity.

H3 K27–Altered Diffuse Midline Glioma

Diffuse midline glioma is an infiltrative glioma that generally arises in the brainstem in pediatric patients (especially the pons, as in diffuse intrinsic pontine glioma) or the thalami or spinal cord in adults. These tumors carry an overall poor prognosis, with less than 10% of individuals surviving 2 years or longer. MRI of diffuse midline glioma shows rim enhancement surrounding central

Cortical Masses With Cystic and Nodular Components[a] TABLE 7-4

Gliomas

- Pilocytic astrocytoma
- Isocitrate dehydrogenase (*IDH*) wild-type glioblastoma (rare)

Glioneuronal tumors

- Ganglioglioma
- Pleomorphic xanthoastrocytoma

Other

- Hemangioblastoma
- Central nervous system metastasis

[a] Modified with permission from Baig MA, et al, Continuum (Minneap Minn).[3] © 2016 American Academy of Neurology.

Copyright © American Academy of Neurology. Unauthorized reproduction of this article is prohibited.

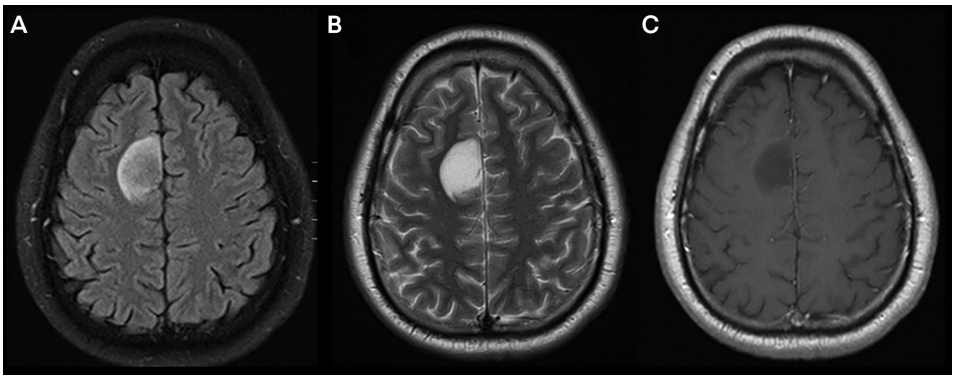

FIGURE 7-4
World Health Organization grade 2 isocitrate dehydrogenase (*IDH*)-mutated astrocytoma. *A,* Axial fluid-attenuated inversion recovery (FLAIR) MRI of the brain shows relative hypointensity within the right frontal mass compared to the T2-weighted images. *B,* Axial T2-weighted MRI shows hyperintensity (T2-FLAIR mismatch sign). *C,* Axial postcontrast T1-weighted MRI shows no abnormal enhancement associated with the tumor.

necrosis in most patients, with poorly defined margins of non–contrast-enhancing portions with heterogeneous FLAIR signal.[33] Specifically, diffuse intrinsic pontine glioma presents as a tumor arising from the pons with FLAIR hyperintensity involving greater than 50% of the ventral pons. The basilar artery may become encased by tumor.

Ependymoma

With an evolving understanding of the molecular and epigenetic features of ependymal tumors, the current iteration of the WHO classification of CNS

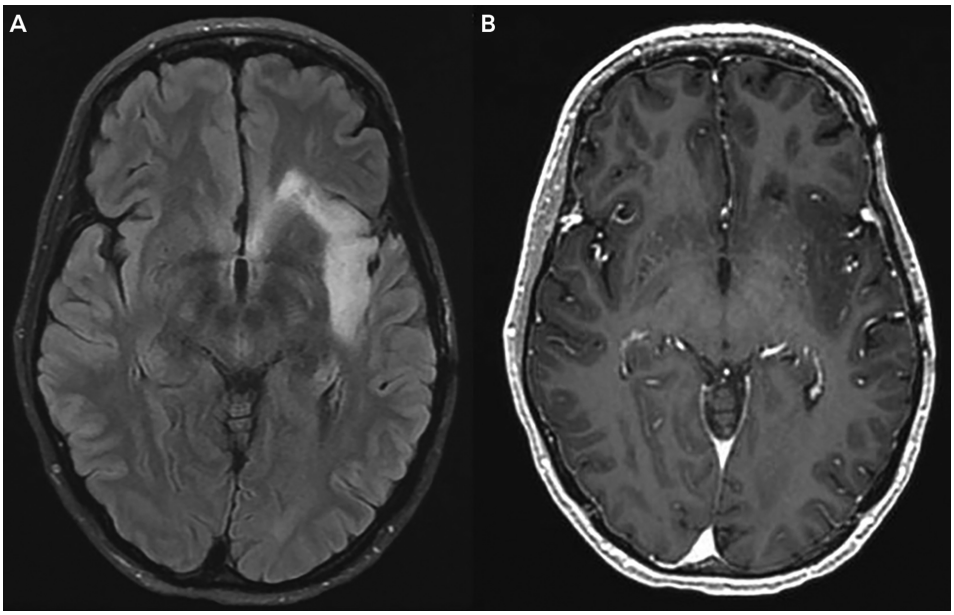

FIGURE 7-5
World Health Organization grade 2 isocitrate dehydrogenase (*IDH*)-mutated, 1p/19q codeleted oligodendroglioma. *A,* Axial fluid-attenuated inversion recovery (FLAIR) MRI reveals a discrete focus of hyperintensity including both insular cortex and subcortical white matter. *B,* Axial postcontrast T1-weighted MRI shows no abnormal enhancement.

Copyright © American Academy of Neurology. Unauthorized reproduction of this article is prohibited.

tumors distinguishes a total of 10 ependymoma subtypes across 3 main anatomic compartments (ie, supratentorial, posterior fossa, and spine). Although prospective data focused on molecular subtype–specific treatment determination are not yet available, the classification distinctions highlight the heterogeneous nature of ependymal tumor biology.

Imaging of ependymal tumors varies primarily by location, not necessarily by molecular subtype. Supratentorial ependymomas generally demonstrate heterogeneous enhancement with internal cysts, calcification, or both. SWI may show evidence of internal hemosiderin, and diffusion restriction may be present in the case of hypercellular tumor. Posterior fossa tumors are primarily found filling the fourth ventricle, with occasional extension into the foramen of Luschka or Magendie. Enhancement patterns are variable in these tumors, and internal cysts and calcifications may be seen (FIGURE 7-6). Spinal ependymomas are intramedullary and enhancing and often have internal cystic change, with less frequent calcification, blood products, or even necrosis. Sixty percent of spinal ependymomas are associated with syrinx. Myxopapillary ependymomas are nearly exclusively found at the conus medullaris or filum terminale. Finally, subependymomas are very well demarcated, hypointense to isointense on T1-weighted images, and hyperintense on T2-weighted images; may have internal calcification or cystic change; and occasionally show small foci of enhancement. TABLE 7-5[3] summarizes the differential diagnosis for intraventricular masses.

Lymphoma of the Central Nervous System

Primary diffuse large B-cell lymphoma of the CNS accounts for only about 3% of all brain tumors, and the peak incidence is during the fifth to seventh decades of life, with a slight male predominance.[2] These tumors are distinguished from immunodeficiency-associated CNS lymphomas, whose frequency has declined as therapies for human immunodeficiency virus (HIV) infection have improved, although they may still be seen with other immunodeficiencies or immunosuppressive therapies. As CNS lymphoma is a diffuse disease, surgery plays little role beyond achieving a diagnosis. Instead, methotrexate-based chemotherapy regimens are the standard induction therapy approach, with consolidation options ranging from high-dose chemotherapy with or without autologous stem cell transplant to low-dose whole-brain radiation therapy. Overall survival is about 3 years according to most published studies, although age is an important factor in prognosis, and some patients (especially younger ones) may be cured.

Imaging patterns are different between primary (or secondary) CNS lymphoma and immunodeficiency-associated CNS lymphoma. In immunocompetent individuals, MRI demonstrates one or more homogeneously enhancing lesions, often with associated restricted diffusion (related to tumor hypercellularity).[34] Nearly 80% of lesions are close to the ventricular ependyma or meningeal surface, and frequent involvement of the basal ganglia, thalamus, or corpus callosum occurs. Although perilesional edema may be present, it is generally less prominent than in gliomas or metastases (CASE 7-2).

Immunodeficiency-associated CNS lymphoma, on the other hand, is more likely to present with multifocality and rim enhancement of lesions (rather than a homogeneous enhancement pattern). Lesions are less likely to be adjacent to ependyma or meningeal surfaces[35] and may be associated with increased edema, or even hemorrhage or necrosis.

KEY POINTS

- *IDH*-mutated astrocytomas commonly exhibit the T2-FLAIR mismatch sign, in which T2-weighted images show a hyperintense tumor but the tumor is less hyperintense on FLAIR images.
- Oligodendrogliomas commonly present with seizures, extend to the cortex, and may reveal internal calcification.
- Glioblastoma is generally characterized by a supratentorial mass lesion with heterogeneous enhancement and surrounding hyperintensity on T2-weighted and FLAIR images; some intratumoral hemosiderin and satellite lesions may exist.
- H3 K27–altered diffuse midline glioma is an aggressive tumor that may arise from any midline structure such as thalamus, brainstem, or spinal cord.
- Ependymomas may arise in the supratentorial space, infratentorial space, or spinal cord and have varying molecular differentiation.
- Central nervous system lymphomas in immunocompetent patients are homogeneously enhancing, whereas immunosuppressed patients present with rim-enhancing lesions with occasional necrosis or hemorrhage.
- Nearly 80% of central nervous system lymphoma lesions are close to the ventricular ependyma or meningeal surface, and frequent involvement of the basal ganglia, thalamus, or corpus callosum occurs.

Copyright © American Academy of Neurology. Unauthorized reproduction of this article is prohibited.

KEY POINTS

- Although hemangioblastomas may be sporadic, evaluation for underlying von Hippel-Lindau syndrome is important.
- Imaging of the entire neuraxis and spinal fluid sampling are necessary for patients with medulloblastoma because of the high rate of disseminated disease.

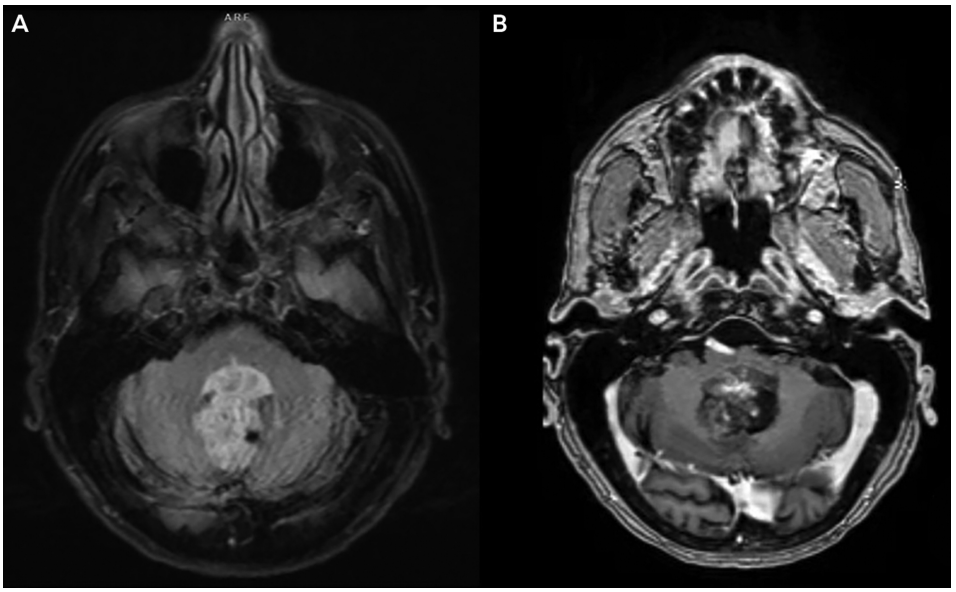

FIGURE 7-6
World Health Organization grade 3 posterior fossa ependymoma. *A,* Axial fluid-attenuated inversion recovery (FLAIR) MRI reveals a hyperintense mass arising from the fourth ventricle (not shown is associated noncommunicating hydrocephalus). *B,* Axial postcontrast T1-weighted MRI shows heterogeneous enhancement of the fourth ventricular mass.

Hemangioblastoma

Hemangioblastomas are histologically benign tumors that are highly vascular and most frequently arise in the cerebellum. Accounting for less than 2% of all CNS tumors, hemangioblastomas are usually sporadic tumors but may be associated with von Hippel-Lindau syndrome (in which case the tumors are usually multiple and widespread).[36] Sporadic hemangioblastomas may be surgically eradicated, whereas those presenting in the setting of von Hippel-Lindau syndrome may be resected individually or treated with belzutifan (hypoxia-inducible factor 2 alpha inhibitor), which has been recently approved by the US Food and Drug Administration (FDA).

Tumors are generally cystic in nature, with a solid mural nodule that appears as isointense on T1-weighted images and hyperintense on T2-weighted images, and often contain serpentine flow voids.[37] The solid portion of the tumor is generally brightly enhancing, whereas the cyst does not enhance. For individuals with von Hippel-Lindau syndrome, imaging of the entire spine and examination of the retina are also recommended.

Medulloblastoma

Medulloblastomas are a type of embryonal tumor that can present at any age but are most common in childhood, with a greater incidence in males than in females.[2] In children, medulloblastomas account for nearly 20% of intracranial tumors, whereas in adults they account for less than 1%.[2] Notably, medulloblastomas may be seen as part of several inherited cancer predisposition syndromes, including Gorlin syndrome (associated with SUFU and PTCH1 germline mutations), Li-Fraumeni syndrome (associated with TP53 germline mutations), familial adenomatous polyposis (associated with germline APC mutations), and others.[38] Medulloblastomas are molecularly categorized into

Copyright © American Academy of Neurology. Unauthorized reproduction of this article is prohibited.

the four primary classifications of wingless and INT-1(WNT)-activated, sonic hedgehog (SHH)-activated and *TP53* wildtype, SHH-activated and *TP53*-mutated, and non-WNT/non-SHH, highlighting the heterogeneity of these tumors both biologically and prognostically. Arising from the fourth ventricle, medulloblastomas are isointense to hypointense on T1-weighted images and isointense on T2-weighted images with avid enhancement with gadolinium and frequent restricted diffusivity. In children, the tumor more often arises from the vermis, whereas in adults it tends to occur laterally in the cerebellar hemispheres. Imaging of the entire neuraxis should be pursued because of the elevated risk of disease dissemination.[39] Treatment for medulloblastomas involves surgical resection followed by a combination of craniospinal radiation therapy and chemotherapy.

Ganglioglioma

A glioneuronal neoplasm, ganglioglioma is a histologically benign, well-demarcated, and relatively slow-growing tumor. Most common in the

Intraventricular Masses[a] TABLE 7-5

Lateral ventricles

- Supratentorial ependymoma
- Subependymoma
- Subependymal giant cell astrocytoma
- Central neurocytoma
- Choroid plexus papilloma (especially in children)
- Choroid plexus carcinoma
- Meningioma
- Metastasis
- Glioblastoma (very rare)

Third ventricle

- Colloid cyst
- Central neurocytoma
- Meningioma
- Metastasis

Fourth ventricle

- Posterior fossa ependymoma
- Metastasis
- Rosette-forming glioneuronal tumors
- Epidermoid cyst
- Choroid plexus papilloma (especially in adults)
- Meningioma

[a] Modified with permission from Baig MA, et al, Continuum (Minneap Minn).[3] © 2016 American Academy of Neurology.

Copyright © American Academy of Neurology. Unauthorized reproduction of this article is prohibited.

CASE 7-2

A 70-year-old right-handed woman presented to the hospital with memory and mood changes. MRI of the brain, with and without contrast, revealed multifocal homogeneously enhancing masses with associated restricted diffusion and surrounding vasogenic edema (FIGURE 7-7).

CTs of the chest, abdomen, and pelvis revealed no other lesions. A biopsy of one of the enhancing intracranial lesions was obtained, which confirmed diffuse large B-cell lymphoma, consistent with primary central nervous system lymphoma. The patient was treated with induction chemotherapy consisting of high-dose methotrexate and rituximab, with remarkable radiographic and clinical improvement. She subsequently underwent high-dose thiotepa-based chemotherapy followed by autologous stem cell rescue. Cranial imaging since then confirms a complete response to therapy with no residual or recurrent disease. Persistent hyperintensity on T2-weighted and fluid-attenuated inversion recovery (FLAIR) images most likely represents gliosis.

COMMENT

This case demonstrates the utility of comprehensive MRI, including diffusion-weighted and apparent diffusion coefficient images as well as postgadolinium images, in the evaluation of central nervous system lymphoma.

Copyright © American Academy of Neurology. Unauthorized reproduction of this article is prohibited.

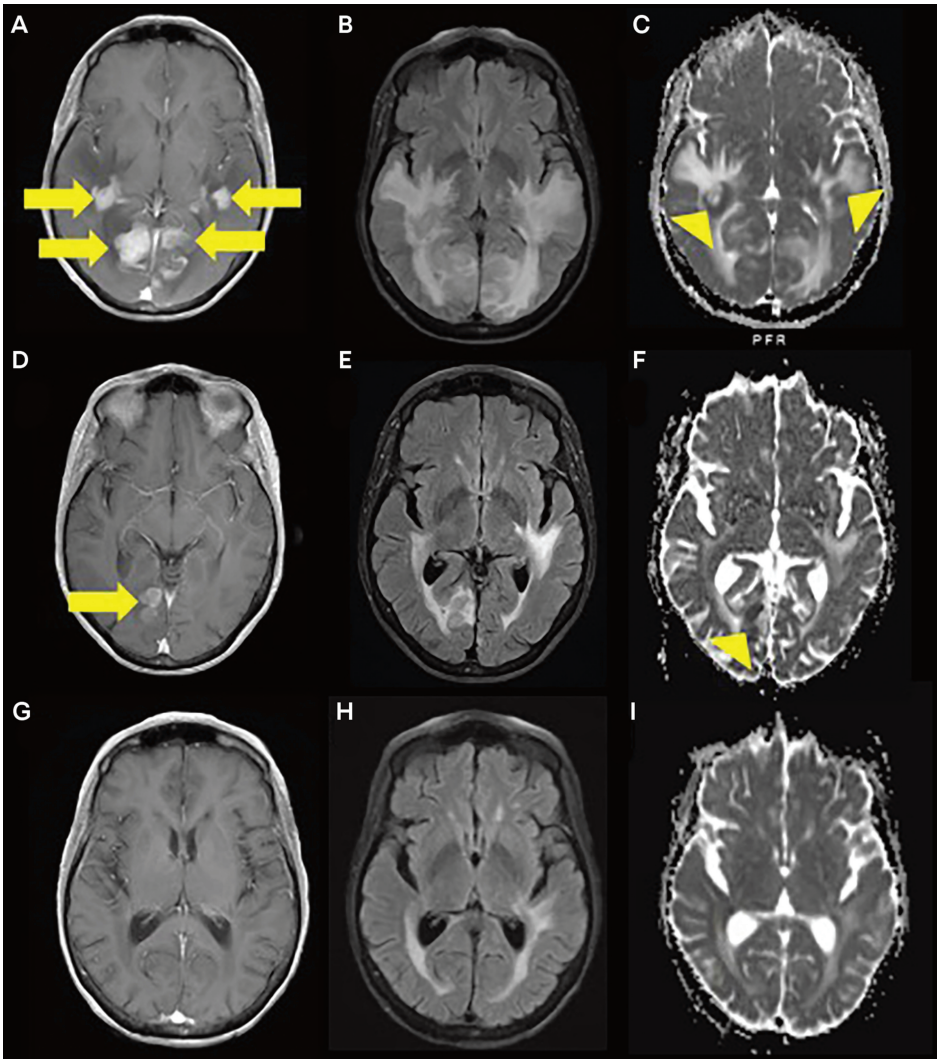

FIGURE 7-7

Imaging of the patient in CASE 7-2 with primary central nervous system lymphoma. Before treatment, axial postcontrast T1-weighted MRI shows multifocal homogeneously enhancing foci (*A*, *arrows*), axial fluid-attenuated inversion recovery (FLAIR) MRI shows hyperintensity associated with the lesions and surrounding the lesions (vasogenic edema) (*B*), and axial apparent diffusion coefficient (ADC) image indicates hypointensity consistent with restricted diffusion (C, *arrowheads*). After 2 months of high-dose methotrexate-based therapy, axial postcontrast T1-weighted MRI shows stark reduction in enhancing foci (*D*, *arrow*), axial FLAIR MRI shows reduced hyperintensity (*E*), and axial ADC image shows reduced restricted diffusion (F, *arrowhead*). After additional methotrexate-based therapy and then high-dose chemotherapy with autologous stem cell transplant, axial postcontrast T1-weighted MRI shows no residual contrast enhancement (*G*), axial FLAIR MRI shows some small residual hyperintensity consistent with gliosis (*H*), and axial ADC image shows no residual restricted diffusion (*I*).

Copyright © American Academy of Neurology. Unauthorized reproduction of this article is prohibited.

adolescent years, gangliogliomas may present in any location throughout the CNS, and supratentorial tumors are frequently associated with seizures. Prognosis is generally very good, with the extent of resection serving as its primary driver. Imaging of gangliogliomas often demonstrates a mix of solid and cystic components with a variably enhancing mural nodule, and calcification may occasionally be observed.[40]

Pleomorphic Xanthoastrocytoma

Generally arising in the temporal lobes, pleomorphic xanthoastroctyomas are rare, intermediate-grade tumors (WHO grades 2 and 3) typically diagnosed in children and young adults. Recurrences are common for these tumors, often with malignant progression. The extent of resection is the primary driver of prognosis, with a 5-year overall survival of 90% for grade 2 tumors and 57% for grade 3 tumors.[41] On imaging, pleomorphic xanthoastroctyomas are usually cystic, cortically located tumors. CT shows variable tumor density with relative hypodensity of associated cysts. MRI shows the solid tumor to be either isointense or hypointense to gray matter on T1-weighted images, with hyperintensity or mixed signal on T2-weighted images. Contrast enhancement of the solid portion of the tumor is moderate to strong. Surrounding edema, if present, may be minimal.

Central Neurocytoma

Central neurocytomas are WHO grade 2 tumors arising intraventricularly, typically attached to the septum pellucidum near the foramen of Monro.[42] These tumors are usually diagnosed in the third decade of life and have a favorable clinical course, which is positively affected by complete resection. On CT, central neurocytomas show mixed solid and cystic structures with frequent calcification, whereas on MRI a characteristic soap-bubble appearance on T2-weighted images is caused by the multicystic structure. With well-defined margins, these tumors demonstrate heterogeneous enhancement, and sometimes vascular flow voids are also present.[42]

Central Nervous System Metastatic Disease

Brain metastases are far more common than primary brain tumors and are increasing in incidence as improved systemic cancer therapies lead to longer postdiagnosis survival.[43] Brain metastases are located in the cerebral hemispheres in 80% of cases, especially in end-arterial border zone locations and at the junction of cortex and subcortical white matter. It is more common to have multiple brain metastases than a single brain metastasis, and it is relatively rare that the brain is the only site of metastasis in the body. Although the development of brain metastases was historically considered an end-stage event, outcomes are now more variable (and frequently more favorable) as a result of the advent of targeted systemic therapies and immunotherapies. The most common sources of brain metastases include small cell lung cancer, non–small cell lung cancer, breast cancer, colorectal cancer, renal cancer, and melanoma.[43] A brain metastasis may be the first tumor identified in a patient with widespread malignancy; therefore, some patients may warrant imaging of the body (chest, abdomen, pelvis) when metastatic brain tumor is highly suspected.

Brain metastases have a variable appearance on MRI but are often isointense to hypointense on T1-weighted images with hyperintensity on T2-weighted images. Some tumors, especially those arising from renal cell carcinoma, melanoma,

Copyright © American Academy of Neurology. Unauthorized reproduction of this article is prohibited.

choriocarcinoma, or papillary thyroid cancer, may show blood products, and other tumors may show restricted diffusion (especially in small, new metastases). Peritumoral edema may be prominent in many cases. After gadolinium injection, enhancement is often seen in a heterogeneous or rimlike pattern with central necrosis. In patients with a differential diagnosis including metastasis versus glioblastoma, perfusion imaging may differentiate pure vasogenic edema from infiltrative glioma in hyperintensity surrounding the tumor on T2-weighted or FLAIR images, thus aiding in presurgical diagnosis.[44]

CONCLUSION

Imaging of brain tumors aids tremendously in diagnosis as well as longitudinal monitoring of treated individuals. MRI with gadolinium is the preferred imaging modality. Contrast enhancement is seen when there is breakdown of the blood-brain barrier and in highly vascular tumors. Although contrast enhancement is seen with many malignant tumors, it is not always indicative of malignancy. For instance, not only is contrast enhancement present in subacute ischemic infarctions, acute demyelination, and other non-neoplastic entities, but it is also seen in various benign tumors such as pilocytic astrocytoma. Restricted diffusion may be indicative of hypercellularity in some tumors but can also be present in ischemic infarctions and abscesses. Perfusion imaging shows variability in relative cerebral blood volume, which may be a proxy for angiogenesis and has been associated with tumor grade. Cerebral blood volume may also aid in differentiation of tumor recurrence or treatment effect. Finally, MR spectroscopy can be helpful in evaluating tumor versus demyelination and may also be useful in studying *IDH*-mutated tumors, specifically through quantitative 2HG analysis.

Structural and functional imaging modalities provide valuable insight into the biology of nervous system pathologies, especially neoplasms. Because imaging is the primary noninvasive tool for disease evaluation and monitoring, incorporation of up-to-date imaging techniques is essential for the modern neuro-oncology practice.

KEY POINTS

- **Pleomorphic xanthoastrocytoma classically presents as a cystic, cortically located tumor with an enhancing nodule.**
- **Brain metastases are usually multiple and within the cerebral hemispheres, especially in end-arterial border zone locations and at the junction of cortex and subcortical white matter.**
- **Very small metastatic tumors may present as foci of restricted diffusion before growing to show definitive enhancing tumors.**
- **Imaging is an essential tool for diagnosing and monitoring intracranial brain tumors.**

REFERENCES

1 Bi WL. Imaging of skull base tumors. Continuum (Minneap Minn) 2023;29(1, Neuroimaging):154-168.

2 Ostrom QT, Cioffi G, Waite K, Kruchko C, Barnholtz-Sloan JS. CBTRUS statistical report: primary brain and other central nervous system tumors diagnosed in the United States in 2014-2018. Neuro Oncol 2021;23(12 Suppl 2): iii1-iii105. doi:10.1093/neuonc/noab200

3 Baig MA, Klein JP, Mechtler LL. Imaging of brain tumors. Continuum (Minneap Minn) 2016; 22(5, Neuroimaging):1529-1552. doi:10.1212/CON.0000000000000388

4 Bitar R, Leung G, Perng R, et al. MR pulse sequences: what every radiologist wants to know but is afraid to ask. Radiographics 2006;26(2): 513-537. doi:10.1148/rg.262055063

5 Ellingson BM, Sahebjam S, Kim HJ, et al. Pretreatment ADC histogram analysis is a predictive imaging biomarker for bevacizumab treatment but not chemotherapy in recurrent glioblastoma. AJNR Am J Neuroradiol 2014;35(4): 673-679. doi:10.3174/ajnr.A3748

6 Wirsching HG, Roelcke U, Weller J, et al. MRI and ^{18}FET-PET predict survival benefit from bevacizumab plus radiotherapy in patients with isocitrate dehydrogenase wild-type glioblastoma: results from the randomized ARTE Trial. Clin Cancer Res 2021;27(1):179-188. doi: 10.1158/1078-0432.CCR-20-2096

7 Kłos J, van Laar PJ, Sinnige PF, et al. Quantifying effects of radiotherapy-induced microvascular injury; review of established and emerging brain MRI techniques. Radiother Oncol 2019;140:41-53. doi:10.1016/j.radonc.2019.05.020

Copyright © American Academy of Neurology. Unauthorized reproduction of this article is prohibited.

8 Boxerman JL, Schmainda KM, Weisskoff RM. Relative cerebral blood volume maps corrected for contrast agent extravasation significantly correlate with glioma tumor grade, whereas uncorrected maps do not. AJNR Am J Neuroradiol 2006;27(4):859-867.

9 Schmainda KM, Zhang Z, Prah M, et al. Dynamic susceptibility contrast MRI measures of relative cerebral blood volume as a prognostic marker for overall survival in recurrent glioblastoma: results from the ACRIN 6677/RTOG 0625 multicenter trial. Neuro Oncol 2015;17(8):1148-1156. doi:10.1093/neuonc/nou364

10 Boxerman JL, Quarles CC, Hu LS, et al. Consensus recommendations for a dynamic susceptibility contrast MRI protocol for use in high-grade gliomas. Neuro Oncol 2020;22(9):1262-1275. doi:10.1093/neuonc/noaa141

11 Andronesi OC, Kim GS, Gerstner E, et al. Detection of 2-hydroxyglutarate in *IDH*-mutated glioma patients by in vivo spectral-editing and 2D correlation magnetic resonance spectroscopy. Sci Transl Med 2012;4(116):116ra4. doi:10.1126/scitranslmed.3002693

12 Andronesi OC, Arrillaga-Romany IC, Ly KI, et al. Pharmacodynamics of mutant-IDH1 inhibitors in glioma patients probed by in vivo 3D MRS imaging of 2-hydroxyglutarate. Nat Commun 2018;9(1):1474. doi:10.1038/s41467-018-03905-6

13 Choi C, Raisanen JM, Ganji SK, et al. Prospective longitudinal analysis of 2-hydroxyglutarate magnetic resonance spectroscopy identifies broad clinical utility for the management of patients with *IDH*-mutant glioma. J Clin Oncol 2016;34(33):4030-4039. doi:10.1200/JCO.2016.67.1222

14 Albert NL, Weller M, Suchorska B, et al. Response Assessment in Neuro-Oncology working group and European Association for Neuro-Oncology recommendations for the clinical use of PET imaging in gliomas. Neuro Oncol 2016;18(9):1199-1208. doi:10.1093/neuonc/now058

15 Beers A, Chang K, Brown J, et al. Sequential neural networks for biologically informed glioma segmentation. In: Medical imaging 2018: image processing. Vol 10574. SPIE; 2018:807-816. doi:10.1117/12.2293941

16 Chang K, Bai HX, Zhou H, et al. Residual convolutional neural network for the determination of *IDH* Status in low- and high-grade gliomas from MR imaging. Clin Cancer Res 2018;24(5):1073-1081. doi:10.1158/1078-0432.CCR-17-2236

17 Chang K, Beers AL, Bai HX, et al. Automatic assessment of glioma burden: a deep learning algorithm for fully automated volumetric and bidimensional measurement. Neuro Oncol 2019;21(11):1412-1422. doi:10.1093/neuonc/noz106

18 Yogananda CGB, Shah BR, Nalawade SS, et al. MRI-based deep-learning method for determining glioma MGMT promoter methylation status. AJNR Am J Neuroradiol 2021;42(5):845-852. doi:10.3174/ajnr.A7029

19 Thust SC, van den Bent MJ, Smits M. Pseudoprogression of brain tumors. J Magn Reson Imaging 2018;48(3):571-589. doi:10.1002/jmri.26171

20 Le Rhun E, Devos P, Boulanger T, et al. The RANO Leptomeningeal Metastasis Group proposal to assess response to treatment: lack of feasibility and clinical utility and a revised proposal. Neuro Oncol 2019;21(5):648-658. doi:10.1093/neuonc/noz024

21 Lin NU, Lee EQ, Aoyama H, et al. Response assessment criteria for brain metastases: proposal from the RANO group. Lancet Oncol 2015;16(6):e270-278. doi:10.1016/S1470-2045(15)70057-4

22 Wen PY, Macdonald DR, Reardon DA, et al. Updated response assessment criteria for high-grade gliomas: response assessment in neuro-oncology working group. J Clin Oncol 2010;28(11):1963-1972. doi:10.1200/JCO.2009.26.3541

23 Louis DN, Perry A, Wesseling P, et al. The 2021 WHO Classification of Tumors of the Central Nervous System: a summary. Neuro Oncol 2021;23(8):1231-1251. doi:10.1093/neuonc/noab106

24 Kondyli M, Larouche V, Saint-Martin C, et al. Trametinib for progressive pediatric low-grade gliomas. J Neurooncol 2018;140(2):435-444. doi:10.1007/s11060-018-2971-9

25 Miller DT, Freedenberg D, Schorry E, et al. Health supervision for children with neurofibromatosis type 1. Pediatrics 2019;143(5):e20190660. doi:10.1542/peds.2019-0660

26 Brat D, Reuss D, von Deimling A. Astrocytoma, *IDH*-mutant. In: WHO classification of tumours, central nervous system tumours. 5th ed. International Agency for Research on Cancer; 2021.

27 Patel SH, Poisson LM, Brat DJ, et al. T2-FLAIR mismatch, an imaging biomarker for *IDH* and 1p/19q status in lower-grade gliomas: a TCGA/TCIA project. Clin Cancer Res 2017;23(20):6078-6085. doi:10.1158/1078-0432.CCR-17-0560

28 Foltyn M, Nieto Taborda KN, Neuberger U, et al. T2/FLAIR-mismatch sign for noninvasive detection of *IDH*-mutant 1p/19q non-codeleted gliomas: validity and pathophysiology. Neurooncol Adv 2020;2(1):vdaa004. doi:10.1093/noajnl/vdaa004

29 Reifenberger G, Louis D, Figarella-Branger D. Oligodendroglioma, *IDH*-mutant and 1p/19q-codeleted. In: WHO classification of tumours, central nervous system tumours. 5th ed. International Agency for Research on Cancer; 2021.

30 Smits M. Imaging of oligodendroglioma. Br J Radiol 2016;89(1060):20150857. doi:10.1259/bjr.20150857

31 Khalid L, Carone M, Dumrongpisutikul N, et al. Imaging characteristics of oligodendrogliomas that predict grade. AJNR Am J Neuroradiol 2012;33(5):852-857. doi:10.3174/ajnr.A2895

Copyright © American Academy of Neurology. Unauthorized reproduction of this article is prohibited.

32 Ohgaki H, Kleihues P. Genetic pathways to primary and secondary glioblastoma. Am J Pathol 2007;170(5):1445-1453. doi:10.2353/ajpath.2007.070011

33 Thust S, Micallef C, Okuchi S, et al. Imaging characteristics of H3 K27M histone-mutant diffuse midline glioma in teenagers and adults. Quant Imaging Med Surg 2021;11(1):43-56. doi:10.21037/qims-19-954

34 Grommes C, Rubenstein JL, DeAngelis LM, Ferreri AJM, Batchelor TT. Comprehensive approach to diagnosis and treatment of newly diagnosed primary CNS lymphoma. Neuro Oncol 2019;21(3):296-305. doi:10.1093/neuonc/noy192

35 Brandsma D, Bromberg JEC. Primary CNS lymphoma in HIV infection. Handb Clin Neurol 2018;152:177-186. doi:10.1016/B978-0-444-63849-6.00014-1

36 Gläsker S. Central nervous system manifestations in VHL: genetics, pathology and clinical phenotypic features. Fam Cancer 2005;4(1):37-42. doi:10.1007/s10689-004-5347-6

37 Cha J, Kim ST, Nam DH, et al. Differentiation of hemangioblastoma from metastatic brain tumor using dynamic contrast-enhanced MR imaging. Clin Neuroradiol 2017;27(3):329-334. doi:10.1007/s00062-016-0508-1

38 Ellison D, Taylor M. Medulloblastoma: introduction. In: WHO Classification of tumours, central nervous system tumours. 5th ed. International Agency for Research on Cancer; 2021.

39 Northcott PA, Robinson GW, Kratz CP, et al. Medulloblastoma. Nat Rev Dis Primers 2019;5(1):11. doi:10.1038/s41572-019-0063-6

40 Abdel Razek AAK, Elsebaie NA, Zamora C, Castillo M. Imaging of neuronal and mixed glioneuronal tumors. J Comput Assist Tomogr 2020;44(3):356-369. doi:10.1097/RCT.0000000000001010

41 Giannini C, Louis D, Figarella-Branger D, et al. Pleomorphic xanthoastrocytoma. In: WHO classification of tumours, central nervous system tumours. 5th ed. International Agency for Research on Cancer; 2021.

42 Wang M, Jia D, Shen J, Zhang J, Li G. Clinical and imaging features of central neurocytomas. J Clin Neurosci 2013;20(5):679-685. doi:10.1016/j.jocn.2012.05.053

43 Tabouret E, Chinot O, Metellus P, et al. Recent trends in epidemiology of brain metastases: an overview. Anticancer Res 2012;32(11):4655-4662.

44 Suh CH, Kim HS, Jung SC, Choi CG, Kim SJ. Perfusion MRI as a diagnostic biomarker for differentiating glioma from brain metastasis: a systematic review and meta-analysis. Eur Radiol 2018;28(9):3819-3831. doi:10.1007/s00330-018-5335-0

DISCLOSURE

Continued from page 171

Network, and the United Council for Neurologic Subspecialties that is relevant to AAN interests or activities. The institution of Dr Jordan has received research support from The Burke Foundation, the Department of Defense, and the National Institutes of Health. Dr Gerstner has received personal compensation in the range of $500 to $4999 for serving on a data safety monitoring board for Midatech Pharma PLC and in the range of $50,000 $99,999 for serving as an officer or member of the board of directors for the Gerstner Family Foundation. The institution of Dr Gerstner has received research support from the National Cancer Institute.

Copyright © American Academy of Neurology. Unauthorized reproduction of this article is prohibited.

REVIEW ARTICLE

CONTINUUM AUDIO INTERVIEW AVAILABLE ONLINE

Imaging in Movement Disorders

By Baijayanta Maiti, MD, PhD; Joel S. Perlmutter, MD

CITE AS:
CONTINUUM (MINNEAP MINN) 2023;29(1, NEUROIMAGING): 194–218.

Address correspondence to Dr Baijayanta Maiti, Department of Neurology, Washington University School of Medicine, Campus Box 8111, 660 S Euclid Ave, Saint Louis, MO 63110, maitib@wustl.edu.

RELATIONSHIP DISCLOSURE:
The institution of Dr Maiti has received research support from the National Center for Advancing Translational Sciences and the National Institute of Neurological Disorders and Stroke of the National Institutes of Health. Dr Perlmutter has received personal compensation in the range of $0 to $499 for serving as an officer or member of the Board of Directors for the Parkinson Study Group, and in the range of $500 to $4999 for serving as an officer or member of the Board of Directors for the CHDI Foundation, as an expert witness for Wood, Cooper and Peterson, LLC, and Simmons and Simmons LLP, as a lecturer for Boston University, as an external advisor for Stanford University, and as a visiting professor with Beth Israel Hospital and the University of Pennsylvania. The institution of Dr Perlmutter has received research support from the American Parkinson Disease
Continued on page 218

UNLABELED USE OF PRODUCTS/INVESTIGATIONAL USE DISCLOSURE:
Drs Maiti and Perlmutter report no disclosures.

© 2023 American Academy of Neurology.

ABSTRACT

OBJECTIVE: This article reviews commonly used imaging modalities in movement disorders, particularly parkinsonism. The review includes the diagnostic utility, role in differential diagnosis, reflection of pathophysiology, and limitations of neuroimaging in the setting of movement disorders. It also introduces promising new imaging modalities and describes the current status of research.

LATEST DEVELOPMENTS: Iron-sensitive MRI sequences and neuromelanin-sensitive MRI can be used to directly assess the integrity of nigral dopaminergic neurons and thus may reflect disease pathology and progression throughout the full range of severity in Parkinson disease (PD). The striatal uptake of presynaptic radiotracers in their terminal axons as currently assessed using clinically approved positron emission tomography (PET) or single-photon emission computed tomography (SPECT) imaging correlates with nigral pathology and disease severity only in early PD. Cholinergic PET, using radiotracers that target the presynaptic vesicular acetylcholine transporter, constitutes a substantial advance and may provide crucial insights into the pathophysiology of clinical symptoms such as dementia, freezing, and falls.

ESSENTIAL POINTS: In the absence of valid, direct, objective biomarkers of intracellular misfolded α-synuclein, PD remains a clinical diagnosis. The clinical utility of PET- or SPECT-based striatal measures is currently limited given their lack of specificity and inability to reflect nigral pathology in moderate to severe PD. These scans may be more sensitive than clinical examination to detect nigrostriatal deficiency that occurs in multiple parkinsonian syndromes and may still be recommended for clinical use in the future to identify prodromal PD if and when disease-modifying treatments become available. Multimodal imaging to evaluate underlying nigral pathology and its functional consequences may hold the key to future advances.

INTRODUCTION

Idiopathic Parkinson disease (PD), the second most common neurodegenerative disorder after Alzheimer disease (AD), is by far the most common cause of parkinsonism and is marked by tremendous clinical heterogeneity. A host of motor features including varying combinations of bradykinesia, rest tremor, rigidity, and postural instability along with

Copyright © American Academy of Neurology. Unauthorized reproduction of this article is prohibited.

associated features such as asymmetric onset and response to levodopa support the clinical diagnosis of PD.[1] A mélange of nonmotor features including rapid eye movement sleep behavior disorder (RBD), olfactory dysfunction, autonomic features, and cognitive dysfunction further adds to the clinical variability. Other less common clinical features such as rapid progression, early postural instability, and lack of sustained response to levodopa may occur in PD and atypical parkinsonisms. Other manifestations may help to identify specific causes of atypical parkinsonisms including early autonomic failure and cerebellar features in multiple system atrophy (MSA), supranuclear vertical gaze palsy primarily affecting downward gaze in progressive supranuclear palsy (PSP), and asymmetric dystonia, myoclonus, cortical sensory features, and language and cognitive dysfunction in corticobasal degeneration (CBD). However, these atypical features are not sensitive, especially early in the disease process, nor are they specific, with considerable overlap among these entities, making the differential diagnosis of early parkinsonism somewhat challenging.[2,3] This article discusses various currently available imaging modalities, focusing primarily on their clinical utility. In addition, the article highlights some ongoing research that could set the stage to further enhance our understanding of the pathophysiology of PD, provide metrics of disease progression, identify targets for novel therapies, and quantify target engagement for such new therapies. Although the primary focus will be on parkinsonism, we will briefly discuss how imaging, especially MRI, can be clinically useful in other movement disorders.

KEY POINTS

- **The pathologic hallmark of Parkinson disease is the intracellular deposition of misfolded α-synuclein; classic motor symptoms of Parkinson disease manifest only after the loss of midbrain nigral dopaminergic neurons crosses a certain threshold.**
- **The nigrostriatal dopaminergic neurons project to the striatum, and substantial loss of striatal dopamine has already occurred by the time the classic motor symptoms of Parkinson disease manifest.**

IMAGING IN PARKINSONISM

The pathologic hallmark of PD is the intraneuronal deposition of misfolded α-synuclein. The spherical intracytoplasmic aggregates are called Lewy bodies, and the spindlelike or threadlike inclusions in the neuronal processes are called Lewy neurites. The pathologic process in the brain begins in the vulnerable neurons in the caudal medulla (with or without involvement of the olfactory bulb or anterior olfactory nucleus), and relentless rostral progression marches in a predictable sequence to ultimately affect the cortex.[4] The classic motor symptoms of PD manifest only after loss of nigrostriatal dopaminergic neurons in the midbrain substantia nigra reaches a certain threshold (about 30% to 35%), leading to reduced dopamine in their terminal axons in the striatum.[5] This article will critically dissect the value of nuclear imaging and MRI in the diagnosis of PD, including presymptomatically, how these studies aid in the differential diagnosis of PD and atypical parkinsonisms, and their ability to serve as a measure of underlying pathology, disease severity, and progression.

Nuclear Imaging in Parkinsonism

The two key components of nuclear imaging are (1) radiotracers, or radiolabeled chemicals (the ones discussed here are primarily ligands that even in very tiny amounts bind the target molecule of interest with very high specificity); and (2) scanners, or cameras that detect the radioactive emissions from the radiotracer in the brain with preferential uptake and retention to desired targets in specific brain regions. Single-photon emission computed tomography (SPECT) uses scanners and radiotracers that are more readily available than those of positron emission tomography (PET), which requires short-lived radioisotopes that must

Copyright © American Academy of Neurology. Unauthorized reproduction of this article is prohibited.

be produced close to the specialized PET scanners; however, PET has a substantially higher resolution than SPECT.

Intuitively, the most direct method of molecular imaging of pathology in PD would be assessment of the integrity of the nigral dopaminergic neurons with a radiotracer that binds selectively and directly to the misfolded α-synuclein. Although vigorous research is currently underway to develop such radiotracers, technical challenges such as off-target binding of potential α-synuclein tracers to misfolded amyloid-β (Aβ) (a frequent coexisting pathology in PD) have slowed this development. In the meantime, molecular imaging has focused on radiotracers targeting presynaptic neurons that project from the substantia nigra dopaminergic neurons to the striatum. A variety of radiotracers have targeted these terminal fields of the nigrostriatal pathway. In 2011, the US Food and Drug Administration (FDA) approved a SPECT radiotracer, [^{123}I]-ioflupane ([^{123}I]-fluoropropyl βCIT), that targets the dopamine transporter (DAT), a presynaptic membrane–bound protein necessary for reuptake of dopamine from the synaptic cleft back into the presynaptic nerve terminal. DAT radiotracers also bind serotonin and noradrenaline reuptake sites and so are not entirely specific for presynaptic dopaminergic neurons. However, dopaminergic terminals in the striatum are far more numerous than those of either serotonin or noradrenaline. Thus, under normal conditions, striatal uptake mostly reflects the integrity of dopaminergic

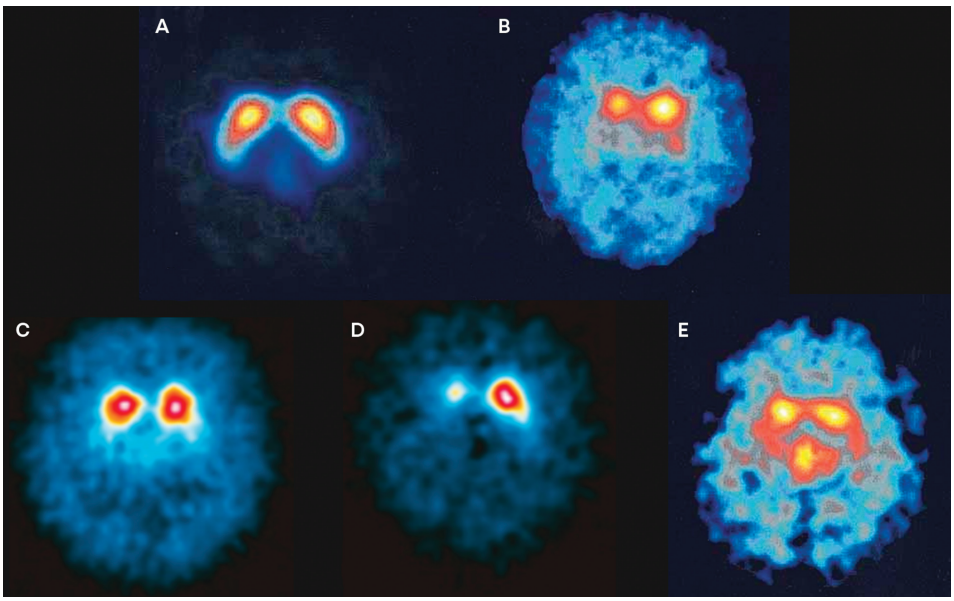

FIGURE 8-1

[^{123}I]β-CIT Dopamine transporter (DAT) single-photon emission computed tomography (SPECT) images at the level of striatum. Uniform (comma-shaped) striatal uptake of DAT tracer in a healthy control (*A*). Asymmetrically (*B*) and symmetrically (*C*) reduced DAT (period shaped) with putamen more affected than caudate nucleus in patients with idiopathic Parkinson disease. Similarly, asymmetrically (*D*) and symmetrically (*E*) reduced DAT can also be seen in patients with multiple system atrophy with predominant parkinsonism. Panels *B, C, D,* and *E* highlight the lack of specificity of DAT-SPECT. Panels *C* and *D* were obtained from patients with pathologically proven diagnoses of Parkinson disease and multiple system atrophy with predominant parkinsonism, respectively.

Panels *A*, *B*, and *E* reprinted with permission from Varrone A, et al, Move Disord.[8] © 2001 International Parkinson and Movement Disorder Society.

Panels *C* and *D reprinted* with permission from Perju-Dumbrava LD, et al, Move Disord.[9] © 2001 Movement Disorder Society.

Copyright © American Academy of Neurology. Unauthorized reproduction of this article is prohibited.

neurons. In 2019, the FDA approved another presynaptic radiotracer, 6-[^{18}F]-fluorodopa, that reflects aromatic amino acid decarboxylase responsible for converting levodopa to dopamine in the nerve terminal for clinical applications; this PET radiotracer has been used in research settings for more than 35 years.

Early in the course of PD, midbrain nigrostriatal degeneration causes reduction of presynaptic striatal markers, including DAT, that relates to the severity of parkinsonism. In individuals with PD, the posterior putamen has an earlier and more severe reduction of striatal markers, reflecting loss of cell bodies in the corresponding part of the substantia nigra.[6,7] This can be identified using either DAT-SPECT or PET, with greater reduction in the posterior putamen compared with the caudate nucleus contralateral to the more affected side in people with early PD (**FIGURE 8-1**[8,9]). At this early stage, striatal uptake correlates with motor symptom severity.[10,11] However, as PD progresses, the relationship becomes more complex, as discussed later in this section.

Molecular imaging of presynaptic markers may help distinguish people with dementia with Lewy bodies (DLB) from those with AD. One study of 33 patients with DLB and 22 with AD that included subsequent pathologic confirmation of diagnosis indicated that antemortem DAT-SPECT scans provided diagnostic accuracy of 86% compared with 79% with a clinical diagnosis of DLB.[12] The specificity of DAT-SPECT (92%) was indeed higher than that of clinical diagnosis (72%), but one might argue that the sensitivity and specificity of clinical diagnosis may vary depending on the clinical setting, such as in a dementia clinic versus a movement disorders clinic. Importantly, 10% of patients with pathologically confirmed DLB had normal DAT-SPECT scans in this study.

Previous studies indicated similar sensitivity of DAT-SPECT and PET using similar presynaptic tracers to detect reduced striatal uptake in patients with PD.[13] This included the detection of reduced striatal uptake contralateral to the clinically unaffected side in early-stage PD[14] as well as in preclinical asymptomatic carriers of mutations implicated in familial PD,[15] thus arguably demonstrating greater sensitivity than clinical examination.

Does this mean that DAT-SPECT scans should be routinely used for the diagnosis of PD? The unequivocal answer is no. Large clinicopathologic correlation analyses documented about 90% sensitivity of an accurate clinical diagnosis of PD, and the positive predictive value of a clinical diagnosis of PD was as high as 98.6% (particularly in advanced PD), compared with only about 71.4% for atypical parkinsonism.[16] A straightforward analysis was performed using the DAT-SPECT data from two large multicenter studies involving patients with PD, those with essential tremor, or healthy controls that ultimately led to the FDA approval of a radioligand for DAT. None of the participants in these studies had a pathologic validation of the diagnosis. The sensitivity, specificity, and positive and negative predictive values for DAT-SPECT diagnosis were calculated assuming that clinical diagnosis was the standard of truth, and a similar analysis was performed for clinical diagnosis assuming that DAT-SPECT diagnosis was the truth. The clinical diagnostic accuracy of PD was noted to be identical to the accuracy of diagnosis based on DAT-SPECT imaging in this analysis.[17] One could argue that DAT-SPECT may enable the diagnosis of PD when the clinical diagnosis is somewhat more challenging, especially early in the disease process. For example, a diagnostic dilemma may arise in certain situations such as in patients with essential tremor (who may present with subtle concurrent parkinsonism) versus early PD, or with the onset of PD in the setting of essential

KEY POINTS

- **A radiotracer specific for α-synuclein may best reflect pathophysiology of motor as well as nonmotor symptoms in Parkinson disease, but such a radiotracer is not yet available.**
- **The only radiotracer approved clinically for single-photon emission computed tomography (SPECT) imaging targets the presynaptic dopamine transporter and hence measures the integrity of terminal axons of the nigrostriatal dopaminergic neurons.**
- **Dopamine transporter (DAT)-SPECT scans demonstrate significantly reduced striatal uptake in the putamen more than the caudate nucleus in Parkinson disease compared with healthy controls; this is usually but not always asymmetric, and this asymmetry may become less pronounced as the disease progresses.**
- **DAT-SPECT may be more sensitive than clinical examination, as significant depletion of terminal axons and striatal dopamine is likely to occur before clinical symptoms of Parkinson disease manifest.**
- **The diagnostic accuracy of DAT-SPECT scans is not significantly different from the accuracy of a clinical diagnosis of Parkinson disease; individuals with normal DAT-SPECT scans may develop Parkinson disease in the future.**

Copyright © American Academy of Neurology. Unauthorized reproduction of this article is prohibited.

CASE 8-1

A 67-year-old woman presented with gradually progressive shaking almost exclusively with action that started in both hands in her forties and interfered with feeding and writing. She did not report any improvement after alcohol intake or any family history of shaking. She always had minor trouble with her balance but denied falls. The examination was notable for an asymmetric kinetic tremor that was worse on the right, no tremor at rest, subtle asymmetric bradykinesia in her hands but no rigidity, and a normal pull test. She was diagnosed with essential tremor. She did not tolerate a trial of primidone and was not a candidate for propranolol given her underlying asthma. She underwent left ventral intermediate thalamic nucleus deep brain stimulation (DBS) with excellent response. About 6 years later, she noticed a worsening of her shaking and gait imbalance. She was walking more slowly, with short steps. She also developed tingling in her feet. The examination was notable for right-hand rest tremor, asymmetric action and postural tremor that was worse on the right, bradykinesia that was not significantly worse than previously, no rigidity, a mildly wide-based gait, and mild retropulsion on the pull test. She also had a symmetric, gradient loss of pinprick and vibration sensation extending up to just above the ankles. Muscle stretch reflexes were reduced at the ankles; plantar responses were flexor bilaterally. MRI of the brain was unremarkable. A trial of carbidopa/levodopa was initiated. In the meantime, she was seen by another movement disorder specialist who ordered dopamine transporter (DAT) single-photon emission computed tomography (SPECT), which reportedly demonstrated reduced striatal DAT uptake. Her parkinsonism did not progress over time, but her gait imbalance significantly worsened. Although cerebellar-type multiple system atrophy remained in the differential diagnosis, the progression of her truncal ataxia in the setting of minimal parkinsonism prompted a search for alternative etiologies. She was ultimately diagnosed with fragile X tremor-ataxia syndrome (FXTAS) based on genetic diagnosis of premutation (72 CGG repeats) in the fragile X mental retardation 1 (*FMR1*) gene.

COMMENT

This patient had minimal objective parkinsonism except for asymmetric rest tremor and mild bradykinesia; levodopa failed to provide any subjective or objective improvement. Left ventral intermediate thalamic nucleus DBS continued to provide moderate reduction of her tremor. Given the atypical findings on her examination and minimal parkinsonism, it was clear that bilateral subthalamic nucleus DBS was not justifiable. An abnormal DAT-SPECT scan does not exclude atypical parkinsonism such as multiple system atrophy, which would not respond to DBS. This case highlights the limited clinical utility of DAT-SPECT given its lack of specificity and further stresses the importance of a meticulous, thorough clinical examination in patients with movement disorders rather than relying solely on imaging to guide management.

Copyright © American Academy of Neurology. Unauthorized reproduction of this article is prohibited.

tremor (patients with essential tremor are more likely to develop incident PD). However, the clinical response (eg, objective clinical improvement of tremor) to an adequate levodopa challenge (≥600 mg/d for 2 weeks) and, on occasion, temporal progression of symptoms usually provide the necessary diagnostic clue. Indeed, in a longitudinal clinical follow-up study of 44 patients with normal DAT-SPECT scans, 5 patients were diagnosed with PD and 3 patients with other degenerative parkinsonisms.[18] A normal striatal uptake early in the disease process may be more common in atypical parkinsonisms; thus caution is warranted against abandoning clinical judgment and overreliance on one imaging measure. Some atypical parkinsonisms such as MSA may respond well to levodopa, especially early in the disease course; thus, depriving such a patient of a trial of levodopa based on a falsely negative scan would be inappropriate. One must bear in mind that a small percentage (about 7.7%) of patients with autopsy-proven PD did not respond to levodopa,[3] but whether a DAT-SPECT scan could change management in such a situation is not entirely clear, especially given that the specificity of presynaptic striatal uptake measures is rather low.

An imaging modality would add value if it could reliably enhance diagnostic accuracy for other neurodegenerative causes of parkinsonism, as this could alter future management. Reduced striatal uptake of DAT, however, is seen not only in all atypical parkinsonisms including MSA, CBD, and PSP but also in other degenerative parkinsonisms, including genetically proven spinocerebellar ataxia type 2 mutations.[19] DAT-SPECT or, for that matter, PET scans with any presynaptic or postsynaptic radiotracers do not reliably enhance the accuracy of differential diagnosis at this time. Although DAT uptake is expected to be normal, abnormal uptake has been reported quite unexpectedly in a substantial number of patients clinically diagnosed with vascular parkinsonism (67.5% with abnormal DAT-SPECT according to some reports) as well as neuroleptic-induced parkinsonism (42% with abnormal scans),[20,21] possibly suggesting underlying neurodegenerative parkinsonism. Although normal striatal uptake on DAT-SPECT may help in the differential diagnosis, the above-mentioned findings limit the clinical utility of DAT-SPECT scans until further research and pathologic validation clarify the conundrum. It should also be remembered that underlying structural abnormalities (eg, strokes), technical issues with acquisition (eg, head positioning in the scanner or head motion during the scan), or interpretation (both visual and semiquantitative) may lead to false-positive DAT-SPECT scans. Medication confounders (especially exposure to stimulants such as cocaine or amphetamines, given that the DAT radiotracers can be cocaine analogs) need to be considered as well. Thus, "treating the scan" instead of using sound clinical reasoning and judgment to treat the patient may be fraught with danger. CASE 8-1 elucidates the diagnostic limitations of DAT-SPECT scans given their lack of specificity.

Hypothetically, one could envisage a paradigm shift in the future in which presynaptic molecular imaging may be recommended as a routine diagnostic tool for people at high risk of PD. For example, reduced striatal uptake of a presynaptic molecular imaging radiotracer indicates a greater risk of phenoconversion to PD in high-risk groups such as those with hyposmia or RBD.[22,23] In these cases, molecular imaging may be more sensitive than clinical examination to identify nigrostriatal injury. Although this could be crucial in identifying at-risk individuals, it becomes clinically relevant only once

KEY POINTS

- **DAT-SPECT scans have low specificity, and abnormal dopamine transporter uptake may be seen in atypical parkinsonism and other neurodegenerative disorders; thus, DAT-SPECT does not aid in the differential diagnosis of parkinsonism, limiting its clinical utility.**
- **False-positive abnormal DAT-SPECT scans may result from underlying strokes, technical issues such as head positioning in the scanner, or exposure to stimulants such as cocaine, amphetamine, or methylphenidate.**
- **Although identification of individuals with prodromal Parkinson disease is valuable from a research perspective, it will be clinically relevant once disease-modifying treatments for Parkinson disease become available.**

Copyright © American Academy of Neurology. Unauthorized reproduction of this article is prohibited.

disease-modifying treatments that could forestall disease onset or slow the progression of parkinsonisms become available.

This potentially greater sensitivity of imaging may help in clinical research by acting as an endophenotype by which to assign subclinical cases to a premanifest group, thereby enhancing genetics research. Similarly, it could facilitate testing of disease-modifying agents in groups that have a high risk of developing PD. However, this approach also restricts the generalizability of the research outcomes to people at such high risk who have demonstrated striatal defects on molecular imaging.

What is perhaps even more critical in such clinical trials involving disease-modifying agents is a reliable, objective, noninvasive in vivo marker of disease severity and progression. Thus, the next question is whether presynaptic SPECT or PET measures reflect pathology and disease progression. The answer is yes, but with critical limitations. Meticulous PET studies in primates with pathologic correlates have clearly shown that striatal uptake of presynaptic radiotracers correlates with striatal dopamine, but the correlation with nigral dopaminergic neurons and motor parkinsonism is lost once the nigral cell loss exceeds a threshold of about 50%. The striatal dopamine drops to near-zero levels around this point.[7] Similar pathologic findings were later confirmed in humans, with virtually complete loss of putaminal dopaminergic neurons within about 4 years after diagnosis.[24]

Albeit with some technical confounders, separate analyses by another group demonstrated that striatal DAT uptake failed to correlate with postmortem measures of either nigral dopaminergic neurons or striatal dopaminergic terminal axons.[25,26] Indeed, similar results have also been reported in multiple PET and SPECT studies with presynaptic radiotracers including DAT,[27] in which the striatal uptake shows a similar flooring effect within around 5 years and correlates with motor symptom severity only early in the clinical course. The change in the longitudinal DAT-SPECT measures failed to correlate with the interim clinical progression as measured by total score on the Movement Disorder Society-Sponsored Revision of the Unified Parkinson's Disease Rating Scale (MDS-UPDRS) in a large cohort of patients with PD, even early in the disease course.[28] Hence, DAT-SPECT imaging measures of striatal uptake may reflect pathology and clinical progression only early in the disease process but not after the nigral cell loss crosses a certain threshold. This is particularly problematic in employing DAT-SPECT as a surrogate measure of disease progression in longitudinal clinical trials to determine the efficacy of neuroprotective agents. Interestingly, PET measures of DAT uptake in primates, when restricted to the midbrain, correlated well with nigral cell loss and motor symptoms throughout the full range of parkinsonism and hence could be a target of an imaging biomarker[29]; further research is warranted.

TRENDS. Given the largely clinical focus of this review, the vast majority of the discussion above regarding nuclear imaging has been restricted to the dopaminergic system and therefore the imaging correlates of motor manifestations in PD. But PD is marked by tremendous clinical heterogeneity, with a vast array of accompanying nonmotor manifestations. Dementia and certain motor symptoms such as gait imbalance and freezing are relatively refractory to levodopa, suggesting the possible involvement of alternative neurotransmitter systems or brain regions beyond the nigrostriatal pathways

Copyright © American Academy of Neurology. Unauthorized reproduction of this article is prohibited.

discussed above. A radioligand specific for oligomeric α-synuclein that could reliably quantify the burden of cortical synucleinopathy would likely better reflect pathophysiology and disease progression even with regard to cognitive dysfunction, but such a tracer remains elusive. Although a comprehensive review is beyond the scope of this article, it briefly discusses a few research trends in the imaging of alternative neurotransmitter systems and proteinopathies that may ultimately provide crucial insights into the pathophysiology of PD. The primary focus here is on the in vivo PET measures of cholinergic pathways and Aβ accumulation.

PROTEINOPATHY-SPECIFIC IMAGING. PET studies using radiotracer N-methyl-[^{11}C]2-(4'-methylaminophenyl)-6-hydroxybenzothiazole, commonly known as Pittsburgh Compound B (PiB), have enabled in vivo quantification of fibrillary Aβ burden. In an initial study limited by a small number of participants in each group, PiB binding potential for predefined cortical regions and mean cortical binding potential were noted to be elevated in an equal proportion of the participants in groups stratified by their cognitive status: healthy controls, PD with normal cognition, PD with mild cognitive impairment, and PD with dementia (PDD) and DLB; the elevated regional PiB binding potential correlated with worse global cognition but did not predict an earlier clinical onset or a more rapid decline in cognition in the participants with Lewy body pathology in this analysis.[30] Whether the elevated PiB uptake reported in multiple initial PET studies reflected the coexistence of classic AD pathology in PD was far from clear; pathologic validation of the PET findings in three individuals with PDD who had PiB PET within 15 months of death clarified this. All three participants had cortical Lewy body pathology; the two PDD participants with abnormally elevated PiB uptake had diffuse Aβ plaques but minimal neuritic plaques and neurofibrillary tangles and hence did not meet the diagnostic criteria of AD[31] (FIGURE 8-2). Thus, this study showed that an abnormal PiB PET was specific for fibrillar Aβ but did not necessarily imply comorbid AD in PDD. Subsequent principal component analysis of PiB PET scans from patients with AD and PD with cognitive impairment demonstrated contrasting patterns of PiB binding, thereby further suggesting different pathophysiologic roles of Aβ in cognitive dysfunction in PD compared with AD.[32] In fact, in a recent study of patients with DLB (with at least core clinical features of the disease), a majority had low Aβ deposition in the setting of diminished striatal DAT uptake.[33] In another study, substantial Aβ accumulation in the setting of cortical synucleinopathy predicted significantly shorter survival than PDD with cortical synucleinopathy only.[34]

Tau deposition has been detected with [^{18}F]-AV-1451. A distinct pattern of AV binding was noted in DLB in the presence of Aβ accumulation; this was marked by greater [^{18}F]-AV-1451 binding in the sensorimotor and visual cortices with lesser tau burden in the lateral and medial temporal cortices as compared with AD.[35] [^{18}F]-AV-1451 uptake may be especially useful in tauopathies such as CBD and PSP. In fact, [^{18}F]-AV-1451 uptake has been shown to be elevated in PSP in multiple cortical and subcortical areas including the precentral cortex, pallidum, dentate nucleus, and midbrain, with increased uptake in longitudinal assays; the clinical progression over time correlated with the rate of midbrain atrophy but not with the

KEY POINTS

- **Striatal dopamine transporter uptake has a flooring effect and may reflect nigral cell loss and clinical severity of Parkinson disease only early in the disease process.**
- **Positron emission tomography (PET) measures of dopamine transporter uptake in the midbrain, unlike the striatum, may reflect nigral cell loss and motor manifestations throughout the full range of parkinsonism.**
- **Pathologic validation of in vivo PET studies is critical for a complete understanding of proteinopathies; increased Pittsburgh Compound B positron emission tomography uptake reflects the accumulation of fibrillary amyloid-β but not necessarily Alzheimer disease pathology in Parkinson disease.**
- **[^{18}F]-AV-1451, a PET tracer of tau, demonstrates increased uptake in progressive supranuclear palsy, a tauopathy, but the increase in uptake over time noted on longitudinal PET scans does not correlate with interim clinical progression of progressive supranuclear palsy.**

Copyright © American Academy of Neurology. Unauthorized reproduction of this article is prohibited.

KEY POINTS

- Radiotracer (-)-5-[^{18}F]-fluoroethoxybenzovesamicol enables quantification of presynaptic cholinergic nerve terminals with good regional specificity; patients with Parkinson disease with a history of falls had greater cholinergic deficits in subcortical structures such as the thalamus and caudate nucleus compared with patients without falls.
- Structural MRI does not show a pattern of atrophy in Parkinson disease that is diagnostic at the individual patient level; MRI in Parkinson disease is indicated if alternative etiologies are suspected.

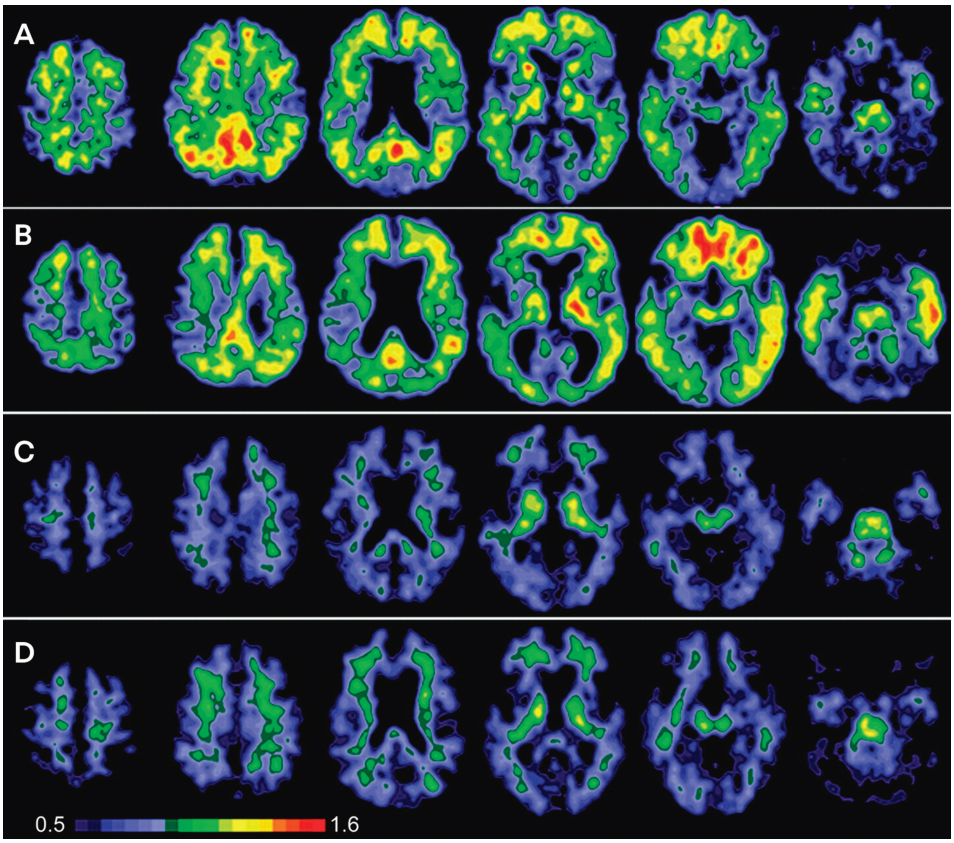

FIGURE 8-2
[^{11}C]–Pittsburgh Compound B (PiB) positron emission tomography (PET) images from three patients with idiopathic Parkinson disease with dementia (PDD) (*A, B, C*) and one healthy control (*D*). The scans of patient 1 (*A*) and patient 2 (*B*) show increased signal in multiple cortical areas, signifying diffuse amyloid burden. The scans of patient 3 (*C*) and patient 4 (*D*) show minimal PiB signal in cortical areas. The PiB retention in white matter is likely secondary to nonspecific PiB binding.
Reprinted with permission from Burack MA, et al, Neurology.[31] © 2010 American Academy of Neurology.

[^{18}F]-AV-1451 uptake.[36] Pathologic validation of the in vivo PET measures, therefore, remains an important prerequisite before drawing definitive pathophysiologic conclusions based on experience with PiB PET.[37]

PET MEASURES OF THE CHOLINERGIC SYSTEM. A substantial advance in cholinergic PET measures has been heralded by radiotracers targeting vesicular acetylcholine transporter (VAChT), enabling qualitative and quantitative analyses of presynaptic cholinergic nerve terminals. The superior regional specificity of (-)-5-[^{18}F]-fluoroethoxybenzovesamicol (FEOBV), a vesamicol analog that selectively binds VAChT, allows critical assessment of subcortical cholinergic deficits as well. In a recent PET study with FEOBV, patients with PD with a history of falls had significantly reduced VAChT expression in the right thalamus, particularly the right lateral geniculate nucleus, right caudate nucleus, and bilateral prefrontal cortices as compared with patients without falls, while patients with PD with freezing had greater cholinergic deficits in the bilateral striatum and limbic archicortex compared with those without freezing.[38] In another study using the same tracer, even though diffuse cholinergic

Copyright © American Academy of Neurology. Unauthorized reproduction of this article is prohibited.

denervation was seen in all patients with PD, the patients with PD who were cognitively healthy had bilaterally increased FEOBV uptake in the hippocampus as compared with patients with PD with mild cognitive impairment, suggesting a possible compensatory upregulation.[39]

Given the advent of these additional radiotracers, much excitement clearly awaits the field in the not-so-distant future. However, a reliable radiotracer specific for oligomeric α-synuclein remains the ultimate diagnostic goal.

MRI in Parkinsonism

Given the clinical focus of this review, this section will primarily consider structural MRI; in addition, a few of the advanced MRI modalities that hold promise but currently remain confined to the research domain will be reviewed briefly.

In general, as highlighted previously, PD remains a clinical diagnosis. Multiple MRI morphometric analyses have delineated PD versus control group differences in cortical thickness involving a variety of cortical regions or volumes of subcortical structures, but these findings are not consistent across studies. Conventional MRI does not consistently show a pattern of atrophy or structural changes that aids in PD diagnosis at an individual level. In fact, brain MRI is not recommended as a part of the routine diagnostic evaluation for a person with a classic clinical presentation consistent with idiopathic PD. However, the authors maintain a low threshold to obtain brain or spine MRI to investigate abnormal clinical findings other than the typical parkinsonian signs that would raise concerns about coexisting pathologies or other causes of parkinsonism, especially if they are potentially treatable (TABLE 8-1). Multiple studies have suggested that medial temporal atrophy could help discriminate AD from DLB, but a recent large-scale analysis revealed that this "hippocampal sparing pattern" on MRI (ie, relatively preserved medial temporal lobes in the presence of atrophy in the posterior cortex, frontal cortex, or both) only marginally enriched the sensitivity of a clinical diagnosis.[40] Conventional MRI may be more useful clinically in the setting of atypical parkinsonism.

MRI FEATURES IN MULTIPLE SYSTEM ATROPHY. MRI features in MSA include atrophy involving the putamen, pons, cerebellum, and middle cerebellar peduncle. Iron deposition in the putamen results in a characteristic hypointensity on

Clinical Indications for Structural Imaging in Parkinsonism TABLE 8-1

Additional clinical features in the setting of parkinsonism that warrant structural MRI, especially if more than one is present

- Acute or subacute onset or rapid progression
- Focal weakness or numbness
- Upper motor neuron signs including spasticity and hyperreflexia, especially if unilateral
- Bulbar or pseudobulbar symptoms, especially early-onset
- Rapidly progressive dementia
- Combination of parkinsonism and other movement disorders including chorea, dystonia, myoclonus, and ataxia, especially if unilateral

Copyright © American Academy of Neurology. Unauthorized reproduction of this article is prohibited.

T2*-weighted images and susceptibility-weighted imaging (SWI), often accompanied laterally by a streak of hyperintensity on T2-weighted images[41]; however, these findings have low sensitivity, especially early in the disease process. In fact, the hyperintense putaminal rim is not specific and can be observed in PD or healthy individuals, especially when images are obtained on MRI scanners with higher magnetic field strengths. Similar hyperintensity has also been described in the other atrophied areas in MSA: T2 hyperintensity in the middle cerebellar peduncle and cruciform T2 hyperintensity in the pons, traditionally referred to as the "hot cross bun" sign, were noted in pathologically proven MSA, but both had low sensitivity[42] (FIGURE 8-3). The middle cerebellar peduncle sign has also been described in fragile X tremor-ataxia syndrome (FXTAS). The hot cross bun sign is another nonspecific finding and has been reported not only in other parkinsonisms but also in patients with spinocerebellar ataxia. In fact, up to 25.7% of people with genetically proven spinocerebellar ataxia type 2 have this finding[43] in addition to cerebellar atrophy. Hence, conventional MRI findings are modestly supportive diagnostically in the appropriate clinical context.

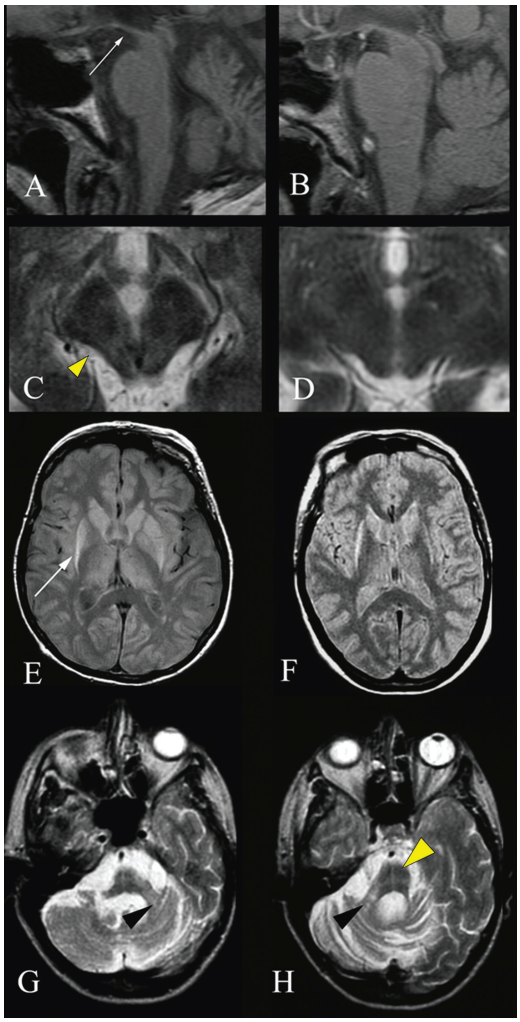

FIGURE 8-3

Structural MRI findings in pathologically confirmed progressive supranuclear palsy (PSP) and multiple system atrophy (MSA). Sagittal T1-weighted image shows the characteristic hummingbird sign (*A, white arrow*) in PSP, in contrast to normal midbrain in Parkinson disease (*B*). Axial T2-weighted image shows characteristic morning glory sign in PSP (*C, yellow arrowhead* showing the concave profile of the midbrain tegmentum), in contrast to normal midbrain in Parkinson disease (*D*). Axial proton density–weighted images (*E, F*) show putaminal atrophy with hyperintense putaminal rim (*E, white arrow*) in MSA. Axial T2-weighted images show middle cerebellar peduncle sign (*G, H, black arrowheads*) and hot cross bun sign in pons (*H, yellow arrowhead*) in MSA.

Reprinted with permission from Massey LA, et al, Move Disord.[42] © 2012 Movement Disorder Society.

MRI FEATURES IN PROGRESSIVE SUPRANUCLEAR PALSY. The infratentorial atrophy in PSP is predominantly noted in the tegmentum of the midbrain and superior cerebellar peduncle; midbrain diameter was noted to differentiate individuals with PD from those with PSP and controls, although overlap with MSA was noted.[44] The midbrain atrophy in pathologically

Copyright © American Academy of Neurology. Unauthorized reproduction of this article is prohibited.

confirmed PSP may manifest on conventional MRI as a "hummingbird" or "giant penguin" sign on a midsagittal slice and as a "morning glory" sign (ie, a concavity of the lateral margin of midbrain tegmentum due to atrophy) in axial slices at the level of the mammillary body (FIGURE 8-3), but these findings have low sensitivity, especially early in the course of the disease.[42] In one case series the morning glory sign was suggested to be associated with vertical supranuclear gaze palsy (the morning glory sign was present in only one of the patients with MSA in this report, who incidentally also had abnormal vertical gaze); however, pathologic validation was not present for any of the clinical diagnoses in that report.[45] Quantitative estimates of the ratio of anteroposterior axes of midbrain to pons in midsagittal plane MRI in pathologically proven cases yielded a significant improvement of sensitivity and specificity; in PSP this ratio was less than 52%, whereas in MSA the ratio was greater than 67%.[46] Inclusion of the ratio of the widths of middle and superior cerebellar peduncles along with the ratio of midsagittal areas of midbrain and pons to generate the Magnetic Resonance Parkinsonism Index and additional consideration of widths of the ventricles may further enhance the sensitivity and specificity of MRI diagnosis of PSP,[47,48] but lack of pathologic validation precludes a definitive conclusion regarding its value in radiologic diagnosis at this time.

Interestingly, the longitudinal rate of progression of regional atrophy based on sequential MRI in clinically diagnosed atypical parkinsonisms revealed the occurrence of pontine atrophy about 20 times faster in MSA compared with controls, while the rate of atrophy of the midbrain in PSP was seven times greater than in healthy controls, suggesting their potential for differential diagnosis of atypical parkinsonism and as a biomarker of clinical progression.[49] Pathologic validation of diagnosis is warranted, however, to confirm these findings.

MRI FEATURES IN CORTICOBASAL DEGENERATION. Several studies have highlighted the asymmetric, predominantly frontoparietal cortical atrophy in CBD, but subsequent clinicopathologic correlation revealed that this MRI finding was neither sensitive (present in only 3 of 14 autopsy-proven cases) nor specific for CBD.[50]

Quantitative volumetric analysis using software-generated automated subcortical segmentation has shown promise in the differential diagnosis of atypical parkinsonsims[51]; further confirmation in larger data sets and pathologic validation of the findings are needed before inferences can be drawn regarding their accuracy at an individual level, especially early in the disease process. Therefore, at present, structural MRI findings in atypical parkinsonisms overall are at best suggestive in the right clinical context.

OTHER CAUSES OF PARKINSONISM. Another important role of MRI in parkinsonism is to exclude alternative etiologies, especially if the clinical findings suggest such a possibility. Although a few such scenarios are delineated here, all the conditions listed in the subsequent section Imaging in Other Movement Disorders can also present with varying degrees of parkinsonism.

VASCULAR PARKINSONISM. Considerable confusion still exists regarding the diagnosis of vascular parkinsonism. Structural lesions such as strokes affecting the substantia nigra or nigrostriatal pathway in the appropriate clinical context are suggestive, but the roles of basal ganglia strokes and small-vessel

KEY POINTS

- **MRI in multiple system atrophy may demonstrate atrophy in the putamen, pons, cerebellum, and middle cerebellar peduncle, but these findings have low sensitivity, especially early in the disease process, and are not specific.**
- **MRI in progressive supranuclear palsy may demonstrate atrophy in the midbrain tegmentum and superior cerebellar peduncle, but these findings have low sensitivity and are not specific; the longitudinal rates of atrophy of the midbrain and pons may aid in the differential diagnosis.**
- **MRI evidence of strokes affecting the substantia nigra or nigrostriatal pathway may suggest a diagnosis of vascular parkinsonism, but the roles of white matter disease and basal ganglia stroke in its etiopathogenesis are less clear.**

Copyright © American Academy of Neurology. Unauthorized reproduction of this article is prohibited.

ischemic white matter disease in the etiopathogenesis of vascular parkinsonism have been questioned.[52] Thus, the MRI findings of lacunar infarcts or small-vessel ischemic white matter changes may not clarify the underlying diagnosis.

NORMAL PRESSURE HYDROCEPHALUS. Although MRI findings are not diagnostic, they can be helpful in the right clinical context. The typical findings in normal pressure hydrocephalus include (1) ventricular enlargement out of proportion to cortical atrophy as measured by an Evans index (ratio of maximal diameter of frontal horns of the lateral ventricles to maximal width of the inner table of the cranium at the same level) of >0.3, (2) periventricular white matter hyperintensities (usually bilateral), (3) a callosal angle measured in the coronal plane at the level of the posterior commissure of between 40 degrees and 90 degrees (a value greater than 90 degrees is suggestive of cortical atrophy), and (4) cerebral aqueductal or fourth ventricular flow void (increased CSF flow results in the loss of typical T2 hyperintensity)[53] (FIGURE 8-4[54,55]).

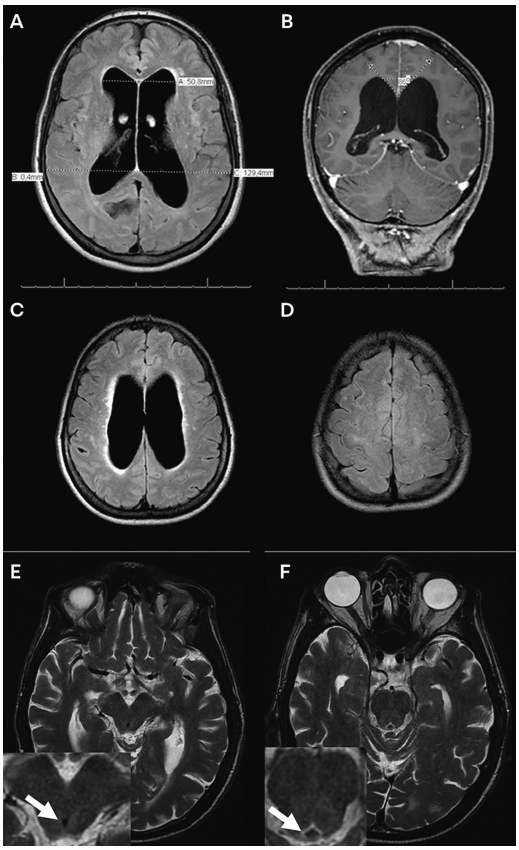

FIGURE 8-4

MRI findings in normal pressure hydrocephalus. *A*, Axial fluid-attenuated inversion recovery (FLAIR) image shows ventriculomegaly with elevated Evans index (ratio of maximal width of frontal horns of the lateral ventricles to maximal diameter of the inner table of the skull at the same level [*dotted lines*]) greater than 0.3. *B*, Coronal T1-weighted image shows reduced callosal angle (*dotted lines*). *C*, Axial FLAIR image shows ventriculomegaly with bilateral periventricular white matter hyperintensities. *D*, Axial FLAIR image shows crowding of the sulci and subarachnoid spaces over the high-convexity and midline surfaces in the frontoparietal regions. Axial T2-weighted images at the level of cerebral aqueduct (*E*) and fourth ventricle (*F*) show flow void (*white arrows in magnified inset*) due to hyperdynamic CSF flow.

Panels *A* through *D* reprinted from Oliveira LM, et al, Dement Neuropsychol.[54]

Panels *E* and *F* modified with permission from Bradley WG, Jr, Semin Ultrasound CT MR.[55] © 2016 Elsevier Inc.

TOXIN-INDUCED PARKINSONISM. Exposure to manganese has been associated with dopaminergic dysfunction, aggregation, and exosomal transmission of misfolded α-synuclein[56] as well as clinical parkinsonism, and thus its study could shed light on the pathophysiology of parkinsonism. Manganese exposure has been associated with increased hyperintensity on T1-weighted images, particularly in the globus pallidus, and the measure of intensity in the globus pallidus

Copyright © American Academy of Neurology. Unauthorized reproduction of this article is prohibited.

(pallidal index) correlates not only with cumulative manganese exposure but also with clinical parkinsonism[57] (FIGURE 8-5[58]).

TRENDS. The PD motor manifestations as discussed earlier appear only after the loss of about 30% to 35% of nigrostriatal neurons. As parkinsonism progresses, midbrain nigral dopaminergic neuronal reduction correlates with the full range of disease severity, whereas striatal measures of these dopaminergic neurons do so only through relatively mild parkinsonism. Thus, molecular imaging measures that reflect nigral dopaminergic neurons not only may detect preclinical PD but also may be good biomarkers of disease severity and longitudinal progression. Hence, direct MRI visualization and quantification of nigral neurons could make a substantial impact on PD research and ultimately have important clinical implications.

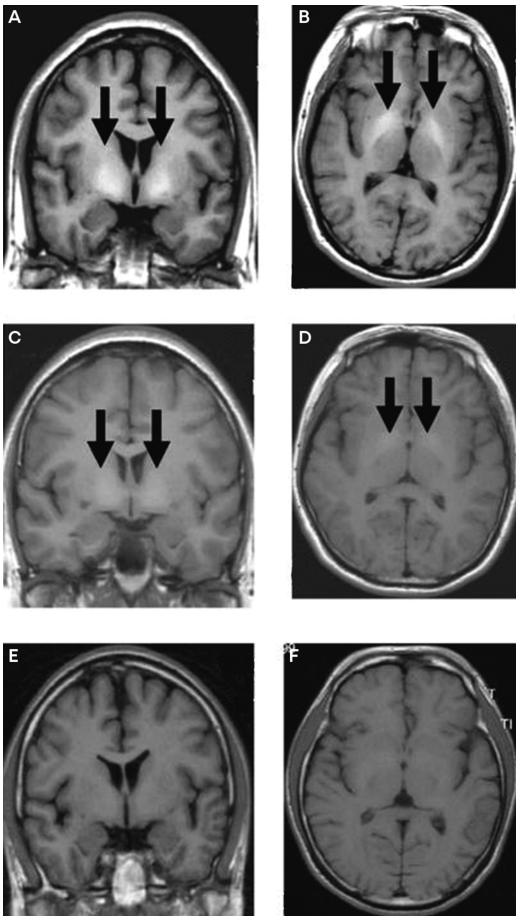

FIGURE 8-5
MRI findings in manganese-exposed workers and control workers. Coronal (*A*) and axial (*B*) T1-weighted images show significantly increased hyperintensity in the globus pallidus (*A, B, arrows*) in a smelting worker exposed to high levels of airborne manganese. Coronal (*C*) and axial (*D*) T-1 weighted images show mildly increased hyperintensity in the globus pallidus (*C, D, arrows*) in a smelting worker exposed to low levels of airborne manganese. Coronal (*E*) and axial (*F*) T-1 weighted images show normal findings in a worker not exposed to manganese.
Reprinted with permission from Jiang Y, et al, Neurotoxicology.[58] © 2006 Elsevier Inc.

IRON-SENSITIVE MRI. Nigrostriatal dopaminergic cells in the substantia nigra pars compacta (SNpc) are clustered into five distinct groups, the largest of which is called nigrasome-1. Pathologic studies have shown the greatest (up to 98%) loss of dopaminergic neurons in nigrasome-1 in PD.[6,59] Nigrasome-1 can be visualized as a hyperintense ovoid signal on iron-sensitive T2*-weighted or SWI MRI sequences at 3T or 7T in healthy controls, whereas the rest of the SNpc appears hypointense; this was further validated via histopathologic analysis.[60] This hyperintensity in the dorsolateral SNpc gives the appearance of a "swallow tail" in healthy controls that is lost in PD, possibly as a result of varying combinations of cell loss, iron deposition, neuromelanin loss, or even a change in the oxidation state of the iron[60,61] (FIGURE 8-6). Subsequent meta-analysis showed that absence of this dorsolateral nigral hyperintensity had a pooled sensitivity and specificity for PD diagnosis versus

KEY POINT

- **Nigrasome-1, the largest group of dopaminergic neurons in the substantia nigra, appears as a hyperintense signal ("swallow tail") in the dorsolateral substantia nigra on iron-sensitive T2*-weighted and susceptibility-weighted imaging (SWI) sequences on high-field MRI.**

Copyright © American Academy of Neurology. Unauthorized reproduction of this article is prohibited.

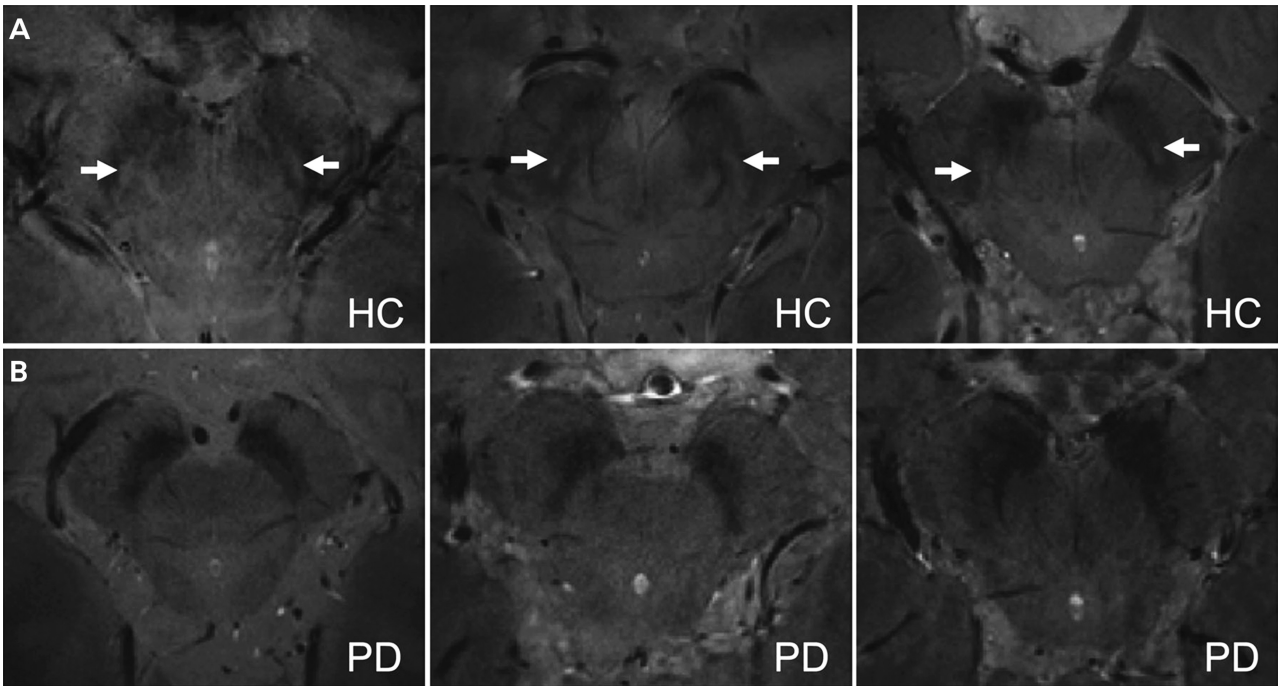

FIGURE 8-6

Iron-sensitive T2*-weighted 7T MRI showing nigrasome-1 in healthy controls (HC) and in patients with Parkinson disease (PD). Dorsolateral nigral hyperintensity (*A*, *arrows*) in the hypointense midbrain substantia nigra gives the appearance of a "swallow tail" and represents nigrasome-1. Dorsolateral nigral hyperintensity is visible in all healthy controls (*A*) but absent in all patients with PD (*B*).

Reprinted with permission from Blazejewska AI, et al, Neurology.[60] © 2013 American Academy of Neurology.

controls of about 94% (on 3T MRI scanners only; the sensitivity was slightly higher if 7T scanners were also included)[62]; quantitative estimation of the dorsolateral nigral hyperintensity may be modestly more sensitive. The dorsolateral nigral hyperintensity was absent in 89% of patients clinically diagnosed with atypical parkinsonism in this meta-analysis; thus, this modality may not be particularly effective in the differential diagnosis of atypical parkinsonism.

In a separate study, the loss of dorsolateral nigral hyperintensity was accompanied by reduced ipsilateral striatal uptake on DAT-SPECT in 104 of the 126 patients with clinically diagnosed PD; no pathologic validation was available to accurately gauge the false positives or false negatives.[63] Loss of dorsolateral nigral hyperintensity on SWI sequences at 3T was observed in patients with idiopathic RBD, consistent with this group's higher risk of developing PD. Interestingly, 5 of the 11 patients with RBD with loss of dorsolateral nigral hyperintensity signal phenoconverted to either parkinsonism or dementia within 18 months.[64] Although these findings are promising, cautious interpretation is warranted given the apparent lack of specificity of the absence of dorsolateral nigral hyperintensity. Not only has loss of dorsolateral nigral hyperintensity been noted in atypical parkinsonisms, but asymmetry and loss of dorsolateral nigral hyperintensity have also been reported in healthy controls[65]; motion artifacts, neighboring microvasculature,[66] and other confounders may contribute to the false-positive reports.

Copyright © American Academy of Neurology. Unauthorized reproduction of this article is prohibited.

NEUROMELANIN-SENSITIVE MRI. Another significant advance has been the advent of neuromelanin-sensitive MRI, which detects signals from paramagnetic neuromelanin-iron complexes. This allows direct quantification of melanin-containing neurons not only in the substantia nigra but also in other extrastriatal sites such as the locus ceruleus, a site of early α-synuclein pathology in PD. Nigral volume loss was described in PD and idiopathic RBD compared with controls using this technique, highlighting its potential as a prodromal marker.[67] In fact, a recent follow-up study documented a longitudinal decline in nigral volume on neuromelanin-sensitive MRI sequences, and the measures correlated with PD duration and severity.[68] This modality holds significant promise, but further large-scale studies and pathologic validation are needed.

RESTING-STATE FUNCTIONAL CONNECTIVITY MRI. Resting-state functional connectivity MRI is a noninvasive MRI technique that measures signal fluctuations due to blood oxygen level–dependent (BOLD) signal changes resulting from spontaneous activity of the brain at rest. These low-frequency fluctuations are strongly and specifically correlated between functionally related brain regions, allowing the investigation of brain organization at a regional as well as a network level. This is particularly relevant for PD in which synucleinopathy is not restricted to the nigrostriatal dopaminergic neurons but also affects multiple anatomic regions and neurotransmitter systems. Striatal resting-state functional connectivity with the brainstem and cerebellum is reduced in PD compared with controls in a graded pattern (posterior putamen greater than anterior putamen greater than caudate nucleus) that reflects the extent of pathologic involvement.[69] A large-scale study investigating functional connectivity group differences in PD across the entire connectome and network level demonstrated the greatest functional connectivity differences across somatomotor, thalamic, and cerebellar networks, with significantly lesser striatal effects.[70] In a study focusing on the cerebellum, the vermis had weaker functional connectivity with the sensorimotor and association cortices in PD compared with healthy controls, and this perturbed functional connectivity correlated with deficits in gait and cognition in patients with PD[71,72] (FIGURE 8-7). Speculatively, altered functional connectivity may be secondary to a local neurotransmitter dysfunction independent from synuclein pathology that is typically not present in the cerebellum. Another study showed that baseline CSF measures of α-synuclein could predict longitudinal decline of sensorimotor networks, whereas the decline in the dorsal attention–frontoparietal internetwork strength correlated with a decline in cognition over time.[73] Importantly, stringent quality assurance measures, especially to eliminate head motion confounders, constitute a critical prerequisite for functional connectivity MRI analyses to avoid spurious conclusions. The functional connectivity MRI studies typically analyze PD versus control group differences and their behavioral correlates and shed light on the pathophysiology of PD, especially when used judiciously and in conjunction with other in vivo measures of pathophysiology such as PET imaging. Considerable research remains to be done for this modality to be effective at the individual patient level; recent findings suggest that this may be feasible.[74]

KEY POINTS

- **Dorsal nigral hyperintensity on iron-sensitive T2*-weighted and SWI is lost in Parkinson disease; this finding may be sensitive but not specific. It may help diagnose prodromal Parkinson disease but does not help in the differential diagnosis of atypical parkinsonisms.**
- **Nigral volume assessed using neuromelanin-sensitive MRI correlates with Parkinson disease duration and severity; decline in nigral volume has been shown on longitudinal scans.**

Copyright © American Academy of Neurology. Unauthorized reproduction of this article is prohibited.

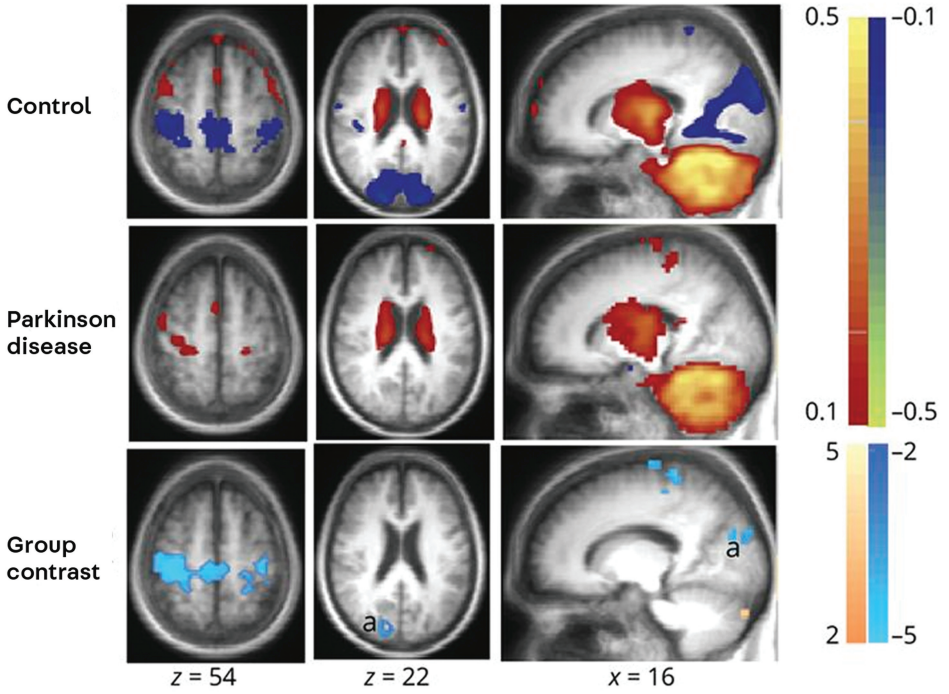

FIGURE 8-7

Vermal resting-state functional connectivity differences between patients with Parkinson disease (PD) and controls. Images show functional connectivity [*z*(*r*)] maps with the vermis seed region averaged over control participants (*top row*) and PD group (*middle row*). Warm (*red/yellow*) and cool (*green/blue*) colors represent positive and negative correlations respectively. Random-effects analysis contrasting the controls and PD group (*bottom row*) shows significant cortical clusters in the sensorimotor cortex and visual association cortex. The vermal functional connectivity with the sensorimotor and association cortices were weaker in the PD group compared with controls.

Modified with permission from Maiti B, et al, Neurology.[71] © 2019 American Academy of Neurology.

IMAGING IN OTHER MOVEMENT DISORDERS

This section primarily reviews the MRI findings of a few clinical conditions that may present with varying combinations of chorea, dystonia, and parkinsonism.

Wilson Disease

Although typical clinical features (eg, Kayser-Fleischer rings, sunflower cataracts), laboratory test results (eg, serum copper, ceruloplasmin, 24-hour urine copper), and genetic testing are used in making a clinical diagnosis of Wilson disease, brain MRI, especially in the presence of neuropsychiatric manifestations, may show characteristic T2-weighted and fluid-attenuated inversion recovery (FLAIR) signal changes in the brainstem, basal ganglia, thalami (concurrent involvement of all three has been suggested to be virtually diagnostic), and white matter. Characteristic MRI findings of the "face of giant panda" in the midbrain, sometimes accompanied by the "face of miniature panda" in the dorsal pons, have been described[75,76] (FIGURE 8-8).

Huntington Disease

In Huntington disease, a constellation of clinical features and family history followed by identification of pathogenic trinucleotide (CAG) repeats in the Huntingtin gene is the usual diagnostic course. MRI may be obtained initially to

Copyright © American Academy of Neurology. Unauthorized reproduction of this article is prohibited.

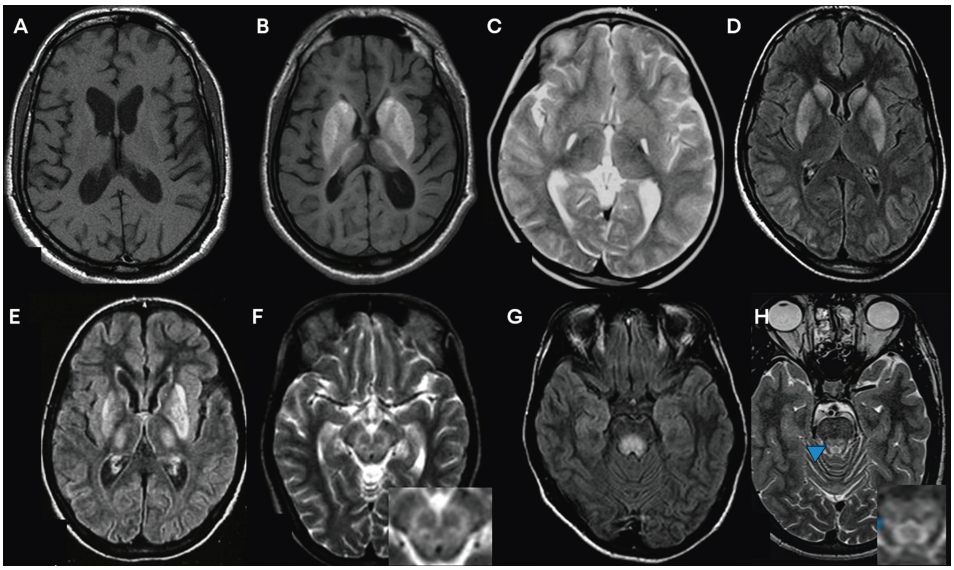

FIGURE 8-8

Characteristic MRI findings in some conditions presenting with varying combinations of dystonia, chorea, and parkinsonism. *A*, Axial T1-weighted image shows atrophy of the caudate nucleus and mild diffuse cortical atrophy in a patient with suspected Huntington disease. *B*, Axial T1-weighted image shows hyperintensity in bilateral caudate nucleus, putamen, globus pallidus, and thalamus in a patient with hepatolenticular degeneration not secondary to Wilson disease. *C*, Axial T2-weighted image shows hyperintensities in the posterior putamen in a patient with a suspected mitochondrial disorder. *D*, Axial fluid-attenuated inversion recovery (FLAIR) image shows hyperintensity in bilateral putamen, caudate nucleus, and globus pallidus in suspected methanol poisoning; note considerable overlap with MRI findings in the setting of non–Wilson disease hepatolenticular degeneration. *E-H*, MRI characteristics in Wilson disease: *E*, Axial FLAIR image shows hyperintensity in bilateral putamen, caudate nucleus, and globus pallidus. *F*, Axial T2-weighted image at the level of the midbrain shows the "face of giant panda" sign (*magnified inset*). *G*, Axial FLAIR image at the level of the midbrain shows hyperintensity in the tectum. *H*, Axial T2-weighted image at the level of the pons shows the "face of miniature panda" sign (*arrowhead* and *magnified inset*) in the dorsal pons.

Panels *A* through *G* modified with permission from Prashanth LK, et al, Move Disord.[76] © 2010 Movement Disorder Society.

Panel *H* modified from Singh P, et al, J Pediatr Neurosci.[75] © 2011 Journal of Pediatric Neurosciences.

exclude phenocopies. The typical structural MRI findings noted in Huntington disease are striatal atrophy involving the caudate head and putamen (FIGURE 8-8). The putamen is typically more involved than the caudate head, and its volume has been suggested to be a more sensitive measure.[77] Striatal atrophy correlates with age at onset, disease duration, and CAG repeat length and may also be evident in presymptomatic Huntington disease gene mutation carriers.[78] It may also be accompanied by varying degrees of cortical atrophy.

Neurodegeneration With Brain Iron Accumulation

Neurodegeneration with brain iron accumulation comprises a group of genetic disorders marked by aberrant brain iron deposition leading to neurodegeneration with varying combinations of chorea, parkinsonism, and dystonia and often with other associated symptoms, including cognitive dysfunction. Neuroferritinopathy and aceruloplasminemia are typically late adult-onset while pantothenate kinase-associated neurodegeneration

Copyright © American Academy of Neurology. Unauthorized reproduction of this article is prohibited.

occasionally presents later in life. Their structural MRI findings are discussed here. In general, the aberrant iron accumulation manifests as T2 and SWI hypointensities, and the relative hypointensity of the globus pallidus and substantia nigra compared with the red nucleus is often a diagnostic clue of abnormal iron deposition.[79]

Pantothenate kinase–associated neurodegeneration may have T2 and SWI hypointensity of the globus pallidus and substantia nigra with a characteristic "eye of the tiger" sign (hyperintense center with surrounding hypointensity of the globus pallidus) that is highly sensitive but not specific; it can also occur in people with neuroferritinopathy, Wilson disease, or MSA.[79-81] MRI in individuals with neuroferritinopathy may show characteristic cavitary lesions in the globus pallidus and putamen. These lesions manifest as T2 hyperintensities often surrounded by a hypointense rim of abnormal iron deposition.[82,83]

Cortical iron deposits result in thin cortical SWI hypointensities termed as "cortical pencil lining."[84] Cavitations and the cortical pencil lining sign are thought to be unique to neuroferritinopathy and may aid in the differential diagnosis. Iron accumulation in the dentate nucleus and occasionally in the caudate nucleus and thalami may also occur in neuroferritinopathy. In people with aceruloplasminemia, MRI typically shows uniform, bilateral T2 and SWI hypointensity of the entire basal ganglia and thalami.[82] Fast spin echo T2-weighted MRI and iron-sensitive (T2*/SWI) sequences can help differentiate these conditions (**FIGURE 8-9**). Even though classic MRI features are highlighted here, it is important to note that the MRI findings vary depending on the stage of the disease process and only nonspecific features may be present in the early or advanced stages of neurodegeneration.[79]

Basal Ganglia Calcifications

Small, symmetric bilateral basal ganglia calcifications are often an incidental imaging finding in the older adult population (up to 20%) and are usually not associated with any clinical symptoms. Rarely, however, extensive bilateral symmetric calcifications in the basal ganglia with or without similar changes in the dentate nucleus, thalamus, or white matter can be seen in the setting of varying combinations of chorea, dystonia, and parkinsonism, often with associated mood and cognitive symptoms. Patients with this syndrome may be diagnosed with primary idiopathic Fahr disease (several genes have been identified) or secondary Fahr syndrome, most commonly due to chronic hypoparathyroidism.[85] Head CT may be more sensitive than routine brain MRI unless SWI (or similar) sequences are included to demonstrate this aberrant calcification[86] (**FIGURE 8-10**).

Functional Movement Disorders

In general, a low threshold should be maintained to obtain MRI of the brain or spine to exclude underlying structural etiologies if the clinical examination suggests such possibilities. Considerable research is underway using structural and functional MRI in functional movement disorders, with a goal of shedding light on the underlying pathophysiology and potentially developing diagnostic biomarkers. Morphometric MRI measures have revealed significant group differences in functional movement disorders involving a variety of cortical and subcortical structures including the striatum, cerebellum, and thalami, but contrasting reports by different groups limit their clinical utility at this time.[87]

Copyright © American Academy of Neurology. Unauthorized reproduction of this article is prohibited.

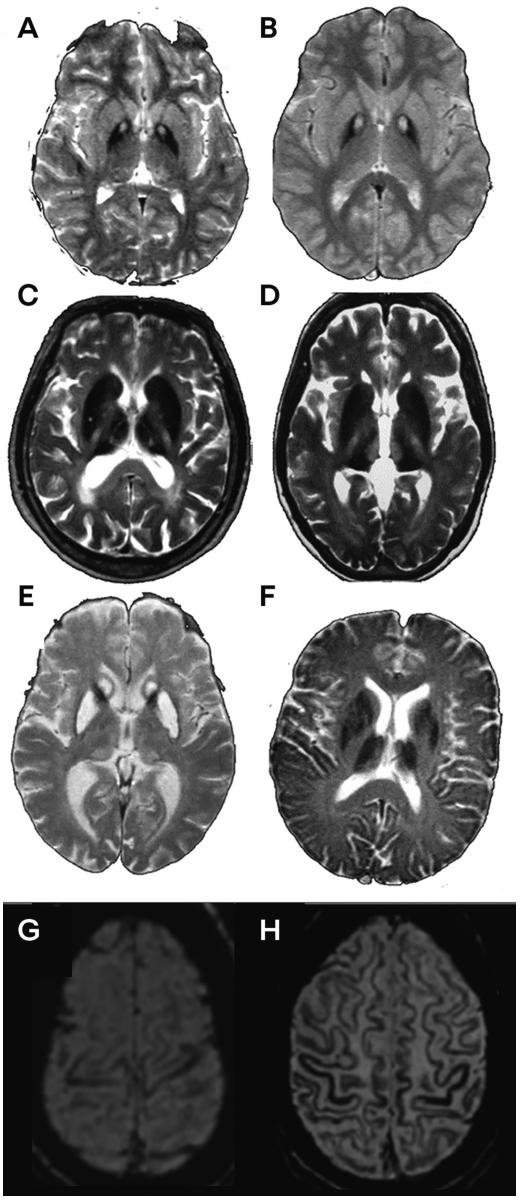

FIGURE 8-9

MRI findings in neurodegeneration with brain iron accumulation. MRI characteristics in pantothenate kinase–associated neurodegeneration (PKAN): Axial fast spin echo (FSE) (*A*) and T2*-weighted (*B*) images show bilateral "eye of the tiger sign" in the globus pallidus in PKAN. MRI characteristics in aceruloplasminemia: Axial FSE (*C*) and T2*-weighted (*D*) images show hypointensity of the globus pallidus, putamen, caudate nucleus, and thalamus in aceruloplasminemia. *E-H*, MRI characteristics in neuroferritinopathy: Axial FSE image (*E*) shows hyperintensity of the caudate nucleus with confluent hyperintensity of the globus pallidus and putamen in neuroferritinopathy. Axial T2*-weighted image (*F*) shows hypointensity of the globus pallidus, putamen, caudate nucleus, and thalamus in neuroferritinopathy. Even though findings on T2*-weighted images may be very similar in neuroferritinopathy and aceruloplasminemia, FSE images readily differentiate these two conditions. Susceptibility-weighted images (SWI) (*G, H*) show "cortical pencil lining" in motor cortices (*G*) and diffuse cortical areas (*H*) in genetically proven neuroferritinopathy.

Panels A-F modified with permission from McNeill A, et al, Neurology.[82] © 2009 American Academy of Neurology.

Parts G-H modified with permission from Batla A, et al, Neurology.[84] © 2015 American Academy of Neurology.

Close clinical follow-up of patients with functional movement disorders is warranted and often further clarifies the diagnosis.

CONCLUSION

In summary, current molecular imaging methods are sensitive measures of onset of pathology in PD, but these measures reflect nigral degeneration and hence disease severity and progression only early in the disease process. Iron-sensitive or neuromelanin-sensitive MRI measures may directly reflect nigral pathology and hold tremendous promise. All of the above-described imaging modalities still have great importance in research, but the lack of specificity limits their clinical utility at this time. Multimodal imaging that reflects both pathology and

Copyright © American Academy of Neurology. Unauthorized reproduction of this article is prohibited.

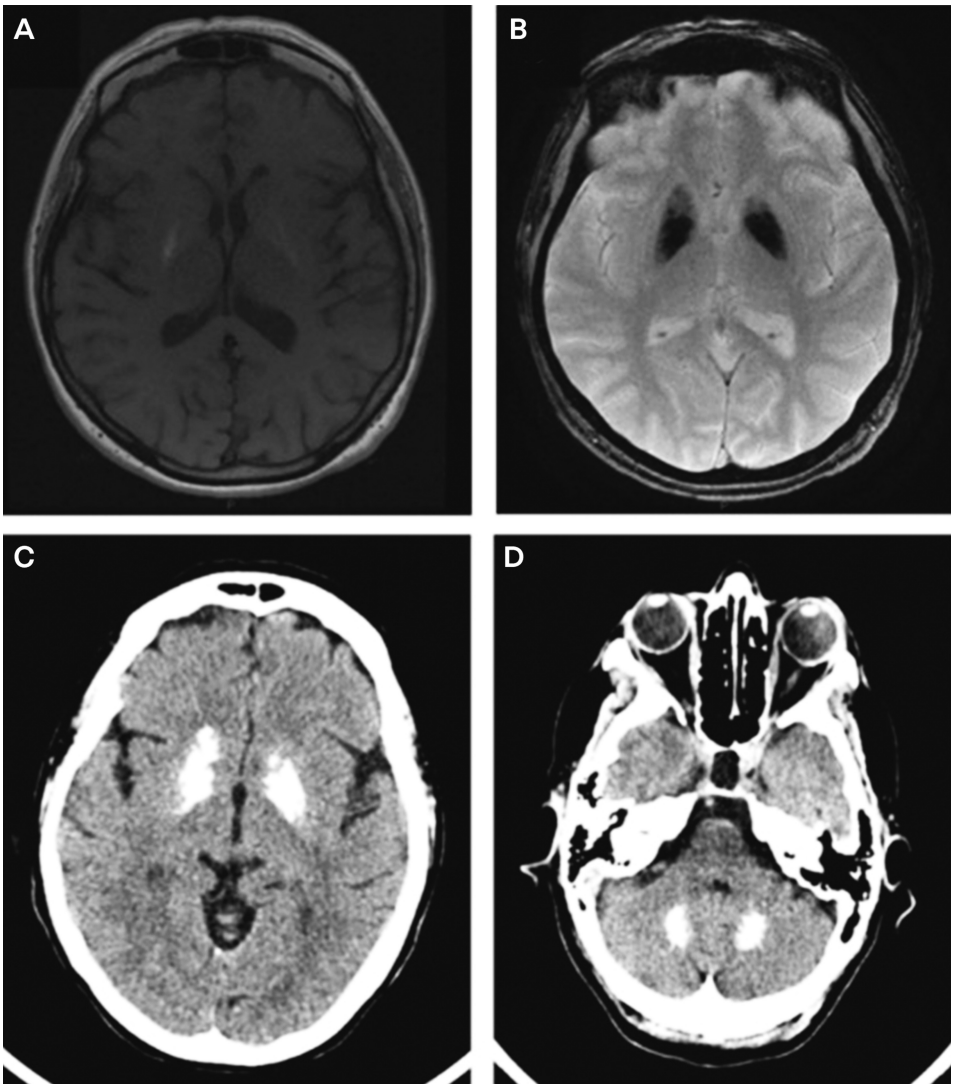

FIGURE 8-10

MRI and head CT findings in basal ganglia calcifications. Axial T1-weighted MRI (*A*) showing hyperintensity in bilateral putamen and caudate. Of note, the intensity of the basal ganglia on T1-weighted MRI diminishes with higher calcium concentration. Axial T2* MRI (*B*) showing marked hypointensity in bilateral basal ganglia. Head CT showing diffuse symmetric calcifications in bilateral basal ganglia (*C*) and dentate nuclei (*D*) of the cerebellum.

Reprinted from Donzuso G, et al, Neurol Sci.[85] © 2019 The Authors.

functional consequences could substantially influence the future course of research. A tracer directly targeting oligomeric α-synuclein remains the ultimate diagnostic goal.

REFERENCES

1 Hughes AJ, Daniel SE, Kilford L, Lees AJ. Accuracy of clinical diagnosis of idiopathic Parkinson's disease: a clinico-pathological study of 100 cases. J Neurol Neurosurg Psychiatry 1992;55(3): 181-184. doi:10.1136/jnnp.55.3.181

2 Martin WRW, Hartlein J, Racette BA, Cairns N, Perlmutter JS. Pathologic correlates of supranuclear gaze palsy with parkinsonism. Parkinsonism Relat Disord 2017;38:68-71. doi: 10.1016/j.parkreldis.2017.02.027

Copyright © American Academy of Neurology. Unauthorized reproduction of this article is prohibited.

3 Martin WRW, Miles M, Zhong Q, et al. Is levodopa response a valid indicator of Parkinson's disease? Mov Disord 2021;36(4):948-954. doi: 10.1002/mds.28406

4 Braak H, Ghebremedhin E, Rüb U, Bratzke H, Del Tredici K. Stages in the development of Parkinson's disease-related pathology. Cell Tissue Res 2004;318(1):121-134. doi:10.1007/s00441-004-0956-9

5 Tabbal SD, Tian L, Karimi M, et al. Low nigrostriatal reserve for motor parkinsonism in nonhuman primates. Exp Neurol 2012;237(2):355-362. doi:10.1016/j.expneurol.2012.07.008

6 Damier P, Hirsch EC, Agid Y, Graybiel AM. The substantia nigra of the human brain. I. Nigrosomes and the nigral matrix, a compartmental organization based on calbindin D(28K) immunohistochemistry. Brain 1999;122(Pt 8):1421-1436. doi:10.1093/brain/122.8.1421

7 Karimi M, Tian L, Brown CA, et al. Validation of nigrostriatal positron emission tomography measures: critical limits. Ann Neurol 2013;73(3):390-396. doi:10.1002/ana.23798

8 Varrone A, Marek KL, Jennings D, Innis RB, Seibyl JP. [(123)I]beta-CIT SPECT imaging demonstrates reduced density of striatal dopamine transporters in Parkinson's disease and multiple system atrophy. Mov Disord 2001;16(6):1023-1032. doi:10.1002/mds.1256

9 Perju-Dumbrava LD, Kovacs GG, Pirker S, et al. Dopamine transporter imaging in autopsy-confirmed Parkinson's disease and multiple system atrophy. Mov Disord 2012;27(1):65-71. doi:10.1002/mds.24000

10 Seibyl JP, Marek KL, Quinlan D, et al. Decreased single-photon emission computed tomographic [123I]beta-CIT striatal uptake correlates with symptom severity in Parkinson's disease. Ann Neurol 1995;38(4):589-598. doi:10.1002/ana.410380407

11 Benamer HT, Patterson J, Wyper DJ, et al. Correlation of Parkinson's disease severity and duration with 123I-FP-CIT SPECT striatal uptake. Mov Disord 2000;15(4):692-698. doi:10.1002/1531-8257(200007)15:4<692::aid-mds1014>3.0.co;2-v

12 Thomas AJ, Attems J, Colloby SJ, et al. Autopsy validation of 123I-FP-CIT dopaminergic neuroimaging for the diagnosis of DLB. Neurology 2017;88(3):276-283. doi:10.1212/WNL.0000000000003512

13 Eshuis SA, Maguire RP, Leenders KL, Jonkman S, Jager PL. Comparison of FP-CIT SPECT with F-DOPA PET in patients with de novo and advanced Parkinson's disease. Eur J Nucl Med Mol Imaging 2006;33(2):200-209. doi:10.1007/s00259-005-1904-y

14 Schwarz J, Linke R, Kerner M, et al. Striatal dopamine transporter binding assessed by [I-123] IPT and single photon emission computed tomography in patients with early Parkinson's disease: implications for a preclinical diagnosis. Arch Neurol 2000;57(2):205-208. doi:10.1001/archneur.57.2.205

15 Adams JR, van Netten H, Schulzer M, et al. PET in LRRK2 mutations: comparison to sporadic Parkinson's disease and evidence for presymptomatic compensation. Brain 2005;128(Pt 12):2777-2785. doi:10.1093/brain/awh607

16 Hughes AJ, Daniel SE, Ben-Shlomo Y, Lees AJ. The accuracy of diagnosis of parkinsonian syndromes in a specialist movement disorder service. Brain 2002;125(Pt 4):861-870. doi:10.1093/brain/awf080

17 de la Fuente-Fernández R. Role of DaTSCAN and clinical diagnosis in Parkinson disease. Neurology 2012;78(10):696-701. doi:10.1212/WNL.0b013e318248e520

18 Serrano Vicente J, García Bernardo L, Durán Barquero C, et al. [Negative predictive value of (123)I Ioflupane SPECT in movement disorders]. Rev Esp Med Nucl 2009;28(1):2-5.

19 Kim YE, Jeon B, Farrer MJ, et al. SCA2 family presenting as typical Parkinson's disease: 34 year follow up. Parkinsonism Relat Disord 2017;40:69-72. doi:10.1016/j.parkreldis.2017.04.003

20 Benítez-Rivero S, Marín-Oyaga VA, García-Solís D, et al. Clinical features and 123I-FP-CIT SPECT imaging in vascular parkinsonism and Parkinson's disease. J Neurol Neurosurg Psychiatry 2013;84(2):122-129. doi:10.1136/jnnp-2012-302618

21 Tinazzi M, Cipriani A, Matinella A, et al. [^{123}I]FP-CIT single photon emission computed tomography findings in drug-induced Parkinsonism. Schizophr Res 2012;139(1-3):40-45. doi:10.1016/j.schres.2012.06.003

22 Iranzo A, Santamaría J, Valldeoriola F, et al. Dopamine transporter imaging deficit predicts early transition to synucleinopathy in idiopathic rapid eye movement sleep behavior disorder. Ann Neurol 2017;82(3):419-428. doi:10.1002/ana.25026

23 Jennings D, Siderowf A, Stern M, et al. Conversion to Parkinson disease in the PARS hyposmic and dopamine transporter-deficit prodromal cohort. JAMA Neurol 2017;74(8):933-940. doi:10.1001/jamaneurol.2017.0985

24 Kordower JH, Olanow CW, Dodiya HB, et al. Disease duration and the integrity of the nigrostriatal system in Parkinson's disease. Brain 2013;136(8):2419-2431. doi:10.1093/brain/awt192

25 Honkanen EA, Saari L, Orte K, et al. No link between striatal dopaminergic axons and dopamine transporter imaging in Parkinson's disease. Mov Disord 2019;34(10):1562-1566. doi:10.1002/mds.27777

Copyright © American Academy of Neurology. Unauthorized reproduction of this article is prohibited.

26 Saari L, Kivinen K, Gardberg M, et al. Dopamine transporter imaging does not predict the number of nigral neurons in Parkinson disease. Neurology 2017;88(15):1461-1467. doi:10.1212/WNL.0000000000003810

27 Nandhagopal R, Kuramoto L, Schulzer M, et al. Longitudinal evolution of compensatory changes in striatal dopamine processing in Parkinson's disease. Brain 2011;134(Pt 11):3290-3298. doi:10.1093/brain/awr233

28 Simuni T, Siderowf A, Lasch S, et al. Longitudinal change of clinical and biological measures in early Parkinson's disease: Parkinson's Progression Markers Initiative Cohort. Movement Disorders 2018;33(5):771-782. doi:10.1002/mds.27361

29 Brown CA, Karimi MK, Tian L, et al. Validation of midbrain positron emission tomography measures for nigrostriatal neurons in macaques. Ann Neurol 2013;74(4):602-610. doi:10.1002/ana.23939

30 Foster ER, Campbell MC, Burack MA, et al. Amyloid imaging of Lewy body-associated disorders. Mov Disord 2010;25(15):2516-2523. doi:10.1002/mds.23393

31 Burack MA, Hartlein J, Flores HP, et al. In vivo amyloid imaging in autopsy-confirmed Parkinson disease with dementia. Neurology 2010;74(1):77-84. doi:10.1212/WNL.0b013e3181c7da8e

32 Campbell MC, Markham J, Flores H, et al. Principal component analysis of PiB distribution in Parkinson and Alzheimer diseases. Neurology 2013;81(6):520-527. doi:10.1212/WNL.0b013e31829e6f94

33 Chen Q, Lowe VJ, Boeve BF, et al. β-Amyloid PET and 123I-FP-CIT SPECT in mild cognitive impairment at risk for Lewy body dementia. Neurology 2021;96(8):e1180-e1189. doi:10.1212/WNL.0000000000011454

34 Kotzbauer PT, Cairns NJ, Campbell MC, et al. Pathologic accumulation of α-synuclein and Aβ in Parkinson disease patients with dementia. Arch Neurol 2012;69(10):1326-1331. doi:10.1001/archneurol.2012.1608

35 Lee SH, Cho H, Choi JY, et al. Distinct patterns of amyloid-dependent tau accumulation in Lewy body diseases. Mov Disord 2018;33(2):262-272. doi:10.1002/mds.27252

36 Whitwell JL, Tosakulwong N, Schwarz CG, et al. MRI Outperforms [18F]AV-1451 PET as a longitudinal biomarker in progressive supranuclear palsy. Mov Disord 2019;34(1):105-113. doi:10.1002/mds.27546

37 Marquié M, Normandin MD, Meltzer AC, et al. Pathological correlations of [F-18]-AV-1451 imaging in non-alzheimer tauopathies. Ann Neurol 2017;81(1):117-128. doi:10.1002/ana.24844

38 Bohnen NI, Kanel P, Zhou Z, et al. Cholinergic system changes of falls and freezing of gait in Parkinson's disease. Ann Neurol 2019;85(4):538-549. doi:10.1002/ana.25430

39 Legault-Denis C, Aghourian M, Soucy JP, et al. Normal cognition in Parkinson's disease may involve hippocampal cholinergic compensation: an exploratory PET imaging study with [18F]-FEOBV. Parkinsonism Relat Disord 2021;91:162-166. doi:10.1016/j.parkreldis.2021.09.018

40 Oppedal K, Ferreira D, Cavallin L, et al. A signature pattern of cortical atrophy in dementia with Lewy bodies: a study on 333 patients from the European DLB consortium. Alzheimers Dement 2019;15(3):400-409. doi:10.1016/j.jalz.2018.09.011

41 Brooks DJ, Seppi K, Neuroimaging Working Group on MSA. Proposed neuroimaging criteria for the diagnosis of multiple system atrophy. Mov Disord 2009;24(7):949-964. doi:10.1002/mds.22413

42 Massey LA, Micallef C, Paviour DC, et al. Conventional magnetic resonance imaging in confirmed progressive supranuclear palsy and multiple system atrophy. Mov Disord 2012;27(14):1754-1762. doi:10.1002/mds.24968

43 Lee YC, Liu CS, Wu HM, et al. The "hot cross bun" sign in the patients with spinocerebellar ataxia. Eur J Neurol 2009;16(4):513-516. doi:10.1111/j.1468-1331.2008.02524.x

44 Warmuth-Metz M, Naumann M, Csoti I, Solymosi L. Measurement of the midbrain diameter on routine magnetic resonance imaging: a simple and accurate method of differentiating between Parkinson disease and progressive supranuclear palsy. Arch Neurol 2001;58(7):1076-1079. doi:10.1001/archneur.58.7.1076

45 Adachi M, Kawanami T, Ohshima H, Sugai Y, Hosoya T. Morning glory sign: a particular MR finding in progressive supranuclear palsy. Magn Reson Med Sci 2004;3(3):125-132. doi:10.2463/mrms.3.125

46 Massey LA, Jäger HR, Paviour DC, et al. The midbrain to pons ratio: a simple and specific MRI sign of progressive supranuclear palsy. Neurology 2013;80(20):1856-1861. doi:10.1212/WNL.0b013e318292a2d2

47 Nigro S, Morelli M, Arabia G, et al. Magnetic resonance parkinsonism index and midbrain to pons ratio: which index better distinguishes progressive supranuclear palsy patients with a low degree of diagnostic certainty from patients with Parkinson disease? Parkinsonism Relat Disord 2017;41:31-36. doi:10.1016/j.parkreldis.2017.05.002

48 Quattrone A, Morelli M, Nigro S, et al. A new MR imaging index for differentiation of progressive supranuclear palsy-parkinsonism from Parkinson's disease. Parkinsonism Relat Disord 2018;54:3-8. doi:10.1016/j.parkreldis.2018.07.016

49 Paviour DC, Price SL, Jahanshahi M, Lees AJ, Fox NC. Longitudinal MRI in progressive supranuclear palsy and multiple system atrophy: rates and regions of atrophy. Brain 2006;129(Pt 4):1040-1049. doi:10.1093/brain/awl021

Copyright © American Academy of Neurology. Unauthorized reproduction of this article is prohibited.

50 Ling H, O'Sullivan SS, Holton JL, et al. Does corticobasal degeneration exist? A clinicopathological re-evaluation. Brain 2010; 133(Pt 7):2045-2057. doi:10.1093/brain/awq123

51 Scherfler C, Göbel G, Müller C, et al. Diagnostic potential of automated subcortical volume segmentation in atypical parkinsonism. Neurology 2016;86(13):1242-1249. doi:10.1212/WNL.0000000000002518

52 Vizcarra JA, Lang AE, Sethi KD, Espay AJ. Vascular parkinsonism: deconstructing a syndrome. Mov Disord 2015;30(7):886-894. doi:10.1002/mds.26263

53 Damasceno BP. Neuroimaging in normal pressure hydrocephalus. Dement Neuropsychol 2015;9(4): 350-355. doi:10.1590/1980-57642015DN94000350

54 Oliveira LM, Nitrini R, Román GC. Normal-pressure hydrocephalus: a critical review. Dement Neuropsychol 2019;13(2):133-143. doi:10.1590/1980-57642018dn13-020001

55 Bradley WG. Magnetic resonance imaging of normal pressure hydrocephalus. Semin Ultrasound CT MR 2016;37(2):120-128. doi:10.1053/j.sult.2016.01.005

56 Harischandra DS, Rokad D, Neal ML, et al. Manganese promotes the aggregation and prion-like cell-to-cell exosomal transmission of α-synuclein. Sci Signal 2019;12(572):eaau4543. doi:10.1126/scisignal.aau4543

57 Criswell SR, Nielsen SS, Warden MN, et al. MRI Signal intensity and parkinsonism in manganese-exposed workers. J Occup Environ Med 2019;61(8):641-645. doi:10.1097/JOM.0000000000001634

58 Jiang Y, Zheng W, Long L, et al. Brain magnetic resonance imaging and manganese concentrations in red blood cells of smelting workers: search for biomarkers of manganese exposure. Neurotoxicology 2007;28(1):126-135. doi:10.1016/j.neuro.2006.08.005

59 Damier P, Hirsch EC, Agid Y, Graybiel AM. The substantia nigra of the human brain. II. Patterns of loss of dopamine-containing neurons in Parkinson's disease. Brain 1999;122(Pt 8): 1437-1448. doi:10.1093/brain/122.8.1437

60 Blazejewska AI, Schwarz ST, Pitiot A, et al. Visualization of nigrosome 1 and its loss in PD: pathoanatomical correlation and in vivo 7 T MRI. Neurology 2013;81(6):534-540. doi:10.1212/WNL.0b013e31829e6fd2

61 Schwarz ST, Afzal M, Morgan PS, et al. The "swallow tail" appearance of the healthy nigrosome - a new accurate test of Parkinson's disease: a case-control and retrospective cross-sectional MRI study at 3T. PLoS One 2014; 9(4):e93814. doi:10.1371/journal.pone.0093814

62 Mahlknecht P, Krismer F, Poewe W, Seppi K. Meta-analysis of dorsolateral nigral hyperintensity on magnetic resonance imaging as a marker for Parkinson's disease. Mov Disord 2017;32(4):619-623. doi:10.1002/mds.26932

63 Bae YJ, Kim JM, Kim E, et al. Loss of nigral hyperintensity on 3 Tesla MRI of parkinsonism: comparison with (123) I-FP-CIT SPECT. Mov Disord 2016;31(5):684-692. doi:10.1002/mds.26584

64 Bae YJ, Kim JM, Kim KJ, et al. Loss of substantia nigra hyperintensity at 3.0-T MR imaging in idiopathic REM sleep behavior disorder: comparison with 123I-FP-CIT SPECT. Radiology 2018;287(1):285-293. doi:10.1148/radiol.2017162486

65 Schmidt MA, Engelhorn T, Marxreiter F, et al. Ultra high-field SWI of the substantia nigra at 7T: reliability and consistency of the swallow-tail sign. BMC Neurol 2017;17(1):194. doi:10.1186/s12883-017-0975-2

66 Kau T, Hametner S, Endmayr V, et al. Microvessels may confound the "swallow tail sign" in normal aged midbrains: a Postmortem 7 T SW-MRI study. J Neuroimaging 2019;29(1):65-69. doi:10.1111/jon.12576

67 Biondetti E, Gaurav R, Yahia-Cherif L, et al. Spatiotemporal changes in substantia nigra neuromelanin content in Parkinson's disease. Brain 2020;143(9):2757-2770. doi:10.1093/brain/awaa216

68 Gaurav R, Yahia-Cherif L, Pyatigorskaya N, et al. Longitudinal changes in neuromelanin MRI signal in Parkinson's disease: a progression marker. Mov Disord 2021;36(7):1592-1602. doi:10.1002/mds.28531

69 Hacker CD, Perlmutter JS, Criswell SR, Ances BM, Snyder AZ. Resting state functional connectivity of the striatum in Parkinson's disease. Brain 2012; 135(Pt 12):3699-3711. doi:10.1093/brain/aws281

70 Gratton C, Koller JM, Shannon W, et al. Emergent functional network effects in Parkinson disease. Cereb Cortex 2019;29(4):1701. doi:10.1093/cercor/bhy229

71 Maiti B, Koller JM, Snyder AZ, et al. Cognitive correlates of cerebellar resting-state functional connectivity in Parkinson disease. Neurology 2020;94(4):e384-e396. doi:10.1212/WNL.0000000000008754

72 Maiti B, Rawson KS, Tanenbaum AB, et al. Functional connectivity of vermis correlates with future gait impairments in Parkinson's disease. Mov Disord 2021;36(11):2559-2568. doi:10.1002/mds.28684

73 Campbell MC, Jackson JJ, Koller JM, et al. Proteinopathy and longitudinal changes in functional connectivity networks in Parkinson disease. Neurology 2020;94(7):e718-e728. doi:10.1212/WNL.0000000000008677

74 Greene DJ, Marek S, Gordon EM, et al. Integrative and network-specific connectivity of the basal ganglia and thalamus defined in individuals. Neuron 2020;105(4):742-758.e6. doi:10.1016/j.neuron.2019.11.012

75 Singh P, Ahluwalia A, Saggar K, Grewal CS. Wilson's disease: MRI features. J Pediatr Neurosci 2011;6(1):27-28. doi:10.4103/1817-1745.84402

Copyright © American Academy of Neurology. Unauthorized reproduction of this article is prohibited.

76 Prashanth LK, Sinha S, Taly AB, Vasudev MK. Do MRI features distinguish Wilson's disease from other early onset extrapyramidal disorders? An analysis of 100 cases. Mov Disord 2010;25(6): 672-678. doi:10.1002/mds.22689

77 Harris GJ, Pearlson GD, Peyser CE, et al. Putamen volume reduction on magnetic resonance imaging exceeds caudate changes in mild Huntington's disease. Ann Neurol 1992;31(1): 69-75. doi:10.1002/ana.410310113

78 Niccolini F, Politis M. Neuroimaging in Huntington's disease. World J Radiol 2014;6(6): 301-312. doi:10.4329/wjr.v6.i6.301

79 Lee JH, Yun JY, Gregory A, Hogarth P, Hayflick SJ. Brain MRI pattern recognition in neurodegeneration with brain iron accumulation. Front Neurol 2020;11:1024. doi:10.3389/fneur.2020.01024

80 Litwin T, Karlinski M, Skowrońska M, Dziezyc K, Gołębiowski M, Członkowska A. MR image mimicking the "eye of the tiger" sign in Wilson's disease. J Neurol 2014;261(5):1025-1027. doi: 10.1007/s00415-014-7322-y

81 Chang MH, Hung WL, Liao YC, Lee YC, Hsieh PF. Eye of the tiger-like MRI in parkinsonian variant of multiple system atrophy. J Neural Transm (Vienna) 2009;116(7):861-866. doi:10.1007/s00702-009-0234-9

82 McNeill A, Birchall D, Hayflick SJ, et al. T2* and FSE MRI distinguishes four subtypes of neurodegeneration with brain iron accumulation. Neurology 2008;70(18):1614-1619. doi:10.1212/01.wnl.0000310985.40011.d6

83 Kumar N, Rizek P, Jog M. Neuroferritinopathy: pathophysiology, presentation, differential diagnoses and management. Tremor Other Hyperkinet Mov (N Y) 2016;6:355. doi:10.7916/D8KK9BHF

84 Batla A, Adams ME, Erro R, et al. Cortical pencil lining in neuroferritinopathy: a diagnostic clue. Neurology 2015;84(17):1816-1818. doi:10.1212/WNL.0000000000001511

85 Donzuso G, Mostile G, Nicoletti A, Zappia M. Basal ganglia calcifications (Fahr's syndrome): related conditions and clinical features. Neurol Sci 2019;40(11):2251-2263. doi:10.1007/s10072-019-03998-x

86 Sahin N, Solak A, Genc B, Kulu U. Fahr disease: use of susceptibility-weighted imaging for diagnostic dilemma with magnetic resonance imaging. Quant Imaging Med Surg 2015;5(4):628-632. doi: 10.3978/j.issn.2223-4292.2015.04.01

87 Sasikumar S, Strafella AP. The neuroimaging evidence of brain abnormalities in functional movement disorders. Brain 2021;144(8): 2278-2283. doi:10.1093/brain/awab131

DISCLOSURE

Continued from page 194

Association, the Barnes-Jewish Hospital Foundation, the CHDI Foundation, the Huntington Disease Society of America, The Michael J Fox Foundation, the National Institutes of Health, the University of California San Diego, and the University of Western Toronto.

Copyright © American Academy of Neurology. Unauthorized reproduction of this article is prohibited.

Neuroimaging in Dementia

By Shannon L. Risacher, PhD; Liana G. Apostolova, MD, MS, FAAN

REVIEW ARTICLE

CONTINUUM AUDIO INTERVIEW AVAILABLE ONLINE

CITE AS:
CONTINUUM (MINNEAP MINN) 2023;29(1, NEUROIMAGING): 219–254.

Address correspondence to Dr Shannon L. Risacher, 355 W 16th St, Indianapolis, IN 46202, srisache@iupui.edu.

RELATIONSHIP DISCLOSURE:
Dr Risacher has received research support from the Alzheimer's Association, New Vision Award, and the National Institute on Aging (K01 AG049050, R01 AG061788, P30 AG010133, and P30 AG072976). Dr Apostolova has received personal compensation in the range of $500 to $4999 for serving as a consultant for Florida Health, General Electric Company, Lilly, the National Institutes of Health (NIH), and NIH Biobank; on a data safety monitoring board for IQVIA Inc; and on advisory boards for Eisai Co, Ltd, F. Hoffman-La Roche Ltd, Genentech, Inc, and TwoLabs, LLC. Dr Apostolova has received personal compensation in the range of $5000 to $9999 for serving on an advisory board for Biogen and in the range of $10,000 to $49,999 for serving as an editor-in-chief for the Alzheimer's Association. An immediate family member of Dr Apostolova has stock in Cassava Sciences, Inc, Golden Seeds, and Semiring. The institution of Dr Apostolova has received research support from *Continued on page 254*

UNLABELED USE OF PRODUCTS/INVESTIGATIONAL USE DISCLOSURE:
Drs Risacher and Apostolova report no disclosures.

© 2023 American Academy of Neurology.

ABSTRACT

OBJECTIVE: **Neurodegenerative diseases are significant health concerns with regard to morbidity and social and economic hardship around the world. This review describes the state of the field of neuroimaging measures as biomarkers for detection and diagnosis of both slowly progressing and rapidly progressing neurodegenerative diseases, specifically Alzheimer disease, vascular cognitive impairment, dementia with Lewy bodies or Parkinson disease dementia, frontotemporal lobar degeneration spectrum disorders, and prion-related diseases. It briefly discusses findings in these diseases in studies using MRI and metabolic and molecular-based imaging (eg, positron emission tomography [PET] and single-photon emission computerized tomography [SPECT]).**

LATEST DEVELOPMENTS: **Neuroimaging studies with MRI and PET have demonstrated differential patterns of brain atrophy and hypometabolism in different neurodegenerative disorders, which can be useful in differential diagnoses. Advanced MRI sequences, such as diffusion-based imaging, and functional MRI (fMRI) provide important information about underlying biological changes in dementia and new directions for development of novel measures for future clinical use. Finally, advancements in molecular imaging allow clinicians and researchers to visualize dementia-related proteinopathies and neurotransmitter levels.**

ESSENTIAL POINTS: **Diagnosis of neurodegenerative diseases is primarily based on symptomatology, although the development of in vivo neuroimaging and fluid biomarkers is changing the scope of clinical diagnosis, as well as the research into these devastating diseases. This article will help inform the reader about the current state of neuroimaging in neurodegenerative diseases, as well as how these tools might be used for differential diagnoses.**

INTRODUCTION

Neuroimaging tools are excellent techniques for evaluating anatomic and functional changes in the brain. The most commonly used neuroimaging technique for evaluating brain changes in dementia is structural MRI, which allows researchers and clinicians to assess both anatomic location and extent of brain atrophy in people with dementia, as well as rule out nondegenerative causes of cognitive impairment. Based on the hydrogen atom spin in water molecules in a strong magnetic field,

Copyright © American Academy of Neurology. Unauthorized reproduction of this article is prohibited.

MRI techniques can also be used to assess integrity and connectivity patterns of brain white matter, extent of and connectivity patterns of brain function during a cognitive task or at rest, cerebral blood flow (CBF), extent and location of cerebrovascular damage, presence and severity of cerebral microbleeds, restricted diffusion in prion diseases, and much more.

The second most commonly used neuroimaging technique to study dementia is positron emission tomography (PET). PET uses radioactive small molecules, called *tracers*, that bind to a target of interest in the tissue of interest. In dementia, PET imaging yields information about ongoing biological processes including brain metabolism, protein aggregation, neurotransmitter systems, neuroinflammation, and other processes. A similar technique, known as single-photon emission computed tomography (SPECT), can be used to measure changes in dopaminergic systems in patients with dementia with Lewy bodies (DLB) or Parkinson disease dementia (PDD). For PET, the major targets are brain levels of key hallmark proteinopathies known to be involved in dementia (eg, amyloid, tau), levels of neurotransmitter receptors and transporters, and glucose metabolism (ie, with fludeoxyglucose [FDG]-PET).

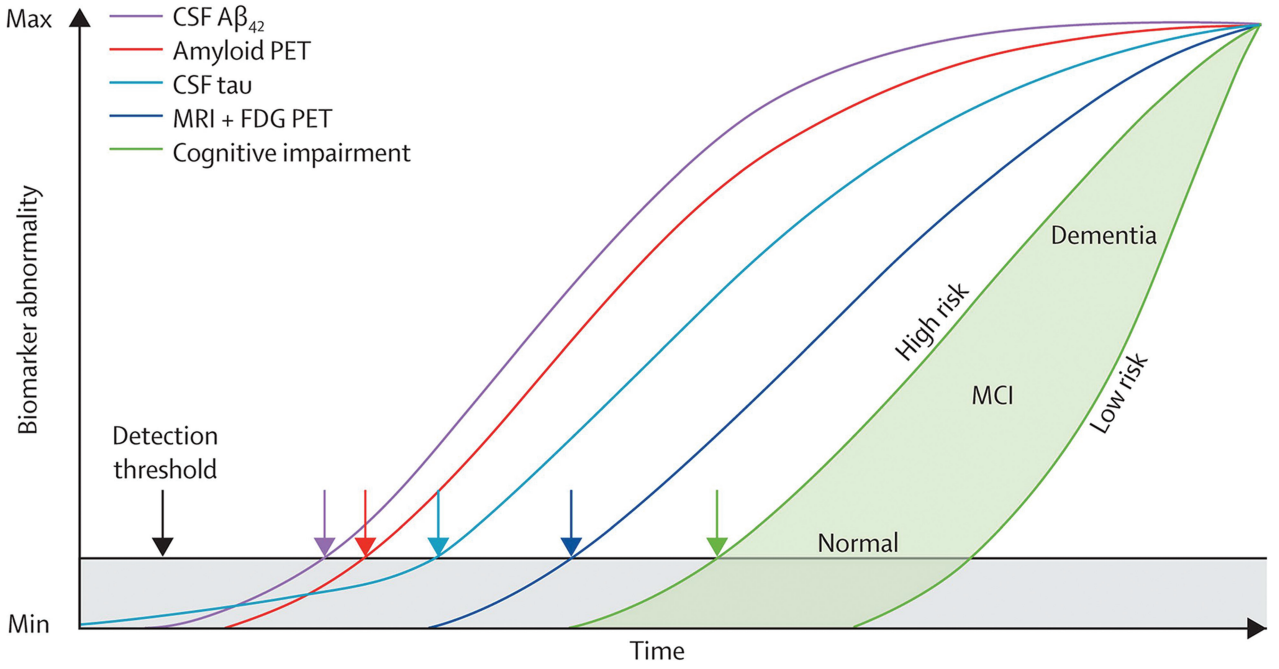

FIGURE 9-1

Hypothetical ordering of Alzheimer disease (AD) biomarkers. The hypothetical ordering of AD biomarkers suggests that the earliest observerable change is increased amyloid deposition, detected first using cerebrospinal fluid (CSF) measures and then by positron emission tomography (PET). Next, changes in tau pathology are observed, as measured by CSF and more recently PET, followed by neurodegenerative changes, measured using structural magnetic resonance imaging (MRI) or fludeoxyglucose (FDG). Finally, changes in cognition are observed with the onset of prodromal AD (ie, mild cognitive impairment [MCI]). All processes are hypothesized to follow a sigmoidal pattern, with initially low levels progressing rapidly once they begin to rise, followed by a plateau at a maximal point.

Aβ = amyloid-β; Max = maximum; Min = minimum.

Reprinted with permission from Jack CR Jr, et al, Lancet Neurol.[2] © 2013 Elsevier Inc.

Copyright © American Academy of Neurology. Unauthorized reproduction of this article is prohibited.

This article reviews neuroimaging findings in selected slow and rapidly progressive dementias, including Alzheimer disease (AD), vascular cognitive impairment, DLB and PDD, frontotemporal lobar degeneration (FTLD) spectrum disorders, and Creutzfeldt-Jakob disease (CJD). It also briefly discusses the potential assistance in differential diagnosis provided by imaging techniques to distinguish dementia types when symptoms are overlapping.

ALZHEIMER DISEASE

AD is the most common age-related dementia and is characterized by the widespread deposition of abnormal amyloid-β (Aβ) in extracellular plaques and tau in intracellular neurofibrillary tangles.[1] Patients with AD also show widespread neuronal loss, gliosis, and immune cell activation, mostly of microglial cells. AD is characterized by progressive cognitive decline, particularly in the memory domain but also in other cognitive domains (eg, executive function, language). Patients with AD show a loss of ability to perform activities of daily living, such as balancing a checkbook, remembering to take medications, and eventually even how to properly dress or bathe themselves. Patients with AD may also show neuropsychiatric symptomatology, including depression, anxiety, and agitation. Currently, three classes of treatments are US Food and Drug Administration (FDA) approved for AD: acetylcholinesterase inhibitors (ie, galantamine, rivastigmine, donepezil), an *N*-methyl-D-aspartate (NMDA) receptor antagonist (memantine), and, most recently, a new medication that is an Aβ-directed antibody that clears Aβ (aducanumab). However, to date, none of these have conclusively been shown to prevent or reverse cognitive decline associated with AD.

Current literature suggests that abnormal protein accumulation, neurodegeneration, and cognitive decline occur over many years to decades. Further, findings suggest that there is a temporally ordered cascade of abnormal changes in various biomarkers of AD as described in the hypothetical ordering of biomarkers proposed by Jack and colleagues[2] (**FIGURE 9-1**). The Jack hypothesis suggests that the first abnormalities are seen in amyloid measured by using either CSF or PET, followed by changes in tau (on CSF or PET) and functional brain changes. Next, abnormal brain atrophy is observed, followed by the clinical symptoms of memory loss and dementia. The long time course between when amyloid and tau abnormalities are detectable and the onset of dementia allows for the characterization of patients who are cognitively normal but show significant amyloid and sometimes tau deposition (preclinical AD), as well as patients with mild impairment in cognition and amyloid and tau deposition (prodromal AD or mild cognitive impairment [MCI] due to AD). These stages of disease show different levels of abnormalities on imaging, as discussed later.

A recent development in characterizing older adults at risk for AD is the amyloid, tau, neurodegeneration (A/T/N) staging system (**TABLE 9-1**[3]).[4] This system categorizes patients by their amyloid status (positive or negative), tau status (positive or negative), and neurodegeneration (positive or negative). The definition of amyloid and tau positivity can be determined by using either CSF or plasma levels of Aβ and phosphorylated tau (pTau) or through PET imaging with tracers that detect Aβ and tau deposition. Neurodegeneration status is more difficult to define because it exists on a spectrum, and some atrophy due to aging is seen in older adults. However, cutoff values for positive or negative neurodegeneration have been established for MRI-based assessments of

KEY POINTS

- **Alzheimer disease (AD) neuroimaging biomarkers become abnormal in a characteristic order where first amyloid deposition is detected on CSF or positron emission tomography (PET), then tau deposition is detected on CSF or PET, followed by changes in atrophy on MRI, and finally cognitive impairment.**
- **A research framework for diagnosing AD by classifying patients based on their amyloid status (positive versus negative), tau status (positive versus negative), and neurodegeneration (positive versus negative), as well as cognitive status, has been proposed and widely adopted.**

Copyright © American Academy of Neurology. Unauthorized reproduction of this article is prohibited.

hippocampal and cortical atrophy, as well as for glucose hypometabolism as measured by FDG-PET. Through the A/T/N characterization system, clinicians or researchers can categorize older adults who are cognitively normal and have preclinical AD as A+, T+ or T-, and N+ or N-. In addition, older adults with cognitive impairment can be categorized as having MCI or dementia due to either AD pathophysiology (A+/T±/N±) or non-AD pathology (A-/T±/N±). Overall, the A/T/N classification system allows researchers and potentially clinicians to better characterize disease burden at the level of the individual and provide a better prediction of disease course and ultimately treatment based on the presence of specific proteinopathies.[4]

MRI Findings in Clinical, Prodromal, and Preclinical Alzheimer Disease

Patients with AD show marked changes on most biomarker measures used for clinical care and research. Patients with AD show widespread degeneration on structural MRI both subcortically, including in the hippocampus, amygdala, basal ganglia, and basal forebrain, and cortically, with the greatest changes in the medial and lateral temporal lobes (FIGURE 9-2A[5]).[6] Changes in subfields of the hippocampus are also evident in patients with AD, including significant atrophy in the subiculum, presubiculum, CA1, CA2/3, and CA4/dentate gyrus.[7] Quantification of cortical atrophy rates in patients with AD suggests an accelerated rate of atrophy, with loss of up to 4.7%/year in the hippocampus and 2%/year in the cortex relative to the approximate normal rate of loss of 1.4% in the hippocampus and less than 1% in the cortex of cognitively normal adults.[8] A recent method for examination of brain white matter myelination uses the ratio

TABLE 9-1 **Amyloid, Tau, and Neurodegeneration Biomarker Classifications by Cognitive Impairment Status[a]**

Biomarker profile[b]	Cognitive stage		
	Cognitively unimpaired	Mild cognitive impairment	Dementia
A- T- (N)-[c]	Normal Alzheimer disease (AD) biomarkers, cognitively unimpaired	Normal AD biomarkers with mild cognitive impairment (MCI)	Normal AD biomarkers with dementia
A+ T- (N)-	Preclinical Alzheimer pathologic change	Alzheimer pathologic change with MCI	Alzheimer pathologic change with dementia
A+ T+ (N)- and A+ T+ (N)+	Preclinical AD	AD with MCI (prodromal AD)	AD with dementia
A+ T- (N)+	Alzheimer and concomitant suspected non-Alzheimer pathologic change, cognitively unimpaired	Alzheimer and concomitant suspected non-Alzheimer pathologic change with MCI	Alzheimer and concomitant suspected non-Alzheimer pathologic change with dementia
A- T+ (N)-, A- T- (N)+, A- T+ (N)+	Non-Alzheimer pathologic change, cognitively unimpaired	Non-Alzheimer pathologic change with MCI	Non-Alzheimer pathologic change with dementia

[a] Modified from Jack CR Jr, et al, Alzheimer Dement.[3] © 2018 The Authors.
[b] Biological classification of patients as amyloid (A) positive or negative (+ or -), tau (T) positive or negative, and neurodegeneration (N) positive or negative across the cognitive impairment spectrum of cognitively unimpaired, MCI, and dementia.
[c] Neurodegeneration (N) is listed in parentheses because of the nonspecificity of the finding of neurodegeneration positive for Alzheimer disease, as neurodegeneration can be caused by several different conditions.

Copyright © American Academy of Neurology. Unauthorized reproduction of this article is prohibited.

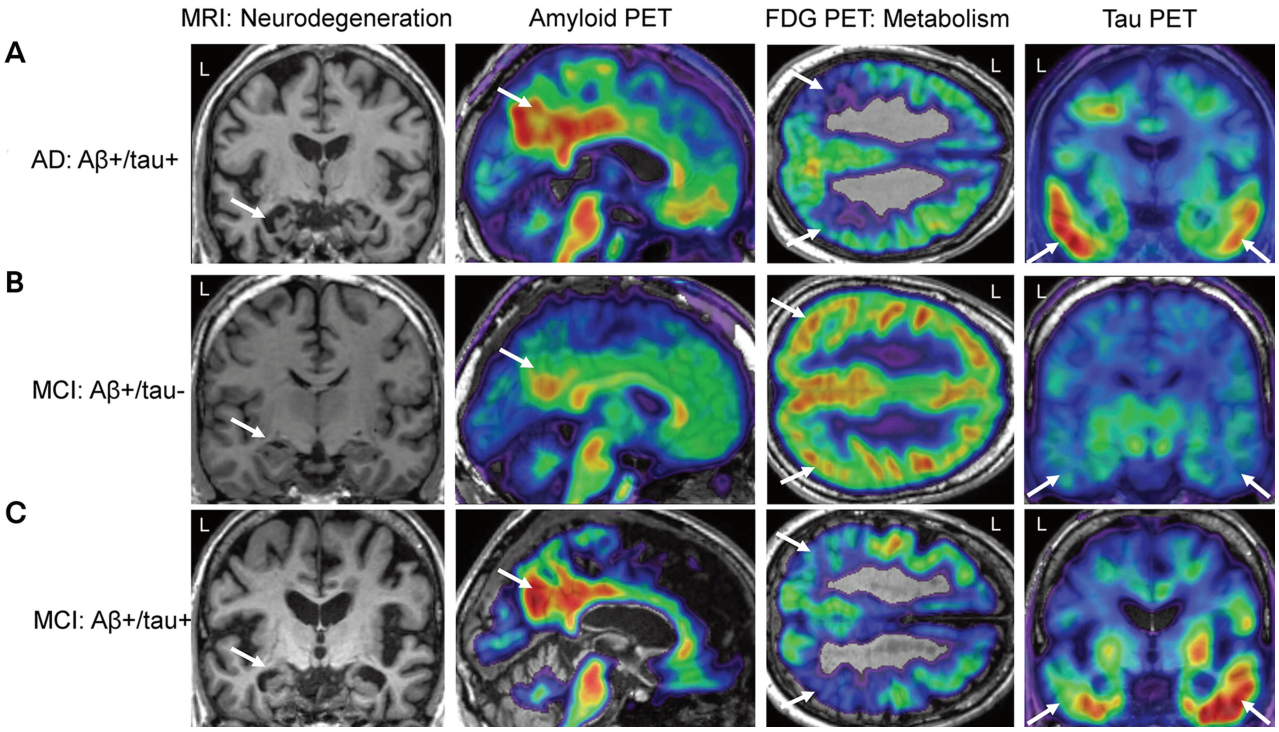

FIGURE 9-2

Neuroimaging biomarkers in patients with mild cognitive impairment (MCI) or Alzheimer disease (AD). Patients with MCI present with varying amounts of amyloid and tau positivity, whereas patients with AD more commonly are amyloid and tau positive. For example, the patient with AD (*A*) is representative of most patients with probable AD, with amyloid positivity (*A*, second column, *arrow*), tau positivity (*A*, fourth column, *arrows*), and marked medial temporal lobe neurodegeneration (*A*, first column, *arrow*) and hypometabolism (*A*, third column, *arrows*). Patients with MCI are more variable. In this example, one patient with MCI (*B*) shows slight medial temporal lobe neurodegeneration (*B*, first column, *arrow*) and lateral parietal glucose hypometabolism (*B*, third column, *arrows*) in the presence of high amyloid deposition (*B*, second column, *arrow*) but minimal tau (*B*, fourth column, *arrows*). However, another patient with MCI (*C*) shows widespread amyloid (*C*, second column, *arrow*) and tau (*C*, fourth column, *arrows*) deposition, as well as medial temporal lobe atrophy (*C*, first column, *arrow*) and parietal hypometabolism (*C*, third column, *arrows*). Neurodegeneration (column 1) and tau deposition (column 4) are shown in a coronal view, amyloid deposition (column 2) is shown in a sagittal view, and hypometabolism (column 3) is shown in an axial view. Note: all example images are taken from the Alzheimer's Disease Neuroimaging Initiative (ADNI) dataset.

Aβ+ = amyloid-β positive; CN = cognitively normal older adult; FDG = fludeoxyglucose; L = left; MRI = magnetic resonance imaging; PET = positron emission tomography; tau- = tau negative; tau+ = tau positive;

Reprinted with permission from Risacher SL, et al, Handb Clin Neurol.[5] © 2019 Elsevier Inc.

of a T1-weighted image intensity value and a T2-weighted image intensity value to assess myelin on a voxel-by-voxel basis. This method, the T1-weighted–to–T2-weighted ratio (T1/T2), shows alterations in cortical white matter in AD, particularly in the temporal lobe, suggesting a loss of myelination in patients with AD.[9]

Other MRI techniques have shown significant impairment in brain structure and function in patients with AD. Diffusion-weighted imaging (DWI) has demonstrated atrophy in widespread cerebral white matter tracts in posterior regions, the corpus callosum, and temporal lobe white matter tracts including the

Copyright © American Academy of Neurology. Unauthorized reproduction of this article is prohibited.

cingulum bundle, uncinate fasciculus, fornix, and superior and inferior longitudinal fasciculi.[10] Brain function is generally measured via functional MRI (fMRI) with blood oxygenation level–dependent (BOLD) imaging and can be done either at rest (resting-state fMRI) or during performance of a cognitive or other task (task-based fMRI). Results from task-based fMRI studies in AD show decreased or even absent activation in the medial temporal lobe, frontal and parietal lobes, and posterior cingulate during episodic memory tasks.[11] Resting-state fMRI studies have also shown widespread impairments in patients with AD, including altered deactivation of the default-mode network, a network of brain regions that are active during a rest state and deactivate on initiation of a cognitive task.[12] Other brain networks such as the salience network and dorsal attention network also show abnormalities in patients with AD.[12] CBF can be measured semiquantitatively using arterial spin labeling MRI techniques. CBF has previously been shown to be reduced in patients with AD relative to those who are cognitively normal, particularly in temporoparietal regions and the hippocampus.[13] Finally, susceptibility-weighted imaging (SWI) techniques analyzed by using a technique called quantitative susceptibility mapping, which is thought to reflect iron deposition in the brain, have demonstrated alterations in patients with AD in the caudate and amygdala that reflect higher levels of iron deposition in these regions.[14] Some individuals with AD also show cerebral microhemorrhages on SWI or similar imaging techniques, which is usually linked to the amount of amyloid deposition, particularly in conditions such as cerebral amyloid angiopathy (CAA).[15]

Amnestic MCI is considered a prodromal stage of AD in many cases, with progression of approximately 50% of patients to a diagnosis of AD dementia within 5 years (illustrated in CASE 9-1). Neuroimaging measures have provided

CASE 9-1

A 72-year-old man presented with symptoms of increasing forgetfulness and word-finding difficulties that had begun in the past 3 years. He and his wife indicated that he was having increasing difficulty remembering appointments and stories recently told to him. Otherwise, his cognition was generally intact, and he was active in his community and with friends and family. However, he was concerned about his symptoms because of a family history of dementia in his mother, who was diagnosed at age 74. On cognitive testing, he showed an isolated memory impairment with normal performance in all other cognitive domains.

COMMENT

This case likely represents mild cognitive impairment due to Alzheimer disease. MRI could rule out treatable conditions and help look for expected atrophy in the medial temporal lobe. A fludeoxyglucose positron emission tomography (FDG-PET) scan could be used and would likely show bilateral lateral parietal hypometabolism. Amyloid PET could also be ordered to determine amyloid status, a positive test suggesting underlying Alzheimer pathology. Overall, the diagnosis would likely be amnestic mild cognitive impairment due to Alzheimer pathology with a positive amyloid scan and medial temporal atrophy.

Copyright © American Academy of Neurology. Unauthorized reproduction of this article is prohibited.

additional evidence of MCI as a transition stage between normal cognition and dementia, showing AD-like patterns of degeneration on structural MRI and deposition of amyloid and tau on molecular imaging that are often less severe than in clinical AD dementia but still markedly different from those in cognitively normal patients. Structural MRI in patients with MCI shows focal atrophy in the medial and lateral temporal lobes, most especially in the entorhinal cortex and hippocampus, which is intermediate in severity between patients who are cognitively normal and patients with clinical AD dementia (FIGURES 9-2B and 9-2C).[6] Structural MRI measures of medial temporal lobe atrophy are also good at predicting future conversion from MCI to AD within a few years.[6] Longitudinally, patients with MCI show more rapid volume loss in the hippocampus and cortex relative to cognitively normal patients but not as severe as the rate of loss seen in patients with clinical AD dementia.[8] Finally, the T1/T2 ratio demonstrates reduced myelin in the bilateral inferior parietal lobule and hippocampus.[9]

Advanced MRI metrics of brain structure and function also show intermediate impairments in patients with MCI that are often reflective of the severity and pattern of symptomatology. DWI measures show white matter degeneration in MCI in tracts that are myelinated later in cerebral development and temporal lobe white matter tracts, including the cingulum, fornix, and superior and inferior longitudinal fasciculi, as well as the corpus callosum.[10] Studies have suggested that these measures of white matter integrity can also predict progression of MCI to AD. Task-based fMRI studies show mixed results in patients with MCI, perhaps linked to varying severity of MCI. Similar mixed results have been seen in resting-state fMRI studies, with differences due to heterogeneity and differential severity.[12] Less impaired patients with MCI may show compensatory hyperactivation in the medial temporal lobe and greater deactivation of the default-mode network during memory tasks and at rest, whereas more impaired patients show patterns of activity similar to those of patients with AD. Arterial spin labeling studies have shown a similar pattern of hyperperfusion in milder forms of MCI and hypoperfusion in more impaired patients with MCI.[13] Finally, quantitative susceptibility mapping has shown mixed results in patients with MCI with one study suggesting increased values representing areas with more iron in cortical regions but not subcortical regions, whereas others found no significant differences in iron deposition in MCI.[14]

Patients with preclinical AD, including cognitively normal patients with significant amyloid deposition (Aβ+ cognitively normal) and cognitively normal patients carrying at least one apolipoprotein E *(APOE)* ε4 allele (*APOE* ε4+ cognitively normal), also show subtle changes in MRI measures of brain structure and function. Studies of structural MRI in preclinical AD have shown mixed findings, with some suggesting mild atrophy in subregions of the hippocampus known to degenerate early in the disease course (eg, subiculum, presubiculum), whereas others have found minimal atrophic changes.[7] Patients with preclinical AD also show an accelerated rate of brain atrophy relative to Aβ- or *APOE* ε4- cognitively normal patients, especially in those who subsequently convert to a diagnosis of MCI or AD dementia.[16] Individuals with preclinical AD also showed a reduced T1/T2 ratio in the right inferior parietal lobule relative to controls without preclinical AD, suggesting altered myelination in this region in the earliest stages of AD.[9]

Advanced neuroimaging techniques have also been applied to preclinical AD populations and suggested ongoing pathologic changes occurring before the

KEY POINTS

- **AD exists on a continuum of cognitive impairment, from cognitively normal individuals with AD pathophysiology (ie, preclinical AD), to mild impairment (mild cognitive impairment [MCI]), and ultimately clinical dementia (clinical AD dementia) with pathology defined by the amyloid, tau, neurodegeneration (A/T/N) framework.**
- **Patients with AD show widespread degeneration on structural MRI both subcortically, including in the hippocampus, amygdala, basal ganglia, and basal forebrain, and cortically, with the greatest changes in the medial and lateral temporal lobes.**
- **Structural MRI in patients with MCI shows focal atrophy in the medial and lateral temporal lobes, most especially in the entorhinal cortex and hippocampus, which is intermediate between cognitively normal patients and patients with clinical AD dementia, which can predict future progression to dementia.**
- **Patients with preclinical AD with normal cognition but positive AD biomarkers or at least one apolipoprotein E ε4 allele (*APOE* ε4) also show subtle changes in MRI measures of brain structure and function.**

Copyright © American Academy of Neurology. Unauthorized reproduction of this article is prohibited.

onset of cognitive symptoms. Specifically, DWI studies have found white matter integrity loss in tracts known to be affected in MCI and clinical AD, including the cingulum and corpus callosum.[17] Task-based fMRI studies in preclinical AD have shown altered activation during memory tasks, as well as both increased and decreased brain connectivity on resting-state fMRI and changes in cortical hubs and modularity.[18] Arterial spin labeling studies in preclinical AD have shown that *APOE* ε4+ cognitively normal patients show areas of both hyperperfusion and hypoperfusion relative to *APOE* ε4- cognitively normal people, with hyperperfusion in the medial temporal lobe, precuneus, and insula and hypoperfusion in the inferior parietal lobe and middle temporal gyri.[19]

Metabolic and Molecular Imaging Findings in Clinical, Prodromal, and Preclinical Alzheimer Disease

FDG-PET studies in patients with AD show hypometabolism in the lateral parietal, temporal, and secondary visual association cortices, with frontal lobe hypometabolism later in the disease and relative sparing of the primary visual cortex and sensorimotor cortex (**FIGURE 9-2A**).[20] As described later, this pattern is distinct from that seen in DLB, PDD, and frontotemporal dementia, assisting with diagnosis in cases with overlapping symptomatology. In fact, the Centers for Medicare & Medicaid Services approves reimbursement for FDG-PET in cases with an uncertainty of diagnosis; FDG-PET provides considerable improvement of diagnostic certainty in patients (approximately 50% to 60%).[21]

On amyloid-specific molecular imaging, patients with AD show widespread amyloid deposition throughout the cortex and later in the striatum (**FIGURE 9-2A**).[20] Stages of amyloid pathology in AD have been described and validated with postmortem data, namely that amyloid deposition begins in medial parietal and frontal regions, then progresses to encompass most of the cortex, finally showing cortical and subcortical amyloid deposition in the striatum.[22] However, given that amyloid deposition can be found in other dementias and even in cognitively normal patients, the diagnostic use of amyloid imaging is best for ruling out AD by a negative scan rather than for use as a positive diagnostic test.

Tau PET imaging is also widely used in research, and one tracer has been approved by the FDA for clinical use ([^{18}F]flortaucipir). Patients with AD show characteristic tau deposition in the medial and lateral temporal and parietal lobes, as well as frontal lobe deposition in more advanced cases (**FIGURE 9-2A**). Significant tau PET tracer uptake is seen in the temporal, parietal, and frontal lobes, whereas the primary sensory and motor cortices are relatively spared.[23] Higher baseline tau PET burden is associated with faster rates of future atrophy, as well as the topographic pattern of where atrophy occurs.[24] Studies have shown that tau PET techniques are able to recreate the topographic patterns of tau deposition, described in seminal work by Braak and Braak,[25] from neuropathologic assessment, especially in Braak stages IV to VI.[26] As tau PET signal and distribution are more closely associated with symptoms of AD than amyloid, tau PET scans provide important information in both classic and atypical presentations of AD (described in more detail later). Longitudinally, patients with AD dementia show accelerated rates of tau accumulation relative to patients with MCI and those who are cognitively normal.[27] The recent development of additional tracers to study synaptic loss (eg, [^{11}C]UCB-J) and neuroinflammation (eg, mitochondrial 18-kDa translocator protein tracers) has provided additional information in patients with AD dementia. These modalities

Copyright © American Academy of Neurology. Unauthorized reproduction of this article is prohibited.

demonstrate synaptic loss in areas known to show neurodegeneration in AD (ie, medial and lateral temporal lobes) and increased neuroinflammation across the cortex.[28,29]

Similar to MRI findings, patients with MCI tend to have intermediate levels of molecular imaging changes relative to cognitively normal people and patients with AD. Patients with MCI show hypometabolism in temporoparietal, posterior cingulate, and parietal regions on FDG-PET, which can predict future progression to dementia (FIGURES 9-2B and 9-2C).[30] As might be expected, 50% to 75% of patients with MCI show widespread amyloid deposition, most prominently in the medial parietal and frontal lobes.[31] Patients with MCI who are amyloid positive show poorer cognition and a faster rate of cognitive decline and progression to dementia than those who are amyloid negative (FIGURES 9-2B and 9-2C).[32] Tau PET studies in patients with MCI show increased signal primarily in the bilateral medial and lateral temporal lobes, with some patients showing deposition in the parietal and secondary visual association areas (similar to Braak stages V and VI).[23] Amyloid-positive patients with MCI show greater tau deposition than amyloid-negative patients with MCI, with very few individuals showing high tau deposition in the absence of amyloid deposition.[33] In fact, amyloid-negative patients with tau positivity in the cortex have recently been postulated to be false-negative amyloid PET cases.[34] Longitudinal studies have suggested that patients with MCI show a more pronounced rate of accumulation of tau relative to cognitively normal people. Finally, patients with MCI show increased neuroinflammation but only minimal changes in synaptic density.[28,29]

Approximately 25% of cognitively normal people older than 65 years show high levels of amyloid deposition. People who are *APOE* ε4+ and cognitively normal are considerably more likely to show amyloid deposition than people who are *APOE* ε4- and cognitively normal.[16] Amyloid deposition in cognitively normal people is associated with a higher risk of cognitive decline.[35] FDG-PET studies in patients with preclinical AD show mixed results, with some studies showing hypometabolism in AD-like distribution (ie, medial temporal lobe, temporoparietal, cingulate) and others showing hypermetabolism in the prefrontal cortex and temporal lobe.[36] The considerable heterogeneity of this group regarding disease stage, likelihood, proximity to an impaired diagnosis (ie, MCI or AD dementia), and any additional risk factors is likely to affect the consistency of the findings. Finally, Aβ+ cognitively normal patients show higher levels of tau deposition and faster rates of tau accumulation than Aβ- cognitively normal patients.[23] Tau in preclinical AD can also be staged similarly to the Braak staging seen in patients with MCI and AD.[37]

New Developments in Alzheimer Disease Neuroimaging

One major area of development in the field of AD is the development of blood-based tests for amyloid and tau, as well as neurodegeneration. Recent advances in fluid assays have led to the development of sensitive plasma-based biomarkers for detection of amyloid and tau along the continuum of AD. Multiple plasma pTau assays for different phosphorylation sites (pTau181, pTau217, pTau231) have been developed and show excellent prediction of clinical diagnosis, as well as the presence of cerebral amyloid and tau deposition. Studies have shown higher levels of pTau and lower Aβ42/Aβ40 ratios in patients with MCI and AD relative to cognitively normal patients.[38] In addition, strong associations between cerebral measures of amyloid and tau (CSF or PET) and

KEY POINTS

- **Metabolic imaging with fludeoxyglucose (FDG)-PET shows bilateral hypometabolism in patients with clinical AD, as well as intermediate changes in patients with MCI. Patients with preclinical AD may also show altered metabolism, including either increased or decreased metabolism in several brain regions.**
- **Amyloid and tau PET imaging allow for visualization of AD pathology across clinical stages, with most clinically diagnosed AD dementia cases showing extensive amyloid and tau binding. The majority of patients with MCI show amyloid binding with some tau binding, and patients with preclinical AD show cortical amyloid binding and minimal tau signal.**
- **One major area of advancement in the field of AD is the development of blood-based tests that detect amyloid and tau in the plasma. These biomarkers provide excellent prediction of clinical status as well as cerebral amyloid and tau deposition, especially with the plasma phosphorylated tau assays.**

Copyright © American Academy of Neurology. Unauthorized reproduction of this article is prohibited.

plasma pTau and Aβ42/Aβ40 ratios have been seen across groups from preclinical AD to clinical AD stages. These measures are being rapidly developed for clinical use and show excellent ability to improve differential diagnosis and diagnostic accuracy, particularly for detecting cerebral amyloid and tau deposition across disease stages.

Patterns of tau and amyloid spread have also been a topic of recent investigations. The patterns of tau deposition seen on PET, which are a set of anatomically dispersed regions in primarily the temporal and parietal lobes, are often similar to the canonical Braak stages.[25] Recent studies have suggested that, instead of spreading locally in neighboring regions, tau may propagate through the brain along functionally and structurally connected networks.[39] This spreading and the associated neuronal loss is thought to be a major factor in the development of cognitive decline because the deposition of the pathologic proteins causes global network failure. Cross-sectional tau PET studies have reported that areas of high tau deposition tend to follow characteristic patterns that significantly overlap with intrinsic functional and structural networks. Specifically, the earliest tau deposition appears to be in the entorhinal cortex, followed by the amygdala, hippocampus, parahippocampal gyri, fusiform, lateral temporal lobe, and finally to the wider cortex. Longitudinal studies using tau PET support these hypotheses, as Aβ+ patients show a higher rate of tau accumulation in more intrinsically connected regions. Overall, this seeding theory of tau spread fits the current data, but larger and longer longitudinal studies are needed to fully understand this hypothesis.

Amyloid data do not fit the propagation model as well as tau PET but do show areas of early versus late amyloid deposition.[40] Early regions of amyloid deposition, such as the anterior temporal lobe, frontal lobe, medial parietal lobe, cingulate, and precuneus, generally precede later regions, such as the insula, other cortical regions, and the striatum. However, the model of amyloid spread is not as strongly supported by the current data, which suggests that amyloid follows a sigmoidal rate of change over time with low to high deposition rate transition occurring approximately 15 to 17 years before the onset of clinical symptoms.[41] Future studies allowing a better understanding of these processes will be crucial for designing treatments to interfere with the spread and deposition of these pathologic proteins in at-risk patients.

Heterogeneity in Patients With Alzheimer Disease

Despite the consistency of results described above, heterogeneity in cognition and imaging findings is common in patients with AD. One type of heterogeneity is the age of onset of dementia, which can be broadly classified as early-onset AD, with an age of onset younger than 65 years, or late-onset AD, with an age of onset at 65 years or older.[1] Early-onset AD is considerably rarer than late-onset AD with only approximately 5% of all patients with AD showing onset before age 65. However, patients with early-onset AD have been shown to have more severe findings on both MRI and metabolic and molecular imaging measures relative to patients with late-onset AD, with more global atrophy, amyloid deposition, and tau deposition at the same level of cognitive impairment.[42] A recent multisite longitudinal neuroimaging study to investigate early-onset AD, the Longitudinal Early-Onset Alzheimer's Disease Study, will provide additional information about the clinical and biomarker course of these patients.[43]

Heterogeneity in the pattern of cognitive symptoms and anatomic patterns of atrophy and tau deposition has also been widely discussed. Although most

Copyright © American Academy of Neurology. Unauthorized reproduction of this article is prohibited.

patients with AD present initially with memory impairments, other presentations with predominant language impairment, visuospatial impairment, and executive impairment are also seen. Patients with early-onset AD are more likely to show nonmemory-predominant cognitive impairment.[44] Rare subtypes of early-onset AD that present with visuospatial impairment (posterior cortical atrophy) and language impairment (logopenic variant primary progressive aphasia [PPA]) show similar patterns of amyloid deposition to those seen in traditional early-onset AD. However, tau deposition and atrophy patterns in posterior cortical atrophy and logopenic PPA show distinct patterns that match the dominant cognitive symptoms. Namely, posterior cortical atrophy is characterized by tau deposition, hypometabolism, and atrophy in posterior brain regions (ie, parietal and occipital lobes), whereas logopenic variant PPA shows left more than right hemisphere tau deposition, hypometabolism, and atrophy, particularly in temporoparietal regions.[45]

An additional atypical amyloid-related disorder is CAA, in which amyloid deposition primarily occurs in the vessel walls of small cerebral arteries and capillaries rather than in the extracellular space. Although commonly co-occurring with AD, primary CAA features a symptomatic and spontaneous local hemorrhage that can cause focal neurologic symptoms, headache, and altered consciousness.[46] MRI findings in CAA show cerebrovascular damage, most especially microhemorrhages and cortical superficial siderosis that can be assessed by using T2* or SWI sequences or both. Further, because CAA is an amyloid-based disorder, amyloid PET scans demonstrate high amyloid deposition,[47] particularly in the occipital lobe, which is generally indistinguishable from positive amyloid scans from traditional AD with parenchymal amyloid. Finally, a tau PET study indicated increased tau deposition in regions with microbleeds and cortical superficial siderosis in patients with CAA.[48]

Heterogeneity occurs in late-onset AD, although not as commonly or as severely as in early-onset AD. Heterogeneity in cognitive symptoms affecting nonmemory domains can be seen in late-onset AD (FIGURE 9-3[44]).[49,50] Patients with these nonmemory-predominant presentations show different atrophy and FDG hypometabolic patterns than those seen in "traditional AD," which correspond to their domain of most impairment (eg, more posterior in visuospatial-predominant late-onset AD, left more than right in language-predominant AD).[51,52] In addition to the cognitive-defined heterogeneity, tau deposition and atrophy patterns have notable heterogeneity following a pattern previously described in neuropathologic studies. In fact, by using both tau deposition on PET and MRI-based assessments of atrophy patterns, the definition of two or three AD subtypes can be described that differ from the traditional AD atrophy pattern.[44,50] Specifically, recent studies in patients with amyloid-positive MCI and AD dementia have suggested the presence of multiple subtypes, including patients with minimal tau deposition or atrophy in any region, patients with a limbic-predominant presentation defined as focal and severe tau deposition and atrophy in the limbic regions with minimal cortical atrophy, and a hippocampal-sparing pattern defined as a heavy tau deposition or severe atrophy in the cortex with relative sparing of tau deposition and atrophy in the hippocampus and medial temporal lobe. Previous studies have suggested important clinical differences between these subtypes, including a faster clinical progression, lesser likelihood of carrying an *APOE* ε4 allele, and earlier age of

KEY POINTS

- **Tau deposition in AD typically follows a staging system originally defined in the pathologic literature (ie, Braak staging). The findings to date suggest that tau may spread through connected networks in the brain that can be measured using functional imaging (eg, functional resting-state imaging) or structural diffusion imaging.**
- **Although most patients with clinical AD present with memory impairment as the primary symptom, heterogeneity of both clinical symptoms and brain atrophy patterns are observed most commonly in patients with early-onset AD (ie, before the age of 65 years).**
- **Three subtypes of AD include logopenic aphasia, posterior cortical atrophy, and cerebral amyloid angiopathy, which often occur at younger ages and have distinct clinical and neuroimaging signatures on MRI and tau PET but not on amyloid PET (which is broadly positive across all forms).**

Copyright © American Academy of Neurology. Unauthorized reproduction of this article is prohibited.

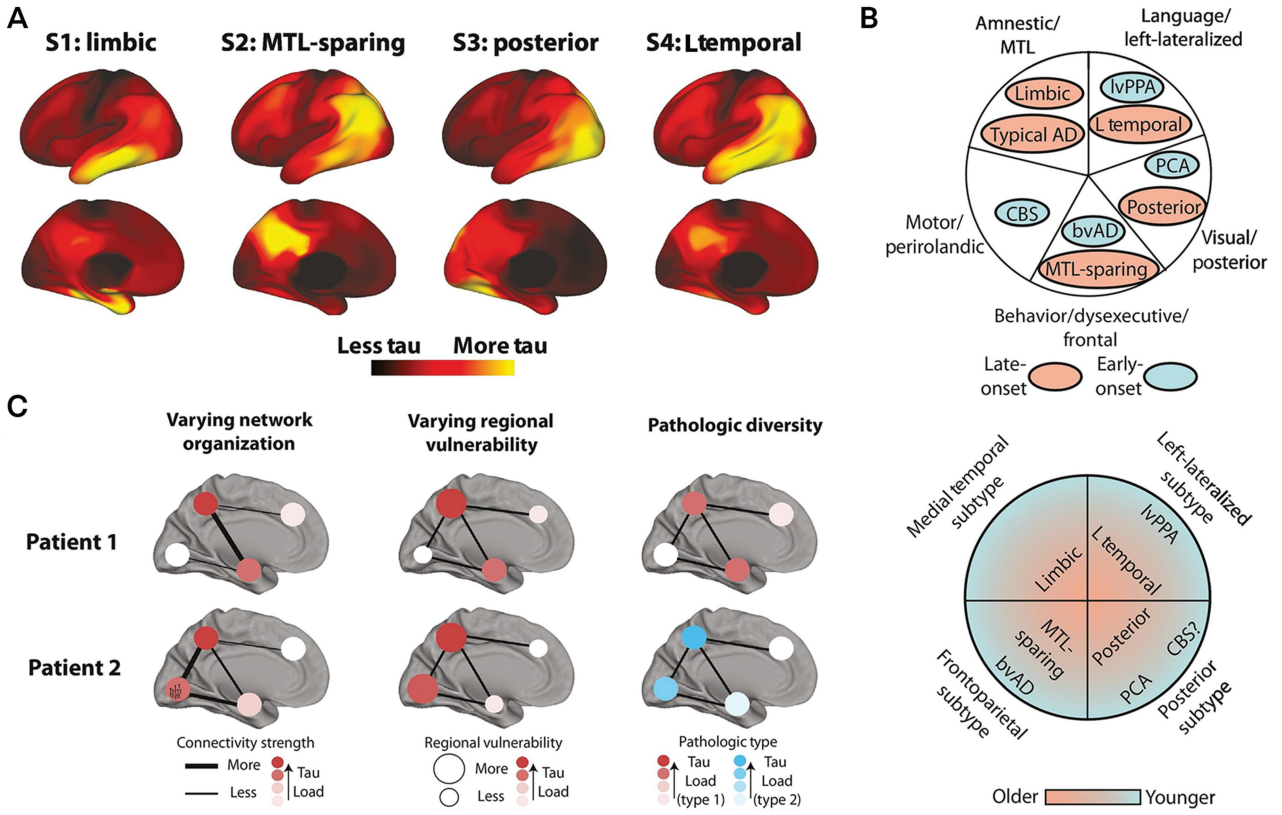

FIGURE 9-3

Conceptualization of heterogeneity in Alzheimer disease (AD). Patients with AD can show heterogeneity in multiple domains, including the patterns of tau deposition, atrophy, and clinical presentation. For example, Vogel and colleagues[49] identified four subtypes (*A*) of tau distribution that mirror those previously seen in studies of brain atrophy.[50] *B* (top), Heterogeneity of phenotypes can be found in late-onset AD, which may often be characterized as a less severe version of the clinically defined atypical variants in early-onset AD, such as logopenic variant primary progressive aphasia (lvPPA), posterior cortical atrophy (PCA), or behavioral variant AD (bvAD). *B* (bottom), Often these heterogeneous atypical phenotypes can be conceptualized as occurring along four different age-associated spectra, such that "atypical" late-onset AD presentations are less extreme expressions of early-onset AD phenotypes. *C*, The causes of these atypical variants are unknown; however, they are hypothesized to be the result of one or more of three different scenarios, including (1) structural variations in axonal connectivity patterns resulting in pathology following an individual network, (2) vulnerabilities in certain regions that cause faster and more severe pathology accumulation in those sites, and (3) the different presentations representing different biological or biophysical diseases causing differential regional spread.

CBS = corticobasal syndrome; L temporal = lateral temporal; MTL = medial temporal lobe; PCA = posterior cortical atrophy; S = subtype.

Reprinted with permission from Vogel JW and Hansson O, Trends Neurosci.[44] © 2022 Elsevier Inc.

onset in hippocampal-sparing AD than traditional AD or limbic-predominant AD. Future treatments developed for AD should consider consistent efficacy in these different subtypes of AD, and perhaps personalized treatments will be needed to address the heterogeneity seen across patients.

VASCULAR COGNITIVE IMPAIRMENT

Vascular cognitive impairment defines dementias that are caused by changes in the cerebrovascular system, including subcortical ischemic vascular dementia,

Copyright © American Academy of Neurology. Unauthorized reproduction of this article is prohibited.

multi-infarct dementia, hemorrhagic dementia, and genetic forms of vascular cognitive impairment such as cerebral autosomal dominant arteriopathy with subcortical infarcts and leukoencephalopathy (CADASIL).[53] The most common type of vascular cognitive impairment is subcortical ischemic vascular dementia, which is often secondary to cardiovascular risk factors such as hypertension, hyperlipidemia, diabetes, and obesity. In subcortical ischemic vascular dementia, cognitive changes are dependent on the location and severity of cerebrovascular damage, strokes, or both. Clinically, patients with vascular cognitive impairment most commonly show impaired executive function and processing speed, as well as potentially headaches, motor changes, apathy, depression, and incontinence, depending on the location and severity of the cerebrovascular insult.

MRI Findings in Vascular Cognitive Impairment

Patients with subcortical ischemic vascular dementia and other types of vascular cognitive impairment most commonly show white matter hyperintensities throughout the white matter of the brain as visualized by T2-weighted or fluid-attenuated inversion recovery (FLAIR) imaging.[54] Other pathologies that can be visualized on MRI include lacunes, prominent perivascular spaces, and cerebral microhemorrhages (FIGURE 9-4). Although these pathologies can be seen in normal aging, the pathology in vascular cognitive impairment or subcortical ischemic vascular dementia is much more severe and widespread than that seen in cognitively normal patients. In addition, patients with vascular cognitive impairment show more extensive white matter hyperintensities and subcortical infarcts and fewer microhemorrhages than patients with CAA. Brain atrophy is also observed globally in gray matter and white matter and is correlated with the extent of white matter hyperintensity burden.[55] DWI studies have also described differences in white matter integrity in vascular cognitive impairment, even in "normal appearing white matter," which are areas of the white matter that do not show apparent cerebrovascular pathology macroscopically and on MRI. Reduced

KEY POINTS

- **Heterogeneity also occurs in late-onset AD, which is linked to different patterns of brain atrophy and FDG hypometabolic patterns. Some of the subtype definitions map to genetic markers (ie, *APOE* ε4), higher rates of clinical progression, and more severe cognitive impairment.**

- **Patients with vascular cognitive impairment most commonly show white matter hyperintensities throughout the white matter of the brain, as well as subcortical infarcts, lacunes, prominent perivascular spaces, and cerebral microhemorrhages on MRI. Although these pathologies can be seen in normal aging, the pathology in vascular cognitive impairment or subcortical ischemic vascular dementia is much more severe and widespread.**

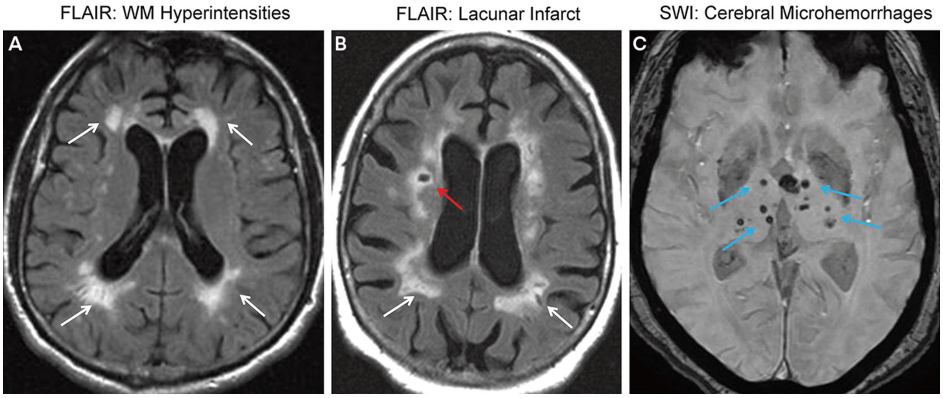

FIGURE 9-4

Example axial MRI scans of vascular cognitive impairment–related pathology. Abnormalities on structural MRI in vascular cognitive impairment are shown on fluid-attenuated inversion recovery (FLAIR) and susceptibility-weighted imaging (SWI). *A*, One example FLAIR image shows white matter (WM) hyperintensities (*white arrows*) in periventricular and subcortical WM regions. *B*, Another FLAIR scan shows a lacunar infarct (*red arrow*) along with WM hyperintensities (*white arrows*). *C*, An example SWI scan shows cerebral microhemorrhages (also known as *microbleeds*) in the basal ganglia and thalamus (*blue arrows*).

Modified with permission from Razek A and Elsebaie N, Clin Imaging.[54] © 2021 Elsevier Inc.

Copyright © American Academy of Neurology. Unauthorized reproduction of this article is prohibited.

white matter integrity in both projection and association fibers in vascular cognitive impairment is associated with severity of dementia, cognitive impairment, motor symptoms, and extent of cerebral atrophy.[56] Both task-based and resting-state fMRI studies have shown alterations in activation and connectivity in patients with vascular cognitive impairment, namely reduced activation during task performance and reduced connectivity of the regions of the cingulate, parietal, and frontal lobes.[57,58] Increased brain connectivity has also been reported, which is associated with the extent of cognitive impairment. Arterial spin labeling studies have shown that a larger white matter hyperintensity burden was associated with lower CBF globally, which was less significant in vascular cognitive impairment without dementia.[59] Finally, quantitative susceptibility mapping has demonstrated higher susceptibility values in vascular cognitive impairment relative to those in cognitively normal patients, especially in the striatum, suggesting greater iron deposition in the caudate and putamen of patients with vascular cognitive impairment.[13] The determination of whether ischemic burden is the primary cause of cognitive impairment or a secondary factor in a clinical patient is difficult considering the high frequency of cerebrovascular disease comorbidity with other disease-causing pathologies. If the patient is negative for other types of copathologies that can be measured in vivo (ie, amyloid, tau) and displays a heavy ischemic burden, that may suggest that the cerebrovascular damage is the primary causative pathology. However, given the current lack of in vivo biomarkers for other important neurodegenerative pathologies (eg, transactive response DNA-binding protein 43 [TDP-43], α-synuclein), some uncertainty remains about concluding that observed vascular damage is the sole cause of cognitive decline.

Metabolic and Molecular Imaging in Vascular Cognitive Impairment

Fewer studies have investigated molecular imaging tools in vascular cognitive impairment because the primary methods for diagnosis and monitoring of

CASE 9-2

A 69-year-old woman presented with a 2-year progressive cognitive decline and sleep difficulties. Recently, she had been experiencing visual hallucinations and advancing motor symptoms, including tremor, muscle rigidity, and balance problems. Her daughter confirmed the symptoms and added that her mother showed increased symptoms of depression and anxiety. Cognitive testing showed memory and executive function impairments, and the neurologic examination showed muscle rigidity and tremor more severe on the left than the right.

COMMENT

This patient likely has dementia with Lewy bodies (DLB). MRI would be ordered to rule out other treatable conditions such as infection and would likely show generalized cerebral atrophy, primarily in posterior regions with relative sparing of the hippocampus. As amyloid and tau PET imaging would be inconclusive because of the frequent co-occurrence of these pathologies in DLB, SPECT imaging targeted to dopamine transporter levels showing reduced uptake in the striatum would help support the diagnosis.

Copyright © American Academy of Neurology. Unauthorized reproduction of this article is prohibited.

vascular cognitive impairment are MRI based. FDG-PET imaging has demonstrated that patients with vascular cognitive impairment have multifocal hypometabolism, which often presents in an asymmetric or scattered pattern or both.[60] This hypometabolism can be cortical or subcortical or both and found near arteries or watershed regions of the brain. Unlike in AD, patients with vascular cognitive impairment may show pronounced hypometabolism in the primary sensorimotor cortex. Amyloid and tau PET studies generally show minimal tracer binding, which can distinguish vascular cognitive impairment from CAA.[53]

COMORBIDITY OF CEREBROVASCULAR DISEASE WITH OTHER DEMENTIA PATHOLOGIES

The majority of dementia cases that come to autopsy have more than one pathologic finding, most commonly AD pathology and small vessel disease, especially in older patients.[61] In life, AD often presents as mixed dementia, reflecting the presence of AD pathophysiology and one or more other suspected pathologies. At this time, only AD and vascular pathologies can be visualized in vivo, because other notable pathologies (eg, α-synuclein, TDP-43, fused in sarcoma [FUS]) can be assessed only at autopsy. Patients with mixed AD and vascular pathologies show greater levels of white matter hyperintensities and more advanced white matter degeneration on structural MRI and DWI relative to those with AD only or vascular cognitive impairment only.[62] Mixed dementia cases have also been shown to have more rapid degeneration in motor function, such as gait and grip strength.[63] Cerebrovascular risk factors in both cognitively impaired patients and cognitively normal patients provide additive risk for cognitive decline, although this may vary by ethnicity, as well as more prominent perivascular spaces and white matter hyperintensities on MRI.[64] Overall, the mixed dementia cases are an important and frequently observed phenomenon that should be considered during the development of novel therapeutic interventions and pharmaceuticals.

PARKINSON DISEASE DEMENTIA AND DEMENTIA WITH LEWY BODIES

Lewy bodies, which represent pathologic protein aggregations of α-synuclein, are the main pathologic characteristic of Parkinson disease (with or without dementia), DLB (illustrated in CASE 9-2), and multiple system atrophy (MSA).[65] These pathologic aggregates may also co-occur in patients with other primary proteinopathies (eg, AD, FTLD) or cerebrovascular damage, leading to mixed pathology, as well as cognitive and motor symptoms. PDD and DLB are diseases along the same continuum with the distinguishing factor being the sequence of onset of motor versus cognitive symptoms. In other words, motor symptoms are diagnosed first in PDD and followed by cognitive impairment, whereas DLB is defined as the opposite (cognitive symptoms came before the motor symptoms). Therefore, the authors of this article discuss these diseases simultaneously, noting that patients with PDD tend to have less severe cerebral pathologies than patients with DLB.[66] DLB-associated and PDD-associated cognitive decline is primarily observed in executive function, attention, and higher-order visuospatial processing domains, which can fluctuate in severity, as well as visual hallucinations and delusions, rapid eye movement (REM) behavior disorder, and parkinsonian symptoms. MSA is a class of rare Lewy body–related diseases, including olivopontocerebellar atrophy, Shy-Drager syndrome, and striatonigral

KEY POINTS

- FDG-PET imaging has demonstrated that patients with vascular cognitive impairment have multifocal hypometabolism, which often presents in an asymmetric or scattered pattern or both. This hypometabolism can be cortical or subcortical or both and found near arteries or watershed regions of the brain.
- The majority of dementia cases that come to autopsy have more than one pathologic finding, most commonly AD pathology and small vessel disease, especially in older patients. In life, AD often presents as mixed dementia, reflecting the presence of AD pathophysiology and one or more other suspected pathologies.
- Parkinson disease dementia (PDD) and dementia with Lewy bodies (DLB) are diseases along the same continuum with the distinguishing factor being the sequence of onset of motor versus cognitive symptoms.

Copyright © American Academy of Neurology. Unauthorized reproduction of this article is prohibited.

degeneration. Patients with MSA show parkinsonian symptoms of varying severity, cerebellar ataxia, and prominent autonomic dysfunction in the case of Shy-Drager syndrome.[67] These patients are now divided into parkinsonian type MSA and cerebellar ataxia type MSA, based on their predominant symptoms.

MRI Findings in Dementia With Lewy Bodies, Parkinson Disease Dementia, and Multiple System Atrophy

Patients with DLB show cortical atrophy on structural MRI, particularly in the insula, middle and posterior cingulate, superior temporal-occipital areas, lateral orbitofrontal lobe, other regions of the frontal lobe, inferior parietal lobe, temporal lobe, and occipital lobe. Patients with PDD show atrophy in similar regions, with less severity in cortical regions than that in patients with DLB.[66] Relative to patients with AD, patients with DLB and PDD show relative sparing of the medial temporal lobe (FIGURE 9-5A). Approximately half of patients with DLB show marked amyloid deposition, suggesting comorbid pathologies.[69] Aβ+ patients with DLB and PDD show more global atrophy than Aβ- patients with DLB and PDD, as do patients with DLB and PDD with comorbid cerebrovascular disease represented by a higher white matter hyperintensity burden.[66] Longitudinally, patients with DLB and PDD show a faster rate of atrophy in the medial temporal lobe, lateral temporal lobes, and temporal-occipital areas, which is generally more

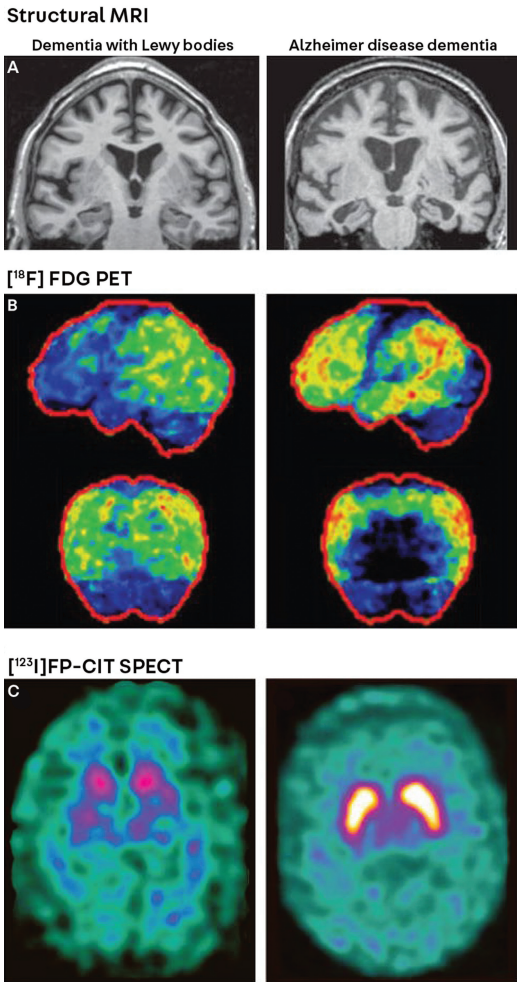

FIGURE 9-5

Imaging findings in dementia with Lewy bodies (DLB) relative to Alzheimer disease (AD). *A*, Representative structural coronal MR images show relatively spared hippocampal volume in the patient with DLB relative to the patient with AD dementia. *B*, Areas of glucose hypometabolism are highlighted (blue to red scale), with the hottest colors showing the areas with the most loss of glucose metabolism. The patient with DLB shows glucose hypometabolism in the primary occipital lobe and parietal lobe, whereas the patient with AD shows mostly lateral parietal and frontal hypometabolism. *C*, [123I]FP-CIT single-photon emission computed tomography (SPECT) imaging of dopamine transporters shows significant reductions in dopaminergic transmission in the striatum of the patient with DLB, with preserved function in the patient with AD.

[18F]FDG = fludeoxyglucose; PET = positron emission tomography.

Modified with permission from Walker Z, et al, Lancet.[68]

© 2015 Elsevier Inc.

Copyright © American Academy of Neurology. Unauthorized reproduction of this article is prohibited.

severe in DLB than PDD.[70] MRI in patients with MSA shows atrophy of the cerebellum, pons, thalamus, substantia nigra, and parietal and occipital lobes.[71] One characteristic (but nonspecific) sign of MSA can be found by using T2-weighted imaging, which shows a cruciform hyperintensity in the pons that is known as the *hot cross buns sign*.[72] Longitudinally, patients with MSA, relative to cognitively normal patients, show increased atrophy rates in the cerebellum, pons, and midbrain, which are associated with declines in cognition[73] and the development of extrapyramidal, cerebellar, and autonomic features.

Advanced MRI studies have also shown alterations in white matter integrity, brain function, CBF, and iron deposition in patients with DLB, PDD, and MSA. In patients with DLB and PDD, DWI studies demonstrate significant loss of white matter integrity in the corpus callosum, longitudinal fasciculi, and frontal, parietal, and occipital white matter, with more severe findings seen in DLB relative to PDD.[74] Reduced structural connectivity in the default-mode network and visual networks are also seen in DLB and PDD.[74] Patients with MSA show reduced white matter integrity in the brainstem, cerebellar, and subcortical regions on DWI, which is associated with the severity of ataxia symptoms.[75] Task-based fMRI studies have observed altered activation in patients with DLB and PDD during visual and executive tasks, including reduced activation in occipital-temporal areas and hyperactivation in the superior temporal sulcus.[76] Patients with PD and MCI showed reduced activation during a working memory task in the middle frontal gyrus and parietal lobule relative to PD patients without cognitive impairment and cognitively normal people.[77] A task-based fMRI study in patients with MSA demonstrated reduced activation in motor control areas during a grip force task.[71] Resting-state fMRI studies in DLB and PDD show reduced functional connectivity in motor-related regions, executive control network, salience network, frontoparietal network, and the default-mode network.[78] Patients with MSA also show altered connectivity on resting-state fMRI studies with areas of both increased and decreased connectivity in motor and sensory regions.[79]

Arterial spin labeling studies in DLB and PDD show hypoperfusion in the cuneus, precuneus, anterior cingulate, and parietal-occipital cortices, as well as the cerebellum and caudate, with relative sparing of the posterior cingulate compared with patients with AD (ie, cingulate island sign).[80] Patients with PD without dementia who convert from normal cognition to MCI have hypoperfusion in the prefrontal cortex and anterior cingulate, which is associated with cognitive function.[81] Patients with MSA have hypoperfusion in the cerebellum, particularly those with cerebellar ataxia type MSA versus parkinsonian type MSA.[82]

Quantitative susceptibility mapping studies have demonstrated increased iron deposition in PDD and DLB, specifically in the brainstem, thalamus, globus pallidum, putamen, and hippocampus, whereas patients with MSA show greater iron deposition in the putamen and brainstem.[13] In addition, the SWI scans used to perform quantitative susceptibility mapping also provide imaging of iron deposition in nigrosomes, which are small bundles of dopaminergic cells in the substantia nigra pars compacta.[83] When intact, this area shows a hyperintense signal that resembles the tail of a swallow, called the *swallow tail sign*. Patients with DLB show a loss of the swallow tail sign on SWI scans.[84]

KEY POINTS

- **Patients with DLB and PDD show widespread cortical atrophy on structural MRI, particularly in the posterior cortical regions and relative sparing of the medial temporal lobe compared with patients with AD.**
- **MRI in patients with multiple system atrophy shows atrophy of the cerebellum, pons, thalamus, substantia nigra, and the parietal and occipital lobes. One characteristic (but nonspecific) sign of multiple system atrophy can be found using T2-weighted imaging, which shows a cruciform hyperintensity in the pons known as the *hot cross buns sign*.**

Copyright © American Academy of Neurology. Unauthorized reproduction of this article is prohibited.

Metabolic and Molecular Imaging in Parkinson Disease Dementia, Dementia With Lewy Bodies, and Multiple System Atrophy

FDG studies in PDD and DLB show hypometabolism in the striatum, cerebellum, frontal and parietal lobes, and the occipital lobe, including the primary visual cortex, with relative sparing of the hippocampus (FIGURE 9-5B).[85] One of the more distinctive patterns in DLB and PDD is the presence of the cingulate island sign, which is a relative preservation of metabolism in the posterior cingulate relative to the surrounding parietal and occipital lobes. Patients with MSA have decreased glucose metabolism in the cerebellum and putamen that does not correlate with dopaminergic changes.[86] Amyloid PET studies have demonstrated amyloid deposition in more than half of patients with DLB but with lesser severity than in patients with AD.[69] Patients with PDD less frequently show amyloid positivity than those with DLB. However, compared with patients with AD, patients with PDD and DLB show more tracer uptake in the primary visual cortex, which is associated with a faster decline in visuospatial function and progression to dementia. Patients with MSA rarely have a positive amyloid PET. Tau PET studies in PDD and DLB show increased tau in the inferior temporal gyrus and precuneus, predominantly in patients with DLB who are amyloid positive.[87] An MSA case study also showed increased tau deposition in the striatum, midbrain, thalamus, and brainstem, as well as frontal, parietal, and temporal lobes.[88] However, tau deposition in these disorders is likely secondary to comorbid amyloid pathology rather than the Lewy body pathology. Finally, a 2021 conference report demonstrated in vivo use of a novel PET tracer called *ACI-12589* that is sensitive and specific to α-synuclein in patients with DLB, PDD, and MSA.[89]

CASE 9-3

A 53-year-old right-handed woman presented with progressive loss of speech generation, grammatical errors, and slowed speech. She recently stopped working as a bank manager because of these difficulties. Her sister reported the changes had been progressing for about 3 years and indicated that the patient had additional problems with decision making and managing finances. Cognitive testing showed grammatical errors and impaired speech production, confrontation naming, and sentence comprehension.

COMMENT

This patient may have progressive nonfluent aphasia, although other language disorders could be considered. MRI scans would be ordered to rule out comorbid or other treatable conditions. If a patient has progressive nonfluent aphasia, notable atrophy will be seen in the left perisylvian and insular regions, as well as the left temporal and inferior frontal lobes. An amyloid positron emission tomography (PET) scan would likely be negative but could help distinguish progressive nonfluent aphasia from logopenic variant Alzheimer disease. Tau PET scans may show increased binding in the left temporal and frontal lobes; however, the disease could be a transactive response DNA-binding protein 43 (TDP-43) proteinopathy as well. Symptomatology and MRI atrophy findings would be the best supportive evidence for the diagnosis.

Copyright © American Academy of Neurology. Unauthorized reproduction of this article is prohibited.

Unique to DLB and other Lewy body diseases, PET and SPECT measures of dopaminergic neurotransmission represent excellent biomarkers for differential diagnosis.[90] Specifically, SPECT and PET studies targeting the dopamine transporter (DAT) with [^{123}I]FP-CIT and dopamine receptors (ie, D2 receptors) have shown reduced tracer binding in the striatum and cortex in DLB and PDD, which can differentiate DLB from AD (FIGURE 9-5C).[91] Some anatomic specificity of dopaminergic alterations has also been observed in PDD and DLB, with decreased DAT binding in the caudate associated with cognitive symptoms, whereas DAT reductions in the putamen are associated with motor symptoms. In MSA, DAT-SPECT shows reduced binding in the striatum that is associated with disease severity and duration in parkinsonian type MSA but not in cerebellar ataxia type MSA.[86] However, none of the imaging measures of dopaminergic neurotransmission can distinguish between different parkinsonian syndromes (eg, DLB, PDD, MSA).

FRONTOTEMPORAL LOBAR DEGENERATION

As the name implies, FTLD diseases feature degeneration of primarily the frontal or temporal lobes or both. Broadly, FTLD disorders can be classified into two forms based on symptomatology: (1) behavioral variant FTLD, in which patients show behavioral disturbances, along with cognitive decline in executive function and, later in the disease, multiple cognitive domains; and (2) PPAs, which feature language impairments of multiple types. One language-predominant FTLD syndrome is semantic dementia, in which patients show aphasia characterized by impairment in semantic memory and single-word comprehension and, later in the disease, behavioral symptoms similar to behavioral variant FTLD. Another is progressive nonfluent aphasia (illustrated in CASE 9-3), featuring speech production difficulties with agrammatism, phonemic errors, and anomia. Finally, logopenic variant PPA is a variant of AD (described earlier) with characteristic word-retrieval problems, phonologic errors, and impaired repetition.[92]

In addition, several FTLD syndromes can feature extrapyramidal or motor symptoms[92] with the FTLD and parkinsonism spectrum. The first disorder is corticobasal degeneration (CBD),[72] which features cognitive impairment, mostly in executive function or aphasia, and markedly asymmetric apraxia, akinesia, limb rigidity, focal myoclonus, dystonia, and alien limb syndrome. Another parkinsonian FTLD is progressive supranuclear palsy (PSP), which features symmetric bradykinesia, truncal rigidity, postural instability, pseudobulbar syndrome with dysarthria and dysphagia, and supranuclear palsy of vertical gaze, as well as cognitive and/or behavioral changes.[72] Finally, FTLD with motor neuron disease, also called *FTLD-amyotrophic lateral sclerosis* (FTLD-ALS), demonstrates progressive muscle weakness and wasting, hyperreflexia, spasticity, and respiratory failure, as well as behavioral and cognitive symptoms.[93] Pathology associated with FTLD is generally caused by pathologic deposition of either tau or TDP-43, a TAR DNA-binding protein. Behavioral variant FTLD, progressive nonfluent aphasia, CBD, and PSP are most commonly associated with tau deposition, whereas semantic dementia and FTLD-ALS are commonly associated with TDP-43 deposition (or in rare cases deposition of FUS protein). Onset of FTLD most commonly occurs before the age of 60, although it can happen later in rare cases. A longitudinal multisite observational clinical and biomarker study, called *The ALLFTD Study*, is ongoing and will

KEY POINTS

- FDG-PET studies in PDD and DLB show hypometabolism in the cortex, including the primary visual cortex, with relative sparing of the hippocampus, most distinctively showing the cingulate island sign, which is a relative preservation of metabolism in the posterior cingulate relative to the surrounding parietal and occipital lobes.
- Unique to DLB and PDD, PET and single-photon emission computed tomography (SPECT) measures of dopaminergic neurotransmission are excellent biomarkers for differential diagnosis, with tracers targeting the dopamine transporter and dopamine receptors (ie, D2 receptors) showing reduced binding in the striatum and cortex.
- Frontotemporal lobar degeneration (FTLD) disorders can be classified into two forms by symptoms: (1) behavioral variant FTLD, in which patients show behavioral disturbances among other symptoms; and (2) primary progressive aphasias, which feature language impairments of multiple types.
- FTLD syndromes can feature extrapyramidal or motor symptoms with the FTLD and parkinsonism spectrum consisting of corticobasal degeneration (CBD) and progressive supranuclear palsy (PSP), as well as FTLD with motor neuron disease (or FTLD-amyotrophic lateral sclerosis).

Copyright © American Academy of Neurology. Unauthorized reproduction of this article is prohibited.

provide new data about important biomarker and pathologic findings in this group of diseases.[94]

MRI Findings in Frontotemporal Lobar Degeneration

Patients with behavioral variant FTLD show frontal and temporal lobe atrophy, including the frontomedial cortex, basal ganglia, anterior insula, thalamus, anterior cingulate, orbitofrontal cortex, and deep gray matter structures (FIGURE 9-6[95]).[96] However, the atrophy pattern observed in behavioral variant FTLD can vary by underlying pathology (ie, tau versus TDP-43).[97] Studies of patients with behavioral variant FTLD due to tauopathy demonstrate atrophy in the prefrontal cortex, temporal lobe, anterior cingulate, and insula, which is typically bilateral but with slightly left more than right atrophy. In extreme cases (eg, Pick disease), the atrophy of the frontal lobes is so pronounced that it gives them a knifelike appearance. Patients with behavioral variant FTLD with TDP-43

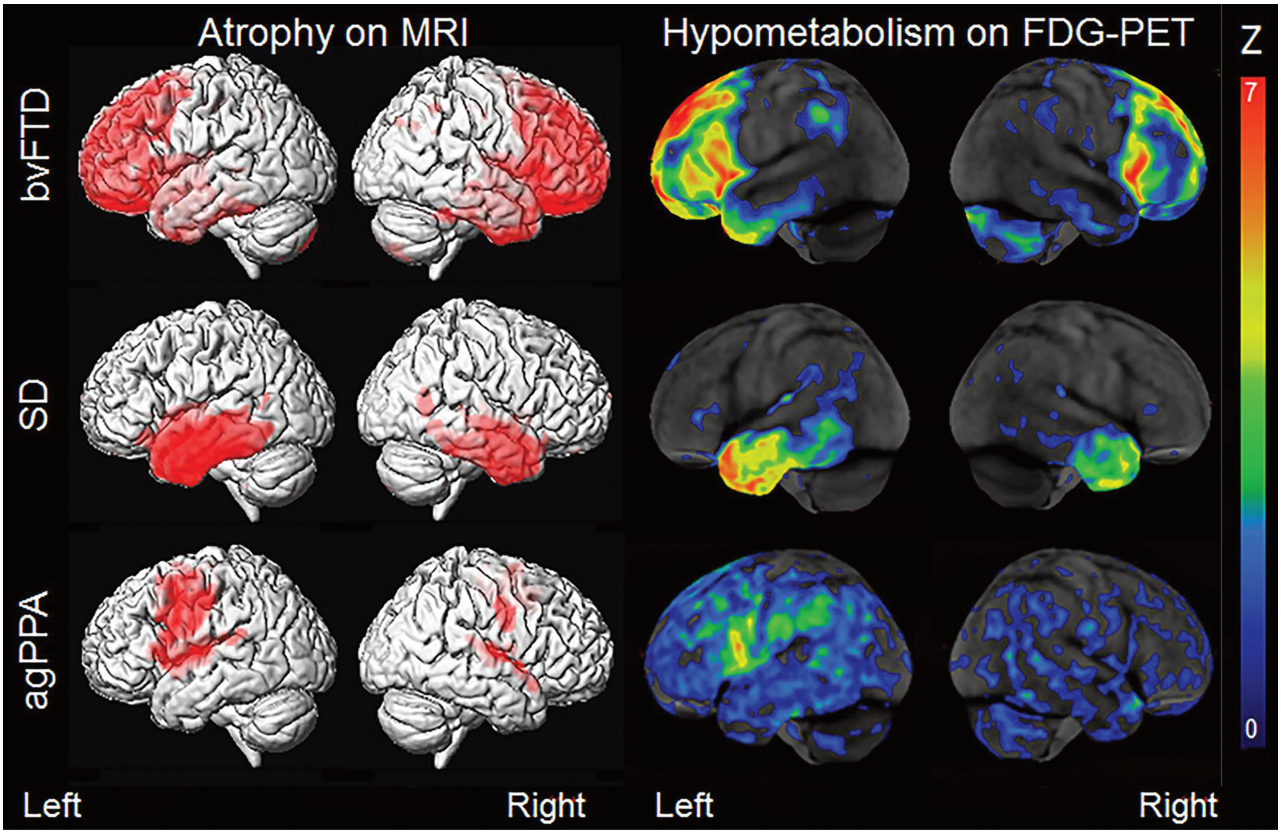

FIGURE 9-6

Atrophy and hypometabolism in frontotemporal dementia spectrum disorders. The two columns on the left show group-level differences between patients with the indicated clinical frontotemporal lobar degeneration (FTLD) syndromes compared with cognitively normal controls visualized on three-dimensional rendered surfaces of the brain (atrophy on MRI). The two columns on the right show hypometabolism in the three FTLD syndromes displayed as z score deficit maps for individual patients compared with controls.

agPPA = agrammatic primary progressive aphasia; bvFTD = behavioral variant frontotemporal dementia; FDG = fludeoxyglucose; MRI = magnetic resonance imaging; PET = positron emission tomography; SD = semantic dementia.

Modified with permission from Whitwell JL, Prog Mol Biol Transl Sci.[95] © 2019 Elsevier Inc.

Copyright © American Academy of Neurology. Unauthorized reproduction of this article is prohibited.

pathology show frontal, temporal, and parietal atrophy, which tends to be asymmetric (either side can be predominant). Differentially, parietal atrophy is greater in patients with TDP-43 behavioral variant FTLD, whereas the frontal atrophy in behavioral variant FTLD due to tauopathy is usually greater than that seen in TDP-43 forms. Longitudinally, patients with behavioral variant FTLD show an increased atrophy rate in the frontal and temporal lobes, regardless of underlying pathology.[98] Alternatively, patients with semantic dementia show focal atrophy of the anterior inferior temporal lobe, with an asymmetric (left more than right) pattern (FIGURE 9-6).[96] Patients with semantic dementia also show atrophy in the left subcallosal area, temporal lobe, amygdala, hippocampus, and perirhinal cortex. Longitudinally, patients with semantic dementia show a high rate of progressive atrophy in the left more than right temporal lobe.[98]

Patients with progressive nonfluent aphasia show asymmetric perisylvian and anterior insular atrophy with the dominant language hemisphere most affected (usually the left hemisphere in right-handed people) (FIGURE 9-6). In addition, atrophy is observed in the frontal operculum (eg, Broca area), temporal pole, lentiform nucleus, inferior and middle frontal gyri, premotor cortex, and the dorsolateral prefrontal cortex, spreading to other frontal, parietal, and temporal lobes, as well as the caudate and thalamus in later stages. If the progressive nonfluent aphasia is caused by a tauopathy, patients have more severe temporal atrophy than in other forms.[97] Longitudinally, the frontal lobe of patients with progressive nonfluent aphasia shows a high rate of atrophy that is twice as fast as even patients with AD.[98]

Patients with CBD show asymmetric atrophy of the frontal and parietal lobes without sparing of the primary motor and sensory cortices, as well as the basal ganglia contralateral to the side most affected with rigidity and apraxia (FIGURE 9-7A).[99] Alternatively, structural MRI studies in patients with PSP show significant midbrain atrophy, particularly in comparison with the neighboring pons, which is more severe than that seen in CBD (FIGURE 9-7B).[99] This atrophy pattern, which is characteristic for PSP, has been described as the *hummingbird sign* on a sagittal view and the *Mickey Mouse sign* or *morning glory sign* on an axial view.[100] Patients with PSP also show atrophy in the posterior frontal lobe, premotor cortex, supplementary motor area, caudate nucleus, brainstem, and cerebellum.[92] Longitudinally, patients with CBD and PSP show accelerated cortical and subcortical atrophy rates, with faster atrophy in CBD than in PSP.[101] Finally, patients with FTLD-ALS show atrophy in the frontal and temporal lobes, as well as the anterior cingulate, occipital lobe, and precentral gyrus, which is more severe in patients with FTLD-ALS than in patients with ALS and no FTLD symptoms.[97]

Abnormalities in patients with FTLD have also been observed on advanced MRI techniques, such as DWI, fMRI, arterial spin labeling, and quantitative susceptibility mapping. DWI studies in behavioral variant FTLD show reduced white matter integrity in the salience network, a set of interconnected regions that includes the anterior cingulate and insula, as well as tracts connecting the frontal and temporal lobes, including the anterior superior longitudinal fasciculus, inferior longitudinal fasciculus, inferior frontal-occipital fasciculus, uncinate fasciculus, anterior cingulum, and parts of the corpus callosum.[102] Diffusion tensor imaging studies of patients with semantic dementia have shown significant white matter integrity loss in the left uncinate fasciculus, left inferior longitudinal fasciculus, and left parahippocampal white matter, with the lowest

KEY POINTS

- Patients with behavioral variant FTLD generally show frontal and temporal lobe atrophy, as well as atrophy in the basal ganglia, thalamus, and other deep gray matter structures, but can vary by underlying pathology (ie, tau versus transactive response DNA-binding protein 43 [TDP-43]).
- Patients with semantic dementia show focal MRI atrophy of the anterior and inferior temporal lobe, with an asymmetric (left more than right) pattern in most cases.
- Patients with progressive nonfluent aphasia show asymmetric perisylvian and anterior insular atrophy with the dominant language hemisphere most affected (usually the left hemisphere in right-handed individuals), as well as in the frontal and temporal lobe (eg, Broca area).
- Patients with CBD show asymmetric atrophy of the frontal and parietal lobes without sparing of the primary motor and sensory cortices, as well as the basal ganglia contralateral to the side most affected with rigidity and apraxia.
- Structural MRI studies in patients with PSP show significant midbrain atrophy, particularly in comparison with the neighboring pons, which is more severe than that seen in CBD. This atrophy pattern has been described as the *hummingbird sign* on sagittal view and the *Mickey Mouse sign* or *morning glory sign* on axial view.

Copyright © American Academy of Neurology. Unauthorized reproduction of this article is prohibited.

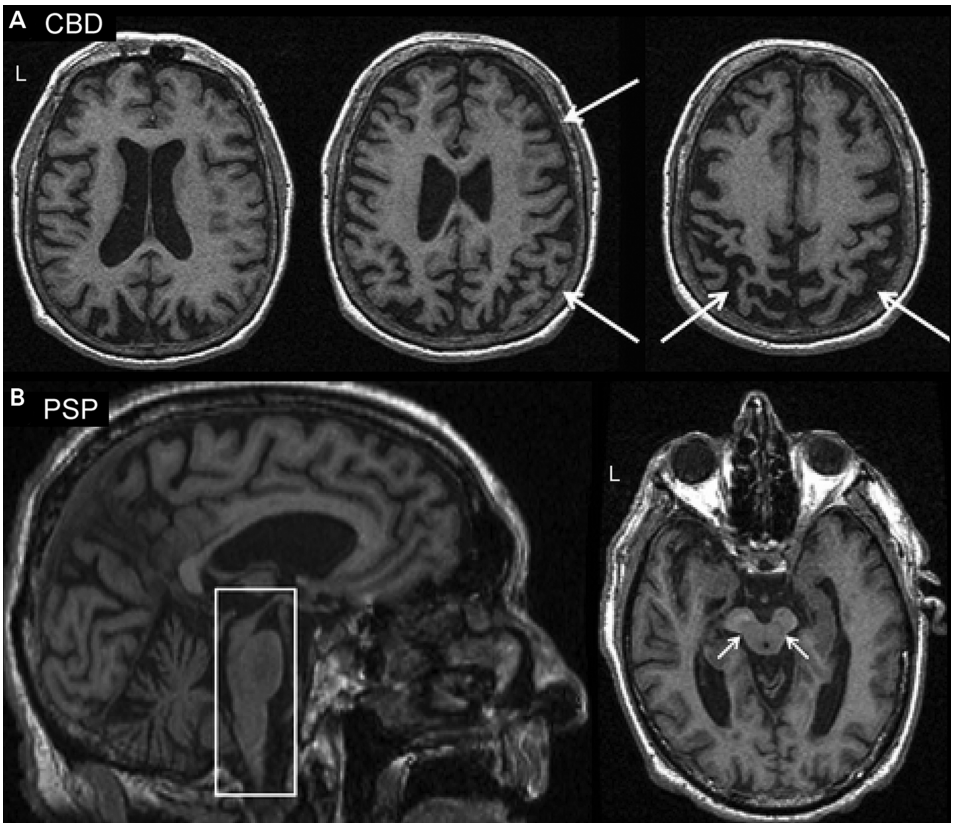

FIGURE 9-7

Structural MRI in corticobasal degeneration (CBD) and progressive supranuclear palsy (PSP). Axial sections from a structural MRI scan from a patient with CBD (*A*) show atrophy in the frontal and parietal lobes (*arrows*), while sagittal and axial views of a structural MRI scan (*B*) from a patient with PSP show two hallmark findings, the hummingbird sign, which represents midbrain atrophy relative to the pons (*box*), and the Mickey Mouse sign or morning glory sign, which represents atrophy of the midbrain (*arrows*).

Modified with permission from Risacher SL and Saykin AJ, Handb Clin Neurol.[5] © 2019 Elsevier Inc.

integrity values in the left anterior temporal lobe.[102] Patients with progressive nonfluent aphasia show white matter degeneration on DWI in frontoparietotemporal pathways, including the uncinate fasciculus, arcuate fasciculus, parts of the superior longitudinal fasciculus, and the superior motor pathway.[102] Decreased white matter integrity in patients with progressive nonfluent aphasia is primarily seen in the regions with gray matter atrophy, including the left perisylvian region, inferior frontal gyrus, insula, and supplementary motor area. In patients with CBD, DWI studies show a loss of white matter integrity in the motor regions of the thalamus, precentral and postcentral gyri, and the bilateral supplementary motor area.[102] Alternatively, patients with PSP show decreased white matter integrity on DWI studies in the superior longitudinal fasciculus, thalamus, cingulum, primary motor cortex, supplementary motor area, and frontal-orbital white matter.[102] Reduced structural connectivity in the cerebellothalamic network is also observed in patients with PSP. Patients with CBD show longitudinal white matter integrity loss in the basal ganglia and cortex, whereas patients with PSP show white matter loss in the superior cerebellar peduncles and caudate.[103] Finally, patients with

Copyright © American Academy of Neurology. Unauthorized reproduction of this article is prohibited.

FTLD-ALS show reduced white matter integrity on DWI studies in the frontal and temporal lobes, corpus callosum, corticospinal tract, inferior longitudinal fasciculus, inferior frontal-occipital fasciculus, and uncinate fasciculus, which are associated with poorer cognition.[104] Longitudinal DWI studies in FTLD-ALS show progressive degeneration of white matter motor tracts.[105]

Task-based fMRI studies in behavioral variant FTLD have shown attenuated frontal activation during working memory, as well as abnormalities during facial expression tasks.[106] In resting-state fMRI studies, patients with behavioral variant FTLD demonstrate significantly reduced salience network connectivity, which predicts worsening behavioral symptoms and dementia, and changes in default-mode network connectivity, although reports have been conflicting.[107] Patients with behavioral variant FTLD also show disrupted internetwork connectivity and a lack of frontal lobe cortical hubs on resting-state fMRI.[108] In task-based fMRI studies, some patients with semantic dementia show impaired activation in temporal regions during reading,[109] whereas others show normal activation.[110] Other task-based fMRI studies have shown impairments in patients with semantic dementia on a variety of language-related tasks, including sound processing, autobiographic memory, and surface dyslexia.[109] Resting-state fMRI studies in patients with semantic dementia show reduced functional connectivity of the left anterior temporal lobe and frontolimbic circuitry, with increased connectivity in local prefrontal cortex networks.[107] Reduced left lateralized functional connectivity in the temporal, occipital, and frontal lobes, as well as in the amygdala, hippocampus, and caudate, were also observed in patients with semantic dementia.

Alternatively, patients with progressive nonfluent aphasia show reduced activation in the posterior inferior frontal cortex during sentence complexity, reading, and comprehension tasks in task-based fMRI studies.[111] Resting-state fMRI studies in progressive nonfluent aphasia show alterations in the inferior frontal and insular speech and language network, as well as language networks more broadly.[112]

Patients with FTLD with motor symptoms also show functional deficits during task-based fMRI of motor tasks. Reduced activation in the premotor cortex, with a corresponding increase in parietal activation, was observed in patients with CBD during a limb apraxia task,[113] whereas patients with PSP have shown altered activation during both a grip-force task and a mental-imagery task (imagining lying, standing, walking, or running), including reduced activation in the basal ganglia, primary motor and premotor cortex, and frontal and temporal lobes.[114] In patients with CBD, a resting-state fMRI study found disruption of multiple resting-state networks, including the lateral visual and auditory networks.[115] Resting-state fMRI studies in patients with PSP have shown decreased functional connectivity in the thalamus, caudate, anterior cingulate, dorsolateral prefrontal cortex, supramarginal gyrus, temporal-occipital cortex, supplementary motor area, and cerebellum. Other resting-state fMRI studies in patients with PSP have demonstrated reduced functional connectivity in the default-mode network and salience network, along with the thalamus, striatum, cerebellum, and premotor cortex.[115] Finally, task-based fMRI studies in patients with FTLD-ALS have demonstrated reduced activation in the frontal lobe, insula, and thalamus during an executive task, in the frontal lobe during an emotional task, and in the frontal lobe, anterior cingulate, supramarginal gyrus, temporal lobe, and occipitotemporal regions during a verbal fluency task.[116]

KEY POINT

- **Patients with FTLD-ALS show atrophy in the frontal and temporal lobes, as well as the anterior cingulate, occipital lobe, and precentral gyrus, which is more severe in patients with FTLD-ALS than in patients with ALS and no FTLD symptoms.**

Copyright © American Academy of Neurology. Unauthorized reproduction of this article is prohibited.

A resting-state fMRI study in presymptomatic FTLD-ALS demonstrated increased functional connectivity between the cerebellum and precuneus, cingulate, and middle frontal lobes.[104]

Studies using arterial spin labeling to measure CBF in FTLD syndromes have demonstrated hypoperfusion in areas that largely overlap with the patterns of atrophy seen in each disease subtype. Specifically, patients with behavioral variant FTLD show hypoperfusion in the frontal and temporal lobes, as well as the anterior cingulate cortex.[117] Patients with semantic dementia show left more than right temporal lobe hypometabolism, including in the anterior temporal lobe, middle temporal gyrus, and fusiform gyrus.[118] Alternatively, an arterial spin labeling study in patients with progressive nonfluent aphasia demonstrated hypoperfusion in the left temporal lobe, insula, frontal pole, and perisylvian region.[118] CBD and PSP both show hypoperfusion in cortical and subcortical regions, as well as the midbrain, relative to that seen in cognitively normal patients.[118] Finally, patients with FTLD-ALS show hypoperfusion in the left frontal and temporal lobes relative to that in patients with ALS without cognitive impairment and cognitively normal people.[119] Quantitative susceptibility mapping studies of iron deposition in FTLD syndromes have primarily been focused on the syndromes with motor symptoms, including CBD, PSP, and FTLD-ALS.[13] Specifically, patients with PSP show increased iron deposition in the striatum, midbrain, and brainstem, whereas patients with CBD show increased susceptibility (representing increased iron) in the corticomedullary junction and superficial gray matter. Finally, patients with FTLD-ALS have consistently shown increased iron deposition in the motor cortex, striatum, brainstem, and hippocampus relative to patients with non-FTLD ALS and cognitively normal patients.

Metabolic and Molecular Imaging in Frontotemporal Lobar Degeneration

The majority of molecular imaging studies in FTLD have been performed with FDG-PET or tau PET tracers because amyloid PET shows no significant signal in patients with FTLD of any type (aside from logopenic variant PPA, discussed earlier). Patients with behavioral variant FTLD show symmetric frontal hypometabolism on FDG-PET, even in the absence of visually apparent atrophy on MRI, which later spreads to the anterior cingulate, parietal lobe, and temporal lobe (**FIGURE 9-6**).[120] The basal ganglia, insula, and thalamus have also shown hypometabolism in patients with behavioral variant FTLD.

FDG-PET studies in semantic dementia have identified reduced metabolism in the left anterior temporal lobe but less significant frontal lobe hypometabolism than in other forms of FTLD (**FIGURE 9-6**).[120] Alternatively, patients with progressive nonfluent aphasia show asymmetric (usually left more than right) frontal cortical hypometabolism in the language-dominant hemisphere, including in the Broca area (**FIGURE 9-6**).[120] Interestingly, left-handed patients may show the reverse pattern, with right more than left frontal hypometabolism, because this may be their language-dominant hemisphere.[121]

FDG-PET studies in CBD show asymmetric hypometabolism in the posterior frontal lobes, paracentral lobule, sensorimotor cortex, thalamus, basal ganglia, middle cingulate, parietal lobe, and substantia nigra, whereas studies in PSP show notable hypometabolism of the prefrontal cortex, caudate, pallidum, thalamus, mesencephalon, and subthalamic nucleus.[122] Thalamic hypometabolism in patients with PSP has been associated with increased postural

Copyright © American Academy of Neurology. Unauthorized reproduction of this article is prohibited.

instability and falls.[123] Finally, patients with FTLD-ALS show hypometabolism in the frontal lobe, superior temporal lobe, parietal lobe, occipital lobe, and insula,[116] which is more severe in FTLD-ALS than in ALS without FTLD.[124] Amyloid PET scans have shown minimal binding in any subtype of FTLD unless comorbid AD pathology exists.

Tau studies in patients with FTLD have shown binding of tracers in multiple phenotypes, including sporadic and familial behavioral variant FTLD, progressive nonfluent aphasia, CBD, PSP, and even in semantic dementia, which is usually linked to TDP-43 deposition (FIGURE 9-8). Sporadic behavioral variant

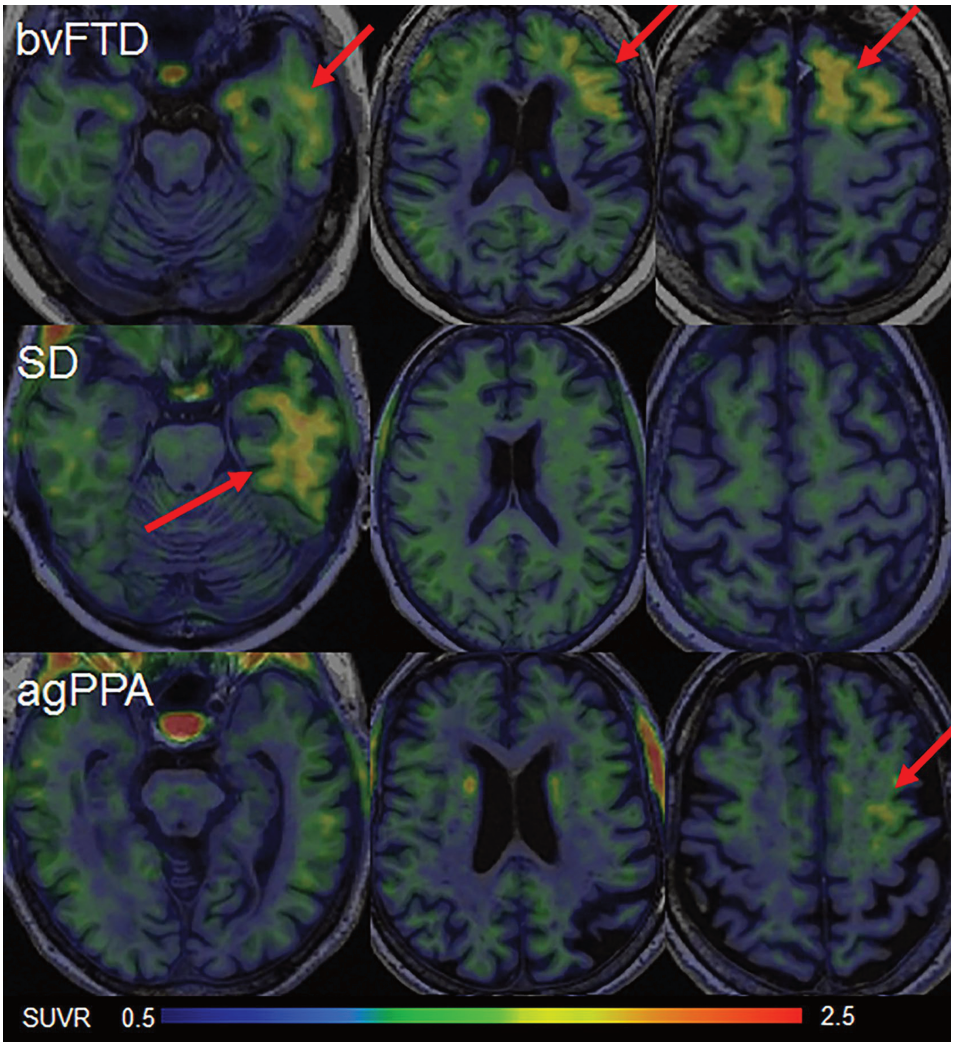

FIGURE 9-8

Axial [^{18}F]flortaucipir positron emission tomography (PET) in frontotemporal dementia spectrum disorders. Imaging of a patient with behavioral variant frontotemporal dementia (bvFTD) shows mild tracer uptake (*arrows*) in the frontotemporal lobes, whereas the imaging of the patient with semantic dementia (SD) shows tracer deposition (*arrow*) predominantly in the left temporal lobe. The imaging of the patient with agrammatic (nonfluent) primary progressive aphasia (agPPA) shows slightly elevated tracer retention (*arrow*) in the left frontal lobe.

SUVR = standardized uptake value ratio.

Modified with permission from Whitwell JL, Prog Mol Biol Transl Sci.[95] © 2019 Elsevier Inc.

KEY POINTS

- **Patients with behavioral variant FTLD show symmetric frontal hypometabolism on FDG-PET, as well as hypometabolism in the anterior cingulate, parietal lobe, and temporal lobe in later stages.**
- **FDG-PET studies in semantic dementia have identified reduced metabolism in the left anterior temporal lobe but less significant frontal lobe hypometabolism than in other forms of FTLD.**
- **Patients with progressive nonfluent aphasia show asymmetric (usually left more than right) frontal cortical hypometabolism in the language-dominant hemisphere, including in the Broca area.**
- **FDG-PET studies in CBD show asymmetric hypometabolism in the posterior frontal lobes, sensorimotor cortex, and subcortical regions.**
- **FDG-PET studies in PSP show notable hypometabolism of the prefrontal cortex, caudate, pallidum, thalamus, mesencephalon, and subthalamic nucleus.**
- **Patients with FTLD-ALS show hypometabolism in the frontal lobe, superior temporal lobe, parietal lobe, occipital lobe, and insula, which is more severe in FTLD-ALS than in ALS without FTLD.**
- **Amyloid PET scans have shown minimal binding in any subtype of FTLD unless comorbid AD pathology exists.**

Copyright © American Academy of Neurology. Unauthorized reproduction of this article is prohibited.

FTLD shows tau deposition in the basal ganglia, anterior cingulate cortex, and insula in about 50% of cases assessed in vivo, perhaps reflecting the variability in the underlying pathology (ie, tau versus TDP-43).[125] However, familial *MAPT* mutations, which result in behavioral variant FTLD secondary to pathologic tau deposition, show high tau signal in the bilateral temporal lobes, anterior cingulate cortex, hippocampus, frontal lobe, and basal ganglia.[126] The extent of tau in *MAPT* mutations is correlated with greater atrophy and varies by tau isoform. Multiple studies in patients with semantic dementia have demonstrated tau tracer uptake in the anterior temporal lobe, fusiform gyrus, and insula, which overlaps with the expected regions of degeneration and TDP-43 deposition. This binding may represent off-target binding to TDP-43, which is the likely underlying pathology causing this condition, or binding to comorbid tau fibrils in the region.[125] Interestingly, a study in a patient carrying a familial *C9orf72* mutation, which generally results in TDP-43 pathology, also showed tau PET tracer binding, suggesting nonspecific binding of the tracer.[127] A 2019 study also reported tau deposition in patients with progressive nonfluent aphasia in the left more than right inferior frontal gyrus.[125] Multiple studies have reported binding of several different tau tracers in patients with CBD or corticobasal syndrome in the premotor cortex, subcortical white matter, and basal ganglia, which was shown to increase in intensity longitudinally with disease progression and found to be more significant in regions contralateral to the more affected side of the body.[125] Finally, tau tracer in the basal ganglia, midbrain, and other subcortical regions was observed in patients with PSP, which was shown to correlate with the amount of clinical impairment in some cases and not in others.[128]

CREUTZFELDT-JAKOB DISEASE AND OTHER PRION DISORDERS

Rapidly progressing neurodegenerative disorders caused by the accumulation of abnormal prion proteins can occur sporadically (sporadic CJD) (illustrated in CASE 9-4), from exposure to food (variant CJD) or tissues (iatrogenic CJD) containing the abnormal prion protein, or because of a genetic variation in the prion protein gene (*PRNP*; familial CJD), Gerstmann-Sträussler-Scheinker disease, or fatal familial insomnia.[129] These diseases feature cognitive and motor

CASE 9-4

A 32-year-old man presented with rapidly progressive cognitive impairment and dementia, loss of balance and coordination, and slurred speech. Cognitive testing showed widespread impairment in multiple domains, and the neurologic examination showed loss of balance and coordination. Bowel and urinary incontinence were also reported. His CSF 14-3-3 protein was elevated, and a real-time quaking-induced conversion (RT-QuIC) assay showed elevated levels of pathologic misfolded prion protein.

COMMENT

This patient likely has sporadic Creutzfeldt-Jakob disease. MRI would be ordered to rule out infectious diseases and would likely show supportive restricted diffusion in the striatum and throughout the cortex, as well as potentially in the thalamus.

Copyright © American Academy of Neurology. Unauthorized reproduction of this article is prohibited.

dysfunction, although other presentations with various symptoms are possible. Specifically, most forms of CJD demonstrate a rapidly progressive dementia and a variety of cerebellar, motor, and extrapyramidal symptoms, as well as myoclonus and ultimately death.

Gerstmann-Sträussler-Scheinker disease is characterized by impairments in executive function, dementia, and numerous motor symptoms including ataxia, balance problems, difficulty walking, incoordination, and sometimes parkinsonian changes. Fatal familial insomnia is primarily associated with a progressive insomnia that causes significant physical and mental decline and ultimately death.

MRI Findings in Creutzfeldt-Jakob Disease and Related Prion Disorders

The primary imaging biomarkers for prion disorders are MRI based, the most sensitive sequence being DWI. All forms of CJD can show restricted diffusion in the basal ganglia, cerebellum, and diffuse regions of the cortex ("ribboning"), most commonly affecting the frontal and parietal lobes (FIGURE 9-9[130]).[131] Cortical involvement is more often asymmetric and does not correspond to arterial perfusion territories. The thalamus may also show restricted diffusion in some cases, although more frequently in patients with variant CJD than sporadic CJD.[131] Restricted diffusion in the pulvinar nucleus of the thalamus relative to the neighboring anterior putamen in patients with variant CJD is called the *hockey stick sign* because of the curvilinear signal abnormality. These measures of restricted diffusion have been shown to be associated with disease duration and severity, as well as the extent of spongiform burden at autopsy. In addition, patients with sporadic CJD show reduced white matter integrity in multiple white matter pathways.[132] A resting-state fMRI study showed increased connectivity in the default-mode network.[133] Arterial spin labeling studies of cerebral perfusion in CJD have also shown hypoperfusion in the cortex, thalamus, and cerebellum.[134]

Patients with Gerstmann-Sträussler-Scheinker disease and some with familial CJD showed mixed results with structural MRI measures, with some showing no

KEY POINTS

- **Tau PET scans have shown less binding in FTLD relative to that seen in AD, potentially because of less sensitivity of the tracers to non-AD tau conformations. However, the tau PET studies generally show higher tau deposition in regions that mirror the location of atrophy across the FTLD spectrum.**

- **The primary imaging biomarkers for prion disorders are MRI based, the most sensitive type being diffusion-weighted imaging (DWI). All forms of CJD can show restricted diffusion in the basal ganglia, cerebellum, and diffuse regions of the cortex ("ribboning"), most commonly affecting the frontal and parietal lobes.**

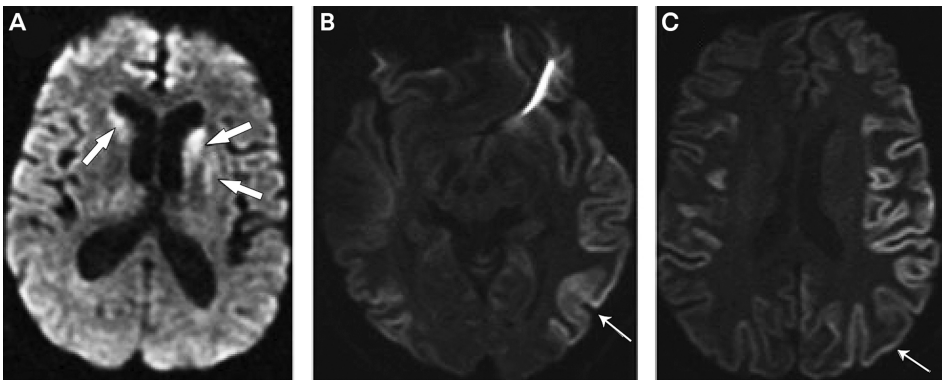

FIGURE 9-9

Structural axial imaging in prion diseases. Diffusion-weighted images (DWI) in patients with sporadic Creutzfeldt-Jakob disease are shown. In the first patient (*A*), hyperintense signal on DWI is observed in the caudate and putamen (*A, thick arrows*), whereas the other two patients (*B*, *C*) show widespread hyperintensities in the cortex, which can often be asymmetric, including in the temporal, parietal, and frontal lobes, referred to as *ribboning* (*B, C, thin arrows*).

Modified with permission from Bertleson JA and Ajtai B, Neurol Clin.[130] © 2014 Elsevier Inc.

Copyright © American Academy of Neurology. Unauthorized reproduction of this article is prohibited.

atrophy and others with generalized cerebral and cerebellar atrophy. However, similar to CJD, hyperintensities on T2-weighted scans are commonly observed in the basal ganglia in Gerstmann-Sträussler-Scheinker disease.[135] Patients with familial CJD also show reduced white matter integrity in multiple white matter pathways, including the corticospinal tract, internal capsule, external capsule, fornix, and posterior thalamic radiations.[135] Finally, patients with fatal familial insomnia may or may not show mild cerebral atrophy but often have restricted diffusion in the thalamus.[135]

Metabolic and Molecular Imaging Findings in Creutzfeldt-Jakob Disease and Related Prion Disorders

FDG-PET studies in all forms of CJD show widespread and often asymmetric hypometabolism in the cortex and cerebellum, with relative sparing of the basal ganglia and thalamus.[136] SPECT and PET studies of cerebral perfusion have also shown cortical hypoperfusion in patients with CJD. The reduced glucose metabolism on FDG-PET in patients with CJD was associated with astrocytosis and reduced perfusion. Patients with familial CJD show reduced metabolism in the postcentral gyri, temporal lobe, and superior parietal lobule before the onset of clinical symptoms.[137] Amyloid and tau PET scans show minimal binding in patients with CJD, suggesting that these tracers are not sensitive to the prion protein deposits.[136,138] In a study with [^{11}C]PK11195, a tracer for neuroinflammatory response, patients with CJD demonstrated upregulated neuroinflammation in the cortex, thalamus, basal ganglia, and cerebellum.[139]

SPECT and FDG-PET studies in patients with Gerstmann-Sträussler-Scheinker disease demonstrate hypoperfusion and hypometabolism throughout the cerebral cortex, especially in the frontal lobe and cerebellum.[140] Like in CJD, amyloid PET scans in patients with Gerstmann-Sträussler-Scheinker disease show no specific binding[141]; however, some variants of Gerstmann-Sträussler-Scheinker disease, including the *PRNP* F198S variant, show tau deposition that is immunochemically identical to that in AD at autopsy. A 2018 study with [^{18}F]flortaucipir showed specific binding in the striatum, thalamus, anterior cingulate cortex, and insula of two patients with Gerstmann-Sträussler-Scheinker disease due to the F198S mutation.[142] Finally, hypometabolism on FDG was observed in the thalamus and cingulate of patients with fatal familial insomnia with relative sparing of the occipital lobes. No amyloid or tau PET scans have been reported in fatal familial insomnia.[135]

DIFFERENTIAL DIAGNOSIS

The differential diagnosis of diseases presenting with or without motor symptoms, such as late-onset AD, atypical AD, CJD, and FTLD, can be improved by using structural MRI and PET techniques. Patterns of atrophy often differ between neurodegenerative disorders and can be used to support a clinical diagnosis. Traditional AD shows the most severe atrophy and tau deposition in bilateral medial temporal lobe and lateral temporal and posterior cortical regions (ie, parietal and secondary visual areas).

Atypical AD cases, such as posterior cortical atrophy and logopenic variant PPA, show more extensive atrophy and tau deposition in other brain regions, specifically posterior brain regions (including the occipital lobe, which is spared in traditional AD) in posterior cortical atrophy and asymmetric (left more than right) temporoparietal atrophy and tau deposition in logopenic variant PPA.

Copyright © American Academy of Neurology. Unauthorized reproduction of this article is prohibited.

Amyloid PET is not useful for differentiating these cases but can assist with differentiating AD syndromes from FTLD, where most patients have negative amyloid scans. In addition, patients with behavioral variant FTLD show more atrophy in the frontal lobe and less in the parietal lobe than do patients with AD; they also show more hypometabolism on FDG-PET, which can be clinically ordered to differentiate these conditions.

Semantic dementia can be distinguished from other neurodegenerative conditions by the highly asymmetric and focal atrophy and hypometabolic pattern in the anterior temporal lobe (left more than right), whereas progressive nonfluent aphasia shows asymmetric (left more than right) atrophy and hypometabolism in the inferior frontal lobe (ie, the Broca area). These focal findings on MRI and FDG-PET, along with a negative amyloid PET scan, provide excellent diagnostic sensitivity for semantic dementia and progressive nonfluent aphasia relative to other FTLD and AD syndromes. Tau PET is less helpful in FTLD because the underlying pathology could be tau (and thus, show binding), TDP-43, or another proteinopathy. Finally, patients with vascular cognitive impairment present with more vascular abnormalities clinically and neuroradiologically, including white matter lesions, than seen in patients with FTLD and AD. Furthermore, FDG-PET hypometabolism in vascular cognitive impairment is seen only in patchy areas that correspond to areas of hypoperfusion, and widespread amyloid deposition is not seen in vascular cognitive impairment in the absence of co-occurring CAA.

Although DLB and PDD have a higher frequency of extrapyramidal symptoms than AD, these disorders can be difficult to distinguish clinically at times. However, patients with DLB have less extensive cortical atrophy than patients with AD and have relative preservation of the medial temporal lobe, which can help in the differential diagnosis between DLB and AD. In addition, patients with DLB show more atrophy of the midbrain and basal ganglia but less frontal lobe atrophy than patients with AD (or FTLD syndromes). Patients with DLB show more hypometabolism in the primary visual cortex relative to patients with AD, which can also be used to distinguish these conditions. Finally, the use of dopaminergic-specific SPECT and PET tracers will distinguish DLB and PDD disorders from AD, as well as FTLD syndromes.

For the neurodegenerative conditions that have extensive motor, extrapyramidal, and cognitive symptoms (FTLD-ALS, CBD, PSP, DLB and PDD, prion diseases), differential diagnosis can be quite challenging because of the overlapping symptoms and areas of pathology. Patients with FTD-ALS show atrophy and reduced perfusion and metabolism in the frontal (including the primary motor area) and temporal lobes, whereas patients with DLB and PDD show greater posterior cortical hypometabolism and atrophy in the parietal and occipital lobes. In addition, patients with DLB and PDD will show decreased dopaminergic neurotransmission in the striatum on PET or SPECT relative to patients with FTLD-ALS. Amyloid and tau PET are likely not helpful for distinguishing FTLD-ALS, DLB, and PDD. However, tau PET tracers could be useful in the differential diagnosis of CBD and PSP, because these conditions show focal signal in disease-related areas, especially the second-generation tau tracers. In addition, PSP shows a characteristic atrophy pattern of the midbrain (noted earlier as the hummingbird sign on a sagittal view and the Mickey Mouse sign on an axial view) that can assist with the differential diagnosis. Finally, sporadic and variant prion diseases can be distinguished from most other

KEY POINTS

- Familial prion protein forms, such as Gerstmann-Sträussler-Scheinker disease and familial CJD, show mixed results with structural MRI measures, with some patients showing no atrophy and others with generalized cerebral and cerebellar atrophy. Patients with fatal familial insomnia may show mild cerebral atrophy and often have restricted diffusion in the thalamus.

- FDG-PET studies in all forms of CJD show widespread and often asymmetric hypometabolism in the cortex and cerebellum, with relative sparing of the basal ganglia and thalamus, whereas familial forms of prion protein disease show cerebral, cerebellar, and subcortical hypometabolism.

- Amyloid and tau PET scans generally show minimal binding in prion protein diseases.

- The differential diagnosis of diseases presenting with or without motor symptoms, such as late-onset AD, atypical AD, CJD, and FTLD, can be improved by using structural MRI and PET techniques.

- Patterns of atrophy and hypometabolism often differ between neurodegenerative disorders and can be used to support a clinical diagnosis, whereas amyloid and tau PET, along with dopaminergic PET or SPECT, can provide support for or rule out a probable diagnosis.

Copyright © American Academy of Neurology. Unauthorized reproduction of this article is prohibited.

dementias by the areas of restricted diffusion seen in the basal ganglia and thalamus on DWI techniques, including the hockey stick sign in the pulvinar of the thalamus in variant CJD. In summary, the combination of both MRI and metabolic and molecular imaging techniques to understand pathology in various neurodegenerative conditions can aid with differential diagnoses in cases with overlapping symptomatology.

CONCLUSION

MRI and molecular imaging techniques provide important information about atrophy patterns and pathologic proteins in multiple types of neurodegenerative conditions, including slower-progressing dementias such as typical and atypical AD, FTLD, and DLB and PDD, as well as rapidly progressing dementias such as CJD and other prion protein disorders. Future studies with novel tracers for important pathologic proteins such as TDP-43, α-synuclein, and others will improve differential diagnoses and the understanding of the clinical course of patients with these devastating diseases.

ACKNOWLEDGMENT

This article was supported by the National Institute on Aging (U01 AG057195, R01 AG057739, and P30 AG072976; Dr Apostolova).

REFERENCES

1 2022 Alzheimer's disease facts and figures. Alzheimers Dement 2022;18(4):700-789. doi: 10.1002/alz.12638

2 Jack CR Jr, Knopman DS, Jagust WJ, et al. Tracking pathophysiological processes in Alzheimer's disease: an updated hypothetical model of dynamic biomarkers. Lancet Neurol 2013;12(2): 207-216. doi:10.1016/S1474-4422(12)70291-0

3 Jack CR Jr, Bennett DA, Blennow K, et al. NIA-AA Research Framework: toward a biological definition of Alzheimer's disease. Alzheimers Dement 2018;14(4):535-562. doi:10.1016/j.jalz.2018.02.018

4 Jack CR Jr, Bennett DA, Blennow K, et al. A/T/N: an unbiased descriptive classification scheme for Alzheimer disease biomarkers. Neurology 2016;87(5):539-547. doi:10.1212/WNL.0000000000002923

5 Risacher SL, Saykin AJ. Neuroimaging in aging and neurologic diseases. Handb Clin Neurol 2019;167: 191-227. doi:10.1016/B978-0-12-804766-8.00012-1

6 Risacher SL, Saykin AJ, West JD, et al. Baseline MRI predictors of conversion from MCI to probable AD in the ADNI cohort. Curr Alzheimer Res 2009;6(4):347-361. doi: 10.2174/156720509788929273

7 Apostolova LG, Dutton RA, Dinov ID, et al. Conversion of mild cognitive impairment to Alzheimer disease predicted by hippocampal atrophy maps. Arch Neurol 2006;63(5):693-699. doi:10.1001/archneur.63.5.693

8 Barnes J, Bartlett JW, van de Pol LA, et al. A meta-analysis of hippocampal atrophy rates in Alzheimer's disease. Neurobiol Aging 2009;30(11): 1711-1723. doi:10.1016/j.neurobiolaging.2008.01.010

9 Luo X, Li K, Zeng Q, et al. Application of T1-/T2-weighted ratio mapping to elucidate intracortical demyelination process in the Alzheimer's disease continuum. Front Neurosci 2019;13:904. doi: 10.3389/fnins.2019.00904

10 Pievani M, Agosta F, Pagani E, et al. Assessment of white matter tract damage in mild cognitive impairment and Alzheimer's disease. Hum Brain Mapp 2010;31(12):1862-1875. doi:10.1002/hbm.20978

11 Sperling RA, Bates JF, Chua EF, et al. fMRI studies of associative encoding in young and elderly controls and mild Alzheimer's disease. J Neurol Neurosurg Psychiatry 2003;74(1):44-50. doi: 10.1136/jnnp.74.1.44

Copyright © American Academy of Neurology. Unauthorized reproduction of this article is prohibited.

12 Zhang L, Zuo XN, Ng KK, et al. Distinct BOLD variability changes in the default mode and salience networks in Alzheimer's disease spectrum and associations with cognitive decline. Sci Rep 2020;10(1):6457. doi:10.1038/s41598-020-63540-4

13 Sierra-Marcos A. Regional cerebral blood flow in mild cognitive impairment and Alzheimer's Disease measured with arterial spin labeling magnetic resonance imaging. Int J Alzheimers Dis 2017;2017:5479597. doi:10.1155/2017/5479597

14 Ravanfar P, Loi SM, Syeda WT, et al. Systematic review: quantitative susceptibility mapping (QSM) of brain iron profile in neurodegenerative diseases. Front Neurosci 2021;15:618435. doi:10.3389/fnins.2021.618435

15 Yamada M. Cerebral amyloid angiopathy: emerging concepts. J Stroke 2015;17(1):17-30. doi:10.5853/jos.2015.17.1.17

16 Risacher SL, Kim S, Nho K, et al. APOE effect on Alzheimer's disease biomarkers in older adults with significant memory concern. Alzheimers Dement 2015;11(12):1417-1429. doi:10.1016/j.jalz.2015.03.003

17 Molinuevo JL, Ripolles P, Simo M, et al. White matter changes in preclinical Alzheimer's disease: a magnetic resonance imaging-diffusion tensor imaging study on cognitively normal older people with positive amyloid beta protein 42 levels. Neurobiol Aging 2014;35(12):2671-2680. doi:10.1016/j.neurobiolaging.2014.05.027

18 Rami L, Sala-Llonch R, Sole-Padulles C, et al. Distinct functional activity of the precuneus and posterior cingulate cortex during encoding in the preclinical stage of Alzheimer's disease. J Alzheimers Dis 2012;31(3):517-526. doi:10.3233/JAD-2012-120223

19 Hays CC, Zlatar ZZ, Wierenga CE. The utility of cerebral blood flow as a biomarker of preclinical Alzheimer's disease. Cell Mol Neurobiol 2016;36(2):167-179. doi:10.1007/s10571-015-0261-z

20 He W, Liu D, Radua J, et al. Meta-analytic comparison between PIB-PET and FDG-PET results in Alzheimer's disease and MCI. Cell Biochem Biophys 2015;71(1):17-26. doi:10.1007/s12013-014-0138-7

21 Minoshima S, Mosci K, Cross D, Thientunyakit T. Brain [F-18]FDG PET for clinical dementia workup: differential diagnosis of Alzheimer's disease and other types of dementing disorders. Semin Nucl Med 2021;51(3):230-240. doi:10.1053/j.semnuclmed.2021.01.002

22 Hanseeuw BJ, Betensky RA, Mormino EC, et al. PET staging of amyloidosis using striatum. Alzheimers Dement 2018;14(10):1281-1292. doi:10.1016/j.jalz.2018.04.011

23 Johnson KA, Schultz A, Betensky RA, et al. Tau positron emission tomographic imaging in aging and early Alzheimer disease. Ann Neurol 2016;79(1):110-119. doi:10.1002/ana.24546

24 La Joie R, Visani AV, Baker SL, et al. Prospective longitudinal atrophy in Alzheimer's disease correlates with the intensity and topography of baseline tau-PET. Sci Transl Med 2020;12(524):5732. doi:10.1126/scitranslmed.aau5732

25 Braak H, Braak E, Bohl J. Staging of Alzheimer-related cortical destruction. Eur Neurol 1993;33(6):403-408. doi:10.1159/000116984

26 Schwarz AJ, Yu P, Miller BB, et al. Regional profiles of the candidate tau PET ligand 18F-AV-1451 recapitulate key features of Braak histopathological stages. Brain 2016;139(Pt 5):1539-1550. doi:10.1093/brain/aww023

27 Ishiki A, Okamura N, Furukawa K, et al. Longitudinal assessment of tau pathology in patients with Alzheimer's disease using [18F]THK-5117 positron emission tomography. PLoS One 2015;10(10):e0140311. doi:10.1371/journal.pone.0140311

28 Gouilly D, Saint-Aubert L, Ribeiro MJ, et al. Neuroinflammation PET imaging of the translocator protein (TSPO) in Alzheimer's disease: an update. Eur J Neurosci 2022;55(5):1322-1343. doi:10.1111/ejn.15613

29 Kong Y, Zhang S, Huang L, et al. Positron emission computed tomography imaging of synaptic vesicle glycoprotein 2A in Alzheimer's disease. Front Aging Neurosci 2021;13:731114. doi:10.3389/fnagi.2021.731114

30 Landau SM, Harvey D, Madison CM, et al. Comparing predictors of conversion and decline in mild cognitive impairment. Neurology 2010;75(3):230-8. doi:10.1212/WNL.0b013e3181e8e8b8

31 Risacher SL, Kim S, Shen L, et al. The role of apolipoprotein E (APOE) genotype in early mild cognitive impairment (E-MCI). Front Aging Neurosci 2013;5:11. doi:10.3389/fnagi.2013.00011

32 Jansen WJ, Ossenkoppele R, Tijms BM, et al. Association of cerebral amyloid-beta aggregation with cognitive functioning in persons without dementia. JAMA Psychiatry 2018;75(1):84-95. doi:10.1001/jamapsychiatry.2017.3391

33 Jack CR, Wiste HJ, Botha H, et al. The bivariate distribution of amyloid-beta and tau: relationship with established neurocognitive clinical syndromes. Brain 2019;142(10):3230-3242. doi:10.1093/brain/awz268

34 Krishnadas N, Dore V, Laws SM, et al. Exploring discordant low amyloid beta and high neocortical tau positron emission tomography cases. Alzheimers Dement (Amst) 2022;14(1):e12326. doi:10.1002/dad2.12326

35 van der Kall LM, Truong T, Burnham SC, et al. Association of beta-amyloid level, clinical progression, and longitudinal cognitive change in normal older individuals. Neurology 2021;96(5):e662-e670. doi:10.1212/WNL.0000000000011222

Copyright © American Academy of Neurology. Unauthorized reproduction of this article is prohibited.

36 Knopman DS, Jack CR Jr, Wiste HJ, et al. 18F-fluorodeoxyglucose positron emission tomography, aging, and apolipoprotein E genotype in cognitively normal persons. Neurobiol Aging 2014;35(9):2096-2106. doi: 10.1016/j.neurobiolaging.2014.03.006

37 Biel D, Brendel M, Rubinski A, et al. Tau-PET and in vivo Braak-staging as prognostic markers of future cognitive decline in cognitively normal to demented individuals. Alzheimers Res Ther 2021; 13(1):137. doi:10.1186/s13195-021-00880-x

38 Leuzy A, Mattsson-Carlgren N, Palmqvist S, et al. Blood-based biomarkers for Alzheimer's disease. EMBO Mol Med 2022;14(1):e14408. doi:10.15252/emmm.202114408

39 Vogel JW, Iturria-Medina Y, Strandberg OT, et al. Spread of pathological tau proteins through communicating neurons in human Alzheimer's disease. Nat Commun 2020;11(1):2612. doi:10.1038/s41467-020-15701-2

40 Collij LE, Heeman F, Salvado G, et al. Multitracer model for staging cortical amyloid deposition using PET imaging. Neurology 2020;95(11): e1538-e1553. doi:10.1212/WNL.0000000000010256

41 Jack CR Jr, Wiste HJ, Lesnick TG, et al. Brain beta-amyloid load approaches a plateau. Neurology 2013;80(10):890-896. doi:10.1212/WNL.0b013e3182840bbe

42 Sirkis DW, Bonham LW, Johnson TP, La Joie R, Yokoyama JS. Dissecting the clinical heterogeneity of early-onset Alzheimer's disease. Mol Psychiatry 2022;27(6):2674-2688. doi:10.1038/s41380-022-01531-9

43 Indiana University School of Medicine. Longitudinal early-onset Alzheimer's disease study. Accessed October 26, 2022. leads-study.medicine.iu.edu/

44 Vogel JW, Hansson O. Subtypes of Alzheimer's disease: questions, controversy, and meaning. Trends Neurosci 2022;45(5):342-345. doi:10.1016/j.tins.2022.02.001

45 Tippett DC, Keser Z. Clinical and neuroimaging characteristics of primary progressive aphasia. Handb Clin Neurol 2022;185:81-97. doi:10.1016/B978-0-12-823384-9.00016-5

46 Gahr M, Nowak DA, Connemann BJ, Schonfeldt-Lecuona C. Cerebral amyloidal angiopathy: a disease with implications for neurology and psychiatry. Brain Res 2013;1519:19-30. doi:10.1016/j.brainres.2013.04.052

47 Charidimou A, Boulouis G, Gurol ME, et al. Emerging concepts in sporadic cerebral amyloid angiopathy. Brain 2017;140(7):1829-1850. doi: 10.1093/brain/awx047

48 Kim HJ, Cho H, Werring DJ, et al. 18F-AV-1451 PET Imaging in three patients with probable cerebral amyloid angiopathy. J Alzheimers Dis 2017;57(3): 711-716. doi:10.3233/JAD-161139

49 Vogel JW, Young AL, Oxtoby NP, et al. Four distinct trajectories of tau deposition identified in Alzheimer's disease. Nat Med 2021;27(5): 871-881. doi:10.1038/s41591-021-01309-6

50 Risacher SL, Anderson WH, Charil A, et al. Alzheimer disease brain atrophy subtypes are associated with cognition and rate of decline. Neurology 2017;89(21):2176-2186. doi:10.1212/WNL.0000000000004670

51 Groot C, Grothe MJ, Mukherjee S, et al. Differential patterns of gray matter volumes and associated gene expression profiles in cognitively-defined Alzheimer's disease subgroups. Neuroimage Clin 2021;30:102660. doi: 10.1016/j.nicl.2021.102660

52 Groot C, Risacher SL, Chen JQA, et al. Differential trajectories of hypometabolism across cognitively-defined Alzheimer's disease subgroups. Neuroimage Clin 2021;31:102725. doi: 10.1016/j.nicl.2021.102725

53 Park JH, Seo SW, Kim C, et al. Pathogenesis of cerebral microbleeds: in vivo imaging of amyloid and subcortical ischemic small vessel disease in 226 individuals with cognitive impairment. Ann Neurol 2013;73(5):584-593. doi:10.1002/ana.23845

54 Razek A, Elsebaie NA. Imaging of vascular cognitive impairment. Clin Imaging 2021;74:45-54. doi:10.1016/j.clinimag.2020.12.038

55 Eckerstrom C, Olsson E, Klasson N, et al. High white matter lesion load is associated with hippocampal atrophy in mild cognitive impairment. Dement Geriatr Cogn Disord 2011; 31(2):132-8. doi:10.1159/000323014

56 Raja R, Rosenberg G, Caprihan A. Review of diffusion MRI studies in chronic white matter diseases. Neurosci Lett 2019;694:198-207. doi: 10.1016/j.neulet.2018.12.007

57 Li C, Zheng J, Wang J, Gui L. Comparison between Alzheimer's disease and subcortical vascular dementia: attentional cortex study in functional magnetic resonance imaging. J Int Med Res 2011; 39(4):1413-1419. doi:10.1177/147323001103900428

58 Liu C, Li C, Yin X, et al. Abnormal intrinsic brain activity patterns in patients with subcortical ischemic vascular dementia. PLoS One 2014;9(2): e87880. doi:10.1371/journal.pone.0087880

59 Shi Y, Thrippleton MJ, Makin SD, et al. Cerebral blood flow in small vessel disease: a systematic review and meta-analysis. J Cereb Blood Flow Metab 2016;36(10):1653-1667. doi: 10.1177/0271678X16662891

60 Heiss WD, Zimmermann-Meinzingen S. PET imaging in the differential diagnosis of vascular dementia. J Neurol Sci 2012;322(1-2):268-273. doi: 10.1016/j.jns.2012.09.023

61 Schneider JA, Arvanitakis Z, Bang W, Bennett DA. Mixed brain pathologies account for most dementia cases in community-dwelling older persons. Neurology 2007;69(24):2197-2204. doi: 10.1212/01.wnl.0000271090.28148.24

Copyright © American Academy of Neurology. Unauthorized reproduction of this article is prohibited.

62 Lee H, Wiggermann V, Rauscher A, et al. Brain imaging abnormalities in mixed Alzheimer's and subcortical vascular dementia. Can J Neurol Sci 2022:1-14. doi:10.1017/cjn.2022.65

63 Oveisgharan S, Yu L, Wang T, et al. Neurodegenerative and cerebrovascular brain pathologies are differentially associated with declining grip strength and gait in older adults. J Gerontol A Biol Sci Med Sci 2022;8:glac128. doi:10.1093/gerona/glac128

64 Rundek T, Del Brutto VJ, Goryawala M, et al. Associations between vascular risk factors and perivascular spaces in adults with intact cognition, mild cognitive impairment, and dementia. J Alzheimers Dis 2022;89(2):437-448. doi:10.3233/JAD-215585

65 Bohnen NI, Muller M, Frey KA. Molecular imaging and updated diagnostic criteria in Lewy body dementias. Curr Neurol Neurosci Rep 2017;17(10):73. doi:10.1007/s11910-017-0789-z

66 de Schipper LJ, Hafkemeijer A, van der Grond J, et al. Regional Structural hippocampal differences between dementia with Lewy bodies and Parkinson's disease. J Parkinsons Dis 2019;9(4):775-783. doi:10.3233/JPD-191600

67 Fanciulli A, Stankovic I, Krismer F, et al. Multiple system atrophy. Int Rev Neurobiol 2019;149:137-192. doi:10.1016/bs.irn.2019.10.004

68 Walker Z, Possin KL, Boeve BF, Aarsland D. Lewy body dementias. Lancet 2015;386(10004):1683-1697. doi:10.1016/S0140-6736(15)00462-6

69 Kantarci K, Lowe VJ, Chen Q, et al. beta-Amyloid PET and neuropathology in dementia with Lewy bodies. Neurology 2020;94(3):e282-e291. doi:10.1212/WNL.0000000000008818

70 O'Brien JT, Paling S, Barber R, et al. Progressive brain atrophy on serial MRI in dementia with Lewy bodies, AD, and vascular dementia. Neurology 2001;56(10):1386-8. doi:10.1212/wnl.56.10.1386

71 Planetta PJ, Kurani AS, Shukla P, et al. Distinct functional and macrostructural brain changes in Parkinson's disease and multiple system atrophy. Hum Brain Mapp 2015;36(3):1165-1179. doi:10.1002/hbm.22694

72 Broski SM, Hunt CH, Johnson GB, et al. Structural and functional imaging in parkinsonian syndromes. Radiographics 2014;34(5):1273-1292. doi:10.1148/rg.345140009

73 Paviour DC, Price SL, Jahanshahi M, Lees AJ, Fox NC. Longitudinal MRI in progressive supranuclear palsy and multiple system atrophy: rates and regions of atrophy. Brain 2006;129(Pt 4):1040-1049. doi:10.1093/brain/awl021

74 Delli Pizzi S, Franciotti R, Taylor JP, et al. Structural connectivity is differently altered in dementia with Lewy body and Alzheimer's disease. Front Aging Neurosci 2015;7:208. doi:10.3389/fnagi.2015.00208

75 Tsukamoto K, Matsusue E, Kanasaki Y, et al. Significance of apparent diffusion coefficient measurement for the differential diagnosis of multiple system atrophy, progressive supranuclear palsy, and Parkinson's disease: evaluation by 3.0-T MR imaging. Neuroradiology 2012;54(9):947-955. doi:10.1007/s00234-012-1009-9

76 Sauer J, ffytche DH, Ballard C, Brown RG, Howard R. Differences between Alzheimer's disease and dementia with Lewy bodies: an fMRI study of task-related brain activity. Brain 2006;129(Pt 7):1780-1788. doi:10.1093/brain/awl102

77 Kawashima S, Shimizu Y, Ueki Y, Matsukawa N. Impairment of the visuospatial working memory in the patients with Parkinson's Disease: an fMRI study. BMC Neurol 2021;21(1):335. doi:10.1186/s12883-021-02366-7

78 Schumacher J, Peraza LR, Firbank M, et al. Functional connectivity in dementia with Lewy bodies: a within- and between-network analysis. Hum Brain Mapp 2018;39(3):1118-1129. doi:10.1002/hbm.23901

79 You H, Wang J, Wang H, et al. Altered regional homogeneity in motor cortices in patients with multiple system atrophy. Neurosci Lett 2011;502(1):18-23. doi:10.1016/j.neulet.2011.07.015

80 Nedelska Z, Senjem ML, Przybelski SA, et al. Regional cortical perfusion on arterial spin labeling MRI in dementia with Lewy bodies: associations with clinical severity, glucose metabolism and tau PET. Neuroimage Clin 2018;19:939-947. doi:10.1016/j.nicl.2018.06.020

81 Wang J, Zhang W, Zhou Y, et al. Altered prefrontal blood flow related with mild cognitive impairment in Parkinson's disease: a longitudinal study. Front Aging Neurosci 2022;14:896191. doi:10.3389/fnagi.2022.896191

82 Zheng W, Ren S, Zhang H, et al. Spatial patterns of decreased cerebral blood flow and functional connectivity in multiple system atrophy (cerebellar-type): a combined arterial spin labeling perfusion and resting state functional magnetic resonance imaging study. Front Neurosci 2019;13:777. doi:10.3389/fnins.2019.00777

83 Kim EY, Sung YH, Lee J. Nigrosome 1 imaging: technical considerations and clinical applications. Br J Radiol 2019;92:20180842. doi:10.1259/bjr.20180842

84 Prange S, Metereau E, Thobois S. Structural imaging in Parkinson's disease: new developments. Curr Neurol Neurosci Rep 2019;19(8):50. doi:10.1007/s11910-019-0964-5

85 Caminiti SP, Sala A, Iaccarino L, et al. Brain glucose metabolism in Lewy body dementia: implications for diagnostic criteria. Alzheimers Res Ther 2019;11(1):20. doi:10.1186/s13195-019-0473-4

Copyright © American Academy of Neurology. Unauthorized reproduction of this article is prohibited.

86 Ko JH, Lee CS, Eidelberg D. Metabolic network expression in parkinsonism: clinical and dopaminergic correlations. J Cereb Blood Flow Metab 2017;37(2):683-693. doi: 10.1177/0271678X16637880

87 Winer JR, Maass A, Pressman P, et al. Associations between tau, beta-amyloid, and cognition in Parkinson disease. JAMA Neurol 2018;75(2):227-235. doi:10.1001/jamaneurol.2017.3713

88 Perez-Soriano A, Arena JE, Dinelle K, et al. PBB3 imaging in Parkinsonian disorders: evidence for binding to tau and other proteins. Mov Disord 2017;32(7):1016-1024. doi:10.1002/mds.27029

89 Capotosti F, Vokali E, Molette J, et al. The development of [18F]ACI-12589, a high affinity and selective alpha-synuclein radiotracer, as a biomarker for Parkinson's disease and other synucleinopathies. Alzheimer's Dement 2021; 17(S5):053943. doi:10.1002/alz.053943

90 Nicastro N, Nencha U, Burkhard PR, Garibotto V. Dopaminergic imaging in degenerative parkinsonisms, an established clinical diagnostic tool. J Neurochem 2021;22:15561. doi:10.1111/jnc.15561

91 Walker Z, Costa DC, Walker RW, et al. Differentiation of dementia with Lewy bodies from Alzheimer's disease using a dopaminergic presynaptic ligand. J Neurol Neurosurg Psychiatry 2002;73(2):134-140. doi:10.1136/jnnp.73.2.134

92 Whitwell JL, Josephs KA. Neuroimaging in frontotemporal lobar degeneration–predicting molecular pathology. Nat Rev Neurol 2012;8(3): 131-142. doi:10.1038/nrneurol.2012.7

93 Ferrari R, Kapogiannis D, Huey ED, Momeni P. FTD and ALS: a tale of two diseases. Curr Alzheimer Res 2011;8(3):273-294. doi: 10.2174/156720511795563700

94 Longitudinal Frontotemporal Lobar Degeneration. The ALLFTD study. Accessed October 26, 2022. allftd.org

95 Whitwell JL. FTD spectrum: neuroimaging across the FTD spectrum. Prog Mol Biol Transl Sci 2019; 165:187-223. doi:10.1016/bs.pmbts.2019.05.009

96 Schroeter ML, Raczka K, Neumann J, Yves von Cramon D. Towards a nosology for frontotemporal lobar degenerations-a meta-analysis involving 267 subjects. Neuroimage 2007;36(3):497-510. doi:10.1016/j.neuroimage.2007.03.024

97 Whitwell JL, Jack CR Jr, Parisi JE, et al. Imaging signatures of molecular pathology in behavioral variant frontotemporal dementia. J Mol Neurosci 2011;45(3):372-378. doi:10.1007/s12031-011-9533-3

98 Krueger CE, Dean DL, Rosen HJ, et al. Longitudinal rates of lobar atrophy in frontotemporal dementia, semantic dementia, and Alzheimer's disease. Alzheimer Dis Assoc Disord 2010;24(1): 43-48. doi:10.1097/WAD.0b013e3181a6f101

99 Perry DC, Brown JA, Possin KL, et al. Clinicopathological correlations in behavioural variant frontotemporal dementia. Brain 2017; 140(12):3329-3345. doi:10.1093/brain/awx254

100 Adachi M, Kawanami T, Ohshima F. The "morning glory sign" should be evaluated using thinly sliced axial images. Magn Reson Med Sci 2007; 6(1):59-60. doi:10.2463/mrms.6.59

101 Whitwell JL, Jack CR Jr, Parisi JE, et al. Rates of cerebral atrophy differ in different degenerative pathologies. Brain 2007;130(Pt 4):1148-1158. doi: 10.1093/brain/awm021

102 Whitwell JL, Avula R, Senjem ML, et al. Gray and white matter water diffusion in the syndromic variants of frontotemporal dementia. Neurology 2010;74(16):1279-1287. doi:10.1212/WNL.0b013e3181d9edde

103 Zhang Y, Walter R, Ng P, et al. Progression of microstructural degeneration in progressive supranuclear palsy and corticobasal syndrome: a longitudinal diffusion tensor imaging study. PLoS One 2016;11(6):e0157218. doi:10.1371/journal.pone.0157218

104 Menke RA, Proudfoot M, Wuu J, et al. Increased functional connectivity common to symptomatic amyotrophic lateral sclerosis and those at genetic risk. J Neurol Neurosurg Psychiatry 2016;87(6):580-588. doi:10.1136/jnnp-2015-311945

105 Verstraete E, Veldink JH, van den Berg LH, van den Heuvel MP. Structural brain network imaging shows expanding disconnection of the motor system in amyotrophic lateral sclerosis. Hum Brain Mapp 2014;35(4):1351-1361. doi: 10.1002/hbm.22258

106 Virani K, Jesso S, Kertesz A, Mitchell D, Finger E. Functional neural correlates of emotional expression processing deficits in behavioural variant frontotemporal dementia. J Psychiatry Neurosci 2013;38(3):174-182. doi:10.1503/jpn.120008

107 Reyes P, Ortega-Merchan MP, Rueda A, et al. Functional connectivity changes in behavioral, semantic, and nonfluent variants of frontotemporal dementia. Behav Neurol 2018; 2018:9684129. doi:10.1155/2018/9684129

108 Agosta F, Sala S, Valsasina P, et al. Brain network connectivity assessed using graph theory in frontotemporal dementia. Neurology 2013;81(2): 134-143. doi:10.1212/WNL.0b013e31829a33f8

109 Wilson SM, Brambati SM, Henry RG, et al. The neural basis of surface dyslexia in semantic dementia. Brain 2009;132(Pt 1):71-86. doi:10.1093/brain/awn300

110 Agosta F, Henry RG, Migliaccio R, et al. Language networks in semantic dementia. Brain 2010; 133(Pt 1):286-299. doi:10.1093/brain/awp233

111 Wilson SM, Dronkers NF, Ogar JM, et al. Neural correlates of syntactic processing in the nonfluent variant of primary progressive aphasia. J Neurosci 2010;30(50):16845-16854. doi: 10.1523/JNEUROSCI.2547-10.2010

Copyright © American Academy of Neurology. Unauthorized reproduction of this article is prohibited.

112 Mandelli ML, Welch AE, Vilaplana E, et al. Altered topology of the functional speech production network in non-fluent/agrammatic variant of PPA. Cortex 2018;108:252-264. doi:10.1016/j.cortex.2018.08.002

113 Beauchet O, Giraux P, Schneider F, et al. Brain abnormalities underlying limb apraxia in corticobasal degeneration: an fMRI study. Dialogues Clin Neurosci 2001;3(3):214-215. doi:10.31887/DCNS.2001.3.3/obeauchet

114 Burciu RG, Ofori E, Shukla P, et al. Distinct patterns of brain activity in progressive supranuclear palsy and Parkinson's disease. Mov Disord 2015;30(9):1248-1258. doi:10.1002/mds.26294

115 Bharti K, Bologna M, Upadhyay N, et al. Abnormal resting-state functional connectivity in progressive supranuclear palsy and corticobasal syndrome. Front Neurol 2017;8:248. doi:10.3389/fneur.2017.00248

116 Turner MR, Grosskreutz J, Kassubek J, et al. Towards a neuroimaging biomarker for amyotrophic lateral sclerosis. Lancet Neurol 2011;10(5):400-403. doi:10.1016/S1474-4422(11)70049-7

117 Tosun D, Schuff N, Jagust W, Weiner MW. Alzheimer's disease neuroimaging. I. Discriminative power of arterial spin labeling magnetic resonance imaging and 18F-fluorodeoxyglucose positron emission tomography changes for amyloid-beta-positive subjects in the Alzheimer's disease continuum. Neurodegener Dis 2016;16(1-2):87-94. doi:10.1159/000439257

118 Ssali T, Anazodo UC, Narciso L, et al. Sensitivity of arterial spin labeling for characterization of longitudinal perfusion changes in frontotemporal dementia and related disorders. Neuroimage Clin 2022;35:102853. doi:10.1016/j.nicl.2021.102853

119 Shen D, Hou B, Xu Y, et al. Brain structural and perfusion signature of amyotrophic lateral sclerosis with varying levels of cognitive deficit. Front Neurol 2018;9:364. doi:10.3389/fneur.2018.00364

120 Malpetti M, Carli G, Sala A, et al. Variant-specific vulnerability in metabolic connectivity and resting-state networks in behavioural variant of frontotemporal dementia. Cortex 2019;120:483-497. doi:10.1016/j.cortex.2019.07.018

121 Drzezga A, Grimmer T, Siebner H, et al. Prominent hypometabolism of the right temporoparietal and frontal cortex in two left-handed patients with primary progressive aphasia. J Neurol 2002;249(9):1263-1267. doi:10.1007/s00415-002-0832-z

122 Mille E, Levin J, Brendel M, et al. Cerebral glucose metabolism and dopaminergic function in patients with corticobasal syndrome. J Neuroimaging 2017;27(2):255-261. doi:10.1111/jon.12391

123 Zwergal A, la Fougere C, Lorenzl S, et al. Postural imbalance and falls in PSP correlate with functional pathology of the thalamus. Neurology 2011;77(2):101-109. doi:10.1212/WNL.0b013e318223c79d

124 Canosa A, Pagani M, Cistaro A, et al. 18F-FDG-PET correlates of cognitive impairment in ALS. Neurology 2016;86(1):44-49. doi:10.1212/WNL.0000000000002242

125 Tsai RM, Bejanin A, Lesman-Segev O, et al. (18)F-flortaucipir (AV-1451) tau PET in frontotemporal dementia syndromes. Alzheimers Res Ther 2019;11(1):13. doi:10.1186/s13195-019-0470-7

126 Smith R, Puschmann A, Scholl M, et al. 18F-AV-1451 tau PET imaging correlates strongly with tau neuropathology in MAPT mutation carriers. Brain 2016;139(Pt 9):2372-2379. doi:10.1093/brain/aww163

127 Bevan-Jones RW, Cope TE, Jones SP, et al. [(18)F]AV-1451 binding is increased in frontotemporal dementia due to *C9orf72* expansion. Ann Clin Transl Neurol 2018;5(10):1292-1296. doi:10.1002/acn3.631

128 Brendel M, Barthel H, van Eimeren T, et al. Assessment of 18F-PI-2620 as a biomarker in progressive supranuclear palsy. JAMA Neurol 2020;77(11):1408-1419. doi:10.1001/jamaneurol.2020.2526

129 Geschwind MD. Prion diseases. Continuum (Minneap Minn) 2015;21(6, Neuroinfectious Disease):1612-1638. doi:10.1212/CON.0000000000000251

130 Bertelson JA, Ajtai B. Neuroimaging of dementia. Neurol Clin 2014;32(1):59-93. doi:10.1016/j.ncl.2013.07.001

131 Krasnianski A, Schulz-Schaeffer WJ, Kallenberg K, et al. Clinical findings and diagnostic tests in the MV2 subtype of sporadic CJD. Brain 2006;129(Pt 9):2288-2296. doi:10.1093/brain/awl123

132 Caverzasi E, Henry RG, Vitali P, et al. Application of quantitative DTI metrics in sporadic CJD. Neuroimage Clin 2014;4:426-435. doi:10.1016/j.nicl.2014.01.011

133 Paoletti M, Caverzasi E, Mandelli ML, et al. Default mode network quantitative diffusion and resting-state functional magnetic resonance imaging correlates in sporadic Creutzfeldt-Jakob disease. Hum Brain Mapp 2022;43(13):4158-4173. doi:10.1002/hbm.25945

134 Yuan J, Wang S, Hu W. Combined findings of FDG-PET and arterial spin labeling in sporadic Creutzfeldt-Jakob disease. Prion 2018;12(5-6):310-314. doi:10.1080/19336896.2018.1525255

135 Letourneau-Guillon L, Wada R, Kucharczyk W. Imaging of prion diseases. J Magn Reson Imaging 2012;35(5):998-1012. doi:10.1002/jmri.23504

Copyright © American Academy of Neurology. Unauthorized reproduction of this article is prohibited.

136 Matias-Guiu JA, Guerrero-Marquez C, Cabrera-Martin MN, et al. Amyloid- and FDG-PET in sporadic Creutzfeldt-Jakob disease: correlation with pathological prion protein in neuropathology. Prion 2017;11(3):205-213. doi: 10.1080/19336896.2017.1314427

137 Lu H, Jing D, Chen Y, et al. Metabolic changes detected by 18F-FDG PET in the preclinical stage of familial Creutzfeldt-Jakob disease. J Alzheimers Dis 2020;77(4):1513-1521. doi: 10.3233/JAD-200576

138 Day GS, Gordon BA, Perrin RJ, et al. In vivo [(18)F]-AV-1451 tau-PET imaging in sporadic Creutzfeldt-Jakob disease. Neurology 2018;90(10): e896-e906. doi:10.1212/ WNL.0000000000005064

139 Iaccarino L, Moresco RM, Presotto L, et al. An In vivo (11)C-(R)-PK11195 PET and In vitro pathology study of microglia activation in Creutzfeldt-Jakob disease. Mol Neurobiol 2018;55(4): 2856-2868. doi:10.1007/s12035-017-0522-6

140 Arata H, Takashima H, Hirano R, et al. Early clinical signs and imaging findings in Gerstmann-Straussler-Scheinker syndrome (Pro102Leu). Neurology 2006;66(11):1672-1678. doi:10.1212/01. wnl.0000218211.85675.18

141 Deters KD, Risacher SL, Yoder KK, et al. [(11)C]PiB PET in Gerstmann-Straussler-Scheinker disease. Am J Nucl Med Mol Imaging 2016;6(1):84-93.

142 Risacher SL, Farlow MR, Bateman DR, et al. Detection of tau in Gerstmann-Straussler-Scheinker disease (PRNP F198S) by [(18)F] Flortaucipir PET. Acta Neuropathol Commun 2018;6(1):114. doi:10.1186/s40478-018-0608-z

DISCLOSURE

Continued from page 219

the Alzheimer's Association, Avid Radiopharmaceuticals, F. Hoffman-La Roche Ltd, Life Molecular Imaging, and the National Institute on Aging (U01 AG057195, R01 AG057739, and P30 AG072976).

Copyright © American Academy of Neurology. Unauthorized reproduction of this article is prohibited.

Imaging of Central Nervous System Autoimmune, Paraneoplastic, and Neuro-rheumatologic Disorders

By Lama Abdel Wahed, MD; Tracey A. Cho, MD, FAAN

REVIEW ARTICLE

CONTINUUM AUDIO INTERVIEW AVAILABLE ONLINE

ABSTRACT

OBJECTIVE: **This article provides an overview of the imaging modalities used in the evaluation of central nervous system (CNS) autoimmune, paraneoplastic, and neuro-rheumatologic disorders. An approach is outlined for interpreting imaging findings in this context, synthesizing a differential diagnosis based on certain imaging patterns, and choosing further imaging for specific diseases.**

LATEST DEVELOPMENTS: **The rapid discovery of new neuronal and glial autoantibodies has revolutionized the autoimmune neurology field and has elucidated imaging patterns characteristic of certain antibody-associated diseases. Many CNS inflammatory diseases, however, lack a definitive biomarker. Clinicians should recognize neuroimaging patterns suggestive of inflammatory disorders, as well as the limitations of imaging. CT, MRI, and positron emission tomography (PET) modalities all play a role in diagnosing autoimmune, paraneoplastic, and neuro-rheumatologic disorders. Additional imaging modalities such as conventional angiography and ultrasonography can be helpful for further evaluation in select situations.**

ESSENTIAL POINTS: **Knowledge of imaging modalities, both structural and functional, is critical in identifying CNS inflammatory diseases quickly and can help avoid invasive testing such as brain biopsy in certain clinical scenarios. Recognizing imaging patterns suggestive of CNS inflammatory diseases can also facilitate the early initiation of appropriate treatments to diminish morbidity and future disability.**

CITE AS:
CONTINUUM (MINNEAP MINN) 2023;29(1, NEUROIMAGING): 255–291.

Address correspondence to Dr Tracey A. Cho, Department of Neurology, University of Iowa Hospitals and Clinics, 200 Hawkins Dr, Iowa City, IA 52242, tracey-cho@uiowa.edu.

RELATIONSHIP DISCLOSURE:
Dr Abdel Wahed has received personal compensation in the range of $0 to $499 for serving as a resident honorary speaker with the Iowa Neurological Association and as an author for MedLink, LLC. Dr Cho has received personal compensation in the range of $500 to $4999 for serving as a consultant for Horizon Therapeutics plc and on a data safety monitoring board for the

Continued on page 291

UNLABELED USE OF PRODUCTS/INVESTIGATIONAL USE DISCLOSURE:
Drs Abdel Wahed and Cho discuss the unlabeled use of corticosteroids for the treatment of autoimmune neurologic diseases that have no US Food and Drug Administration–approved medications.

© 2023 American Academy of Neurology.

Copyright © American Academy of Neurology. Unauthorized reproduction of this article is prohibited.

INTRODUCTION

Central nervous system (CNS) autoimmune, paraneoplastic, and neuro-rheumatologic disorders, which are referred to as *neuroinflammatory diseases* in this article, are a heterogeneous group of pathologies that often require extensive testing, complex decision-making, and multidisciplinary care. With the rapidly increasing discovery of neuronal, synaptic, and onconeural autoantibodies, along with more targeted and effective immune-based therapies, recognizing clinical and radiographic patterns of neuroinflammatory diseases is critical for timely diagnosis and initiation of treatment. Certain clinical features can be quite useful in recognizing specific diseases, such as the orofacial dyskinesias in *N*-methyl-D-aspartate (NMDA) receptor encephalitis or the pathognomonic faciobrachial dystonic seizures seen in leucine-rich glioma inactivated 1 (LGI1) antibody

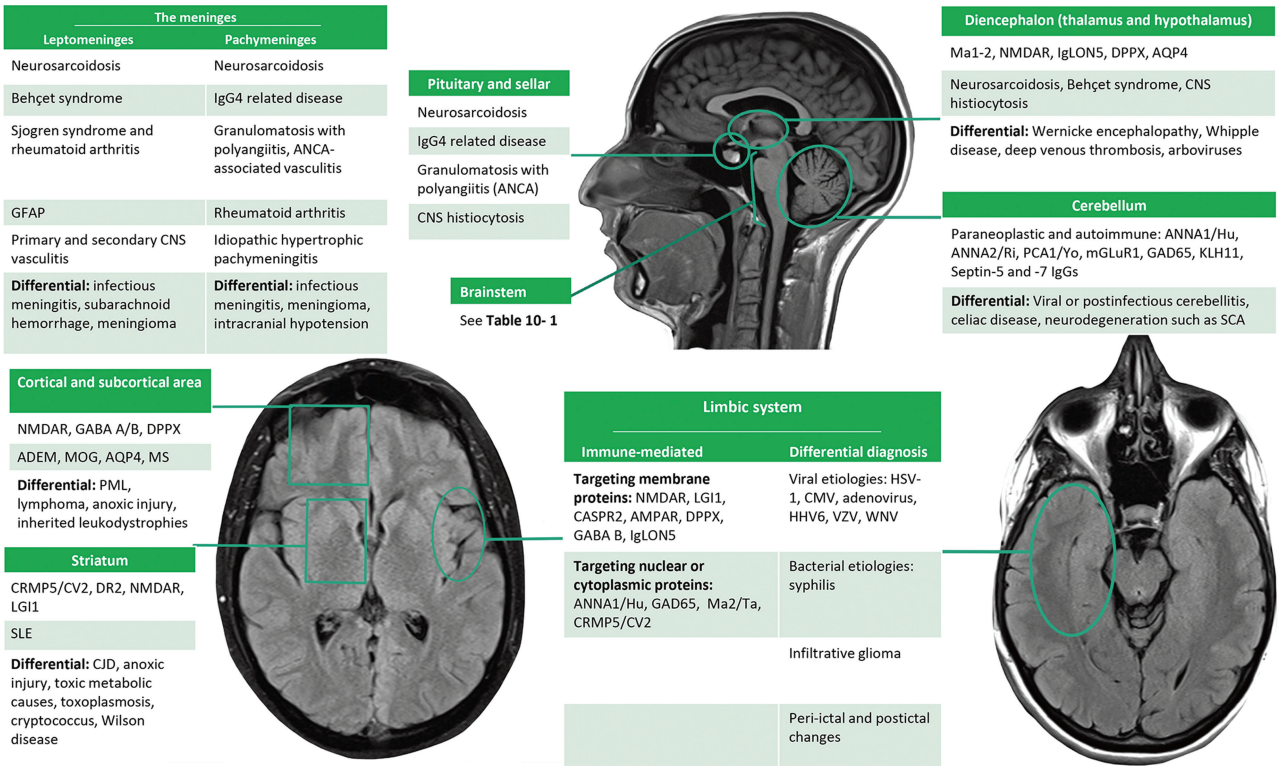

FIGURE 10-1

Autoimmune and inflammatory central nervous system (CNS) disorders and radiographic differential diagnoses based on typical location.

ADEM = acute disseminated encephalomyelitis; AMPAR = α-amino-3-hydroxy-5-methyl-4-isoxazolepropionic acid receptor; ANCA = antineutrophil cytoplasmic antibody; ANNA1 = antineuronal nuclear antibody type 1; ANNA2 = antineuronal nuclear autoantibody type 2; AQP4 = aquaporin-4; CASPR2 = contactin-associated proteinlike 2; CJD = Creutzfeldt-Jakob disease; CRMP5 = collapsin response mediator protein-5; CMV = cytomegalovirus; DR2 = dopamine receptor 2; DPPX = dipeptidyl-peptidase-like protein 6; GABA A/B = γ-aminobutyric acid type A or γ-aminobutyric acid type B; GABAR = γ-aminobutyric acid receptor; GAD65 = glutamic acid decarboxylase 65; GFAP = glial fibrillary acidic protein; HHV6 = human herpes virus 6; HSV-1 = herpes simplex virus type 1; IgG = immunoglobulin G; IgLON5 = immunoglobulin-like cell adhesion molecule 5; KLH11 = kelch-like protein 11; LGI1 = leucine-rich glioma inactivated; mGLUR1 = metabotropic glutamate receptor 1; MOG = myelin oligodendrocyte glycoprotein; MS = multiple sclerosis; NMDAR = *N*-methyl-D-aspartate receptor; PCA1 = Purkinje cell antibody 1; PML = progressive multifocal leukoencephalopathy; SCA = spinocerebellar ataxia; SLE = systemic lupus erythematosus; VZV = varicella-zoster virus; WNV = West Nile virus.

Copyright © American Academy of Neurology. Unauthorized reproduction of this article is prohibited.

encephalitis. Others have specific biomarkers such as aquaporin-4 antibodies in neuromyelitis optica spectrum disorder (NMOSD) or NMDA receptor antibodies in NMDA receptor encephalitis. In many cases, however, definitive clinical patterns and laboratory assays are lacking or nonspecific. For instance, headache and altered mental status can occur with encephalitis, leptomeningitis, pachymeningitis, or vasculitis. In such cases, neuroimaging is essential to help localize the syndrome and, thus, the differential diagnosis (FIGURE 10-1). In other cases, the neurologic syndrome is part of a systemic disease process, and imaging of non-neurologic sites can be helpful in identifying a systemic disease or an extra-CNS target for biopsy.

As with any neurologic disease process, the approach to CNS inflammatory diseases begins with identifying the tempo and progression of the process and the localization within the CNS. The choice of imaging will vary depending on whether the underlying disease is, for example, a chronic, relapsing spinal cord process or a subacute meningeal process. The clinician must also understand how imaging can help identify the core pathologic process in CNS inflammatory diseases, including inflammation, edema, gliosis, and atrophy, and the compartment within which the pathology predominates, whether parenchymal, meningeal, ventricular, or vascular.[1] When a systemic or paraneoplastic process is suspected, imaging of additional sites may include the use of metabolic imaging (positron emission tomography [PET]) or ultrasound, in addition to CT and MRI.

As with any biomarker, imaging findings must be interpreted in the context of the time course and clinical localization of the patient's symptoms. The sensitivity and specificity of neuroimaging in neuroinflammatory disease vary significantly. For instance, MRI in NMDA receptor encephalitis is frequently normal or nonspecific throughout the course of the disease, whereas dorsal pial enhancement of the spinal cord is particularly characteristic of active spinal cord neurosarcoidosis. Understanding and accurately selecting the appropriate neuroimaging modality are essential in evaluating any patient presenting with a suspected inflammatory CNS disease.

CSF analysis provides crucial data to support the presence of a neuroinflammatory process. Lumbar puncture should not be delayed in favor of MRI in acute presentations with high clinical suspicion for bacterial meningitis. In most other neuroinflammatory diseases when lumbar puncture is not emergent, MRI is often acquired prior to lumbar puncture to better characterize the disease process and guide CSF testing. In situations where MRI is delayed, however, lumbar puncture should be pursued when suspicion is high. Despite anecdotal concern for dural contrast enhancement as a result of lumbar puncture, dural enhancement is rare after a single nontraumatic lumbar puncture, especially if MRI is performed within 2 days.[2,3] Another strategy to limit traumatic lumbar puncture and a potentially confounding MRI contrast pattern is using point-of-care ultrasound guidance, both for site-marking and real-time guidance. This is especially important in patients who are obese (body mass index above 35 kg/m^2) with less palpable anatomic landmarks.[4]

KEY POINT

- Neuroimaging, especially MRI, can help identify the central nervous system (CNS) compartments predominantly involved in suspected autoimmune or inflammatory disease: parenchymal, meningeal, ventricular, or vascular.

CT IN NEUROINFLAMMATORY DISEASE

Head CT is a good first step to rule out large structural abnormalities such as masses, hemorrhage, calcifications, bony abnormalities, or hydrocephalus; however, its diagnostic value is limited by its poor resolution and suboptimal soft tissue discrimination leading to lower sensitivity and specificity. Brain MRI is

Copyright © American Academy of Neurology. Unauthorized reproduction of this article is prohibited.

almost always indicated to more thoroughly evaluate subtle findings. When MRI is contraindicated or unavailable, head CT with contrast may be helpful in identifying highly vascular or inflammatory lesions. CT is also particularly useful when the disease process involves bone.

CT angiography provides excellent visualization of the integrity and caliber of vessels based on the time elapsed from contrast administration: early for arterial and delayed for venous phases. This noninvasive method is important in evaluating large vessel obstructions, aneurysms and vascular malformations, dissection, vasospasm, and vasculopathies such as CNS vasculitis (FIGURE 10-2). Small and some medium vessel vasculitides may be missed on CT angiograms, so clinicians must recognize the limitations of resolution when CNS vasculitis is highly suspected.

MRI IN NEUROINFLAMMATORY DISEASE

The T2 fluid-attenuated inversion recovery (FLAIR) sequence is useful in identifying sites of altered water content, including demyelination, edema, inflammation, or gliosis; sagittal and coronal FLAIR may help visualize more specific patterns of abnormality such as lesion orientation away from the ventricular surface, or involvement of the corpus callosum. Some of these pathologies are reversible, and the evolution of FLAIR signal change can help elucidate the suspected pathologic process. High T2 contrast sequences such as fast imaging employing steady state acquisition (FIESTA) or constructive interference in steady state (CISS) highlight the contrast between CSF and other structures such as blood vessels and cranial nerves in the basal cisterns and can help identify lesions of these structures. Postcontrast T1 enhancement indicates increased vascularity or blood-brain barrier disruption due to inflammation.

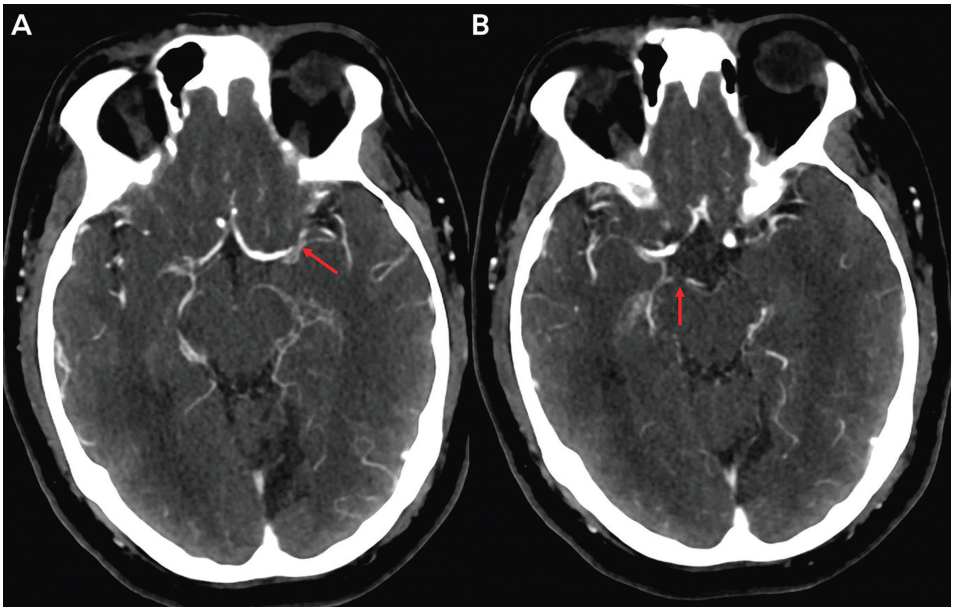

FIGURE 10-2
Axial CT angiography of the head demonstrating severe focal narrowing of the distal M1 segment of the left middle cerebral artery (*A*, *arrow*) and severe stenosis of the P2 segment of the right posterior cerebral artery (*B*, *arrow*) in a patient with multifocal vasculopathy (*other areas not visualized here*) secondary to immune checkpoint inhibitor vasculitis.

Copyright © American Academy of Neurology. Unauthorized reproduction of this article is prohibited.

High-resolution, thin-slice, three-dimensional sequences can be helpful in distinguishing extra-axial from intraparenchymal processes and provide better resolution of the brainstem and cranial nerve structures. High-resolution susceptibility-weighted imaging (SWI) can identify blood within structures such as venules, as well as sites of microhemorrhage. Diffusion-weighted imaging (DWI) can highlight acute infarcts as well as acute demyelination, abscess, and some (generally high-grade) neoplasms.

POSITRON EMISSION TOMOGRAPHY IN NEUROINFLAMMATORY DISEASE

PET using fludeoxyglucose (FDG-PET) can visualize increased metabolic activity in inflamed or hyperactive neuronal tissue (status epilepticus) or decreased metabolism in damaged or dysfunctional tissue. The pattern of uptake often relates to the stage and clinical manifestations of encephalitis, with earlier stages associated with hypermetabolism and later stages with hypometabolism.[5,6] PET may be useful in cases of suspected autoimmune encephalitis when MRI is negative; however, noninflammatory status epilepticus, postictal states, and neurodegenerative diseases may also show similar patterns of hypermetabolism or hypometabolism.

SYNDROMIC APPROACH TO IMAGING

As discussed previously, identifying the predominant compartment affected by inflammation can help narrow the differential substantially. This section discusses imaging findings in specific syndromes of the CNS.

Leptomeningitis

Leptomeningitis is defined as inflammation of the CSF in the subarachnoid space (arachnoid and pia mater) and typically manifests as gyriform or serpentine enhancement following the sulci on postcontrast CT or MRI T1-weighted sequences (FIGURE 10-3). Sulcal enhancement can be hard to differentiate from the normal appearance of vessels tracking along the sulci, so it is important to evaluate images in different planes (ie, axial, sagittal, and coronal). Care should also be taken to ensure that T1-hyperintense signal is not present on precontrast images (and, thus, not truly enhancing on postcontrast images), as can be seen with methemoglobin (subacute hemorrhage), fatty or highly proteinaceous lesions (laminar necrosis), or melanin (metastatic melanoma). FLAIR can show nonsuppression of CSF signal in the sulci manifested by hypertense signal tracking along the sulci. SWI can help distinguish gadolinium enhancement of the meninges from subtle subdural or subarachnoid hemorrhage and calcifications.[7] Clinical history should also focus on any prior traumatic events or neurosurgical procedures, in which the breakdown of the blood-brain barrier can lead to meningeal enhancement in the short term.

Most causes of acute meningitis are viral and bacterial, whereas subacute and chronic meningitis have a much wider range of differential diagnoses that includes systemic autoimmune diseases such as sarcoidosis and rheumatologic diseases, including rheumatoid arthritis.[8,9] Sarcoidosis is a multisystem granulomatous inflammatory disorder. Neurologic involvement most commonly presents as cranial neuropathies in up to 75% of patients with adjacent leptomeningeal enhancement[10] and as subacute to chronic meningitis syndrome in up to 40%. In a study of MRI in 100 patients with neurosarcoidosis, 47%

KEY POINTS

- CT angiography provides good anatomic resolution of large and some medium-size vessels but has poor resolution for smaller vessels.
- Leptomeningitis typically manifests as gyriform or serpentine enhancement following the sulci.
- When assessing extra-axial postcontrast T1-hyperintense lesions, it is important to review in the context of other sequences including T1 precontrast, fluid-attenuated inversion recovery (FLAIR), and susceptibility-weighted imaging (SWI).
- Trauma or neurosurgery may lead to meningeal enhancement in the short term.
- Neurosarcoidosis should be suspected in patients with subacute onset of multiple cranial neuropathies with basal meningitis on MRI.

Copyright © American Academy of Neurology. Unauthorized reproduction of this article is prohibited.

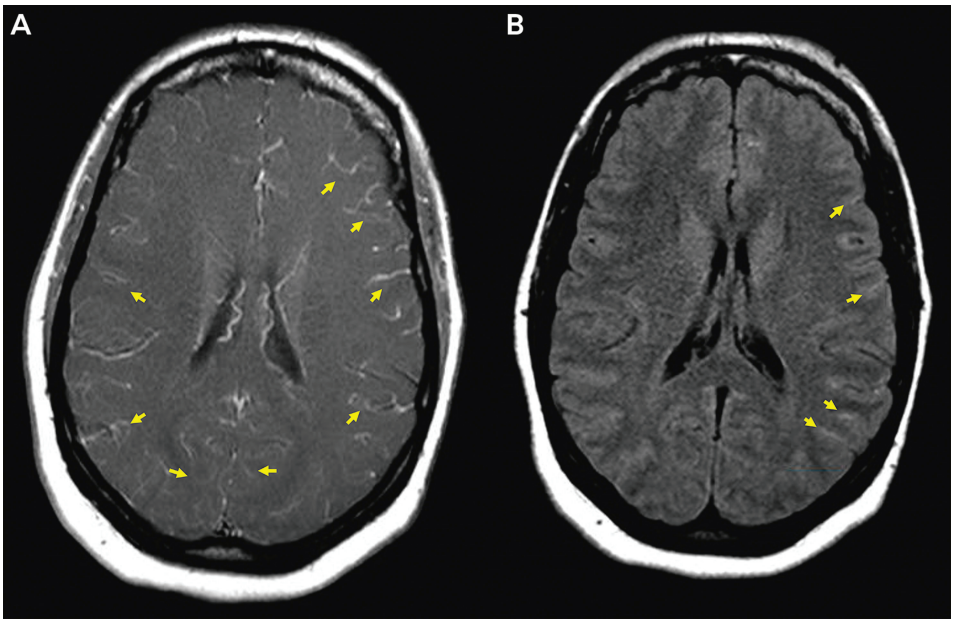

FIGURE 10-3
Axial brain MRI of a patient with autoimmune meningoencephalitis. *A*, Postcontrast T1-weighted MRI showing diffuse leptomeningeal enhancement (*arrows*). *B*, T2 fluid-attenuated inversion recovery (FLAIR) sequence from the same patient with nonsuppression of the CSF signal; note the hyperintensities tracking along the sulci (*arrows*).

showed leptomeningeal enhancement with approximately one-quarter of those patients demonstrating a basal localization (FIGURE 10-4).[11] CNS involvement in rheumatoid arthritis is extremely rare but can manifest as aseptic meningitis with corresponding MRI changes.[12] Rheumatoid meningitis can happen at any time in the course of rheumatoid arthritis.[13] Extension of leptomeningitis into the spinal column may indicate infectious etiologies, such as herpesviruses, tuberculosis, and syphilis among others,[14] but can also be seen in inflammatory diseases such as neurosarcoidosis.

Pachymeningitis

Pachymeningitis refers to inflammation of the dura mater. On MRI, postcontrast T1 images show enhancement of the dura, with or without involvement of the underlying leptomeninges (FIGURE 10-5). The pattern of enhancement may be diffuse or focal, and smooth or nodular. Processes that can mimic inflammatory pachymeningitis include intracranial hypotension, meningioma, and postoperative reactive granulation tissue. Intracranial hypotension, whether spontaneous or traumatic (caused by lumbar puncture, trauma, or neurosurgery), usually manifests clinically with positional headache that is exacerbated in upright positions and radiographically with diffuse and smooth dural enhancement. Other imaging clues include a full sella, crowded pons, and low-lying cerebellar tonsils.[15] Intralesional calcifications and surrounding hyperostosis or bony destruction may be helpful clues to distinguishing meningiomas from inflammatory diseases.[7] Trauma or neurosurgical procedures may lead to chronic granulation tissue and neovascularity causing dural enhancement for years after the procedure.[7] Cranial neuropathies, both clinical and radiographic, are a common feature of skull base pachymeningitis; dural

Copyright © American Academy of Neurology. Unauthorized reproduction of this article is prohibited.

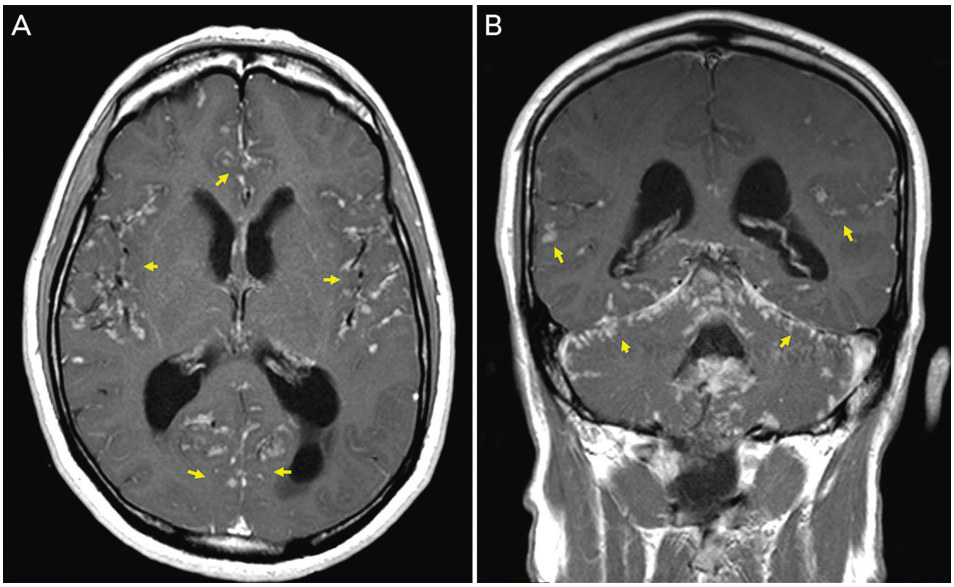

FIGURE 10-4
Axial (*A*) and coronal (*B*) postcontrast T1-weighted MRI showing nodular leptomeningeal enhancement (*A, B, arrows*) most prominently affecting the basal cisterns in a patient with probable neurosarcoidosis (lymph node biopsy positive).

KEY POINTS

- Meningioma is often associated with intralesional calcifications and surrounding hyperostosis or bony destruction, which helps distinguish it from focal pachymeningitis.
- Cranial neuropathies, both clinical and radiographic, are a common feature of skull base meningitis.

thickening can lead to mass effect and compression and vascular compromise of the cranial nerves.[7]

Pachymeningitis may occur as a direct extension of leptomeningitis in several infections including Lyme disease, syphilis, and tuberculosis; in these cases, the presence of prominent CSF inflammation and an acute to subacute time course suggest the infectious mechanism. Isolated dural involvement is more commonly associated with autoimmune and rheumatologic diseases.[9] Sarcoidosis, in addition to causing aseptic leptomeningitis, is an important cause of pachymeningitis. In the previously mentioned imaging study of 100 patients with neurosarcoidosis, pachymeningitis was reported in 32%.[11] Neurosarcoidosis may cause both diffuse and nodular patterns (FIGURE 10-6) and may be associated with simultaneous leptomeningitis or obstructive hydrocephalus.[16]

IgG4-related disease is another important cause of pachymeningitis. It is a chronic progressive autoimmune multisystem disease that frequently involves the pancreas, biliary tract, and kidneys. Pachymeningitis is the most common neurologic manifestation, either as isolated dural disease or with extension

FIGURE 10-5
Axial postcontrast T1-weighted MRI showing dural enhancement with diffuse smooth dural thickening (*arrows*) in a patient with idiopathic pachymeningitis.

Copyright © American Academy of Neurology. Unauthorized reproduction of this article is prohibited.

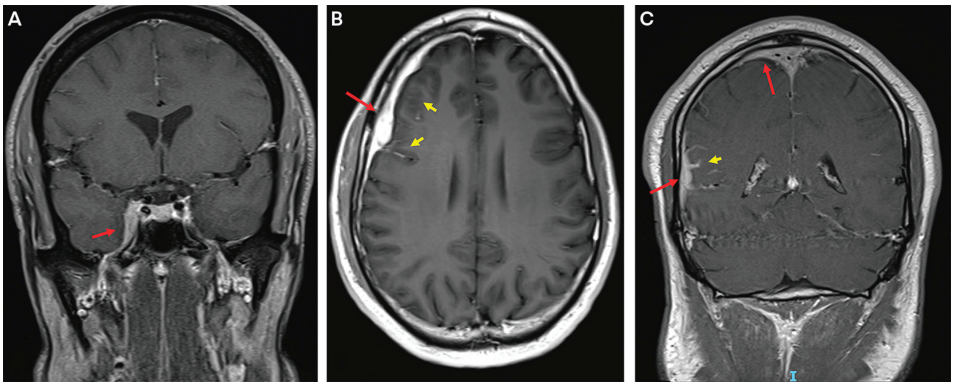

FIGURE 10-6

Three patients with various forms of dural neurosarcoidosis. Coronal postcontrast T1-weighted MRI showing right cavernous sinus dural masslike inflammation (*A, red arrow*) in a patient with right abducens and trigeminal palsies due to possible neurosarcoidosis. Axial (*B*) and coronal (*C*) postcontrast T1-weighted MRI showing dural-based inflammation and focal pachymeningeal enhancement (*B, C, red arrows*) and adjacent leptomeningeal enhancement (*B, C, yellow arrows*) in two patients with neurosarcoidosis.

to adjacent orbital, sinus, and hypothalamopituitary tissues. Dural lesions in IgG4-related disease may be hyperdense on noncontrast CT, mimicking subdural hematoma (FIGURE 10-7). On MRI, lesions may have nodular enhancement and thickening, which may be misdiagnosed as meningioma if focal (FIGURE 10-8). IgG4-related disease (and neurosarcoidosis) can cause hypophysitis and cavernous sinus disease, with nodular enhancing lesions (FIGURE 10-9).

Idiopathic hypertrophic pachymeningitis has been reported with varying presentations and with both diffuse and nodular involvement. As the name suggests, the radiographic and pathologic pattern is hypertrophic, but no identifiable underlying disease is identified. Many cases of idiopathic hypertrophic pachymeningitis are likely due to previously undiagnosed IgG4-related disease.[17]

Granulomatosis with polyangiitis, often associated with antineutrophil cytoplasmic antibodies (ANCAs), may also cause pachymeningitis. CNS involvement may occur in up to 15% of patients with ANCA-associated vasculitis. Hypertrophic pachymeningitis is a typical CNS manifestation, often accompanied by multiple ipsilateral cranial neuropathies. The dura may be affected by direct extension from involved sinuses, which can be a clue to the diagnosis (FIGURE 10-10).[18] The term *CNS-limited ANCA-associated vasculitis* has been used for a specific subset of patients with myeloperoxidase antibody–ANCA-positive vasculitis, with a predilection for older women in a hypertrophic meningitis pattern with less severe neurologic damage and lower rates of generalized disease.[19]

Encephalitis

Encephalitis refers to inflammation of the brain parenchyma. It may be diffuse or focal. Acute encephalitis is frequently caused by viruses, with herpes simplex virus (HSV) type 1 and West Nile virus being the most common. Encephalitis may also occur in the setting of systemic autoimmune diseases, such as sarcoidosis or Behçet syndrome. Autoimmune encephalitis is an umbrella term for a group of noninfectious, immune-mediated brain disorders that typically

Copyright © American Academy of Neurology. Unauthorized reproduction of this article is prohibited.

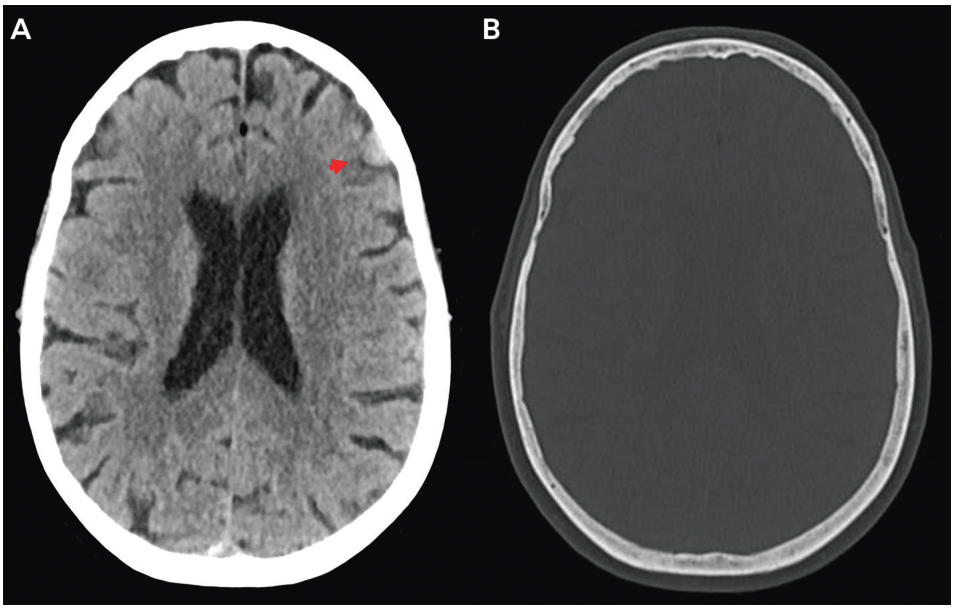

FIGURE 10-7
Axial brain CT without contrast in a patient with biopsy-proven IgG4-related disease. *A*, Brain window showing a left frontal dural hyperdensity (*arrow*) that was initially misdiagnosed as a small subdural hematoma. *B*, Bone window of the same CT scan to demonstrate the lack of changes in the overlying bone that might be seen in other diseases such as meningioma.

KEY POINTS

- IgG4-related disease (as well as neurosarcoidosis) can cause hypophysitis and cavernous sinus disease.
- Direct extension of granulomatous inflammation from sinus to dura is a clue to antineutrophil cytoplasmic antibody–associated vasculitis.
- CNS-limited antineutrophil cytoplasmic antibody–associated vasculitis is typically associated with a hypertrophic meningitis in older women with positive myeloperoxidase antibody.

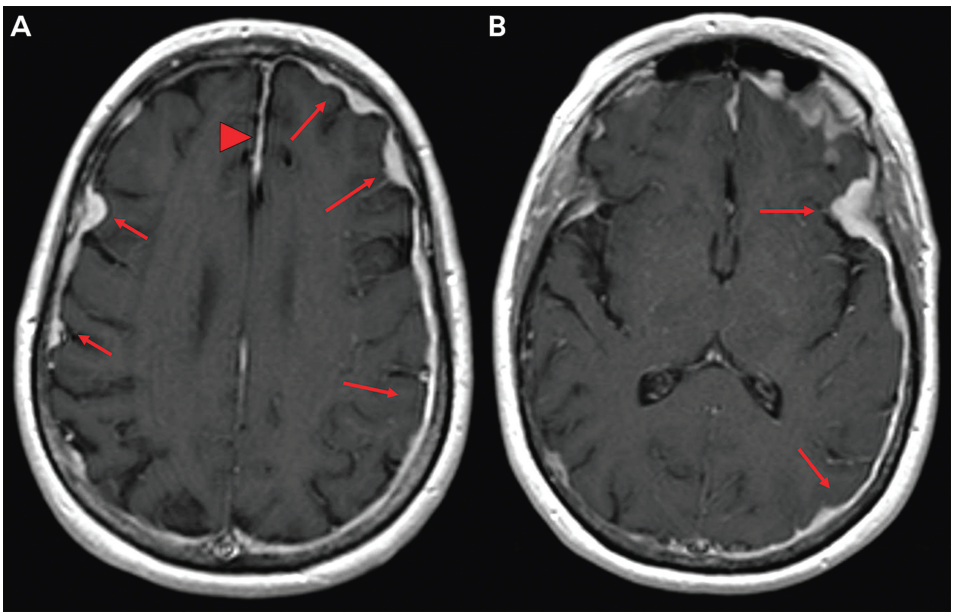

FIGURE 10-8
Axial postcontrast T1-weighted MRI showing numerous dural-based lesions along the bilateral convexity (*A*, *B*, *arrows*) and falx (*A*, *arrowhead*) in a patient with hypertrophic pachymeningitis secondary to biopsy-proven IgG4-related disease.

Copyright © American Academy of Neurology. Unauthorized reproduction of this article is prohibited.

KEY POINTS

- Brain MRI in NMDA receptor encephalitis is normal in most patients.
- Compared with autoimmune encephalitis, herpes simplex virus encephalitis is more likely to be unilateral or asymmetric and to have accompanying diffusion-weighted imaging restriction and enhancement.
- Lack of prodromal symptoms, rapid clinical improvement with antiseizure medications alone, and noninflammatory CSF are all clues to distinguish peri-ictal MRI changes from limbic autoimmune encephalitis.

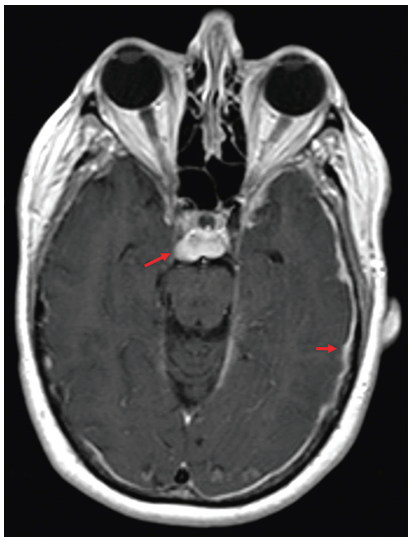

FIGURE 10-9
Axial postcontrast T1-weighted MRI showing a pituitary lesion and dural thickening and enhancement (*arrows*) in a patient with hypertrophic pachymeningitis secondary to biopsy-proven IgG4-related disease.

present with subacute (over 6 to 12 weeks) cognitive or behavioral changes, seizures, or focal neurologic deficits.[20] Autoimmune encephalitis most commonly affects the cortex and deep gray matter but may also involve white matter, meninges, or the spinal cord.[21] The underlying pathophysiology may involve a pathologic autoantibody to neuronal or glial surface antigens, a cytotoxic process targeting onconeural intracellular antigens with an accompanying paraneoplastic antibody marker, an unknown T cell–mediated process, or a yet unidentified autoantibody.[12]

Autoimmune encephalitis may be categorized based on the topography of pathology (FIGURE 10-1).

LIMBIC AUTOIMMUNE ENCEPHALITIS. Limbic autoimmune encephalitis is characterized by anterograde memory loss, behavioral or psychiatric symptoms, and seizures because of the involvement of the medial temporal lobes. Typical imaging findings include T2 hyperintensity in bilateral mesial temporal lobes (FIGURE 10-11). Limbic encephalitis due to LGI1 is one of the most commonly identified forms of autoimmune encephalitis with this imaging appearance, although several other antibody associations have been noted with bilateral temporal lobe predilection. Importantly, brain MRI is normal in most patients

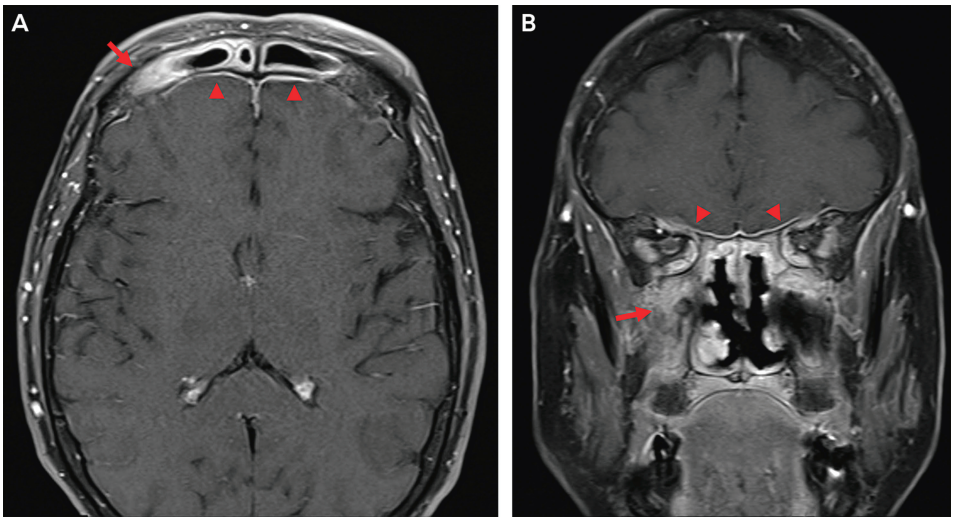

FIGURE 10-10
Axial (*A*) and coronal (*B*) postcontrast T1-weighted MRI showing frontal and maxillary sinus inflammation (*A, B, arrows*) and subjacent dural enhancement (*A, B, arrowheads*) in a patient with multiple cranial neuropathies as the initial presentation of granulomatous polyangiitis (antineutrophil cytoplasmic antibody positive).

Copyright © American Academy of Neurology. Unauthorized reproduction of this article is prohibited.

with NMDA receptor encephalitis despite typical involvement of limbic (among other) areas and the frequency of seizures. It is estimated that up to 89% of patients with NMDA receptor encephalitis have normal initial MRI, and up to 77% upon follow-up MRI (median Day 25).[22]

HSV encephalitis is a potential radiographic mimicker of limbic autoimmune encephalitis. In addition to the clinical clues of a more fulminant clinical course and fever at presentation, on MRI HSV encephalitis is more likely to be unilateral or asymmetric and to have accompanying DWI restriction and enhancement (FIGURE 10-12). When HSV encephalitis MRI changes are bilateral, extensive involvement is typically seen beyond the medial temporal lobe on the side initially affected before spreading to the contralateral temporal lobe.[23,24]

Another challenging radiographic differential diagnosis includes the reversible MRI changes that can be seen in the hippocampi and deep gray matter after seizure activity from any cause, especially given the frequency of seizures as a complication of autoimmune encephalitis. These peri-ictal MRI changes can include T2-hyperintense signal, restricted diffusion on DWI, postcontrast T1 enhancement, and mass effect from edema. The MRI changes may persist for 2 weeks to 5 months before either complete resolution or evolution into gliosis and focal atrophy occur.[25] The lack of prodromal symptoms before the seizure, rapid clinical improvement with antiseizure medications alone, and noninflammatory CSF are helpful clues to differentiate peri-ictal MRI changes from limbic autoimmune encephalitis.

NMDA receptor encephalitis is the most common cause of autoimmune encephalitis. It typically presents with a flulike prodrome followed by an onset of psychiatric and behavioral changes such as anxiety, depression, and psychosis and progresses over time to amnesia, seizures, autonomic dysfunction, and abnormal involuntary movements such as orofacial dyskinesias.[21] Although MRI in NMDA receptor encephalitis is often normal, it can sometimes present as large, poorly demarcated lesions with no or minimal enhancement, located throughout the brain including the cortex, white matter, and deep gray matter.[21]

Patients with Hashimoto encephalopathy present with altered mental status, seizures, myoclonus, hallucinations, or strokelike episodes. Serum antithyroid

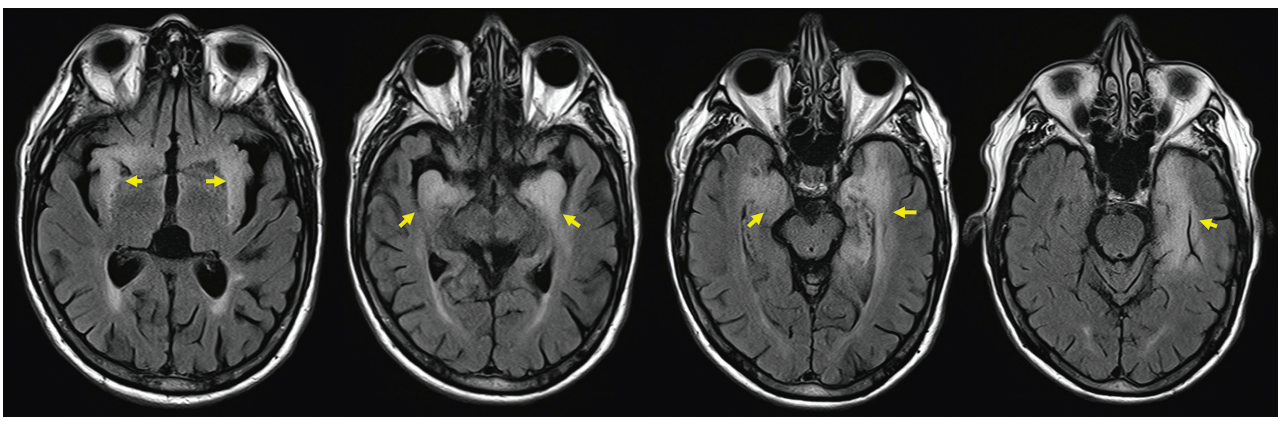

FIGURE 10-11

Axial T2 fluid-attenuated inversion recovery (FLAIR) magnetic resonance images demonstrating abnormal hyperintensities (*arrows*) in the bilateral insula and mesiotemporal lobes in a patient with seronegative limbic encephalitis. No associated abnormality was seen on diffusion-weighted imaging (DWI) (*not shown*).

Copyright © American Academy of Neurology. Unauthorized reproduction of this article is prohibited.

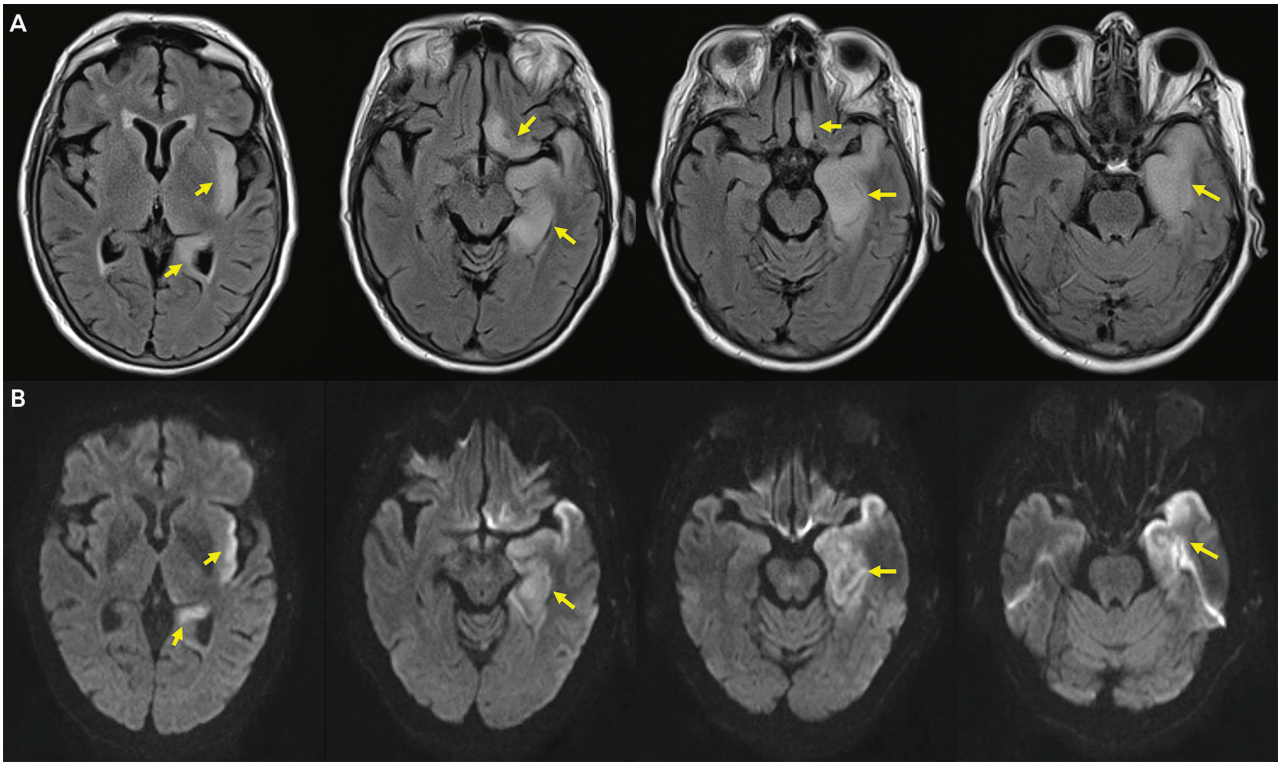

FIGURE 10-12
Axial brain MRI of a patient with herpes simplex virus encephalitis. *A*, T2 fluid-attenuated inversion recovery (FLAIR) magnetic resonance images showing markedly asymmetric abnormal hyperintensity (*arrows*) in the left insula, medial temporal, and inferior frontal areas. *B*, Diffusion-weighted imaging (DWI) showing restricted diffusion (*arrows*) in the same areas.

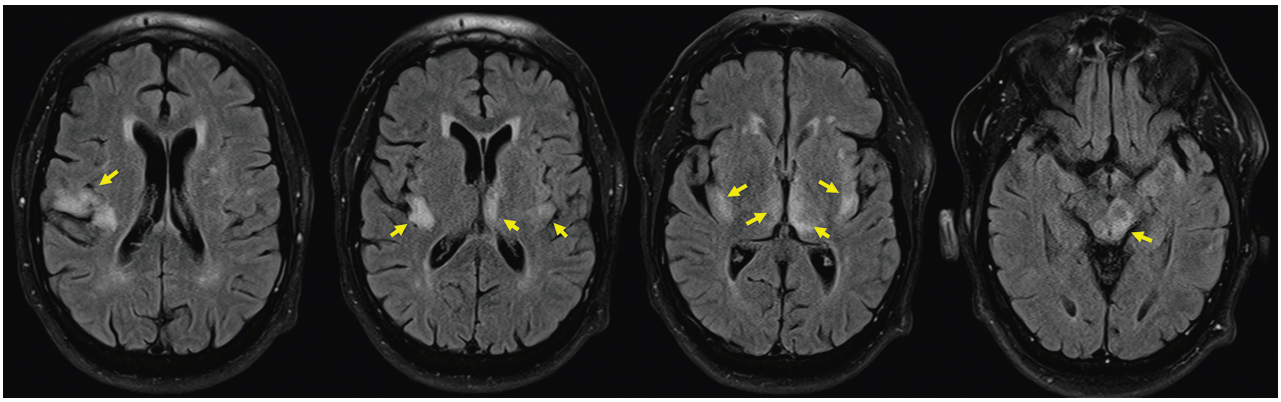

FIGURE 10-13
Axial T2 fluid-attenuated inversion recovery (FLAIR) magnetic resonance images showing scattered hyperintensities (arrows) in the right parietal lobe, bilateral insula, bilateral thalami (more prominent on the left), and left midbrain in a patient with encephalitis secondary to exposure to immune checkpoint inhibitor therapy.

Copyright © American Academy of Neurology. Unauthorized reproduction of this article is prohibited.

peroxidase or thyroglobulin antibodies or both are elevated, although this is associated with subclinical or only mildly overt thyroid disease. These thyroid antibodies are thought to be a biomarker of an immune-mediated process but are not part of the CNS pathology. About 50% of patients with Hashimoto encephalopathy have a normal brain MRI. The Graus 2016 criteria for diagnosis of Hashimoto encephalopathy stipulate that MRI is normal or shows only nonspecific findings such as cerebral atrophy and subcortical white matter changes.[20] Those with hippocampal or temporal lobe hyperintensities on FLAIR should raise the suspicion for either postictal edema or seronegative autoimmune encephalitis.[20,26]

When autoimmune encephalitis is suspected but brain MRI is normal, fludeoxyglucose positron emission tomography (FDG-PET) of the brain can be a more sensitive biomarker in detecting focal or multifocal brain abnormalities, with studies reporting a sensitivity of 87% compared with 56% for MRI.[5] Most PET imaging in limbic autoimmune encephalitis shows abnormalities within the basal ganglia and mesiotemporal lobes, with varying hypermetabolism or hypometabolism depending on the syndrome and stage of the illness. A gradient of anterior hypermetabolism to posterior cortical hypometabolism, especially in the medial and lateral occipital lobes, has been described in NMDA receptor encephalitis.[27] In Rasmussen encephalitis, a pattern of hemispheric hypometabolism, out of proportion to the atrophy seen on MRI, can help make the diagnosis.[5] Despite the utility of PET in diagnosing these forms of autoimmune encephalitis, clinicians must be aware that hypometabolic foci are nonspecific and may be seen commonly postictally and in older patients with neurodegenerative disease.[28]

Although the presence of bilateral temporal lobe FLAIR hyperintensities is typical enough to make a diagnosis of limbic autoimmune encephalitis even in the absence of neuronal antibodies (once viral etiologies have been sufficiently ruled out), other MRI patterns including cortical, subcortical, deep (striatal and diencephalic), brainstem, and cerebellar involvement are less specific and support only possible or probable autoimmune encephalitis unless a clinically relevant autoantibody is positive.[20]

SUBCORTICAL IMMUNE-MEDIATED DISEASE. Subcortical immune-mediated disease is most commonly caused by demyelinating disorders such as acute disseminated encephalomyelitis (ADEM), myelin oligodendrocyte glycoprotein (MOG)–associated disorder, and multiple sclerosis. Rarely, however, autoimmune encephalitis can present with subcortical predominance, for example, with immune checkpoint inhibitor–induced encephalitis (FIGURE 10-13). Conversely, cortical involvement or "cortical encephalitis" can sometimes occur with predominantly subcortical syndromes, especially ADEM and MOG-associated disorder (FIGURE 10-14).

An important diagnostic consideration for subacute, predominantly subcortical encephalitis is progressive multifocal leukoencephalopathy caused by JC virus infection, most commonly associated with immunocompromise including human immunodeficiency virus (HIV) infection, lymphoproliferative diseases, and natalizumab therapy in patients with multiple sclerosis. MRI FLAIR sequences are the most sensitive for detecting progressive multifocal leukoencephalopathy lesions, which typically involve subcortical and juxtacortical white matter hyperintensities with early involvement of the U fibers.

KEY POINTS

- About 50% of patients with Hashimoto encephalopathy have a normal brain MRI.
- Fludeoxyglucose positron emission tomography (FDG-PET) of the brain can be a more sensitive biomarker than brain MRI for detecting focal or multifocal brain abnormalities in autoimmune encephalitis.
- A gradient of anterior hypermetabolism to posterior cortical hypometabolism, especially in the medial and lateral occipital lobes, has been described in NMDA receptor encephalitis.
- Hypometabolic PET patterns are not specific to autoimmune encephalitis and are seen commonly in the postictal state and in older patients with neurodegenerative disease.
- Once viral causes are ruled out, the presence of bilateral temporal lobe FLAIR hyperintensities is sufficient to diagnose definite limbic autoimmune encephalitis even in the absence of neuronal antibodies.

Copyright © American Academy of Neurology. Unauthorized reproduction of this article is prohibited.

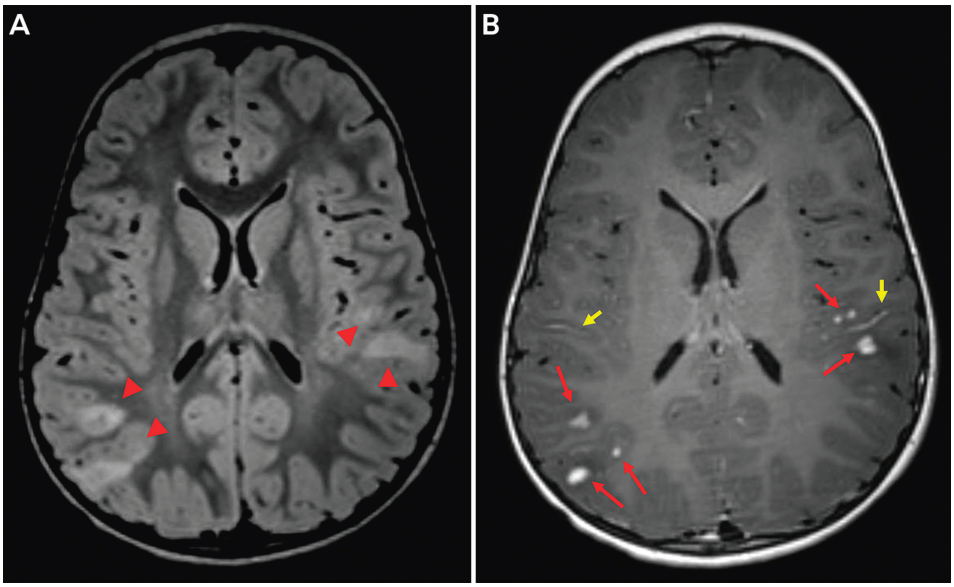

FIGURE 10-14
Axial T2 fluid-attenuated inversion recovery (FLAIR) (*A*) and postcontrast T1-weighted (*B*) MRI demonstrating "fluffy" cortical and subcortical lesions *(A, red arrowheads)* with associated parenchymal (B, red arrows) and leptomeningeal enhancement *(B, yellow arrows)* in a patient with myelin oligodendrocyte glycoprotein–associated acute disseminated encephalomyelitis (ADEM) with concurrent positive anti–*N*-methyl-D-aspartate (NMDA) receptor antibody.

Lesions are usually isointense or hypointense lesions on T1-weighted imaging with variable enhancement depending on the state of the host's immune system (nonenhancing with severe immunocompromise and patchy enhancement in patients with mild immunosuppression or reconstituting immune systems) (FIGURE 10-15). Serial imaging shows asymmetric enlargement of lesions, coalescence, and appearance of new lesions, hence the name *multifocal*.[29]

MULTIPLE AND CONFLUENT CORTICAL AND SUBCORTICAL DISEASE. Multiple and confluent cortical and subcortical FLAIR hyperintensities are a hallmark of encephalitis with autoantibodies to γ-aminobutyric acid type A ($GABA_A$) receptor, typically presenting as drug-resistant epilepsy and epilepsia partialis continua.[30] In contrast to $GABA_B$ receptor encephalitis, which tends to show no abnormalities on MRI, $GABA_A$ receptor encephalitis demonstrates these multifocal lesions in the frontal and temporal lobes and bilateral cingulate gyri without abnormal enhancement, diffusion restriction, or mass effect (FIGURE 10-16).[31] In children with refractory epilepsia partialis continua, subcortical T2 changes restricted to one hemisphere should raise concern for Rasmussen encephalitis, which typically presents early on as edema and nonenhancing hyperintensity on FLAIR imaging, especially in the insular and peri-insular regions, followed by severe hemispheric atrophy as the disease progresses.[32]

INVOLVEMENT OF DEEP GRAY MATTER. Involvement of the deep gray matter in encephalitis may be divided into striatal and diencephalic. Clinically, these syndromes are easily distinguished from limbic encephalitis. Striatal encephalitis tends to manifest with movement disorders such as chorea in association with anticollapsin response mediator protein-5 (CRMP5 or CV2) antibodies, typically

Copyright © American Academy of Neurology. Unauthorized reproduction of this article is prohibited.

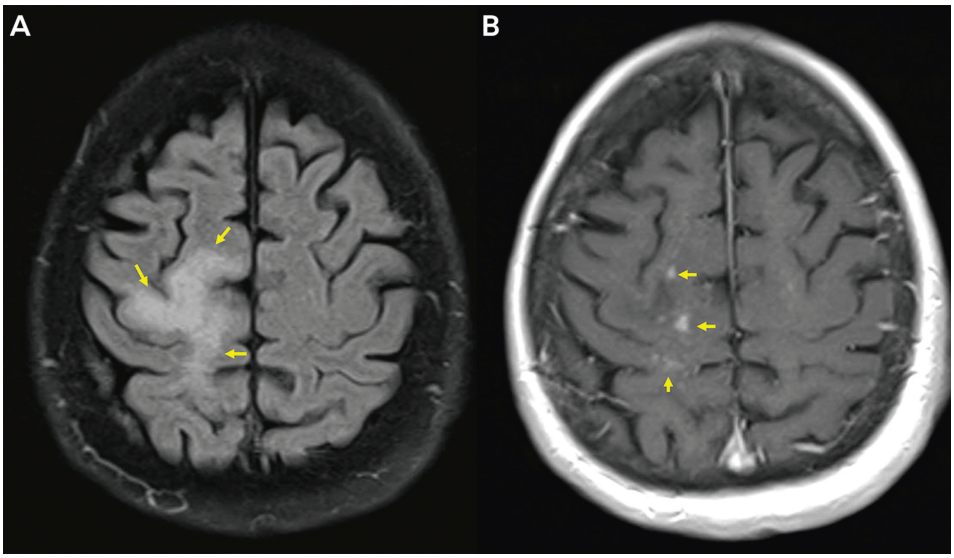

FIGURE 10-15
Axial T2 fluid-attenuated inversion recovery (FLAIR) (*A*) MRI showing right frontal juxtacortical and subcortical T2-hyperintense signal change (*A, arrows*) and axial postcontrast T1-weighted (*B*) MRI showing central hypointense signal with patchy enhancement (*B, arrows*) in a patient with biopsy-proven progressive multifocal leukoencephalopathy without known immunocompromise.

KEY POINT

- Multiple and confluent cortical and subcortical FLAIR hyperintensities are a hallmark of encephalitis with autoantibodies to γ-aminobutyric acid type A ($GABA_A$) receptor.

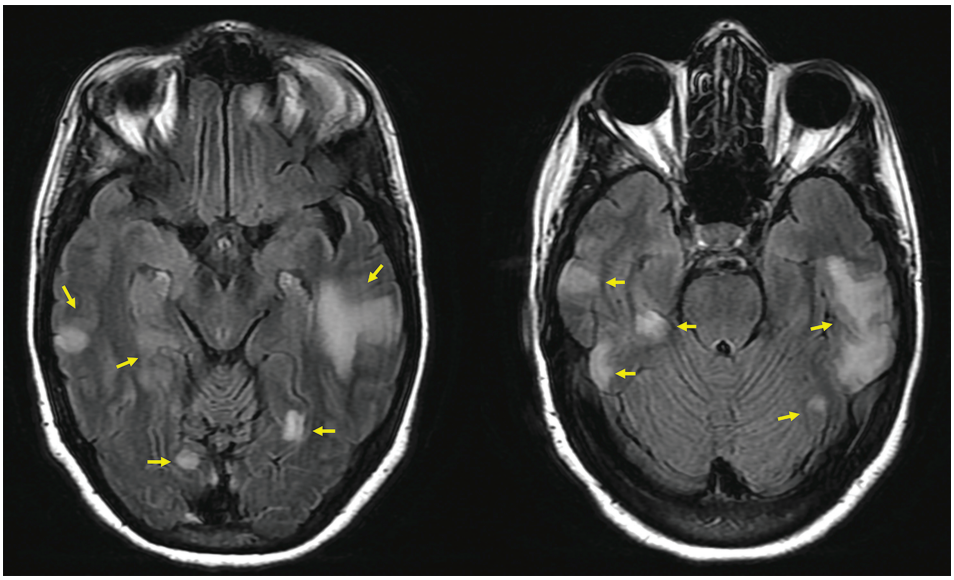

FIGURE 10-16
Axial T2 fluid-attenuated inversion recovery (FLAIR) MRI showing several abnormal cortical and subcortical hyperintensities (*arrows*), without enhancement (*not shown*), in a patient with γ-aminobutyric acid type A ($GABA_A$) receptor encephalitis.
Images courtesy of Christine Gill, MD.

Copyright © American Academy of Neurology. Unauthorized reproduction of this article is prohibited.

heralding an occult small cell lung cancer. Cases of extensive T2-hyperintense symmetric signal affecting the bilateral caudate and putamen have been reported with extension into the anterior limbs of the internal capsules.[33,34] Dopamine D_2 receptor encephalitis also manifests with basal ganglia T2 hyperintensities on MRI in 50% of patients with this autoantibody and mainly presents in adolescents as subacute parkinsonism and dystonia after an infection such as β-hemolytic streptococcus and mycoplasma.[35] Diencephalic encephalitis manifests with sleep disturbances (narcolepsy-cataplexy) and autonomic and hormonal disturbances due to the involvement of the hypothalamus. Anti-Ma2–associated encephalitis, commonly associated with testicular germ cell tumors, characteristically targets the diencephalon. Brain MRI is abnormal in up to 74% of patients with positive anti-Ma antibodies; in those with a diencephalic presentation, MRI may show T2 hyperintensities with variable enhancement in the medial thalami and midbrain (FIGURE 10-17).[36] For clinical or radiographic subacute hypothalamic inflammatory syndromes, neurosarcoidosis should also be considered; involvement of the pituitary stalk and gland in addition to the hypothalamus can be a clue to this diagnosis.

Glial fibrillary acidic protein (GFAP) astrocytopathy is an autoimmune encephalitis that may manifest with meningitis, encephalitis, myelitis, and optic neuritis.[37] It has been associated with periventricular linear radial enhancement

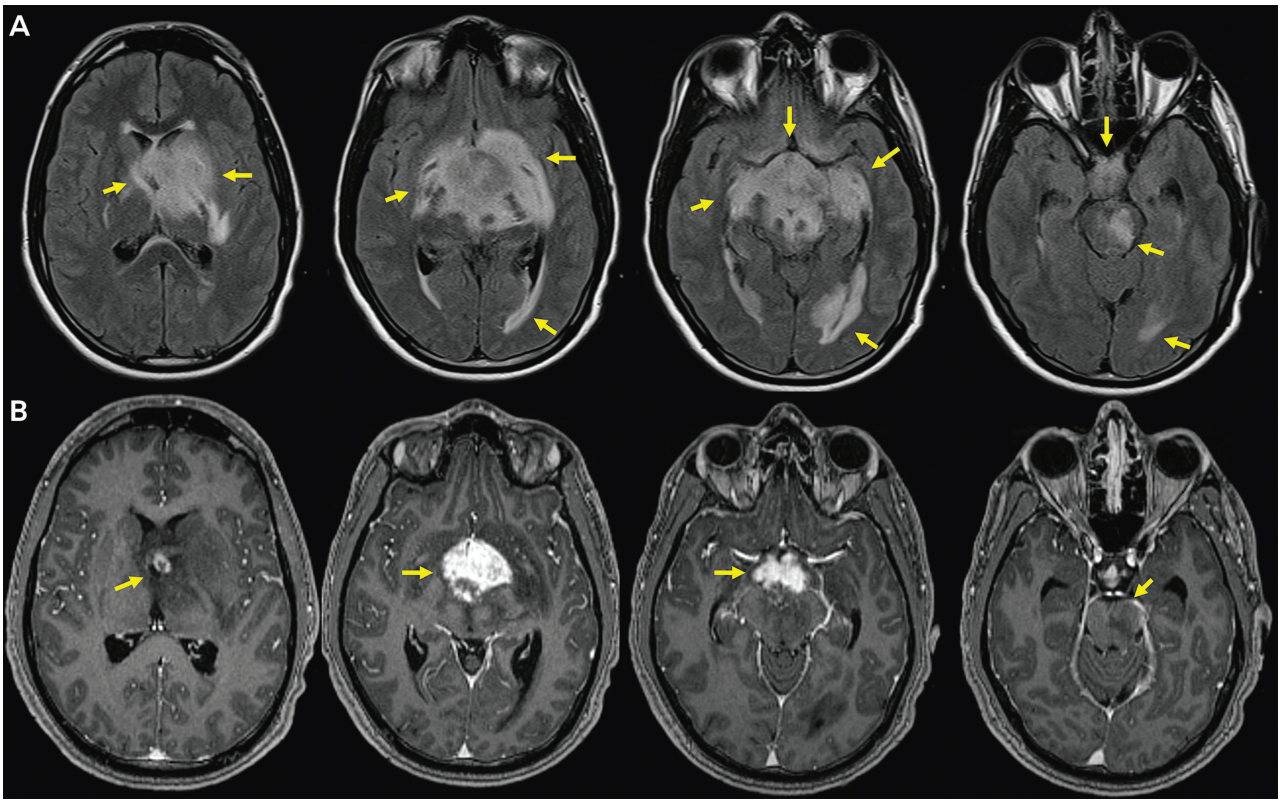

FIGURE 10-17

Axial T2 fluid-attenuated inversion recovery (FLAIR) (*A*) and axial postcontrast T1-weighted (*B*) MRIs revealing a suprasellar, diencephalic T2-hyperintense lesion (*A, arrows*) that is avidly enhancing (*B, arrows*), with mass effect and resultant obstructive hydrocephalus in a patient with anti-Ma2 encephalitis and nonseminomatous germ cell tumor found in the mediastinum.

Copyright © American Academy of Neurology. Unauthorized reproduction of this article is prohibited.

on MRI postcontrast T1-weighted imaging, a distinctive radiographic finding that should raise suspicion for the culprit autoantibody; this finding has also been described in the cerebellum and brainstem.[37,38] Patients with GFAP astrocytopathy may also harbor other autoantibodies such as NMDA receptor IgG (CASE 10-1).

BRAINSTEM AND CEREBELLAR INFLAMMATORY PATHOLOGIES. Brainstem and cerebellar inflammatory pathologies tend to present with acute to subacute ataxia, cranial neuropathies, bulbar dysfunction, and pyramidal weakness.[39] Inflammation of hindbrain structures (pons, medulla, and cerebellum) is sometimes termed *rhombencephalitis*, but many processes also affect the midbrain. For simplicity, many authors use the term *brainstem encephalitis* to indicate midbrain and hindbrain inflammation. Of note, for posterior fossa structures, subtle T2 hyperintensity may be more easily appreciated on conventional T2-weighted MRI than on FLAIR sequences.

Listeria monocytogenes is the most common cause of infectious brainstem encephalitis, with tropism for the tissue surrounding the fourth ventricle. On MRI, T1 hypointensity and T2 hyperintensity are typical; if present, rim-enhancing lesions with central restricted diffusion suggestive of abscess are a strong clue to the diagnosis. Although HSV type 1 preferentially involves the limbic system, extralimbic brainstem involvement may also occur. Acute to subacute onset with fever and inflammatory CSF should prompt consideration and treatment for *Listeria* infection or HSV encephalitis in cases with clinical and radiographic evidence for brainstem encephalitis until these are excluded.[39]

Autoimmune brainstem pathologies are diverse, and MRI can offer helpful clues, even if normal (TABLE 10-1[40,41]). Behçet syndrome is a systemic vascular inflammatory disease with hallmark features including recurrent oral ulcers and combinations of genital ulcers, uveitis, or skin changes. When the CNS is involved (neuro-Behçet syndrome), the disorder has a predilection for the corticospinal tracts in the midbrain and pons, with variable rostral extension into the internal capsule or caudal extension into the medulla and spinal cord. The underlying inflammatory process in venules leads to an MRI pattern including T2 hyperintensity and edema sparing the red nucleus, patchy postcontrast T1 enhancement, and punctate foci of susceptibility artifact on SWI (FIGURE 10-19).[42]

Another immune-mediated syndrome with a tropism for the brainstem is chronic lymphocytic inflammation with pontine perivascular enhancement responsive to steroids (CLIPPERS). This idiopathic immune-mediated disorder is marked by a subacute brainstem syndrome with MRI showing a unique pattern of multiple small (<3 mm) FLAIR–hyperintense foci with matching homogenous or curvilinear enhancement mostly restricted to the pons (although it may extend rostrally or caudally). By definition, the clinical syndrome and lesions improve markedly with corticosteroids.[43] Pathologies that can radiographically mimic CLIPPERS include CNS lymphoma and granulomatous diseases such as CNS tuberculosis and neurosarcoidosis, all of which may have a similar punctate or curvilinear enhancement pattern reflecting a perivascular location and may respond (at least initially) to corticosteroids (FIGURE 10-20). CNS tuberculosis and neurosarcoidosis are often associated with meningitis and accompanying leptomeningeal enhancement, which is less common with CLIPPERS. Susac syndrome is an endotheliopathy defined by a triad of encephalopathy, retinal vasculitis, and

KEY POINTS

- Striatal encephalitis with anti-collapsin response mediator protein 5 (CRMP5 or CV2) antibodies may be associated with extensive T2-hyperintense symmetric signal affecting the bilateral caudate and putamen.
- Paraneoplastic diencephalic encephalitis associated with Ma2 antibodies may cause T2 hyperintensities in the medial thalami and midbrain.
- Glial fibrillary acidic protein (GFAP) astrocytopathy is associated with a hallmark MRI finding of periventricular linear radial enhancement on postcontrast T1-weighted sequences.
- For posterior fossa structures, subtle T2 hyperintensity may be more easily appreciated on conventional T2-weighted MRI than on FLAIR sequences.
- Rim-enhancing lesions with central restricted diffusion suggestive of abscess are clues to *Listeria* infection as the cause of brainstem encephalitis.
- Neuro-Behçet syndrome may be associated with T2 hyperintensity in the ventral pons and midbrain, sparing the red nucleus.

Copyright © American Academy of Neurology. Unauthorized reproduction of this article is prohibited.

CASE 10-1

A 23-year-old woman developed headache and confusion followed by bursts of aggression, forgetfulness, and insomnia over a few days. In the emergency department, she was tachycardic, tachypneic, and febrile to 38.6°C (101.5°F). She was started on empiric treatment for meningitis and encephalitis with antibiotics and acyclovir. She progressed rapidly to stupor and developed abnormal stereotypical movements of bilateral eyelids, mouth opening and closing, and inverse ocular bobbing. Lumbar puncture revealed normal glucose adjusted for serum, an elevated protein concentration of 135 mg/dL, and lymphocytic pleocytosis with 331 cells/mm^3; infectious multiplex polymerase chain reaction (PCR) assay was negative which prompted discontinuation of the empiric antibiotics and acyclovir. Brain MRI with contrast revealed diffuse leptomeningeal enhancement, as well as periventricular linear radial enhancement (FIGURE 10-18). EEG was significant for diffuse slowing without epileptiform discharges. Autoimmune encephalitis was suspected, and empiric treatment was initiated with methylprednisolone 1000 mg IV daily for 5 days and concomitant IV immunoglobulins (IVIg) 2 g/kg administered in divided doses over 2 consecutive days. The autoantibody panel returned positive for both anti–*N*-methyl-D-aspartate (NMDA) receptor antibody and anti–glial fibrillary acidic protein (GFAP) antibody in both the serum and CSF. Tumor screening with fludeoxyglucose positron emission tomography (FDG-PET) of her whole body and transvaginal ultrasonography was negative. Because of paroxysmal sympathetic hyperactivity requiring intensive care, the patient was started sequentially on rituximab followed 2 weeks later by cyclophosphamide.

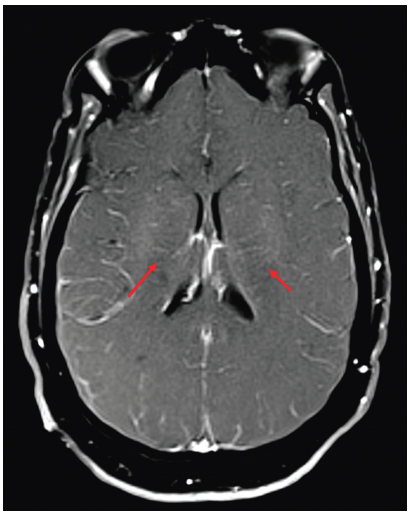

FIGURE 10-18
Axial postcontrast T1-weighted MRI showing diffuse leptomeningeal enhancement with characteristic radial linear enhancement perpendicular to the lateral ventricles (*arrows*) in the patient in CASE 10-1 with *N*-methyl-D-aspartate (NMDA) receptor encephalitis with concomitant glial fibrillary acidic protein (GFAP) meningoencephalitis.

COMMENT

It is most likely that this patient's MRI and CSF findings are driven by GFAP meningoencephalitis, whereas her clinical picture is driven by NMDA receptor encephalitis. The patient improved slowly with aggressive symptomatic treatment of her autonomic instability, as well as the immunosuppressant therapies. She was discharged from the hospital after several months in the ICU with a tracheostomy and a percutaneous gastrostomy tube for enteral feeding with plans for physical therapy.

Copyright © American Academy of Neurology. Unauthorized reproduction of this article is prohibited.

Brainstem Inflammatory Syndromes[a]

TABLE 10-1

Characteristics	Inflammatory differential diagnosis	Noninflammatory differential diagnosis
Topography and size of lesion		
Well-defined, peripheral, and ovoid, especially when affecting specific tracts (medial longitudinal fasciculus, trigeminal fascicles)	Multiple sclerosis	Ischemic infarcts
Circumventricular lesion (abutting third and fourth ventricles) Linear lesions along the dorsal medulla (area postrema)	Neuromyelitis optica spectrum disorder (NMOSD)	Not applicable (NA)
Extension into the diencephalon	NMOSD, neuro-Behçet syndrome	Wernicke encephalopathy, Whipple disease
Space-occupying lesion	Tumefactive demyelination, central nervous system (CNS) vasculitis, CNS histiocytosis	Glioma
Asymmetric, hazy, or "fluffy" lesions that are poorly demarcated	Myelin oligodendrocyte glycoprotein (MOG)-associated disorder, acute disseminated encephalomyelitis (ADEM), neuro-Behçet syndrome	Whipple disease, herpes simplex virus (HSV) encephalitis, small vessel ischemic changes (especially when central pontine)
Brainstem atrophy	Chronic multiple sclerosis or NMOSD, neuro-Behçet syndrome, chronic lymphocytic inflammation with pontine perivascular enhancement responsive to steroids (CLIPPERS)	Neurodegenerative causes such as Alexander disease
Pattern of enhancement		
Punctate and curvilinear	CLIPPERS, Susac syndrome	NA
Nodular	Neurosarcoidosis, CNS vasculitis	NA
Open ring	CNS demyelination	NA
Meningeal and cranial neuropathies	Neurosarcoidosis, IgG4-related disease, vasculitis	Tuberculosis meningitis, Lyme meningitis
Other sequences		
Diffusion restriction	Acute demyelination, neuro-Behçet syndrome, Susac syndrome, vasculitis	Lymphoma, abscess, acute ischemia, central pontine myelinolysis
T1 hypointensity	NMOSD	NA
Microhemorrhages on susceptibility-weight imaging (SWI) or gradient echo (GRE)	Inflammatory cerebral amyloid angiopathy (reported in the thalamus and cerebellum)[41]	HSV encephalitis

[a] Data from Law LY, et al, Neurology.[40]

Copyright © American Academy of Neurology. Unauthorized reproduction of this article is prohibited.

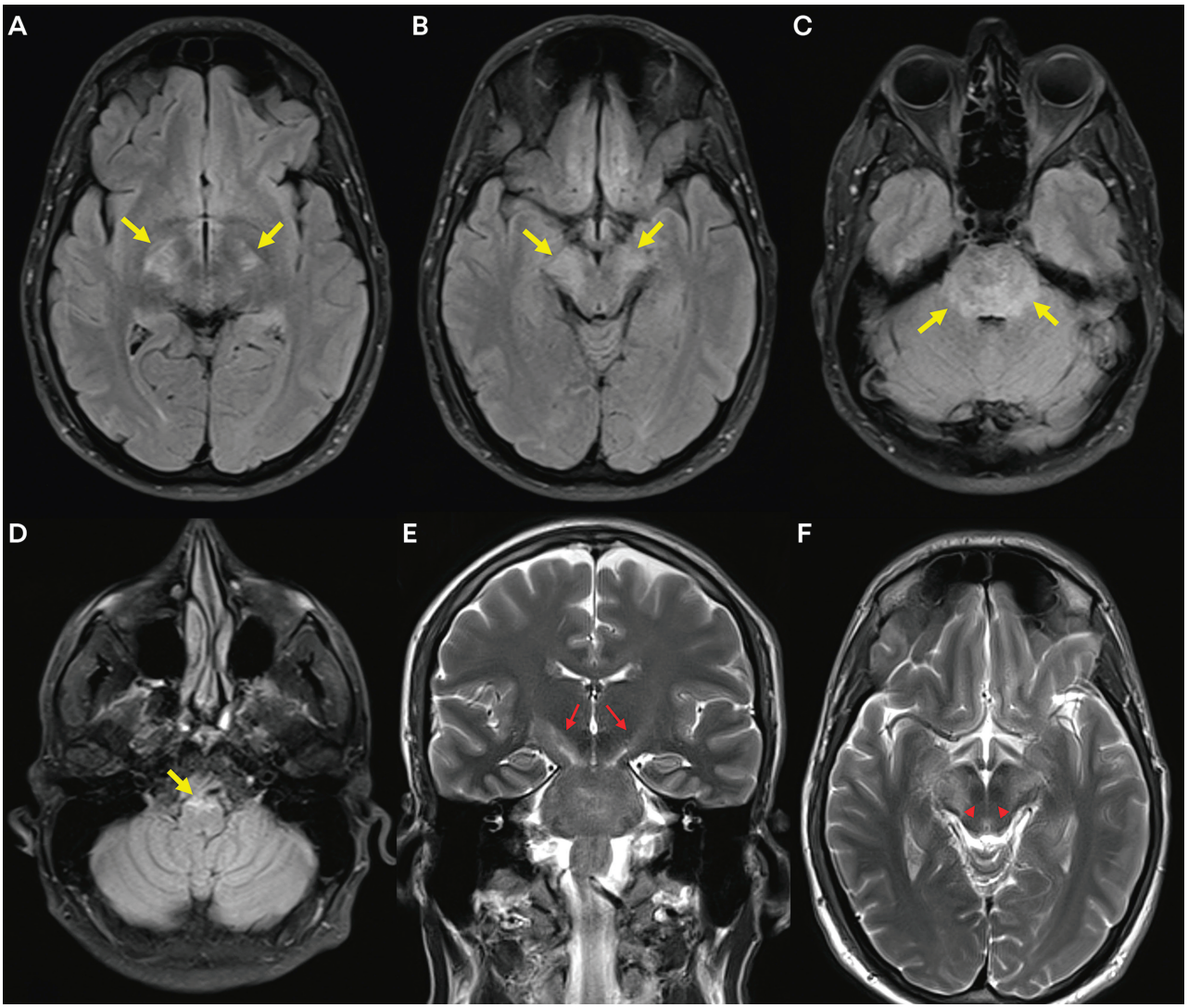

FIGURE 10-19

Brain MRI of a patient with neuro-Behçet syndrome. Axial T2-fluid-attenuated inversion recovery (FLAIR) MRI showing abnormal T2-hyperintense signal (A, B, C, D, yellow arrows) in the right more than left internal capsule (*A*), midbrain (*B*), pons (*C*), and medulla (*D*). Coronal (*E*) and axial (*F*) T2-weighted MRI highlights the corticospinal tract tropism *(E, red arrows)* and sparing of red nuclei *(F, red arrowheads).*

sensorineural hearing loss. It may involve the brainstem with punctate T2-hyperintense foci and curvilinear enhancement; unlike CLIPPERS, however, the foci restrict diffusion acutely and are often accompanied by T2-hyperintense round lesions in the corpus callosum (snowball lesions) (FIGURE 10-21).[44]

Aquaporin-4 IgG-positive NMOSD may present with a brainstem syndrome, typically with symptoms referable to the area postrema in the medulla or circumventricular region around the third ventricle, which is rich in aquaporin-4 channels. MRI demonstrates T2 hyperintensity in the dorsal medulla or rostral midbrain, with minimal or patchy enhancement (FIGURE 10-22). MOG-associated disorder may also present with an area postrema

Copyright © American Academy of Neurology. Unauthorized reproduction of this article is prohibited.

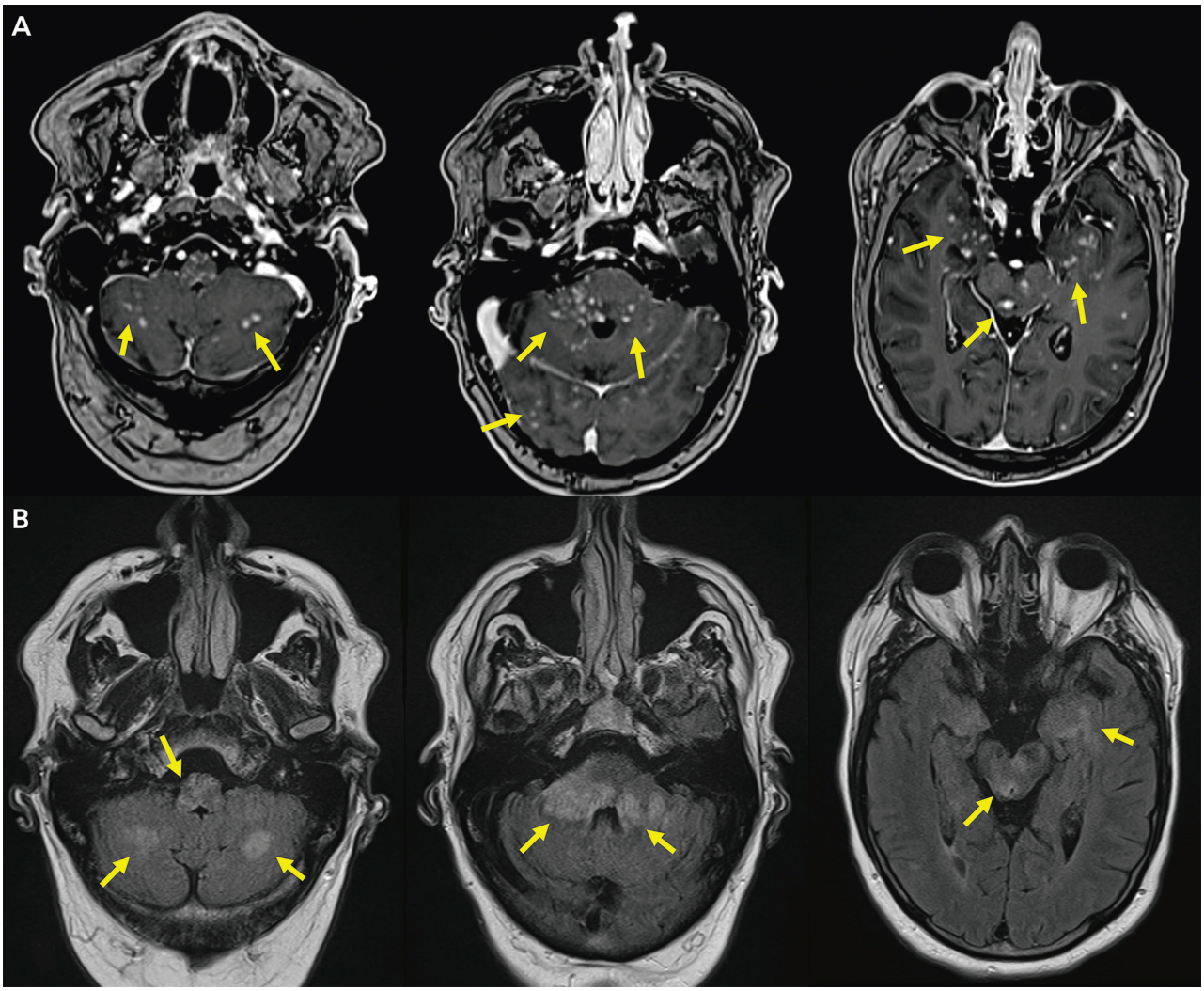

FIGURE 10-20

Axial postcontrast T1-weighted (*A*) MRIs showing multifocal punctate "scattershot" lesions (*A, arrows*) with accompanying abnormal hyperintense signal (*B, arrows*) on axial T2 fluid-attenuated inversion recovery (FLAIR) images throughout the brainstem, cerebellum, and cerebral hemispheres, as well as spinal cord (*not shown*) in a patient with probable neurosarcoidosis.

syndrome. Both NMOSD and MOG-associated disorder may present with associated optic neuritis or longitudinally extensive transverse myelitis, which are clues to the diagnosis.[40]

Some patients present with clinical symptoms and signs that localize to the brainstem, but MRI is normal, initially and on subsequent scans. Several immune-mediated brainstem pathologies may be MRI negative. Bickerstaff brainstem encephalitis is defined by a triad of ataxia, bilateral external ophthalmoplegia, and encephalopathy and is considered a variant of Guillain-Barré syndrome. As with the related Guillain-Barré syndrome variant Miller-Fisher syndrome, anti-GQ1b antibody in the serum or CSF is specific for the disease. Although MRI is usually normal, Bickerstaff brainstem encephalitis can be associated with MRI changes in up to 30% of patients,

Copyright © American Academy of Neurology. Unauthorized reproduction of this article is prohibited.

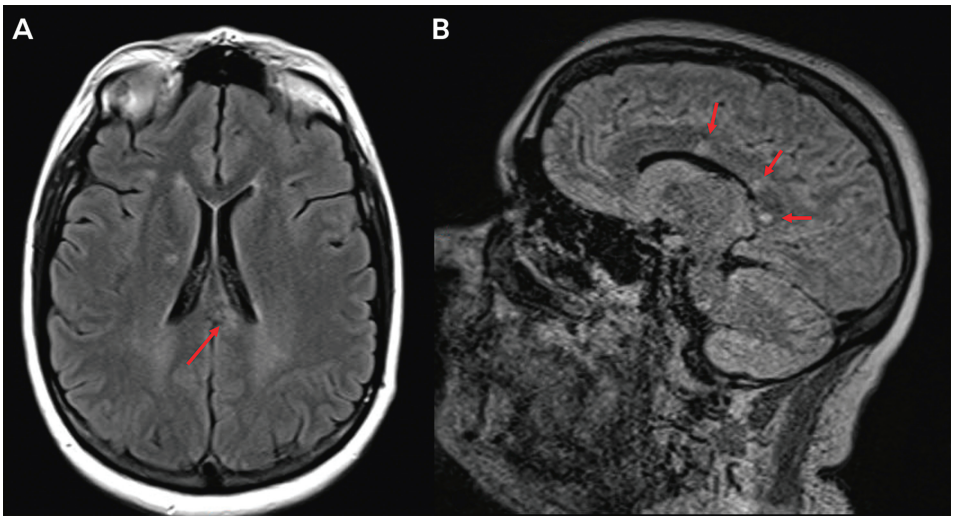

FIGURE 10-21
Axial (*A*) and sagittal (*B*) T2 fluid-attenuated inversion recovery (FLAIR) sequences demonstrating "snowball" T2 hyperintensities in the corpus callosum (*A, B, arrows*) in a patient with Susac syndrome.

including waxing and waning T2-hyperintense lesions throughout the brainstem (especially in the midbrain).[40]

Patients with anti-IgLON5 disease present with parasomnia and breathing difficulty during sleep preceded or accompanied by bulbar symptoms resembling motor neuron disease, gait abnormalities, oculomotor problems resembling progressive supranuclear palsy, and cognitive decline. Brain MRI is typically unremarkable but may show mild atrophy of the brainstem and cerebellum.[45]

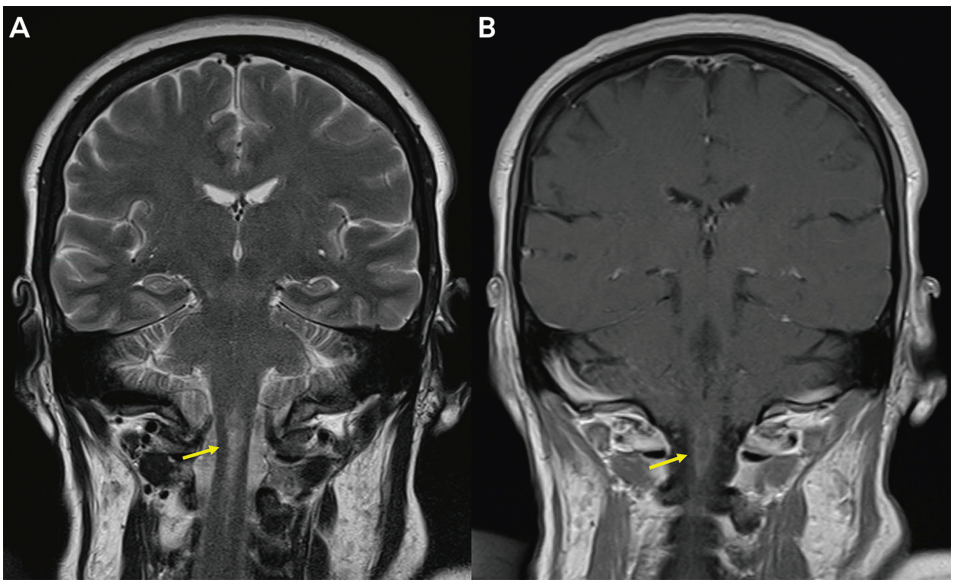

FIGURE 10-22
Coronal T2-weighted (*A*) MRI showing abnormal hyperintensity in the dorsal medulla (*A*, *arrow*) with corresponding coronal T1 postcontrast enhancement (*B*, *arrow*) in a patient with aquaporin-4 IgG positive neuromyelitis optica spectrum disorder presenting with area postrema syndrome (refractory vomiting).

Copyright © American Academy of Neurology. Unauthorized reproduction of this article is prohibited.

Paraneoplastic brainstem encephalitis secondary to onconeural antibodies is also associated with a normal or nonspecific brain MRI. Kelch-like protein 11 antibody in seminoma-associated paraneoplastic encephalitis presents with ataxia and cochleovestibulopathy but normal MRI.[46] Anti-ANNA1 (anti-Hu)–associated encephalitis, which classically presents with limbic encephalitis and neuronopathy in the setting of small cell lung cancer, can present as isolated brainstem encephalitis with normal MRI and central hypoventilation (Ondine's curse).[47] Anti-ANNA2 (anti-Ri) is an onconeural antibody targeting intracellular antigens usually associated with breast cancer. Patients may present with opsoclonus-myoclonus-ataxia syndrome, but brain MRI typically either is normal or shows nonspecific changes in the brainstem.[48]

Immune-mediated cerebellar syndromes may be paraneoplastic or autoimmune. Paraneoplastic cerebellar degeneration is the second most common CNS paraneoplastic syndrome following limbic encephalitis; it is associated with nearly 30 different autoantibodies and multiple types of malignancy.[49,50] Rapidly progressive cerebellar ataxia is typically associated with anti-Yo (also known as *Purkinje cell antibody 1*) antibody, whereas a more diffuse encephalomyelitis is associated with ANNA1 (anti-Hu) antibodies.[50] MRI findings depend on the phase of the disease but are typically mild, with acute paraneoplastic cerebellar degeneration showing normal MRI or mild T2 hyperintensities in the cerebellar hemispheres, whereas the more chronic phases demonstrate cerebellar atrophy best seen on T1 sequences (FIGURE 10-23).[50]

Autoimmune cerebellar ataxias include gluten ataxia, postinfectious cerebellitis (especially in children), and opsoclonus-myoclonus-ataxia syndrome, with or without causative neuronal antibodies.[51] Some of the most commonly associated autoantibodies with autoimmune cerebellar ataxia are anti–glutamic acid decarboxylase 65 (GAD65), anti–contactin-associated proteinlike 2 (CASPR2), and anti–metabotropic glutamate receptor (mGLuR1). Most of these have normal MRI early in the disease but may demonstrate enhancement or T2-hyperintense

KEY POINTS

- MRI is often normal early in the course of paraneoplastic cerebellar degeneration although mild T2 hyperintensities may be seen in the cerebellar hemispheres.
- The most commonly associated autoantibodies with autoimmune cerebellar ataxia are anti–glutamic acid decarboxylase 65 (GAD65), anti–contactin-associated proteinlike 2 (CASPR2), and anti–metabotropic glutamate receptor (mGLuR1).
- Approximately 50% of patients with neuropsychiatric lupus have abnormal brain MRI, most commonly manifesting as nonspecific white matter periventricular and subcortical T2 hyperintensities.

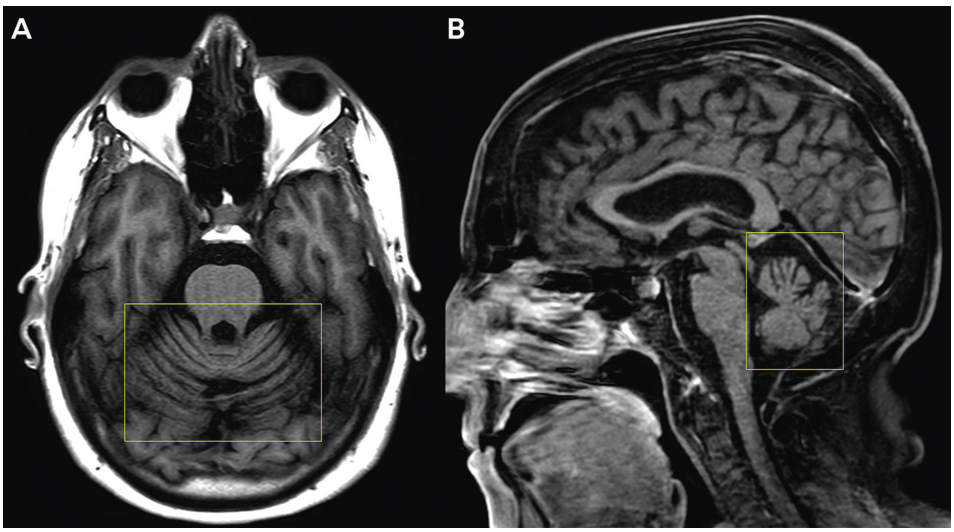

FIGURE 10-23
Axial (*A*) and sagittal (*B*) T1-weighted MRIs showing diffuse cerebellar atrophy (*A, B, inside rectangles*) in a patient with subacute ataxia in the setting of presumed seronegative paraneoplastic cerebellar degeneration with occult endometrial cancer.

Copyright © American Academy of Neurology. Unauthorized reproduction of this article is prohibited.

signal along cerebellar folia (FIGURE 10-24); patients with autoimmune cerebellar ataxias develop cerebellar atrophy over time, especially with GAD65.[52]

Systemic Autoimmunity With Neuroimaging Abnormalities

Several neurologic syndromes and imaging abnormalities have been associated with systemic autoimmune and connective tissue diseases. Neuropsychiatric manifestations of systemic lupus erythematosus (SLE) are attributed to multiple etiologies such as vasculopathy, thromboembolism, demyelination, and direct neural autoimmune damage.[13] Concurrent antiphospholipid syndrome in patients with SLE increases the risk of large and small vessel infarcts and arterial stenosis and is associated with more abnormalities on MRI than in patients with SLE but without antiphospholipid syndrome.[53] Approximately 50% of patients with neuropsychiatric lupus have abnormal brain MRI, most commonly manifesting as white matter periventricular and subcortical T2 hyperintensities. These changes are nonspecific and indistinguishable from microvascular ischemic changes seen with aging or leukoaraiosis.[13] The central vein sign is an imaging biomarker for multiple sclerosis in which a vein passing through the white matter lesion is visualized on SWI in keeping with the venular origin of inflammatory lesions; this finding is generally absent in SLE.[54] Cerebral atrophy and confluent white matter lesions that are either periventricular or striatal have also been reported.[12,55] Patients can also have imaging abnormalities related to complications such as postictal changes after seizures or large vessel occlusions.[56] No clear autoantibodies have been established with direct CNS pathogenicity in SLE; however, elevated antiribosomal P antibodies have been associated with CNS manifestations of SLE, and at least some cases of neuropsychiatric SLE are caused by NMDA receptor encephalitis with corresponding CSF NMDA receptor IgG antibodies.[57,58]

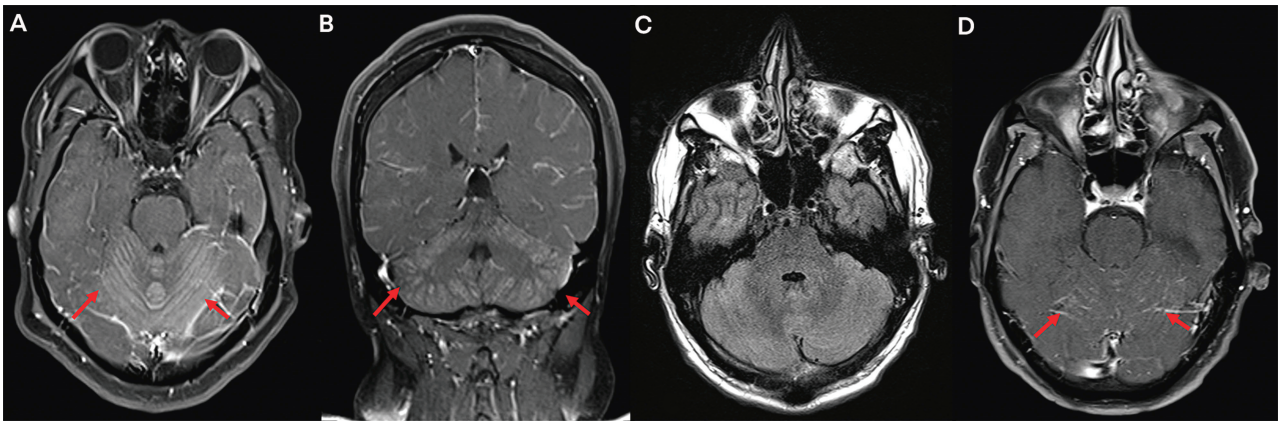

FIGURE 10-24

Brain MRI from two patients with immune-mediated cerebellar ataxia. Axial (*A*) and coronal (*B*) postcontrast T1-weighted MRI showing diffuse leptomeningeal enhancement most prominently in the bilateral cerebellar hemispheres (*A*, *B*, *arrows*) in a patient with postinfectious cerebellitis. Axial T2 fluid-attenuated inversion recovery (FLAIR) (*C*) sequence showing subtle sulcal T2 nonsuppression along the cerebellar folia with associated postcontrast T1 enhancement (*D*, *arrows*) in a patient with acute cerebellar ataxia with septin and immunoglobulin-G (IgG) autoantibodies specific for ρ GTPase activating protein 26 (ARHGAP26, also known as *GTPase regulator associated with focal adhesion kinase* [GRAF1]) (GRAF/ARHGAP) antibodies in CSF.

Copyright © American Academy of Neurology. Unauthorized reproduction of this article is prohibited.

Sjögren syndrome (SS) is a systemic inflammatory disease affecting the exocrine glands. CNS involvement in Sjögren syndrome historically has been attributed to immune-mediated demyelination and vasculopathy. Subcortical and periventricular white matter T2 hyperintensities are the most common MRI feature, present in up to 70% of patients with Sjögren syndrome.[59] Compared with multiple sclerosis, basal ganglia lesions are more common and corpus callosum lesions are rare; however, the findings are nonspecific, and the link to Sjögren syndrome is unclear.[13,60] Relapsing demyelinating syndromes in patients with Sjögren syndrome are most often caused by comorbid multiple sclerosis or NMOSD with MRI features typical for those diseases. All patients with Sjögren syndrome who have optic neuritis or transverse myelitis should be tested for serum anti-aquaporin-4 IgG antibodies and MOG IgG (anti–myelin oligodendrocyte glycoprotein antibody).[13]

KEY POINTS

- Neuromyelitis optica spectrum disorder (NMOSD) may occur in association with Sjögren syndrome, and patients with optic neuritis or transverse myelitis should be tested for serum aquaporin-4 IgG and myelin oligodendrocyte glycoprotein IgG.
- Brain MRI is abnormal in 95% to 100% of patients with CNS vasculitis.
- Digital subtraction angiography is the most sensitive modality for vascular luminal changes in CNS vasculitis, including alternating areas of stenosis and dilation in at least two separate vascular distributions.

Cerebral Vasculitis

CNS vasculitis refers to a group of inflammatory disorders that affect the walls of the cerebral vessels. They may be classified based on the size of the vessel affected, histopathologic findings, and the underlying inflammatory disease, which may be systemic or isolated to the CNS. *Primary angiitis of the CNS* refers to inflammation affecting the vessels of the brain or spinal cord without overt systemic vasculitis or an underlying potential cause. Secondary CNS vasculitis occurs in the setting of a systemic vasculitis or CNS infection (such as syphilis, tuberculosis, and varicella-zoster virus).[61] Depending on the cause, patients may present with subacute onset of progressive headache, cognitive impairment, and neuropsychiatric disturbances or multifocal cerebral infarcts across multiple vascular territories. Imaging may help differentiate CNS vasculitis from mimics such as intracranial atherosclerosis, vasospasm such as in reversible cerebral vasoconstriction syndrome (RCVS), and noninflammatory vasculopathies such as cerebral autosomal dominant arteriopathy with subcortical infarcts and leukoencephalopathy (CADASIL).[61]

MRI is abnormal in 95% to 100% of patients with CNS vasculitis, so a negative MRI can essentially exclude the diagnosis. Typical findings include infarcts of varying ages in multiple vascular territories with foci of restricted diffusion acutely and T2-hyperintense foci from subacute to chronic infarcts. Ischemic lesions are sometimes accompanied by subarachnoid or intraparenchymal hemorrhagic lesions.[62] Prominent meningeal gadolinium enhancement is usually associated with negative angiography (because of involvement of small meningeal arteries) but may have a more favorable response to immunosuppressive therapy.[61,63] Tumorlike infiltrative lesions have been described in 4% to 11% of patients with primary angiitis of the CNS with neoplasm as the most common differential diagnosis. A biopsy is typically required for diagnosis in these cases (FIGURE 10-25).[62,64]

Angiography, whether magnetic resonance, CT, or digital subtraction angiography (DSA), may be abnormal in cases involving medium to large vessels. For large vessel irregularities (ie, carotid involvement in Takayasu or giant cell arteritis), PET may be useful in confirming the inflammatory nature of the vasculopathy (FIGURE 10-26).[65] DSA is the most sensitive modality for identifying vascular luminal changes, classically manifesting in CNS vasculitis as alternating areas of stenosis and dilation in at least two separate vascular distributions, a pattern sometimes referred to as *beading* (FIGURE 10-27). These

Copyright © American Academy of Neurology. Unauthorized reproduction of this article is prohibited.

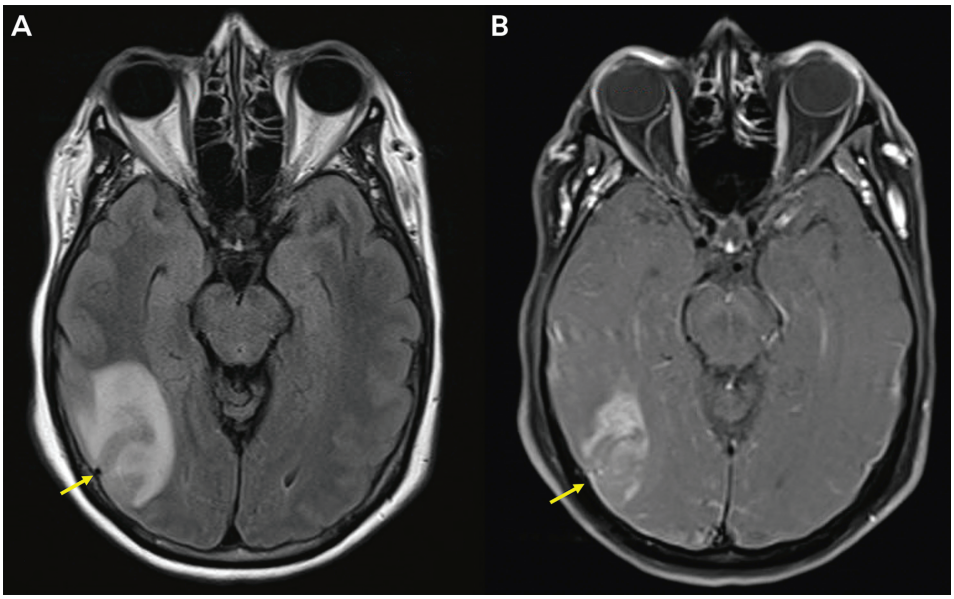

FIGURE 10-25
Axial T2 fluid-attenuated inversion recovery (FLAIR) (*A*) and axial postcontrast T1-weighted (*B*) MRI reveal a right temporo-occipital hyperintense lesion with heterogenous enhancement (*A, B, arrows*) in a patient with biopsy-proven central nervous system vasculitis.

changes are nonspecific, however, and may occur in noninflammatory medium and large vessel vasculopathies. Furthermore, DSA cannot detect changes in distal vessels of smaller caliber (<500 μm in diameter). One study of 60 patients with primary angiitis of the CNS showed that 23% had biopsy-proven angiitis without any visible imaging manifestations of vasculopathy.[62] DSA carries a small risk of complications including emboli, puncture site hematoma or pseudoaneurysm, and radiation exposure.[63] Brain and meningeal biopsy is the gold standard for diagnosis, although it also has limited sensitivity. CSF

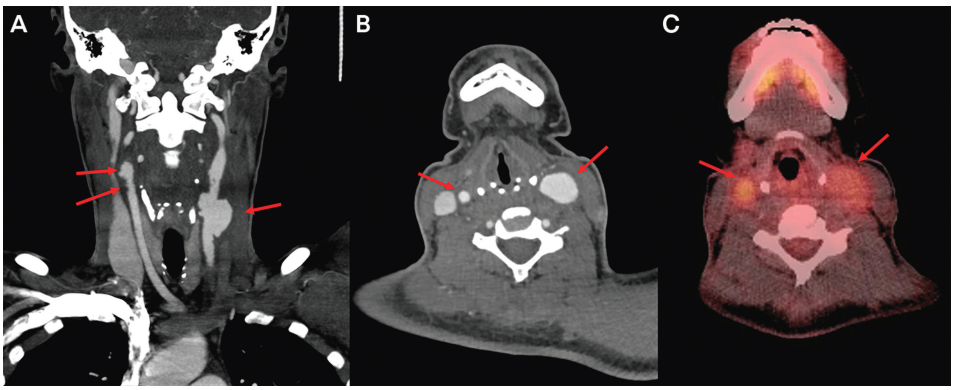

FIGURE 10-26
Imaging of a patient with Takayasu arteritis. Coronal (*A*) and axial (*B*) CT angiography images of the neck showing diffuse irregularity of the carotid walls (A, B, *arrows*) with thickened appearance and pseudoaneurysm of the left common carotid. *C*, Axial fludeoxyglucose positron emission tomography (FDG-PET) of the same patient demonstrates abnormal FDG uptake in both common carotid arteries (*arrows*), worse on the left, consistent with large vessel vasculitis.

Copyright © American Academy of Neurology. Unauthorized reproduction of this article is prohibited.

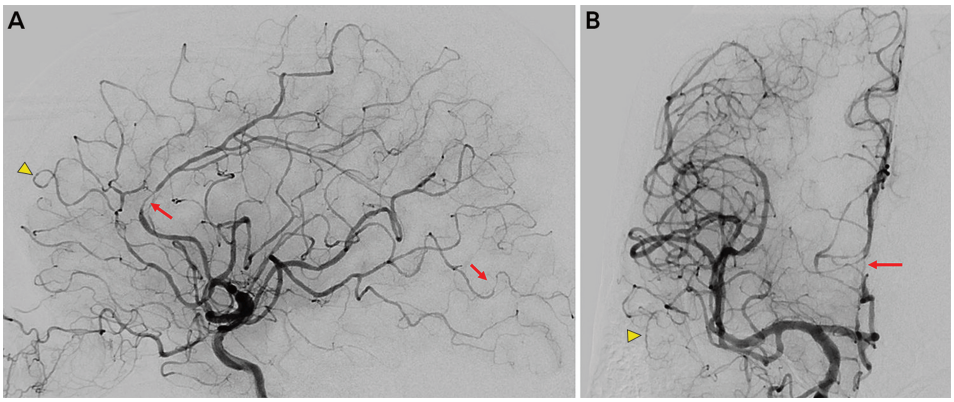

FIGURE 10-27
Right common carotid injection sagittal (*A*) and anterior-posterior (*B*) digital subtraction angiography shows diffuse medium vessel vasculopathy including luminal narrowing and irregularities (*A, B, red arrows*) and "beading" (*A, B, yellow arrowheads*) in anterior and posterior circulation in a patient with parainfectious central nervous vasculitis.

KEY POINT

- High-resolution MRI with vessel wall imaging may be helpful in demonstrating enhancement of the vessel walls in vasculitis, but the modality has limited specificity.

analysis may be helpful if inflammation is present but can be normal, even in biopsy-proven cases.

High-resolution MRI with vessel wall imaging, also known as the *black blood sequence*, was developed as a noninvasive method to assess vessel wall inflammation through concurrent suppression of both CSF and luminal contrast to highlight any postcontrast enhancement in affected vessel walls. In CNS vasculitis, vessel wall imaging may show multifocal areas of concentric wall thickening and enhancement, especially where a caliber change has occurred (FIGURE 10-28). This method is not specific, however, because other noninflammatory vasculopathies can present similarly, including intracranial

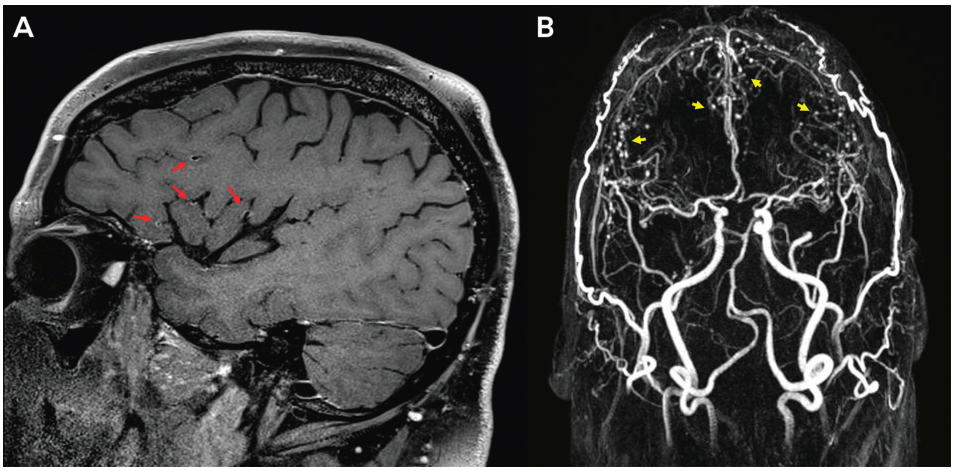

FIGURE 10-28
Sagittal high-resolution 3T MRI (*A*) and coronal magnetic resonance angiography (*B*) with vessel wall imaging showing multifocal peripheral segmental concentric wall thickening and enhancement (*A, red arrows*) and coronal oblique postcontrast vessel reconstruction imaging showing diffuse vasculopathy with microaneurysm formation (*B, yellow arrows*) in a patient with aseptic meningitis, increased intracranial pressure, headaches, and punctate infarcts due to possible neurosarcoidosis.

Copyright © American Academy of Neurology. Unauthorized reproduction of this article is prohibited.

atherosclerosis, arterial dissection, postthrombectomy changes, and RCVS. Some studies suggest that atherosclerotic lesions typically have eccentric wall enhancement whereas vasculitis shows circumferential enhancement. Vessel wall enhancement in RCVS is typically subtle or absent.[66]

Although small vessel vasculitis can be hard to diagnose without a biopsy, certain subtypes have characteristic imaging patterns that can aid in diagnosis. Susac syndrome, as noted earlier, may involve encephalopathy, branch retinal artery occlusion, and sensorineural hearing loss. Callosal T2 hyperintensities and acutely diffusion-restricting "snowball-like" lesions in the corpus callosum are highly suggestive of this diagnosis in the right clinical setting (FIGURE 10-21). Parenchymal, leptomeningeal, and perivascular enhancement have also been described in Susac syndrome.[44,67] The presence of microhemorrhages, asymmetric white matter T2-hyperintense signal change, and focal leptomeningeal enhancement is suggestive of cerebral amyloid angiopathy-related inflammation or amyloid β–related angiitis, manifestations of an immune reaction to amyloid deposition in the brain perivascular parenchyma (cerebral amyloid angiopathy-related inflammation) or vessel walls (amyloid β–related angiitis).[63,68] SWI typically shows microhemorrhages with or without superficial siderosis. In cerebral amyloid angiopathy-related inflammation, confluent and asymmetric T2 hyperintensities in cortical and subcortical areas are characteristic, often extending to the U fibers.[68] Focal gadolinium enhancement of the leptomeninges is frequently seen in amyloid β–related angiitis and may also be present in cerebral amyloid angiopathy-related inflammation (FIGURE 10-29).[69]

Myelitis

Myelitis, or inflammation of the spinal cord, may present acutely over hours, subacutely over weeks, or in rare cases chronically over months. Suspected myelopathy based on clinical course and examination findings warrants imaging

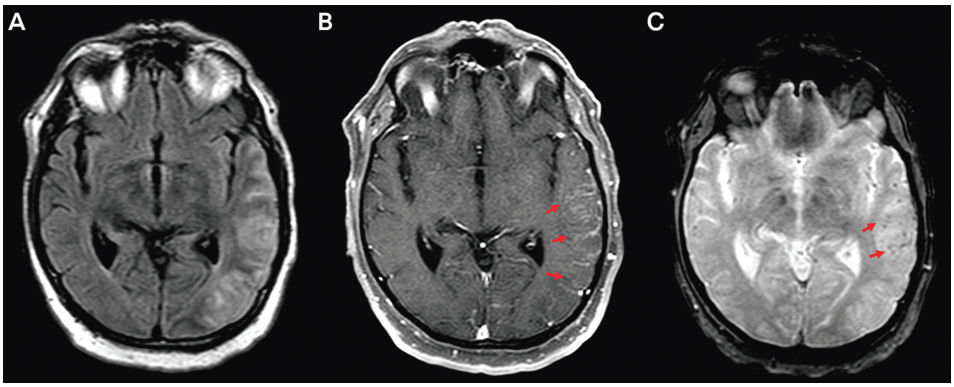

FIGURE 10-29

MRI of a patient with probable cerebral amyloid angiopathy associated–related inflammation. *A*, Axial T2 fluid-attenuated inversion recovery (FLAIR) MRI showing abnormal hyperintensity in the left temporal region that is mainly cortical, with nonsuppression of the sulcal CSF. *B*, Axial postcontrast T1-weighted MRI showing associated leptomeningeal contrast enhancement (*arrows*). *C*, Axial gradient echo image showing multiple microhemorrhages (*arrows*) (these are better visualized on susceptibility-weighted imaging, but this sequence was not done on this patient).

Copyright © American Academy of Neurology. Unauthorized reproduction of this article is prohibited.

to exclude structural compromise and to assess for patterns that might suggest the underlying etiology. Spinal MRI is the most sensitive imaging modality to evaluate myelopathy and is essential in ruling out spinal cord compression in the acute setting. If MRI is contraindicated, CT myelography can exclude spinal cord compression. PET has poor resolution for spinal cord disorders and is rarely used as a modality focused on spinal cord pathology; when used to assess for sarcoidosis or neoplasm, both inflammatory and neoplastic pathologies may be associated with increased spinal cord glucose uptake.[70] MRI can help characterize lesions in terms of location (spinal level), rostral-caudal extent (short segment versus longitudinally extensive), transverse extent (transverse myelitis versus partial myelitis), and topography (eg, hemicord, anterior horn, posterior column).[70-72] The pattern of gadolinium enhancement may also provide clues to diagnosis. Myelitis typically manifests as T2 hyperintensity with or without cord edema and enhancement. DWI may reveal restricted diffusion in spinal cord infarction. In cases of suspected myelitis with negative MRI initially, repeat MRI should be considered because some forms of myelitis, as well as spinal cord infarct, may be associated with normal MRI early but evolve over days.

Short-segment partial transverse myelitis is most typical of multiple sclerosis. Neurosarcoidosis, NMOSD, and MOG-associated disorder all typically cause longitudinally extensive transverse myelitis. Neurosarcoidosis is distinguished by a unique pattern of subpial dorsal enhancement with or without central canal enhancement (trident sign) (FIGURE 10-30) and may also be associated with meningitis at the base of the brain (CASE 10-2).[73,74] Persistent gadolinium enhancement on posttreatment MRI (often lasting more than 2 months) is more typical for

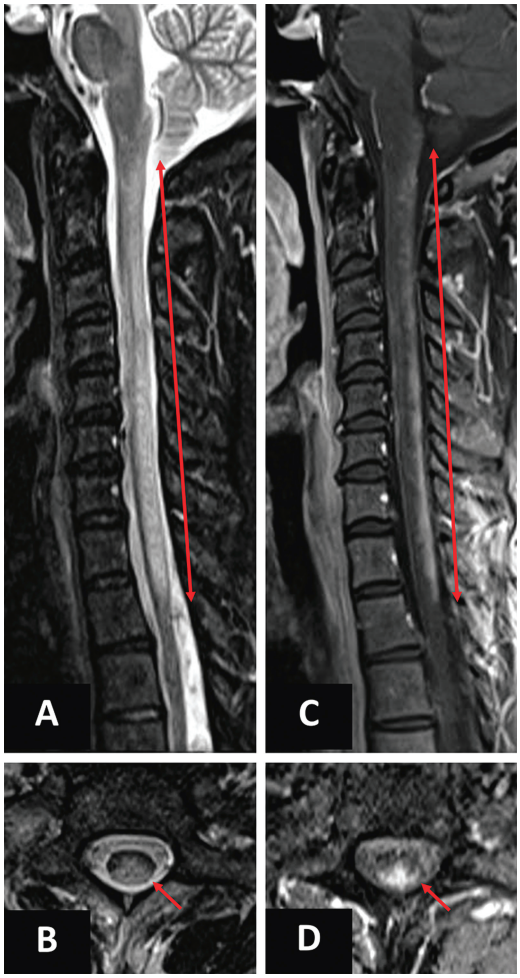

FIGURE 10-30
Sagittal (*A*) and axial (*B*) T2-weighted MRI showing longitudinally extensive spinal cord T2 signal change from C1 to T2 (*A, double arrow*; *B, arrow*). Sagittal (*C, double arrow*) and axial (*D*) postcontrast T1-weighted MRI showing dorsal (and to a lesser extent ventral) subpial enhancement with associated central canal enhancement forming the trident sign (*D, arrow*) in a patient with probable neurosarcoidosis.

KEY POINTS

- Findings of callosal T2 hyperintensities or "snowball-like" lesions in the corpus callosum in the context of encephalopathy, branch retinal artery occlusion, and hearing loss are highly suggestive of Susac syndrome.
- Confluent and asymmetric T2 hyperintensities in cortical and subcortical areas, in association with microhemorrhage on SWI, are characteristic of cerebral amyloid angiopathy-related inflammation.
- MRI is helpful in determining the length of the lesion (short versus longitudinally extensive transverse myelitis), width (partial versus transverse), and location (eccentric, central, hemicord, anterior versus posterior, conus, tracts, or meningeal).
- The trident sign, which has been described in relation to neurosarcoidosis, demonstrates leptomeningeal or dorsal subpial enhancement that may or may not involve the central canal.
- Involvement of the conus medullaris is a clue to myelin oligodendrocyte glycoprotein-associated disorder as the cause of longitudinally extensive transverse myelitis.
- CT of the chest, abdomen, and pelvis with iodine contrast is a generally accepted first method of screening for occult malignancy or systemic inflammation (eg, sarcoidosis).

Copyright © American Academy of Neurology. Unauthorized reproduction of this article is prohibited.

neurosarcoidosis than demyelinating diseases including multiple sclerosis and NMOSD.[75] NMOSD spinal cord lesions are characteristically located centrally in the cord with varying enhancement patterns and may be associated with edema or expansion of the cord (FIGURE 10-32); meningeal enhancement is not typical. Longitudinally extensive transverse myelitis in MOG-associated

CASE 10-2

A 38-year-old woman presented with a 1-month history of headache, blurred vision in her left eye, low-grade fever of 38.5°C (101.3°F), and lethargy. Ten days before her admission, she developed back pain, urinary retention, tingling in her upper and lower extremities, and abdominal discomfort and was able to ambulate only with assistance. MRI of the brain and orbits showed left optic sheath enhancement and leptomeningeal enhancement in the interpeduncular fossa, pons, and medulla, consistent with basal meningitis. Spinal MRI showed longitudinally extensive T2 hyperintensity with associated subpial and central canal enhancement consistent with the trident sign (FIGURE 10-31). Serum aquaporin-4 IgG and myelin oligodendrocyte glycoprotein (MOG) IgG were negative. CSF analysis showed low glucose concentration at 31 mg/dL, elevated protein at 126 mg/dL, and lymphocytic pleocytosis with 159 cells/mm^3. Whole-body CT followed by whole-body fludeoxyglucose positron emission tomography (FDG-PET) did not identify a hypermetabolic focus. A diagnosis of possible neurosarcoidosis was made. The patient was treated with methylprednisolone 1000 mg IV daily for 5 days with complete improvement. She was continued on an oral prednisone taper over 3 months, as well as maintenance adalimumab subcutaneous injections.

COMMENT

This patient had findings on MRI characteristic of neurosarcoidosis, including basal meningitis, optic sheath enhancement, and longitudinally extensive transverse myelitis with meningeal enhancement. The CSF profile was also supportive of neurosarcoidosis, especially the low glucose. PET-CT did not reveal any systemic focus for possible biopsy, but given the highly characteristic imaging pattern, spinal cord biopsy was not pursued, and she was treated empirically for possible neurosarcoidosis.

Copyright © American Academy of Neurology. Unauthorized reproduction of this article is prohibited.

disease should be suspected when a central gray matter pattern manifests as an H shape on axial T2-weighted MRI or when the conus medullaris is involved (FIGURE 10-33).[76] Although rare, paraneoplastic myelitis may involve specific spinal cord tracts (dorsal or lateral columns) with long linear segments of T2 hyperintensity and enhancement (TABLE 10-2[71,77,78]).

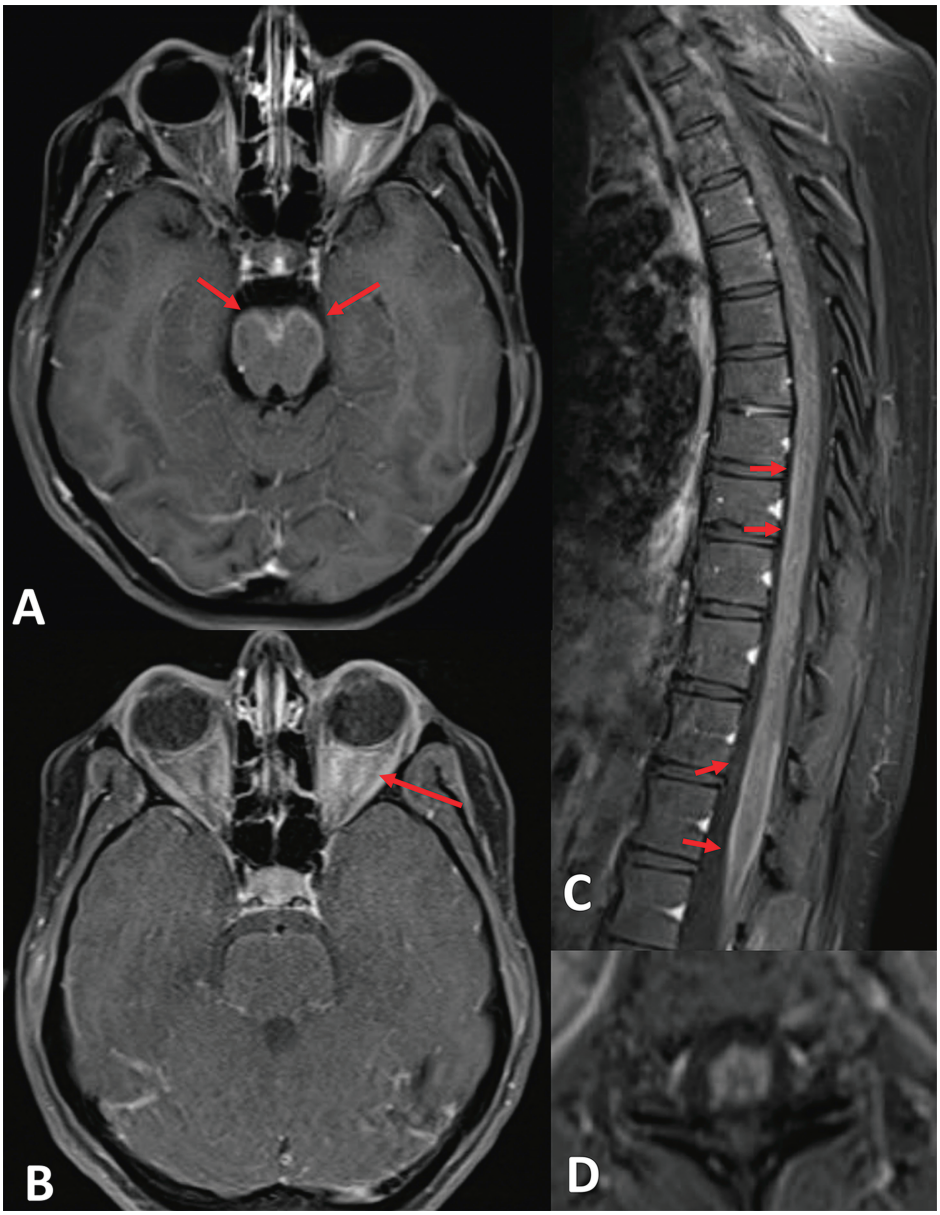

FIGURE 10-31
Imaging of the patient in CASE 10-2. Axial postcontrast T1-weighted MRI showing leptomeningeal enhancement in the interpeduncular cistern (*A*, *arrows*) and left optic perineural enhancement (*B*, *arrow*). Sagittal (*C*) and axial (*D*) postcontrast T1-weighted MRI showing subpial and central canal enhancement (*C*, *arrows*).

Copyright © American Academy of Neurology. Unauthorized reproduction of this article is prohibited.

FIGURE 10-32
Sagittal (*A*) and axial (*B*) thoracic spine T2-weighted MRI showing longitudinally extensive spinal cord signal change and edema in all visualized levels (*B, arrow*). Sagittal (*C*) and axial (*D*) postcontrast T1-weighted MRI showing parenchymal rim enhancement (*D, arrow*) in a patient with aquaporin-4 IgG positive neuromyelitis optica spectrum disorder.

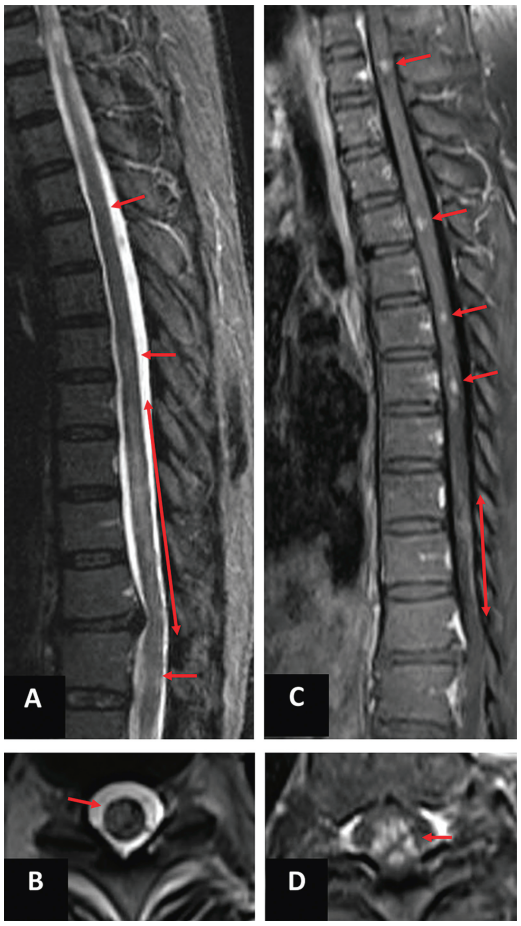

FIGURE 10-33
Sagittal (*A*) and axial (*B*) thoracic spine T2-weighted MRI showing patchy longitudinally extensive cord signal change involving the conus medullaris (*A, double arrow* for the longitudinal segment, *short arrows* demonstrating patchy short segments; *B, arrow*). Sagittal (*C*) and axial (*D*) postcontrast T1-weighted MRI showing nodular parenchymal enhancement (*C, double arrow, arrows; D, arrow*) in a patient with myelin oligodendrocyte glycoprotein IgG–associated disease.

EXTRANEURAL IMAGING MODALITIES IN AUTOIMMUNE NEUROLOGY

CT of the chest, abdomen, and pelvis with iodine contrast is useful for screening when an occult malignancy or systemic etiology such as sarcoidosis is suspected. It has the advantage of being readily available at most centers and providing good spatial resolution. FDG-PET of the whole body may be useful in detecting smaller occult malignancies or foci of inflammation in patients with negative body CT screen; in some centers, PET is combined with CT as first-line screening. In some cases, including FDG-PET of the brain with the body is appropriate, especially when an autoimmune or paraneoplastic encephalitis is suspected but MRI is negative.

When the neurologic syndrome is suggestive of or proven to be paraneoplastic in origin and tumors of the ovaries or testicles are suspected,

Copyright © American Academy of Neurology. Unauthorized reproduction of this article is prohibited.

ultrasonography is preferred over CT for screening. When suspicion for these malignancies is high (eg, in the setting of NMDA receptor encephalitis), a transvaginal approach for ovarian assessment is more sensitive than pelvic ultrasound.[79]

CONCLUSION

Neuroimaging is essential in the evaluation of patients with inflammatory, autoimmune, and paraneoplastic neurologic disorders. Familiarity with the

Imaging Patterns in Myelitis[a]

TABLE 10-2

Disorder	>Size	Most common MRI characteristics
Multiple sclerosis	Small and ovoid, lesions may become confluent in progressive forms	Eccentric "partial myelitis," enhancement is either homogenous or ringlike
Neuromyelitis optica	Longitudinally extensive transverse myelitis (LETM), may be short segment	Central "bright and spotty" T2 lesions, present cord edema and may be hypointense on T1-weighted MRI, enhancement may be ringlike in one-third of cases[77]
Myelin oligodendrocyte glycoprotein–IgG associated myelitis	LETM, may be short segment	Can involve the conus medullaris, lesions are often restricted to the gray matter on T2-weighted MRI (the H sign), enhancement is faint and patchy
Parainfectious and idiopathic	Variable, may be LETM in the setting of acute disseminated encephalomyelitis (ADEM)	Nonspecific, can be limited to the gray matter on T2-weighted MRI in acute flaccid myelitis (the H sign)
Neurosarcoidosis	LETM	Pial enhancement, typically dorsal, may cause the trident sign appearance with central canal involvement on axial postcontrast T1-weighted MRI
In the setting of rheumatologic disorders	Variable	Systemic lupus erythematosus (SLE): typically associated with NMOSD but may be associated with SLE flares in the setting of negative aquaporin-4 IgG Behçet myelitis: can cause a distinctive hyperintense rim with hypointense core on T2-weighted MRI (the bagel sign); the motor neuron sign was also described, affecting just the anterior horn cells symmetrically[13] Sjögren myelitis: typically associated with NMOSD but may occur in the setting of negative aquaporin-4 IgG
Paraneoplastic	Usually LETM	May involve gray matter or a tractopathy on T2-weighted MRI (ie, myelopathies associated with amphiphysin and collapsin response mediator protein-5 [CRMP5] antibodies)[78]
Anti–glial fibrillary acidic protein (GFAP)	Usually LETM	Central thin linear enhancement along the central canal on sagittal postcontrast T1-weighted MRI

IgG = immunoglobulin G; MRI = magnetic resonance imaging.
[a] Modified with permission from Abdel-Wahed L, Cho TA, Semin Neurol.[71] © 2021 Thieme.

Copyright © American Academy of Neurology. Unauthorized reproduction of this article is prohibited.

specific findings on imaging modalities, appropriate yield, and expected changes with treatment are important in differentiating the underlying inflammatory etiologies. Given the incomplete sensitivity and delay in result reporting for neuronal autoantibody testing, neuroimaging may allow empiric treatment in the right clinical setting, resulting in potential avoidance of long-term morbidity.

REFERENCES

1 Sattarnezhad N, Klein JP. Imaging. In: Cho TA, Bhattacharyya S, Helfgott S, eds. Neurorheumatology: a comprehenisve guide to immune mediated disorders of the nervous system. Springer International Publishing; 2019: 11-20.

2 Mark IT, Dillon WP, Richie MB, Villanueva-Meyer JE. MRI findings after recent image-guided lumbar puncture: the rate of dural enhancement and subdural collections. AJNR Am J Neuroradiol 2022;43(5):784-788. doi:10.3174/ajnr.A7496

3 Wesley SF, Garcia-Santibanez R, Liang J, Pyburn D. Incidence of meningeal enhancement on brain MRI secondary to lumbar puncture. Neurol Clin Pract 2016;6(4):315-320. doi:10.1212/CPJ.0000000000000262

4 Soni NJ, Franco-Sadud R, Schnobrich D, et al. Ultrasound guidance for lumbar puncture. Neurol Clin Pract 2016;6(4):358-368. doi:10.1212/CPJ.0000000000000265

5 Bordonne M, Chawki MB, Doyen M, et al. Brain (18)F-FDG PET for the diagnosis of autoimmune encephalitis: a systematic review and a meta-analysis. Eur J Nucl Med Mol Imaging 2021;48(12): 3847-3858. doi:10.1007/s00259-021-05299-y

6 Probasco JC, Solnes L, Nalluri A, et al. Abnormal brain metabolism on FDG-PET/CT is a common early finding in autoimmune encephalitis. Neurol Neuroimmunol Neuroinflamm 2017;4(4):e352. doi:10.1212/NXI.0000000000000352

7 Kirmi O, Sheerin F, Patel N. Imaging of the meninges and the extra-axial spaces. Semin Ultrasound CT MRI 2009;30(6):565-593. doi:10.1053/j.sult.2009.08.007

8 Smirniotopoulos JG, Murphy FM, Rushing EJ, Rees JH, Schroeder JW. Patterns of contrast enhancement in the brain and meninges. Radiographics 2007;27(2):525-551. doi:10.1148/rg.272065155

9 Carruthers R, Carruthers M, Della-Torre E. IgG4-related disease and other causes of inflammatory meningeal disease. Semin Neurol 2014;34(4):395-404. doi:10.1055/s-0034-1390388

10 Bradshaw MJ, Pawate S, Koth LL, Cho TA, Gelfand JM. Neurosarcoidosis: pathophysiology, diagnosis, and treatment. Neurol Neuroimmunol Neuroinflamm 2021;8(6):1084. doi:10.1212/NXI.0000000000001084

11 Bathla G, Freeman CW, Moritani T, et al. Retrospective, dual-centre review of imaging findings in neurosarcoidosis at presentation: prevalence and imaging sub-types. Clin Radiol 2020;75(10):796.e791-796.e799. doi:10.1016/j.crad.2020.05.008

12 Shadmani G, Simkins TJ, Assadsangabi R, et al. Autoimmune diseases of the brain, imaging and clinical review. Neuroradiol J 2022;35(2):152-169. doi:10.1177/19714009211042879

13 Kandemirli SG, Bathla G. Neuroimaging findings in rheumatologic disorders. J Neurol Sci 2021;427: 117531. doi:10.1016/j.jns.2021.117531

14 Amukotuwa SA, Cook MJ. Chapter 40—spinal disease: neuoplastic, degenerative, and infective spinal cord diseases and spinal cord compression. In: Schapira AHV, Byrne E, DiMauro S, et al, eds. Neurology and Clinical Neuroscience. Mosby; 2007:511-538.

15 Antony J, Hacking C, Jeffree RL. Pachymeningeal enhancement-a comprehensive review of literature. Neurosurg Rev 2015;38(4):649-659. doi:10.1007/s10143-015-0646-y

16 Agnihotri SP, Singhal T, Stern BJ, Cho TA. Neurosarcoidosis. Semin Neurol 2014;34(4): 386-394. doi:10.1055/s-0034-1390387

17 Wallace ZS, Carruthers MN, Khosroshahi A, et al. IgG4-related disease and hypertrophic pachymeningitis. Medicine 2013;92(4):206-216. doi:10.1097/MD.0b013e31829cce35

18 Pakalniskis MG, Berg AD, Policeni BA, et al. The many faces of granulomatosis with polyangiitis: a review of the head and neck imaging manifestations. AJR Am J Roentgenol 2015;205(6): W619-W629. doi:10.2214/AJR.14.13864

19 Zheng Y, Zhang Y, Cai M, et al. Central nervous system involvement in ANCA-associated vasculitis: what neurologists need to know. Front Neurol 2018;9:1166. doi:10.3389/fneur.2018.01166

20 Graus F, Titulaer MJ, Balu R, et al. A clinical approach to diagnosis of autoimmune encephalitis. Lancet Neurol 2016;15(4):391-404. doi:10.1016/S1474-4422(15)00401-9

21 Abboud H, Probasco JC, Irani S, et al. Autoimmune encephalitis: proposed best practice recommendations for diagnosis and acute management. J Neurol Neurosurg Psychiatry 2021;92(7):757-768. doi:10.1136/jnnp-2020-325300

Copyright © American Academy of Neurology. Unauthorized reproduction of this article is prohibited.

22 Irani SR, Bera K, Waters P, et al. *N*-methyl-D-aspartate antibody encephalitis: temporal progression of clinical and paraclinical observations in a predominantly non-paraneoplastic disorder of both sexes. Brain 2010;133(Pt 6):1655-1667. doi:10.1093/brain/awq113

23 Chow FC, Glaser CA, Sheriff H, et al. Use of clinical and neuroimaging characteristics to distinguish temporal lobe herpes simplex encephalitis from its mimics. Clin Infect Dis 2015; 60(9):1377-1383. doi:10.1093/cid/civ051

24 Renard D, Nerrant E, Lechiche C. DWI and FLAIR imaging in herpes simplex encephalitis: a comparative and topographical analysis. J Neurol 2015;262(9):2101-2105. doi:10.1007/s00415-015-7818-0

25 Cianfoni A, Caulo M, Cerase A, et al. Seizure-induced brain lesions: a wide spectrum of variably reversible MRI abnormalities. Eur J Radiol 2013;82(11):1964-1972. doi:10.1016/j.ejrad.2013.05.020

26 Mattozzi S, Sabater L, Escudero D, et al. Hashimoto encephalopathy in the 21st century. Neurology 2020;94(2):e217-e224. doi:10.1212/WNL.0000000000008785

27 Probasco JC, Solnes L, Nalluri A, et al. Decreased occipital lobe metabolism by FDG-PET/CT: an anti-NMDA receptor encephalitis biomarker. Neurol Neuroimmunol Neuroinflamm 2018;5(1): e413. doi:10.1212/NXI.0000000000000413

28 Lotan E, Friedman KP, Davidson T, Shepherd TM. Brain 18F-FDG-PET: utility in the diagnosis of dementia and epilepsy. Isr Med Assoc J 2020; 22(3):178-184.

29 Cortese I, Reich DS, Nath A. Progressive multifocal leukoencephalopathy and the spectrum of JC virus-related disease. Nat Rev Neurol 2021;17(1):37-51. doi:10.1038/s41582-020-00427-y

30 Gillinder L, Britton J. Autoimmune-associated seizures. Continuum (Minneap Minn) 2022; 28(2, Epilepsy):363-398. doi:10.1212/CON.0000000000001079

31 Deng B, Cai M, Qiu Y, et al. MRI characteristics of autoimmune encephalitis with autoantibodies to GABAA receptor: a case series. Neurol Neuroimmunol Neuroinflamm 2022;9(3):1158. doi:10.1212/NXI.0000000000001158

32 Cay-Martinez KC, Hickman RA, McKhann Ii GM, Provenzano FA, Sands TT. Rasmussen encephalitis: an update. Semin Neurol 2020; 40(2):201-210. doi:10.1055/s-0040-1708504

33 Crespo-Burillo JA, Hernando-Quintana N, Ruiz-Palomino P, Martin-Martinez J. Chorea secondary to striatal encephalitis due to anti-CV2/CRMP5 antibodies. Case description and review of the literature. Neurologia 2015;30(7): 451-453. doi:10.1016/j.nrl.2013.10.007

34 Vaswani PA, Kimchi EY, Hung AY. CRMP-5-IgG associated paraneoplastic chorea. Mov Disord Clin Pract 2020;7(6):713-715. doi:10.1002/mdc3.13019

35 Marinas JE, Matveychuk D, Dursun SM, Baker GB. Neuroimmunological antibody-mediated encephalitis and implications for diagnosis and therapy in neuropsychiatry. Acta Neuropsychiatr 2020;32(4):177-185. doi:10.1017/neu.2019.50

36 Dalmau J, Graus F, Villarejo A, et al. Clinical analysis of anti-Ma2-associated encephalitis. Brain 2004;127(Pt 8):1831-1844. doi:10.1093/brain/awh203

37 Kunchok A, Zekeridou A, McKeon A. Autoimmune glial fibrillary acidic protein astrocytopathy. Curr Opin Neurol 2019;32(3):452-458. doi:10.1097/WCO.0000000000000676

38 Mirian A, Sharma M, Budhram A. linear radial brainstem enhancement in autoimmune glial fibrillary acidic protein astrocytopathy. JAMA Neurol 2022;79(1):82-83. doi:10.1001/jamaneurol.2021.4054

39 Sotoudeh H, Razaei A, Saadatpour Z, et al. Brainstem encephalitis. The role of imaging in diagnosis. Curr Probl Diagn Radiol 2021;50(6): 946-960. doi:10.1067/j.cpradiol.2020.09.004

40 Law LY, Riminton DS, Nguyen M, et al. The spectrum of immune-mediated and inflammatory lesions of the brainstem: clues to diagnosis. Neurology 27 2019;93(9):390-405. doi:10.1212/WNL.0000000000008015

41 Grasso D, Castorani G, Borreggine C, Simeone A, De Blasi R. Cerebral amyloid angiopathy related inflammation: a little known but not to be underestimated disease. Radiol Case Rep 2021; 16(9):2514-2521. doi:10.1016/j.radcr.2021.05.080

42 Koçer N, Islak C, Siva A, et al. CNS involvement in neuro-Behcet syndrome: an MR study. AJNR Am J Neuroradiol 1999;20(6):1015-1024.

43 Tobin WO, Guo Y, Krecke KN, et al. Diagnostic criteria for chronic lymphocytic inflammation with pontine perivascular enhancement responsive to steroids (CLIPPERS). Brain 2017; 140(9):2415-2425. doi:10.1093/brain/awx200

44 Susac JO, Murtagh FR, Egan RA, et al. MRI findings in Susac's syndrome. Neurology 2003; 61(12):1783-1787. doi:10.1212/01.wnl.0000103880.29693.48

45 Gaig C, Graus F, Compta Y, et al. Clinical manifestations of the anti-IgLON5 disease. Neurology 2017;88(18):1736-1743. doi:10.1212/WNL.0000000000003887

46 Mandel-Brehm C, Dubey D, Kryzer TJ, et al. Kelch-like protein 11 antibodies in seminoma-associated paraneoplastic encephalitis. N Engl J Med 2019;381(1):47-54. doi:10.1056/NEJMoa1816721

47 Saiz A, Bruna J, Stourac P, et al. Anti-Hu-associated brainstem encephalitis. J Neurol Neurosurg Psychiatry 2009;80(4):404-407. doi:10.1136/jnnp.2008.158246

Copyright © American Academy of Neurology. Unauthorized reproduction of this article is prohibited.

48 Simard C, Vogrig A, Joubert B, et al. Clinical spectrum and diagnostic pitfalls of neurologic syndromes with Ri antibodies. Neurol Neuroimmunol Neuroinflamm 2020;7(3):699. doi:10.1212/NXI.0000000000000699

49 Vogrig A, Gigli GL, Segatti S, et al. Epidemiology of paraneoplastic neurological syndromes: a population-based study. J Neurol 2020;267(1): 26-35. doi:10.1007/s00415-019-09544-1

50 Loehrer PA, Zieger L, Simon OJ. Update on paraneoplastic cerebellar degeneration. Brain Sci 2021;11(11):414. doi:10.3390/brainsci11111414

51 Hadjivassiliou M, Graus F, Honnorat J, et al. Diagnostic criteria for primary autoimmune cerebellar ataxia-guidelines from an international task force on immune-mediated cerebellar ataxias. Cerebellum 2020;19(4):605-610. doi:10.1007/s12311-020-01132-8

52 Joubert B, Honnorat J. Nonparaneoplastic autoimmune cerebellar ataxias. Curr Opin Neurol 2019;32(3):484-492. doi:10.1097/WCO.0000000000000678

53 Kaichi Y, Kakeda S, Moriya J, et al. Brain MR findings in patients with systemic lupus erythematosus with and without antiphospholipid antibody syndrome. AJNR Am J Neuroradiol 2014;35(1):100-105. doi:10.3174/ajnr.A3645

54 Sinnecker T, Clarke MA, Meier D, et al. Evaluation of the central vein sign as a diagnostic imaging biomarker in multiple sclerosis. JAMA Neurol 2019;76(12):1446-1456. doi:10.1001/jamaneurol.2019.2478

55 Kelley BP, Corrigan JJ, Patel SC, Griffith BD. Neuropsychiatric lupus with antibody-mediated striatal encephalitis. AJNR Am J Neuroradiol 2018; 39(12):2263-2269. doi:10.3174/ajnr.A5842

56 Sarbu N, Alobeidi F, Toledano P, et al. Brain abnormalities in newly diagnosed neuropsychiatric lupus: systematic MRI approach and correlation with clinical and laboratory data in a large multicenter cohort. Autoimmun Rev 2015;14(2):153-159. doi:10.1016/j.autrev.2014.11.001

57 Kayser MS, Dalmau J. The emerging link between autoimmune disorders and neuropsychiatric disease. J Neuropsychiatry Clin Neurosci 2011; 23(1):90-97. doi:10.1176/jnp.23.1.jnp90

58 Deijns SJ, Broen JCA, Kruyt ND, et al. The immunologic etiology of psychiatric manifestations in systemic lupus erythematosus: a narrative review on the role of the blood brain barrier, antibodies, cytokines and chemokines. Autoimmun Rev 2020;19(8):102592. doi:10.1016/j.autrev.2020.102592

59 Delalande S, de Seze J, Fauchais AL, et al. Neurologic manifestations in primary Sjogren syndrome: a study of 82 patients. Medicine 2004;83(5):280-291. doi:10.1097/01.md.0000141099.53742.16

60 Goglin S, Cho TA. Clinical approach to neuro-rheumatology. J Neurol Sci 2021;431:120048. doi: 10.1016/j.jns.2021.120048

61 Gill CM PA, Cho TA. Central nervous system vasculitis. In: Neuroimmunology. Springer International Publishing; 2021:385-404.

62 Boulouis G, de Boysson H, Zuber M, et al. Primary angiitis of the central nervous system: magnetic resonance imaging spectrum of parenchymal, meningeal, and vascular lesions at baseline. Stroke 2017;48(5):1248-1255. doi:10.1161/STROKEAHA.116.016194

63 Beuker C, Schmidt A, Strunk D, et al. Primary angiitis of the central nervous system: diagnosis and treatment. Ther Adv Neurol Disord 2018;11: 1756286418785071. doi:10.1177/1756286418785071

64 Molloy ES, Singhal AB, Calabrese LH. Tumour-like mass lesion: an under-recognised presentation of primary angiitis of the central nervous system. Ann Rheum Dis 2008;67(12):1732-1735. doi:10.1136/ard.2008.096800

65 Al-Louzi O, Hauptman H, Saidha S. Biopsy-negative PET-positive giant-cell arteritis. Neurology 2014;83(18):1674-1676. doi:10.1212/WNL.0000000000000940

66 Leao DJ, Agarwal A, Mohan S, Bathla G. Intracranial vessel wall imaging: applications, interpretation, and pitfalls. Clin Radiol 2020; 75(10):730-739. doi:10.1016/j.crad.2020.02.006

67 Sarbu N, Shih RY, Jones RV, et al. White matter diseases with radiologic-pathologic correlation. Radiographics 2016;36(5):1426-1447. doi:10.1148/rg.2016160031

68 Chwalisz BK. Cerebral amyloid angiopathy and related inflammatory disorders. J Neurol Sci 2021; 424:117425. doi:10.1016/j.jns.2021.117425

69 Salvarani C, Morris JM, Giannini C, et al. Imaging findings of cerebral amyloid angiopathy, abeta-related angiitis (ABRA), and cerebral amyloid angiopathy-related inflammation: a single-institution 25-year experience. Medicine 2016;95(20):e3613. doi:10.1097/MD.0000000000003613

70 Diehn FE, Krecke KN. Neuroimaging of spinal cord and cauda equina disorders. Continuum (Minneap Minn) 2021;27(1, Spinal Cord Disorders): 225-263. doi:10.1212/CON.0000000000000926

71 Abdel-Wahed L, Cho TA. Immune-mediated myelopathies: a review of etiologies, diagnostic approach, and therapeutic management. Semin Neurol 2021;41(3):269-279. doi:10.1055/s-0041-1725152

72 Lopez-Chiriboga S, Flanagan EP. Myelitis and other autoimmune myelopathies. Continuum (Minneapolis Minn) 2021; 27(1, Spinal Cord Disorders):62-92. 10.1212/CON.0000000000000900

Copyright © American Academy of Neurology. Unauthorized reproduction of this article is prohibited.

73 Nesbit GM, Miller GM, Baker HL Jr, Ebersold MJ, Scheithauer BW. Spinal cord sarcoidosis: a new finding at MR imaging with Gd-DTPA enhancement. Radiology 1989;173(3):839-843. doi:10.1148/radiology.173.3.2813795

74 Zalewski NL, Krecke KN, Weinshenker BG, et al. Central canal enhancement and the trident sign in spinal cord sarcoidosis. Neurology 2016;87(7): 743-744. doi:10.1212/WNL.0000000000002992

75 Flanagan EP, Kaufmann TJ, Krecke KN, et al. Discriminating long myelitis of neuromyelitis optica from sarcoidosis. Ann Neurol 2016;79(3): 437-447. doi:10.1002/ana.24582

76 Dubey D, Pittock SJ, Krecke KN, et al. Clinical, radiologic, and prognostic features of myelitis associated with myelin oligodendrocyte glycoprotein autoantibody. JAMA Neurol 2019; 76(3):301-309. doi:10.1001/jamaneurol.2018.4053

77 Zalewski NL, Morris PP, Weinshenker BG, et al. Ring-enhancing spinal cord lesions in neuromyelitis optica spectrum disorders. J Neurol Neurosurg Psychiatry 2017;88(3):218-225. doi:10.1136/jnnp-2016-314738

78 Flanagan EP, McKeon A, Lennon VA, et al. Paraneoplastic isolated myelopathy: clinical course and neuroimaging clues. Neurology 2011; 76(24):2089-2095. doi:10.1212/WNL.0b013e31821f468f

79 Linnoila JJ. Imaging in autoimmune neurology. Semin Neurol 2018;38(3):371-378. doi:10.1055/s-0038-1660476

DISCLOSURE

Continued from page 255

National Institutes of Health and has received publishing royalties from a publication relating to health care. The institution of an immediate family member of Dr Cho has received research support from the National Institutes of Health.

Copyright © American Academy of Neurology. Unauthorized reproduction of this article is prohibited.

REVIEW ARTICLE

CONTINUUM AUDIO INTERVIEW AVAILABLE ONLINE

Imaging of Central Nervous System Demyelinating Disorders

By Jan-Mendelt Tillema, MD

ABSTRACT

OBJECTIVE: **This article summarizes neuroimaging findings in demyelinating disease, the most common being multiple sclerosis. Revisions to criteria and treatment options have been ongoing, and MRI plays a pivotal role in diagnosis and disease monitoring. The common antibody-mediated demyelinating disorders with their respective classic imaging features are reviewed, as well as the differential diagnostic considerations on imaging.**

LATEST DEVELOPMENTS: **The clinical criteria of demyelinating disease rely heavily on imaging with MRI. With novel antibody detection, the range of clinical demyelinating syndromes has expanded, most recently with myelin oligodendrocyte glycoprotein–IgG antibodies. Imaging has improved our understanding of the pathophysiology of multiple sclerosis and disease progression, and further research is underway. The importance of increased detection of pathology outside of the classic lesions will have an important role as therapeutic options are expanding.**

ESSENTIAL POINTS: **MRI has a crucial role in the diagnostic criteria and differentiation among common demyelinating disorders and syndromes. This article reviews the typical imaging features and clinical scenarios that assist in accurate diagnosis, differentiation between demyelinating diseases and other white matter diseases, the importance of standardized MRI protocols in clinical practice, and novel imaging techniques.**

CITE AS:
CONTINUUM (MINNEAP MINN) 2023;29(1, NEUROIMAGING): 292–323.

Address correspondence to Dr Jan-Mendelt Tillema 200 First St SW, Rochester, MN 55905, Tillema.JanMendelt@mayo.edu.

RELATIONSHIP DISCLOSURE:
Dr Tillema reports no disclosure.

UNLABELED USE OF PRODUCTS/INVESTIGATIONAL USE DISCLOSURE:
Dr Tillema reports no disclosure.

© 2023 American Academy of Neurology.

INTRODUCTION

Since the introduction of MRI, the technical development and availability of scanners reflect their pivotal noninvasive investigational role in demyelinating disorders of the central nervous system (CNS), highlighted by the number of publications on their use. The advances in MRI have resulted in earlier and more accurate diagnosis of multiple sclerosis (MS) and provide the ability to noninvasively detect subclinical disease activity. MRI findings are a major outcome measure in therapeutic clinical trials. Furthermore, MRI has expanded the spectrum of demyelinating disorders with specific imaging criteria for antibody-mediated demyelinating disorders, such as neuromyelitis optica spectrum disorders (NMOSD) and myelin oligodendrocyte glycoprotein (MOG)–associated disorders.

Copyright © American Academy of Neurology. Unauthorized reproduction of this article is prohibited.

This article reviews the role of MRI in the evaluation of the most common CNS demyelinating disorders, including diagnosis, differentiation, protocols, and advanced and future directions. Many aspects of MS have remained elusive to capture, but research with advanced imaging and processing techniques has and will continue to improve our understanding of the disease. The main focus here is on the current clinical (conventional) techniques used to assist in diagnosis and management and imaging as a tool in combination with sound clinical judgment. The role of MRI has increased over the years in the clinical criteria for diagnosing demyelinating disease.

KEY POINTS

- **MRI plays a pivotal role in the diagnostic criteria for central nervous system (CNS) demyelinating disorders.**
- **In patients with multiple sclerosis (MS), normal-appearing white matter and gray matter are now well known to harbor both demyelinating and neurodegenerative pathology.**
- **Earlier diagnosis and treatment monitoring for MS rely greatly on MRI. Despite these advances, the diagnosis and distinction between MS phenotypes remain a clinical assessment.**

ROLE OF MRI IN DIAGNOSIS OF DEMYELINATING DISEASE

This section summarizes the most common demyelinating disorders including clinical criteria and classic or typical imaging features.

Multiple Sclerosis

MS is the most common demyelinating disease. It is a chronic life-long disease, mainly characterized by immune-mediated inflammatory demyelination of the CNS, predominantly affecting white matter although there are long-recognized pathologic[1] and now well-established MRI involvement of the cortical and subcortical gray matter.[2] In patients with MS, normal-appearing white matter and gray matter are now well known to harbor both demyelinating and neurodegenerative pathology. This is apparent with atrophy, axonal loss, and diminished integrity of healthy-appearing tissue on pathology and MRI. These pathologic changes outside of the classic lesions have been detected by advanced neuroimaging techniques.

The main clinical MS phenotypes include clinically isolated syndrome (CIS), relapsing-remitting MS (RRMS), secondary progressive MS (SPMS), and primary progressive MS (PPMS); additionally, separate criteria exist for radiologically isolated syndrome (RIS).

Relapsing-Remitting Multiple Sclerosis and Clinically Isolated Syndrome

The clinical symptoms of a demyelinating attack of CIS and MS (synonymous with *relapse* or *exacerbation*) have a subacute onset, typically with a gradual increase over a few days. By definition, an attack lasts longer than 24 hours. Without objective evidence of an attack, the diagnosis of CIS and RRMS cannot be made. The attack cannot be explained by an infection and occurs in the absence of a fever. These attacks can affect sensory, motor, bladder, cerebellar, and cranial nerve function. Classic presentations include unilateral optic neuritis, focal supratentorial, brainstem or cerebellar syndrome, or a partial myelopathy.[3] A (hyper)acute onset of symptoms should immediately raise concerns for other neurologic disorders. Heat sensitivity (Uhthoff phenomenon) is defined as a worsening of symptoms in the setting of infection or overheating; this and the Lhermitte sign, a shocklike sensation down the spine with flexion of the neck, are commonly encountered. Fatigue, mood disorders, and cognitive dysfunction are important features of MS, often affecting quality of life, but are nonspecific findings that do not comprise an initial attack. Other clinical features that are considered atypical include early pediatric onset (age younger than 12 years), extrapyramidal features, ophthalmoplegia, bilateral vision loss, complete myelopathy, headache, encephalopathy, seizures, or progressive cognitive dysfunction.

Copyright © American Academy of Neurology. Unauthorized reproduction of this article is prohibited.

TABLE 11-1

Diagnostic Criteria for Multiple Sclerosis[a]

Clinical findings

- **Clinical attack is mandatory. Patients meet relapsing-remitting multiple sclerosis criteria with**
- **Single attack with objective evidence of central nervous system (CNS) demyelinating event and presence of both (mandatory) dissemination in space and time by either**
  - ≥2 lesions with dissemination in time demonstrated by either
    - → A distinct additional attack
    - → Either MRI or CSF dissemination in time criteria
  - 1 lesion with evidence of both dissemination in space and dissemination in time on subsequent follow-up
    - → Dissemination in space demonstrated by
      - Additional new attack at a different CNS site
      - Follow-up MRI with new lesions, now fulfilling dissemination in space MRI criteria
    - → Dissemination in time demonstrated by
      - An additional new clinical attack
      - MRI or CSF demonstration of dissemination in time with MRI lesion according to dissemination in space criteria
    - → Dissemination in time requires either fulfillment of MRI dissemination in time criteria OR abnormalities in CSF (presence of CSF unique oligoclonal bands)
- **Multiple (≥2) distinct anatomic attacks with evidence of**
  - MRI criteria fulfilling dissemination in space criteria
  - >1 lesion with both attacks having objective anatomically distinct clinical attacks
  - >1 lesion with an additional clinical attack in a different CNS site (clinically or radiographically)
- **Reasonable exclusion of other conditions that would explain clinical or imaging findings**

MRI findings of dissemination in space

- **Round or ovoid T2-hyperintense lesions, well-circumscribed, ≥3 mm^2**
- **MRI involvement in ≥2 of 4 locations**
  - ≥1 infratentorial lesion
  - ≥1 juxtacortical (abutting cortex) or cortical lesion
  - ≥1 periventricular lesion (abutting ventricle)
  - ≥1 spinal cord lesion
- **Exclusion of another explanation for imaging findings**

MRI findings of dissemination in time

- **New T2-hyperintense lesion irrespective of timing**
- **Presence of simultaneous enhancing and nonenhancing lesions on MRI**

CSF = cerebrospinal fluid; MRI = magnetic resonance imaging.
[a] These criteria are according to and modified from the current operational 2017 McDonald criteria.[6] The components of these include the criteria combining clinical, imaging, and laboratory CSF investigations.

Copyright © American Academy of Neurology. Unauthorized reproduction of this article is prohibited.

RELAPSING-REMITTING MULTIPLE SCLEROSIS. RRMS is the most common phenotype of MS at the onset of the disease and diagnosis, constituting approximately 85% to 90% of patients with MS.[4,5] Clearly defined attacks are followed by complete or incomplete recovery. The severity of the persistent deficits is variable, with only a very small number of patients (fewer than 1%) requiring new gait assistance after recovery.

CLINICALLY ISOLATED SYNDROME. *CIS* is defined as a monophasic clinical episode, consistent with an objective demyelinating attack of the CNS, which occurs in a patient who is not known to have MS.[6] The patient can be diagnosed with MS; thus, the CIS is the first attack of MS, if MS criteria of dissemination in space and time are met. The clinical symptoms can be monofocal (restricted to a single CNS location) or multifocal. In CIS, when a second attack or new lesion on MRI is found, MS criteria are also met. With revisions of the MS criteria over time, most recently in 2017,[6] MS is diagnosed earlier, lowering the incidence of CIS. The criteria are summarized in TABLE 11-1.

Radiologically Isolated Syndrome

RIS is a condition with radiographic findings of demyelination in the absence of clear symptoms consistent with demyelination. The incidence of RIS increased with the rising use of MRI in clinical practice, and over the years, conversion to MS has become better understood. Common MRI indications that result in incidental demyelinating findings include headaches, trauma, and epilepsy. To meet the diagnosis, both (negative) clinical criteria and imaging criteria need to be met. The imaging criteria are more robust than the current MS criteria revisions, in keeping with the 2001 McDonald MRI criteria for dissemination in space.[7] Criteria for RIS are summarized in TABLE 11-2.[8]

Importantly, the risk of conversion to clinically definite MS, whether to RRMS or PPMS, has been seen with the following risk factors: onset age younger than 37 years, presence of gadolinium enhancement on index scan, or the presence of spinal cord lesions on MRI.[9] This overall risk of conversion is estimated to be 19%.[9] CASE 11-1 reviews some of the characteristic RIS findings, workup, and follow-up. Treatment of RIS is generally recommended to be provided by neurologists with expertise in MS. To date, no specific evidence-based recommendations for treatment exist, but ongoing clinical trials are investigating the use of disease-modifying therapy.[10]

Progressive Multiple Sclerosis

Progressive MS is a clinically defined phenotype with gradual progressive neurologic decline. Imaging criteria are part of PPMS diagnostic criteria. Cerebral lesion burden is typically lower, and it has more emphasis on spinal cord involvement. The other classic progressive MS phenotype is SPMS, which is classified as a progressive disease course preceded by RRMS. Patients with PPMS have had progressive disease from onset with gradual neurologic decline for more than 1 year. The median age of presentation in PPMS is about 40 years and occurs in about 10% to 15% of all patients with MS. In patients with SPMS, there is not a single clinical event or investigation that predicts progression. Patients with progressive MS can still have subsequent disease activity in the form of relapses or new MRI activity, although these are much less common. Progression

KEY POINTS

- In MS, radiologic activity can exist without any clinical activity. One of the diagnoses that has gained traction with this pattern is radiologically isolated syndrome, in which MRI lesions are present in asymptomatic patients.
- The risk of conversion to clinically definite MS, whether to relasping-remitting MS or primary progressive MS, is increased with the following risk factors: onset age younger than 37 years, presence of gadolinium enhancement on index scan, or the presence of spinal cord lesions on MRI.
- Patients with progressive MS can still have subsequent disease activity in the form of relapses or new MRI activity, although these are much less common.

Copyright © American Academy of Neurology. Unauthorized reproduction of this article is prohibited.

differs from disease worsening as detailed later in this article. Criteria are reviewed in TABLE 11-3.[6]

Brain Lesions on MRI in Multiple Sclerosis

Brain lesions are the most common demyelinating lesion and are required for all phenotypes, with the exception of PPMS, for which spinal cord lesions may suffice. This section reviews typical features of conventional lesion detection; advanced methods are discussed later in this article. MRI has become the most essential investigational tool in MS with the advances made over the past 3 decades. Two-dimensional acquisitions are still commonly used, have excellent quality on most 1.5T and 3T scanners, and are sensitive to lesion detection; however, with advances in imaging, two-dimensional scans are increasingly replaced by three-dimensional techniques, with simultaneous multislice or undersampling acquisition techniques increasing speed and quality. The overall approach to an attack of a suspected demyelinating disease focuses on the affected CNS structure. For both diagnostic and prognostic reasons, expansion to other areas of the CNS is subsequently recommended. In children or older patients requiring sedation, structures covered on initial imaging may be more extensive to avoid repeat sedation.

The T2-hyperintense lesion is the cardinal feature of demyelinating lesions and is visualized with a T2-weighted image, classically with two-dimensional acquisition, or with fluid-attenuated inversion recovery (FLAIR). By definition,

TABLE 11-2 Diagnostic Criteria for Radiologically Isolated Syndrome[a]

Clinical findings

- **Absence of remitting clinical symptoms consistent with neurologic dysfunction (ie, no clinical attack suggestive of demyelination)**
- **Abnormalities not accounting for clinical impairment in social, occupational, or generalized areas of dysfunction**
- **MRI abnormalities are not related to direct physiologic effects of substances (recreational drugs, toxic exposure) or medical condition**
- **The central nervous system (CNS) abnormalities are not accounted for by another disease process**

MRI findings

- **Ovoid well-circumscribed lesions (with or without corpus callosum involvement)**
- **Lesions are T2 hyperintense, ≥3 mm^2, fulfilling 2001 Barkhof-Tintoré criteria[7]**
  - ≥9 T2-hyperintense lesions or ≥ 1 gadolinium-enhancing lesion
  - ≥1 infratentorial lesion
  - ≥1 juxtacortical lesion
  - ≥3 periventricular lesions
- **CNS white matter abnormalities not consistent with the pattern of vascular disease**
- **Exclusion of MRI phenotypes suggestive of leukoaraiosis or extensive white matter pathology that lack involvement of the corpus callosum**

MRI = magnetic resonance imaging.
[a] Modified with permission from Okuda DT, et al, Neurology.[8] © 2009 American Academy of Neurology.

Copyright © American Academy of Neurology. Unauthorized reproduction of this article is prohibited.

a lesion needs to be greater than 3 mm in diameter. Classic MS lesions are round or ovoid and well circumscribed in the chronic stage. T2 hyperintensities are obviously not limited to MS; other pathologic processes with, for example, edema, ischemic disease, gliosis, and neoplastic growth, have T2 prolongation. Similarly, four immunohistopathological phenotypes exist,[11,12] and they are distinguished based on cellular and humoral immune responses on histopathology; however, MRI appearance on T2-weighted sequences and contrast-enhancing patterns do not necessarily distinguish among these different phenotypes. With this lack of pathologic specificity, lesion location and configuration are key. Lesions that are large or ill circumscribed; have irregular borders, hemispheric symmetry, or extensive gray matter involvement; or are

CASE 11-1

A 27-year-old woman with a long-standing history of headaches presented to her primary care physician with a minor concussion after a sports-related injury. She had worse headaches with some intermittent blurring of her vision. An MRI demonstrated multiple lesions, and she was subsequently referred to neurology. A detailed history revealed the injury was accidental, not related to neurologic deficits, and that the fluctuating blurred vision was painless, short in duration, and decreasing in frequency. The patient had no prior deficits neurologically, and she was in excellent general health without any substance use or abuse or any systemic comorbid disease. Her neurologic examination was normal. Noncontrast brain MRI revealed 11 total lesions. Typical ovoid lesions were well circumscribed and distributed throughout the brain, with lesions noted in juxtacortical white matter (4 lesions), periventricular white matter (3 lesions), and deep white matter (3 lesions). Subsequent contrasted images and cervical spine MRI showed a small nonenhancing lesion at C3. CSF was normal. The diagnosis of radiologically isolated syndrome was made, and the patient was followed clinically. In the next few years, she had no symptoms until she presented with vision loss, which at that time was unilateral and constant with a gradual build-up and a visual acuity of 20/50 with a relative afferent pupillary defect on the affected side. Orbital MRI confirmed an optic nerve lesion, and MRI of the brain showed three new lesions.

COMMENT

This patient presented with imaging findings suggestive of multiple sclerosis (MS) demyelination but lacked any objective clinical features of MS. The necessity of the initial MRI and CSF analysis is debatable; nonetheless, she had multiple lesions, more than nine in three of four characteristic locations, meeting imaging criteria for RIS at onset. At follow-up, she was diagnosed with optic neuritis and had three new lesions on the brain MRI. This patient had converted and met all diagnostic criteria for relapsing-remitting MS and was subsequently started on treatment. This case illustrates the presence of two of three risk factors for conversion (age and spinal cord involvement but not gadolinium enhancement on the index scan).

Copyright © American Academy of Neurology. Unauthorized reproduction of this article is prohibited.

outside the typical distribution should raise concerns.[13] After resolution of the initial edema and inflammation, lesions remain stable in size, unless new disease activity occurs in the same site (ie, smoldering or enlarging lesions).

Typical location and distribution definitions are reflected in the diagnostic criteria.[6] Despite wide use, the recognition of specific lesion location and appearance is not always interpreted correctly, even by MS experts.[13] Definitions are as follows: Periventricular lesions seem to arise from the ventricle. Periventricular lesions are commonly ovoid, with the long axis perpendicular to the ventricle (Dawson finger). They are required to abut the ventricle and are restricted to the white matter (ie, should not be confined solely to basal ganglia). If normal white matter is seen between the lesions and the ventricle, the lesions are not considered to be periventricular and would not add to the diagnostic MRI criteria. Similarly, juxtacortical lesions are required to abut the cortex, without normal-appearing white matter between them. Otherwise, they are subcortical and do not satisfy diagnostic MRI criteria. Juxtacortical lesions are best seen with higher-resolution imaging, often in the sagittal plane. Deep white matter lesions or subcortical lesions are seen commonly in MS, but specificity is low. Thus, when lesions are in an isolated or predominantly subcortical distribution, alternative diagnoses require stronger consideration. Infratentorial lesions are found in the brainstem, cerebellar peduncle, or cerebellum and typically appear near the surface. Classically, infratentorial lesions are better visible on two-dimensional T2-weighted imaging compared with two-dimensional FLAIR. With recent advances in three-dimensional FLAIR imaging, when quality is sufficient, this sequence is actually as sensitive or better than axial two-dimensional T2-weighted images, despite the higher signal-to-noise ratio in the latter.[14] Examples of typical brain lesions are shown in **FIGURE 11-1**.

One of the additions to the 2017 MS criteria included cortical lesions being able to replace juxtacortical lesions. With two-dimensional acquisitions, cortical lesions are barely detectable. Advances in high-resolution three-dimensional imaging sequences have improved lesion detection. The majority of reliably detected lesions are leukocortical. High-quality three-dimensional FLAIR, at 3T more so than double inversion recovery and phase-sensitive inversion recovery, has the best ability to detect cortical MS lesions. An example is shown in **FIGURE 11-2**. The majority of cortical lesions remain undetectable.

TABLE 11-3 **Diagnostic Criteria for Progressive Multiple Sclerosis[a,b]**

Clinical criteria

- >1 year of disability progression (either retrospective or prospective) which is independent of a clinical relapse with ≥2 of three of the following findings:
- CSF: oligoclonal bands present
- MRI: presence of ≥1 T2-hyperintense lesions in periventricular, (juxta)cortical, or infratentorial regions
- MRI: presence of ≥2 distinct T2-hyperintense spinal cord lesions

CSF = cerebrospinal fluid; MRI = magnetic resonance imaging.
[a] Modified with permission from Thompson AJ, et al, Lancet Neurol.[6] © 2018 Elsevier Inc.
[b] The clinical and imaging diagnostic features of primary and secondary progressive multiple sclerosis.[6]

Copyright © American Academy of Neurology. Unauthorized reproduction of this article is prohibited.

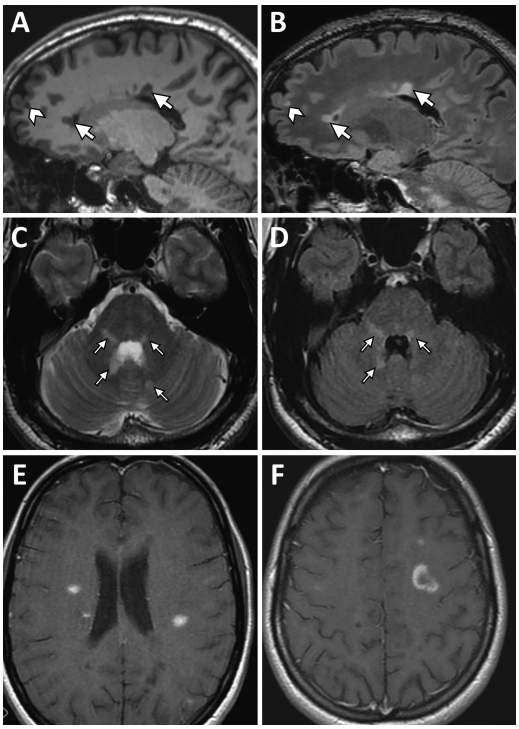

FIGURE 11-1

Typical brain lesions in multiple sclerosis (MS) from a patient with relapsing-remitting MS. Sagittal fluid-attenuated inversion recovery (FLAIR) (*A*) and T1-weighted (*B*) MRI were both acquired with three-dimensional 1-mm isotropic sequences. Typical periventricular (*A, B, arrows*) and juxtacortical (*A, B, arrowheads*) lesions are noted. Axial T2-weighted (*C*) and FLAIR (*D*) images show infratentorial lesions (cerebellum and cerebellar peduncle lesions; *C, D, arrows*). Note that the FLAIR (*D*) image reveals the majority of the lesions, but at a much lower contrast-to-noise ratio, exemplifying that the fourth lesion is barely visible on FLAIR images (hence the missing fourth arrow in *D*). In the bottom row are two typical postgadolinium enhancement patterns, with solid (*E*) and open-ring (*F*) enhancement. Note that in the latter the opening is facing toward the cortical gray matter.

Caution is necessary for potential false-positive (typically smaller or subpial) lesions, highlighted by poor interrater reliability for detection with double inversion recovery (greater than 50%).[15]

T1-hypointense lesions can be present in both acute and chronic lesion stages. Recognizing and distinguishing acute lesions from chronic "black holes" is important. A difficulty in interpretation is that the sequences used, as well as the timing of MRI, have a role in detection. Unlike T2-weighted images, conventionally acquired two-dimensional T1-weighted images have more protocol and scanner variability, affecting the signal-to-noise ratio; thus, they demonstrate potential inconsistencies in the extent or severity of the apparent hypointensity. With currently commonly applied three-dimensional sequences, the acquisition can be harmonized better across scanners, with typically greater gray-to-white differentiation. In the acute stage, the T1 hypointensity reflects demyelination, inflammation, and excess extracellular fluid. The long-term follow-up (longer than 3 months) appearance of T1-hypointense lesions, known as *black holes*, presents in approximately 30% of lesions and is associated with more destructive pathologic properties with less remyelination and repair and more axonal loss.[16]

Gadolinium-enhancing brain lesions in MS are classically thought of as active lesions. The leakage of gadolinium through the blood-brain barrier is related to the subacute inflammation. Enhancing lesions provide a window into recent inflammatory activity; enhancement is observed in the first 4 to 6 weeks of lesion formation. The presence and amount of enhancement are related to the contrast agent, dosing, timing between administration and imaging, timing from lesion onset, and lesion pathology. Persistent enhancement over time should raise doubts about the diagnosis of MS, increasing consideration for alternative diagnoses, such as sarcoidosis or neoplasm. Classic patterns of enhancement are

KEY POINTS

- **Classic MS lesions are round or ovoid and well circumscribed in the chronic stage.**
- **With recent advances in three-dimensional fluid-attenuated inversion recovery (FLAIR) imaging, when quality is sufficient, this sequence is actually as sensitive or better than axial two-dimensional T2-weighted images.**
- **High-quality three-dimensional FLAIR at 3T, more so than double inversion recovery and phase-sensitive inversion recovery, has the best ability to detect cortical MS lesions.**

Copyright © American Academy of Neurology. Unauthorized reproduction of this article is prohibited.

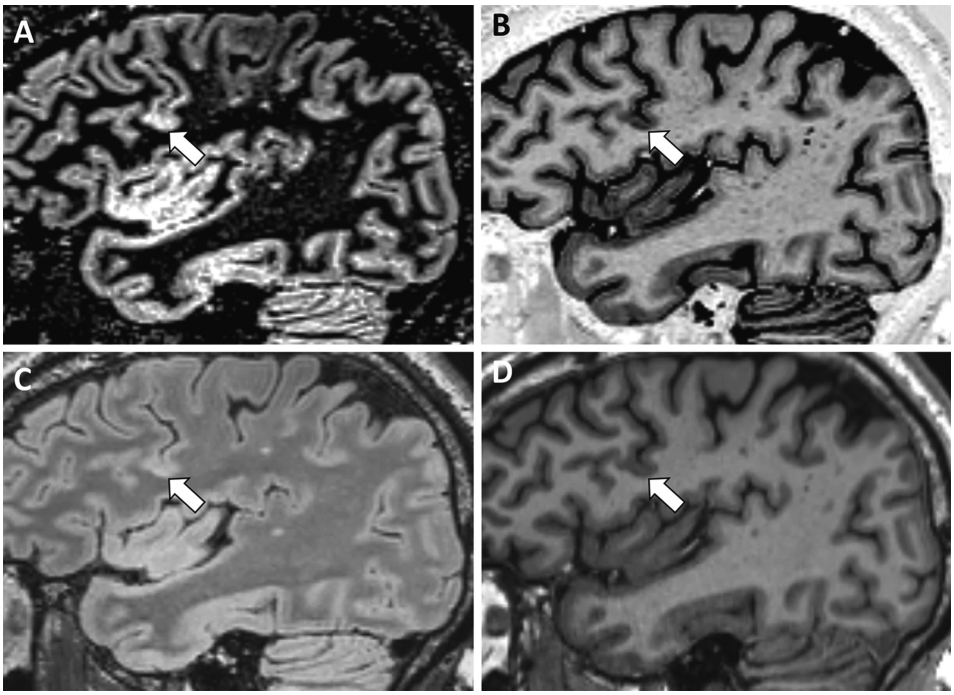

FIGURE 11-2

Examples of cortical lesions in multiple sclerosis (MS). The top row shows a typical leukocortical lesion. In double-inversion recovery (DIR) (*A*) and phase-sensitive inversion recovery (PSIR) (*B*), the cortical lesion (*A, B, arrows*) is best seen and localized with PSIR. Sagittal three-dimensional-acquired FLAIR (*C*) and three-dimensional-acquired T1-weighted magnetization-prepared rapid gradient echo (MPRAGE) (*D*) images have the same resolution in the same patient. The lesion (*C, D, arrows*) is visible but not as prominent as noted in the sequences that have been used most in research and have the highest sensitivity to lesion detection. Of note, as seen in the DIR images (*A*), based on the quality of the acquired images, quite significant noise can be present, leading to concern for false-positive detection as exemplified by the poor interrater agreement in these images alone. Some caution with identifying smaller lesions in particular is warranted.

homogenous, heterogeneous or nodular, and (open) ring. The latter two are more commonly seen in larger lesions; examples are shown in FIGURE 11-1. Open-ring enhancement is highly specific to MS with a pattern in which the opening is facing the gray matter.[17]

Tumefactive demyelinating lesions are larger lesions, by definition 2.5 cm or greater in diameter. At presentation, these can represent a clinical challenge, and biopsy is often considered. Interpretation of conventional scans has improved, and in some patients, biopsy could therefore be avoided. Tumefactive lesions themselves do not necessarily distinguish between demyelinating disease phenotype of MS or NMO, but features outside of the lesion may. Differentiation from neoplastic disease and infection improves with consideration of contrast-enhancing pattern, diffusion imaging (peripheral restriction), and T2 pattern recognition as shown in FIGURE 11-3. Baló concentric sclerosis is a distinct phenotype, both pathologically and radiographically. The initial disease course can be more aggressive and approached similarly. Despite this, the long-term outcome is not necessarily poor.[18,19]

Copyright © American Academy of Neurology. Unauthorized reproduction of this article is prohibited.

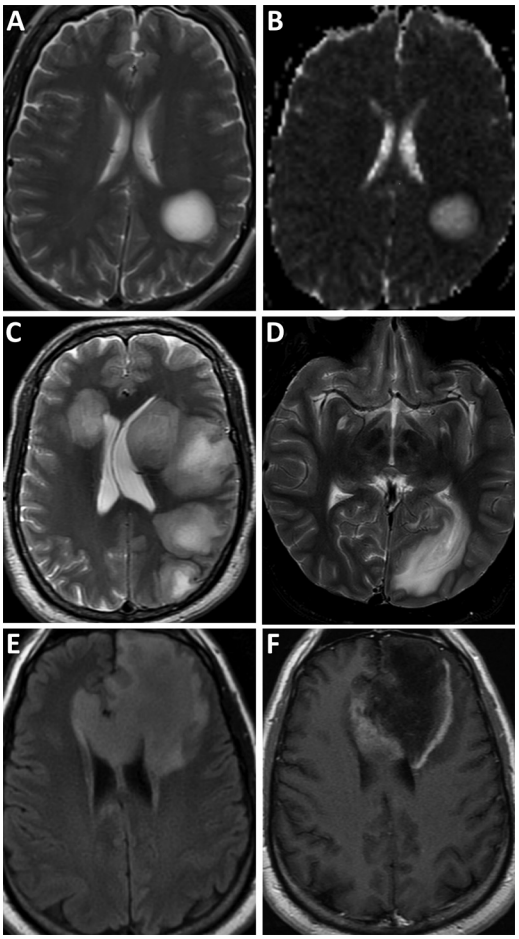

FIGURE 11-3

Examples of findings in axial MRI in tumefactive demyelination, in this case, all with biopsy-proven pathology consistent with multiple sclerosis. Findings on a T2-weighted (*A*) image with a corresponding rim of apparent diffusion coefficient (ADC) restriction (*B*), correlating to the edge of the actual lesion can be seen, in places surrounded by further edema. Diffusion-weighted imaging with ADC (*B*) can be helpful and has been reported to assist in distinguishing from abscess and neoplastic disease. *Panel C* shows the possibility of significant mass effect with large lesions and surrounding edema, and *panel D* shows a few rings of intralesional T2-hypointense signal change, which are concentric rims that can be seen in Baló concentric sclerosis. *Panels E and F* show again the possibility of mass effect and the butterfly spread of demyelinating lesions as possible lesion distribution with patchy ringlike enhancement.

Optic Nerve Imaging

Optic neuritis is a common presentation of MS, but it also may occur in a large percentage of other demyelinating disorders. Optic neuritis is a clinical diagnosis, and imaging is helpful but not necessary to make the diagnosis.

ROLE OF MRI IN OPTIC NEURITIS. When optic neuritis is suspected, dedicated orbital imaging should be obtained, with fat suppression to suppress orbital fat tissue. Clinical and imaging phenotypes can help distinguish between disease phenotypes, as shown in FIGURE 11-3.

Classic attacks of optic neuritis in MS are unilateral, affecting a short segment of the nerve, with moderate vision loss. As with everything, overlap and variation are present. Pediatric patients can have more significant vision loss and atypical presentations.[20] The opposite of some of these classic findings is seen in antibody-mediated optic neuritis. In those patients, vision loss and papilledema are more prominent, and in the majority, the visible length of inflammation covers more than 50% of the nerve with frequent bilateral involvement. A critically important feature of imaging in optic neuritis is the addition of additional brain coverage when MS is suspected. An attack of optic neuritis can be considered an attack of MS in the clinical criteria. But importantly, the optic nerve lesion (even when enhancing) is not considered an MRI criterion. In patients with isolated optic neuritis, the conversion risk to MS is about 25% over 15 years in the absence of brain lesions.[21] Examples of typical lesions are shown in FIGURE 11-4.

KEY POINTS

- Open-ring enhancement is highly specific to MS with a pattern in which the opening is facing the gray matter.
- In patients with isolated optic neuritis, the conversion risk to MS is about 25% over 15 years in the absence of brain lesions.
- Optic nerve lesions can have an extensive course throughout the optic nerve, particularly in antibody-mediated optic neuritis (myelin oligodendrocyte glycoprotein and neuromyelitis optica).

Copyright © American Academy of Neurology. Unauthorized reproduction of this article is prohibited.

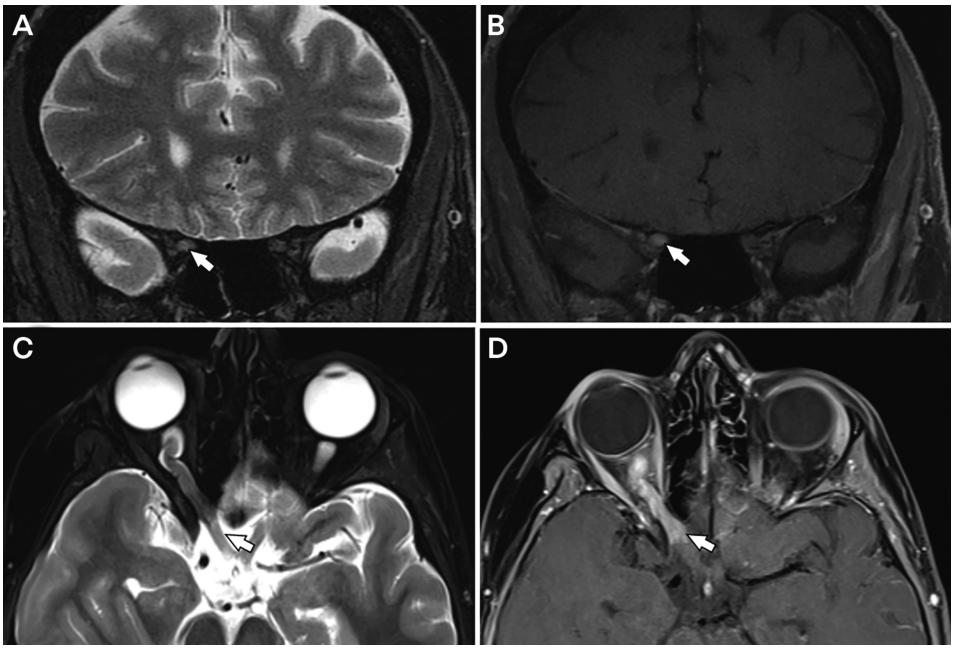

FIGURE 11-4

Optic neuritis in multiple sclerosis (MS) and other demyelinating syndromes. Typical imaging features of optic neuritis are shown in MS and myelin oligodendrocyte glycoprotein (MOG)–associated disorder. The coronal sequences are sensitive enough to detect the T2 signal change and gadolinium enhancement of the nerve. Lesions are seen in a patient with MS with coronal T2 fat saturation (*A, arrow*) and coronal postcontrast T1 fat saturation (*B, arrow*) images. These lesions are typically focal and less than 50% of the length of the nerve compared with lesions in antibody-mediated optic neuritis (MOG/neuromyelitis optica [NMO]), which more often have greater than 50% of the nerve involved and more often have bilateral involvement. The extensive involvement is shown in a patient with MOG-associated disorder with axial MRI obtained with fat saturation sequences on T2 (*C*) and postcontrast T1 (*D*) and *arrows* indicating the lesions. MOG-associated disorder and NMO are commonly associated with less severe vision loss. In MOG-associated disorder, the lesions tend to predominantly affect the anterior optic pathways, which may explain the more common presence of optic disc edema, where NMO spectrum disorder lesions tend to more commonly affect the posterior optic pathways or lesions isolated to the optic chiasm.

ROLE OF IMAGING WITH OPTICAL COHERENCE TOMOGRAPHY IN MULTIPLE SCLEROSIS. Optical coherence tomography (OCT) in demyelinating disease is a noninvasive tool to measure the thickness of distinct layers of the eye, including the retinal nerve fiber layers and ganglion cell inner plexiform layer. OCT can show retinal nerve fiber layer thickening in the acute stage of optic neuritis. After resolution of the attack or in the setting of the presence of a previous attack, thinning of both layers is noted, with the extent correlating to residual vision loss. OCT is highly sensitive in the detection of possible previous optic nerve lesions or attacks.[22] The utility in monitoring and extent of detecting subclinical activity remain to be determined.

Spinal Cord Imaging

In transverse myelitis, MRI has great utility in diagnosis and differentiating among inflammatory demyelinating syndromes (potentially seen in all RIS, MS, NMO, MOG, and acute disseminated encephalomyelitis [ADEM] settings). Transverse myelitis can be isolated, as in CIS, or idiopathic. The necessity for imaging may be urgent, especially when the onset is rapid, after trauma, when

Copyright © American Academy of Neurology. Unauthorized reproduction of this article is prohibited.

associated with significant back pain, or after surgery. Compressive lesions require urgent neurosurgical evaluation. Other suspected etiologies have specific imaging findings and require a different expansion of workup. Because the differential diagnosis is broad and complex, the most common diagnoses (toxic or metabolic,[23] ischemic,[24] neoplastic or paraneoplastic, and other myelopathies) were discussed in the February 2021 *Continuum* Spinal Cord Disorders issue, including other inflammatory myelopathies.[25]

In demyelinating disorders, transverse myelitis presents subacutely. A common onset is with paraparesis, quadriparesis, sensory loss below the localization of the lesion, or neurogenic bladder and bowel dysfunction. Time from the development to nadir should be longer than 1 hour and less than 21 days, and symptoms need to be longer than 24 hours in duration. Transverse myelitis can be partial or complete (clinically and holocord on axial imaging), but in MS, it is typically partial. MRI in MS commonly shows ovoid lesions, greater than 3 mm in diameter, and no more than 1 vertebral segment (FIGURE 11-4). The lesions are often localized in a dorsal or lateral location and are seen most commonly in the cervical spinal cord, but they can occur anywhere in thoracic cord and conus medullaris. T1-hypointense lesions are rare. More commonly, subtle spinal cord atrophy can be seen, caving in on sagittal images or with flattening of the round surfaces on axial images. Helpful imaging sequences include sagittal T2-weighted fast spin echo and short tau inversion recovery (STIR). Axial imaging with T2-weighted proton density has a high signal-to-noise ratio and is most helpful in the exact localization of the section and tracts involved.

KEY POINT

- Optical coherence tomography is highly sensitive in the detection of possible previous optic nerve lesions or attacks.

DIFFERENTIATION FROM OTHER DEMYELINATING SYNDROMES

The imaging features of MS are specific and differ from other demyelinating disorders. This section describes the imaging findings in other demyelinating diseases.

Neuromyelitis Optica Spectrum Disorder

The classic recognition of NMO initially was based on distinct clinical and imaging features. After the breakthrough antibody discovery of aquaporin-4 (AQP4)-IgG,[26] recognition of different phenotypes has refined the spectrum. NMOSD is much more common in female patients (10:1) compared with MS (3:1), and it has a disproportionate incidence that is much higher in Black patients.[27] The NMOSD criteria include the presence of AQP4-IgG (seropositive NMOSD) and cases in which the antibody could not be detected (seronegative NMOSD). Because antibody detection assays have improved, the current cell-based assays with the highest sensitivity and specificity are recommended. Criteria for NMOSD are reviewed in TABLE 11-4.[3,28]

MRI of the spinal cord is a key component in the diagnosis of NMOSD, characteristically demonstrating longitudinally extensive transverse myelitis (LETM), a lesion expanding over three or more spinal cord segments. Lesions commonly have a strongly inflammatory component with a swollen appearance of the affected cord. The potentially severe destructive properties of lesions are notable in clinical and imaging investigations. Patients with NMOSD generally have more severe attacks with poorer recovery, and the lesions are more extensive than in typical MS or MOG-associated disorder. The extensive transverse lesion size is noted on axial images (FIGURE 11-5), where again more

Copyright © American Academy of Neurology. Unauthorized reproduction of this article is prohibited.

TABLE 11-4

Diagnostic Criteria for Neuromyelitis Optica[a,b]

Core clinical characteristics

- **Optic neuritis**
- **Acute myelitis**
- **Area postrema syndrome**
- **Acute brainstem syndrome**
- **Symptomatic narcolepsy or acute diencephalic clinical syndrome with typical MRI lesions**
- **Symptomatic cerebral syndrome with typical MRI lesions**

Seropositive neuromyelitis optica spectrum disorder (NMOSD)

- **Clinical**
  - ≥1 core clinical attack
  - Aquaporin-4 (AQP4)–IgG antibodies positive or detected
  - Exclusion of another alternative diagnoses
- **MRI**
  - Obtained to confirm lesions, but none of the MRI criteria are necessary for the diagnosis

Seronegative NMOSD (AQP4-IgG not detected or unknown)

- **Clinical**
  - ≥2 core clinical characteristics as the result of >1 attack when all the following are met:
    - ≥1 being optic neuritis, transverse myelitis, or area postrema syndrome
    - Dissemination in space (≥2 different core characteristics)
    - Additional MRI requirements
  - AQP4-IgG testing negative or not available
  - Exclusion of other diagnoses
- **MRI**
  - In the case of acute optic neuritis
    - Brain MRI normal or nonspecific
    - MRI orbit with >50% optic nerve length or chiasm involved
  - In the case of acute myelitis
    - Lesion in ≥3 vertebral segments
    - Atrophy in ≥3 vertebral segments in the case of a previous attack
  - In the case of area postrema syndrome
    - Dorsal medulla or area postrema lesion present
  - In the case of acute brainstem syndrome
    - MRI-visible periependymal brainstem lesion

Ig = immunoglobulin G; MRI = magnetic resonance imaging.

[a] Modified with permission from Wingerchuk DM, et al, Neurology.[28] © 2015 American Academy of Neurology.

[b] The table shows the somewhat complex criteria for NMO, with understandable scrutiny for specificity when AQP4-IgG is absent. The most common sites that are involved are circumventricular locations, which are rich in AQP4 water channels. These correlate to the variety of clinical phenotypes that are seen in NMO, such as endocrinopathies, syndrome of inappropriate secretion of antidiuretic hormone (SIADH), autonomic changes, excessive daytime sleepiness and narcolepsy, and encephalopathy. Cortical and limbic encephalitis can present with seizures and encephalopathy. Posterior reversible encephalopathy syndrome (PRES) has been seen.

Copyright © American Academy of Neurology. Unauthorized reproduction of this article is prohibited.

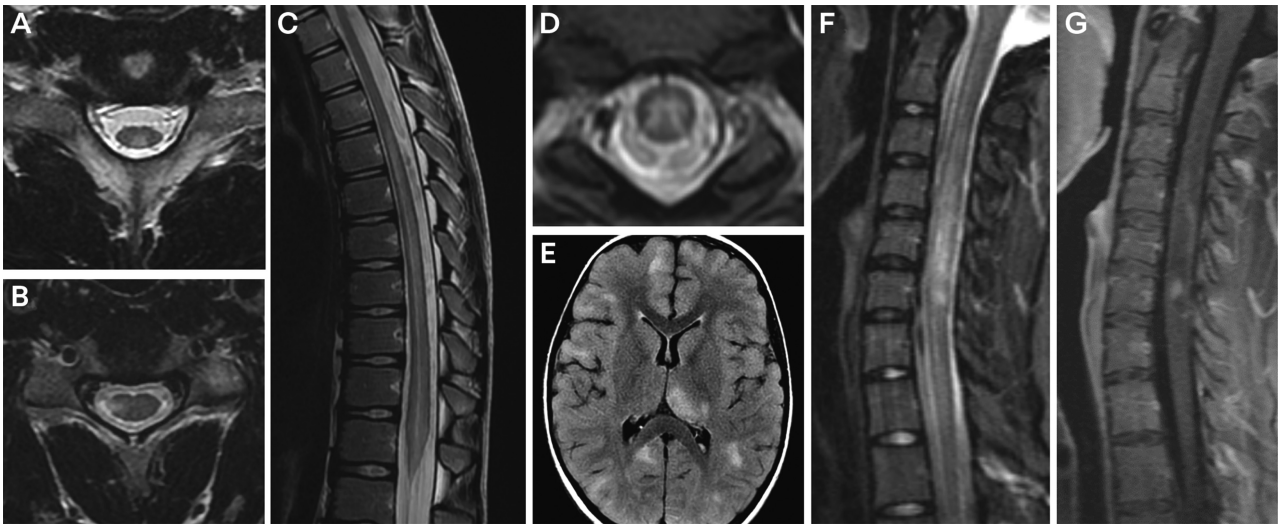

FIGURE 11-5

Typical distribution of spinal cord lesions in demyelinating disorders. In multiple sclerosis, a typical short-segment ovoid-shaped (craniocaudal direction) lesion with localization of the involved tracts is best seen on axial images: a lateral localized lesion (*A*) and a dorsal localized lesion (*B*). *C, D,* Spinal cord involvement in myelin oligodendrocyte glycoprotein–associated disorder. The longitudinal lesion expands over multiple vertebral segments (*C*) and involves part of the cord, mainly in the central distribution. This penlike stripe on sagittal sequences can be further localized on axial images (*D*) to the central gray matter predominantly. *E,* In this case, the associated brain MRI shows features that are consistent with acute disseminated encephalomyelitis (ADEM). The multiple lesions include both gray matter (cortical and deep) and white matter and are less well circumscribed. This combined presentation is possible, but either transverse myelitis or ADEM can be seen as an isolated presentation. An extensive spinal cord lesion of neuromyelitis optica (NMO) is shown in sagittal T2-weighted (*F*) and postcontrast T1-weighted (*G*) images. The lesion can be more extensive than the one noted, which just extends three vertebral segments (a short spinal cord lesion does not rule out NMO) and has a swollen appearance with extensive, patchy signal change. The associated enhancement can be patchy (*G*).

extensive involvement is noted in this plane. The cord often demonstrates expansile enlargement and more common central or holocord involvement. Although common and classic, LETM is not a requirement for diagnosis, and shorter-segment lesions can be seen in NMO either in combination with LETM elsewhere or in isolation.[29]

Optic neuritis attacks seen in NMO tend to be more severe than in MS. Lesions are commonly bilateral and extensive (more than 50% longer) and tend to isolate to or across the optic chiasm.[30] Optic neuritis in NMO also has more destructive findings and correlates with poorer outcomes.

Assessment of brain involvement is important in NMOSD, as outlined in the clinical criteria. A few specific clinical phenotypes with associated imaging have been included in NMOSD. When characteristic lesions are seen in isolation, NMSOD should be on the differential diagnosis, as seen in CASE 11-2. Brain lesions tend to be larger, ill circumscribed, and not typically distributed as in MS. The presentation is variable, and imaging features can be relatively quiet in clinical correlation, but most have a more severe presentation. Age of onset is variable, with one-third of adult patients, compared with about two-thirds of pediatric patients, having cerebral involvement.[31]

Copyright © American Academy of Neurology. Unauthorized reproduction of this article is prohibited.

CASE 11-2

An 18-year-old woman presented to the emergency department with ongoing nausea and vomiting. An initial diagnosis of viral gastroenteritis was made, and she was found to have hyponatremia (sodium concentration, 128 mmol/L). After rehydration and antiemetics, she was discharged home. She returned the next day with ongoing symptoms, described by her family as significant fatigue and confusion consistent with worsening encephalopathy. Her serum sodium was low again, and based on serum/urine sodium ratios, the diagnosis of syndrome of inappropriate secretion of antidiuretic hormone (SIADH) was made. Further systemic workup was unrevealing, but brain imaging showed T2 hyperintensities that were isolated to the subthalamic area (FIGURE 11-3B) without contrast enhancement. A wide range of diagnostic considerations, mainly including infectious, neoplastic, and inflammatory causes, was considered. Appropriate treatment slowly corrected the hyponatremia, and antiemetics were continued. A lumbar puncture was performed with CSF demonstrating a lymphocytic pleocytosis (white blood cell count, 89 cells/mm^3), but further studies including infectious polymerase chain reaction (PCR) panels were negative, as were oligoclonal bands. The concern for a viral infection or parainfectious process remained, and she was treated initially with IV immunoglobulin (IVIg). Her condition continued to worsen throughout the first few days of her hospitalization, prompting repeat imaging. At that time, she was more encephalopathic, had hypersomnia during the day with narcoleptic features, and on examination had upper motor neuron findings affecting the left arm. Repeat imaging showed significant expansion of the subthalamic lesion, expansion of the cerebral lesions, and a cervical spinal cord lesion spreading across two vertebral segments. Further testing was positive for neuromyelitis optica (NMO) in CSF and serum.

COMMENT

The patient had a clear diencephalic presentation with initial SIADH, followed by encephalopathy and narcolepsy. At follow-up imaging, she had newly developed LETM. All these are hallmark features of NMO. Although not the most common, initial presentation with diencephalic or isolated brain involvement can be seen. The severity of these abnormalities and the illustrated rapid potential progression of the disease make early recognition and testing important in this clinical scenario. Endocrinopathies may be seen with this presentation. Sleepiness and narcolepsy are also associated with this presentation, as well as encephalopathy and seizures. IVIg is not the appropriate therapy for NMO spectrum disorders, and this was promptly switched to IV steroids and plasma exchange. The patient recovered fully and was placed on B cell–depleting therapy without any further attacks to date.

Copyright © American Academy of Neurology. Unauthorized reproduction of this article is prohibited.

Acute Disseminated Encephalomyelitis

Acute disseminated encephalomyelitis (ADEM) is an acute demyelinating disease predominantly affecting children.[32,33] Clinical onset in about three-fourths of patients is preceded by a viral illness. Patients with ADEM present with acute, new-onset polyfocal CNS involvement requiring both clinical and imaging evidence, and encephalopathy must be present (TABLE 11-5).[32] In cases in which encephalopathy is absent, the confusing term *ADEM-like* has been used, but when antibodies are found, the syndromes associated with them should be the diagnosis; otherwise, a better clinical description would be CIS. Symptoms at presentation can include involvement of the optic nerve, cerebrum, brainstem, cerebellum, and spinal cord. Motor impairment with hemiparesis and long tract signs are the most common presenting signs.[34] Nausea and vomiting are more likely caused by a viral illness rather than area postrema involvement as seen in NMO. CSF typically shows nonspecific inflammatory markers, and oligoclonal bands are much less common, typically present in fewer than 10% of affected patients.[33]

Brain lesions in ADEM have distinct imaging features. Many of the lesions can be large and are typically very poorly demarcated ("fluffy") in appearance. Importantly, the lesions affect both white matter and gray matter, most

Diagnostic Criteria for Acute Disseminated Encephalomyelitis[a,b] TABLE 11-5

Clinical findings

- **Monophasic acute disseminated encephalomyelitis (ADEM)**
  - A first polyfocal objective clinical central nervous system event, presumed inflammatory demyelinating
  - Encephalopathy that is not explained by fever, seizures, or systemic illness
  - No new clinical or MRI findings >3 months from onset
  - Brain MRI is abnormal
- **Multiphasic ADEM**
  - A second bout of ADEM but limited to 2 attacks total
  - The second attack is >3 months after the first one
  - Objective new evidence on MRI and clinically, either with new or reemergence or worsening of previous symptoms

MRI findings

- **Diffuse, ill-defined, or poorly demarcated large lesion (>1 cm)**
- **Predominant white matter involvement**
- **Deep gray matter lesions can be present**
- **T1-hypointense lesions are rare**

MRI = magnetic resonance imaging.

[a] Modified from Krupp LB, et al, Mult Scler.[32] © 2013 The Authors.

[b] In ADEM, the criteria in the table are adapted from the international operational criteria for ADEM in children. As observed, some of these criteria are more loosely defined compared with neuromyelitis optica and multiple sclerosis criteria. With recognition of myelin oligodendrocyte glycoprotein (MOG)–associated disorder, revision of these and development of MOG-associated disorder criteria are necessary and expected to follow.

Copyright © American Academy of Neurology. Unauthorized reproduction of this article is prohibited.

CASE 11-3

A 9-year-old previously healthy boy presented to the emergency department with a history of generalized mild headache and gradually worsening encephalopathy. Symptoms started after a febrile illness 1 to 2 weeks before, with gastroenteritis symptoms in addition to general malaise. He had nausea and intermittent vomiting, which lasted 2 to 3 days. During the emergency department visit, he was noted to have some right leg weakness, which continued to gradually worsen over the next day. He was admitted, and brain MRI showed seven ill-circumscribed fluffy-appearing lesions affecting deep white matter, leukocortical locations, and thalamus. These were larger (about 2 to 3 cm in diameter) and did not enhance. The spinal cord MRI showed a longitudinally extensive lesion from C7 to T5, predominantly affecting the gray matter as noted on axial imaging. CSF analysis showed mild pleocytosis with neutrophil predominance, mildly elevated protein, and negative oligoclonal bands. Aquaporin-4-IgG testing was negative. He was diagnosed with acute disseminated encephalomyelitis (ADEM), was treated with high-dose IV methylprednisolone for 5 days (typical dosing is 30 mg/kg/d in children, with a maximum daily dose of a typical adult dose of 1000 mg, administered for the duration of a 3- to 5-day treatment regimen), was placed on an oral steroid taper for 4 weeks. His condition improved promptly without residual deficits. Approximately 6 weeks after discharge, off steroids and back to baseline since discharge, he presented with an attack consistent with optic neuritis. On examination, he had 20/100 visual acuity in his right eye, 20/40 in his left eye, and loss of color vision. He had significant papilledema, more so on the right side, with a right relative afferent pupillary defect. MRI showed enhancement of the right anterior section of the optic nerve and a smaller patchy enhancement in the left optic nerve. Again, he was treated with IV methylprednisolone and rapidly improved without a need for second-line therapy. Initially, the working diagnosis was seronegative neuromyelitis optica spectrum disorder (NMOSD) because NMO antibody testing was negative at first. Myelin oligodendrocyte glycoprotein (MOG)-IgG antibodies were present with a high titer, and the diagnosis was correctly revised to MOG-associated disorder.

COMMENT

The case highlights some important features that are strongly consistent with MOG-associated disorder. A presentation with ADEM is common in children and has no sex predilection as seen with NMO and multiple sclerosis. Commonly in this scenario, rapid improvement with steroids is seen, but therapy needs escalation if this is not the case. The duration of steroid tapers has no specific evidence-based guidance, and the described taper in this case would not be atypical. Soon after completion of the taper, symptoms recurred. Optic neuritis is often present at recurrence, and patients can present with more severe deficits in visual acuity and more severe papilledema, especially younger patients. MOG-IgG antibodies were tested and were positive at a high titer (1:1000; laboratory reference norm, ≤1:20), confirming the diagnosis of MOG-associated disorder.

Copyright © American Academy of Neurology. Unauthorized reproduction of this article is prohibited.

commonly with leukocortical lesions and deep gray matter lesions. In the latter, the most common location is the thalamus. Enhancement is reported in up to 30% of lesions.[34] Examples are shown in FIGURE 11-5.

Spinal cord involvement in ADEM, when present, is typically an LETM. These confluent intramedullary lesions commonly extend over several vertebral segments.[33,34] When LETM lesions are more restricted to the central gray matter, MOG-associated disorder or acute flaccid myelitis should be considered.

Optic nerve involvement in combination with ADEM should raise suspicion for MOG-associated disorder. Given the relatively recent discovery of MOG-associated disorder antibodies, little is known about the exact incidence of optic neuritis in isolated ADEM. When optic neuritis is present, the typical distribution is more extensive than with MS, is bilateral, and often involves anterior segments.

Myelin Oligodendrocyte Glycoprotein–Associated Disorder

MOG-associated disorder is an acute demyelinating disorder now considered a distinct entity. It disproportionately affects younger (including pediatric) patients. Diagnostic criteria have been proposed by a single center,[35] but formal international criteria have not yet been established. Typical presentations that should prompt MOG-IgG testing are optic neuritis, myelitis, encephalitis including brainstem encephalitis, or any combination of these, but it is not recommended when the phenotype is typical for MS. In adults, the most common attack is optic neuritis, whereas in children the most common presentation is ADEM (68%).[36] Cranial nerve involvement outside of optic neuritis is only rarely encountered[37] in contrast to MS.

Cell-based assays have much improved and are now recommended with titer documentation as the most specific measure. As diagnostic criteria and phenotypes have not been fully established, false-positive results deserve a note of caution, especially at low titers. Recognition of MOG-associated disorder as a separate diagnostic entity is important because the treatment and prognosis differ (an example of this is provided in CASE 11-3). Overlap has reclassified some of these patients. Of patients who were classified as having seronegative NMOSD, about one-third met MOG-associated disorder criteria. Conversely, only 20% to 30% of patients with MOG-associated disorder would formally meet criteria for NMOSD.[38] About 50% of patients with ADEM tested positive for MOG-associated disorder.[36] Coexisting antibody of NMO and MOG is rare (<1%), and in those cases, diagnosis should lean toward NMO given the clinical implications. Other coexisting autoimmunity is rare[39] but is seen occasionally with *N*-methyl-D-aspartate (NMDA) receptor antibodies.[40]

IMAGING IN MYELIN OLIGODENDROCYTE GLYCOPROTEIN–ASSOCIATED DISORDER. MRI has had a great impact on differentiation between the demyelinating syndromes. In MOG-associated disorders, multiple specific markers may be present that can assist in differentiation from other conditions.

Brain imaging often has features similar to the presentation of ADEM as described earlier. When present, enhancement tends to be heterogeneous or patchy. Other isolated cerebral (non-ADEM) lesions typically are small, ill circumscribed, and frequently transient, resolving over time on MRI. In children, a phenotype with extensive confluent white matter involvement has been noted, typically with persistence of signal change and poor outcome.[41]

KEY POINTS

- MRI features in other (antibody-mediated) demyelinating disorders can have distinct characteristics that help distinguish these disorders from MS.
- Acute disseminated encephalomyelitis (ADEM) and optic neuritis are the most common presenting phenotypes of myelin oligodendrocyte glycoprotein–associated disorder.
- Myelin oligodendrocyte glycoprotein–associated disorder lesions can differ from those in neuromyelitis optica and predominantly affect the central gray matter, which is best noted on axial imaging.

Copyright © American Academy of Neurology. Unauthorized reproduction of this article is prohibited.

Meningeal enhancement is relatively common, present in about 10% of adults and up to one-third of children with MOG-associated disorder.[42,43] Rarely, encephalitis with predominant cortical edema and leptomeningeal enhancement can be seen; in these cases, 80% of patients have unilateral (clinical and imaging) involvement throughout the affected hemisphere. which some have referred to as *unilateral cortical FLAIR-hyperintense lesions in anti-MOG–associated encephalitis with seizures* (FLAMES). Posterior fossa involvement on imaging may include large lesions, most commonly in the cerebellar peduncles. When present, these are associated with other lesions.[44]

Spinal cord involvement is an important feature of MOG-associated disorder. The lesions are almost always longitudinally extensive (LETM). When lesions are short or unilateral, another diagnosis (ie, MS) should be considered. Lesions can differ from NMO, with MOG-associated disorder predominantly affecting the central gray matter, which is best noted on axial imaging. In about one-third of cases, transverse myelitis is completely isolated to the gray matter.[45] Additionally, conus involvement is more common. Enhancement is present in about 50% of acute cases but, when present, tends to be less avid than with NMO and MS. Interestingly, cauda equina and peripheral nerve root involvement is encountered in MOG-associated disorder but not in NMO or MS.[46] When present, it is associated with lower motor neuron signs, and the differential diagnosis should include acute flaccid myelitis.

Optic nerve involvement has features comparable with NMO in lesion length. Similarities include bilateral involvement (approximately 50%) and commonly

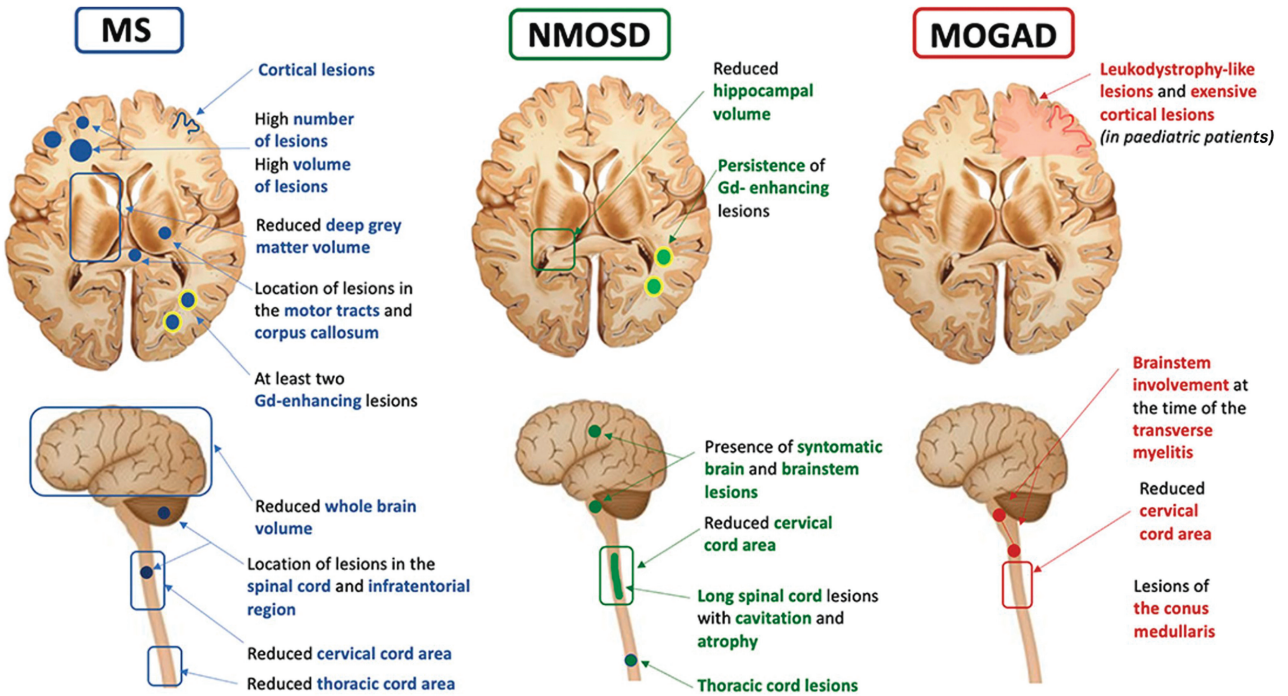

FIGURE 11-6

Indicators of poor prognosis for different demyelinating disease phenotypes.

Gd = gadolinium; MOGAD = myelin oligodendrocyte glycoprotein–associated disorder; MS = multiple sclerosis; NMOSD = neuromyelitis optica spectrum disorders.

Reprinted with permission from Cortese R, et al, Front Neurol.[52] © 2021 Frontiers Media S. A.

Copyright © American Academy of Neurology. Unauthorized reproduction of this article is prohibited.

longitudinally extensive (greater than 50% length) lesions with a more prominent anterior distribution.[47] In MOG-associated disorder, papilledema is more commonly noted clinically and on OCT.[48] In addition, optic nerve sheath enhancement and orbital fatty tissue enhancement can be seen.

ROLE OF MRI IN PROGNOSIS, TREATMENT, AND OUTCOME

In addition to its diagnostic utility, MRI has had an increasing role in finding imaging markers that can be associated with specific outcome measures. This section reviews further advances in imaging that may provide direction in the future.

As noted earlier, MRI is helpful in differentiation between demyelinating syndromes of the acute attack. Therapy decisions are based on clinical features of the attack, but differentiation to specific syndromes may provide further guidance for next-step therapies. First-line therapy for all clinically significant attacks (whether this is MS, NMO, MOG, or ADEM) is high-dose (usually IV) corticosteroid treatment, typically with IV methylprednisolone. In the absence of a full response or in severe attacks of NMO and MS, the next option is subsequent or simultaneous plasma exchange; in MOG-associated disorder and ADEM, treatment escalation can be alternatively done with IVIg.

Recovery, Outcome, and MRI Monitoring in Antibody-Mediated Demyelinating Disease

Long-term outcomes depend to an extent on the clinical attack severity, severity seen in imaging, and early recovery from the attack. In MOG-associated disorder and NMO, severity at the nadir of attacks is worse than in MS. For example, one-third of patients use a wheelchair at the nadir of myelitis in antibody-mediated LETM. With prompt treatment in particular, the recovery of attacks of MOG-associated disorder tends to be better than with both MS and NMO.[49] In particular, NMOSD has poor long-term outcomes with clinical disability in up to 80% of patients.[50] Specific treatment recommendations are detailed elsewhere, but for antibody-mediated disease, it is universally accepted that lifelong treatment is currently recommended for NMO, whereas MOG-associated disease may require a more tailored approach with less aggressive long-term therapy. MRI surveillance is typically not felt to be helpful in antibody-mediated demyelinating disease and should be reserved for when new symptoms suggestive of attacks present, unless the diagnosis is uncertain, in which case follow-up imaging can be helpful in NMOSD. In ADEM, MRI lesions completely or partially resolve for up to 90% of patients.[51] A 2021 article nicely summarized the currently known factors on imaging for MS, NMO, and MOG-associated disease,[52] as shown in **FIGURE 11-6**. Asymptomatic lesions are seen in MS, whereas in NMOSD, this only rarely occurs.[53]

Prognosis, Treatment, and Disease Monitoring in Multiple Sclerosis

In the past several decades conventional MRI markers have been the subject of numerous studies looking for prognostic markers of disability accumulation. The term *clinico-radiological paradox*[54] described the low correlation between the number of lesions and clinical severity. The well-established and expanding medication options in MS are too extensive to review here, including options now available for both SPMS and PPMS. MRI has a significant role in disease surveillance because many brain, and even spinal cord, lesions are silent without clinical correlation.

KEY POINTS

- **MRI surveillance is typically not felt to be helpful in antibody-mediated demyelinating disease and should be reserved for when new symptoms suggestive of attacks present unless the diagnosis is uncertain.**
- **Novel MRI acquisition and processing techniques have distinguished some lesion signatures with potential prognostic properties, some of which are slowly finding their way into clinical practice.**

Copyright © American Academy of Neurology. Unauthorized reproduction of this article is prohibited.

A clinical distinction exists among disease activity, worsening, and disease progression. Important components of the current clinical MS phenotype descriptions are disease modifiers, which highlight the differences among disease activity, worsening, and progression. *Disease activity* is defined as new clinical and imaging features consistent with newly developed, enlarging, or contrast-enhancing lesions. *Disease worsening* is an increase in impairment regardless of whether it is from residual symptoms from a new clinical attack or a gradual progression. The term *disease progression* should be reserved for ongoing progression alone, to be used solely in progressive MS phenotypes.[4,5]

"No evidence of disease activity" is an outcome measure that is now commonly used and important to distinguish between therapy options. The role

CASE 11-4

A 37-year-old man reported to the neurology clinic after being referred by his primary care provider for a gradual history of worsening gait abnormalities, leg stiffness on both sides, and concerns of clumsiness and memory problems. During the neurologic evaluation, it became apparent that a gradually worsening paraparesis was evolving over the past 4 years, which was confirmed with objective findings on examination with spasticity, a mild upper motor neuron pattern of weakness affecting his legs equally, and extensor plantar reflex responses. The patient also described and exhibited findings of a cerebellar ataxia on examination. His mental status examination revealed deficits in recall and attention, and at times he had difficulty with providing a linear history. MRI demonstrated extensive symmetric bilateral periventricular T2 hyperintensities and no juxtacortical, infratentorial, or spinal cord lesions. The lesions had diffuse mild associated T1-hypointense signal, and no enhancement was present. The cervical and thoracic spinal cord demonstrated atrophy without T2 signal hyperintensities. CSF was normal, with no oligoclonal bands identified. Optical coherence tomography was normal. The patient was referred to genetics, and a leukodystrophy genetic panel showed a pathogenic mutation in the *GFAP* gene.

COMMENT

The clinical presentation could be easily misinterpreted as progressive MS with the patient's gradual decline, but his syndrome was not specific. The brain lesions were not typical of MS without a clear lesion formation. Often the radiologic report will include demyelinating pathology on the differential diagnosis, but diagnosis should incorporate all other features. In the absence of oligoclonal bands and distinct spinal cord lesions, the diagnostic criteria for MS are not met, and testing or referral to genetics is the best next step. Confluent, symmetric lesions without clear involvement of other locations should raise concerns and further testing. In this case, spinal cord atrophy was seen but not specific. The genetic testing led to the diagnosis of Alexander disease, a neurodegenerative disease affecting the central nervous system that can have demyelinating features and a progressive debilitating course.

Copyright © American Academy of Neurology. Unauthorized reproduction of this article is prohibited.

of imaging again is additive to the clinical features (attack or progression); evidence of new lesions and more recently atrophy measures are discussed further later in this article.

MRI plays an important role in the decision to change therapy, but specific recommendations vary and there are no consensus recommendations; in one study, about two-thirds of MS experts would consider a change in therapy with more than two new lesions in 2 years in an asymptomatic patient, and about half would consider this with one new gadolinium-enhancing lesion in the same clinical scenario.[55]

Progressive multifocal leukoencephalopathy in MS is an important consideration in the monitoring of some medications. In particular, treatment with natalizumab needs specific follow-up given the increased risk of progressive multifocal leukoencephalopathy. With other therapies (fingolimod, dimethyl fumarate, B cell–depleting therapy), progressive multifocal leukoencephalopathy has been described but in such low numbers that specific monitoring is not necessarily protocolized. The risk stratification for natalizumab recommends regular imaging surveillance.

KEY POINT

● **Newer MRI techniques better capture disease that can be visualized beyond the white matter lesions noted on conventional MRI. Lesions can be found in the cerebral cortex with specific acquisitions.**

FURTHER IMAGING INSIGHT AND FUTURE DIRECTIONS

Not all imaging techniques can be discussed here, but some of the main considerations are reviewed next.

Smoldering Lesions

Despite minimal to no apparent change on standard imaging, including with contrast, ongoing inflammatory demyelination can be present in lesions; this is referred to as *smoldering activity*. This important feature on pathology can be found, in particular, in progressive MS phenotypes.[11] Because of this continual pathologic change, efforts to improve radiologic detection are ongoing. Specifically, magnetic susceptibility-based imaging techniques and magnetization transfer ratios are potentially promising sequences for the future of treatment decisions regarding these lesions.

Lesion Specificity

As reviewed, standard imaging techniques may not differentiate demyelinating lesions from nonspecific or chronic ischemic lesions. Morphology on high-resolution and newer imaging techniques has been used to improve this specificity. Findings initially seen on ultra-high-field (ie, 7T) imaging have been translated back to 3T studies. Susceptibility-weighted techniques have been studied and reviewed the most as a potential clinical tool. This has led to development of the central vein sign, with the notion that lesions often arise in a perivenular pattern. This central vein appearance in white matter lesions is less commonly seen in nonspecific MRI lesions (eg, migraine) and NMO lesions. Susceptibility-weighted imaging also can detect another finding of interest: paramagnetic rim lesions. The clinical utility of these techniques remains of interest for potential implementation in clinical practice and, in some centers, is already part of the evaluation.

White Matter Integrity

Subtle chronic tissue changes (degeneration and demyelination) occur in MS. Conventional FLAIR, T2-weighted, and T1-weighted techniques lack the

Copyright © American Academy of Neurology. Unauthorized reproduction of this article is prohibited.

TABLE 11-6 **Differential Diagnoses and Imaging Red Flags for Central Nervous System Demyelinating Disease[a]**

Imaging finding	Diagnostic consideration
Brain: white matter lesions	
Symmetric distribution or appearance	Genetic leukoencephalopathies
Extensive, symmetric, posterior predominance	Early onset adrenoleukodystrophy (ALD)
Extensive, symmetric, frontal predominance	Alexander disease, late-onset ALD
Diffuse white matter change with possible (not necessary) gadolinium enhancement	ALD, Alexander disease, Krabbe disease
Large lesion	Neoplasm, abscess, tumefactive multiple sclerosis (MS), Behçet syndrome, encephalitis, progressive multifocal leukoencephalopathy (PML)
Mass effect	Malignancy, tumefactive MS, abscess
Complete ring of gadolinium enhancement	Glioblastoma, metastases, central nervous system (CNS) abscess
Apparent diffusion coefficient solid or central restriction	Abscess
Apparent diffusion coefficient restricted rim	Tumefactive MS
Concentric rings	Baló concentric sclerosis
Poorly defined margins	Acute disseminated encephalomyelitis (ADEM), myelin oligodendrocyte glycoprotein (MOG), neuromyelitis optica (NMO)
Progressively enlarging, lacking mass effect	PML
White matter lesion with persistent or worsening enhancement	Sarcoidosis, CNS lymphoproliferative disease (lymphoma), glioma, vasculitis
All lesions enhancing	Vasculitis, sarcoidosis
Deep T1-hypointense lesion (lacunar)	Ischemic stroke, Susac syndrome, cerebral autosomal dominant arteriopathy with subcortical infarcts and leukoencephalopathy (CADASIL), cerebral autosomal recessive arteriopathy with subcortical infarcts and leukoencephalopathy (CARASIL)
Diffusion restriction (can involve both white matter and gray matter)	Stroke, mitochondrial disorders, vasculitis
(Micro)hemorrhages	Amyloid angiopathy, amyloid-β–related angiitis, CADASIL, vasculitis, acute hemorrhagic encephalomyelitis (AHEM)
Anterior temporal diffuse T2 signal change	CADASIL, CARASIL
External capsule involvement	CADASIL, CARASIL
Corpus callosum involvement (diffuse)	Susac syndrome, glioblastoma, genetic leukoencephalopathy
Calcifications (CT most sensitive)	Infection (**t**oxoplasmosis, **o**ther infections, **r**ubella, **c**ytomegalovirus infection, and **h**erpes simplex [TORCH]), cysticercosis
Lactate peak on MR spectroscopy	Leukoencephalopathy with brainstem and spinal cord involvement with elevated lactate (LBSL), mitochondrial disorders

CONTINUED ON PAGE 315

Copyright © American Academy of Neurology. Unauthorized reproduction of this article is prohibited.

CONTINUED FROM PAGE 314

Imaging finding	Diagnostic consideration
Predominant subcortical and deep white matter	Small vessel disease, leukoaraiosis, vasculitis, PML
Multiple cranial nerve enhancement	Sarcoidosis, chronic meningitis, infections (tuberculosis, borreliosis)
Prominent Virchow-Robin spaces	Primary angiitis in the CNS, hyperhomocysteinemia
Large predominant brainstem lesion	Behçet syndrome, glioma
Brain: cortical and deep gray matter	
Significant meningeal enhancement	Sarcoidosis, chronic meningitis, MOG-associated disorder, vasculitis, lymphoproliferative disease
Deep gray matter involvement or hazy mixed cortical and subcortical hazy strokelike lesion	Mitochondrial disorders, vasculitis, ADEM
Deep gray involvement	
Dentate nucleus	Cerebrotendinous xanthomatosis
Basal ganglia, multiple lesions	Mitochondrial disease, hypomyelination with atrophy of the basal ganglia and cerebellum, Susac syndrome, Behçet syndrome
Hazy thalamic predominant T2 hyperintensities	Viral encephalitis, ADEM, mitochondrial disorders
Hypothalamus (diabetes insipidus)	NMO, histiocytosis (eg, Langerhans cell histiocytosis), sarcoidosis, paraneoplastic disorders
T1-hyperintense pulvinar	Fabry disease
Spinal cord	
Diffuse longitudinal (extensive) signal change	LBSL, adult polyglucosan body disease (APBD), Alexander disease
Prominent or predominant atrophy (without discrete lesions)	Adrenomyeloneuropathy (AMN), genetic leukoencephalopathy, neurodegenerative (eg, primary lateral sclerosis, hereditary spastic paraplegia), APBD
Extensive signal change–specific tractopathy	Paraneoplastic disorders, leukoencephalopathy
Extensive dorsal or posterior columns spinal cord	Vitamin B_{12} deficiency, copper deficiency, paraneoplastic disorders
Atrophy of cervical cord and medulla with preserved pons (tadpole sign)	Alexander disease
Anterior or central gray matter signal change	Ischemic, MOG-associated disorder, acute flaccid myelitis, infectious (eg, enterovirus)
Other organ involvement (clinical and imaging)	
Bone lesions	Histiocytosis, including Erdheim-Chester disease
Pulmonary involvement	Sarcoidosis, granulomatosis
Cardiac involvement	Embolic stroke, multiple abscesses, mitochondrial disorders
Retinopathy	Mitochondrial disorders, vasculitis, genetic (eg, neuronal ceroid lipofuscinosis), Susac syndrome

CONTINUED ON PAGE 316

Copyright © American Academy of Neurology. Unauthorized reproduction of this article is prohibited.

CONTINUED FROM PAGE 315

Imaging finding	Diagnostic consideration
Myopathy	Mitochondrial disorders, NMO (rare)
Peripheral neuropathy	APBD, ALD, AMN, metachromatic leukodystrophy
Renal disease	Mitochondrial disorders, systemic lupus erythematosus, Fabry disease, vasculitis
Mucosal or genital ulcerations	Behçet syndrome
Sicca	Sjögren syndrome
Uveitis	Granulomatosis (eg, sarcoidosis), Behçet syndrome, lymphoma

CT = computed tomography; MR = magnetic resonance.
[a] Data from Geraldes R, et al, Nat Rev Neurol[62] and from Tillema JM and Pirko I, Ther Adv Neurol Disord.[63]

ability to clearly visualize these changes, but subtle changes are sometimes described as "dirty white matter." Quantitative measures of advanced MRI techniques (eg, diffusion tensor imaging) and MR spectroscopy have identified what is known in pathology as normal-appearing white matter involvement. These features have been shown to be associated with disease course and outcome, similar to some of the earlier-mentioned quantitative strategies. It is apparent that refined and reliable measures are needed before implementation, but they hold great promise in assisting in an individualized targeted approach.

Brain Atrophy

Early recognition of brain atrophy is noted by widening or enlargement of the third and lateral ventricles. Subsequently, with the development of automated quantitative volumetric techniques, deep gray matter volume loss (in particular, the thalamus) and cortical thinning have been replicated multiple times. These changes have been seen in the earliest phenotypes of MS and have been associated clearly with severity and disability progression in MS. These relevant measures have been incorporated in measures of no evidence of disease activity and are often already implemented in clinical practice. This field is progressing, and robust techniques (commonly supported by artificial intelligence) to automatically report lesion burden and longitudinal atrophy measures have been commercialized. It deserves some caution, given some of the fluctuations and error margins that affect the results and interpretation. These factors include, but are not limited to, physiology (eg, dehydration), technical factors (eg, scanner, sequence, and upgrade variability), computation (eg, the software used), or medications (eg, corticosteroids). Like other promising imaging technologies described above, it requires further optimization to clearly guide therapy decisions.

Spinal Cord Atrophy

Similar to brain atrophy, spinal cord atrophy has been increasingly recognized and better characterized over time. When the atrophy appears in isolation

Copyright © American Academy of Neurology. Unauthorized reproduction of this article is prohibited.

and without lesions, other conditions should be considered. Cord atrophy can be visible on conventional imaging, and when present in any of the demyelinating disorders, prognosis and outcome are worse.[56] Quantitative measures are gaining traction with both manual[57] and automated approaches. Especially with automated processing, a scan of the brain that has a visual field including the upper sections of the spinal cord will suffice in quantification around C2. As with imaging of brain atrophy, technical improvements are necessary before practical standardized implementation.

Cortical Lesions and Demyelination

Detection of cortical lesions and technical challenges were briefly reviewed earlier in this article. Studies previously have shown poor correlation with pathologic detection (ie, only 18% of lesions were detected with double inversion recovery).[58] Despite this limitation, the visualization has revolutionized understanding of cortical involvement in MS and is seen as early as in RIS and pediatric MS. A limitation in clinical practice is the sensitivity to mainly leukocortical lesions, which have more widespread demyelination throughout the normal-appearing gray matter, and (at times extensive) subpial lesions, which go undetected even with 7T imaging. As cortical involvement has been associated with disability progression, the combination with atrophy detection conceivably could provide clinical insight into what currently goes unnoticed on MRI.

Leptomeningeal gadolinium-enhancing lesions have been found to be associated more with progressive MS. The future possible clinical utility is unknown, but these lesions may be present despite more efficacious and aggressive pharmacotherapy and could provide further insight into disease progression. Whether disease monitoring would be within the realm of possibilities remains to be determined.

Solitary Lesions

Special consideration is given to spinal cord and brainstem lesions that result in progressive long tract and myelopathic features. The term *solitary sclerosis* has been coined to describe this condition.[59,60] In current criteria, the isolated brainstem lesions in combination with CSF abnormalities could qualify, but solitary spinal cord lesions with or without an attack and subsequent progression is an ongoing area of research interest. Further understanding of the pathophysiology of this entity and whether it could be incorporated into the primary progressive MS phenotype requires further research and discussion.

Diagnostic Uncertainty or Misdiagnosis

As mentioned multiple times throughout this article, sound clinical judgment is needed for all aspects of diagnosis in patients suspected of having demyelinating disease. MS criteria were designed to apply in a scenario in which the a priori chance of MS is high and not initially to specifically distinguish it from all other neurologic diagnoses. Objective clinical information is necessary in all diagnoses, whether it is identification of cardinal features of a relapse or identification of nonspecific symptoms. The radiologist's perspective differs from that of clinical neurologists, and clinical correlation is key. MRI lesion appearance and location definitions can be overlooked in haste, wrongly applied, or misinterpreted, even in experienced

KEY POINTS

- **Quantitative measures of advanced MRI techniques (eg, diffusion tensor imaging) and MR spectroscopy have identified what is known in pathology as normal-appearing white matter involvement.**
- **Atrophy has been reported throughout the central nervous system in MS, affecting whole brain volume and, in particular, the thalamus.**
- **Spinal cord lesions can be present without clinical symptoms in MS, and the most common location of spinal cord lesions is within the cervical spinal cord.**

Copyright © American Academy of Neurology. Unauthorized reproduction of this article is prohibited.

hands.[13] The misdiagnosis of MS is relevant and is not entirely uncommon.[61] In complex cases, it may require subspecialty consultation in the setting of ever-changing diagnostic and therapeutic approaches. An example is described in CASE 11-4.

Imaging Differential Diagnosis or Red Flags

In certain clinical scenarios, some radiographic features may prompt alternative diagnostic considerations, despite radiologic reports raising the possibility of demyelination. These findings have been reviewed as "red flags" in multiple publications and are summarized in TABLE 11-6.[62,63]

TABLE 11-7 **Imaging Protocol Recommendations for Multiple Sclerosis[a,b]**

	Protocol	Use in diagnosis	Use in disease monitoring
Brain MRI Preferred (if available) at 3T, otherwise at least 1.5T High-quality three-dimensional–acquired sequences when available (eg, fluid-attenuated inversion recovery [FLAIR], T1 magnetization-prepared rapid gradient echo [MPRAGE], fast spoiled gradient-echo) with possibility for multiplanar reconstruction Axial images with ≤3-mm slice thickness, ≤1 mm × ≤1 mm in-plane resolution (except diffusion-weighted imaging [DWI], ≤5 mm) Field of view covering the whole brain, including upper cervical cord if possible	Two-dimensional axial T2 (turbo spin echo [TSE] or fast spin echo [FSE])	Recommended	Optional (if three-dimensional FLAIR not available)
	Three-dimensional FLAIR	Recommended (if available)	Recommended (if available)
	Two-dimensional axial FLAIR	If three-dimensional FLAIR not available	If three-dimensional FLAIR not available
	Two-dimensional sagittal FLAIR	If three-dimensional FLAIR not available	If three-dimensional FLAIR not available
	T1 (axial or three-dimensional) postcontrast	Recommended	Optional
	DWI	Optional	Optional
	Double inversion recovery (DIR) or phase-sensitive inversion recovery (PSIR)	Optional	Optional
	Three-dimensional T1-weighted, high-resolution	Optional	Optional
	Susceptibility-weighted imaging	Optional	Not required
Optic nerve MRI At least 1.5T, field of view including optic nerve and optic chiasm Slice thickness ≤3 mm (preferred ≤2 mm), without gap, with ≤1 mm × ≤1 mm in-plane resolution Use only when indicated (ie, not necessary for multiple sclerosis diagnosis per se)	Axial and coronal T2-weighted (need fat suppression)	Optional	Not required
	Axial and coronal postcontrast T1-weighted (need fat suppression)	Optional	Not required

CONTINUED ON PAGE 319

Copyright © American Academy of Neurology. Unauthorized reproduction of this article is prohibited.

Field Strength Considerations

Field strength for the acquisition of MR imaging of the brain and spine should be a minimum of 1.5T. The best clinical utility is with high- and stable-quality imaging from the available scanner rather than simply higher field strength. Novel rapid three-dimensional acquisitions are best performed on 3T scanners. These techniques additionally allow for accurate side-to-side comparison at follow-up with increased sensitivity in lesion detection. Nonetheless, evidence is not sufficient that higher-field-strength scanners lead to better MS care. Optimization in cooperation with radiologists and physics experts and obtaining the best image quality are overall more important than the actual field strength.

CONTINUED FROM PAGE 318

	Protocol	Use in diagnosis	Use in disease monitoring
Spinal cord At least 1.5T (3T has no additional value), covering cervical and thoracolumbar cord Sagittal ≤3 mm, axial ≤5 mm, in-plane with ≤1 mm × ≤1 mm resolution	≥2 of 3: sagittal T2-weighted (TSE/FSE), proton density (TSE/FSE), or short tau inversion recovery (STIR)	Recommended	Optional
	Sagittal T1-weighted after contrast	Recommended	Optional
	Sagittal three-dimensional T1-weighted (PSIR, MPRAGE)	Optional (cervical)	Optional
	Axial T2-weighted (TSE/FSE) or gradient recalled echo (GRE)	Optional	Optional
	Sagittal T1-weighted (TSE/FSE) before contrast	Optional	Optional
	Axial T1-weighted after contrast	Optional	Optional

[a] Modified with permission from Wattjes MP, et al, Lancet Neurol.[64] © 2021 Elsevier Inc.

[b] The MRI protocol recommendations specifically for multiple sclerosis, revised from the 2021 Magnetic Resonance Imaging in Multiple Sclerosis study group, Consortium of Multiple Sclerosis Centres, and North American Imaging in Multiple Sclerosis Cooperative MRI guidelines working group consensus recommendations. These are applicable and sufficient for assisting in the differential diagnosis of other demyelinating diseases. As noted, the recommended minimal sequences are limited, and the majority of the sequences are optional and often helpful when the differential diagnosis is not clear. Specific attention for disease monitoring for high-risk medications (eg, treatment for progressive multifocal leukoencephalopathy) includes recommended brain protocol with axial and sagittal three-dimensional FLAIR if available or two-dimensional FLAIR imaging as minimal recommended sequences.

Copyright © American Academy of Neurology. Unauthorized reproduction of this article is prohibited.

KEY POINTS

- The differential diagnosis should remain broad when the presentation is atypical or in the setting of imaging red flags.
- Harmonization of MRI protocols with the minimal required sequences is highlighted in consensus statements from MS experts, incorporating both diagnostic and disease monitoring purposes in MS.

Ultra-high field strength (greater than 3T) is mostly performed with 7T scanners, which are predominantly still reserved for research.

PROTOCOLIZED IMAGING APPROACH TO DEMYELINATING DISEASE

The clinical diagnosis mainly relies on conventional sequences. With this, the minimal imaging necessary to make the diagnosis and provide follow-up was reviewed by international panels first in 2016 and subsequently jointly published in 2021.[64] This protocolized approach provides some simplification and specific guidelines, including appendices with scanning parameters. It is important to note that this is specific to MS (when a priori chance is high or diagnosis is already made), thus requiring further liberal expansion for other considerations. Diagnostic and follow-up protocols were adapted from these recommendations and are summarized in TABLE 11-7.

CONCLUSION

In differentiation of demyelinating diagnoses, MRI plays a critical role. Reliable interpretation and implementation will continue to improve care. It is certainly without doubt that MRI in demyelinating disease will continue to bring better understanding of the pathophysiology, classification, and mainly prognostication and insight into treatment options to positively alter the clinical trajectory for patients. Imaging will be incorporated into an individualized approach with sound evidence-based stratification, supporting both clinical neurologists and patients in decision making.

REFERENCES

1 Kutzelnigg A, Faber-Rod JC, Bauer J, et al. Widespread demyelination in the cerebellar cortex in multiple sclerosis. Brain Pathol 2007; 17(1):38-44. doi:10.1111/j.1750-3639.2006.00041.x

2 Pirko I, Lucchinetti CF, Sriram S, Bakshi R. Gray matter involvement in multiple sclerosis. Neurology 2007;68(9):634-642. doi:10.1212/01.wnl.0000250267.85698.7a

3 Brownlee WJ, Hardy TA, Fazekas F, Miller DH. Diagnosis of multiple sclerosis: progress and challenges. Lancet 2017;389(10076):1336-1346. doi:10.1016/S0140-6736(16)30959-X

4 Lublin FD, Reingold SC, Cohen JA, et al. Defining the clinical course of multiple sclerosis: the 2013 revisions. Neurology 2014;83(3):278-286. doi:10.1212/WNL.0000000000000560

5 Lublin FD, Coetzee T, Cohen JA, Marrie RA, Thompson AJ, International Advisory Committee on Clinical Trials in MS. The 2013 clinical course descriptors for multiple sclerosis: a clarification. Neurology 2020;94(24):1088-1092. doi:10.1212/WNL.0000000000009636

6 Thompson AJ, Banwell BL, Barkhof F, et al. Diagnosis of multiple sclerosis: 2017 revisions of the McDonald criteria. Lancet Neurol 2018;17(2): 162-173. doi:10.1016/S1474-4422(17)30470-2

7 McDonald WI, Compston A, Edan G, et al. Recommended diagnostic criteria for multiple sclerosis: guidelines from the International Panel on the diagnosis of multiple sclerosis. Ann Neurol 2001;50(1):121-127. doi:10.1002/ana.1032

8 Okuda DT, Mowry EM, Beheshtian A, et al. Incidental MRI anomalies suggestive of multiple sclerosis: the radiologically isolated syndrome. Neurology 2009;72(9):800-805. doi:10.1212/01.wnl.0000335764.14513.1a

9 Lebrun-Frenay C, Rollot F, Mondot L, et al. Risk factors and time to clinical symptoms of multiple sclerosis among patients with radiologically isolated syndrome. JAMA Netw Open 2021;4(10): e2128271. doi:10.1001/jamanetworkopen.2021.28271

10 Okuda DT, Kantarci O, Lebrun-Frenay C, et al. Dimethyl fumarate delays multiple sclerosis in radiologically isolated syndrome [published online November 18, 2022]. Ann Neurol. doi:10.1002/ana.26555

11 Frischer JM, Weigand SD, Guo Y, et al. Clinical and pathological insights into the dynamic nature of the white matter multiple sclerosis plaque. Ann Neurol 2015;78(5):710-721. doi:10.1002/ana.24497

Copyright © American Academy of Neurology. Unauthorized reproduction of this article is prohibited.

12 Lucchinetti C, Bruck W, Parisi J, et al. Heterogeneity of multiple sclerosis lesions: implications for the pathogenesis of demyelination. Ann Neurol 2000;47(6):707-717. doi:10.1002/1531-8249(200006)47:6<707::aid-ana3>3.0.co;2-q

13 Solomon AJ, Pettigrew R, Naismith RT, et al. Challenges in multiple sclerosis diagnosis: misunderstanding and misapplication of the McDonald criteria. Mult Scler 2021;27(2):250-258. doi:10.1177/1352458520910496

14 Wang KY, Uribe TA, Lincoln CM. Comparing lesion detection of infratentorial multiple sclerosis lesions between T2-weighted spin-echo, 2D-FLAIR, and 3D-FLAIR sequences. Clin Imaging 2018;51:229-234. doi:10.1016/j.clinimag.2018.05.017

15 Geurts JJ, Roosendaal SD, Calabrese M, et al. Consensus recommendations for MS cortical lesion scoring using double inversion recovery MRI. Neurology 2011;76(5):418-424. doi:10.1212/WNL.0b013e31820a0cc4

16 Bitsch A, Kuhlmann T, Stadelmann C, et al. A longitudinal MRI study of histopathologically defined hypointense multiple sclerosis lesions. Ann Neurol 2001;49(6):793-796. doi:10.1002/ana.1053

17 Masdeu JC, Drayer BP, Anderson RE, et al. Multiple sclerosis–when and how to image. American College of Radiology. ACR Appropriateness Criteria. Radiology 2000;21(5 Suppl):547-562.

18 Kalinowska-Lyszczarz A, Tillema JM, Tobin WO, et al. Long-term clinical, MRI, and cognitive follow-up in a large cohort of pathologically confirmed, predominantly tumefactive multiple sclerosis. Mult Scler 2022;28(3):441-452. doi:10.1177/13524585211024162

19 Pittock SJ, McClelland RL, Achenbach SJ, et al. Clinical course, pathological correlations, and outcome of biopsy proved inflammatory demyelinating disease. J Neurol Neurosurg Psychiatry 2005;76(12):1693-1697. doi:10.1136/jnnp.2004.060624

20 Yeh EA, Graves JS, Benson LA, Wassmer E, Waldman A. Pediatric optic neuritis. Neurology 2016;87(9 Supplement 2):S53-S58. doi: 10.1212/WNL.0000000000002822

21 Optic Neuritis Study Group. Visual function 15 years after optic neuritis: a final follow-up report from the Optic Neuritis Treatment Trial. Ophthalmology 2008;115(6):1079-1082.e5. doi:10.1016/j.ophtha.2007.08.004

22 Xu SC, Kardon RH, Leavitt JA, et al. Optical coherence tomography is highly sensitive in detecting prior optic neuritis. Neurology 2019;92(6):e527-e535. doi:10.1212/WNL.0000000000006873

23 Parks NE. Metabolic and toxic myelopathies. Continuum (Minneap Minn) 2021;27(1, Spinal Cord Disorders):143-162. doi:10.1212/CON.0000000000000963

24 Zalewski NL. Vascular myelopathies. Continuum (Minneap Minn) 2021;27(1, Spinal Cord Disorders):30-61. doi:10.1212/CON.0000000000000905

25 Lopez Chiriboga S, Flanagan EP. Myelitis and other autoimmune myelopathies. Continuum (Minneap Minn) 2021;27(1, Spinal Cord Disorders):62-92. doi:10.1212/CON.0000000000000900

26 Lennon VA, Wingerchuk DM, Kryzer TJ, et al. A serum autoantibody marker of neuromyelitis optica: distinction from multiple sclerosis. Lancet 2004;364(9451):2106-2112. doi:10.1016/S0140-6736(04)17551-X

27 Flanagan EP, Cabre P, Weinshenker BG, et al. Epidemiology of aquaporin-4 autoimmunity and neuromyelitis optica spectrum. Ann Neurol 2016;79(5):775-783. doi:10.1002/ana.24617

28 Wingerchuk DM, Banwell B, Bennett JL, et al. International consensus diagnostic criteria for neuromyelitis optica spectrum disorders. Neurology 2015;85(2):177-189. doi:10.1212/WNL.0000000000001729

29 Flanagan EP, Weinshenker BG. Myelitis in neuromyelitis optica spectrum disorder: the long and the short of it. Mult Scler 2017;23(3):360-361. doi:10.1177/1352458517692888

30 Akaishi T, Sato DK, Nakashima I, et al. MRI and retinal abnormalities in isolated optic neuritis with myelin oligodendrocyte glycoprotein and aquaporin-4 antibodies: a comparative study. J Neurol Neurosurg Psychiatry 2016;87(4):446-448. doi:10.1136/jnnp-2014-310206

31 Tillema JM, McKeon A. The spectrum of neuromyelitis optica (NMO) in childhood. J Child Neurol 2012;27(11):1437-1447. doi:10.1177/0883073812451495

32 Krupp LB, Tardieu M, Amato MP, et al. International Pediatric Multiple Sclerosis Study Group criteria for pediatric multiple sclerosis and immune-mediated central nervous system demyelinating disorders: revisions to the 2007 definitions. Mult Scler 2013;19(10):1261-1267. doi:10.1177/1352458513484547

33 Pohl D, Alper G, Van Haren K, et al. Acute disseminated encephalomyelitis: updates on an inflammatory CNS syndrome. Neurology 2016;87(9 Suppl 2):S38-S45. doi:10.1212/WNL.0000000000002825

34 Tenembaum S, Chamoles N, Fejerman N. Acute disseminated encephalomyelitis: a long-term follow-up study of 84 pediatric patients. Neurology 2002;59(8):1224-1231. doi:10.1212/wnl.59.8.1224

35 Lopez-Chiriboga AS, Majed M, Fryer J, et al. Association of MOG-IgG serostatus with relapse after acute disseminated encephalomyelitis and proposed diagnostic criteria for MOG-IgG-associated disorders. JAMA Neurol 2018;75(11):1355-1363. doi:10.1001/jamaneurol.2018.1814

Copyright © American Academy of Neurology. Unauthorized reproduction of this article is prohibited.

36 Armangue T, Olive-Cirera G, Martinez-Hernandez E, et al. Associations of paediatric demyelinating and encephalitic syndromes with myelin oligodendrocyte glycoprotein antibodies: a multicentre observational study. Lancet Neurol 2020;19(3):234-246. doi:10.1016/S1474-4422(19)30488-0

37 Cobo-Calvo A, Ayrignac X, Kerschen P, et al. Cranial nerve involvement in patients with MOG antibody-associated disease. Neurol Neuroimmunol Neuroinflamm 2019;6(2):e543. doi:10.1212/NXI.0000000000000543

38 Hacohen Y, Palace J. Time to separate MOG-Ab-associated disease from AQP4-Ab-positive neuromyelitis optica spectrum disorder. Neurology 22 2018;90(21):947-948. doi:10.1212/WNL.0000000000005619

39 Kunchok A, Flanagan EP, Snyder M, et al. Coexisting systemic and organ-specific autoimmunity in MOG-IgG1-associated disorders versus AQP4-IgG+ NMOSD. Mult Scler 2021;27(4):630-635. doi:10.1177/1352458520933884

40 Kunchok A, Flanagan EP, Krecke KN, et al. MOG-IgG1 and co-existence of neuronal autoantibodies. Mult Scler 2021;27(8):1175-1186. doi:10.1177/1352458520951046

41 Hacohen Y, Rossor T, Mankad K, et al. 'Leukodystrophy-like' phenotype in children with myelin oligodendrocyte glycoprotein antibody-associated disease. Dev Med Child Neurol 2018;60(4):417-423. doi:10.1111/dmcn.13649

42 Cobo-Calvo A, Ruiz A, Maillart E, et al. Clinical spectrum and prognostic value of CNS MOG autoimmunity in adults: the MOGADOR study. Neurology 2018;90(21):e1858-e1869. doi:10.1212/WNL.0000000000005560

43 Gadde JA, Wolf DS, Keller S, Gombolay GY. Rate of leptomeningeal enhancement in pediatric myelin oligodendrocyte glycoprotein antibody-associated encephalomyelitis. J Child Neurol 2021;36(11):1042-1046. doi:10.1177/08830738211025867

44 Banks SA, Morris PP, Chen JJ, et al. Brainstem and cerebellar involvement in MOG-IgG-associated disorder versus aquaporin-4-IgG and MS. J Neurol Neurosurg Psychiatry 2020:jnnp-2020-325121. doi: 10.1136/jnnp-2020-325121

45 Dubey D, Pittock SJ, Krecke KN, et al. Clinical, radiologic, and prognostic features of myelitis associated with myelin oligodendrocyte glycoprotein autoantibody. JAMA Neurol 2019;76(3):301-309. doi:10.1001/jamaneurol.2018.4053

46 Rinaldi S, Davies A, Fehmi J, et al. Overlapping central and peripheral nervous system syndromes in MOG antibody-associated disorders. Neurol Neuroimmunol Neuroinflamm 2021;8(1):e924. doi:10.1212/NXI.0000000000000924

47 Ramanathan S, Prelog K, Barnes EH, et al. Radiological differentiation of optic neuritis with myelin oligodendrocyte glycoprotein antibodies, aquaporin-4 antibodies, and multiple sclerosis. Mult Sclerr 2016;22(4):470-482. doi:10.1177/1352458515593406

48 Chen JJ, Bhatti MT. Clinical phenotype, radiological features, and treatment of myelin oligodendrocyte glycoprotein-immunoglobulin G (MOG-IgG) optic neuritis. Curr Opin Neurol 2020;33(1):47-54. doi:10.1097/WCO.0000000000000766

49 Chen JJ, Flanagan EP, Jitprapaikulsan J, et al. Myelin oligodendrocyte glycoprotein antibody-positive optic neuritis: clinical characteristics, radiologic clues, and outcome. Am J Ophthalmol 2018;195:8-15. doi:10.1016/j.ajo.2018.07.020

50 Kleiter I, Gahlen A, Borisow N, et al. Neuromyelitis optica: evaluation of 871 attacks and 1,153 treatment courses. Ann Neurol 2016;79(2):206-216. doi:10.1002/ana.24554

51 Dale RC, de Sousa C, Chong WK, et al. Acute disseminated encephalomyelitis, multiphasic disseminated encephalomyelitis and multiple sclerosis in children. Brain 2000;123(Pt 12):2407-2422. doi:10.1093/brain/123.12.2407

52 Cortese R, Giorgio A, Severa G, De Stefano N. MRI prognostic factors in multiple sclerosis, neuromyelitis optica spectrum disorder, and myelin oligodendrocyte antibody disease. Front Neurol 2021;12:679881. doi:10.3389/fneur.2021.679881

53 Flanagan EP, Weinshenker BG, Krecke KN, Pittock SJ. Asymptomatic myelitis in neuromyelitis optica and autoimmune aquaporin-4 channelopathy. Neurol Clin Pract 2015;5(2):175-177. doi:10.1212/CPJ.0000000000000104

54 Barkhof F. The clinico-radiological paradox in multiple sclerosis revisited. Curr Opin Neurol 2002;15(3):239-245. doi:10.1097/00019052-200206000-00003

55 Tornatore C, Phillips JT, Khan O, Miller AE, Hughes M. Consensus opinion of US neurologists on practice patterns in RIS, CIS, and RRMS: evolution of treatment practices. Neurol Clin Pract 2016;6(4):329-338. doi:10.1212/CPJ.0000000000000254

56 Valsasina P, Aboulwafa M, Preziosa P, et al. Cervical Cord t1-weighted hypointense lesions at MR Imaging in multiple sclerosis: relationship to cord atrophy and disability. Radiology 2018;288(1):234-244. doi:10.1148/radiol.2018172311

57 Zeydan B, Gu X, Atkinson EJ, et al. Cervical spinal cord atrophy: an early marker of progressive MS onset. Neurol Neuroimmunol Neuroinflamm 2018;5(2):e435. doi:10.1212/NXI.0000000000000435

58 Seewann A, Kooi EJ, Roosendaal SD, et al. Postmortem verification of MS cortical lesion detection with 3D DIR. Neurology 2012;78(5):302-308. doi:10.1212/WNL.0b013e31824528a0

Copyright © American Academy of Neurology. Unauthorized reproduction of this article is prohibited.

59 Keegan BM, Kaufmann TJ, Weinshenker BG, et al. Progressive solitary sclerosis: gradual motor impairment from a single CNS demyelinating lesion. Neurology 2016;87(16):1713-1719. doi:10.1212/WNL.0000000000003235

60 Lee LE, Chan JK, Nevill E, et al. Advanced imaging findings in progressive solitary sclerosis: a single lesion or a global disease? Mult Scler J Exp Transl Clin 2019;5(1):2055217318824612. doi: 10.1177/2055217318824612

61 Solomon AJ, Bourdette DN, Cross AH, et al. The contemporary spectrum of multiple sclerosis misdiagnosis: a multicenter study. Neurology 2016;87(13):1393-1399. doi:10.1212/WNL.0000000000003152

62 Geraldes R, Ciccarelli O, Barkhof F, et al. The current role of MRI in differentiating multiple sclerosis from its imaging mimics. Nat Rev Neurol 2018;14(4):199-213. doi: 10.1038/nrneurol.2018.14

63 Tillema JM, Pirko I. Neuroradiological evaluation of demyelinating disease. Ther Adv Neurol Disord 2013;6(4):249-268. doi: 10.1177/1756285613478870

64 Wattjes MP, Ciccarelli O, Reich DS, et al. 2021 MAGNIMS-CMSC-NAIMS consensus recommendations on the use of MRI in patients with multiple sclerosis. Lancet Neurol 2021;20(8): 653-670. doi:10.1016/S1474-4422(21)00095-8

Copyright © American Academy of Neurology. Unauthorized reproduction of this article is prohibited.

REVIEW ARTICLE

CONTINUUM AUDIO INTERVIEW AVAILABLE ONLINE

VIDEO CONTENT AVAILABLE ONLINE

Diagnostic Ultrasonography in Neurology

By Elsa Azevedo, MD, PhD

ABSTRACT

OBJECTIVE: **Ultrasonography allows neurologists to complement clinical information with additional useful, easily acquired, real-time data. This article highlights its clinical applications in neurology.**

LATEST DEVELOPMENTS: **Diagnostic ultrasonography is expanding its applications with smaller and better devices. Most indications in neurology relate to cerebrovascular evaluations. Ultrasonography contributes to the etiologic evaluation and is helpful for hemodynamic diagnosis of brain or eye ischemia. It can accurately characterize cervical vascular atherosclerosis, dissection, vasculitis, or other rarer disorders. Ultrasonography can aid in the diagnosis of intracranial large vessel stenosis or occlusion and evaluation of collateral pathways and indirect hemodynamic signs of more proximal and distal pathology. Transcranial Doppler (TCD) is the most sensitive method for detecting paradoxical emboli from a systemic right-left shunt such as a patent foramen ovale. TCD is mandatory for sickle cell disease surveillance, guiding the timing for preventive transfusion. In subarachnoid hemorrhage, TCD is useful in monitoring vasospasm and adapting treatment. Some arteriovenous shunts can be detected by ultrasonography. Cerebral vasoregulation studies are another developing field of interest. TCD enables monitoring of hemodynamic changes related to intracranial hypertension and can diagnose cerebral circulatory arrest. Optic nerve sheath measurement and brain midline deviation are ultrasonography-detectable signs of intracranial hypertension. Most importantly, ultrasonography allows for easily repeated monitoring of evolving clinical conditions or during and after interventions.**

ESSENTIAL POINTS: **Diagnostic ultrasonography is an invaluable tool in neurology, used as an extension of the clinical examination. It helps diagnose and monitor many conditions, allowing for more data-driven and rapid treatment interventions.**

CITE AS:
CONTINUUM (MINNEAP MINN) 2023;29(1, NEUROIMAGING): 324–363.

Address correspondence to Dr Elsa Azevedo, Department of Neurology, Centro Hospitalar Universitário de São João, Alameda Professor Hernani Monteiro, 4200-319 Porto, Portugal, elsa.azevedo@chsj.min-saude.pt.

RELATIONSHIP DISCLOSURE:
Dr Azevedo reports no disclosure.

UNLABELED USE OF PRODUCTS/INVESTIGATIONAL USE DISCLOSURE:
Dr Azevedo reports no disclosure.

© 2023 American Academy of Neurology.

Copyright © American Academy of Neurology. Unauthorized reproduction of this article is prohibited.

INTRODUCTION

Ultrasonography in neurology, or *neurosonology*, is the medical science dedicated to the use of ultrasonography for the study of the nervous system.

Neurosonology is a technique used by physicians as an extension of the clinical examination. It is commonly used for the evaluation of cerebrovascular diseases, where it establishes the diagnosis or provides complementary hemodynamic information to computed tomography angiography (CTA) or magnetic resonance angiography (MRA). It is also used in several other applications, such as in the study of the peripheral nervous system, and guides neurointerventional procedures (such as echo-guided injection of botulinum toxin or lumbar puncture).

The main advantages of this tool are related to its (1) being performed at the patient's bedside, if appropriate, avoiding travel when patients are unstable; (2) giving real-time information, allowing immediate clinical action; (3) being noninvasive, with no ionizing radiation, with no sedation needed even for children or some agitated patients, not being influenced by central nervous system depressants, and having no iodinated contrast exposure or contrast side-effects; (4) being easily repeated to monitor changes and allowing monitoring during therapeutic and other interventions; (5) being a comparatively inexpensive method; (6) allowing the neurologist to demonstrate changes to the patient during the procedure; and (7) most importantly, giving accurate and validated information. As practice and hands-on experience with a device offer the best instruction, an interesting feature of ultrasonography is that the beginner can learn the first steps by evaluating their own vessels and other structures. As with other techniques, it requires an experienced operator.

For intracranial studies, one main limitation is the intact skull that prevents a good ultrasound window in about 10% to 20% of patients, particularly in older women, although for vascular studies this can be overcome by echo contrast agents.

KEY POINTS

- Neurosonology can be used as an extension of the clinical neurologic examination.
- Advantages of neurosonology are that it can be performed at the bedside, is noninvasive, provides real-time accurate information, and allows continuous monitoring.
- An ultrasound machine that provides B-mode echography, color imaging of the vessels, and blood flow velocities spectrum allows extracranial and many intracranial applications, including vascular and parenchymal studies.

GENERAL TECHNICAL REQUIREMENTS FOR NEUROSONOLOGY

Two main devices are used in neurosonology. First are ultrasound machines that provide at least three pieces of information: B-mode echography, color imaging of the vessels, and blood flow velocities spectrum. B-mode (brightness mode) generates an echographic grayscale image. A superimposed color-Doppler mode shows the blood flow direction and its velocity, through the Doppler effect, which is the frequency difference of the transmitted and reflected ultrasound proportional to the velocity of moving erythrocytes. Power-Doppler mode uses the signal intensity of the returning Doppler signal instead of frequency shift, providing a color map superimposed on a B-mode image. Spectral analysis shows the graphic distribution of direction and velocities in moving erythrocytes over time. Some indices are very useful in clinical practice, such as the resistance (systolic flow velocity minus the diastolic velocity divided by the systolic velocity) and the pulsatility (systolic flow velocity minus the diastolic velocity divided by the mean velocity) indices, which give clues about upstream and downstream pathology. This device is used for extracranial and many intracranial applications, such as extracranial color Doppler sonography and transcranial color sonography, and for parenchymal studies.

Copyright © American Academy of Neurology. Unauthorized reproduction of this article is prohibited.

TABLE 12-1

Main Applications of Neurosonology

Settings

- Prediction of vascular risk in primary prevention (atherosclerosis, sickle cell disease)
- Acute ischemic stroke and eye ischemic syndrome (etiology, hemodynamic monitoring)
- Monitoring of vasospasm in subarachnoid hemorrhage
- Monitoring during and after cerebrovascular interventions
- Neurocritical care monitoring
- Suspicion of temporal arteritis or dural fistula
- Brain parenchyma studies in neonatal pathology and in some movement disorders
- Eye pathology
- Neuromuscular diseases

Extracranial

- Neck vessel atherosclerotic disease (intima-media thickness, atherosclerotic plaques)
- Arterial dissection, fibromuscular dysplasia
- Cervical and temporal arteritis
- Transient perivascular inflammation of the carotid artery syndrome
- Isolated thrombus
- Signs of arteriovenous shunts (eg, dural fistula)
- Subclavian steal phenomenon
- Other indirect hemodynamic signs of upstream (eg, aortic valvular disease, proximal stenosis) and downstream (eg, distal occlusion) lesions
- Neuromuscular diseases
- Echo-guided interventions (botulinum toxin, lumbar puncture)

Intracranial

- Intracranial arterial stenosis and occlusions (atherosclerosis, arteritis, embolus)
- Cerebral hemodynamics in sickle cell disease
- Intracranial impact of extracranial disease collateralization pathways (circle of Willis, ophthalmic artery, inversion of vertebral flow direction)
- Microembolic signal detection
- Right-to-left shunt assessment (eg, patent foramen ovale, arteriovenous pulmonary fistula)
- Cerebral vasospasm in subarachnoid hemorrhage
- Reversible cerebral vasoconstriction syndrome
- Hemodynamic monitoring during and after interventions
- Cerebral vasoreactivity, autoregulation, and neurovascular coupling studies
- Intracranial hypertension and brain death
- Venous studies
- Eye (vascular or optic nerve pathology)
- Brain parenchyma studies, such as in neonatal pathology and in some movement disorders

Copyright © American Academy of Neurology. Unauthorized reproduction of this article is prohibited.

A second device is the transcranial Doppler (TCD) device examining only the Doppler effect through its spectral analysis. It does not provide echo-imaging information ("blind" TCD). Nevertheless, this smaller device, with smaller probes, is very useful for the evaluation of hemodynamics because it allows hands-free and bilateral monitoring of cerebral hemodynamics with a headframe.

Pulsed-waved linear-array probes of approximately 5 MHz to 13 MHz are used for evaluating the cervical vessels. Probes of at least 15 MHz to 20 MHz are used for more superficial vessels, such as the temporal arteries. Because intracranial vessels are deeper, lower frequencies are needed, so for transcranial examinations, 1.5-MHz to 3.5-MHz probes are used.

The cervical vessels (the common, internal, and external carotids and vertebral arteries) are usually examined with the patient in a supine position, neck slightly extended and laterally rotated. The intracranial structures are approached through three main windows: orbital (for ophthalmic artery, carotid siphon, and optical nerve), temporal (for distal internal carotid; middle, anterior, and posterior cerebral arteries; and brain parenchyma), and occipital (for intracranial segments of vertebral arteries and the basilar artery). When the skull does not have good windows for ultrasonography, clinicians can use commercial IV transpulmonary ultrasound contrast agents that improve the detection of flow in intracranial vessels.

KEY POINTS

- **A transcranial Doppler device providing only Doppler spectral analysis is a smaller device that allows hands-free and bilateral monitoring of cerebral hemodynamics with a headframe.**
- **Atherosclerosis, sickle cell disease, brain and eye ischemia, subarachnoid hemorrhage, suspicion of temporal arteritis or dural fistulas, intracranial hypertension, and cerebral circulatory arrest are some of the settings for neurovascular ultrasonography.**

MAIN APPLICATIONS OF NEUROSONOLOGY

After clinical history and neurologic examination, neurosonology allows the physician to look further right away, inside the patient. TABLE 12-1 lists the main applications of neurosonology.

This article discusses neurovascular ultrasonography as the main application of neurosonology. In primary prevention, it predicts vascular risk (eg, atherosclerosis, sickle cell disease). In the setting of brain or eye ischemia, it contributes to etiologic and hemodynamic diagnosis, which is useful in hyperacute phase monitoring and for secondary prevention. The temporal arteries can also be rapidly evaluated by ultrasonography. In subarachnoid hemorrhage, TCD allows for monitoring of vasospasm, guiding treatment options. Some arteriovenous shunts, such as dural arteriovenous fistulas in patients with pulsatile tinnitus, are easily perceived by hemodynamic features in ultrasonography. In neurocritical care, TCD enables monitoring of hemodynamic changes associated with intracranial hypertension and can diagnose cerebral circulatory arrest with high accuracy. Optic nerve sheath measurement and brain midline deviation are other ultrasonography-detectable signs of intracranial hypertension. Neurosonology allows for easily repeated monitoring of clinical conditions or during and after interventions.

Brain parenchyma may also be studied with ultrasonography, as in neonatal pathology and potentially in movement disorders. Additionally, ultrasonography allows for guidance of peripheral neurointervention procedures and the study of the peripheral nervous system.[1]

New trends, such as ultraportable devices, ultrafast-ultrasonography, ultrasound perfusion imaging, cerebral hemodynamic and vasoregulation studies applied to guiding decisions, and the concept of point-of-care ultrasonography for neurology, are other developing fields of interest.

Copyright © American Academy of Neurology. Unauthorized reproduction of this article is prohibited.

KEY POINTS

- A comprehensive cerebrovascular ultrasonographic evaluation should include cervical as well as intracranial vessels.
- The degree of stenosis of a cervical internal carotid atherosclerotic plaque can be measured by direct morphologic and velocimetric parameters, as well as by indirect criteria.
- Compensatory intracranial collateral circuits (ophthalmic, anterior communicating, and posterior communicating arteries) provide indirect signs of the hemodynamic effect of a cervical carotid stenosis.

NEUROVASCULAR ULTRASONOGRAPHY

Ultrasonography can be thought of as a brain stethoscope providing insight into cerebrovascular hemodynamics.

A comprehensive cerebrovascular evaluation includes cervical as well as intracranial vessels (FIGURE 12-1), both morphologic and hemodynamic features at the cervical level, and hemodynamics concerning the intracranial vessels. With this approach, neurosonology can help answer important clinical questions in acute stroke settings, from etiology to monitoring in several steps, as listed in TABLE 12-2.

Extracranial Neurovascular Ultrasonography

At the cervical level, it is possible to accurately assess morphologic changes of carotid and vertebral arteries, along with their hemodynamic functional performance.

ATHEROSCLEROTIC DISEASE. Cervical vascular ultrasonography is useful for diagnosing atherosclerotic disease, measuring intima-media thickness, as a systemic marker of atherosclerosis, and atherosclerotic plaque characterization and its hemodynamic effects. TABLE 12-3 reviews the criteria for defining the degree of stenosis of a cervical internal carotid atherosclerotic plaque, most frequently occurring in the carotid bulb.[2] Other similar criteria have been published,[3] but all are essentially based on the morphologic assessment of the degree of luminal stenosis, which can be measured by methods used in angiographic studies such as NASCET (the North American Symptomatic

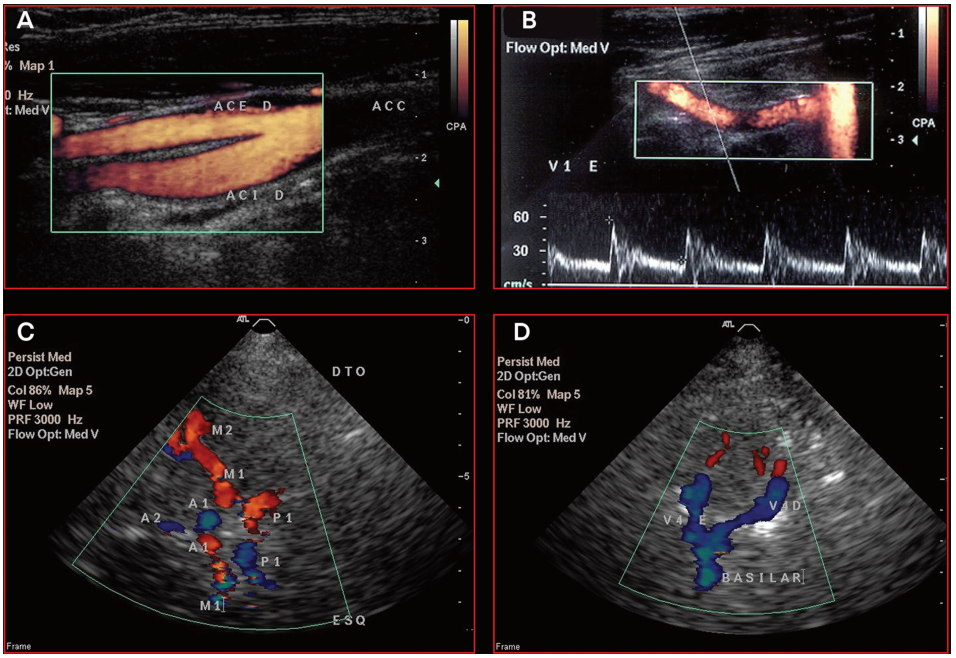

FIGURE 12-1

Normal cervical and brain vessels. *A*, Bifurcation of common (ACC) into external (ACE) and internal (ACI) carotid arteries. *B*, Vertebral artery (V1) starting at the subclavian artery. *C*, Transcranial temporal window: right and left segments of middle (M1, M2), anterior (A1, A2), and posterior (P1) cerebral arteries. *D*, Transcranial occipital window: intracranial vertebral (V4) and basilar arteries.

Copyright © American Academy of Neurology. Unauthorized reproduction of this article is prohibited.

Carotid Endarterectomy Trial) and ECST (the European Carotid Surgery Trial) (FIGURE 12-2),[4] complemented by hemodynamic assessment. Hemodynamics are assessed by the blood flow velocity at the most stenotic point, comparison with proximal and more distal segments, and the appreciation of possible intracranial compensatory collateral circuits (ophthalmic, anterior communicating, and posterior communicating arteries), which provide indirect signs of the hemodynamic effect of the stenosis.

The following should be considered for carotid stenosis evaluation: (1) if a good visualization of the stenotic channel is possible, morphologic criteria can be prioritized, although hemodynamics should also be evaluated; (2) if visualization of the stenotic channel is difficult, the velocimetric direct and indirect criteria should be prioritized; and (3) intracranial signs of compensatory collateral circuits favor a high degree of stenosis. In carotid occlusion, no velocity signal is present for at least 1.5 cm, and at least one of the compensatory intracranial collateral circuit signals must be present.

Beyond the degree of stenosis, ultrasonography provides other parameters related to stroke risk attributable to a given carotid stenosis (stenosis of greater than 50%, progression of degree of stenosis, plaque surface ulceration, hypoechogenic and vascularized plaque, cerebral microembolic signals, bad intracranial collateralization, and exhaustion of cerebral vasoreactivity), that inform a decision regarding the need for revascularization. The mechanism of stroke can be a decrease in distal perfusion pressure or a carotid atheroembolism.

Questions That May be Addressed by Neurosonology in the Setting of Acute Stroke TABLE 12-2

- Has a large artery occlusion occurred? Do not delay the CTA (computed tomography angiography)!
- How are the cerebral hemodynamics?
- Is the artery opening with thrombolysis?
- Was the revascularization hemodynamically satisfactory?
- Has an artery reoccluded?
- Was the stroke caused by an atherosclerotic lesion? Does it have a criterion for revascularization?
- Is a dissection hemodynamically unstable and a candidate for revascularization?
- Has a cerebral hyperperfusion syndrome developed after cerebral artery revascularization or after carotid endarterectomy?
- Are clues for a cardioembolic etiology present?
- Is a patent foramen ovale present and worth closing?
- Is a cerebral vasoconstriction syndrome, vasculitis, or more rare syndrome such as moyamoya syndrome likely?
- Are any arteriovenous malformation clues present in a patient with an intracranial hemorrhage?
- Have subarachnoid hemorrhage vasospasm criteria for endovascular treatment been evaluated?
- Are hemodynamic or optic nerve sheath signs of increased intracranial pressure present?
- Are signs of cerebral circulatory arrest present?

Copyright © American Academy of Neurology. Unauthorized reproduction of this article is prohibited.

A higher degree of stenosis is related to both mechanisms, whereas unstable plaques (characterized by irregular surface, hypoechogenic signal, vascularization as evaluated with contrast agents, or those that generate microembolic signals) tend to be more associated with embolism formation, and a lack of good distal compensatory blood flow increases the risk of severe hypoperfusion. FIGURE 12-3 illustrates some examples of unstable symptomatic carotid plaques.

Cervical vertebral artery stenosis is most frequent at its ostium. Its severity can be assessed by the decrease in lumen diameter and by blood flow velocity at the stenotic segment and more distally. In the case of severe stenosis or occlusion, the contralateral vertebral artery may compensate by providing flow in an inverted

TABLE 12-3 **Criteria to Define Degree of Stenosis in Internal Carotid Atherosclerotic Plaque**[a]

	Degree of stenosis as defined by NASCET (the North American Symptomatic Carotid Endarterectomy Trial), %						
	10-40	50	60	70	80	90	Occlusion
Main criteria							
1 B-mode image, diameter	Applicable	Possibly applicable					Imaging of occluded artery
2 Color Doppler image	Plaque delineation	Flow	Flow	Flow	Flow	Flow	Absence of flow
3 PSV threshold, cm/s		125		230		NA	NA
4a PSV average, cm/s	≤160	210	240	330	370	Variable	NA
4b PSV poststenotic, cm/s				≥50	<50	<30	NA
5 Collateral flow (periorbital arteries or circle of Willis)				Possible	Present	Present	Present
Additional criteria							
6 Prestenotic flow (diastole) (CCA)				Possibly reduced	Reduced	Reduced	Reduced
7 Poststenotic flow disturbances (severity and length)		Moderate	Pronounced	Pronounced	Pronounced	Variable	NA
8 End-diastolic flow velocity in the stenosis (cm/s)			<100	>100		Variable	NA
9 Carotid ratio ICA/CCA	<2	≥2	≥2	>4	>4	Variable	NA

CCA = common carotid artery; ICA = internal carotid artery; NA = not applicable; PSV = peak systolic velocity.
[a] Modified with permission from von Reutern GM, et al, Stroke.[2] © 2012 American Heart Association.

Copyright © American Academy of Neurology. Unauthorized reproduction of this article is prohibited.

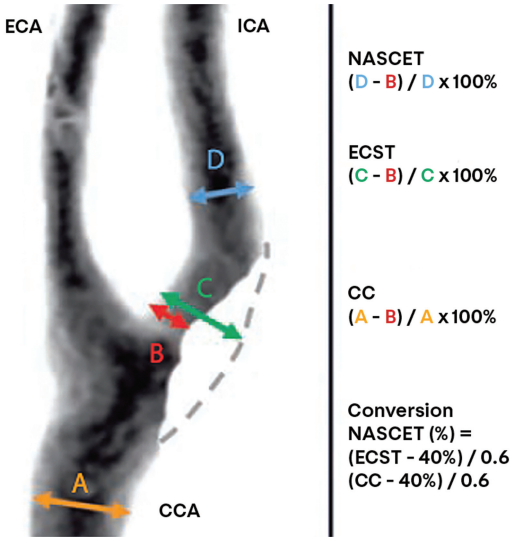

FIGURE 12-2

Assessment of the degree of luminal stenosis, measured by methods used in NASCET (the North American Symptomatic Carotid Endarterectomy Trial) and ECST (the European Carotid Surgery Trial) angiographic studies.

CC = common carotid method; CCA = common carotid artery; ECA = external carotid artery; ICA = internal carotid artery.

Reprinted with permission from Valdueza JM, et al.[4] © 2017 Thieme Medical Publishers, Inc.

direction into the intracranial segment of the affected vertebral artery. It is more difficult to establish velocimetric criteria for vertebral stenosis because physiologic asymmetry in arterial diameter is frequent.[5] This asymmetry dictates blood flow velocity variation, with a lower velocity and higher resistance index in the narrower side.

In occlusion or tight stenosis of the proximal subclavian artery proximal to the vertebral artery ostium, the arm might be perfused by an inverted flow from the ipsilateral vertebral artery, while the contralateral vertebral artery has a compensatory high blood flow velocity. This is called a *subclavian steal effect* and, when symptomatic, *subclavian steal syndrome*. FIGURE 12-4 illustrates this phenomenon.[4]

CASE 12-1 is an example of a clinical case in which ultrasonography provided insight into multifocal atherosclerosis, subclavian steal effect, and paroxysmal atrial fibrillation.

KEY POINTS

- **Higher degrees of stenosis are related to both the decrease in distal perfusion pressure and atheroembolism. Atheroembolic risk is further linked to unstable plaque features.**
- **Cervical vertebral artery stenosis can be assessed by the decrease in lumen diameter and measurement of blood flow velocity at the stenotic segment and more distally.**
- **Subclavian steal effect consists of inverted flow from the ipsilateral vertebral artery when a tight stenosis or occlusion of the proximal subclavian artery is present.**
- **Ultrasound signs of dissection may include an enlarged artery with an eccentric hypoechogenic luminal stenosis, tapering stenosis ending in a string sign, floating intimal flap, and double lumen appearance, with to-and-fro aspect in color and spectral Doppler in the false lumen.**

ARTERIAL DISSECTION. Arterial dissection is the cause of approximately 2.5% of all cases of cerebral ischemia and the second leading cause of stroke in young adults. Cervical vascular ultrasonography can disclose signs of arterial dissection, both directly and indirectly. Usually, an intimal tear has occurred, leading to an intramural hematoma, provoking an enlargement of the artery with a variable degree of eccentric intraluminal stenosis or even occlusion. Dissections frequently occur at the postbulbar distal cervical or cervicocranial levels due to neck mobility and trauma against bone surfaces. Direct ultrasound dissection signs include an enlarged artery with an eccentric hypoechogenic luminal stenosis, sometimes a tapering stenosis ending in a string sign, and a floating intimal flap. Another possible finding is a double lumen appearance, with a to-and-fro aspect in color and spectral Doppler in the false lumen. However, distal dissections might be detected mainly through hemodynamic signs either by finding a stenotic carotid flow acceleration in a distal retromandibular approach or indirectly finding a significantly higher resistance index in the cervical carotid segment, meaning an occlusion or high-degree stenosis is present distally. TCD may also add hemodynamic information. Doppler ultrasonography might be important to check if a dissection is hemodynamically unstable and if the patient may be a candidate for revascularization.

Overall, the sensitivity, specificity, and positive and negative predictive values for color Doppler sonography to diagnose patients with a spontaneous internal

Copyright © American Academy of Neurology. Unauthorized reproduction of this article is prohibited.

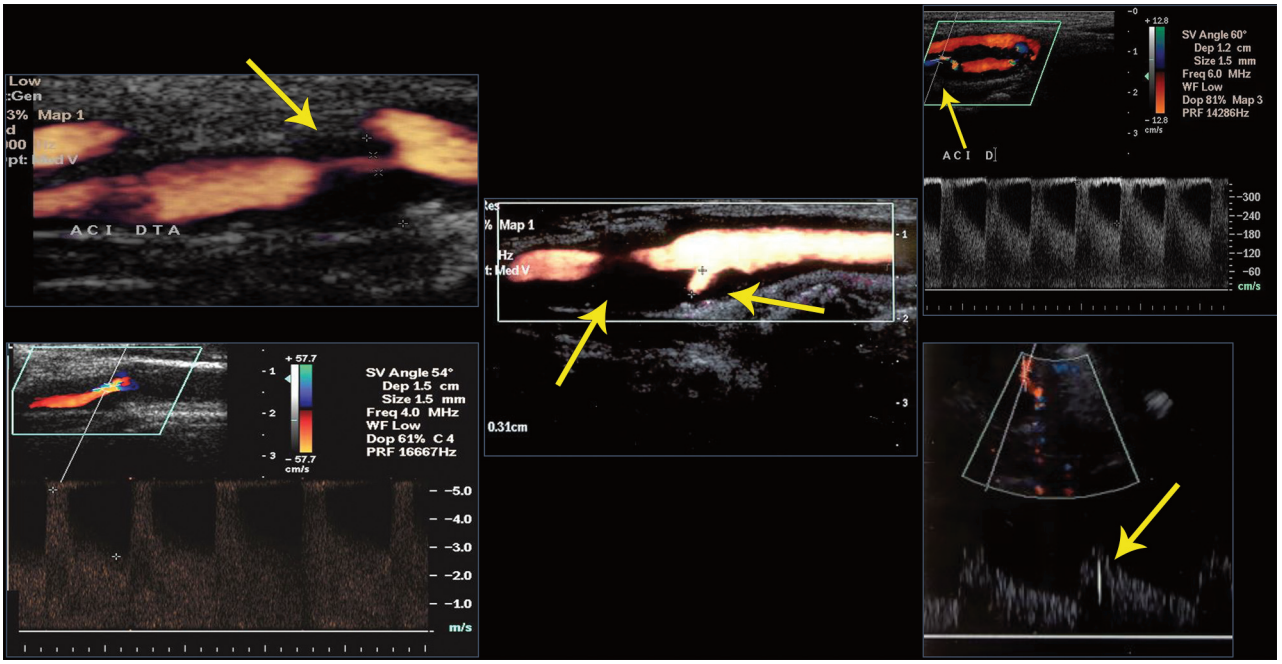

FIGURE 12-3

Examples of unstable symptomatic carotid plaques. *Left*, Subocclusive hypoechogenic stenosis (*arrow*) with high flow acceleration. *Middle*, Highly stenotic hypoechogenic and ulcerated plaque (*arrows*). *Right*, Highly stenotic active plaque with a microembolic signal in the ipsilateral middle cerebral artery (*arrows*).

ACI = internal carotid artery; DTA = right side.

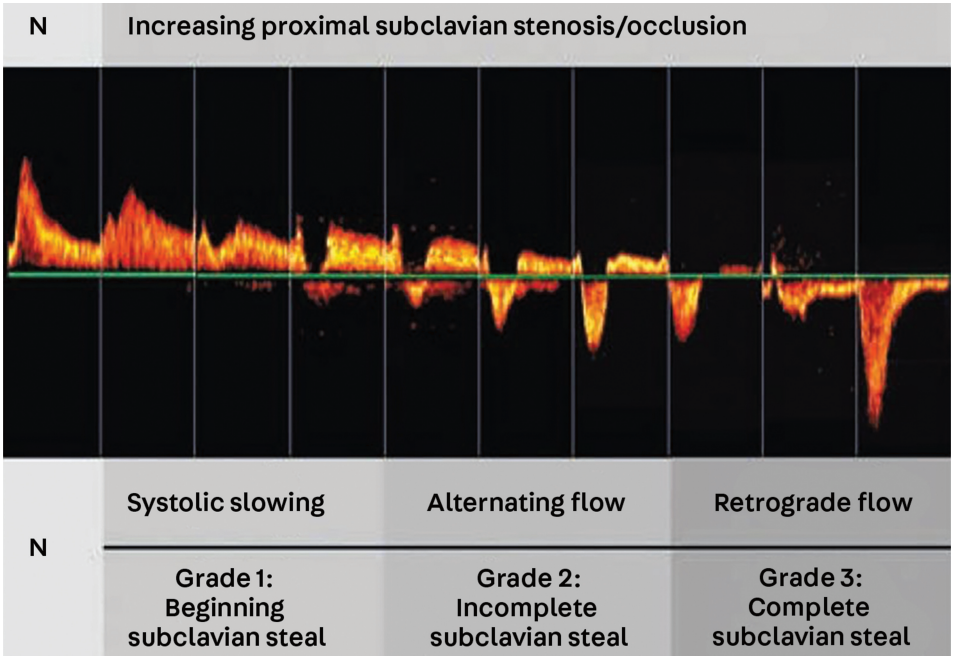

FIGURE 12-4

Illustration of subclavian steal phenomenon and its effect on vertebral artery blood flow.

N = normal.

Reprinted with permission from Valdueza JM, et al.[4] © 2017 Thieme Medical Publishers, Inc.

Copyright © American Academy of Neurology. Unauthorized reproduction of this article is prohibited.

carotid artery dissection causing carotid territory ischemia were 96%, 94%, 92%, and 97%, respectively.[6] Nevertheless, as carotid dissection lesions are often high in the neck or intracranial where ultrasonography lacks morphologic resolution, the diagnosis is better confirmed with other angiographic techniques. MRI is best suited to visualize the intramural hematoma characteristic of an arterial dissection.

In vertebral arteries, finding direct signs of dissection might be more challenging but is possible in the V1, V2, and sometimes in V3 segments, although dissection might be identified only by hemodynamic changes.

In some cases of aortic dissection, the dissection ascends to the proximal common carotid arteries. FIGURE 12-7, VIDEO 12-1, and VIDEO 12-2 show some ultrasonography examples of cervical carotid and vertebral dissection.[7]

VASCULITIS. Systemic vasculitis might also affect the cervical arteries. In this case, concentric hypoechogenic vessel wall thickening is present, with blood flow acceleration if the intraluminal stenosis is significant, which may lead to vessel occlusion. Takayasu arteritis is an uncommon vasculitis affecting the aorta and main branches, with wall thickness in the typical macaroni sign (concentric thickening of the arterial wall with a regular surface and intermediate echogenicity). In clinical practice, the most common adult form of vasculitis is giant cell arteritis (GCA). GCA frequently causes an intense and sustained headache, affecting the temporal branch of the external carotid artery, where arterial changes can be detected by ultrasonography. In suspected cases, a hypoechogenic noncompressible wall thickening (the halo sign, seen in FIGURE 12-8) has a high diagnostic accuracy of 77% sensitivity and 96% specificity[8]; the bilateral halo sign has even higher diagnostic accuracy. This disease frequently affects other branches of the external carotid artery, the ophthalmic circulation, and sometimes the vertebral arteries, potentially leading to amaurosis and posterior circulation stroke.

Monitoring response to treatment with ultrasonography is important and will become crucial as new treatments for GCA involving interleukin 6 inhibition may impair the usefulness of measuring C-reactive protein and erythrocyte sedimentation rate as follow-up parameters. TABLE 12-4[9] shows cutoff values for ultrasound intima-media thickness in GCA, and FIGURE 12-8 shows clinical examples of GCA.[10]

TRANSIENT PERIVASCULAR INFLAMMATION OF THE CAROTID ARTERY AND MURAL THROMBI. A more recently described inflammatory entity is transient perivascular inflammation of the carotid artery syndrome,[11] characterized by carotid pain associated with an eccentric carotid stenosis, disappearing within a few weeks spontaneously or after treatment with anti-inflammatory medications.

Other potential transient stenotic lesions should be excluded, such as a carotid dissection or an isolated nonocclusive mural floating thrombus in the absence of atherosclerosis. These mural thrombi might appear associated with thrombophilia and disappear by lysis, spontaneously, or after anticoagulation therapy (FIGURE 12-9).

FIBROMUSCULAR DYSPLASIA AND CAROTID WEB. Fibromuscular dysplasia is a rare, idiopathic, noninflammatory, and nonatherosclerotic fibrous or fibromuscular thickening of the arterial wall. Any layer of the vessel wall may be affected,

KEY POINTS

- Concentric hypoechogenic vessel wall thickening is the sonographic hallmark of vasculitis.
- Giant cell arteritis is the most common form of large and medium vessel vasculitis affecting adults, characterized by a hypoechogenic noncompressible thickening of the wall (the halo sign) in the temporal branch of the external carotid artery.
- Transient perivascular inflammation of the carotid artery syndrome associates carotid pain with an eccentric carotid stenosis, disappearing within a few weeks spontaneously or after treatment with anti-inflammatory drugs.
- Isolated hypoechogenic mural thrombi might appear associated with thrombophilia and disappear by lysis, spontaneously, or after anticoagulation therapy.

Copyright © American Academy of Neurology. Unauthorized reproduction of this article is prohibited.

CASE 12-1

A 68-year-old man who had a history of smoking and medication-controlled hypertension presented with transient left arm paresis and periods of dizziness. The neurologic examination was normal. Ultrasonography showed a left-sided carotid occlusion and intracranial collateralization to its territory through the anterior communicating artery, although maintaining a dampened flow in the left middle cerebral artery. It also demonstrated a right-sided significant carotid stenosis, a left-sided subclavian steal effect, and probable paroxysmal atrial fibrillation (FIGURE 12-5 and FIGURE 12-6). This information led to several secondary prevention measures after the transient ischemic attack. The patient started direct anticoagulant therapy, and a 24-hour ECG confirmed paroxysmal atrial fibrillation. His low-density lipoprotein cholesterol was 205 mg/dL, and he started statin therapy. Arterial hypertension was well controlled with medications. Right carotid revascularization surgery was performed. MR angiography confirmed a left subclavian proximal near-occlusion that was treated with stenting. The patient stopped smoking with the help of transdermal nicotine. All intracranial hemodynamics were improved on a follow-up examination, and the patient remained asymptomatic.

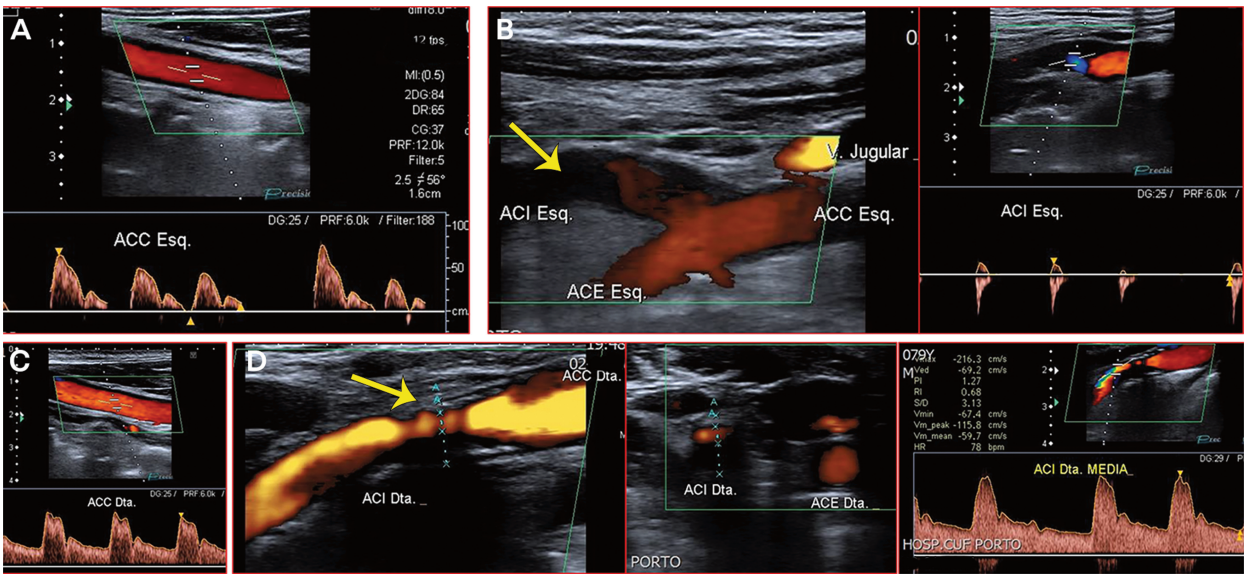

FIGURE 12-5

Ultrasonography of the patient in CASE 12-1 with multifocal atherosclerosis and paroxysmal atrial fibrillation. Left-sided cervical carotid arteries (*A*): common carotid artery (ACC) velocities spectral analysis with high resistance flow suggesting a downstream occlusion and cardiac arrhythmia suggestive of atrial fibrillation. *B*, Internal carotid artery occlusion (*arrow*). Right-sided cervical carotid arteries (*C*): common carotid artery (ACI) with normal flow (*D*) and internal carotid artery with a 70% stenosis (*arrow*), with focal flow acceleration.

ACE = external carotid artery; Dta = right side; Esq = left side.

Copyright © American Academy of Neurology. Unauthorized reproduction of this article is prohibited.

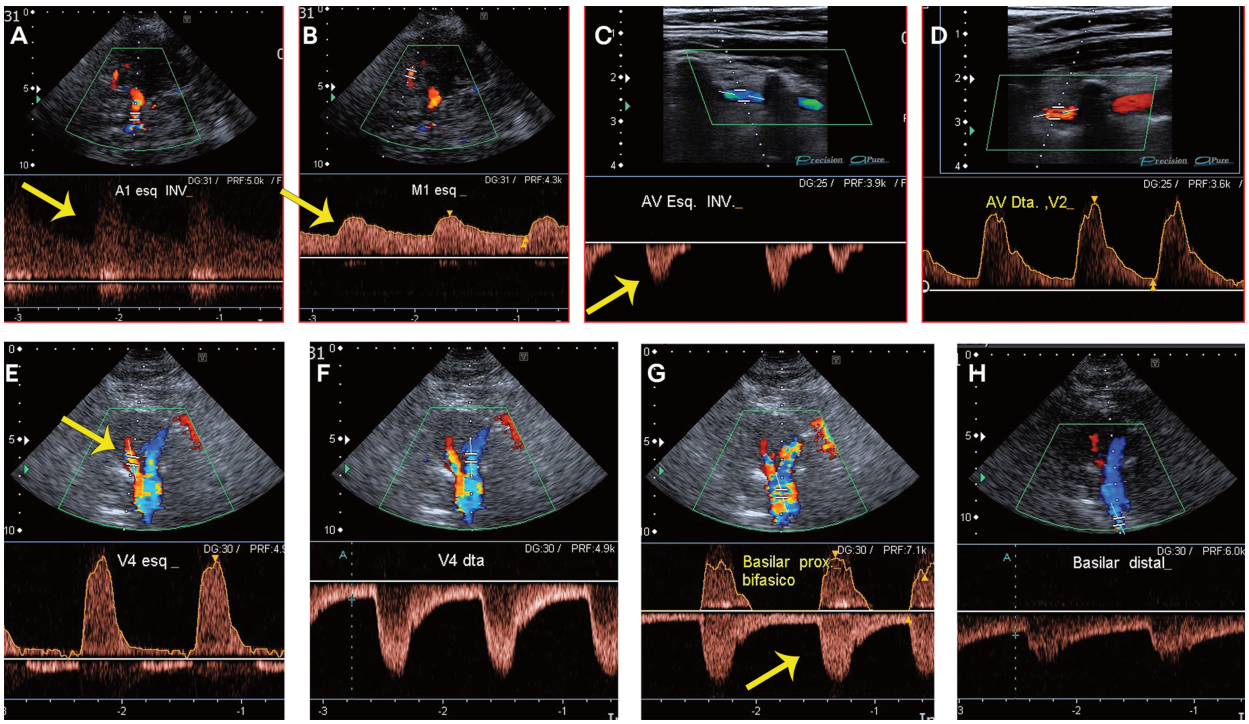

FIGURE 12-6

Ultrasonography of the patient in CASE 12-1 with multifocal atherosclerosis and paroxysmal atrial fibrillation. Intracranial collateralization through the anterior communicating artery with turbulent and inverted flow direction in left A1 segment (*A*, *arrow*), with partial compensation of left M1 flow (dampened) (*B*, *arrow*). Cervical vertebral arteries: left vertebral artery with inverted flow direction (*C*, *arrow*) and cardiac arrhythmia; right vertebral artery with normal direction and globally accelerated flow (*D*). Intracranial vertebral arteries (V4) and basilar artery: left V4 with inverted flow direction (*E*, *arrow* in color Doppler red, in contrast to the contralateral, in blue); right V4 with normal direction flow (*F*); biphasic flow at proximal basilar (*G*, *arrow*), as part of the flow from right V4 goes to left V4, and part follows to distal basilar; distal basilar with normal flow direction (*H*).

AV = vertebral artery; dta = right side; esq = left side; INV = inverted flow.

COMMENT

This case exemplifies how useful a noninvasive ultrasound cerebrovascular examination can be for timely detection of lesions, leading to targeted therapeutic and preventive treatments.

Copyright © American Academy of Neurology. Unauthorized reproduction of this article is prohibited.

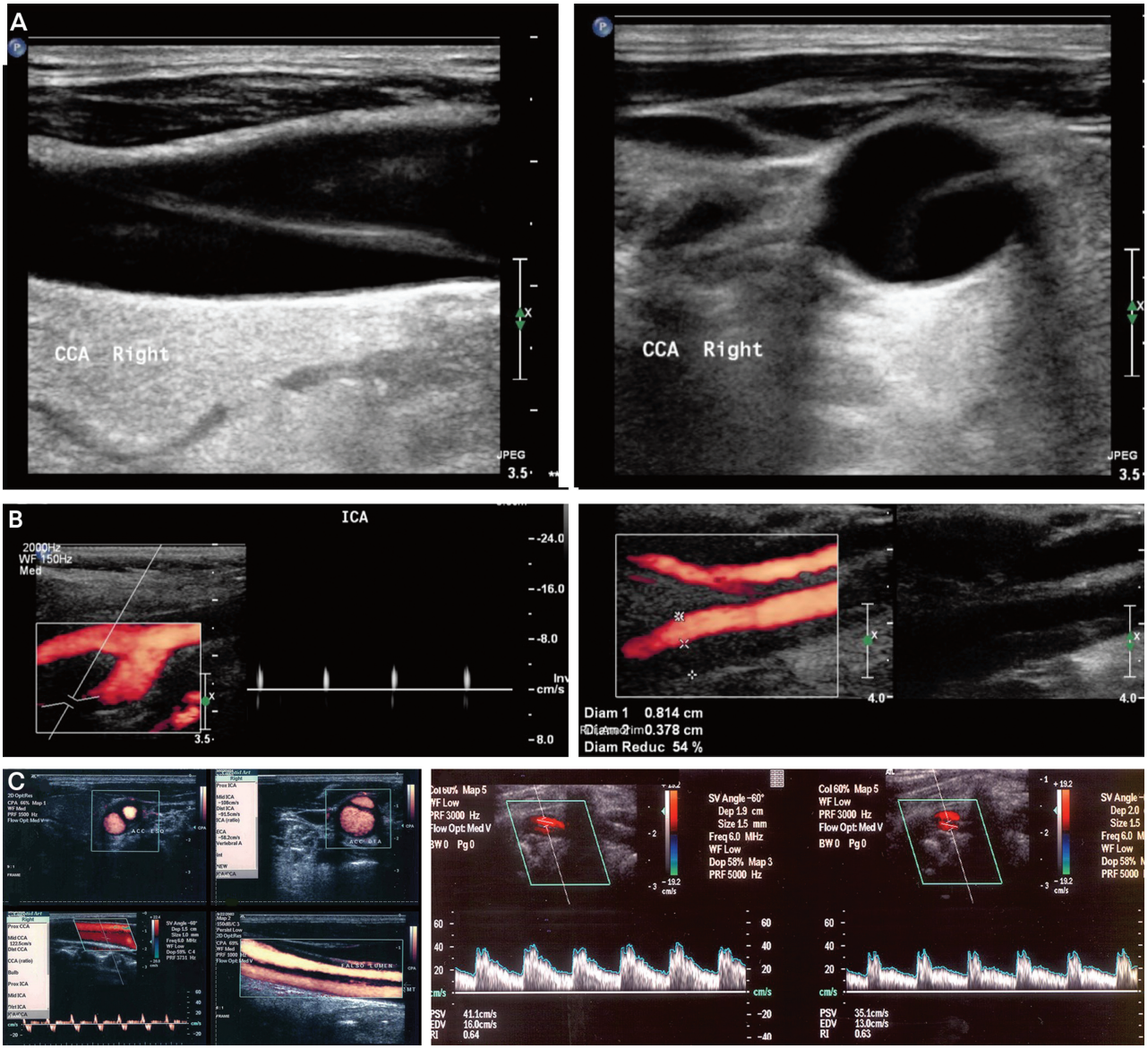

FIGURE 12-7

Examples of cervical carotid and vertebral dissection. *A*, Common carotid artery (CCA) dissection as an extension of aortic dissection; also see VIDEO 12-1 and VIDEO 12-2 with a floating intimal flap. *B*, Internal carotid artery (ICA) dissection with postbulbar occlusion (*left*) and with hypoechogenic tapering distal cervical stenosis (*right*). *C*, CCA (*left*) and vertebral (*right*) dissections with a double lumen.

Panel C reprinted with permission from Azevedo E and Castro P.[7] © 2014 John Wiley & Sons, Inc.

resulting in arterial stenosis, occlusion, aneurysm, or dissection. It most commonly affects the renal and extracranial carotid and vertebral arteries, where it can cause headache or pulsatile tinnitus. Ultrasonography may reveal the characteristic alternation of stenoses and dilations, causing a string-of-beads appearance, associated with velocity shifts in the mid to distal cervical internal carotid artery and the vertebral arteries. Although a sinusoidal curve in the internal carotid artery is not specific to fibromuscular dysplasia, its presence on a carotid ultrasonogram in a patient younger than 70 years of age should alert to the possibility of fibromuscular dysplasia.[12]

Copyright © American Academy of Neurology. Unauthorized reproduction of this article is prohibited.

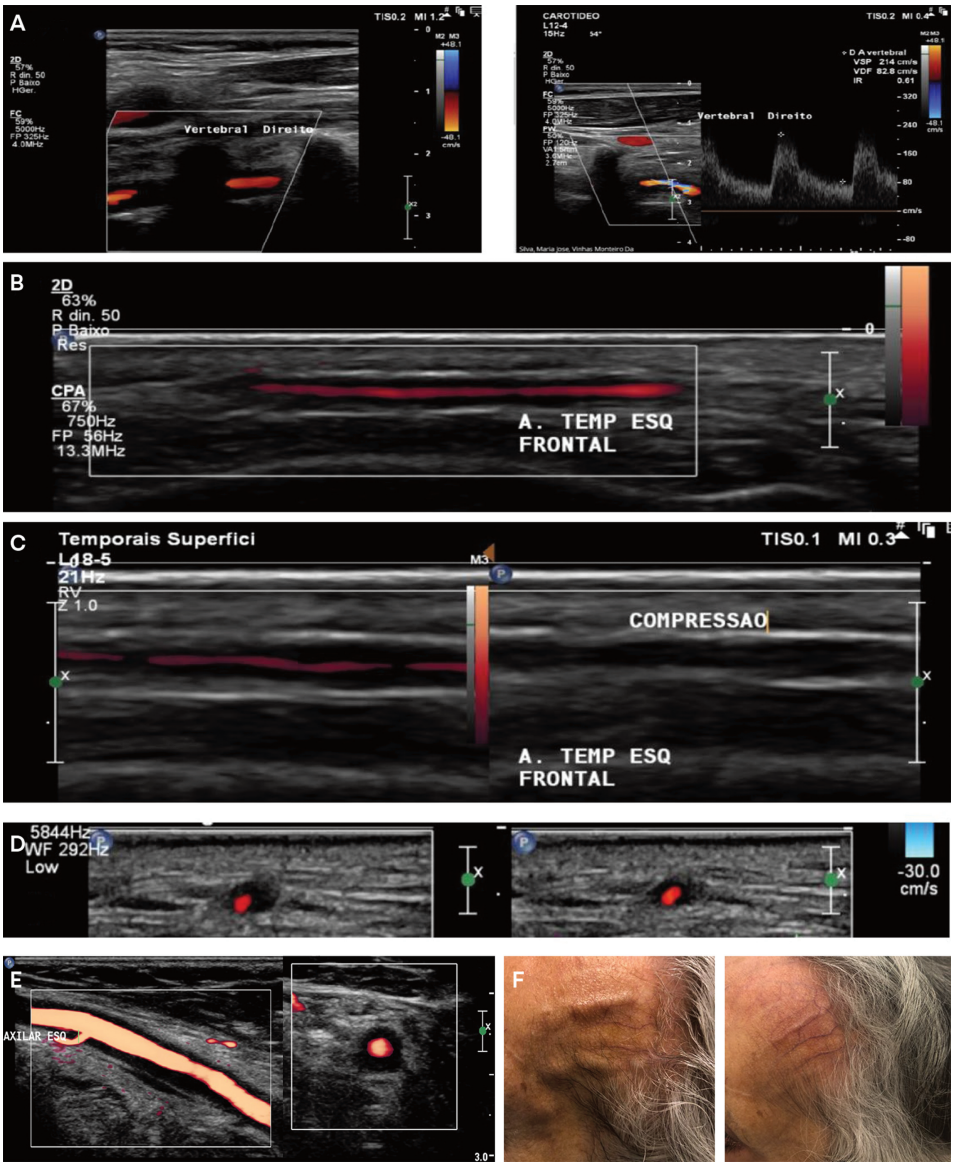

FIGURE 12-8

Examples of the halo sign in giant cell arteritis in an older woman with a vertebrobasilar stroke and high inflammatory biomarkers. *A*, Concentric hypoechogenic thickness of the vertebral artery walls, in some segments associated with a blood flow velocity acceleration, which is suggestive of vasculitis. *B*, The superficial temporal arteries also showed concentric hypoechogenic thickness of the walls that was suggestive of giant cell arteritis. *C*, Compression led to the disappearance of the residual lumen, but the wall thickness was maintained. *D*, The typical halo sign in a cross-sectional view. *E*, An axillary artery was also affected and shows the typical halo sign. *F*, Appearance of the branches of the temporal artery before (*left*) and after (*right*) starting corticosteroid treatment.

KEY POINTS

- **Fibromuscular dysplasia is suspected by a string-of-beads appearance in the distal cervical internal carotid artery and the vertebral arteries.**
- **Carotid webs are potentially thrombogenic and may be implicated in ischemic stroke. Sonographically it appears as a shelf-like membrane in the posterior aspect of the internal carotid artery bulb into the lumen, just beyond the carotid bifurcation.**

Carotid webs, shown in FIGURE 12-10, are rare variants of fibromuscular dysplasia, defined as a thin, linear membrane that extends from the posterior aspect of the internal carotid artery bulb into the lumen, located just beyond the carotid bifurcation. It is highly thrombogenic and may be implicated in ischemic stroke. Carotid ultrasonography may detect the carotid web as a shelf-like echogenic lesion, although conventional angiography remains the

Copyright © American Academy of Neurology. Unauthorized reproduction of this article is prohibited.

gold standard examination. Meticulous sonographic technique, appropriate education, and a high index of suspicion are necessary to differentiate the carotid web from arterial dissection, focal atherosclerotic plaque, and mural thrombus.[13,14]

ARTERIOVENOUS SHUNTS. Doppler ultrasonography can reveal signs of arteriovenous pathologic shunts. Normally, the internal carotid artery has a lower resistance than the external carotid artery. When the external carotid artery demonstrates high velocity and low resistance, one of its branches might be involved in an arteriovenous shunt, namely a fistula between the occipital artery and a dural sinus (FIGURE 12-11). The same type of hemodynamic changes can raise the suspicion of arteriovenous shunts in other vessels. Ultrasound screening for dural arteriovenous fistula in patients with pulsatile tinnitus revealed sensitivity, specificity, and positive and negative predictive values of 96%, 100%, 100%, and 98%, respectively. The isolated use of a low external carotid artery resistance index showed a sensitivity of 81%.[15,16] These data are summarized in TABLE 12-5.

Intracranial Neurovascular Ultrasonography

Even with transcranial color sonography, it is not possible to study the intracranial arterial wall with ultrasonography. However, TCD and transcranial color sonography contribute important hemodynamic information to the understanding of clinical situations and are also tools for research. At an intracranial level, vascular ultrasonography mainly allows for the detection of flow direction, the measurement of blood flow velocities, and some hemodynamic indices in the main basal arteries of the brain.

COMPENSATORY INTRACRANIAL COLLATERAL CIRCUITS OF PROXIMAL STENO-OCCLUSIVE DISEASE. TCD and transcranial color sonography allow for the detection of intracranial arterial stenosis and occlusions and the hemodynamic effects of downstream and upstream disease.

In the setting of an extracranial carotid and vertebral stenosis or occlusion, TCD and transcranial color sonography can identify compensatory intracranial collateral circuits. The following may be seen in the setting of carotid steno-occlusive disease: an inversion of ophthalmic flow direction perfused by branches

TABLE 12-4

Cutoff Values for Ultrasonography Intima-Media Thickness in Giant Cell Arthritis

Anatomic region	Cutoff intima-media thickness, mm
Common superficial temporal artery (TA)	0.42
Frontal branch of TA	0.34
Parietal branch of TA	0.29
Axillary artery	1.0

[a] Reprinted with permission from Schafer VS, et al, Rheumatology (Oxford).[9] © 2017 Oxford University Press.

Copyright © American Academy of Neurology. Unauthorized reproduction of this article is prohibited.

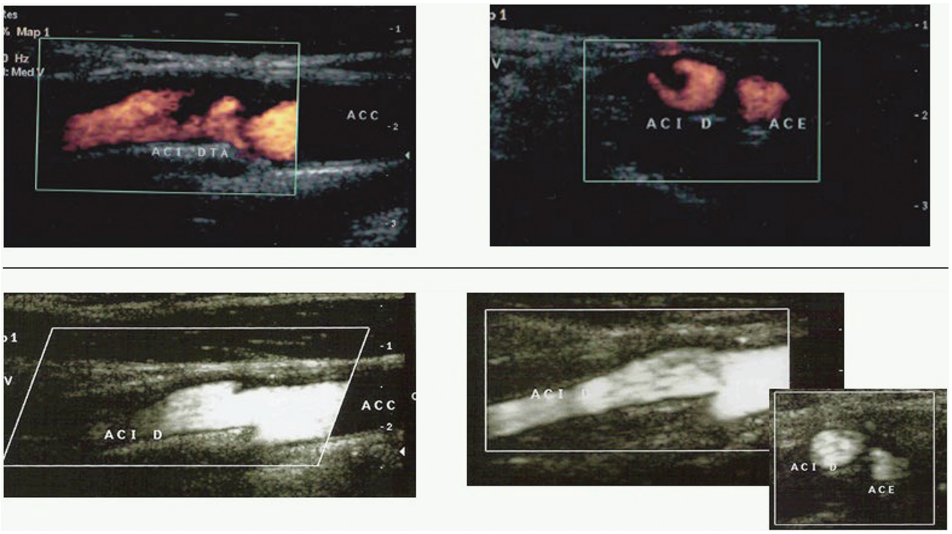

FIGURE 12-9

Floating mural thrombi in the absence of atherosclerosis. A 36-year-old woman was admitted 48 hours after having an acute left faciobrachial paresis due to a cortical frontal ischemic stroke. *Top*, Ultrasonography showed, in the right carotid artery, mobile mural material suggestive of nonocclusive thrombi, homogeneously hypoechogenic, and a relatively narrow wall pedicle. An anticoagulant was prescribed. *Bottom*, Spontaneous revascularization occurred after 1 week, and treatment was shifted to aspirin.

ACC = common carotid artery; ACE = external carotid artery; ACI = internal carotid artery; DTA = right side.

KEY POINTS

- **When the external carotid artery shows high velocity and low resistance, an arteriovenous shunt may be suspected, especially in a patient with pulsatile tinnitus.**
- **The thrombolysis in brain ischemia score helps in evaluation of the flow conditions in the symptomatic intracranial artery in acute ischemic stroke, namely before and after recanalization treatment.**
- **Systolic and mean blood flow velocity cut-offs help diagnose intracranial stenosis and stratify it as <50%, >50%, and >70%.**

of the external carotid artery, an inversion of flow direction in the A1 segment of the anterior cerebral artery of the affected side and acceleration in the contralateral (collateralization through the anterior communicating artery), and collateralization through the ipsilateral posterior communicating artery (marked by increase blood flow velocity in the P1 segment of posterior carotid artery). For cervical vertebral steno-occlusive disease, an inversion of flow direction in the distal intracranial vertebral artery, perfused by the contralateral vertebral artery, may be seen.

THROMBOLYSIS IN BRAIN ISCHEMIA SCORE. In the setting of hyperacute ischemic stroke, the TCD thrombolysis in brain ischemia score relates the spectral Doppler wave with the distance to the point of arterial occlusion or identifies a local significant stenosis (FIGURE 12-12). Thrombolysis in brain ischemia waveforms are graded according to flow as follows: 0, absent; 1, minimal; 2, blunted; 3, dampened; 4, stenotic; and 5, normal. This score is useful for monitoring intracranial large vessel occlusion, recanalization, or even an eventual reocclusion, in acute stroke.[17]

INTRACRANIAL STENOSIS. Intracranial stenosis is detected by a focal systolic-diastolic acceleration of blood flow velocity. Comparing data from transcranial color sonography and catheter angiography allows cutoff systolic blood flow velocity values for intracranial stenosis, reliably being able to detect 50% or greater and less than 50% basal cerebral artery narrowing (TABLE 12-6).[18] Other authors have validated mean blood flow velocity detected by TCD with angiographic changes. They have also highlighted the importance of the ratio between blood flow velocity in the most stenotic point and the previous

Copyright © American Academy of Neurology. Unauthorized reproduction of this article is prohibited.

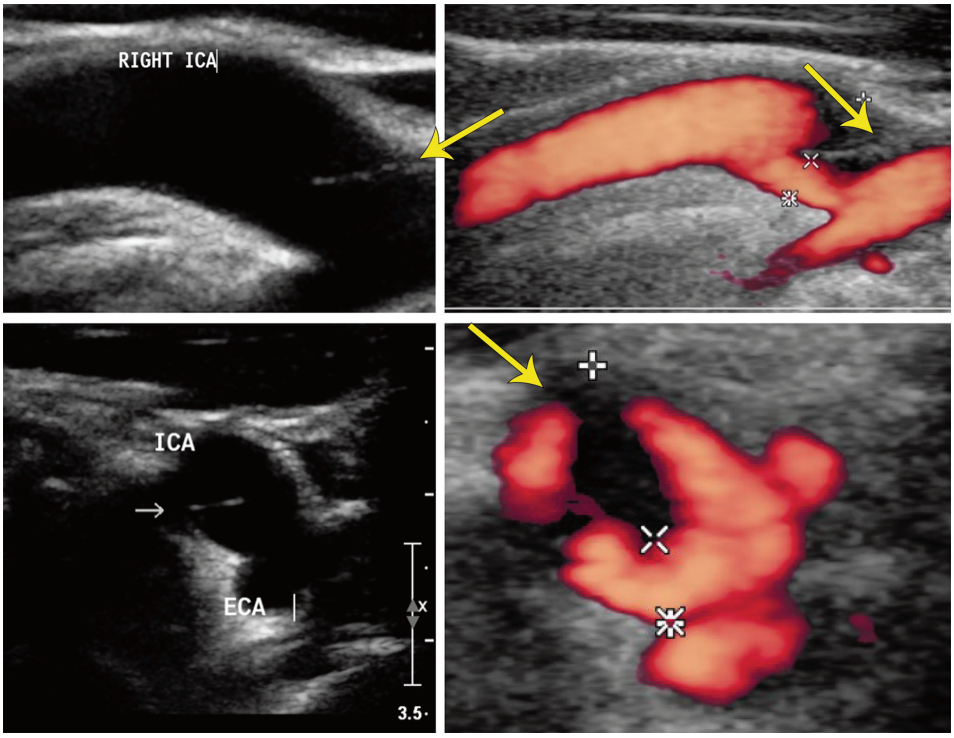

FIGURE 12-10

Carotid web in a 42-year-old woman with a middle cerebral artery ischemic stroke successfully treated with thrombectomy. Ultrasonography revealed a thin, linear, protruding membrane in the posterior aspect of the internal carotid artery (ICA) bulb (*arrows*). *Top*, Longitudinal view. *Bottom*, Cross-sectional view.

ECA = external carotid artery.

lesion-free segment (a ratio greater than 2 related to more than 50% stenosis, greater than 3 related to more than 70% stenosis), as shown in TABLE 12-7.[19]

Nevertheless, if a stenosis occurs after another critical stenosis, blood flow velocity might not proportionally increase, and if the lumen is long and narrow, rather than focally narrow, the blood flow velocity might be decreased instead.[20]

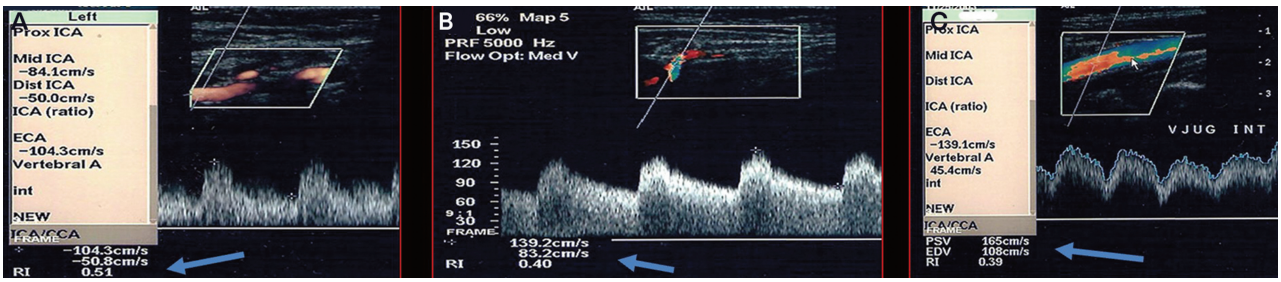

FIGURE 12-11

Ultrasonography from a patient with pulsatile tinnitus and a dural arteriovenous fistula. *A*, External carotid artery (ECA) with a low resistance flow (resistance index 0.51; *arrow*). *B*, The ECA's occipital branch demonstrated higher velocities and even lower resistance index (0.40; *arrow*). *C*, Ipsilateral jugular vein with high-velocity flow, draining the fistula (*arrow*).

CCA = common carotid artery; ICA = internal carotid artery.

Copyright © American Academy of Neurology. Unauthorized reproduction of this article is prohibited.

A middle cerebral artery branch occlusion can be suspected when the M1 segment has lower blood flow velocity than the ipsilateral anterior cerebral artery and contralateral M1 segment. TCD or transcranial color sonography can detect stenosis or occlusion of intracranial vessels in patients with acute ischemic stroke with high sensitivity and specificity, and guide the need for more invasive vascular neuroimaging.[21]

However, ultrasound diagnosis of an intracranial stenosis does not specify its nature (eg, atherosclerotic or other). Factors favoring an atherosclerotic nature are very focal blood flow velocity acceleration, the absence of short-term relevant fluctuations of blood flow velocity, and the presence of atherosclerotic pathology in extracranial vessels. Factors favoring nonatherosclerotic vasculopathy (embolus, dissection, vasospasm, vasculitis) include changing blood flow velocity over time, within days to a few months.

Some findings are suggestive of a cardioembolic source of emboli[22]: a nonlacunar stroke syndrome, absence of extracranial atherosclerosis, initial documentation of stenosis or occlusion in the middle cerebral artery or basilar bifurcation with early (hours to a few days) spontaneous recanalization, and documentation of microembolic signals to bilateral vessels of the cerebral circulation. The diagnosis of patent foramen ovale (PFO) with TCD is described later in this article.

Regarding intracranial vasculitis, one of the sonographic clues to the diagnosis is finding segmental blood flow velocity acceleration in different vessels, especially if no atherosclerosis is present in cervical vessels and if it is a dynamic process with velocities changing in the short term. Although rare in adults, intracranial vasculitis is an important cause of stroke in children, sometimes associated with infections as in the case of tuberculous cerebral vasculitis shown in CASE 12-2, where transcranial color sonography helped detect the focal vascular changes.

Another rare cause of intracranial steno-occlusive disease is moyamoya disease, found mostly in the Asian population, although a moyamoyalike phenomenon (moyamoya syndrome) is sometimes associated with other conditions. With ultrasonography, suspicion for this syndrome is raised with occlusion or tight stenosis of the distal intracranial internal carotid artery or even

Ultrasonographic Criteria for Arteriovenous Fistula[a] TABLE 12-5

General suspicion of an arteriovenous fistula

- Artery with increased velocity and decreased resistance index
- Artery with decreased resistance index compared to the other side
- Increased jugular vein drainage on the same side

Suspicion of dural arteriovenous fistula

- Resistance index in external carotid artery (ECA) < 0.7 and resistance index in internal carotid artery (ICA)/ECA > 0.9 (sensitivity, 55%; specificity, 88%)[14]
- Diastolic velocity in the ECA > 21 cm/s[16]

[a] Data from Tsai LK, et al, Ultrasound Med Biol.[15]

Copyright © American Academy of Neurology. Unauthorized reproduction of this article is prohibited.

Grade 0: Absent	Absent flow signals are defined by the lack of regular pulsatile flow signals despite varying degrees of background noise
Grade 1: Minimal	Systolic spikes of variable velocity and duration Absent diastolic flow during all cardiac cycles based on a visual interpretation of periods of no flow during end diastole; reverberating flow is a type of minimal flow
Grade 2: Blunted	Flattened systolic flow acceleration of variable duration compared to control Positive end diastolic velocity and pulsatility index <1.2
Grade 3: Dampened	Normal systolic flow acceleration Positive end diastolic velocity Decreased mean flow velocities (MFV) by >30% compared to control
Grade 4: Stenotic	MFV of >80 cm/s AND velocity difference of >30% compared to the control side or If both affected and comparison sides have MFV <80 cm/s due to low end diastolic velocities, MFV >30% compared to the control side AND signs of turbulence
Grade 5: Normal	<30% mean velocity difference compared to control Similar waveform shapes compared to control

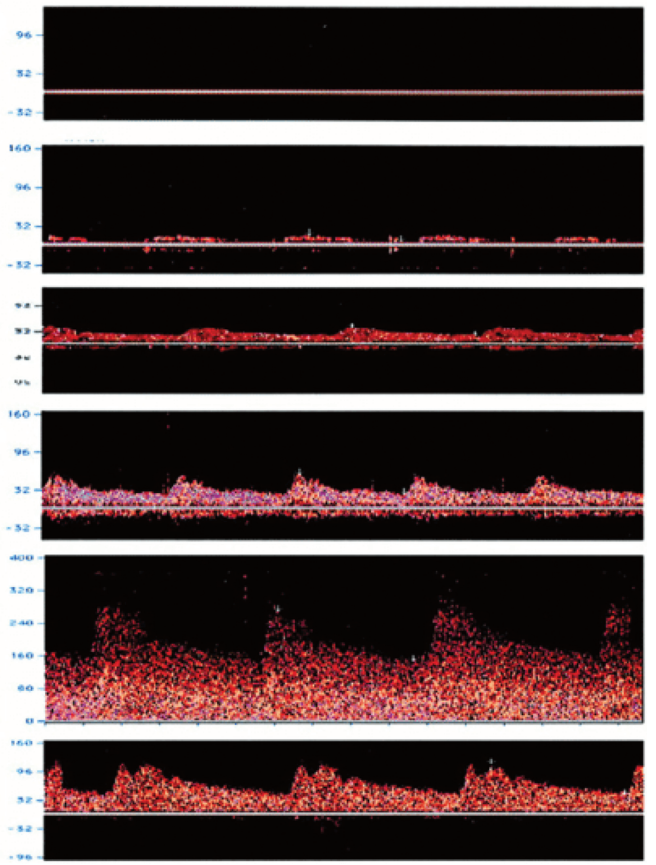

FIGURE 12-12
Thrombolysis in brain ischemia score.
Reprinted with permission from Demchuk AM, et al, Stroke.[17] © 2001 American Heart Association.

at the ostium of the middle cerebral artery and anterior cerebral artery. The changes are often bilateral.

SICKLE CELL DISEASE. The STOP (Stroke Prevention Trial in Sickle Cell Anemia) trial demonstrated that screening children with TCD and treating those with abnormal TCD velocities with regular blood transfusion may result in a 10-fold decrease in the prevalence of strokes in children.[23] The burden of neurologic complications of sickle cell disease in Africa is most likely underestimated.[24]

The threshold for regular blood transfusion therapy is two nonimaging TCD measurements of 200 cm/s or greater time-averaged mean of the maximum blood flow velocity measurement or a single TCD measurement greater than 220 cm/s in the proximal portion of the middle cerebral artery or the distal portion of the internal carotid artery. As recommended by the American Society of Hematology, annual TCD screening should be offered for children (aged 2 to 16 years) with sickle cell disease of the type *HbSS* (those with two genes, one from each parent, that code for hemoglobin S) or of the type Sβ0 (sickle beta 0) thalassemia.[25]

SUBARACHNOID HEMORRHAGE. Patients with subarachnoid hemorrhage (SAH) are at risk of delayed cerebral ischemia and cerebral infarction, usually occurring between days 4 and 14. Focal hypoperfusion from reversible cerebral arterial

Copyright © American Academy of Neurology. Unauthorized reproduction of this article is prohibited.

Cutoff Peak Systolic Blood Flow Velocity Values for Intracranial Stenosis by Transcranial Color Sonography[a]

TABLE 12-6

	Ultrasonography					Angiography	
	PSV cutoff, cm/s	Sensitivity, %	Specificity, %	Positive predictive value, %	Negative predictive value, %	Number of patients studied	Mean ± SD degree (range)
Ultrasonic detection of ≥50% intracranial stenoses (n = 31) with angiography as standard of reference							
ACA	≥155	100	100	100	100	4	60 ± 8 (52-71)
MCA	≥220	100	100	100	100	11	67 ± 11 (50-80)
PCA	≥145	100	100	100	91	10	63 ± 7 (50-72)
BA	≥140	100	100	100	100	3	67 ± 14 (53-85)
VA	≥120	100	100	100	100	3	69 ± 14 (55-84)
Ultrasonic detection of <50% intracranial stenoses (n = 38) with angiography as standard of reference							
ACA[b]	≥120	100	99	73	100	5	38 ± 12 (20-47)
MCA	≥155	94	100	95	100	18	36 ± 8 (22-48)
PCA	≥100	100	100	100	100	5	29 ± 12 (13-41)
BA	≥100	100	100	100	100	4	33 ± 4 (29-37)
VA	≥90	100	100	100	100	5	32 ± 6 (25-39)

ACA = anterior cerebral artery; BA = basilar artery; MCA = middle cerebral artery; PCA = posterior cerebral artery; PSV = peak systolic velocity; VA = vertebral artery.

[a] Modified with permission from Baumgartner RW, et al, Stroke.[18] © 1999 American Heart Association.

[b] One stenosed anterior cerebral artery was missed because of an inadequate temporal bone window.

Cutoff Mean Blood Flow Velocity Values for Intracranial Stenosis by Transcranial Doppler[a]

TABLE 12-7

Artery	Stenosis ≥ 50% (MFV, SPR)	Stenosis ≥ 70% (MFV, SPR)
Middle cerebral artery	≥ 100 cm/s, ≥2	≥ 120 cm/s, ≥3
Anterior cerebral artery	≥ 80 cm/s, ≥2	Not applicable, ≥3
Posterior cerebral artery	≥ 80 cm/s, ≥2	Not applicable, ≥3
Basilar artery	≥ 90 cm/s, ≥2	≥ 110 cm/s, ≥3
Vertebral artery	≥ 90 cm/s, ≥2	≥ 110 cm/s, ≥3

MFV = mean flow velocity; SPR = stenotic/prestenotic mean flow velocity ratio.

[a] Data from Zhao L, et al, Stroke.[19]

Copyright © American Academy of Neurology. Unauthorized reproduction of this article is prohibited.

CASE 12-2

A 20-month-old girl had recurrent fever in the previous 4 months, weight loss, and cervical lymphadenopathy. After worsening lethargy, irritability, and vomiting over several days, she was brought to the emergency department. Neurologic examination disclosed altered mental status and signs of meningeal irritation. Brain MRI showed focal punctiform restriction of diffusion on the DWI study (FIGURE 12-13). CSF findings included elevated total nucleated cell count (108 cells/mm^3), with neutrophil predominance (71%), elevated total protein level (85 mg/dL), and reduced glucose level (26 mg/dL). In transcranial color sonography, blood flow velocity showed several changes, namely abnormally increased velocity in the left A1 segment and low velocity in the right P2 segment, predicting ischemic lesions that were later seen on head CT. The overall picture suggested cerebral vasculitis. An interferon gamma release assay, tuberculin skin test, and *Mycobacterium tuberculosis* polymerase chain reaction (PCR) sputum smears were positive. The child started antituberculosis therapy with isoniazid, rifampin, pyrazinamide, and ethambutol.

COMMENT

This case exemplifies the usefulness of monitoring cerebral hemodynamics in neurocritical care patients in whom the clinical course may be dynamic. This evaluation is complementary to other neuroimaging examinations, increasing the overall understanding of the ongoing pathophysiology.

Copyright © American Academy of Neurology. Unauthorized reproduction of this article is prohibited.

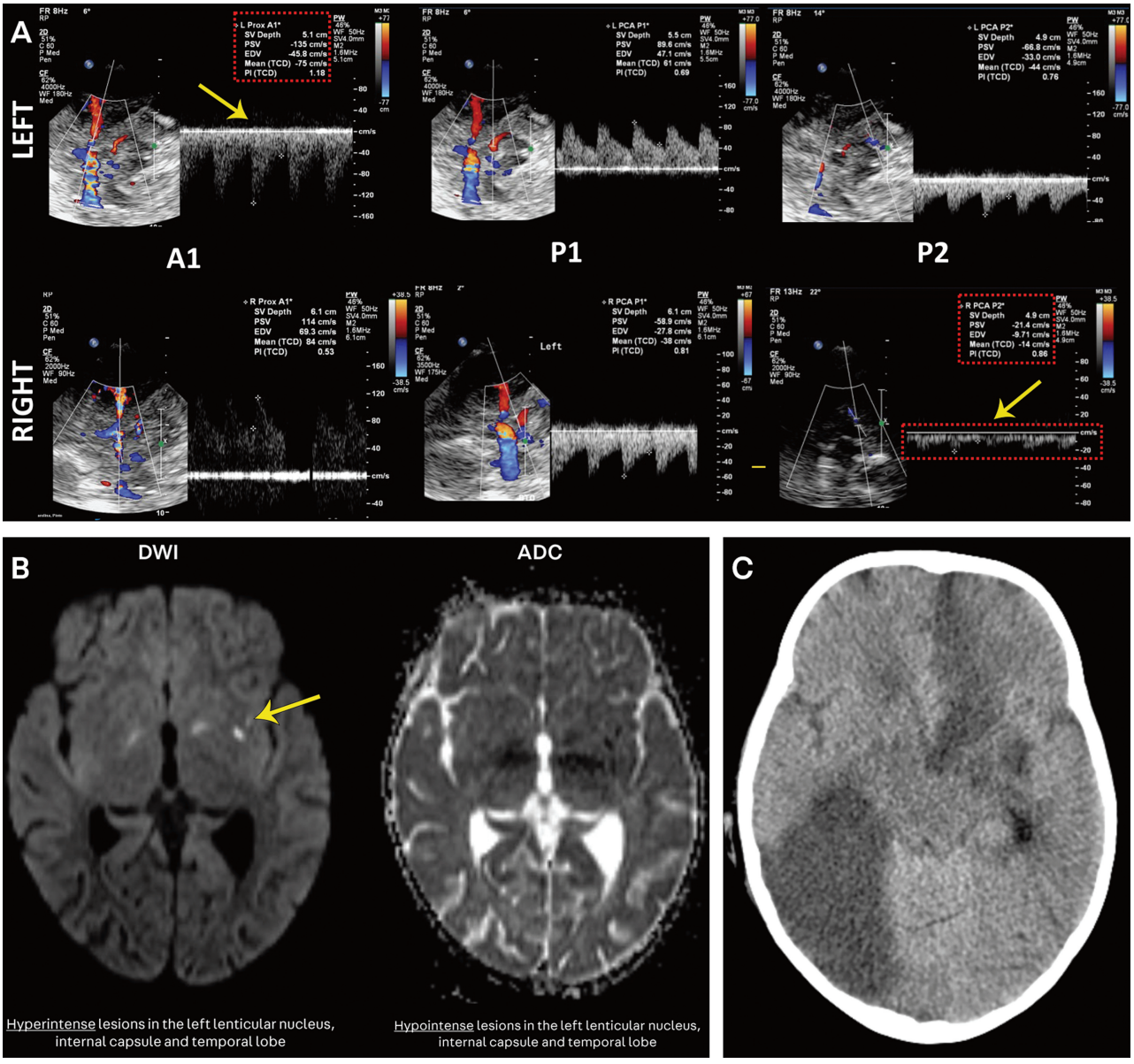

FIGURE 12-13

Imaging from the patient in CASE 12-2. Tuberculous cerebral vasculitis shown in the initial transcranial color sonography with high velocity in the left anterior cerebral artery suggestive of stenosis and low velocity in the right posterior cerebral artery suggestive of a distal lesion (*A*, *arrows*). Initial axial diffusion-weighted (DWI) (*arrow*) and apparent diffusion coefficient (ADC) MRI (*B*), and axial CT scan (*C*) 7 days after admission, with global edema and bigger infarct areas in the left anterior cerebral artery and right posterior cerebral artery territories.

Copyright © American Academy of Neurology. Unauthorized reproduction of this article is prohibited.

vasospasm due to exposure of the arteries to perivascular blood is likely to play a relevant causal role. Although angiography is the gold standard for detecting vasospasm, TCD evidence of vasospasm is a good predictor of delayed cerebral ischemia in aneurysmal SAH, with a 90% sensitivity and 71% specificity.[26] TCD is more appropriate for repetitive screenings with the American Heart Association/American Stroke Association guidelines recommending it as a technique for monitoring vasospasm.[27]

Vasospasm causes a blood flow velocity increase in the affected segments. To correctly distinguish it from other physiologic and pathologic conditions that could result in elevated blood flow velocity, such as hyperemia and hypertension, a hemispheric ratio of the mean blood flow velocity in the middle cerebral artery and distal ipsilateral extracranial internal carotid artery is applied (TABLE 12-8).[28] Elevations of blood flow velocity in both the middle cerebral artery and internal carotid artery would result in a hemispheric ratio less than 3, whereas vasospasm would preferentially elevate middle cerebral artery blood flow velocity. Vasospasm is considered mild if the hemispheric ratio is 3 to 6 and severe if it is greater than 6. Regarding the posterior circulation, the detection of more than 50% vasospasm in the basilar artery with a mean blood flow volume greater than 85 cm/s and a modified ratio (basilar artery/vertebral artery) greater than 3 have been shown to have a sensitivity of 92% and specificity of 97%.[29] TABLE 12-8 and TABLE 12-9 show TCD vasospasm criteria in SAH,[28] and FIGURE 12-14 illustrates sequential blood flow velocity changes due to vasospasm in a case of SAH.

Cerebral ultrasound perfusion imaging has been recently found to be a feasible technique to detect cerebral hypoperfusion after SAH, which might lead to

TABLE 12-8

Transcranial Doppler Vasospasm Criteria for the Middle Cerebral Artery[a]

Mean flow velocity (MFV), cm/s	Middle cerebral artery/internal carotid artery MFV ratio	Interpretation
<120	≤3	Hyperemia
>80	3-4	Hyperemia + possible mild spasm
≥120	3-4	Mild spasm + hyperemia
≥120	4-5	Moderate spasm + hyperemia
≥120	5-6	Moderate spasm
≥180	6	Moderate to severe spasm
≥200	≥6	Severe spasm
>200	4-6	Moderate spasm + hyperemia
>200	3-4	Hyperemia + mild (often residual) spasm
>200	<3	Hyperemia

[a] Reprinted with permission from Alexandrov AV.[28] © 2004 John Wiley & Sons.

Copyright © American Academy of Neurology. Unauthorized reproduction of this article is prohibited.

delayed cerebral ischemia.[30] TCD is also useful for follow-up hemodynamics after endovascular intervention in vasospasm.

REVERSIBLE VASOCONSTRICTION SYNDROME. TCD can diagnose vasoconstriction related to reversible vasoconstriction syndrome (RCVS) in the proximal cerebral arteries, although it often fails when the affected arteries are more distal. Follow-up monitoring of blood flow velocity using TCD may help identify patients with more extensive vasoconstriction and higher risk of developing neurologic complications related to RCVS.[31] Velocities are not usually as high as in SAH vasospasm (only a minority have mean blood flow velocity in the middle cerebral artery greater than 120 cm/s and a hemispheric ratio greater than 3), but they maintain a high plateau at the mean time of headache remission (day 22) and remain abnormal even 10 days after headache resolution,[32] so monitoring the blood flow velocity changes in the time course may be more useful than the isolated values.

THERAPY MONITORING WITH TRANSCRANIAL DOPPLER. Cerebral hemodynamic monitoring is an important application of ultrasonography. Beyond monitoring hemodynamic changes during acute stroke and in the neurocritical setting, TCD permits real-time monitoring of the effect of drugs and other treatments, such as thrombolytic and endovascular therapy in acute ischemic stroke or antiedematous measures in the intensive care patient. TCD also allows for monitoring of emboli and changes in perfusion during interventions such as carotid revascularization and cardiac surgery. A higher blood flow velocity in a successfully recanalized middle cerebral artery, compared with the contralateral side, indicates a risk for postinterventional intracerebral hemorrhage and worse prognosis.[33]

INTRACRANIAL HYPERTENSION AND CEREBRAL CIRCULATORY ARREST. Although TCD and transcranial color sonography do not allow for measurement of intracranial pressure (ICP) itself, they can provide indirect information regarding changes in ICP. In normal conditions and as an organ of low resistance, the brain is well

Transcranial Doppler Vasospasm Criteria for Intracranial Arteries[a] TABLE 12-9

	Arterial mean flow velocity, cm/s		
	Possible vasospasm	Probable vasospasm	Definite vasospasm
Internal carotid artery	>80	>110	>130
Anterior cerebral artery	>90	>110	>120
Posterior cerebral artery	>60	>80	>90
Basilar artery	>70	>90	>100
Vertebral artery	>60	>80	>90

[a] Reprinted with permission from Alexandrov AV.[28] © John Wiley & Sons.

Copyright © American Academy of Neurology. Unauthorized reproduction of this article is prohibited.

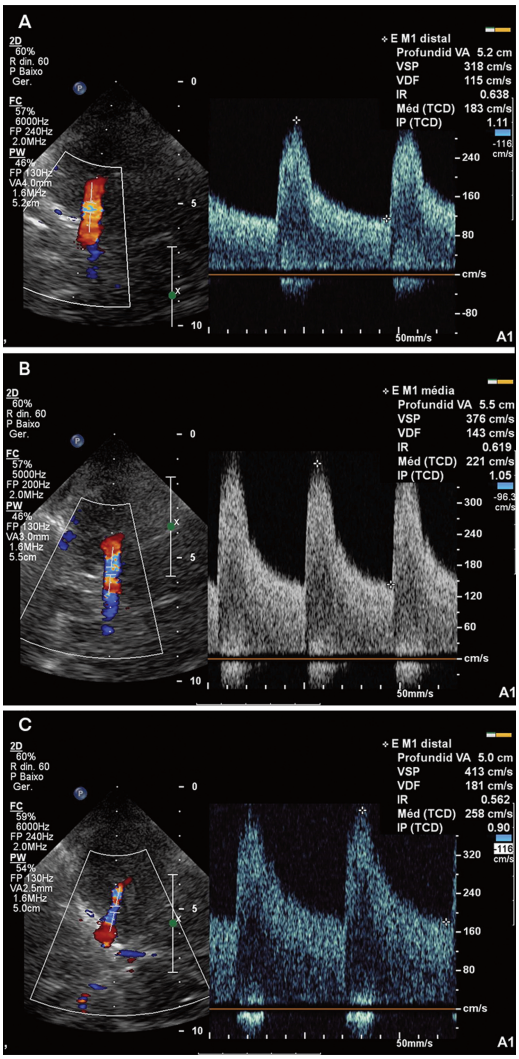

FIGURE 12-14
A case of subarachnoid hemorrhage with a sequential velocity increase due to vasospasm on days 7 (*A*), 9 (*B*), and 11 (*C*).

perfused during the full cardiac cycle. As ICP increases, the cerebral blood flow velocity during diastole decreases, disappears, and even reverses; systolic blood flow velocity also decreases. When positive diastolic blood flow velocity is still present in the main cerebral arteries, increasing blood pressure and decreasing ICP might improve cerebral blood flow and eventually the clinical condition. At least 30 minutes without diastolic positive blood flow velocity and decreased systolic blood flow velocity in both middle cerebral arteries and the basilar artery indicates cerebral circulatory arrest, and clinical brain death tests will likely be positive.[34] TABLE 12-10 shows the criteria for cerebral circulatory arrest by TCD, and FIGURE 12-15 shows a case of cerebral circulatory arrest.

Limitations of this examination might be poor bone windows for ultrasonography and distortion of vascular structures. In cases of very high intracranial hypertension and no detectable intracranial flow with TCD and transcranial color

TABLE 12-10 **Criteria for Cerebral Circulatory Arrest by Transcranial Doppler[a]**

- Biphasic flow with diastolic reflux
- Flow only with protosystolic peaks with velocity lower than 50 cm/s
- Flow with an intermediate pattern between the two criteria above

[a] Any of the three flow patterns in the table might be present in cerebral circulatory arrest diagnosis by transcranial Doppler. To achieve criteria for cerebral circulatory arrest, any of these flow patterns should be recorded in three intracerebral arteries from different territories, in both carotid territories (usually in the middle cerebral arteries) and in the vertebrobasilar (usually in the basilar artery). If the blood flow velocity cannot be registered with transcranial Doppler because of excessive intracranial pressure, the above criteria might be found in cervical internal carotid and vertebral arteries. This pattern should be continuously present for at least 30 minutes.

Copyright © American Academy of Neurology. Unauthorized reproduction of this article is prohibited.

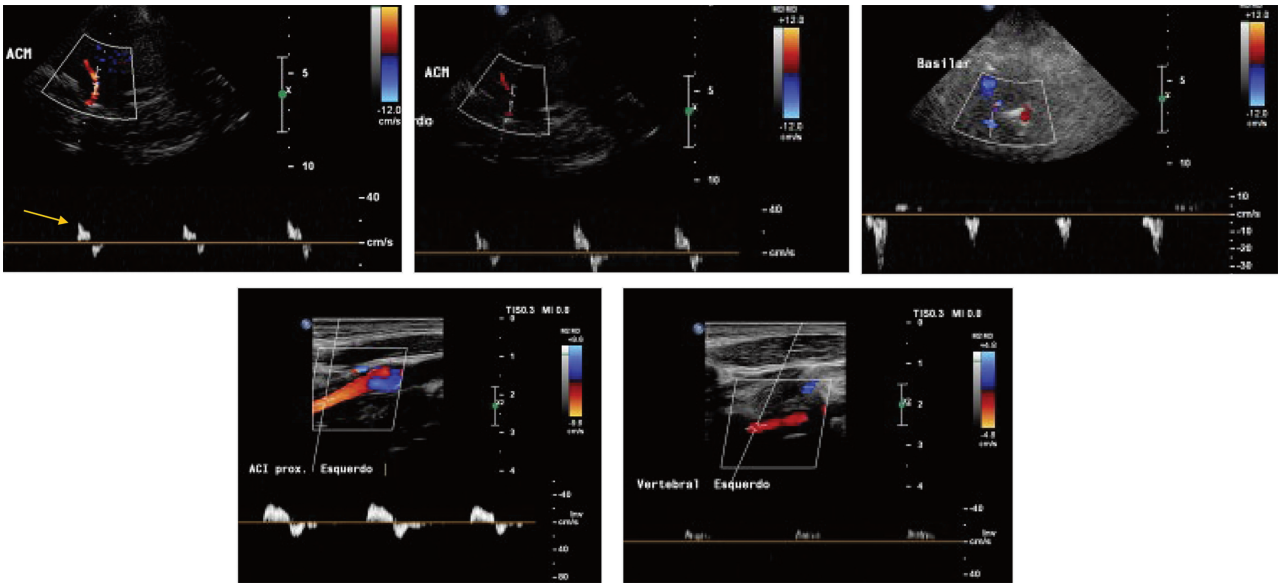

FIGURE 12-15

Cerebral circulatory arrest ultrasonography shows only protosystolic peaks with a velocity lower than 50 cm/s and the absence of diastolic flow (*arrow*) in both the middle cerebral (ACM) and basilar arteries (*top*) and in extracranial internal carotid (ACI) and vertebral arteries (*bottom*).

sonography, the flow patterns referred to earlier can be observed in extracranial carotid and vertebral artery color Doppler sonography.

Although ultrasonography is not influenced by central nervous system depressants, it is influenced by the patient's hemodynamic status, $PaCO_2$, and temperature. Therefore, the examination should be performed with systolic blood pressure greater than 90 to 100 mm Hg, with PCO_2 35 to 45 mm Hg, and temperature greater than 32°C (89.6°F).

TCD and transcranial color sonography have approximately 100% specificity for cerebral circulatory arrest confirmation, provided they are performed by an experienced operator with the aforementioned criteria and in the context of suspected clinical brain death. Sensitivity is approximately 90% because false negatives may be associated with irreversible brainstem damage without a major impact on ICP.[35]

TCD and transcranial color sonography are not validated for diagnosis of cerebral circulatory arrest in children, although the findings are similar.[36]

TCD can be used to support a diagnosis of brain death in patients on extracorporeal membrane oxygenation who have sufficient cardiac contractility or an intra-aortic balloon pump to produce pulsatile flow. TCD utility in patients on extracorporeal membrane oxygenation who have low left ventricular ejection fraction needs further study.[37]

Beyond the blood flow velocity features, brain and eye sonography also contribute to the evaluation of a patient with elevated ICP, informing eventual midline shift with space-occupying lesions, and optic nerve changes (see the Neuro-orbital Ultrasonography section).

TRANSCRANIAL DOPPLER FOR DIAGNOSIS OF RIGHT-TO-LEFT CARDIAC SHUNT. PFO is present in approximately 25% of the general population and can be a cause of

Copyright © American Academy of Neurology. Unauthorized reproduction of this article is prohibited.

stroke through a paradoxical cerebral embolism. TCD and a nontranspulmonary gaseous contrast injection is a reliable and less invasive alternative to the gold standard transesophageal echocardiography (TEE) for diagnosis of PFO and enables the detection of eventual extracardiac right-to-left shunt. A well-agitated mixture of 9 mL of saline and 1 mL of air, in a three-way stopcock, is injected into the brachial vein. The examination is performed during the resting state and, unless strongly positive, repeated after the Valsalva maneuver.

In the presence of a right-to-left shunt, the contrast bypasses the pulmonary circulation and causes microembolic signals (high-intensity signals of short duration) to be detected in the middle cerebral artery by TCD, visualized in the velocity spectrum, and heard as "blips" seconds after the injection (FIGURE 12-16 and VIDEO 12-3). The time of occurrence and number of microembolic signals are used to assess the shunt location (intracardiac if early after injection, extracardiac if later) and the size and functional relevance of the right-to-left shunt. The following scale may be used to grade the size of the shunt: (1) negative; (2) 1 to 10 microembolic signals; (3) more than 10 microembolic signals and no curtain; and (4) curtain (shower of microembolic signals with no single bubble being identified).[38] The size of a PFO measured by TEE correlates with the amount of microembolic signals on TCD.[39] Nontranspulmonary gaseous contrast injection TCD is more sensitive than TEE in detecting PFO because medication-induced sedation and the esophageal probe used in TEE prevent an adequate Valsalva maneuver. The pooled sensitivity and specificity of TCD for a PFO are 96.1% and 92.4%, respectively.[40] However, TEE and TCD are complementary and should be applied jointly to detect a PFO and to characterize its morphologic features.

Microembolic Signal Detection by Transcranial Doppler

TCD can detect and quantify the burden of embolization (microembolic signals) driven by large artery disease and cardioembolic sources. Although these microemboli are clinically silent, they may be clinically important by indicating

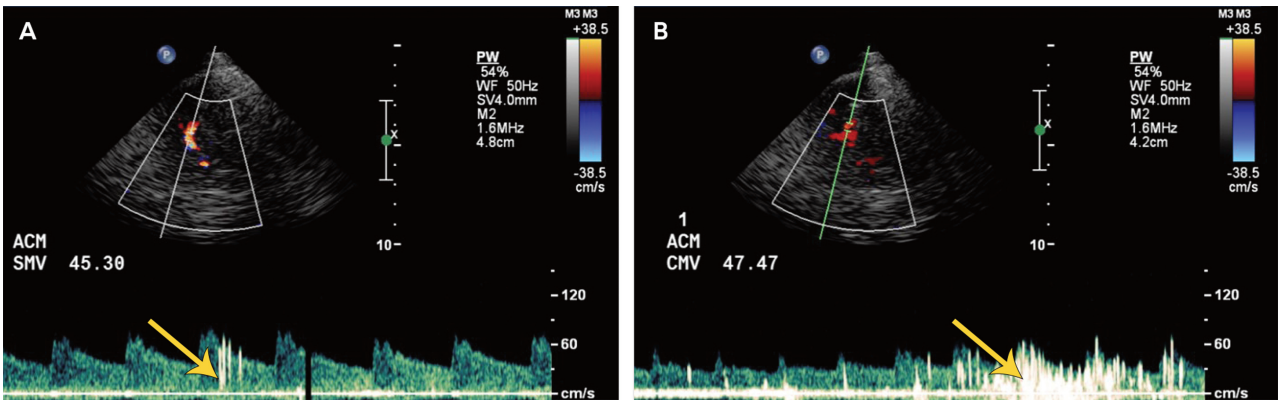

FIGURE 12-16

Detection with transcranial color sonography of a right-to-left cardiac shunt, caused by a patent foramen ovale. *A*, Four microembolic signals are visible in the velocity spectrum (*arrow*) of the middle cerebral artery, a few seconds after the gaseous contrast injection in a brachial vein. *B*, Repetition of the injection is followed by the Valsalva maneuver with the early appearance of a curtain of microembolic signals (*arrow*).

ACM = middle cerebral artery; CMV = with Valsalva maneuver; SMV = without Valsalva maneuver.

Copyright © American Academy of Neurology. Unauthorized reproduction of this article is prohibited.

stroke risk because they are associated with a sixfold to eightfold increase in the risk of recurrent vascular events after acute stroke.[41] Many studies have detected microembolic signals in patients with symptomatic carotid stenosis, and their presence correlates with recent symptoms, ulcerated plaques, and high-grade stenosis. In asymptomatic carotid stenosis, microembolic signals are less frequent and data are less robust.[42] As noted earlier, microembolic signal detection is also useful during carotid endarterectomy and cardiac surgery. This technique is increasingly used to guide patient management and as a surrogate marker of antithrombotic drug efficacy.[43,44]

Microembolic signal monitoring is performed over 30 to 60 minutes, usually with bilateral 2-MHz probes fixed in a headframe. Currently, robotized probes allow the patient to move and walk while being monitored, making longer evaluations easier.

Dynamic Vasoregulation Assessment

The cerebral distal arteriolar system is responsible for vasomotor regulation and maintenance of appropriate perfusion of a given volume of cerebral tissue. When this regulation is disturbed or exhausted, the risk of ischemia, edema, and hemorrhage increases. Dynamic vasoregulation assessment may be performed with ultrasonography. Data analysis is becoming more user friendly, allowing this important information to increase knowledge about patient risk and support clinical decision making, particularly in acute stroke and in patients in the intensive care unit.

CEREBRAL AUTOREGULATION. Cerebral autoregulation is one the main cerebrovascular regulating principles, allowing, in normal conditions, stable cerebral blood flow within a wide range of systemic blood pressure variation (within about 50 to 150 mm Hg mean arterial pressure). Cerebral autoregulation may be assessed via spontaneous fluctuations of blood pressure (by arterial line or plethysmography) and blood flow velocity measurement with TCD. As previously mentioned, the TCD is performed with bilateral 2-MHz probes fixed in a headframe to prevent probe sliding and loss of signal. Then, with transfer function analysis, cerebral autoregulation in the frequency domain can be characterized by three parameters: phase, gain, and coherence (FIGURE 12-17). More effective cerebral autoregulation is evidenced by lower coherence and gain and higher phase. In the intensive care setting, in patients with an ICP catheter, the pressure-reactivity index can be derived instead.

Worse cerebral autoregulation correlates with increased risk of hemorrhagic transformation, larger infarcts, and worse outcome in ischemic stroke.[45] Cerebral autoregulation operates slowly (requires at least 6 to 10 seconds) at low frequencies. No cutoff between normal and abnormal cerebral autoregulation has been validated, but a phase shift inferior to 30 degrees has been proposed to represent cerebral autoregulation failure, matching the cutoff for worse outcome in a cohort of patients with ischemic stroke.[46,47]

CEREBRAL VASOREACTIVITY. Cerebral vasoreactivity, or vasomotor reactivity, is an index of blood flow velocity response to a vasomodulatory stimulus (eg, to acetazolamide or carbon dioxide). The easiest way to evaluate vasomotor reactivity is by monitoring blood flow velocity with the previously described bilateral TCD probes in a headframe while changing $PaCO_2$ because carbon

KEY POINTS

- Transcranial Doppler (TCD) and transcranial color sonography can accurately detect significant intracranial artery stenosis and occlusion.
- Atherosclerotic stenosis has a more focal and stable blood flow velocity increase than dynamic intracranial stenoses such as those caused by an embolus, dissection, vasospasm, or vasculitis.
- In children with sickle cell disease, screening with TCD for high blood flow velocity (≥200 cm/s) and treatment with regular blood transfusion may result in a 10-fold decrease in the prevalence of strokes.
- Annual TCD screening should be offered for children aged 2 to 16 years with sickle cell disease of the types *HbSS* or Sβ0 thalassemia.
- In patients with subarachnoid hemorrhage, vasospasm can be monitored with TCD, which helps adjust medical and intervention therapy aiming to prevent delayed cerebral ischemia and cerebral infarction.
- TCD can diagnose vasoconstriction related to reversible cerebral vasoconstriction syndrome in the proximal cerebral arteries, although there are no standardized blood flow velocity criteria.
- Changes in blood flow velocity over time in patients with reversible cerebral vasoconstriction syndrome may be more informative than the isolated values.

Copyright © American Academy of Neurology. Unauthorized reproduction of this article is prohibited.

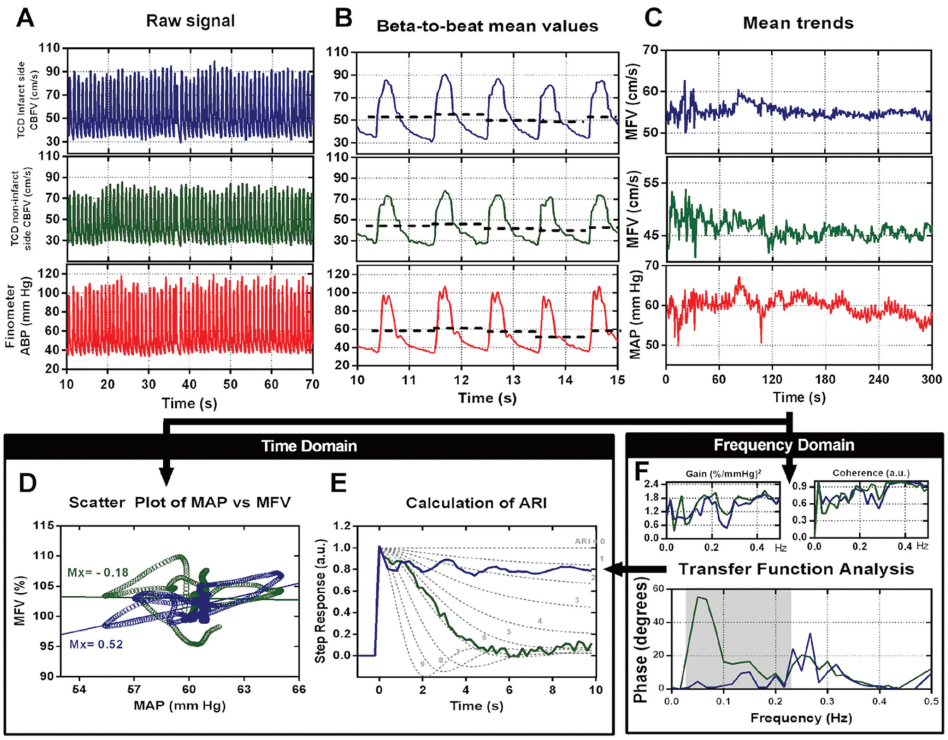

FIGURE 12-17

Cerebral autoregulation (CA) calculation. Calculation of various CA index values within 6 hours of stroke onset in a patient with the total territory of the middle cerebral artery (MCA) affected. The continuous signals of transcranial Doppler (TCD) (*A*) cerebral blood flow velocity (CBFV) from affected (*blue*) and unaffected (*green*) MCA territories and arterial blood pressure (ABP, *red*) are inspected (*B*) and mean values calculated (mean blood flow velocity [MFV] and mean arterial pressure [MAP], respectively). From 300 seconds of these time series (*C*), CA can be calculated in time and frequency domains. In the first case (*D*), MFV is plotted against MAP and a Pearson correlation coefficient is obtained (Mx). Note Mx = 0.52 in the affected hemisphere, while Mx = −0.18 on the contralateral side, meaning CA is worse on the affected side (*E*). In the frequency domain (*F*), the transfer function analysis outputs are coherence, gain, and phase. CA is highly impaired on the affected side. The patient had a hemorrhagic transformation at 24 hours and remained bedridden (3-month modified Rankin scale of 5).

ARI = autoregulation index.

Reprinted with permission from Castro P, et al, Curr Atheroscler Rep.[45] © 2018 Springer Nature.

dioxide is a potent cerebral vasodilator. This can be achieved by either giving the patient a carbon dioxide-rich air mixture to breathe or inducing hypoventilation and hyperventilation.

A simple bedside test to assess vasomotor reactivity is to perform a breath-hold test. After a period of rest and a normal inspiration, the patient remains in apnea for approximately 30 seconds (or a minimum of 24 seconds). Then the breath-hold index is calculated, using mean blood flow velocity (MFV) values: [(maximum MFV at end of apnea – baseline MFV) / baseline MFV)] × 100, divided by apnea time in seconds.

Carbon dioxide vasomotor reactivity can also be assessed with continued monitoring of mean blood flow velocity changes by TCD and end-tidal carbon dioxide by capnography (FIGURE 12-18[48]).[49]

The grade of vasomotor reactivity has been linked to prognosis in patients in critical care settings. Importantly, vasomotor reactivity can help in deciding

Copyright © American Academy of Neurology. Unauthorized reproduction of this article is prohibited.

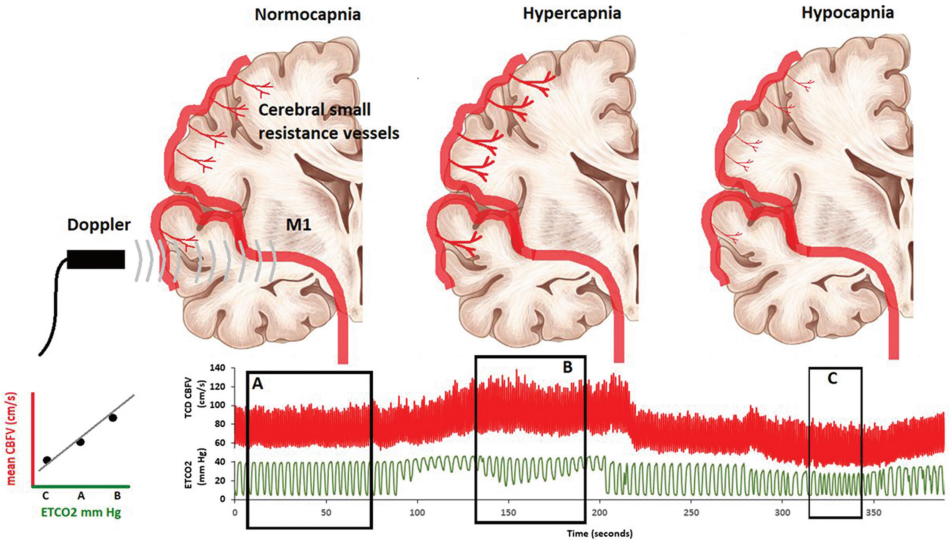

FIGURE 12-18

Carbon dioxide vasoreactivity testing. Compared with normocapnia, in hypercapnia the small resistance vessels dilate, and the blood flow velocity measured proximally at the middle cerebral artery increases. The opposite occurs with hypocapnia.

CBFV = cerebral blood flow velocity; ETCO2 = end-tidal carbon dioxide; TCD = transcranial Doppler. Reprinted with permission from Castro P and Azevedo E, Neurosonology in Critical Care.[48]

© 2022 Springer Nature.

about treatment of a carotid stenosis because it might be helpful to understand if compensatory vasodilatation is exhausted and determine the stroke risk and urgency of revascularization. A cutoff of the breath-hold index distinguishing between impaired and normal cerebrovascular reactivity was determined to be 0.69.[50]

When vasomotor reactivity is disturbed or exhausted, a "reversed Robin Hood" effect may occur: hypercapnia will cause vasodilatation on the unaffected side but not in the affected one, thus shifting the cerebral blood pool to nonischemic areas.[51]

NEUROVASCULAR COUPLING. Functional TCD is a tool designed to measure the increase of local cerebral blood flow due to regional cortical neuronal activation and is accomplished by neurovascular coupling at the neurovascular unit. Dysfunction of neurovascular coupling might occur in the early and presymptomatic stages of cerebrovascular pathology.[52]

Functional TCD can also be used to evaluate cerebral laterality, which is sometimes needed when deciding on a neurosurgical intervention. It is performed by monitoring both middle cerebral arteries while the patient is performing a language task, and a significantly higher increase in blood flow velocity will be seen in the dominant hemisphere middle cerebral artery.

Venous Disease

Raised blood flow velocity in collateral venous drainage is the most frequent sonographic finding in patients with cerebral venous sinus thrombosis. Interpretation of blood flow velocity in venous ultrasonography must be done carefully because some physiologic (arachnoid granulations, physiologic

KEY POINTS

- TCD can be used to monitor cerebral hemodynamics during acute stroke and in the neurocritical setting, as well as before, during, and after therapeutic interventions.
- TCD and transcranial color sonography allow for monitoring intracranial pressure changes. With intracranial pressure increase, cerebral blood flow velocity, mainly diastolic, decreases.
- Cerebral circulatory arrest is indicated by no diastolic flow for at least 30 minutes in the middle cerebral arteries and the basilar artery, and decreased systolic blood flow velocity.
- TCD and transcranial color sonography are highly accurate ancillary tests for cerebral circulatory arrest confirmation.
- TCD and a nontranspulmonary gaseous contrast injection are a reliable and less invasive complement to gold standard transesophageal echocardiography in the diagnosis of a patent foramen ovale and enable the detection of extracardiac right-to-left shunt.
- The size of a patent foramen ovale measured by transesophageal echocardiography correlates with the amount of microembolic signals observed by TCD.

Copyright © American Academy of Neurology. Unauthorized reproduction of this article is prohibited.

asymmetries) and pathologic conditions (arteriovenous malformations or dural fistulas) might also contribute to flow increase. Moreover, in approximately 30% of cases of cerebral venous thrombosis, no pathologic ultrasound findings can be found.[53]

Neck ultrasound evaluation of venous outflow might also provide useful information regarding the insufficiency of the venous system or an obstruction due to thrombosis. The compression ultrasound maneuver has been shown to be a highly reliable tool in the diagnosis of internal jugular vein thrombosis.[54]

NEURO-ORBITAL ULTRASONOGRAPHY

Ultrasonography of the optic nerve sheath diameter and papilla in search for signs of increased ICP, measurement of pupil reactivity, and the analysis of orbital vascularization are all potential ultrasonographic applications. This can be performed with the same probe as for the cervical carotid examination (linear-array probe of 6 MHz to 12 MHz). The optic nerve serves as a landmark and is easily detected as a hypoechogenic structure near the distal pole of the globe with hyperechoic striped bands at its edges (sheath). B-mode ultrasound markers at the outer edges of the hyperechoic striped bands or at the transitions from the single dark region to the hyperechoic retrobulbar fat (FIGURE 12-19) yield the highest sensitivity of optic nerve sheath diameter measurements for increased ICP.[55]

The standard point of measurement of the optic nerve sheath diameter is approximately 3 mm behind the papilla. Normal values for the optic nerve sheath diameter are 4 to 5 mm. Large discrepancies may be caused by incorrect positioning of the markers. An increased optic nerve sheath diameter indicates an increase in ICP. During the same examination, the clinician can also assess the presence of papilledema, that is, the prominence of the papilla (FIGURE 12-19), with the normal value of less than 0.5 mm. In several neurologic conditions, including in neurocritical settings, pupillometry can be done with ultrasonography with very good accuracy.[56]

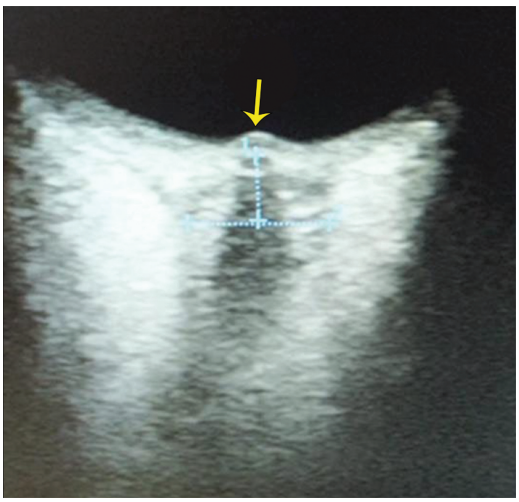

FIGURE 12-19
Ultrasonography from a patient with chronic cerebral venous thrombosis with an enlarged optic nerve sheath and elevated papilla (*arrow*) suggestive of intracranial hypertension.

Regarding vascular disease in acute vision loss, in addition to assessing for a carotid stenosis, blood flow velocity can be evaluated in the central retinal artery running within the optic nerve. Sometimes it is possible to identify a calcified embolus (suggestive of arterial plaque embolism) lodging in the central retinal artery just behind the papilla. This spot sign correlates with a lower probability of revascularization, spontaneously or with a thrombolytic, and a worse prognosis for visual recovery, as exemplified in CASE 12-3.

Copyright © American Academy of Neurology. Unauthorized reproduction of this article is prohibited.

Also, evaluation of the orbital vessels may give important clues to vascular pathology elsewhere. As discussed earlier, inversion of ophthalmic artery flow direction suggests a critical cervical internal carotid stenosis. The inversion and arterialization of the flow in the superior ophthalmic vein provide clues for a carotid-cavernous fistula in a patient with pulsatile tinnitus, cavernous sinus syndrome, exophthalmos, or chemosis (FIGURE 12-21).

ULTRASONOGRAPHY OF THE PERIPHERAL NERVOUS SYSTEM

Neuromuscular ultrasonography is an increasingly used application of ultrasound. It allows the clinician to view most nerves and muscles in real time and to detect anomalies through changes in size, echogenicity, and vascularity. It is useful in compressive, demyelinating, and traumatic neuropathies and can quickly and noninvasively assess muscle dysfunction.[1]

Ultrasonography allows the clinician to evaluate muscles and nerves both in static and dynamic conditions, which provides information about pathologic features and is also important in identifying the structures.

The classic ultrasound finding of affected muscle, resulting from either a primary neurogenic or myopathic disorder, is increased brightness and reduced size. Dynamic ultrasonography reveals fasciculations, an important finding in early amyotrophic lateral sclerosis.[1]

In carpal tunnel syndrome, as in entrapment neuropathies in general, a hypoechoic focal nerve enlargement occurs either proximal or distal to the site of entrapment.

In traumatic neuropathies, ultrasonography is useful in distinguishing transected nerves from those with anatomic continuity.

In more generalized neuropathies, ultrasonography might show nerve enlargement, which is useful for detecting hypertrophic hereditary (as in Charcot-Marie-Tooth disease) or inflammatory neuropathies (as in chronic inflammatory demyelinating polyradiculoneuropathy and multifocal motor neuropathy).[1]

Ultrasonography can provide real-time guidance for needle placement and can sometimes make a diagnosis when electromyography is not tolerated or is no longer informative.[57]

New technologic advances show promise in the field of neuromuscular ultrasonopraphy.[58] Ultra-high-resolution ultrasonography enables imaging of the nerve at the fascicular level. Shear wave elastography imaging can provide measures of tissue stiffness that can act as a surrogate measure of nerve and muscle health. Photoacoustic imaging may overcome neuromuscular ultrasonography's current lack of contrast agents to detect inflammation and other functional changes within nerve and muscle, while artificial intelligence stands to address operator dependency and improve diagnostic imaging.

ULTRASONOGRAPHY FOR GUIDING PROCEDURES

In addition to the usefulness of ultrasonography to guide safer and faster vascular catheterization, especially in the context of neurocritical care, it is also useful to guide other interventions in neurologic clinical practice.

Echo-Guided Lumbar Puncture

Lumbar puncture is commonly used as a diagnostic and therapeutic procedure in neurologic diseases and routinely performed based on landmarks.

KEY POINTS

- Microembolic signal monitoring is useful in evaluating arterial lesion stroke risk and as a surrogate marker of antithrombotic drug efficacy.
- Microembolic signal monitoring is performed over 30 to 60 minutes, usually with bilateral 2-MHz probes fixed in a headframe.
- Reduced cerebral autoregulation is associated with worse outcome in acute stroke and in the neurocritical care setting.
- Functional TCD studies may allow identification of the dominant hemisphere and identification of early neurovascular unit dysfunction in cerebrovascular pathologies.
- Raised flow velocities in collateral venous drainage are the most frequent finding in patients with cerebral venous sinus thrombosis, although it has low sensitivity.
- Ultrasound evaluation of the optic nerve allows for detection of signs of increased intracranial pressure, namely increased optic nerve sheath diameter and raised papilla.
- Especially in the neurocritical care setting, ultrasonography can be useful for the measurement of pupil reactivity.
- Analysis of orbital vascularization may provide evidence of central retina artery occlusion, which has a worse prognosis if an embolic echogenic spot sign is present.

Copyright © American Academy of Neurology. Unauthorized reproduction of this article is prohibited.

Nevertheless, in patients with unfavorable anatomy, such as obesity or spinal deformities, its success rate decreases. Ultrasound imaging of the lumbar spine might help guide lumbar puncture by revealing the anatomic landmarks and select the widest interspinous space, as is shown in FIGURE 12-22.[59] Previous studies have provided evidence supporting its use for patients with a body mass index of 25 kg/m^2 or greater, as well as in neonates.[59,60]

Ultrasonography in Headache and Painful Cranial Neuropathies

Minimally invasive techniques such as peripheral nerve blocks may provide pain relief in headaches refractory to pharmacologic therapy as well as decrease systemic side effects of pharmacologic therapy. Cranial neuropathies such as supraorbital, auriculotemporal, or the more common occipital neuropathies also benefit from peripheral nerve blocks as a diagnostic and treatment approach. Ultrasound-guided peripheral nerve blocks might allow a more precise location of the nerve, reducing the anesthetic volumes needed and avoiding blockage of closer nerves and nonspecific analgesic effects due to intramuscular spread.[61,62]

CASE 12-3

A 73-year-old man with hypertension, diabetes, and dyslipidemia presented to the emergency department with sudden acute vision loss in his right eye. He also reported chronic mild to moderate headache for several months. He was diagnosed with acute retinal ischemia and discharged with aspirin. One month later, he presented again with sudden visual loss, at that time in his left eye, that had occurred 60 minutes earlier. Because he did not recover from the previous episode, he had complete vision loss. The ultrasound examination showed a bilateral retrobulbar hyperechoic spot signal and absent flow in both central retinal arteries (FIGURE 12-20). This confirmed the ischemic and embolic nature of the retinal ischemic events, arguing against an arteritic etiology. Temporal artery ultrasonography was normal, as was the sedimentation rate.

COMMENT

This case exemplifies that the presence of the hyperechoic embolic material is a sign of a worse prognosis and of unlikely spontaneous revascularization and of the importance of a rapid search for the cause of vision loss, including for an embolic source, to reduce the risk of a recurrence of ischemic events. This patient was found to have a severe aortic arch stenosis as the cause of the embolic episodes and did not recover from blindness at follow-up.

Copyright © American Academy of Neurology. Unauthorized reproduction of this article is prohibited.

Ultrasonography in Botulinum Neurotoxin Injection

To improve quality of life, patients with focal dystonia or spasticity are treated with intramuscular botulinum neurotoxin injections. Several studies show low accuracy of muscle selection when anatomic landmarks are used.[63] To maximize the efficacy of treatment, an accurate selection of muscles is critical. In this setting, ultrasonography allows clinicians to unequivocally identify target muscles for botulinum neurotoxin injection and to better select the site of administration, which may lead to a more effective treatment and a lower risk of iatrogenic effects, such as dysphagia.[64,65]

FUTURE TRENDS

Some new trends, such as ultraportable devices, ultrafast ultrasonography, ultrasonography perfusion imaging, and cerebral hemodynamic and vasoregulation studies applied to guiding decisions, as well as the concept of point-of-care ultrasonography for neurology, are other developing fields of interest.

Ultraportable ultrasonography devices allow more flexible and faster neurovascular studies, not only at the patient's bedside but also in other environments such as the emergency department, the radiography suite, or

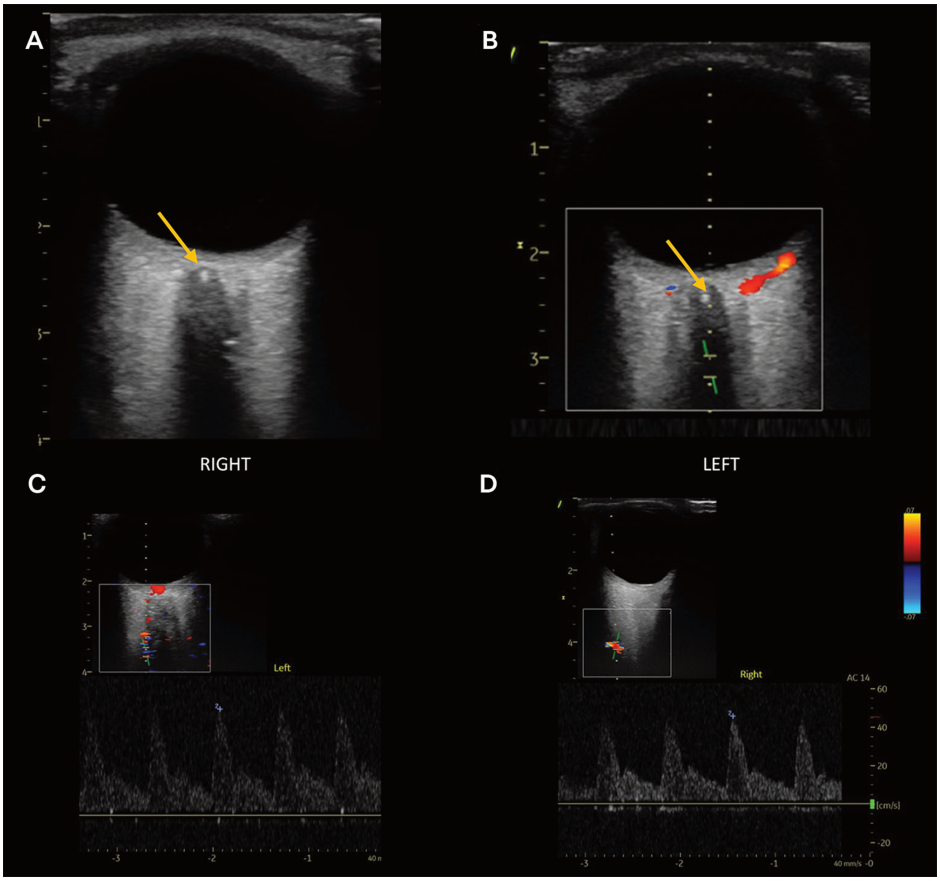

FIGURE 12-20

Sequential bilateral loss of vision. *A*, *B*, Bilateral retrobulbar spot sign (*arrows*) and absent flow in both central retinal arteries. *C*, *D*, Preserved flow in ophthalmic arteries.

Copyright © American Academy of Neurology. Unauthorized reproduction of this article is prohibited.

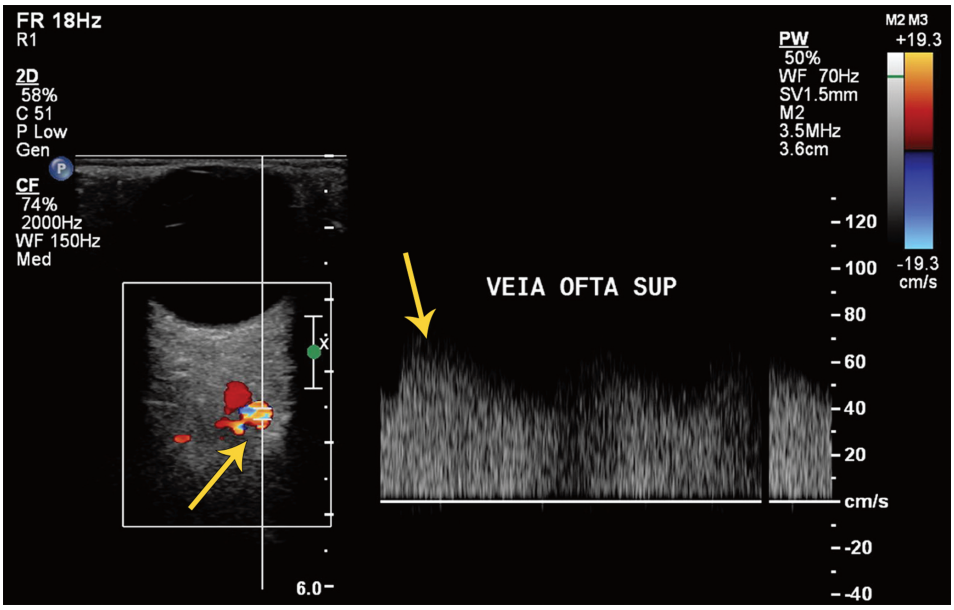

FIGURE 12-21
Carotid cavernous fistula: "arterialized" (pulsatile flow on right side, *arrow*) superior ophthalmic vein (left side, *arrow*).

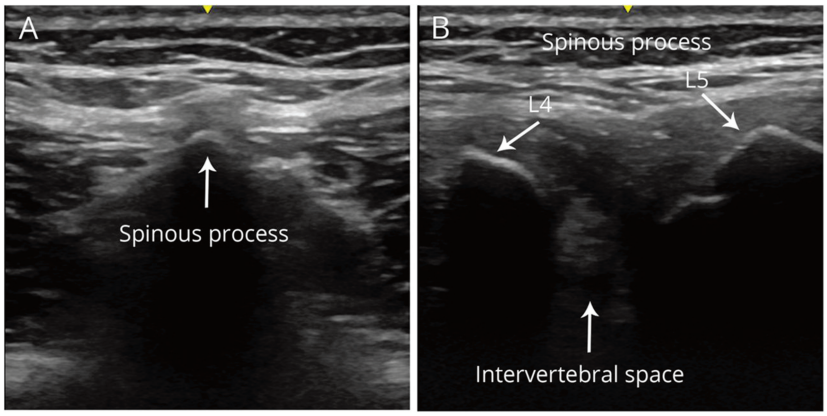

FIGURE 12-22
Ultrasound-guided lumbar puncture. *A*, Transverse view of lumbar spine ultrasound image. An ultrasound probe was first placed on the lumbar area perpendicular to the axis of spinous process, with slow movements of the transducer allowing identification of the spinous processes; it showed the typical hypoechoic crescent shape of the spinous process with posterior acoustic shadowing. *B*, Longitudinal view of lumbar spine ultrasound image. After locating the spinous process in the center and a mark is drawn, the transducer was rotated 90 degrees to align the ultrasound beam longitudinally over the midline and was moved along to find the widest interspinous space: crescent-shaped structures are identified as the "eyebrow" shape, indicating spinous processes. Centered between these spinous processes is the intervertebral space with visible superior and inferior borders.
Reprinted with permission from Li Y, et al, Neurol Clin Pract.[59] © 2020 American Academy of Neurology.

Copyright © American Academy of Neurology. Unauthorized reproduction of this article is prohibited.

even in the ambulance. Point-of-care ultrasonography is a goal-directed and -focused ultrasound examination performed where the patient is being observed and treated, to obtain in real time a prompt answer to a specific clinical question related to neurologic symptoms, or for supporting procedures (eg, image-guidance).[66]

Ultrasonic cerebral perfusion imaging permits improved vessel imaging and contrast-enhanced tissue imaging. Studies performed in a stroke setting allow following up brain perfusion status and effect of recanalization therapeutics. Trials such as the ongoing SONAS Ultrasound for Detecting Stroke,[67] which uses a portable ultrasound machine and a semiquantitative algorithm to detect a large vessel occlusion in a prehospital setting, may expand the application of these procedures into clinical practice. Moreover, ultrasonic cerebral perfusion imaging might help delineate the border of intracerebral hemorrhage for more valid volume measurement.

Ultrafast ultrasonography enables transcranial imaging of deep vasculature in the adult brain at microscopic resolution and the quantification of hemodynamic parameters. It will facilitate the understanding of brain hemodynamics and how vascular abnormalities in the brain are related to neurologic pathologies.[68] New ultrasonography cerebral hemodynamic and vasoregulation studies are promising for guiding clinical decisions, as in the acute stroke setting, as well as in the noninvasive assessment of ICP.[46,47,69]

CONCLUSION

Diagnostic ultrasonography in neurology enables the physician to better understand a clinical case using a noninvasive and accurate tool that can be used at a patient's bedside.

Neurovascular ultrasonography provides morphologic and hemodynamic information, complementing data from CT or MRI. As ultrasonography examinations can be easily repeated, they are ideal for monitoring an unstable patient or during and after interventions. Recently, brain and eye sonography have added new applications, namely for ICP assessment.

Diagnostic ultrasonography can be a powerful tool for morbidity and mortality prevention. In adults, it allows early detection of atherosclerosis and the opportunity to prevent progression to stroke with timely aggressive control of vascular risk factors. In children with sickle cell disease, it is important to have access to TCD screening to select patients for transfusion and reduce the risk of stroke. In conclusion, diagnostic ultrasonography helps neurologists provide select patients better and more timely treatment.

USEFUL WEBSITES

THE AMERICAN SOCIETY OF NEUROIMAGING
The mission of the American Society of Neuroimaging is to provide neuroimaging informatics education, certification, support, and guidance to neurologists and other neuroscience clinicians, technologists, sonographers, and researchers. It aims to ensure all individuals with neurologic disorders have access to experts in neuroimaging and neurosonology.

asnweb.org

EUROPEAN SOCIETY OF NEUROSONOLOGY AND CEREBRAL HEMODYNAMICS
The European Society of Neurosonology and Cerebral Hemodynamics brings together the professionals most dedicated to the use of ultrasound in neurology and is very active in the dissemination of neurosonology, in the certification of professionals, in the constitution of study groups and multicenter initiatives to promote the practice, and teaching and research in the area.

esnch.org/

Copyright © American Academy of Neurology. Unauthorized reproduction of this article is prohibited.

VIDEO LEGENDS

VIDEO 12-1
Video shows a common carotid artery dissection as an extension of aortic dissection. The intimal flap of the dissection is visible as an echogenic (white) linear moving image within the artery in a longitudinal view of the proximal common carotid artery.

ACC prox. Direito = right proximal common carotid artery.

© 2023 American Academy of Neurology.

VIDEO 12-2
Video shows a common carotid artery dissection as an extension of aortic dissection. The intimal flap of the dissection is visible as an echogenic (white) linear moving image within the artery, in a cross-sectional view of the proximal common carotid artery.

© 2023 American Academy of Neurology.

VIDEO 12-3
Video shows microembolic signals in a patient with a patent foramen ovale. While monitoring middle cerebral artery (red area in the video) blood flow velocity (bottom), a nontranspulmonary microbubble solution was injected into an arm vein. At 12 seconds, microembolic signals are visible in the velocity spectrum as high-intensity signals; simultaneous typical "blip" sounds are heard. Between 18 and 28 seconds, the patient is doing a Valsalva maneuver, which is reflected in a decrease in blood flow velocity in the spectrum, and some more microembolic signals follow.

© 2023 American Academy of Neurology.

REFERENCES

1 Walker FO. Ultrasonography in peripheral nervous system diagnosis. Continuum (Minneap Minn) 2017;23(5, Peripheral Nerve and Motor Neuron Disorders):1276-1294. doi:10.1212/CON.0000000000000522

2 von Reutern GM, Goertler MW, Bornstein NM, et al. Grading carotid stenosis using ultrasonic methods. Stroke 2012;43(3):916-921. doi:10.1161/STROKEAHA.111.636084

3 Barlinn K, Floegel T, Kitzler HH, et al. Multi-parametric ultrasound criteria for internal carotid artery disease-comparison with CT angiography. Neuroradiology 2016;58(9):845-851. doi:10.1007/s00234-016-1706-x

4 Valdueza JS, Roehl J, Connolly F, Klingebiel R. Neurosonology and neuroimaging of stroke. 2nd ed. Thieme; 2017.

5 Bartels E, Fuchs HH, Flügel KA. Duplex ultrasonography of vertebral arteries: examination, technique, normal values, and clinical applications. Angiology 1992;43(3 Pt 1):169-180. doi:10.1177/000331979204300301

6 Benninger DH, Georgiadis D, Gandjour J, Baumgartner RW. Accuracy of color duplex ultrasound diagnosis of spontaneous carotid dissection causing ischemia. Stroke 2006;37(2):377-381. doi:10.1161/01.STR.0000198811.65068.16

7 Azevedo EC. Novel applications of ultrasound vascular imaging. In: Vascular imaging of the central nervous system: physical principles, clinical applications, and emerging techniques. 1st ed. John Wiley & Sons, Inc; 2014.

8 Duftner C, Dejaco C, Sepriano A, Falzon L, Schmidt WA, Ramiro S. Imaging in diagnosis, outcome prediction and monitoring of large vessel vasculitis: a systematic literature review and meta-analysis informing the EULAR recommendations. RMD Open 2018;4(1):e000612. doi:10.1136/rmdopen-2017-000612

9 Schäfer VS, Juche A, Ramiro S, Krause A, Schmidt WA. Ultrasound cut-off values for intima-media thickness of temporal, facial and axillary arteries in giant cell arteritis. Rheumatology (Oxford) 2017;56(9):1479-1483. doi:10.1093/rheumatology/kex143

10 Soares C, Costa A, Santos R, et al. Clinical, laboratory and ultrasonographic interrelations in giant cell arteritis. J Stroke Cerebrovasc Dis 2021;30(4):105601. doi:10.1016/j.jstrokecerebrovasdis.2021.105601

11 Lecler A, Obadia M, Savatovsky J, et al. TIPIC syndrome: beyond the myth of carotidynia, a new distinct unclassified entity. AJNR Am J Neuroradiol 2017;38(7):1391-1398. doi:10.3174/ajnr.A5214

12 Olin JW, Gornik HL, Bacharach JM, et al. Fibromuscular dysplasia: state of the science and critical unanswered questions: a scientific statement from the American Heart Association. Circulation 2014;129(9):1048-1078. doi:10.1161/01.cir.0000442577.96802.8c

13 Coutinho JM, Derkatch S, Potvin ARJ, et al. Carotid artery web and ischemic stroke: a case-control study. Neurology 2017;88(1):65-69. doi:10.1212/WNL.0000000000003464

14 Kim SJ, Nogueira RG, Haussen DC. Current understanding and gaps in research of carotid webs in ischemic strokes: a review. JAMA Neurol 2019;76(3):355-361. doi:10.1001/jamaneurol.2018.3366

Copyright © American Academy of Neurology. Unauthorized reproduction of this article is prohibited.

15 Tsai LK, Yeh SJ, Tang SC, et al. Validity of carotid duplex sonography in screening for intracranial dural arteriovenous fistula among patients with pulsatile tinnitus. Ultrasound Med Biol 2016;42(2):407-412. doi:10.1016/j.ultrasmedbio.2015.10.013

16 Yeh SJ, Tsai LK, Jeng JS. Clinical and carotid ultrasonographic features of intracranial dural arteriovenous fistulas in patients with and without pulsatile tinnitus. J Neuroimaging 2010;20(4):354-358. doi:10.1111/j.1552-6569.2009.00379.x

17 Demchuk AM, Burgin WS, Christou I, et al. Thrombolysis in brain ischemia (TIBI) transcranial Doppler flow grades predict clinical severity, early recovery, and mortality in patients treated with intravenous tissue plasminogen activator. Stroke 2001;32(1):89-93. doi:10.1161/01.str.32.1.89

18 Baumgartner RW, Mattle HP, Schroth G. Assessment of >/=50% and <50% intracranial stenoses by transcranial color-coded duplex sonography. Stroke 1999;30(1):87-92. doi:10.1161/01.str.30.1.87

19 Zhao L, Barlinn K, Sharma VK, et al. Velocity criteria for intracranial stenosis revisited: an international multicenter study of transcranial Doppler and digital subtraction angiography. Stroke 2011;42(12):3429-3434. doi:10.1161/STROKEAHA.111.621235

20 Zhang J, Wang L, Chen Y, Wang S, Cui L. Non-invasive detection of diffuse intracranial vertebrobasilar artery stenosis: a prospective comparison with digital subtraction angiography. Ultrasound Med Biol 2022;48(3):554-564. doi:10.1016/j.ultrasmedbio.2021.11.015

21 Mattioni A, Cenciarelli S, Eusebi P, et al. Transcranial Doppler sonography for detecting stenosis or occlusion of intracranial arteries in people with acute ischaemic stroke. Cochrane Database Syst Rev 2020;2:CD010722. doi:10.1002/14651858.CD010722.pub2

22 Azevedo E. Neurosonology in atrial fibrillation. In: Atrial fibrillation: causes, diagnosis and treatment options. Nova Science Publishers, Inc; 2014.

23 Enninful-Eghan H, Moore RH, Ichord R, Smith-Whitley K, Kwiatkowski JL. Transcranial Doppler ultrasonography and prophylactic transfusion program is effective in preventing overt stroke in children with sickle cell disease. J Pediatr 2010;157(3):479-484. doi:10.1016/j.jpeds.2010.03.007

24 Noubiap JJ, Mengnjo MK, Nicastro N, Kamtchum-Tatuene J. Neurologic complications of sickle cell disease in Africa: a systematic review and meta-analysis. Neurology 2017;89(14):1516-1524. doi:10.1212/WNL.0000000000004537

25 DeBaun MR, Jordan LC, King AA, et al. American Society of Hematology 2020 guidelines for sickle cell disease: prevention, diagnosis, and treatment of cerebrovascular disease in children and adults. Blood Adv 2020;4(8):1554-1588. doi:10.1182/bloodadvances.2019001142

26 Kumar G, Shahripour RB, Harrigan MR. Vasospasm on transcranial Doppler is predictive of delayed cerebral ischemia in aneurysmal subarachnoid hemorrhage: a systematic review and meta-analysis. J Neurosurg 2016;124(5):1257-1264. doi:10.3171/2015.4.JNS15428

27 Connolly ES, Rabinstein AA, Carhuapoma JR, et al. Guidelines for the management of aneurysmal subarachnoid hemorrhage: a guideline for healthcare professionals from the American Heart Association/american Stroke Association. Stroke 2012;43(6):1711-1737. doi:10.1161/STR.0b013e3182587839

28 Alexandrov A, ed. Cerebrovascular ultrasound in stroke prevention and treatment. Blackwell; 2004.

29 Sviri GE, Ghodke B, Britz GW, et al. Transcranial Doppler grading criteria for basilar artery vasospasm. Neurosurgery 2006;59(2):360-366. doi:10.1227/01.NEU.0000223502.93013.6E

30 Fung C, Heiland DH, Reitmeir R, et al. Ultrasound perfusion imaging for the detection of cerebral hypoperfusion after aneurysmal subarachnoid hemorrhage. Neurocrit Care 2022;37(1):149-159. doi:10.1007/s12028-022-01460-z

31 Boitet R, de Gaalon S, Duflos C, et al. Long-term outcomes after reversible cerebral vasoconstriction syndrome. Stroke 2020;51(2):670-673. doi:10.1161/STROKEAHA.119.027703

32 Chen SP, Fuh JL, Chang FC, et al. Transcranial color doppler study for reversible cerebral vasoconstriction syndromes. Ann Neurol 2008;63(6):751-757. doi:10.1002/ana.21384

33 Kneihsl M, Niederkorn K, Deutschmann H, et al. Increased middle cerebral artery mean blood flow velocity index after stroke thrombectomy indicates increased risk for intracranial hemorrhage. J Neurointerv Surg 2018;10(9):882-887. doi:10.1136/neurintsurg-2017-013617

34 Ducrocq X, Hassler W, Moritake K, et al. Consensus opinion on diagnosis of cerebral circulatory arrest using Doppler-sonography: Task Force Group on cerebral death of the Neurosonology Research Group of the World Federation of Neurology. J Neurol Sci 1998;159(2):145-150. doi:10.1016/s0022-510x(98)00158-0

35 Chang JJ, Tsivgoulis G, Katsanos AH, Malkoff MD, Alexandrov AV. Diagnostic accuracy of transcranial doppler for brain death confirmation: systematic review and meta-analysis. AJNR Am J Neuroradiol 2016;37(3):408-414. doi:10.3174/ajnr.A4548

36 Lewis A, Kirschen MP. Brain death/death by neurologic criteria determination. Continuum (Minneap Minn) 2021;27(5, Neurocritical Care):1444-1464. doi:10.1212/CON.0000000000000987

37 Migdady I, Shoskes A, Amin M, et al. Determination of brain death in patients undergoing short-term mechanical circulatory support devices. Heart Lung Circ 2022;31(2):239-245. doi:10.1016/j.hlc.2021.05.100

Copyright © American Academy of Neurology. Unauthorized reproduction of this article is prohibited.

38 Jauss M, Zanette E. Detection of right-to-left shunt with ultrasound contrast agent and transcranial Doppler sonography. Cerebrovasc Dis 2000;10(6):490-496. doi:10.1159/000016119

39 Telman G, Yalonetsky S, Kouperberg E, et al. Size of PFO and amount of microembolic signals in patients with ischaemic stroke or TIA. Eur J Neurol 2008;15(9):969-972. doi:10.1111/j.1468-1331.2008.02232.x

40 Katsanos AH, Psaltopoulou T, Sergentanis TN, et al. Transcranial Doppler versus transthoracic echocardiography for the detection of patent foramen ovale in patients with cryptogenic cerebral ischemia: a systematic review and diagnostic test accuracy meta-analysis. Ann Neurol 2016;79(4):625-635. doi:10.1002/ana.24609

41 Sheriff F, Diz-Lopes M, Khawaja A, et al. Microemboli after successful thrombectomy do not affect outcome but predict new embolic events. Stroke 2020;51(1):154-161. doi:10.1161/STROKEAHA.119.025856

42 King A, Markus HS. Doppler embolic signals in cerebrovascular disease and prediction of stroke risk: a systematic review and meta-analysis. Stroke 2009;40(12):3711-3717. doi:10.1161/STROKEAHA.109.563056

43 Markus HS, Droste DW, Kaps M, et al. Dual antiplatelet therapy with clopidogrel and aspirin in symptomatic carotid stenosis evaluated using doppler embolic signal detection: the Clopidogrel and Aspirin for Reduction of Emboli in Symptomatic Carotid Stenosis (CARESS) trial. Circulation 2005;111(17):2233-2240. doi:10.1161/01.CIR.0000163561.90680.1C

44 Wong KSL, Chen C, Fu J, et al. Clopidogrel plus aspirin versus aspirin alone for reducing embolisation in patients with acute symptomatic cerebral or carotid artery stenosis (CLAIR study): a randomised, open-label, blinded-endpoint trial. Lancet Neurol 2010;9(5):489-497. doi:10.1016/S1474-4422(10)70060-0

45 Castro P, Azevedo E, Sorond F. Cerebral autoregulation in stroke. Curr Atheroscler Rep 2018;20(8):37. doi:10.1007/s11883-018-0739-5

46 Castro P, Azevedo E, Serrador J, Rocha I, Sorond F. Hemorrhagic transformation and cerebral edema in acute ischemic stroke: link to cerebral autoregulation. J Neurol Sci 2017;372:256-261. doi:10.1016/j.jns.2016.11.065

47 Castro P, Serrador JM, Rocha I, Sorond F, Azevedo E. Efficacy of cerebral autoregulation in early ischemic stroke predicts smaller infarcts and better outcome. Front Neurol 2017;8:113. doi:10.3389/fneur.2017.00113

48 Castro P, Azevedo E. Acute neurologic injury in ICU: vasomotor reactivity testing by transcranial Doppler (TCD/TCCS). In: Neurosonology in critical care. Springer; 2022:333-340.

49 Madureira J, Castro P, Azevedo E. Demographic and systemic hemodynamic influences in mechanisms of cerebrovascular regulation in healthy adults. J Stroke Cerebrovasc Dis 2017;26(3):500-508. doi:10.1016/j.jstrokecerebrovasdis.2016.12.003

50 Silvestrini M, Vernieri F, Pasqualetti P, et al. Impaired cerebral vasoreactivity and risk of stroke in patients with asymptomatic carotid artery stenosis. JAMA 2000;283(16):2122-2127. doi:10.1001/jama.283.16.2122

51 Alexandrov AV, Sharma VK, Lao AY, et al. Reversed Robin Hood syndrome in acute ischemic stroke patients. Stroke 2007;38(11):3045-3048. doi:10.1161/STROKEAHA.107.482810

52 Monteiro A, Castro P, Pereira G, et al. Neurovascular coupling is impaired in hypertensive and diabetic subjects without symptomatic cerebrovascular disease. Front Aging Neurosci 2021;13:728007. doi:10.3389/fnagi.2021.728007

53 Stolz EP. Role of ultrasound in diagnosis and management of cerebral vein and sinus thrombosis. Front Neurol Neurosci 2008;23:112-121. doi:10.1159/000111373

54 Prandoni P, Polistena P, Bernardi E, et al. Upper-extremity deep vein thrombosis. Risk factors, diagnosis, and complications. Arch Intern Med 1997;157(1):57-62. PMID: 8996041

55 Stevens RRF, Gommer ED, Aries MJH, et al. Optic nerve sheath diameter assessment by neurosonology: a review of methodologic discrepancies. J Neuroimaging 2021;31(5):814-825. doi:10.1111/jon.12906

56 Farina F, Vosko MR, Baracchini C, et al. Ultrasound examination of the pupil - a new tool for the neuro-ophthalmological assessment. Ultraschall Med 2021;42(1):84-91. doi:10.1055/a-1208-1482

57 van Alfen N, Mah JK. Neuromuscular ultrasound: a new tool in your toolbox. Can J Neurol Sci 2018;45(5):504-515. doi:10.1017/cjn.2018.269

58 Hobson-Webb LD. Emerging technologies in neuromuscular ultrasound. Muscle Nerve 2020;61(6):719-725. doi:10.1002/mus.26819

59 Li Y, Carandang RA, Ade S, Flahive J, Daniello K. Ultrasound-guided lumbar puncture improves success rate and efficiency in overweight patients. Neurol Clin Pract 2020;10(4):307-313. doi:10.1212/CPJ.0000000000000725

60 Stoller JZ, Fraga MV. Real-time ultrasound-guided lumbar puncture in the neonatal intensive care unit. J Perinatol 2021;41(10):2495-2498. doi:10.1038/s41372-021-01152-0

61 Greher M, Moriggl B, Curatolo M, Kirchmair L, Eichenberger U. Sonographic visualization and ultrasound-guided blockade of the greater occipital nerve: a comparison of two selective techniques confirmed by anatomical dissection. Br J Anaesth 2010;104(5):637-642. doi:10.1093/bja/aeq052

Copyright © American Academy of Neurology. Unauthorized reproduction of this article is prohibited.

62 Palamar D, Uluduz D, Saip S, et al. Ultrasound-guided greater occipital nerve block: an efficient technique in chronic refractory migraine without aura? Pain Physician 2015;18(2):153-162. PMID: 25794201

63 Molloy FM, Shill HA, Kaelin-Lang A, Karp BI. Accuracy of muscle localization without EMG: implications for treatment of limb dystonia. Neurology 2002;58(5):805-807. doi:10.1212/wnl.58.5.805

64 Henzel MK, Munin MC, Niyonkuru C, et al. Comparison of surface and ultrasound localization to identify forearm flexor muscles for botulinum toxin injections. PM R 2010;2(7):642-646. doi:10.1016/j.pmrj.2010.05.002

65 Hong JS, Sathe GG, Niyonkuru C, Munin MC. Elimination of dysphagia using ultrasound guidance for botulinum toxin injections in cervical dystonia. Muscle Nerve 2012;46(4):535-539. doi:10.1002/mus.23409

66 Valaikiene J, Schlachetzki F, Azevedo E, et al. Point-of-care ultrasound in neurology - report of the EAN SPN/ESNCH/ERcNsono Neuro-POCUS Working Group. Ultraschall Med 2022;43(4):354-366. doi:10.1055/a-1816-8548

67 ClinicalTrials.gov. SONAS ultrasound for detecting stroke (NCT03296852). Updated March 26, 2019. Accessed December 9, 2022. clinicaltrials.gov/ct2/show/NCT03296852

68 Demené C, Robin J, Dizeux A, et al. Transcranial ultrafast ultrasound localization microscopy of brain vasculature in patients. Nat Biomed Eng 2021;5(3):219-228. doi:10.1038/s41551-021-00697-x

69 Schmidt B, Czosnyka M, Cardim D, Czosnyka Z, Rosengarten B. Is lumbar puncture needed? Noninvasive assessment of ICP facilitates decision making in patients with suspected idiopathic intracranial hypertension [published online September 8, 2021]. Ultraschall Med. doi:10.1055/a-1586-6487

Copyright © American Academy of Neurology. Unauthorized reproduction of this article is prohibited.

Copyright © American Academy of Neurology. Unauthorized reproduction of this article is prohibited.

SELF-ASSESSMENT AND CME

Instructions for Completing *Continuum* Postreading Self-Assessment and CME Test

For information on *Continuum* Audio CME, go to continuum.audio-digest.org.

You must be a *Continuum* subscriber or have purchased a back issue to earn self-assessment and CME (SA-CME) credit for this issue. Institutional access does not include individual CME. To earn credits, complete the Postreading Self-Assessment and CME Test in one of three ways:

1 **Go to** contінpub.com/CME and complete the test online (available to subscribers only)

2 **Read** through the questions in the issue and mark your answers on the adjacent tally sheet before entering them online at continpub.com/CME, or

3 **Email** ContinuumCME@aan.com for online access if you are a nonsubscriber who has a single issue.

Participants have up to 3 years from the date of publication online to earn *AMA PRA Category 1 Credit*™ from this issue.

US Participants
The ABPN has reviewed *Continuum: Lifelong Learning in Neurology* and has approved this product as part of a comprehensive lifelong learning and self-assessment program, which is mandated by the ABMS as a necessary component of Continuing Certification (CC).

US participants may earn up to 20 *AMA PRA Category 1 Credits* in SA-CME by completing the Postreading Self-Assessment and CME Test. AAN members can view and download a report of SA-CME credits earned on the AAN's NeuroTracker™ on aan.com within 2 business days. AAN nonmember subscribers may request a transcript of credits earned by contacting AAN Member Services at memberservices@aan.com or (800) 879-1960.

Canadian Participants
This program is an Accredited Self-Assessment Program (Section 3) as defined by the Maintenance of Certification Program of the Royal College of Physicians and Surgeons of Canada and approved by the University of Calgary Office of Continuing Medical Education and Professional Development.

Canadian participants should visit MAINPORT (www.mainport.org) to record learning and outcomes. Canadian participants can claim a maximum of 20 hours per issue (credits are automatically calculated).

For all questions regarding *Continuum* CME, email ContinuumCME@aan.com or call (612) 928-6348.

Continuum®

TALLY SHEET

Postreading Self-Assessment and CME Test Responses

After completing this tally sheet, please enter your answers online at continpub.com/CME.

NEUROIMAGING
Vol. 29 No. 1 February 2023

1	A	B	C	D	E	21	A	B	C	D	E
2	A	B	C	D	E	22	A	B	C	D	E
3	A	B	C	D	E	23	A	B	C	D	E
4	A	B	C	D	E	24	A	B	C	D	E
5	A	B	C	D	E	25	A	B	C	D	E
6	A	B	C	D	E	26	A	B	C	D	E
7	A	B	C	D	E	27	A	B	C	D	E
8	A	B	C	D	E	28	A	B	C	D	E
9	A	B	C	D	E	29	A	B	C	D	E
10	A	B	C	D	E	30	A	B	C	D	E
11	A	B	C	D	E	31	A	B	C	D	E
12	A	B	C	D	E	32	A	B	C	D	E
13	A	B	C	D	E	33	A	B	C	D	E
14	A	B	C	D	E	34	A	B	C	D	E
15	A	B	C	D	E	35	A	B	C	D	E
16	A	B	C	D	E	36	A	B	C	D	E
17	A	B	C	D	E	37	A	B	C	D	E
18	A	B	C	D	E	38	A	B	C	D	E
19	A	B	C	D	E	39	A	B	C	D	E
20	A	B	C	D	E	40	A	B	C	D	E

Copyright © American Academy of Neurology. Unauthorized reproduction of this article is prohibited.

Copyright © American Academy of Neurology. Unauthorized reproduction of this article is prohibited.

Postreading Self-Assessment and CME Test

By Nuri Jacoby, MD; Allison L. Weathers, MD, FAAN

NEUROIMAGING

The *Continuum* Postreading Self-Assessment and CME Test is an integral part of the issue that is intended to stimulate thought and help participants assess general understanding of the material presented in this issue. The Postreading Self-Assessment and CME Test is also approved by the American Board of Psychiatry and Neurology (ABPN) to meet the Lifelong Learning (CME), Self-Assessment (SA) (part 2) component for Continuing Certification (CC).

For each item, select the single best response. A tally sheet is provided with this issue to allow the option of marking answers before entering them online at continpub.com/CME. Nonsubscribers who have purchased single back issues should email ContinuumCME@aan.com for instructions to complete this test online.

US PARTICIPANTS: Upon the completion of the Postreading Self-Assessment and CME Test and issue evaluation online at continpub.com/CME, participants may earn up to 20 *AMA PRA Category 1 Credits*™ toward SA-CME. US participants have up to 3 years from the date of publication online to earn SA-CME credits.

CANADIAN PARTICIPANTS: This program is an Accredited Self-Assessment Program (Section 3) as defined by the Maintenance of Certification Program of the Royal College of Physicians and Surgeons of Canada and approved by the University of Calgary Office of Continuing Medical Education and Professional Development. Refer to the CME tab on ContinuumJournal.com for dates of accreditation. Canadian participants should visit MAINPORT (mainport.org) to record learning and outcomes. Canadian participants can claim a maximum of 20 hours per issue (credits are automatically calculated).

Copyright © American Academy of Neurology. Unauthorized reproduction of this article is prohibited.

ARTICLE 1: THE RIGHT IMAGING PROTOCOL FOR THE RIGHT PATIENT

1 Which of the following is a limitation of the American College of Radiology Appropriateness Criteria?

A it does not include recommendations for whether contrast should be used
B it does not include vessel imaging in its recommendations
C it does not recommend disease-specific protocols
D it is not evidence based
E it updates its recommendations only once every 10 years

ARTICLE 2: SAFETY CONSIDERATIONS IN MRI AND CT

2 Which of the following components of MRI is most associated with the risk of patient burns?

A cryogen-based cooling system
B main magnetic field
C radiofrequency amplifier
D time-varying gradient magnetic field
E time-varying radiofrequency magnetic field

3 If appropriate scanning conditions are met, a 70-year-old patient with which of the following conditions would be able to safely have an MRI of the lumbar spine without prescanning investigation or intervention?

A history of cardiac arrhythmia diagnosed in childhood with placement of a pacemaker that has not required replacement
B intractable epilepsy with failed vagus nerve stimulator placement with retained lead
C remote workplace accident that resulted in a retained 1-cm piece of metal embedded in the left calf
D severe hypertension managed with clonidine patches
E type 1 diabetes managed by insulin pump

Copyright © American Academy of Neurology. Unauthorized reproduction of this article is prohibited.

4 **A 46-year-old man presents to the emergency department with the acute onset of left face and arm weakness. The emergency department provider discusses with the patient the concern for stroke and informs him that he will be taken shortly for a CT of the head in which multiple scans will be obtained to look at the brain and its vessels (head CT, CT angiography, and CT perfusion). The patient expresses that he is worried about radiation exposure and cancer risk because he has relatives on both sides of his family who have had cancer. What is the most appropriate way to counsel this patient on his risk so that he can make an informed decision?**

A explain that it is only the accumulated dose of radiation exposure that matters when deciding whether to obtain a diagnostic CT and provide reassurance that he should be fine if this is his first CT
B given the time sensitivity of obtaining images, provide an estimated prediction of the patient's hypothetical cancer risk and place a referral for outpatient genetic consultation for more detailed discussion
C obtain a detailed family history including ages at cancer diagnosis so that a personalized quantitative estimate of risk can be provided before imaging
D provide reassurance that, given the low doses of radiation used in diagnostic CT, the risk of cancer is known to be very small and reiterate why CT is important in the workup of suspected stroke
E share with the patient specific data derived from epidemiologic studies and predictive risk models

5 **What is a potential safety risk of applying aggressive CT radiation dose reduction (eg, more than 50%) when noise reduction techniques such as iterative reconstruction and deep learning–based methods are implemented on the scanner?**

A increased scanning times
B lack of efficacy with vascular imaging
C limits windowing capabilities
D low-contrast lesions may be missed
E mild changes in ventricular size may be missed

Copyright © American Academy of Neurology. Unauthorized reproduction of this article is prohibited.

ARTICLE 3: IMAGING OF CENTRAL NERVOUS SYSTEM ISCHEMIA

6 **What is the recommended Alberta Stroke Programme Early CT Score (ASPECTS) needed to proceed with mechanical thrombectomy without additional advanced imaging in a patient with a large vessel occlusion presenting within 6 hours of the last known well time?**

A ≥3
B ≥4
C ≥5
D ≥6
E ≥7

7 **Which imaging study provides the most accuracy in determining a posterior circulation Alberta Stroke Programme Early CT Score (ASPECTS)?**

A brain MRI
B CT angiogram source images
C MR angiogram source images
D MR perfusion
E noncontrast head CT

8 **Which of the following is a benefit of using multiphase CT angiography in place of traditionally timed CT angiography?**

A better visualization of arterial dissection
B decreased radiation
C improved assessment of collateral circulation
D improved evaluation of posterior circulation
E quicker scan time

9 **Which of the following CT perfusion findings indicate an ischemic penumbra?**

A decreased cerebral blood flow, increased mean transit time, and decreased cerebral blood volume
B decreased cerebral blood flow, increased mean transit time, and normal cerebral blood volume
C decreased cerebral blood flow, normal mean transit time, and decreased cerebral blood volume
D normal cerebral blood flow, increased mean transit time, and decreased cerebral blood volume
E normal cerebral blood flow, normal mean transit time, and normal cerebral blood volume

Copyright © American Academy of Neurology. Unauthorized reproduction of this article is prohibited.

10 **A 75-year-old man presents with acute onset ataxia that he noticed when standing up to walk 45 minutes before presentation to the emergency department. On examination, he has right finger-to-nose dysmetria and right heel-to-shin dysmetria, as well as an ataxic gait. Head CT and CT angiogram are both normal. Brain MRI 90 minutes after symptom onset is normal. Which of the following tests is most likely to be diagnostic of the patient's symptoms?**

A anti-glutamic acid decarboxylase (GAD) antibody
B head MR angiography
C lumbar puncture
D repeat brain MRI
E vitamin E

ARTICLE 4: IMAGING OF CENTRAL NERVOUS SYSTEM HEMORRHAGE

11 **Which of the following diseases may impact the utility of noncontrast head CT in detecting an acute central nervous system hemorrhage?**

A congestive heart failure
B diabetes mellitus type 1
C hypercholesterolemia
D hypothyroidism
E iron deficiency anemia

12 **The spot sign's clinical value in patients with intracerebral hemorrhage is most accurately described by which of the following?**

A a component of the Intracerebral Hemorrhage Stroke Score, it is a key factor in the decision to limit life-sustaining measures
B frequently precedes neurologic deterioration prompting consideration of transfer to a higher level of care
C signifies a ruptured underlying arteriovenous malformation prompting emergent neurosurgical intervention
D stability or reduction in size between initial imaging and repeat imaging 12 hours later portends a good prognosis
E strongly correlates with 30-day mortality

13 **Which of the following is a limitation of transcranial color-coded duplex as compared with transcranial Doppler ultrasound?**

A angle correction is not possible
B does not allow for structural imaging
C machines are less portable
D requires advanced technical skills and additional experience to perform
E serial monitoring of subdural hematomas is not possible

Copyright © American Academy of Neurology. Unauthorized reproduction of this article is prohibited.

ARTICLE 5: IMAGING IN EPILEPSY

14 **A 4-year-old girl presents with seizures since she was 6 months old. During her seizures, she turns her head to the right and extends her right arm. She is currently on levetiracetam and oxcarbazepine with moderate control of seizures. Brain MRI completed 3 years ago was normal. EEG has shown interictal slowing over the left frontal region. What is the next best step in management?**

A addition of clobazam
B ictal subtraction single-photon emission computerized tomography (SPECT)
C magnetoencephalography
D repeat brain MRI with dedicated three-dimensional epilepsy protocol
E video-EEG with positron emission tomography (PET)

15 **A 22-year-old man presents with seizures that consist of staring spells associated with fumbling hand movements for the past year and a sense of déjà vu. He recently had an epilepsy protocol MRI of the brain, which was read as normal, with a comment that attention was paid to the hippocampus. When looking at the MRI of this patient, which of the following regions should also be carefully analyzed?**

A amygdala, temporal pole, and the parahippocampal gyrus
B dorsal posterior cingulate gyrus
C inferior parietal lobe
D orbitofrontal cortex
E prefrontal cortex

16 **An 18-year-old man with epilepsy has a brain MRI that shows a cystic lesion in the right superior temporal sulcus with an enhancing mural nodule and calcifications noted on susceptibility-weighted imaging. What is the most likely diagnosis?**

A angiocentric glioma
B dysembryoplastic neuroepithelial tumor
C ganglioglioma
D oligodendroglioma
E pleomorphic xanthoastrocytoma

Copyright © American Academy of Neurology. Unauthorized reproduction of this article is prohibited.

ARTICLE 6: IMAGING OF SKULL BASE TUMORS

17 Which radiologic feature of solitary fibrous tumors can help distinguish them from meningioma on MRI?

A avid contrast enhancement
B hyperostosis
C intratumoral calcifications
D multiple enhancing pachymeningeal foci
E prominent flow voids

18 Which of the following radiographic features is characteristically shared between chordomas and chondrosarcomas?

A hyperintense appearance on T2-weighted MRI
B midline origin with expansion occurring posteriorly and laterally
C paramedian eccentric growth through the skull base
D prominent restricted diffusion demonstrated on diffusion-weighted MRI
E pronounced calcification seen on CT

19 Which of the following skull base lesions appears hyperintense on unenhanced T1-weighted MRI?

A arachnoid cysts
B dermoid cysts
C epidermoid cysts
D pituitary microadenoma
E schwannoma

ARTICLE 7: IMAGING OF BRAIN TUMORS

20 Measurement of oncometabolite 2-hydroxyglutarate (2HG) by MR spectroscopy can be helpful in diagnosing a glioma that has a mutation of which gene?

A *ATRX*
B *BRAF*
C *IDH*
D *TERT*
E *TP53*

Copyright © American Academy of Neurology. Unauthorized reproduction of this article is prohibited.

21 **Which of the following imaging findings favors pseudoprogression rather than tumor progression?**

A decreased *N*-acetylaspartate on MR spectroscopy
B decreased uptake on amino acid positron emission tomography (PET)
C elevated cerebral blood volume on perfusion imaging
D increased choline-to-creatine ratio on MR spectroscopy
E low apparent diffusion coefficient on MRI

22 **A 68-year-old woman with past medical history of hypertension presents with 1 month of worsening cognitive symptoms. Brain MRI demonstrates periventricular, multifocal, homogeneously enhancing lesions with restricted diffusion and mild surrounding vasogenic edema. What is the most likely diagnosis?**

A astrocytoma, *IDH* mutation
B central nervous system lymphoma
C central nervous system metastases
D ependymoma
E glioblastoma, *IDH* wild-type

23 **A 22-year-old man presents with mildly unsteady gait and worsening morning headaches for the past few weeks. Family history is notable for his mother having a brain tumor although he does not know the details. Brain MRI demonstrates a cystic lesion in the right cerebellum with a solid enhancing mural nodule. Given the most likely diagnosis, what annual screening is recommended?**

A audiometry
B dermatologic examination
C pulmonary function tests
D retinal screening
E transthoracic echocardiogram

24 **Which of the following tumors is often located within the fourth ventricle?**

A central neurocytoma
B colloid cyst
C ependymoma
D lymphoma
E subependymal giant cell astrocytoma

Copyright © American Academy of Neurology. Unauthorized reproduction of this article is prohibited.

ARTICLE 8: IMAGING IN MOVEMENT DISORDERS

25 Which of the following best describes the relationship between the findings on dopamine transporter single-photon emission computed tomography (DAT-SPECT) and the severity of motor signs of idiopathic Parkinson disease?

A striatal uptake correlates with motor severity in a constant manner throughout the entire disease course
B striatal uptake correlates with motor severity late in the disease course (after a minimum of 5 years of clinical symptoms)
C striatal uptake correlates with motor severity only in the early stages of disease
D striatal uptake has not been found to correlate with any pre- or postmortem measures of motor severity
E striatal uptake strongly correlates with postmortem measures of striatal dopaminergic terminal axons, although it does not correlate with clinical assessment

26 Which of the following medications can result in a false-positive dopamine transporter single-photon emission computed tomography (DAT-SPECT) scan?

A amphetamine
B colchicine
C levothyroxine
D lorazepam
E meloxicam

ARTICLE 9: NEUROIMAGING IN DEMENTIA

27 Which of the following regions becomes positive in amyloid imaging in the later stages of Alzheimer disease?

A cerebellum
B periaqueductal gray
C striatum
D substantia nigra
E thalamus

Copyright © American Academy of Neurology. Unauthorized reproduction of this article is prohibited.

28 **A 78-year-old man presents with 1 year of mild cognitive changes noted by his family, as well as frequent falls. His spouse notes that while sleeping the patient appears scared and looks like he is fighting someone in his dreams. Examination is notable for bradykinesia and rigidity in his right arm and mild shuffling gait. Brain MRI is normal. What finding would be expected on a fludeoxyglucose positron emission tomography (FDG-PET)?**

A cingulate island sign
B global hypoperfusion
C hyperperfusion in bilateral occipital lobes
D hypoperfusion in bilateral precuneus
E hypoperfusion in the cerebellum

29 **Decreased dopamine transporter binding to what structure is associated with cognitive symptoms in Parkinson disease dementia?**

A caudate
B cerebellum
C pons
D putamen
E subthalamic nucleus

30 **A 53-year-old man presents with 18 months of progressive language impairment with marked difficulty repeating sentences and frequent pauses to find the right word. Brain MRI is unrevealing. Which of the following studies would be most helpful to establish the diagnosis?**

A amyloid positron emission tomography (PET)
B diffusion tensor imaging
C dopamine transporter single-photon emission computed tomography (DAT-SPECT) scan
D fludeoxyglucose positron emission tomography (FDG-PET)
E MRI of the brain

Copyright © American Academy of Neurology. Unauthorized reproduction of this article is prohibited.

31 **A 67-year-old woman presents with several months of progressive headaches and multiple cranial neuropathies. In addition to her neurologic findings on examination, she is observed to be jaundiced and cachectic and to have enlargement of the parotid and submandibular glands. Systemic imaging has revealed bile duct lesions, a "sausage-shaped pancreas," and renal lesions. Serum IgG4 concentration is 10 times the upper limit of normal. Which of the following neuroimaging findings would be most expected in this patient?**

A enhancement of the pons on postcontrast T1-weighted MRI
B hyperdense dural lesions on noncontrast CT
C hyperintense basal ganglia lesions on precontrast T1-weighted MRI
D hypodense parenchymal lesions on noncontrast CT
E restricted diffusion of the corpus callosum on diffusion-weighted MRI

32 **Findings of unilateral hemispheric hypometabolism on brain fludeoxyglucose positron emission tomography (FDG-PET) is most consistent with which of the following diagnoses?**

A herpes simplex virus encephalitis
B immune checkpoint inhibitor–induced encephalitis
C leucine-rich glioma inactivated protein 1 (LGI1) antibody encephalitis
D *N*-methyl-D-aspartate receptor encephalitis
E Rasmussen encephalitis

33 **What is the most appropriate next step in the workup of a 20-year-old man with subacute onset of excessive daytime sleepiness and autonomic disturbances who is found to have hyperintensities with associated enhancement of the medial thalami and midbrain on brain MRI?**

A brain biopsy
B CT of the chest
C MRI of the spine
D positron emission tomography (PET) of the brain
E testicular ultrasonography

Copyright © American Academy of Neurology. Unauthorized reproduction of this article is prohibited.

34 Which of the following best describes the utility of the black blood MRI sequence?

A can diagnose spinal cord infarct earlier than traditional MRI
B differentiates cerebral amyloid angiopathy–related inflammation from amyloid-β–related angiitis
C differentiates reversible cerebral vasoconstriction syndrome from cerebral autosomal dominant arteriopathy with subcortical infarcts and leukoencephalopathy
D noninvasively assesses vessel wall inflammation in patients with suspected vasculitis
E tracks treatment response in Takayasu arteritis

ARTICLE 11: IMAGING OF CENTRAL NERVOUS SYSTEM DEMYELINATING DISORDERS

35 Which of the following MRI findings is required as part of the diagnosis of radiologically isolated syndrome?

A greater than or equal to one enhancing lesion
B greater than or equal to two juxtacortical lesions
C greater than or equal to three periventricular lesions
D MRI involvement in at least two of four typical locations
E presence of simultaneous enhancing and nonenhancing lesions on MRI

36 In suspected multiple sclerosis lesions that show gadolinium enhancement, what is the typical duration after which alternative etiologies should be considered more carefully?

A 2 to 4 weeks
B 4 to 6 weeks
C 6 to 8 weeks
D 8 to 10 weeks
E 10 to 12 weeks

Copyright © American Academy of Neurology. Unauthorized reproduction of this article is prohibited.

37 **A 41-year-old woman presents with 4 days of worsening confusion, sleepiness, nausea, and vomiting, as well as pain and gradual worsening vision in her right eye. The patient and her family report no recent illness. Examination reveals severe fluctuating encephalopathy, and visual acuity testing when the patients is more lucid shows she has light perception only in the right eye. Laboratory values are notable for sodium at 123 mmol/L, and brain MRI shows T2 hyperintensities in the subthalamic area, as well as extensive T2 hyperintensities of the right optic nerve that are greater than 75% of its length. Lumbar puncture and other blood tests are pending. What is the recommended treatment for this patient?**

A IV immunoglobulin
B methylprednisolone
C methylprednisolone and IV immunoglobulin
D methylprednisolone and plasma exchange
E plasma exchange

38 **An 18-year-old man with no significant past medical history presents with 3 days of weakness and numbness in his legs, as well as urinary retention. MRI reveals a T8-L2 T2-hyperintense lesion that predominantly affects the central grey matter and does not demonstrate enhancement. No flow voids are present. Based on the history and imaging findings, which of the following is the most likely diagnosis?**

A myelin oligodendrocyte glycoprotein (MOG)–associated disorder
B multiple sclerosis
C neuromyelitis optica spectrum disorder
D neurosarcoidosis
E spinal dural arteriovenous fistula

ARTICLE 12: DIAGNOSTIC ULTRASONOGRAPHY IN NEUROLOGY

39 **The presence of which of the following signs on extracranial neurovascular ultrasonography is highly specific for the diagnosis of giant cell arteritis?**

A halo sign
B macaroni sign
C microembolic signals
D S-curve sign
E string sign

Copyright © American Academy of Neurology. Unauthorized reproduction of this article is prohibited.

40 **The time-averaged mean of the maximum blood flow velocity is most useful to guide management decisions in children in which of the following diseases?**

A idiopathic intracranial hypertension
B moyamoya disease
C sickle cell disease
D transient perivascular inflammation of the carotid artery
E vertebral dissection

Copyright © American Academy of Neurology. Unauthorized reproduction of this article is prohibited.

Postreading Self-Assessment and CME Test—Preferred Responses

By Nuri Jacoby, MD; Allison L. Weathers, MD, FAAN

NEUROIMAGING

Following are the preferred responses to the questions in the Postreading Self-Assessment and CME Test in this *Continuum* issue. The preferred response is followed by an explanation and a reference with which you may seek more specific information. You are encouraged to review the responses and explanations carefully to evaluate your general understanding of the article topic. The comments and references included with each question are intended to encourage independent study.

US PARTICIPANTS: Upon completion of the Postreading Self-Assessment and CME Test and issue evaluation online at continpub.com/CME, participants may earn up to 20 *AMA PRA Category 1 Credits*™ toward SA-CME. US participants have up to 3 years from the date of publication online to earn SA-CME credits.

CANADIAN PARTICIPANTS: This program is an Accredited Self-Assessment Program (Section 3) as defined by the Maintenance of Certification Program of the Royal College of Physicians and Surgeons of Canada and approved by the University of Calgary Office of Continuing Medical Education and Professional Development. Refer to the CME tab on ContinuumJournal.com for dates of accreditation. Canadian participants should visit MAINPORT (mainport.org) to record learning and outcomes. Canadian participants can claim a maximum of 20 hours per issue (credits are automatically calculated).

Copyright © American Academy of Neurology. Unauthorized reproduction of this article is prohibited.

ARTICLE 1: THE RIGHT IMAGING PROTOCOL FOR THE RIGHT PATIENT

1 The preferred response is **C (it does not recommend disease-specific protocols).** Although the American College of Radiology Appropriateness Criteria provide general recommendations and can begin to help a clinician determine the correct imaging modality for a patient, it does not recommend disease-specific protocols. For more information, refer to **page 16** of the *Continuum* article "The Right Imaging Protocol for the Right Patient."

ARTICLE 2: SAFETY CONSIDERATIONS IN MRI AND CT

2 The preferred response is **E (time-varying radiofrequency magnetic field).** The radiofrequency coils are closest to the patient-adjacent bore wall and are the component that is associated with heating and burns, which are the most common type of MRI safety events (as reported to the US Food and Drug Administration [FDA]). Proximity to the bore wall and skin-to-skin contact increase the risk of this adverse event. For more information, refer to **page 29** of the *Continuum* article "Safety Considerations in MRI and CT."

3 The preferred response is **C (remote workplace accident that resulted in a retained 1-cm piece of metal embedded in the left calf).** Small (less than 2 cm) metallic foreign bodies, shrapnel, and bullets are considered MRI-conditional, as long as they are not in proximity to or within a vital structure. Scarring and formation of dense connective tissue over time prevent displacement, and at commonly used magnet strengths (1.5T and 3T), significant heating does not occur for a fragment of that size. For implanted devices to be considered MRI-conditional, the exact make, model, and status of all components must be first identified. Foil-backed medication patches may heat, resulting in burns, and would need to be removed before scanning. For more information, refer to **page 39** of the *Continuum* article "Safety Considerations in MRI and CT."

Copyright © American Academy of Neurology. Unauthorized reproduction of this article is prohibited.

4 The preferred response is **D (provide reassurance that, given the low doses of radiation used in diagnostic CT, the risk of cancer is known to be very small and reiterate why CT is important in the workup of suspected stroke).** It is important that patients feel safe in receiving clinically appropriate medical imaging and that they are not inadvertently deterred, given the potential of negative consequences. The cancer risk from the very low radiation doses used in diagnostic CT is known to be very small, without a clear consensus on the exact risk. Therefore, providing specific data (whether a personalized quantitative estimate of risk or detailed discussion of the literature) when counseling patients is strongly discouraged by the major radiation protection organizations. Accumulated radiation dose from prior imaging examinations should also not be factored into current imaging decisions. Only the utility and appropriateness of the modality based on the patient's current clinical picture and the potential benefits of the imaging should be considered. For more information, refer to **pages 44-45** of the *Continuum* article "Safety Considerations in MRI and CT."

5 The preferred response is **D (low-contrast lesions may be missed).** The use of techniques such as iterative reconstruction and deep learning–based noise reduction methods can be used to improve image quality and as a way to achieve radiation dose reduction while maintaining baseline image quality. However, if too aggressive a dose reduction (beyond 20% to 30%) is used, low-contrast lesions may be missed. For more information, refer to **pages 46-47** of the *Continuum* article "Safety Considerations in MRI and CT."

ARTICLE 3: IMAGING OF CENTRAL NERVOUS SYSTEM ISCHEMIA

6 The preferred response is **D (≥6).** American Heart Association/American Stroke Association guidelines recommend an Alberta Stroke Programme Early CT Score (ASPECTS) of greater than or equal to 6 to proceed with mechanical thrombectomy without advanced imaging for patients presenting within 6 hours of last known well time. This criterion was used in three of four clinical trials that demonstrated a benefit of endovascular therapy in patients presenting with large vessel occlusions in this time window. For more information, refer to **page 57** of the *Continuum* article "Imaging of Central Nervous System Ischemia."

Copyright © American Academy of Neurology. Unauthorized reproduction of this article is prohibited.

7 The preferred response is **B (CT angiogram source images).** The Alberta Stroke Programme Early CT Score (ASPECTS) is a CT-based scoring system, excluding answer choices A, C, and D. While it is possible to calculate posterior-circulation ASPECTS on a noncontrast head CT, significant beam hardening artifact in the posterior fossa often limits accuracy. Using CT angiogram source images limits that artifact and can, therefore, provide a more accurate posterior-circulation ASPECTS. For more information, refer to **page 57** of the *Continuum* article "Imaging of Central Nervous System Ischemia."

8 The preferred response is **C (improved assessment of collateral circulation).** In multiphase CT angiography, three sets of images are acquired, instead of the sole arterial time point done in traditionally timed CT angiography. This results in improved visualization of the collateral circulation. For more information, refer to **page 60** of the *Continuum* article "Imaging of Central Nervous System Ischemia."

9 The preferred response is **B (decreased cerebral blood flow, increased mean transit time, and normal cerebral blood volume).** An ischemic penumbra is characterized by decreased cerebral blood flow, increased mean transit time, and normal or increased cerebral blood volume. For more information, refer to **page 62** of the *Continuum* article "Imaging of Central Nervous System Ischemia."

10 The preferred response is **D (repeat brain MRI).** Of patients with acute ischemic strokes, 6.8% may be diffusion-weighted imaging (DWI) negative. This most commonly occurs with hyperacute strokes with MRI occurring less than 2 hours after symptom onset, as well as with small, posterior circulation strokes. As the brain MRI in this patient was obtained 90 minutes after symptom onset and high clinical suspicion for posterior circulation ischemia remained, a repeat brain MRI is recommended. For more information, refer to **page 64** of the *Continuum* article "Imaging of Central Nervous System Ischemia."

Copyright © American Academy of Neurology. Unauthorized reproduction of this article is prohibited.

ARTICLE 4: IMAGING OF CENTRAL NERVOUS SYSTEM HEMORRHAGE

11 The preferred answer is **E (iron deficiency anemia).** Acute blood is hyperdense on CT because of the iron in hemoglobin. Iron deficiency anemia may make it more difficult to detect acute hemorrhage as it will not appear as hyperdense. Of the options provided, iron deficiency anemia is the best response. For more information, refer to **page 74** of the *Continuum* article "Imaging of Central Nervous System Hemorrhage."

12 The preferred answer is **B (frequently precedes neurologic deterioration prompting consideration of transfer to a higher level of care).** The spot sign is a focal area of increased density within the larger area of hemorrhage seen on CT angiography. It is caused by contrast extravasation and is a predictor of hemorrhage expansion, which often results in clinical neurologic deterioration. Therefore, its finding should prompt consideration of transfer to a higher level of care, such as a neurocritical care unit. For more information, refer to **pages 80-81** of the *Continuum* article "Imaging of Central Nervous System Hemorrhage."

13 The preferred answer is **C (machines are less portable).** The advantage of transcranial color-coded duplex over transcranial doppler ultrasound (TCD) is that it provides a real-time structural imaging aspect. This in turn enables serial monitoring of subdural hematomas and intraparenchymal hematomas. Transcranial color-coded duplex requires less technical skill and experience in comparison with TCD. A transcranial color-coded duplex software package is added to a standard ultrasound cart used for peripheral vascular imaging or body ultrasound, which are much larger and less portable than TCD machines. For more information, refer to **page 77** of the *Continuum* article "Imaging of Central Nervous System Hemorrhage."

Copyright © American Academy of Neurology. Unauthorized reproduction of this article is prohibited.

ARTICLE 5: IMAGING IN EPILEPSY

14 The preferred response is **D (repeat brain MRI with dedicated three-dimensional epilepsy protocol).** Certain abnormalities on brain MRI such as focal cortical dysplasia are not evident from infancy to 18 months of age. This is because of the dynamic changes in myelination that occur during this period, resulting in a lack of delineation between the gray and white matter. Therefore, all patients with epilepsy who are 2 years old and older with a prior normal brain MRI should have a follow-up International League Against Epilepsy–endorsed Harmonized Neuroimaging of Epilepsy Structural Sequences (HARNESS) MRI. For more information, refer to **page 113** of the *Continuum* article "Imaging in Epilepsy."

15 The preferred response is **A (amygdala, temporal pole, and the parahippocampal gyrus).** Given the automatisms and the sense of déjà vu, the temporal lobe is the most likely localization. Besides the hippocampus, evaluation of the amygdala, parahippocampal gyrus, and temporal polar cortex is critical when assessing for seizures with the clinical symptomatology pointing toward the temporal lobe as an etiology. For more information, refer to **page 125** of the *Continuum* article "Imaging in Epilepsy."

16 The preferred response is **C (ganglioglioma).** Gangliogliomas typically are cystic lesions with an enhancing mural nodule, with 30% to 50% demonstrating calcifications. Although pleomorphic xanthoastrocytomas can have a similar appearance on MRI, they are not associated with calcifications and often have leptomeningeal involvement. For more information, refer to **page 134** of the *Continuum* article "Imaging in Epilepsy."

ARTICLE 6: IMAGING OF SKULL BASE TUMORS

17 The preferred response is **E (prominent flow voids).** Solitary fibrous tumors (formerly known as *hemangiopericytomas*) can be strikingly similar in appearance to meningiomas on neuroimaging, making them difficult to distinguish on radiologic assessment alone. A notable distinction is that solitary fibrous tumors are highly vascular with associated prominent flow voids on T2-weighted MRI. The appearance of solitary fibrous tumors on postcontrast T1-weighted MRI can be identical to that of meningioma as both will have avid contrast enhancement. Solitary fibrous tumors tend to cause bony erosion instead of hyperostosis and intratumoral calcification. For more information, refer to **page 162** of the *Continuum* article "Imaging of Skull Base Tumors."

Copyright © American Academy of Neurology. Unauthorized reproduction of this article is prohibited.

18 The preferred response is **A (hyperintense appearance on T2-weighted MRI).** Chordomas and chondrosarcomas both appear hyperintense on T2-weighted MRI and are hypointense or isointense on T1-weighted images. The other options provided are associated with one or the other tumor type and can be used to help differentiate these on neuroimaging. For more information, refer to **page 168** of the *Continuum* article "Imaging of Skull Base Tumors."

19 The preferred response is **B (dermoid cysts).** Because dermoid cysts contain fatty elements, they appear hyperintense on unenhanced T1-weighted MRI. The other options provided appear hypointense to isointense. For more information, refer to **page 168** of the *Continuum* article "Imaging of Skull Base Tumors."

ARTICLE 7: IMAGING OF BRAIN TUMORS

20 The preferred response choice is **C (*IDH*).** Measurement of 2-hydroxyglutarate (2HG) is present in *IDH*-mutated gliomas. Although still primarily used for research, this new MR spectroscopy technique has the potential to aid in diagnosis and interpretation of tumor response to treatment for *IDH*-mutated gliomas. For more information, refer to **page 175** of the *Continuum* article "Imaging of Brain Tumors."

21 The preferred response is **B (decreased uptake on amino acid positron emission tomography [PET]).** Although no single imaging technique is the gold standard in differentiating tumor progression and pseudoprogression, studies have suggested some findings that favor one over the other. A decreased uptake on amino acid PET is associated with pseudoprogression. All other answer choices are more often associated with tumor progression. For more information, refer to **page 177** of the *Continuum* article "Imaging of Brain Tumors."

22 The preferred response is **B (central nervous system lymphoma).** The MRI characteristics of homogeneously enhancing periventricular lesions with restricted diffusion are most consistent with central nervous system lymphoma in an immunocompetent patient. For more information, refer to **page 185** of the *Continuum* article "Imaging of Brain Tumors."

Copyright © American Academy of Neurology. Unauthorized reproduction of this article is prohibited.

23 The preferred response is **D (retinal screening).** The MRI features are most consistent with a hemangioblastoma. Given the positive family history, the most likely diagnosis is von Hippel-Lindau syndrome. Patients with von Hippel-Lindau syndrome need annual retinal screening because retinal capillary hemangioblastomas occur in up to 80% of these patients. For more information, refer to **page 186** of the *Continuum* article "Imaging of Brain Tumors."

24 The preferred response is **C (ependymoma).** Ependymomas may occur in three compartments: supratentorial, posterior fossa, and spine. Posterior fossa ependymomas are primarily localized to the fourth ventricle. Other etiologies of fourth ventricular masses are metastasis, glioneuronal tumors, epidermoid cysts, choroid plexus papilloma, and meningiomas. For more information, refer to **page 185** of the *Continuum* article "Imaging of Brain Tumors."

ARTICLE 8: IMAGING IN MOVEMENT DISORDERS

25 The preferred response is **C (striatal uptake correlates with motor severity only in the early stages of disease).** In patients with early Parkinson disease, dopamine transporter single-photon emission computed tomography (DAT-SPECT) scans typically show greater reduction in striatal uptake in the posterior putamen compared with the caudate contralateral to the more clinically affected side, with correlation between striatal uptake and motor severity. This striatal DAT uptake has a flooring effect, and the correlation does not persist in later disease stages, once nigral cell loss exceeds a certain threshold. Striatal DAT uptake has not been shown to correlate with postmortem measures of striatal dopaminergic terminal axons. For more information, refer to **page 200** of the *Continuum* article "Imaging in Movement Disorders."

26 The preferred response is **A (amphetamine).** Several medications, including stimulants such as amphetamine, dextroamphetamine, and cocaine, can serve as confounders in the interpretation of dopamine transporter single-photon emission computed tomography (DAT-SPECT) scans. This occurs because the radiotracers used in these scans can be cocaine analogues, and stimulant medications such as methylphenidate, amphetamine, and dextroamphetamine can reduce the availability of DATs for binding to such tracers, thus resulting in falsely reduced striatal uptake. For more information, refer to **page 199** of the *Continuum* article "Imaging in Movement Disorders."

Copyright © American Academy of Neurology. Unauthorized reproduction of this article is prohibited.

27 The preferred response is **C (striatum).** Amyloid pathology, which can be seen on molecular imaging and postmortem, begins in the medial parietal and frontal regions, then progresses to most of the cortex, followed by subcortical deposition in the striatum. For more information, refer to **page 226** of the *Continuum* article "Neuroimaging in Dementia."

28 The preferred response is **A (cingulate island sign).** The clinical features of this patient are consistent with a diagnosis of dementia with Lewy bodies. Fludeoxyglucose positron emission tomography (FDG-PET) in patients with dementia with Lewy bodies shows hypoperfusion in the striatum, cerebellum, frontal and parietal lobes, and the occipital lobe, with sparing of the posterior cingulate gyrus, called the *cingulate island sign*. For more information, refer to **page 242** of the *Continuum* article "Neuroimaging in Dementia."

29 The preferred response is **A (caudate).** Dopamine transporter scans can be helpful in the diagnosis of dementia with Lewy bodies and Parkinson disease dementia with reduced tracer binding in the striatum and cortex. Decreased DAT binding in the caudate, specifically, has been associated with cognitive symptoms in these patients. For more information, refer to **page 237** of the *Continuum* article "Neuroimaging in Dementia."

30 The preferred response is **A (amyloid positron emission tomography [PET]).** This patient presents with a slowly progressive aphasia, consistent with a primary progressive aphasia (PPA). Of the three PPAs, his clinical picture is most consistent with logopenic variant PPA, a variant of Alzheimer disease. Although brain MRI can be helpful because it may show variable types of atrophy among the three subtypes of PPA, an amyloid PET scan would be positive in logopenic variant PPA and negative in the other two, most clearly establishing the diagnosis. For more information, refer to **page 236** of the *Continuum* article "Neuroimaging in Dementia."

Copyright © American Academy of Neurology. Unauthorized reproduction of this article is prohibited.

ARTICLE 10: IMAGING OF CENTRAL NERVOUS SYSTEM AUTOIMMUNE, PARANEOPLASTIC, AND NEURO-RHEUMATOLOGIC DISORDERS

31 The preferred response is **B (hyperdense dural lesions on noncontrast CT).** The patient's presentation is consistent with a diagnosis of IgG4-related disease, a progressive disease that can involve the dura and meninges, orbits, pancreas, biliary tract, and kidneys among other organs. The most frequent neurologic manifestation is pachymeningitis with dural lesions appearing as hyperdense on noncontrast CT, a finding that can be mistaken for subdural hematoma. For more information, refer to **pages 261-262** of the *Continuum* article "Imaging of Central Nervous System Autoimmune, Paraneoplastic, and Neuro-rheumatologic Disorders."

32 The preferred response is **E (Rasmussen encephalitis).** Brain fludeoxyglucose positron emission tomography (FDG-PET) can show hemispheric hypometabolism in Rasmussen encephalitis that is out of proportion to the degree of atrophy seen on MRI, which can help solidify the diagnosis. For more information, refer to **page 267** of the *Continuum* article "Imaging of Central Nervous System Autoimmune, Paraneoplastic, and Neuro-rheumatologic Disorders."

33 The preferred response is **E (testicular ultrasonography).** The patient's presentation and MRI findings are most consistent with a diagnosis of anti-Ma2–associated encephalitis, which is characterized by diencephalon and brainstem dysfunction. Anti-Ma2–associated encephalitis is most commonly associated with testicular germ-cell tumors. Therefore, of the options provided, testicular ultrasonography is the most appropriate next step in the workup of this patient. For more information, refer to **page 270** of the *Continuum* article "Imaging of Central Nervous System Autoimmune, Paraneoplastic, and Neuro-rheumatologic Disorders."

Copyright © American Academy of Neurology. Unauthorized reproduction of this article is prohibited.

34 The preferred response is **D (noninvasively assesses vessel wall inflammation in patients with suspected vasculitis).** The black blood MRI sequence is the informal name for high-resolution MRI with vessel wall imaging. Vessel wall imaging is a noninvasive method of assessing vessel wall inflammation. This is accomplished through the simultaneous suppression of CSF and luminal contrast, which makes postcontrast enhancement in affected vessel walls more apparent. In patients with central nervous system vasculitis, multifocal areas of concentric wall thickening and enhancement corresponding to areas with a caliber change may be seen on vessel wall imaging. Although noninflammatory vasculopathies may have a similar appearance on vessel wall imaging, the pattern of wall enhancement (circumferential for vasculitis) and degree of enhancement may help differentiate between these diagnoses. For more information, refer to **pages 281-282** of the *Continuum* article "Imaging of Central Nervous System Autoimmune, Paraneoplastic, and Neuro-rheumatologic Disorders."

ARTICLE 11: IMAGING OF CENTRAL NERVOUS SYSTEM DEMYELINATING DISORDERS

35 The preferred response is **C (greater than or equal to three periventricular lesions).** The imaging criteria for radiologically isolated syndrome follow the 2001 McDonald MRI criteria for dissemination in space, which is stricter than the 2017 revised McDonald criteria. To fulfill the criteria, nine or more T2 hyperintense lesions or one or more enhancing lesions, one or more infratentorial lesions, one or more juxtacortical lesions, and three or more periventricular lesions must be present. For more information, refer to **page 296** of the *Continuum* article "Imaging of Central Nervous System Demyelinating Disorders."

36 The preferred response is **B (4 to 6 weeks).** Active multiple sclerosis lesions enhance for 4 to 6 weeks after lesion formation. For more information, refer to **page 299** of the *Continuum* article "Imaging of Central Nervous System Demyelinating Disorders."

Copyright © American Academy of Neurology. Unauthorized reproduction of this article is prohibited.

37 The preferred response is **D (methylprednisolone and plasma exchange).** This patient's clinical presentation is most consistent with neuromyelitis optica spectrum disorder given the optic neuritis with MRI showing greater than 50% of the nerve length being involved and the acute diencephalic clinical syndrome. As it can take time for aquaporin-4-IgG antibody results, it is recommended to start empiric treatment. Given the severity of the presentation, the recommended treatment would be to initiate steroids and plasma exchange. For more information, refer to **page 305** of the *Continuum* article "Imaging of Central Nervous System Demyelinating Disorders."

38 The preferred response is **A (myelin oligodendrocyte glycoprotein [MOG]-associated disorder).** All answer choices except for multiple sclerosis commonly present with a longitudinally extensive transverse myelitis. The MRI findings, however, are most suggestive of MOG-associated disorder, specifically the lack of enhancement and the lesion predominantly affecting the central grey matter. For more information, refer to **page 310** of the *Continuum* article "Imaging of Central Nervous System Demyelinating Disorders."

ARTICLE 12: DIAGNOSTIC ULTRASONOGRAPHY IN NEUROLOGY

39 The preferred response is **A (halo sign).** The halo sign results from hypoechogenic noncompressible wall thickening of the temporal arteries that can be visualized on extracranial neurovascular ultrasonography. This sign has been found in some studies to have a 96% specificity and 77% sensitivity for the diagnosis of giant cell arteritis when detected unilaterally. The diagnostic value increases when the halo sign is present bilaterally. For more information, refer to **page 333** of the *Continuum* article "Diagnostic Ultrasonography in Neurology."

40 The preferred response is **C (sickle cell disease).** Annual screening with transcranial Doppler sonography is recommended for children with sickle cell disease and sickle beta-thalassemia as regular screening and subsequent transfusion of patients with abnormal transcranial Doppler velocities has been shown to decrease the prevalence of strokes. A single time-averaged mean of the maximum blood flow velocity measurement of greater than 220 cm/s detected in the proximal portion of the middle cerebral artery or the distal portion of the internal carotid artery should prompt blood transfusion. Alternatively, transfusion would also be indicated with the finding of two nonimaging transcranial Doppler measurements greater than or equal to 200 cm/s. For more information, refer to **page 342** of the *Continuum* article "Diagnostic Ultrasonography in Neurology."

Copyright © American Academy of Neurology. Unauthorized reproduction of this article is prohibited.

LEARNING OBJECTIVES AND CORE COMPETENCIES

Learning Objectives

Upon completion of this *Continuum: Lifelong Learning in Neurology* Neuroimaging issue, participants will be able to:

- Describe governing rules for choosing an imaging modality or a specific imaging protocol in an individual patient, with emphasis on the limitations of predefined protocols and the importance of clinical context
- Describe the physical and procedural safety risks of MRI and CT, which are essential imaging modalities for the diagnosis of neurologic disease
- Describe the imaging modalities used in the evaluation of patients presenting with acute ischemic stroke, including technical considerations, interpretation, and clinical utility of each modality
- Describe the role of neuroimaging in guiding identification of central nervous system hemorrhage, aiding in identification of hemorrhage etiology, and guiding subsequent medical decision making
- Describe a methodical approach to the integration of neuroimaging in the clinical care of patients with epilepsy
- Discuss the classic imaging features of common skull base tumors and their implications in surveillance, as well as management of these tumors
- Describe essential imaging modalities in the treatment of patients with brain tumors and recognize common imaging patterns for tumors and certain clinical scenarios
- Recognize abnormal findings on conventional clinical imaging in movement disorders and critically evaluate their relationship with pathology, utility, and limitations; and describe some other imaging modalities used in research and recent findings
- Identify and describe neuroimaging findings in the most common age-related dementias
- Describe the imaging patterns typical of autoimmune and inflammatory brain and spinal cord diseases, causes of the limbic encephalitis pattern on MRI, and findings on MRI that can help distinguish causes of myelitis
- Discuss the role of MRI in both the diagnosis and prognosis of multiple sclerosis and antibody-mediated demyelinating diseases such as myelin oligodendrocyte glycoprotein–associated disorder, acquired disseminated encephalomyelitis, and neuromyelitis optica
- Discuss the technical requirements, applications, and limitations of ultrasonography in central nervous system neurology

Core Competencies

This *Continuum: Lifelong Learning in Neurology* Neuroimaging issue covers the following core competencies:

- Patient Care and Procedural Skills
- Medical Knowledge
- Practice-Based Learning and Improvement
- Interpersonal and Communication Skills
- Professionalism
- Systems-Based Practice

Copyright © American Academy of Neurology. Unauthorized reproduction of this article is prohibited.

LIST OF ABBREVIATIONS

Neuroimaging

2HG	2-hydroxyglutarate
^{99m}Tc-ECD	Technetium 99m–ethyl cysteinate dimer
^{99m}Tc-HMPAO	Technetium 99m–hexamethylpropyleneamine oxime
A/T/N	Amyloid, tau, neurodegeneration
AAN	American Academy of Neurology
Aβ	Amyloid-β
ACR	American College of Radiology
ACTH	Adrenocorticotropic hormone
AD	Alzheimer disease
ADC	Apparent diffusion coefficient
ADEM	Acute disseminated encephalomyelitis
AHA	American Heart Association
ALARA	As low as reasonably achievable
ALS	Amyotrophic lateral sclerosis
ANCA	Antineutrophil cytoplasmic antibody
APOE	Apolipoprotein E
APOE ε4	Apolipoprotein E ε4 allele
APT	Amide proton transfer
AQP4	Aquaporin-4
ASA	American Stroke Association
ASPECTS	Alberta Stroke Programme Early CT Score
AVM	Arteriovenous malformation
BOLD	Blood oxygenation level dependent
CA	Cornu ammonis
CAA	Cerebral amyloid angiopathy
CADASIL	Cerebral autosomal dominant arteriopathy with subcortical infarcts and leukoencephalopathy
CASPR2	Contactin-associated proteinlike 2
CBD	Corticobasal degeneration
CIS	Clinically isolated syndrome
CJD	Creutzfeldt-Jakob disease
CLIPPERS	Chronic lymphocytic inflammation with pontine perivascular enhancement responsive to steroids
CNS	Central nervous system
CRMP5	Collapsin response mediator protein-5
CSF	Cerebrospinal fluid
CT	Computed tomography
CTA	Computed tomography angiography
$CTDI_{vol}$	CT dose index
CTP	Computed tomography perfusion
DAT	Dopamine transporter
DBS	Deep brain stimulation
DLB	Dementia with Lewy bodies
DNET	Dysembryoplastic neuroepithelial tumor
DSA	Digital subtraction angiography
DWI	Diffusion-weighted imaging
ECG	Electrocardiogram
ECMO	Extracorporeal membrane oxygenation
EEG	Electroencephalogram
ESCAPE	Endovascular Treatment for Small Core and Anterior Circulation Proximal Occlusion
EVD	External ventricular drainage
FDA	US Food and Drug Administration
FDG-PET	Fludeoxyglucose positron emission tomography
FEOBV	(-)-5-[^{18}F]-fluoroethoxybenzovesamicol
FIESTA	Fast imaging employing steady state acquisition
FLAIR	Fluid-attenuated inversion recovery
FLAMES	Fluid-attenuated inversion recovery–hyperintense lesions in anti–myelin oligodendrocyte glycoprotein–associated encephalitis with seizures
fMRI	Functional magnetic resonance imaging
FSE	Fast spin echo
FTLD	Frontotemporal lobar degeneration
FUS	Fused in sarcoma
FXTAS	Fragile X tremor-ataxia syndrome
GABA	γ-Aminobutyric acid
GAD65	Glutamic acid decarboxylase 65
GCA	Giant cell arteritis
GFAP	Glial fibrillary acidic protein
GRE	Gradient recalled echo
HARNESS	Harmonized neuroimaging of epilepsy structural sequences
HIV	Human immunodeficiency virus
ICH	Intracerebral hemorrhage
ICP	Intracranial pressure
IDH	Isocitrate dehydrogenase
IgG4	Immunoglobulin G4
ILAE	International League Against Epilepsy
IV	Intravenous
IVH	Intraventricular hemorrhage
IVIg	Intravenous immunoglobulin
LETM	Longitudinally extensive transverse myelitis
LGI1	Leucine-rich glioma inactivated 1
MAGNIMS	Magnetic Resonance Imaging in Multiple Sclerosis
MCA	Middle cerebral artery
MEG	Magnetoencephalography
MGMT	*O*-6-methylguanine-DNA methyltransferase
MOG	Myelin oligodendrocyte glycoprotein
MPRAGE	Magnetization-prepared rapid gradient echo
MRA	Magnetic resonance angiography
MRI	Magnetic resonance imaging
MRV	Magnetic resonance venography
MS	Multiple sclerosis
MSA	Multiple system atrophy
mTICI	Modified Thrombolysis in Cerebral Infarction
mTOR	Mammalian target of rapamycin
NAA	*N*-acetylaspartate
NF1	Neurofibromatosis type 1
NF2	Neurofibromatosis type 2
NMDA	*N*-methyl-D-aspartate
NMOSD	Neuromyelitis optica spectrum disorder
OCT	Optical coherence tomography
pc-ASPECTS	Posterior-circulation ASPECTS
PD	Parkinson disease
PDD	Parkinson disease with dementia
PET	Positron emission tomography
PiB	Pittsburgh Compound B
PKAN	Pantothenate kinase–associated neurodegeneration
PPA	Primary progressive aphasia
PPMS	Primary progressive multiple sclerosis
PSP	Progressive supranuclear palsy
pTau	Phosphorylated tau
RANO	Response Assessment in Neuro-Oncology
RBD	Rapid eye movement sleep behavior disorder
RCVS	Reversible cerebral vasoconstriction syndrome
REM	Rapid eye movement
RIS	Radiologically isolated syndrome
RRMS	Relapsing-remitting multiple sclerosis
SAH	Subarachnoid hemorrhage
SCA	Spinocerebellar ataxia
SCA2	Spinocerebellar ataxia type 2
SEGA	Subependymal giant cell astrocytoma
SIADH	Syndrome of inappropriate secretion of antidiuretic hormone
SISCOM	Subtraction ictal single-photon emission computerized tomography coregistered to magnetic resonance imaging
SLE	Systemic lupus erythematosus
SNpc	Substantia nigra pars compacta
SPECT	Single-photon emission computed tomography
SPMS	Secondary progressive multiple sclerosis
STIR	Short tau inversion recovery
SWI	Susceptibility-weighted imaging
TCD	Transcranial Doppler ultrasonography
TDP-43	Transactive response DNA-binding protein 43
TEE	Transesophageal echocardiography
tPA	Tissue plasminogen activator
TRANCE	Triggered angiography non–contrast-enhanced
TSH	Thyroid-stimulating hormone
VAChT	Vesicular acetylcholine transporter
VEGF	Vascular endothelial growth factor
VNS	Vagus nerve stimulation
VWI	Vessel wall imaging
WAKE-UP	Efficacy and Safety of MRI-based Thrombolysis in Wake-up stroke
WHO	World Health Organization

© 2023 American Academy of Neurology.

Copyright © American Academy of Neurology. Unauthorized reproduction of this article is prohibited.

Continuum
LIFELONG LEARNING IN NEUROLOGY®

AMERICAN ACADEMY OF NEUROLOGY®

NEUROIMAGING

ARTICLE 1: THE RIGHT IMAGING PROTOCOL FOR THE RIGHT PATIENT

Nandor K. Pinter, MD. Continuum (Minneap Minn). February 2023;
29 (1 Neuroimaging):16–26.

ABSTRACT

OBJECTIVE:

This article provides a high-level overview of the challenge of choosing the right imaging approach for an individual patient. It also presents a generalizable approach that can be applied to practice regardless of specific imaging technologies.

ESSENTIAL POINTS:

This article constitutes an introduction to the in-depth, topic-focused analyses in the rest of this issue. It examines the broad principles that guide placing a patient on the right diagnostic trajectory, illustrated with real-life examples of current protocol recommendations and cases of advanced imaging techniques, as well as some thought experiments. Thinking about diagnostic imaging strictly in terms of imaging protocols is often inefficient because these protocols can be vague and have numerous variations. Broadly defined protocols may be sufficient, but their successful use often depends largely on the particular circumstances, with special emphasis on the relationship between neurologists and radiologists.

KEY POINTS

- The American College of Radiology Appropriateness Criteria provide a good starting point for finding the right imaging modality. The American College of Radiology does not prescribe disease-specific protocols.
- Imaging protocols are not generally applicable laws but rather rules that may be adapted to the circumstances.
- Communication is key for two main reasons: (1) the default imaging approach may need to be changed based on relevant clinical data, and (2) communication can facilitate focused examinations and reporting.
- Even if MRI would be the method of choice, in urgent cases CT may be preferred.
- One should always follow the "as low as reasonably achievable" principle with studies that use ionizing radiation.
- Providing MRI safety information for patients with implants improves safety.
- Contrast agents do not automatically make a scan more informative, and clinical gain versus safety risks should always be considered.

Copyright © American Academy of Neurology. Unauthorized reproduction of this article is prohibited.

- Disease-specific imaging protocols are mostly born out of necessity and refer to a distinct way of manipulating conventional image acquisition or reconstruction in order to produce specific views that highlight pathologic features of the disease. Real disease-specific imaging operates with biomarkers.
- Imaging technologies advance, causing clinical protocols to change. A powerful future technology could rewrite prevailing practices regarding what is considered "right" imaging, or even eliminate the question entirely. This will depend on many factors, an important one being the inertia of the medical industry and practices.
- *MRI protocol optimization* is the process of creating a disease-specific protocol via iterative customization of imaging sequences. It can provide significant added value, but the process can be lengthy and resource-intensive. The optimization must be driven by clinical outcome and achieved through a systematic approach.

ARTICLE 2: SAFETY CONSIDERATIONS IN MRI AND CT

Robert E. Watson, MD, PhD; Lifeng Yu, PhD. Continuum (Minneap Minn). February 2023; 29 (1 Neuroimaging):27–53.

ABSTRACT

OBJECTIVE:

MRI and CT are indispensable imaging modalities for the evaluation of patients with neurologic disease, and each is particularly well suited to address specific clinical questions. Although both of these imaging modalities have excellent safety profiles in clinical use as a result of concerted and dedicated efforts, each has potential physical and procedural risks that the practitioner should be aware of, which are described in this article.

LATEST DEVELOPMENTS:

Recent advancements have been made in understanding and reducing safety risks with MR and CT. The magnetic fields in MRI create risks for dangerous projectile accidents, radiofrequency burns, and deleterious interactions with implanted devices, and serious patient injuries and deaths have occurred. Ionizing radiation in CT may be associated with shorter-term deterministic effects on biological tissues at extremely high doses and longer-term stochastic effects related to mutagenesis and carcinogenesis at low doses. The cancer risk of radiation exposure in diagnostic CT is considered extremely low, and the benefit of an appropriately indicated CT examination far outweighs the potential risk. Continuing major efforts are centered on improving image quality and the diagnostic power of CT while concurrently keeping radiation doses as low as reasonably achievable.

ESSENTIAL POINTS:

An understanding of these MRI and CT safety issues that are central to contemporary radiology practice is essential for the safe and effective treatment of patients with neurologic disease.

KEY POINTS

- The three different magnetic fields involved in the creation of MRIs are each associated with defined safety risks.
- The MRI room is one of the most dangerous environments in the hospital.
- The magnet is always "on." The tremendously powerful magnetic field creates a dangerous projectile risk in the MRI room regardless of whether a patient is being scanned or not.

Copyright © American Academy of Neurology. Unauthorized reproduction of this article is prohibited.

- Only trained MRI personnel should enter the magnet room in a patient emergency (eg, cardiopulmonary arrest).
- Accurate information about a patient's implanted devices should be provided to the MRI team with the MRI order.
- Physical spaces related to MRI are defined by a four-zone model. Access to zone III (the technologist control area) and zone IV (the magnet room) is restricted.
- Implanted devices are designated as MR-safe, MR-conditional, or MR-unsafe.
- Well-designed MRI safety systems and procedures must be in place and rigorously followed to prevent serious safety events and accidents involving dangerous projectiles, burns, and unplanned scanning of implanted devices.
- The magnetic fields around the opening of an MRI bore are not uniform; rather, a steep gradient exists in the forces as the magnet is approached.
- Older intracranial aneurysm clips contained ferromagnetic metal, resulting in patient deaths during MRI.
- Heating and burns related to the radiofrequency field are the most common type of MRI safety events.
- Foil-backed medication patches can cause burns during MRI.
- Scanning a patient with an MR-unsafe device or with an MR-conditional device without abiding by the conditions for safe scanning can lead to serious patient injury or death.
- Intrathecal pumps are the type of device associated with the greatest number of patient deaths during MRI in recent years.
- Patients with pacemakers and defibrillators can increasingly be safely scanned if important safety measures are strictly adhered to.
- An insulin pump exposed to MRI is likely unreliable and could lead to serious hyperglycemia or hypoglycemia.
- Displacement of an intraocular ferromagnetic foreign body during MRI can lead to blindness.
- No deleterious clinical effects of gadolinium retention have yet been identified, although continued study of this issue is important.
- Radiation dose in CT is commonly quantified in terms of scanner radiation output, patient absorbed dose, and effective dose.
- Two types of biological effects from radiation exposure in CT occur. One is the deterministic effect (tissue reaction), and the other is the stochastic effect (cancer induction and hereditary effect).
- Deterministic effects rarely occur in diagnostic CT examinations except for some prolonged CT-guided interventional procedures. The risk of radiation exposure in CT refers mostly to stochastic effect.
- At low levels of radiation, considerable uncertainty exists regarding the risk of cancer induction. It was stated in a report by the National Academy of Sciences that at doses of 100 mSv or less, "statistical limitations make it difficult to evaluate cancer risk in humans."
- It is generally believed that quantitative estimation of cancer risk for an individual patient receiving a radiation dose of less than 100 mSv during CT does not bring clinical value to the patient.
- To maximize the benefit-to-risk ratio, it is still best practice to use the lowest possible radiation dose at each CT examination while generating images with sufficient diagnostic quality. Two basic principles must be followed for managing radiation dose in CT: justification and optimization.
- Commonly used radiation dose–reduction techniques include automatic tube current modulation, automatic tube potential selection, iterative reconstruction, and deep learning–based noise reduction.
- CT operators are required to receive appropriate training on scanner operation, radiation exposure, and emergency procedures.
- The presence of implanted electronic devices should not preclude a clinically justified CT scan. However, to reduce the potential risk of interference between electronic devices and CT radiation, some precautions are needed.

Copyright © American Academy of Neurology. Unauthorized reproduction of this article is prohibited.

ARTICLE 3: IMAGING OF CENTRAL NERVOUS SYSTEM ISCHEMIA

Julie G. Shulman, MD; Mohamad Abdalkader, MD.
Continuum (Minneap Minn). February 2023; 29 (1 Neuroimaging):54–72.

ABSTRACT

OBJECTIVE:

This article describes imaging modalities used in the evaluation of patients presenting with symptoms of acute ischemic stroke.

LATEST DEVELOPMENTS:

The year 2015 marked the beginning of a new era in acute stroke care with the widespread adoption of mechanical thrombectomy. Subsequent randomized controlled trials in 2017 and 2018 brought the stroke community even further into this new territory with the expansion of the eligibility window for thrombectomy using imaging-based patient selection, which led to an increase in the use of perfusion imaging. Now, after several years of routine use, the debate is ongoing as to when this additional imaging is truly required and when it results in unnecessary delays in time-sensitive stroke care. At this time, more than ever, a robust understanding of neuroimaging techniques, applications, and interpretation is essential for the practicing neurologist.

ESSENTIAL POINTS:

CT-based imaging is the first step in most centers for the evaluation of patients presenting with symptoms of acute stroke because of its wide availability, speed, and safety. Noncontrast head CT alone is sufficient for IV thrombolysis decision making. CT angiography is very sensitive for the detection of large-vessel occlusion and can be used reliably to make this determination. Advanced imaging including multiphase CT angiography, CT perfusion, MRI, and MR perfusion can provide additional information useful for therapeutic decision making in specific clinical scenarios. In all cases, it is essential that neuroimaging be performed and interpreted rapidly to allow for timely reperfusion therapy.

KEY POINTS

- Early ischemic changes evident on noncontrast CT include obscuration of the lentiform nucleus, loss of the gray-white boundary in the insula (insular ribbon sign), and effacement of the cortical sulci (cortical ribbon sign).
- The Alberta Stroke Programme Early CT Score (ASPECTS) is a quantitative assessment of early ischemic changes calculated by visual inspection of 10 specific neuroanatomic regions on noncontrast CT. The maximum score of 10 indicates no evidence of early ischemia.
- The American Heart Association/American Stroke Association guidelines recommend proceeding with mechanical thrombectomy for patients with large-vessel occlusion stroke and an Alberta Stroke Programme Early CT Score (ASPECTS) of 6 or greater who present within 6 hours of last known well time, without additional advanced imaging.
- The posterior-circulation Alberta Stroke Programme Early CT Score (ASPECTS) is a 10-point scale that assesses eight brain regions supplied by the vertebrobasilar system for evidence of early ischemic changes. It has been shown to improve detection of ischemia and predict functional outcome.
- The hyperdense vessel sign can be seen on noncontrast CT and is highly specific for large-vessel occlusion.

Copyright © American Academy of Neurology. Unauthorized reproduction of this article is prohibited.

- It is recommended to proceed with CT angiography before measuring a serum creatinine level in patients eligible for mechanical thrombectomy without known renal impairment to avoid unnecessary delays in reperfusion.
- CT angiography is extremely accurate for detecting large-vessel occlusion, with sensitivity and specificity of approximately 98%.
- Multiphase CT angiography can be used to obtain a more robust assessment of a patient's collateral circulation. Quality of collateral flow has been shown to correlate with rate of infarct growth and predict prognosis in some studies.
- CT perfusion uses three parameters to assess a given brain region: cerebral blood flow, cerebral blood volume, and mean transit time. Postprocessing software creates maps based on these measures to approximate the size and location of the infarct core and the ischemic penumbra.
- MRI is more sensitive and specific than CT for the identification of acute stroke and can detect ischemia as early as a few minutes after stroke onset.
- In true restricted diffusion seen in acute ischemic stroke, a region of increased diffusion-weighted imaging signal correlates with a region of low signal intensity on the apparent diffusion coefficient image.
- Diffusion-weighted imaging–negative stroke is rare and most frequently seen in patients with small, posterior-circulation, or hyperacute strokes. Repeat diffusion-weighted imaging is recommended if there is a strong clinical suspicion of ischemia.
- Diffusion-weighted imaging positivity appears within the first few minutes after stroke onset, whereas fluid-attenuated inversion recovery (FLAIR) signal changes take longer to develop. This mismatch has been used to estimate stroke onset and select patients for thrombolysis.
- Acute intraarterial thrombus produces susceptibility artifact and blooming on gradient recalled echo or susceptibility-weighted MRI. This finding is similar to the "hyperdense vessel sign" seen on noncontrast CT and is strongly suggestive of large-vessel occlusion.
- The modified Thrombolysis in Cerebral Infarction scale is used to describe the degree of reperfusion achieved after mechanical thrombectomy. A score of 2b, 2c, or 3 is considered successful reperfusion.

ARTICLE 4: IMAGING OF CENTRAL NERVOUS SYSTEM HEMORRHAGE

Ryan Hakimi, DO, MS, NVS, RPNI, CPB, FNCS, FCCM.
Continuum (Minneap Minn). February 2023; 29 (1 Neuroimaging):73–103.

ABSTRACT

OBJECTIVE:

This article aims to familiarize the reader with the various types of nontraumatic central nervous system (CNS) hemorrhage and the various neuroimaging modalities used to help diagnose and manage them.

LATEST DEVELOPMENTS:

According to the 2019 Global Burden of Diseases, Injuries, and Risk Factors Study, intraparenchymal hemorrhage accounts for 28% of the global stroke burden. In the United States, hemorrhagic stroke makes up 13% of all strokes. The incidence of intraparenchymal hemorrhage increases substantially with age; thus, despite improvements in blood pressure control through various public health measures, the incidence is not decreasing as the population ages. In fact, in the most recent longitudinal study of aging, autopsy findings showed intraparenchymal hemorrhage and cerebral amyloid angiopathy in 30% to 35% of patients.

Copyright © American Academy of Neurology. Unauthorized reproduction of this article is prohibited.

ESSENTIAL POINTS:

Rapid identification of CNS hemorrhage, which includes intraparenchymal hemorrhage, intraventricular hemorrhage, and subarachnoid hemorrhage, requires either head CT or brain MRI. Once hemorrhage is identified on the screening neuroimaging study, the pattern of blood in conjunction with the history and physical examination can guide subsequent neuroimaging, laboratory, and ancillary tests as part of the etiologic assessment. After determination of the cause, the chief aims of the treatment regimen are reducing hemorrhage expansion and preventing subsequent complications such as cytotoxic cerebral edema, brain compression, and obstructive hydrocephalus. In addition, nontraumatic spinal cord hemorrhage will also be briefly discussed.

KEY POINTS

- Intracranial hemorrhage may be subdivided into spontaneous intraparenchymal hemorrhage, aneurysmal subarachnoid hemorrhage, and intraventricular hemorrhage.
- The pattern of hemorrhage in conjunction with the history and physical examination can guide subsequent neuroimaging, laboratory, and ancillary tests as part of the etiologic assessment.
- Communication about central nervous system hemorrhage noted on head CT should include the type, location, acuity (acute or chronic), volume of the lesion, presence or absence of intraventricular hemorrhage, and extent of cerebral edema and brain compression.
- Compared with head CT, brain MRI has greater sensitivity for the detection of central nervous system hemorrhage, as it identifies both acute and chronic hemorrhages, which are noted as hypointensities on two-dimensional gradient recalled echo (GRE) T2*-weighted imaging and susceptibility-weighted imaging (SWI), or three-dimensional GRE imaging.
- Digital subtraction angiography offers 99% sensitivity and specificity in identifying underlying vascular lesions in cases of central nervous system hemorrhage.
- Transcranial Doppler ultrasonography can predict symptomatic vasospasm and has high sensitivity, specificity, and positive and negative predictive values.
- Head CT angiography with or without venography is recommended in patients without hypertension who are less than 70 years old and present with a lobar intraparenchymal hemorrhage, as one in seven to one in four patients will have an underlying vascular etiology.
- When intraventricular hemorrhage is noted in isolation, digital subtraction angiography and brain MRI are warranted.
- Primary intraparenchymal hemorrhage is most commonly due to arteriosclerosis.
- Hemorrhage volume is calculated using the ABC/2 method.
- When using 0.5-cm slice thickness, the volume of the central nervous system hemorrhage is calculated by multiplying A, B, and C and dividing by 4.
- One-third of patients with intraparenchymal hemorrhage will have hemorrhage expansion within 3 hours of the index scan.
- Head CT angiography immediately after the noncontrast head CT can allow for quick identification of patients at high risk for rapid hemorrhage expansion when the spot sign is noted.
- The ICH Score is a standard communication tool for describing the patient's clinical condition and is used to document the patient's extent of illness for purposes of quality assurance and mortality risk stratification.
- The 2022 American Heart Association/American Stroke Association guidelines recommend that the ICH Score not be used in isolation as the basis for limiting life-sustaining measures.
- Cerebral amyloid angiopathy is the most common secondary cause of intraparenchymal hemorrhage.
- For diagnosing cerebral amyloid angiopathy, brain MRI is most revealing, with cortical microhemorrhages and superficial siderosis noted on SWI or T2* sequences.
- The risk of recurrent hemorrhage is higher in patients with central nervous system hemorrhage with underlying cerebral amyloid angiopathy (7.39% per year) than in those with central nervous system hemorrhage due to other causes (1.1% per year).

Copyright © American Academy of Neurology. Unauthorized reproduction of this article is prohibited.

- Besides a ruptured aneurysm, other etiologies of subarachnoid hemorrhage include arteriovenous malformation, fistula, intracranial dissection, cerebral venous sinus thrombosis, reversible cerebral vasoconstriction syndrome, vasculitis, use of antithrombotic or sympathomimetic drugs, and to a lesser degree uncontrolled hypertension.
- The clinical neurologic examination and the extent of hemorrhage in patients with subarachnoid hemorrhage are communicated and documented using the Hunt and Hess scale and the modified Fisher scale, respectively.
- Advances in SWI sequences now provide a useful adjunct in ruling out subarachnoid hemorrhage in patients whose clinical history is consistent with an aneurysmal subarachnoid hemorrhage but whose head CT and head and neck CT angiography are normal.
- Isolated intraventricular hemorrhage warrants additional advanced neuroimaging, including brain MRI with gadolinium, to exclude a choroid plexus tumor or another underlying structural mass lesion. If the MRI is unrevealing, digital subtraction angiography is needed to exclude an intraventricular vascular lesion such as a choroidal artery aneurysm or arteriovenous malformation.
- Asymmetry in venous sinuses is common, and identification of asymmetry between one transverse sinus and its contralateral sinus may be quite normal for a given individual and not signify disease.
- With improving care provided by stroke, neuroendovascular, and neurocritical care teams, the risk of symptomatic hemorrhagic transformation of an ischemic stroke is declining and currently stands at approximately 1% to 3%.
- Intracerebral hemorrhage secondary to septic emboli is overall an uncommon condition and is most frequently seen in immunocompromised individuals, patients with prosthetic heart valves, and IV drug users.

ARTICLE 5: NEUROIMAGING IN ADULTS AND CHILDREN WITH EPILEPSY

Erasmo A. Passaro, MD. Continuum (Minneap Minn). February 2023;
29 (1 Neuroimaging):104–155.

ABSTRACT

OBJECTIVE:

This article discusses the fundamental importance of optimal epilepsy imaging using the International League Against Epilepsy–endorsed Harmonized Neuroimaging of Epilepsy Structural Sequences (HARNESS) protocol and the use of multimodality imaging in the evaluation of patients with drug-resistant epilepsy. It outlines a methodical approach to evaluating these images, particularly in the context of clinical information.

LATEST DEVELOPMENTS:

Epilepsy imaging is rapidly evolving, and a high-resolution epilepsy protocol MRI is essential in evaluating newly diagnosed, chronic, and drug-resistant epilepsy. The article reviews the spectrum of relevant MRI findings in epilepsy and their clinical significance. Integrating multimodality imaging is a powerful tool in the presurgical evaluation of epilepsy, particularly in "MRI-negative" cases. For example, correlation of clinical phenomenology, video-EEG with positron emission tomography (PET), ictal subtraction single-photon emission computerized tomography (SPECT), magnetoencephalography (MEG), functional MRI, and advanced neuroimaging such as MRI texture analysis and voxel-based morphometry enhances the identification of subtle cortical lesions such as focal cortical dysplasias to optimize epilepsy localization and selection of optimal surgical candidates.

Copyright © American Academy of Neurology. Unauthorized reproduction of this article is prohibited.

ESSENTIAL POINTS:

The neurologist has a unique role in understanding the clinical history and seizure phenomenology, which are the cornerstones of neuroanatomic localization. When integrated with advanced neuroimaging, the clinical context has a profound impact on identifying subtle MRI lesions or finding the "epileptogenic" lesion when multiple lesions are present. Patients with an identified lesion on MRI have a 2.5-fold improved chance of achieving seizure freedom with epilepsy surgery compared with those without a lesion.

This clinical–radiographic integration is essential to accurate classification, localization, determination of long-term prognosis for seizure control, and identification of candidates for epilepsy surgery to reduce seizure burden or attain seizure freedom.

KEY POINTS

- MRI is essential to classify epilepsy as focal or generalized and guides treatment decisions.
- Clinical anatomic correlation of epileptic auras and seizure phenomenology can increase the yield of identifying a structural abnormality on MRI, particularly when the finding is subtle.
- In patients with new-onset seizures, epilepsy protocol MRI identifies a cause in 53% of cases.
- In patients with chronic focal epilepsy who had a standard MRI, an abnormality was found in 49%. In those who had an epilepsy protocol MRI, an abnormality was found in 72%.
- An epilepsy protocol MRI and an interpretation by an expert neuroradiologist increased the yield of identifying a lesion from 39% to a striking 85% in patients with drug-resistant epilepsy.
- By using an 8-channel phased-array head coil at 3T, 48% more lesions were identified than with a routine 1.5T MRI. In patients with prior epilepsy protocol, 1.5T MRI was interpreted as normal, and 3T phased-array MRI resulted in the detection of a new lesion in 65% of patients.
- The International League Against Epilepsy Neuroimaging Task Force 2019 guidelines for optimal imaging should be followed for all patients with epilepsy using a Harmonized Neuroimaging of Epilepsy Structural Sequences (HARNESS) 3T MRI protocol.
- Many MRI findings are subtle, and the clinician must correlate their relevance to clinical history and clinical neurophysiology.
- In a patient with a single unprovoked seizure, an abnormal MRI showing pathology that causes epilepsy increases the risk for a recurrent seizure twofold and, according to the International League Against Epilepsy, the patient would be classified as having epilepsy even with a normal EEG and would warrant treatment with an antiseizure medication.
- In patients with chronic epilepsy who are seizure-free for 2 or more years, prolonged remission of epilepsy off antiseizure medication is approximately 65%. However, when an etiology is known, the chance for remission is less than 50%.
- MRI can show certain pathologic substrates that predict a poor prognosis for long-term seizure control, such as hippocampal sclerosis, malformations of cortical development, and cavernous malformations.
- In one study, greater than 10% of patients died within 2 years of developing medically intractable epilepsy. Fewer than 2% of patients who may have benefited from epilepsy surgery received it.
- Patients with long-term-epilepsy–associated neuroepithelial tumors, vascular malformation, or hippocampal sclerosis attained seizure freedom rates 2 years after surgery ranging from 71% to 77%.
- Finding a lesion on MRI improves surgical seizure-free success 2.5-fold.
- Children younger than the age of 2 years require a different MRI protocol because of the dynamic changes in myelination during this period. From infancy to 18 months, fluid-attenuated inversion recovery (FLAIR) MRI is less informative since the gray and white matter blend in because of reduced myelination and water content.
- Hippocampal sclerosis is characterized by neuronal loss and gliosis and is seen in 36.4% of all epilepsy surgical specimens, 44.5% of those from adults and 15.0% from children.
- High-resolution MRI is 80% to 90% sensitive for identifying hippocampal sclerosis by visual analysis.
- Although most patients with temporal lobe epilepsy show marked hippocampal sclerosis on pathologic examination, 40% demonstrate no significant cell loss and gliotic changes only.

Copyright © American Academy of Neurology. Unauthorized reproduction of this article is prohibited.

- The frequency of temporal polar cortex abnormalities was found to range from 28% to 66% in patients with drug-resistant temporal lobe epilepsy, usually ipsilateral to the side of hippocampal sclerosis.
- The amygdala can be abnormally enlarged in patients with epilepsy, indicating amygdalar dysplasia, hamartoma, gliosis, or a low-grade neoplasm or developmental tumor. In amygdalar enlargement, pathology findings include dysplasia with hypertrophic, clustered neurons or astrocytic gliosis.
- Malformations of cortical development are classified into three groups based on the main developmental stage affected, with consideration that alteration of early developmental events often affects later events.
- Malformations of cortical development account for the most common surgical pathologies in children and the third most common in adults undergoing epilepsy surgery, with focal cortical dysplasia representing almost 75% of all malformation of cortical development cases.
- Focal cortical dysplasia type II has been described as a "bottom-of-sulcus dysplasia" resulting from dysplastic features maximal at the sulcal depth, tapering to a relatively normal gyral crown.
- A cleft dimple complex can be a clue to identifying a focal cortical dysplasia. It is defined as the cortex buckling inward, away from the brain surface, with a prominent space between the cortex and leptomeninges (cleft and dimple).
- Focal cortical dysplasia type IIa and type IIb are associated with germline mutations in the mammalian target of rapamycin (mTOR) pathway. These mutations include but are not limited to *DEPDC5*, *NPRL2*, and *NPRL3* mutations and, in some cases, can be associated with multiple cortical dysplasias, some of which are MRI occult.
- Grey matter nodular heterotopia refers to a collection of neurons in an abnormal location such as the subcortical white matter and subependymal region or under normal-appearing cortex in a laminar pattern. On MRI, the lesions are gray matter isointense on both T1- and T2-weighted sequences.
- Polymicrogyria consists of an excessive number of small gyri with shallow sulci. Polymicrogyria can be (1) focal and limited; (2) focal, unilateral, and extensive; (3) bilateral and symmetric; (4) bilateral and asymmetric; (5) multifocal; or (6) diffuse. MRI shows numerous small gyri with shallow sulci, and the cortical-subcortical junction is often irregular.
- In patients with intractable epilepsy treated with epilepsy surgery, neoplasms account for approximately 22% of cases, with long-term-epilepsy–associated tumors accounting for the majority and ganglioglioma the most common.
- Long-term-epilepsy–associated tumors most commonly occur in the temporal lobe with a mean age of 16 years at seizure onset. They can be associated with focal cortical dysplasia type 1 with cortical disorganization in 80% of patients with long-term-epilepsy–associated tumors and type II cortical dysplasia in 11%.
- Hypothalamic hamartomas are rare, occurring in 1 in 200,000 children. They are typically located between the infundibular stalk anteriorly and the mamillary bodies posteriorly. They are T1 hypointense and T2 hyperintense on MRI. In one-third of cases, they present with gelastic seizures.
- Temporal lobe encephaloceles are herniations of the temporal lobe and meninges through the dura and the skull; they account for 0.30% of patients with newly diagnosed epilepsy and 2.0% to 5.5% of patients with drug-resistant epilepsy.
- Cavernous malformations are composed of well-circumscribed vascular spaces with blood in varying stages of evolution.
- Susceptibility-weighted imaging (SWI) capitalizes on the paramagnetic properties of deoxygenated blood. SWI helps detect microhemorrhages from remote trauma or cavernous malformations and identifies calcification.
- Coregistering positron emission tomography (PET) to three-dimensional epilepsy protocol MRI optimizes the identification of subtle focal cortical dysplasias or helps localize the epileptogenic region.
- Subtraction ictal single-photon emission computerized tomography (SPECT) coregistered to MRI (SISCOM) is a technique in which the interictal SPECT is subtracted from the ictal SPECT and then coregistered to MRI, which enhances the sensitivity, specificity, and interreader reliability of localizing epileptogenic regions and lesions.

Copyright © American Academy of Neurology. Unauthorized reproduction of this article is prohibited.

- SPECT can show larger regions of cerebral hyperperfusion than the actual epileptogenic region, reflecting regions of seizure propagation rather than onset.
- Functional MRI (fMRI) acquisitions use the blood oxygen level-dependent (BOLD) effect to indirectly infer brain activity through task-related increases in cerebral blood flow via T2* acquisitions.
- Task-based fMRI is widely used in presurgical evaluation to determine language hemispheric dominance, often in planned temporal lobe resection in the dominant hemisphere.
- Magnetoencephalography and magnetic source imaging use direct electrophysiologic measurements of neural activity recording of the magnetic field outside the scalp on a millisecond basis. It is highly accurate in the localization of interictal epileptiform discharges and is more sensitive to tangential dipoles than radial dipoles recorded by scalp EEG.
- Patients with a single tight cluster of dipoles have improved localization compared with patients with scattered dipoles. The MEG coregistered to a three-dimensional epilepsy protocol MRI shows the relationship of the spike dipoles to the cortical anatomy.
- Magnetoencephalography can direct the clinician to identify subtle cortical dysplasia or guide intracranial electrode placement to optimize surgical localization, particularly in MRI-negative patients.
- Multimodality imaging is most useful in MRI-negative epilepsies, where the surgical seizure-free outcome can be 20% or less. It can optimize localization in conjunction with video-EEG and seizure phenomenology, guide intracranial EEG implantation, and, in some cases, identify a previously missed subtle focal cortical dysplasia.
- Fludeoxyglucose positron emission tomography (FDG-PET) shows a functional deficit zone that can be larger than the epileptogenic zone, but in some cases such patterns may have predictive value for a surgical seizure-free outcome.
- Texture analysis using voxel-based modeling of gray-white matter blurring and gray matter intensity from three-dimensional T1-weighted MRI increases the identification of focal cortical dysplasia type II by 40% compared with visual analysis.

ARTICLE 6: IMAGING OF SKULL BASE TUMORS

Wenya Linda Bi, MD, PhD. Continuum (Minneap Minn). February 2023;
29 (1 Neuroimaging):156–170.

ABSTRACT

OBJECTIVE:

This article provides an overview of imaging modalities and findings associated with common skull base tumors including meningiomas and how to use imaging features to guide surveillance and treatment decision making.

LATEST DEVELOPMENTS:

Ease of access to cranial imaging has led to a higher number of incidentally diagnosed skull base tumors, which merit careful consideration for management with observation or treatment. The point of origin of the tumor dictates the pattern of anatomic displacement and involvement by the tumor as it grows. Careful study of vascular encroachment on CT angiography, as well as the pattern and extent of bony invasion on CT, abets treatment planning. Quantitative analyses of imaging, such as with radiomics, may further elucidate phenotype-genotype associations in the future.

Copyright © American Academy of Neurology. Unauthorized reproduction of this article is prohibited.

ESSENTIAL POINTS:

Combinatorial application of CT and MRI analyses improves the diagnosis of skull base tumors, clarifies their point of origin, and dictates the extent of treatment needed.

KEY POINTS

- Skull base tumors refer to both tumors whose cell of origin is outside of the brain parenchyma as well as tumors that are physically located in or near the base of the skull.
- Many skull base tumors, such as meningiomas or pituitary microadenomas, are incidentally diagnosed and may be safely observed as the initial strategy.
- The point of origin of skull base tumors dictates their relationship with adjacent nerves, vessels, and the brain because relative anatomic relationships are usually maintained even while absolute anatomic positions are distorted.
- Meningiomas frequently involve the adjacent bone, which should be specifically examined on surveillance imaging.
- Venous sinus occlusion through natural growth of a meningioma leads to rerouting of venous drainage from cortical veins at the anterior and posterior limits of the occluded sinus and does not result in venous infarction on its own.
- Enlarging benign meningiomas typically grow 1 to 2 mm per year; rates faster than this raise concern for more atypical behavior.
- A meningioma growth rate exceeding that of benign meningioma trajectories, irregular tumor shape, intratumoral heterogeneity including the presence of central necrosis or hemorrhage, a knobby or ill-defined pattern of tumor-brain interface, and potentially the extent of peritumoral edema all raise concern for more aggressive behavior.
- Falcine and parasagittal meningiomas are more likely to be higher grade whereas midline anterior skull base meningiomas tend to be benign.
- Solitary fibrous tumors, formerly termed *hemangiopericytoma*, are a highly vascular mimic of meningiomas and may metastasize outside of the central nervous system.
- Schwannomas demonstrate variable growth rates, with cystic and neurofibromatosis type 2–associated tumors more likely to exhibit faster growth.
- Although contrast-enhanced T1-weighted MRI remains the most common modality to visualize schwannomas, T2-weighted MRI may be suitable for long-term surveillance of schwannoma growth.
- Rathke cleft cysts and neurohypophysial tumors push the pituitary stalk anteriorly, as best appreciated on sagittal imaging, because of their origin posterior to the adenohypophysis.
- Craniopharyngiomas in children are almost exclusively adamantinomatous whereas papillary craniopharyngiomas are found in adults, commonly with a $BRAF^{V600E}$ mutation.
- Chondrosarcomas exhibit pronounced calcification in comparison to chordomas and are typically eccentric toward one side as opposed to midline.
- Epidermoid cysts are best characterized by their avid restricted diffusion on diffusion-weighted imaging sequences.
- Radiomic analyses of conventional tumor imaging may augment the prediction of biological signatures in the future.

Copyright © American Academy of Neurology. Unauthorized reproduction of this article is prohibited.

ARTICLE 7: IMAGING OF BRAIN TUMORS

Justin T. Jordan, MD, MPH, FAAN; Elizabeth R. Gerstner, MD.
Continuum (Minneap Minn). February 2023; 29 (1 Neuroimaging):171–193.

ABSTRACT

OBJECTIVE:

This article focuses on neuroimaging as an essential tool for diagnosing brain tumors and monitoring response to treatment.

LATEST DEVELOPMENTS:

Neuroimaging is useful at all stages of brain tumor care. Technologic advances have improved the clinical diagnostic capability of neuroimaging as a vital complement to history, examination, and pathologic assessment. Presurgical evaluations are enriched by novel imaging techniques, through improved differential diagnosis and better surgical planning using functional MRI (fMRI) and diffusion tensor imaging. The common clinical challenge of differentiating tumor progression from treatment-related inflammatory change is aided by novel uses of perfusion imaging, susceptibility-weighted imaging (SWI), spectroscopy, and new positron emission tomography (PET) tracers.

ESSENTIAL POINTS:

Using the most up-to-date imaging techniques will facilitate high-quality clinical practice in the care of patients with brain tumors.

KEY POINTS

- Approximately 25,000 primary malignant brain tumors are diagnosed each year in the United States.
- Glioblastoma is the most common malignant primary intracranial brain tumor in adults.
- Keeping a broad differential diagnosis is important for mass lesions, including abscesses, strokes, or inflammatory disease.
- Although CT may show acute changes such as stroke or hemorrhage, gadolinium-enhanced MRI is the preferred imaging modality for brain tumors.
- T1-weighted, T2-weighted, and fluid-attenuated inversion recovery (FLAIR) sequences are critical to diagnosing and treating patients with brain tumors.
- Diffusion-weighted imaging may be helpful to detect ischemic strokes, hypercellularity within tumors (especially lymphomas and high-grade gliomas), and perioperative devitalized tissues.
- Susceptibility-weighted imaging is helpful to identify calcifications in low-grade tumors or hemorrhage in typically higher-grade tumors.
- Perfusion imaging may help visualize vascularity and help distinguish between low- and high-grade tumors, as well as between tumor growth and inflammatory changes.
- MR spectroscopy that measures 2-hydroxyglutarate may aid in diagnosing an isocitrate dehydrogenase (*IDH*)-mutated tumor and may improve monitoring of treatment response.
- Functional MRI is useful for determining the anatomic location of brain activity for various tasks such as speaking or motor function and may help surgical planning.
- Amino acid positron emission tomography (PET) tracers may aid in distinguishing tumor growth from inflammatory changes.
- Pseudoprogression in high-grade gliomas is often associated with increased contrast enhancement and hyperintensity on T2-weighted and FLAIR images and is caused by inflammatory change.
- Distinguishing tumor progression from inflammatory change is a frequent challenge, and a thorough evaluation may incorporate perfusion MRI, amino acid positron emission tomography, or MR spectroscopy.

Copyright © American Academy of Neurology. Unauthorized reproduction of this article is prohibited.

- Lower-grade tumors may exhibit inflammatory radiation change through slow progression of hyperintensity on FLAIR images.
- Drugs targeting vascular endothelial growth factor (VEGF) such as bevacizumab may reduce enhancement and hyperintensity on FLAIR images temporarily for high-grade gliomas, a phenomenon known as pseudoresponse.
- Based on expert consensus, the Response Assessment in Neuro-Oncology criteria provide a standardized framework for monitoring brain tumor treatment response.
- Despite their nonmalignant behavior, pilocytic astrocytomas present as heterogeneously enhancing nodules with adjacent cystic structures.
- Subependymal giant cell astrocytomas are a classic feature of tuberous sclerosis complex and are generally found near the foramen of Monro.
- *IDH*-mutated astrocytomas commonly exhibit the T2-FLAIR mismatch sign, in which T2-weighted images show a hyperintense tumor but the tumor is less hyperintense on FLAIR images.
- Oligodendrogliomas commonly present with seizures, extend to the cortex, and may reveal internal calcification.
- Glioblastoma is generally characterized by a supratentorial mass lesion with heterogeneous enhancement and surrounding hyperintensity on T2-weighted and FLAIR images; some intratumoral hemosiderin and satellite lesions may exist.
- H3 K27–altered diffuse midline glioma is an aggressive tumor that may arise from any midline structure such as thalamus, brainstem, or spinal cord.
- Ependymomas may arise in the supratentorial space, infratentorial space, or spinal cord and have varying molecular differentiation.
- Central nervous system lymphomas in immunocompetent patients are homogeneously enhancing, whereas immunosuppressed patients present with rim-enhancing lesions with occasional necrosis or hemorrhage.
- Nearly 80% of central nervous system lymphoma lesions are close to the ventricular ependyma or meningeal surface, and frequent involvement of the basal ganglia, thalamus, or corpus callosum occurs.
- Although hemangioblastomas may be sporadic, evaluation for underlying von Hippel-Lindau syndrome is important.
- Imaging of the entire neuraxis and spinal fluid sampling are necessary for patients with medulloblastoma because of the high rate of disseminated disease.
- Pleomorphic xanthoastrocytoma classically presents as a cystic, cortically located tumor with an enhancing nodule.
- Brain metastases are usually multiple and within the cerebral hemispheres, especially in end-arterial border zone locations and at the junction of cortex and subcortical white matter.
- Very small metastatic tumors may present as foci of restricted diffusion before growing to show definitive enhancing tumors.
- Imaging is an essential tool for diagnosing and monitoring intracranial brain tumors.

Copyright © American Academy of Neurology. Unauthorized reproduction of this article is prohibited.

ARTICLE 8: IMAGING IN MOVEMENT DISORDERS

Baijayanta Maiti, MD, PhD; Joel S. Perlmutter, MD.
Continuum (Minneap Minn). February 2023; 29 (1 Neuroimaging):194–218.

ABSTRACT

OBJECTIVE:

This article reviews commonly used imaging modalities in movement disorders, particularly parkinsonism. The review includes the diagnostic utility, role in differential diagnosis, reflection of pathophysiology, and limitations of neuroimaging in the setting of movement disorders. It also introduces promising new imaging modalities and describes the current status of research.

LATEST DEVELOPMENTS:

Iron-sensitive MRI sequences and neuromelanin-sensitive MRI can be used to directly assess the integrity of nigral dopaminergic neurons and thus may reflect disease pathology and progression throughout the full range of severity in Parkinson disease (PD). The striatal uptake of presynaptic radiotracers in their terminal axons as currently assessed using clinically approved positron emission tomography (PET) or single-photon emission computed tomography (SPECT) imaging correlates with nigral pathology and disease severity only in early PD. Cholinergic PET, using radiotracers that target the presynaptic vesicular acetylcholine transporter, constitutes a substantial advance and may provide crucial insights into the pathophysiology of clinical symptoms such as dementia, freezing, and falls.

ESSENTIAL POINTS:

In the absence of valid, direct, objective biomarkers of intracellular misfolded α-synuclein, PD remains a clinical diagnosis. The clinical utility of PET- or SPECT-based striatal measures is currently limited given their lack of specificity and inability to reflect nigral pathology in moderate to severe PD. These scans may be more sensitive than clinical examination to detect nigrostriatal deficiency that occurs in multiple parkinsonian syndromes and may still be recommended for clinical use in the future to identify prodromal PD if and when disease-modifying treatments become available. Multimodal imaging to evaluate underlying nigral pathology and its functional consequences may hold the key to future advances.

KEY POINTS

- The pathologic hallmark of Parkinson disease is the intracellular deposition of misfolded α-synuclein; classic motor symptoms of Parkinson disease manifest only after the loss of midbrain nigral dopaminergic neurons crosses a certain threshold.
- The nigrostriatal dopaminergic neurons project to the striatum, and substantial loss of striatal dopamine has already occurred by the time the classic motor symptoms of Parkinson disease manifest.
- A radiotracer specific for α-synuclein may best reflect pathophysiology of motor as well as nonmotor symptoms in Parkinson disease, but such a radiotracer is not yet available.
- The only radiotracer approved clinically for single-photon emission computed tomography (SPECT) imaging targets the presynaptic dopamine transporter and hence measures the integrity of terminal axons of the nigrostriatal dopaminergic neurons.
- Dopamine transporter (DAT)-SPECT scans demonstrate significantly reduced striatal uptake in the putamen more than the caudate nucleus in Parkinson disease compared with healthy controls; this is usually but not always asymmetric, and this asymmetry may become less pronounced as the disease progresses.

Copyright © American Academy of Neurology. Unauthorized reproduction of this article is prohibited.

- DAT-SPECT may be more sensitive than clinical examination, as significant depletion of terminal axons and striatal dopamine is likely to occur before clinical symptoms of Parkinson disease manifest.
- The diagnostic accuracy of DAT-SPECT scans is not significantly different from the accuracy of a clinical diagnosis of Parkinson disease; individuals with normal DAT-SPECT scans may develop Parkinson disease in the future.
- DAT-SPECT scans have low specificity, and abnormal dopamine transporter uptake may be seen in atypical parkinsonism and other neurodegenerative disorders; thus, DAT-SPECT does not aid in the differential diagnosis of parkinsonism, limiting its clinical utility.
- False-positive abnormal DAT-SPECT scans may result from underlying strokes, technical issues such as head positioning in the scanner, or exposure to stimulants such as cocaine, amphetamine, or methylphenidate.
- Although identification of individuals with prodromal Parkinson disease is valuable from a research perspective, it will be clinically relevant once disease-modifying treatments for Parkinson disease become available.
- Striatal dopamine transporter uptake has a flooring effect and may reflect nigral cell loss and clinical severity of Parkinson disease only early in the disease process.
- Positron emission tomography (PET) measures of dopamine transporter uptake in the midbrain, unlike the striatum, may reflect nigral cell loss and motor manifestations throughout the full range of parkinsonism.
- Pathologic validation of in vivo PET studies is critical for a complete understanding of proteinopathies; increased Pittsburgh Compound B positron emission tomography uptake reflects the accumulation of fibrillary amyloid-β but not necessarily Alzheimer disease pathology in Parkinson disease.
- [^{18}F]-AV-1451, a PET tracer of tau, demonstrates increased uptake in progressive supranuclear palsy, a tauopathy, but the increase in uptake over time noted on longitudinal PET scans does not correlate with interim clinical progression of progressive supranuclear palsy.
- Radiotracer (-)-5-[^{18}F]-fluoroethoxybenzovesamicol enables quantification of presynaptic cholinergic nerve terminals with good regional specificity; patients with Parkinson disease with a history of falls had greater cholinergic deficits in subcortical structures such as the thalamus and caudate nucleus compared with patients without falls.
- Structural MRI does not show a pattern of atrophy in Parkinson disease that is diagnostic at the individual patient level; MRI in Parkinson disease is indicated if alternative etiologies are suspected.
- MRI in multiple system atrophy may demonstrate atrophy in the putamen, pons, cerebellum, and middle cerebellar peduncle, but these findings have low sensitivity, especially early in the disease process, and are not specific.
- MRI in progressive supranuclear palsy may demonstrate atrophy in the midbrain tegmentum and superior cerebellar peduncle, but these findings have low sensitivity and are not specific; the longitudinal rates of atrophy of the midbrain and pons may aid in the differential diagnosis.
- MRI evidence of strokes affecting the substantia nigra or nigrostriatal pathway may suggest a diagnosis of vascular parkinsonism, but the roles of white matter disease and basal ganglia stroke in its etiopathogenesis are less clear.
- Nigrasome-1, the largest group of dopaminergic neurons in the substantia nigra, appears as a hyperintense signal ("swallow tail") in the dorsolateral substantia nigra on iron-sensitive T2*-weighted and susceptibility-weighted imaging (SWI) sequences on high-field MRI.
- Dorsal nigral hyperintensity on iron-sensitive T2*-weighted and SWI is lost in Parkinson disease; this finding may be sensitive but not specific. It may help diagnose prodromal Parkinson disease but does not help in the differential diagnosis of atypical parkinsonisms.
- Nigral volume assessed using neuromelanin-sensitive MRI correlates with Parkinson disease duration and severity; decline in nigral volume has been shown on longitudinal scans.

Copyright © American Academy of Neurology. Unauthorized reproduction of this article is prohibited.

ARTICLE 9: NEUROIMAGING IN DEMENTIA

Shannon L. Risacher, PhD; Liana G. Apostolova, MD, MS, FAAN.
Continuum (Minneap Minn). February 2023; 29 (1 Neuroimaging):219–254.

ABSTRACT

OBJECTIVE:

Neurodegenerative diseases are significant health concerns with regard to morbidity and social and economic hardship around the world. This review describes the state of the field of neuroimaging measures as biomarkers for detection and diagnosis of both slowly progressing and rapidly progressing neurodegenerative diseases, specifically Alzheimer disease, vascular cognitive impairment, dementia with Lewy bodies or Parkinson disease dementia, frontotemporal lobar degeneration spectrum disorders, and prion-related diseases. It briefly discusses findings in these diseases in studies using MRI and metabolic and molecular-based imaging (eg, positron emission tomography [PET] and single-photon emission computerized tomography [SPECT]).

LATEST DEVELOPMENTS:

Neuroimaging studies with MRI and PET have demonstrated differential patterns of brain atrophy and hypometabolism in different neurodegenerative disorders, which can be useful in differential diagnoses. Advanced MRI sequences, such as diffusion-based imaging, and functional MRI (fMRI) provide important information about underlying biological changes in dementia and new directions for development of novel measures for future clinical use. Finally, advancements in molecular imaging allow clinicians and researchers to visualize dementia-related proteinopathies and neurotransmitter levels.

ESSENTIAL POINTS:

Diagnosis of neurodegenerative diseases is primarily based on symptomatology, although the development of in vivo neuroimaging and fluid biomarkers is changing the scope of clinical diagnosis, as well as the research into these devastating diseases. This article will help inform the reader about the current state of neuroimaging in neurodegenerative diseases, as well as how these tools might be used for differential diagnoses.

KEY POINTS

- **Alzheimer disease (AD) neuroimaging biomarkers become abnormal in a characteristic order where first amyloid deposition is detected on CSF or positron emission tomography (PET), then tau deposition is detected on CSF or PET, followed by changes in atrophy on MRI, and finally cognitive impairment.**
- **A research framework for diagnosing AD by classifying patients based on their amyloid status (positive versus negative), tau status (positive versus negative), and neurodegeneration (positive versus negative), as well as cognitive status, has been proposed and widely adopted.**
- **AD exists on a continuum of cognitive impairment, from cognitively normal individuals with AD pathophysiology (ie, preclinical AD), to mild impairment (mild cognitive impairment [MCI]), and ultimately clinical dementia (clinical AD dementia) with pathology defined by the amyloid, tau, neurodegeneration (A/T/N) framework.**
- **Patients with AD show widespread degeneration on structural MRI both subcortically, including in the hippocampus, amygdala, basal ganglia, and basal forebrain, and cortically, with the greatest changes in the medial and lateral temporal lobes.**

Copyright © American Academy of Neurology. Unauthorized reproduction of this article is prohibited.

- Structural MRI in patients with MCI shows focal atrophy in the medial and lateral temporal lobes, most especially in the entorhinal cortex and hippocampus, which is intermediate between cognitively normal patients and patients with clinical AD dementia, which can predict future progression to dementia.
- Patients with preclinical AD with normal cognition but positive AD biomarkers or at least one apolipoprotein E ε4 allele (*APOE* ε4) also show subtle changes in MRI measures of brain structure and function.
- Metabolic imaging with fludeoxyglucose (FDG)-PET shows bilateral hypometabolism in patients with clinical AD, as well as intermediate changes in patients with MCI. Patients with preclinical AD may also show altered metabolism, including either increased or decreased metabolism in several brain regions.
- Amyloid and tau PET imaging allow for visualization of AD pathology across clinical stages, with most clinically diagnosed AD dementia cases showing extensive amyloid and tau binding. The majority of patients with MCI show amyloid binding with some tau binding, and patients with preclinical AD show cortical amyloid binding and minimal tau signal.
- One major area of advancement in the field of AD is the development of blood-based tests that detect amyloid and tau in the plasma. These biomarkers provide excellent prediction of clinical status as well as cerebral amyloid and tau deposition, especially with the plasma phosphorylated tau assays.
- Tau deposition in AD typically follows a staging system originally defined in the pathologic literature (ie, Braak staging). The findings to date suggest that tau may spread through connected networks in the brain that can be measured using functional imaging (eg, functional resting-state imaging) or structural diffusion imaging.
- Although most patients with clinical AD present with memory impairment as the primary symptom, heterogeneity of both clinical symptoms and brain atrophy patterns are observed most commonly in patients with early-onset AD (ie, before the age of 65 years).
- Three subtypes of AD include logopenic aphasia, posterior cortical atrophy, and cerebral amyloid angiopathy, which often occur at younger ages and have distinct clinical and neuroimaging signatures on MRI and tau PET but not on amyloid PET (which is broadly positive across all forms).
- Heterogeneity also occurs in late-onset AD, which is linked to different patterns of brain atrophy and FDG hypometabolic patterns. Some of the subtype definitions map to genetic markers (ie, *APOE* ε4), higher rates of clinical progression, and more severe cognitive impairment.
- Patients with vascular cognitive impairment most commonly show white matter hyperintensities throughout the white matter of the brain, as well as subcortical infarcts, lacunes, prominent perivascular spaces, and cerebral microhemorrhages on MRI. Although these pathologies can be seen in normal aging, the pathology in vascular cognitive impairment or subcortical ischemic vascular dementia is much more severe and widespread.
- FDG-PET imaging has demonstrated that patients with vascular cognitive impairment have multifocal hypometabolism, which often presents in an asymmetric or scattered pattern or both. This hypometabolism can be cortical or subcortical or both and found near arteries or watershed regions of the brain.
- The majority of dementia cases that come to autopsy have more than one pathologic finding, most commonly AD pathology and small vessel disease, especially in older patients. In life, AD often presents as mixed dementia, reflecting the presence of AD pathophysiology and one or more other suspected pathologies.
- Parkinson disease dementia (PDD) and dementia with Lewy bodies (DLB) are diseases along the same continuum with the distinguishing factor being the sequence of onset of motor versus cognitive symptoms.
- Patients with DLB and PDD show widespread cortical atrophy on structural MRI, particularly in the posterior cortical regions and relative sparing of the medial temporal lobe compared with patients with AD.
- MRI in patients with multiple system atrophy shows atrophy of the cerebellum, pons, thalamus, substantia nigra, and the parietal and occipital lobes. One characteristic (but nonspecific) sign of multiple system atrophy can be found using T2-weighted imaging, which shows a cruciform hyperintensity in the pons known as the *hot cross buns sign*.
- FDG-PET studies in PDD and DLB show hypometabolism in the cortex, including the primary visual cortex, with relative sparing of the hippocampus, most distinctively showing the cingulate island sign, which is a relative preservation of metabolism in the posterior cingulate relative to the surrounding parietal and occipital lobes.

Copyright © American Academy of Neurology. Unauthorized reproduction of this article is prohibited.

- Unique to DLB and PDD, PET and single-photon emission computed tomography (SPECT) measures of dopaminergic neurotransmission are excellent biomarkers for differential diagnosis, with tracers targeting the dopamine transporter and dopamine receptors (ie, D2 receptors) showing reduced binding in the striatum and cortex.
- Frontotemporal lobar degeneration (FTLD) disorders can be classified into two forms by symptoms: (1) behavioral variant FTLD, in which patients show behavioral disturbances among other symptoms; and (2) primary progressive aphasias, which feature language impairments of multiple types.
- FTLD syndromes can feature extrapyramidal or motor symptoms with the FTLD and parkinsonism spectrum consisting of corticobasal degeneration (CBD) and progressive supranuclear palsy (PSP), as well as FTLD with motor neuron disease (or FTLD-amyotrophic lateral sclerosis).
- Patients with behavioral variant FTLD generally show frontal and temporal lobe atrophy, as well as atrophy in the basal ganglia, thalamus, and other deep gray matter structures, but can vary by underlying pathology (ie, tau versus transactive response DNA-binding protein 43 [TDP-43]).
- Patients with semantic dementia show focal MRI atrophy of the anterior and inferior temporal lobe, with an asymmetric (left more than right) pattern in most cases.
- Patients with progressive nonfluent aphasia show asymmetric perisylvian and anterior insular atrophy with the dominant language hemisphere most affected (usually the left hemisphere in right-handed individuals), as well as in the frontal and temporal lobe (eg, Broca area).
- Patients with CBD show asymmetric atrophy of the frontal and parietal lobes without sparing of the primary motor and sensory cortices, as well as the basal ganglia contralateral to the side most affected with rigidity and apraxia.
- Structural MRI studies in patients with PSP show significant midbrain atrophy, particularly in comparison with the neighboring pons, which is more severe than that seen in CBD. This atrophy pattern has been described as the *hummingbird sign* on sagittal view and the *Mickey Mouse sign* or *morning glory sign* on axial view.
- Patients with FTLD-ALS show atrophy in the frontal and temporal lobes, as well as the anterior cingulate, occipital lobe, and precentral gyrus, which is more severe in patients with FTLD-ALS than in patients with ALS and no FTLD symptoms.
- Patients with behavioral variant FTLD show symmetric frontal hypometabolism on FDG-PET, as well as hypometabolism in the anterior cingulate, parietal lobe, and temporal lobe in later stages.
- FDG-PET studies in semantic dementia have identified reduced metabolism in the left anterior temporal lobe but less significant frontal lobe hypometabolism than in other forms of FTLD.
- Patients with progressive nonfluent aphasia show asymmetric (usually left more than right) frontal cortical hypometabolism in the language-dominant hemisphere, including in the Broca area.
- FDG-PET studies in CBD show asymmetric hypometabolism in the posterior frontal lobes, sensorimotor cortex, and subcortical regions.
- FDG-PET studies in PSP show notable hypometabolism of the prefrontal cortex, caudate, pallidum, thalamus, mesencephalon, and subthalamic nucleus.
- Patients with FTLD-ALS show hypometabolism in the frontal lobe, superior temporal lobe, parietal lobe, occipital lobe, and insula, which is more severe in FTLD-ALS than in ALS without FTLD.
- Amyloid PET scans have shown minimal binding in any subtype of FTLD unless comorbid AD pathology exists.
- Tau PET scans have shown less binding in FTLD relative to that seen in AD, potentially because of less sensitivity of the tracers to non-AD tau conformations. However, the tau PET studies generally show higher tau deposition in regions that mirror the location of atrophy across the FTLD spectrum.
- The primary imaging biomarkers for prion disorders are MRI based, the most sensitive type being diffusion-weighted imaging (DWI). All forms of CJD can show restricted diffusion in the basal ganglia, cerebellum, and diffuse regions of the cortex ("ribboning"), most commonly affecting the frontal and parietal lobes.
- Familial prion protein forms, such as Gerstmann-Sträussler-Scheinker disease and familial CJD, show mixed results with structural MRI measures, with some patients showing no atrophy and others with generalized

Copyright © American Academy of Neurology. Unauthorized reproduction of this article is prohibited.

cerebral and cerebellar atrophy. Patients with fatal familial insomnia may show mild cerebral atrophy and often have restricted diffusion in the thalamus.

- FDG-PET studies in all forms of CJD show widespread and often asymmetric hypometabolism in the cortex and cerebellum, with relative sparing of the basal ganglia and thalamus, whereas familial forms of prion protein disease show cerebral, cerebellar, and subcortical hypometabolism.
- Amyloid and tau PET scans generally show minimal binding in prion protein diseases.
- The differential diagnosis of diseases presenting with or without motor symptoms, such as late-onset AD, atypical AD, CJD, and FTLD, can be improved by using structural MRI and PET techniques.
- Patterns of atrophy and hypometabolism often differ between neurodegenerative disorders and can be used to support a clinical diagnosis, whereas amyloid and tau PET, along with dopaminergic PET or SPECT, can provide support for or rule out a probable diagnosis.

ARTICLE 10: IMAGING OF CENTRAL NERVOUS SYSTEM AUTOIMMUNE, PARANEOPLASTIC, AND NEURO-RHEUMATOLOGIC DISORDERS

Lama Abdel Wahed, MD; Tracey A. Cho, MD, FAAN.
Continuum (Minneap Minn). February 2023; 29 (1 Neuroimaging):255–291.

ABSTRACT

OBJECTIVE:

This article provides an overview of the imaging modalities used in the evaluation of central nervous system (CNS) autoimmune, paraneoplastic, and neuro-rheumatologic disorders. An approach is outlined for interpreting imaging findings in this context, synthesizing a differential diagnosis based on certain imaging patterns, and choosing further imaging for specific diseases.

LATEST DEVELOPMENTS:

The rapid discovery of new neuronal and glial autoantibodies has revolutionized the autoimmune neurology field and has elucidated imaging patterns characteristic of certain antibody-associated diseases. Many CNS inflammatory diseases, however, lack a definitive biomarker. Clinicians should recognize neuroimaging patterns suggestive of inflammatory disorders, as well as the limitations of imaging. CT, MRI, and positron emission tomography (PET) modalities all play a role in diagnosing autoimmune, paraneoplastic, and neuro-rheumatologic disorders. Additional imaging modalities such as conventional angiography and ultrasonography can be helpful for further evaluation in select situations.

ESSENTIAL POINTS:

Knowledge of imaging modalities, both structural and functional, is critical in identifying CNS inflammatory diseases quickly and can help avoid invasive testing such as brain biopsy in certain clinical scenarios. Recognizing imaging patterns suggestive of CNS inflammatory diseases can also facilitate the early initiation of appropriate treatments to diminish morbidity and future disability.

Copyright © American Academy of Neurology. Unauthorized reproduction of this article is prohibited.

KEY POINTS

- Neuroimaging, especially MRI, can help identify the central nervous system (CNS) compartments predominantly involved in suspected autoimmune or inflammatory disease: parenchymal, meningeal, ventricular, or vascular.
- CT angiography provides good anatomic resolution of large and some medium-size vessels but has poor resolution for smaller vessels.
- Leptomeningitis typically manifests as gyriform or serpentine enhancement following the sulci.
- When assessing extra-axial postcontrast T1-hyperintense lesions, it is important to review in the context of other sequences including T1 precontrast, fluid-attenuated inversion recovery (FLAIR), and susceptibility-weighted imaging (SWI).
- Trauma or neurosurgery may lead to meningeal enhancement in the short term.
- Neurosarcoidosis should be suspected in patients with subacute onset of multiple cranial neuropathies with basal meningitis on MRI.
- Meningioma is often associated with intralesional calcifications and surrounding hyperostosis or bony destruction, which helps distinguish it from focal pachymeningitis.
- Cranial neuropathies, both clinical and radiographic, are a common feature of skull base meningitis.
- IgG4-related disease (as well as neurosarcoidosis) can cause hypophysitis and cavernous sinus disease.
- Direct extension of granulomatous inflammation from sinus to dura is a clue to antineutrophil cytoplasmic antibody–associated vasculitis.
- CNS-limited antineutrophil cytoplasmic antibody–associated vasculitis is typically associated with a hypertrophic meningitis in older women with positive myeloperoxidase antibody.
- Brain MRI in NMDA receptor encephalitis is normal in most patients.
- Compared with autoimmune encephalitis, herpes simplex virus encephalitis is more likely to be unilateral or asymmetric and to have accompanying diffusion-weighted imaging restriction and enhancement.
- Lack of prodromal symptoms, rapid clinical improvement with antiseizure medications alone, and noninflammatory CSF are all clues to distinguish peri-ictal MRI changes from limbic autoimmune encephalitis.
- About 50% of patients with Hashimoto encephalopathy have a normal brain MRI.
- Fludeoxyglucose positron emission tomography (FDG-PET) of the brain can be a more sensitive biomarker than brain MRI for detecting focal or multifocal brain abnormalities in autoimmune encephalitis.
- A gradient of anterior hypermetabolism to posterior cortical hypometabolism, especially in the medial and lateral occipital lobes, has been described in NMDA receptor encephalitis.
- Hypometabolic PET patterns are not specific to autoimmune encephalitis and are seen commonly in the postictal state and in older patients with neurodegenerative disease.
- Once viral causes are ruled out, the presence of bilateral temporal lobe FLAIR hyperintensities is sufficient to diagnose definite limbic autoimmune encephalitis even in the absence of neuronal antibodies.
- Multiple and confluent cortical and subcortical FLAIR hyperintensities are a hallmark of encephalitis with autoantibodies to γ-aminobutyric acid type A ($GABA_A$) receptor.
- Striatal encephalitis with anti-collapsin response mediator protein 5 (CRMP5 or CV2) antibodies may be associated with extensive T2-hyperintense symmetric signal affecting the bilateral caudate and putamen.
- Paraneoplastic diencephalic encephalitis associated with Ma2 antibodies may cause T2 hyperintensities in the medial thalami and midbrain.
- Glial fibrillary acidic protein (GFAP) astrocytopathy is associated with a hallmark MRI finding of periventricular linear radial enhancement on postcontrast T1-weighted sequences.
- For posterior fossa structures, subtle T2 hyperintensity may be more easily appreciated on conventional T2-weighted MRI than on FLAIR sequences.
- Rim-enhancing lesions with central restricted diffusion suggestive of abscess are clues to *Listeria* infection as the cause of brainstem encephalitis.
- Neuro-Behçet syndrome may be associated with T2 hyperintensity in the ventral pons and midbrain, sparing the red nucleus.

Copyright © American Academy of Neurology. Unauthorized reproduction of this article is prohibited.

- MRI is often normal early in the course of paraneoplastic cerebellar degeneration although mild T2 hyperintensities may be seen in the cerebellar hemispheres.
- The most commonly associated autoantibodies with autoimmune cerebellar ataxia are anti–glutamic acid decarboxylase 65 (GAD65), anti–contactin-associated proteinlike 2 (CASPR2), and anti–metabotropic glutamate receptor (mGLuR1).
- Approximately 50% of patients with neuropsychiatric lupus have abnormal brain MRI, most commonly manifesting as nonspecific white matter periventricular and subcortical T2 hyperintensities.
- Neuromyelitis optica spectrum disorder (NMOSD) may occur in association with Sjögren syndrome, and patients with optic neuritis or transverse myelitis should be tested for serum aquaporin-4 IgG and myelin oligodendrocyte glycoprotein IgG.
- Brain MRI is abnormal in 95% to 100% of patients with CNS vasculitis.
- Digital subtraction angiography is the most sensitive modality for vascular luminal changes in CNS vasculitis, including alternating areas of stenosis and dilation in at least two separate vascular distributions.
- High-resolution MRI with vessel wall imaging may be helpful in demonstrating enhancement of the vessel walls in vasculitis, but the modality has limited specificity.
- Findings of callosal T2 hyperintensities or "snowball-like" lesions in the corpus callosum in the context of encephalopathy, branch retinal artery occlusion, and hearing loss are highly suggestive of Susac syndrome.
- Confluent and asymmetric T2 hyperintensities in cortical and subcortical areas, in association with microhemorrhage on SWI, are characteristic of cerebral amyloid angiopathy-related inflammation.
- MRI is helpful in determining the length of the lesion (short versus longitudinally extensive transverse myelitis), width (partial versus transverse), and location (eccentric, central, hemicord, anterior versus posterior, conus, tracts, or meningeal).
- The trident sign, which has been described in relation to neurosarcoidosis, demonstrates leptomeningeal or dorsal subpial enhancement that may or may not involve the central canal.
- Involvement of the conus medullaris is a clue to myelin oligodendrocyte glycoprotein-associated disorder as the cause of longitudinally extensive transverse myelitis.
- CT of the chest, abdomen, and pelvis with iodine contrast is a generally accepted first method of screening for occult malignancy or systemic inflammation (eg, sarcoidosis).

ARTICLE 11: IMAGING OF CENTRAL NERVOUS SYSTEM DEMYELINATING DISORDERS

Jan-Mendelt Tillema, MD. Continuum (Minneap Minn). February 2023; 29 (1 Neuroimaging):292–323.

ABSTRACT

OBJECTIVE:

This article summarizes neuroimaging findings in demyelinating disease, the most common being multiple sclerosis. Revisions to criteria and treatment options have been ongoing, and MRI plays a pivotal role in diagnosis and disease monitoring. The common antibody-mediated demyelinating disorders with their respective classic imaging features are reviewed, as well as the differential diagnostic considerations on imaging.

Copyright © American Academy of Neurology. Unauthorized reproduction of this article is prohibited.

LATEST DEVELOPMENTS:

The clinical criteria of demyelinating disease rely heavily on imaging with MRI. With novel antibody detection, the range of clinical demyelinating syndromes has expanded, most recently with myelin oligodendrocyte glycoprotein–IgG antibodies. Imaging has improved our understanding of the pathophysiology of multiple sclerosis and disease progression, and further research is underway. The importance of increased detection of pathology outside of the classic lesions will have an important role as therapeutic options are expanding.

ESSENTIAL POINTS:

MRI has a crucial role in the diagnostic criteria and differentiation among common demyelinating disorders and syndromes. This article reviews the typical imaging features and clinical scenarios that assist in accurate diagnosis, differentiation between demyelinating diseases and other white matter diseases, the importance of standardized MRI protocols in clinical practice, and novel imaging techniques.

KEY POINTS

- MRI plays a pivotal role in the diagnostic criteria for central nervous system (CNS) demyelinating disorders.
- In patients with multiple sclerosis (MS), normal-appearing white matter and gray matter are now well known to harbor both demyelinating and neurodegenerative pathology.
- Earlier diagnosis and treatment monitoring for MS rely greatly on MRI. Despite these advances, the diagnosis and distinction between MS phenotypes remain a clinical assessment.
- In MS, radiologic activity can exist without any clinical activity. One of the diagnoses that has gained traction with this pattern is radiologically isolated syndrome, in which MRI lesions are present in asymptomatic patients.
- The risk of conversion to clinically definite MS, whether to relasping-remitting MS or primary progressive MS, is increased with the following risk factors: onset age younger than 37 years, presence of gadolinium enhancement on index scan, or the presence of spinal cord lesions on MRI.
- Patients with progressive MS can still have subsequent disease activity in the form of relapses or new MRI activity, although these are much less common.
- Classic MS lesions are round or ovoid and well circumscribed in the chronic stage.
- With recent advances in three-dimensional fluid-attenuated inversion recovery (FLAIR) imaging, when quality is sufficient, this sequence is actually as sensitive or better than axial two-dimensional T2-weighted images.
- High-quality three-dimensional FLAIR at 3T, more so than double inversion recovery and phase-sensitive inversion recovery, has the best ability to detect cortical MS lesions.
- Open-ring enhancement is highly specific to MS with a pattern in which the opening is facing the gray matter.
- In patients with isolated optic neuritis, the conversion risk to MS is about 25% over 15 years in the absence of brain lesions.
- Optic nerve lesions can have an extensive course throughout the optic nerve, particularly in antibody-mediated optic neuritis (myelin oligodendrocyte glycoprotein and neuromyelitis optica).
- Optical coherence tomography is highly sensitive in the detection of possible previous optic nerve lesions or attacks.
- MRI features in other (antibody-mediated) demyelinating disorders can have distinct characteristics that help distinguish these disorders from MS.
- Acute disseminated encephalomyelitis (ADEM) and optic neuritis are the most common presenting phenotypes of myelin oligodendrocyte glycoprotein–associated disorder.
- Myelin oligodendrocyte glycoprotein–associated disorder lesions can differ from those in neuromyelitis optica and predominantly affect the central gray matter, which is best noted on axial imaging.
- MRI surveillance is typically not felt to be helpful in antibody-mediated demyelinating disease and should be reserved for when new symptoms suggestive of attacks present unless the diagnosis is uncertain.

Copyright © American Academy of Neurology. Unauthorized reproduction of this article is prohibited.

- Novel MRI acquisition and processing techniques have distinguished some lesion signatures with potential prognostic properties, some of which are slowly finding their way into clinical practice.
- Newer MRI techniques better capture disease that can be visualized beyond the white matter lesions noted on conventional MRI. Lesions can be found in the cerebral cortex with specific acquisitions.
- Quantitative measures of advanced MRI techniques (eg, diffusion tensor imaging) and MR spectroscopy have identified what is known in pathology as normal-appearing white matter involvement.
- Atrophy has been reported throughout the central nervous system in MS, affecting whole brain volume and, in particular, the thalamus.
- Spinal cord lesions can be present without clinical symptoms in MS, and the most common location of spinal cord lesions is within the cervical spinal cord.
- The differential diagnosis should remain broad when the presentation is atypical or in the setting of imaging red flags.
- Harmonization of MRI protocols with the minimal required sequences is highlighted in consensus statements from MS experts, incorporating both diagnostic and disease monitoring purposes in MS.

ARTICLE 12: DIAGNOSTIC ULTRASONOGRAPHY IN NEUROLOGY

Elsa Azevedo, MD, PhD. Continuum (Minneap Minn). February 2023;
29 (1 Neuroimaging):324-363.

ABSTRACT

OBJECTIVE:

Ultrasonography allows neurologists to complement clinical information with additional useful, easily acquired, real-time data. This article highlights its clinical applications in neurology.

LATEST DEVELOPMENTS:

Diagnostic ultrasonography is expanding its applications with smaller and better devices. Most indications in neurology relate to cerebrovascular evaluations. Ultrasonography contributes to the etiologic evaluation and is helpful for hemodynamic diagnosis of brain or eye ischemia. It can accurately characterize cervical vascular atherosclerosis, dissection, vasculitis, or other rarer disorders. Ultrasonography can aid in the diagnosis of intracranial large vessel stenosis or occlusion and evaluation of collateral pathways and indirect hemodynamic signs of more proximal and distal pathology. Transcranial Doppler (TCD) is the most sensitive method for detecting paradoxical emboli from a systemic right-left shunt such as a patent foramen ovale. TCD is mandatory for sickle cell disease surveillance, guiding the timing for preventive transfusion. In subarachnoid hemorrhage, TCD is useful in monitoring vasospasm and adapting treatment. Some arteriovenous shunts can be detected by ultrasonography. Cerebral vasoregulation studies are another developing field of interest. TCD enables monitoring of hemodynamic changes related to intracranial hypertension and can diagnose cerebral circulatory arrest. Optic nerve sheath measurement and brain midline deviation are ultrasonography-detectable signs of intracranial hypertension. Most importantly, ultrasonography allows for easily repeated monitoring of evolving clinical conditions or during and after interventions.

Copyright © American Academy of Neurology. Unauthorized reproduction of this article is prohibited.

ESSENTIAL POINTS:

Diagnostic ultrasonography is an invaluable tool in neurology, used as an extension of the clinical examination. It helps diagnose and monitor many conditions, allowing for more data-driven and rapid treatment interventions.

KEY POINTS

- Neurosonology can be used as an extension of the clinical neurologic examination.
- Advantages of neurosonology are that it can be performed at the bedside, is noninvasive, provides real-time accurate information, and allows continuous monitoring.
- An ultrasound machine that provides B-mode echography, color imaging of the vessels, and blood flow velocities spectrum allows extracranial and many intracranial applications, including vascular and parenchymal studies.
- A transcranial Doppler device providing only Doppler spectral analysis is a smaller device that allows hands-free and bilateral monitoring of cerebral hemodynamics with a headframe.
- Atherosclerosis, sickle cell disease, brain and eye ischemia, subarachnoid hemorrhage, suspicion of temporal arteritis or dural fistulas, intracranial hypertension, and cerebral circulatory arrest are some of the settings for neurovascular ultrasonography.
- A comprehensive cerebrovascular ultrasonographic evaluation should include cervical as well as intracranial vessels.
- The degree of stenosis of a cervical internal carotid atherosclerotic plaque can be measured by direct morphologic and velocimetric parameters, as well as by indirect criteria.
- Compensatory intracranial collateral circuits (ophthalmic, anterior communicating, and posterior communicating arteries) provide indirect signs of the hemodynamic effect of a cervical carotid stenosis.
- Higher degrees of stenosis are related to both the decrease in distal perfusion pressure and atheroembolism. Atheroembolic risk is further linked to unstable plaque features.
- Cervical vertebral artery stenosis can be assessed by the decrease in lumen diameter and measurement of blood flow velocity at the stenotic segment and more distally.
- Subclavian steal effect consists of inverted flow from the ipsilateral vertebral artery when a tight stenosis or occlusion of the proximal subclavian artery is present.
- Ultrasound signs of dissection may include an enlarged artery with an eccentric hypoechogenic luminal stenosis, tapering stenosis ending in a string sign, floating intimal flap, and double lumen appearance, with to-and-fro aspect in color and spectral Doppler in the false lumen.
- Concentric hypoechogenic vessel wall thickening is the sonographic hallmark of vasculitis.
- Giant cell arteritis is the most common form of large and medium vessel vasculitis affecting adults, characterized by a hypoechogenic noncompressible thickening of the wall (the halo sign) in the temporal branch of the external carotid artery.
- Transient perivascular inflammation of the carotid artery syndrome associates carotid pain with an eccentric carotid stenosis, disappearing within a few weeks spontaneously or after treatment with anti-inflammatory drugs.
- Isolated hypoechogenic mural thrombi might appear associated with thrombophilia and disappear by lysis, spontaneously, or after anticoagulation therapy.
- Fibromuscular dysplasia is suspected by a string-of-beads appearance in the distal cervical internal carotid artery and the vertebral arteries.
- Carotid webs are potentially thrombogenic and may be implicated in ischemic stroke. Sonographically it appears as a shelf-like membrane in the posterior aspect of the internal carotid artery bulb into the lumen, just beyond the carotid bifurcation.
- When the external carotid artery shows high velocity and low resistance, an arteriovenous shunt may be suspected, especially in a patient with pulsatile tinnitus.
- The thrombolysis in brain ischemia score helps in evaluation of the flow conditions in the symptomatic intracranial artery in acute ischemic stroke, namely before and after recanalization treatment.

Copyright © American Academy of Neurology. Unauthorized reproduction of this article is prohibited.

- Systolic and mean blood flow velocity cut-offs help diagnose intracranial stenosis and stratify it as <50%, >50%, and>70%.
- Transcranial Doppler (TCD) and transcranial color sonography can accurately detect significant intracranial artery stenosis and occlusion.
- Atherosclerotic stenosis has a more focal and stable blood flow velocity increase than dynamic intracranial stenoses such as those caused by an embolus, dissection, vasospasm, or vasculitis.
- In children with sickle cell disease, screening with TCD for high blood flow velocity (≥200 cm/s) and treatment with regular blood transfusion may result in a 10-fold decrease in the prevalence of strokes.
- Annual TCD screening should be offered for children aged 2 to 16 years with sickle cell disease of the types *HbSS* or Sβ0 thalassemia.
- In patients with subarachnoid hemorrhage, vasospasm can be monitored with TCD, which helps adjust medical and intervention therapy aiming to prevent delayed cerebral ischemia and cerebral infarction.
- TCD can diagnose vasoconstriction related to reversible cerebral vasoconstriction syndrome in the proximal cerebral arteries, although there are no standardized blood flow velocity criteria.
- Changes in blood flow velocity over time in patients with reversible cerebral vasoconstriction syndrome may be more informative than the isolated values.
- TCD can be used to monitor cerebral hemodynamics during acute stroke and in the neurocritical setting, as well as before, during, and after therapeutic interventions.
- TCD and transcranial color sonography allow for monitoring intracranial pressure changes. With intracranial pressure increase, cerebral blood flow velocity, mainly diastolic, decreases.
- Cerebral circulatory arrest is indicated by no diastolic flow for at least 30 minutes in the middle cerebral arteries and the basilar artery, and decreased systolic blood flow velocity.
- TCD and transcranial color sonography are highly accurate ancillary tests for cerebral circulatory arrest confirmation.
- TCD and a nontranspulmonary gaseous contrast injection are a reliable and less invasive complement to gold standard transesophageal echocardiography in the diagnosis of a patent foramen ovale and enable the detection of extracardiac right-to-left shunt.
- The size of a patent foramen ovale measured by transesophageal echocardiography correlates with the amount of microembolic signals observed by TCD.
- Microembolic signal monitoring is useful in evaluating arterial lesion stroke risk and as a surrogate marker of antithrombotic drug efficacy.
- Microembolic signal monitoring is performed over 30 to 60 minutes, usually with bilateral 2-MHz probes fixed in a headframe.
- Reduced cerebral autoregulation is associated with worse outcome in acute stroke and in the neurocritical care setting.
- Functional TCD studies may allow identification of the dominant hemisphere and identification of early neurovascular unit dysfunction in cerebrovascular pathologies.
- Raised flow velocities in collateral venous drainage are the most frequent finding in patients with cerebral venous sinus thrombosis, although it has low sensitivity.
- Ultrasound evaluation of the optic nerve allows for detection of signs of increased intracranial pressure, namely increased optic nerve sheath diameter and raised papilla.
- Especially in the neurocritical care setting, ultrasonography can be useful for the measurement of pupil reactivity.
- Analysis of orbital vascularization may provide evidence of central retina artery occlusion, which has a worse prognosis if an embolic echogenic spot sign is present.

Copyright © American Academy of Neurology. Unauthorized reproduction of this article is prohibited.

Issue Overview

Neuroimaging, Volume 29, Number 1, February 2023

Continuum: Lifelong Learning in Neurology® is designed to help practicing neurologists stay abreast of advances in the field while simultaneously developing lifelong self-directed learning skills.

Learning Objectives

Upon completion of this *Continuum: Lifelong Learning in Neurology* Neuroimaging issue, participants will be able to:

- Describe governing rules for choosing an imaging modality or a specific imaging protocol in an individual patient, with emphasis on the limitations of predefined protocols and the importance of clinical context
- Describe the physical and procedural safety risks of MRI and CT, which are essential imaging modalities for the diagnosis of neurologic disease
- Describe the imaging modalities used in the evaluation of patients presenting with acute ischemic stroke, including technical considerations, interpretation, and clinical utility of each modality
- Describe the role of neuroimaging in guiding identification of central nervous system hemorrhage, aiding in identification of hemorrhage etiology, and guiding subsequent medical decision making
- Describe a methodical approach to the integration of neuroimaging in the clinical care of patients with epilepsy
- Discuss the classic imaging features of common skull base tumors and their implications in surveillance, as well as management of these tumors
- Describe essential imaging modalities in the treatment of patients with brain tumors and recognize common imaging patterns for tumors and certain clinical scenarios
- Recognize abnormal findings on conventional clinical imaging in movement disorders and critically evaluate their relationship with pathology, utility, and limitations; and describe some other imaging modalities used in research and recent findings
- Identify and describe neuroimaging findings in the most common age-related dementias
- Describe the imaging patterns typical of autoimmune and inflammatory brain and spinal cord diseases, causes of the limbic encephalitis pattern on MRI, and findings on MRI that can help distinguish causes of myelitis
- Discuss the role of MRI in both the diagnosis and prognosis of multiple sclerosis and antibody-mediated demyelinating diseases such as myelin oligodendrocyte glycoprotein–associated disorder, acquired disseminated encephalomyelitis, and neuromyelitis optica
- Discuss the technical requirements, applications, and limitations of ultrasonography in central nervous system neurology

Copyright © American Academy of Neurology. Unauthorized reproduction of this article is prohibited.

Core Competencies

This *Continuum: Lifelong Learning in Neurology* Neuroimaging issue covers the following core competencies:

- Patient Care and Procedural Skills
- Medical Knowledge
- Practice-Based Learning and Improvement
- Interpersonal and Communication Skills
- Professionalism
- Systems-Based Practice

Copyright © American Academy of Neurology. Unauthorized reproduction of this article is prohibited.

Contributors

Joshua P. Klein, MD, PhD, FANA, FASN, FAAN, *Guest Editor*

Vice Chair, Clinical Affairs, and Chief, Division of Hospital Neurology, Department of Neurology, Brigham and Women's Hospital; Associate Professor of Neurology and Radiology, Harvard Medical School, Boston, Massachusetts

Relationship Disclosure: Dr Klein has received personal compensation in the range of $5000 to $9999 for serving as an editor, associate editor, or editorial advisory board member for Oakstone Publishing and in the range of $10,000 to $49,999 for serving as an editor, associate editor, or editorial advisory board member for AudioDigest, McGraw Hill, and SAGE Publications. Dr Klein has received publishing royalties in the range of $10,000 to $49,000 from a publication relating to health care. Dr Klein has received personal compensation in the range of $100,000 to $499,999 for serving as an expert witness for various law firms.

Unlabeled Use of Products/Investigational Use Disclosure: Dr Klein reports no disclosure.

Mohamad Abdalkader, MD

Assistant Professor of Radiology, Boston Medical Center, Boston University School of Medicine, Boston, Massachusetts

Relationship Disclosure: Dr Abdalkader reports no disclosure.

Unlabeled Use of Products/Investigational Use Disclosure: Dr Abdalkader reports no disclosure.

Lama Abdel Wahed, MD

Clinical Assistant Professor of Neurology, University of Iowa Carver College of Medicine; Associate Residency Program Director, Associate Clerkship Director, University of Iowa Healthcare, Iowa City, Iowa

Relationship Disclosure: Dr Abdel Wahed has received personal compensation in the range of $0 to $499 for serving as a resident honorary speaker with the Iowa Neurological Association and as an author for MedLink, LLC.

Unlabeled Use of Products/Investigational Use Disclosure: Dr Abdel Wahed discusses the unlabeled use of corticosteroids for the treatment of autoimmune neurologic diseases that have no US Food and Drug Administration–approved medications.

Liana G. Apostolova, MD, MS, FAAN

Indiana University Distinguished Professor, Barbara and Peer Baekgaard Professor in Alzheimer's Disease Research, Indiana University School of Medicine, Indianapolis, Indiana

Relationship Disclosure: Dr Apostolova has received personal compensation in the range of $500 to $4999 for serving as a consultant for Florida Health, General Electric Company, Lilly, the National Institutes of Health (NIH), and NIH Biobank; on a data safety monitoring board for IQVIA Inc; and on advisory boards for Eisai Co, Ltd, F. Hoffman-La Roche Ltd, Genentech, Inc, and TwoLabs, LLC. Dr Apostolova has received personal compensation in the range of $5000 to $9999 for serving on an advisory board for Biogen and in the range of $10,000 to $49,999 for serving as an editor-in-chief for the Alzheimer’s Association. An immediate family member of Dr Apostolova has stock in Cassava Sciences, Inc, Golden Seeds, and Semiring. The institution of Dr Apostolova has received research support from the Alzheimer’s Association, Avid Radiopharmaceuticals, F. Hoffman-La Roche Ltd, Life Molecular Imaging, and the National Institute on Aging.

Unlabeled Use of Products/Investigational Use Disclosure: Dr Apostolova reports no disclosure.

Elsa Azevedo, MD, PhD

Department of Neurology, Centro Hospitalar Universitário de São João; Department of Clinical Neurosciences and Mental Health, Faculty of Medicine of University of Porto, Porto, Portugal

Relationship Disclosure: Dr Azevedo reports no disclosure.

Copyright © American Academy of Neurology. Unauthorized reproduction of this article is prohibited.

Unlabeled Use of Products/Investigational Use Disclosure: Dr Azevedo reports no disclosure.

Wenya Linda Bi, MD, PhD
Assistant Professor of Neurosurgery, Harvard Medical School, Brigham and Women's Hospital, Boston, Massachusetts

Relationship Disclosure: Dr Bi reports no disclosure.

Unlabeled Use of Products/Investigational Use Disclosure: Dr Bi reports no disclosure.

Tracey A. Cho, MD, FAAN
Clinical Professor of Neurology, University of Iowa Carver College of Medicine; Director, Neuroimmunology Division, University of Iowa Healthcare, Iowa City, Iowa

Relationship Disclosure: Dr Cho has received personal compensation in the range of $500 to $4999 for serving as a consultant for Horizon Therapeutics plc and on a data safety monitoring board for the National Institutes of Health and has received publishing royalties from a publication relating to health care. The institution of an immediate family member of Dr Cho has received research support from the National Institutes of Health.

Unlabeled Use of Products/Investigational Use Disclosure: Dr Cho discusses the unlabeled use of corticosteroids for the treatment of autoimmune neurologic diseases that have no US Food and Drug Administration–approved medications.

Elizabeth R. Gerstner, MD
Associate Professor of Neurology, Harvard Medical School; Associate Neurologist, Massachusetts General Hospital, Boston, Massachusetts

Relationship Disclosure: Dr Gerstner has received personal compensation in the range of $500 to $4999 for serving on a data safety monitoring board for Midatech Pharma PLC and in the range of $50,000 to $99,999 for serving as an officer or member of the board of directors for the Gerstner Family Foundation. The institution of Dr Gerstner has received research support from the National Cancer Institute.

Unlabeled Use of Products/Investigational Use Disclosure: Dr Gerstner discusses the unlabeled/investigational use of mitogen-associated protein kinase (MAPK) pathway with MAP-ERK kinase (MEK) inhibitors for the treatment of MAP kinase-altered tumors and various MRI and positron emission tomography (PET) techniques not approved for the imaging of brain tumors.

Ryan Hakimi, DO, MS, NVS, RPNI, CPB, FNCS, FCCM
Director, Neuro ICU and Transcranial Doppler Ultrasound Services, Prisma Health-Upstate; Professor, Department of Medicine (Neurology Division), University of South Carolina School of Medicine-Greenville, Greenville, South Carolina

Relationship Disclosure: Dr Hakimi has received personal compensation in the range of $0 to $499 for serving as a delegate in the American Medical Association House of Delegates for the American Society of Neuroimaging and in the range of $500 to $4999 for serving as the immediate past president for the South Carolina Osteopathic Medical Society and as a medical reviewer for the Office of Disciplinary Counsel in the South Carolina Department of Labor, Licensing and Regulation and has received publishing royalties from Osler, Hoskin & Harcourt LLP. Dr Hakimi has a noncompensated relationship as an annual meeting course committee member with the Neurocritical Care Society that is relevant to AAN interests or activities.

Unlabeled Use of Products/Investigational Use Disclosure: Dr Hakimi reports no disclosure.

Justin T. Jordan, MD, MPH, FAAN
Clinical Director, Stephen E. and Catherine Pappas Center for Neuro-Oncology at Massachusetts General Hospital; Director, Family Center for Neurofibromatosis Massachusetts General Hospital; Assistant Professor of Neurology, Harvard Medical School, Boston, Massachusetts

Relationship Disclosure: Dr Jordan has received personal compensation in the range of $0 to $499 for serving as a consultant for Atheneum Partners, EM Partners, GLG Pharma, and Guidepoint Global, LLC; in the range of $500 to

Copyright © American Academy of Neurology. Unauthorized reproduction of this article is prohibited.

$4999 for serving as a consultant for Creative Educational Concepts, LLC, and Texas Health Resources; and in the range of $5000 to $9999 for serving as a consultant for Children's Tumor Foundation, Navio Theragnostics, Inc, and Recursion and on a scientific advisory board for Recursion. Dr Jordan has stock in The Doctor Lounge and Navio Theragnostics, Inc, has received publishing royalties from Elsevier, and has noncompensated relationships as a board member with ABA Academy, Neurofibromatosis Northeast, Neurofibromatosis Network, and the United Council for Neurologic Subspecialties that is relevant to AAN interests or activities. The institution of Dr Jordan has received research support from The Burke Foundation, the Department of Defense, and the National Institutes of Health.

Unlabeled Use of Products/Investigational Use Disclosure: Dr Jordan discusses the unlabeled/investigational use of mitogen-associated protein kinase (MAPK) pathway with MAP-ERK kinase (MEK) inhibitors for the treatment of MAP kinase-altered tumors and various MRI and positron emission tomography (PET) techniques not approved for the imaging of brain tumors.

Baijayanta Maiti, MD, PhD
Assistant Professor of Neurology, Washington University in St. Louis School of Medicine, St. Louis, Missouri

Relationship Disclosure: The institution of Dr Maiti has received research support from the National Center for Advancing Translational Sciences and the National Institute of Neurological Disorders and Stroke of the National Institutes of Health.

Unlabeled Use of Products/Investigational Use Disclosure: Dr Maiti reports no disclosure.

Erasmo A. Passaro, MD
Professor of Neurology, University of South Florida, Tampa; Director, Epilepsy Program, Bayfront Health; Medical Director, Epilepsy Surgery, Johns Hopkins All Children's Hospital; St Petersburg, Florida

Relationship Disclosure: Dr Passaro has received personal compensation in the range of $0 to $499 for serving on a speakers bureau and as a consultant for Neurelis, Inc; in the range of $500 to $4999 for serving on speakers bureaus and as a consultant for Eisai Co, Ltd, and Sunovion Pharmaceuticals, Inc; and in the range of $5000 to $9999 for serving on speakers bureaus and as a consultant for SK Life Science, Inc, and UCB, Inc.

Unlabeled Use of Products/Investigational Use Disclosure: Dr Passaro reports no disclosure.

Joel S. Perlmutter, MD
Elliot Stein Family Professor Neurology; Head of Movement Disorders; Professor of Radiology, Neuroscience, Physical Therapy, Occupational Therapy, Washington University in St. Louis School of Medicine, St. Louis, Missouri

Relationship Disclosure: Dr Perlmutter has received personal compensation in the range of $0 to $499 for serving as an officer or member of the Board of Directors for the Parkinson Study Group, and in the range of $500 to $4999 for serving as an officer or member of the Board of Directors for the CHDI Foundation, as an expert witness for Wood, Cooper and Peterson, LLC, and Simmons and Simmons LLP, as a lecturer for Boston University, as an external advisor for Stanford University, and as a visiting professor with Beth Israel Hospital and the University of Pennsylvania. The institution of Dr Perlmutter has received research support from the American Parkinson Disease Association, the Barnes-Jewish Hospital Foundation, the CHDI Foundation, the Huntington Disease Society of America, The Michael J Fox Foundation, the National Institutes of Health, the University of California San Diego, and the University of Western Toronto.

Unlabeled Use of Products/Investigational Use Disclosure: Dr Perlmutter reports no disclosure.

Nandor K. Pinter, MD
Director, Neuroimaging Research, Dent Neurologic Institute, Amherst; Research Associate Professor, Department of Neurosurgery, Jacobs School of Medicine and Biomedical Sciences, University at Buffalo, Buffalo, New York; University of Amsterdam Medical Center, VUmc, Department of Radiology, Amsterdam, The Netherlands

Copyright © American Academy of Neurology. Unauthorized reproduction of this article is prohibited.

Relationship Disclosure: Dr Pinter has received personal compensation in the range of $5000 to $10,000 for serving as a consultant for Koninklijke Philips N.V. and in the range of $10,000 to $49,000 for serving as a consultant for NeuroNetPro. The institution of Dr Pinter has received research support from the Dent Family Foundation and Koninklijke Philips N.V.

Unlabeled Use of Products/Investigational Use Disclosure: Dr Pinter reports no disclosure.

Shannon L. Risacher, PhD
Associate Professor of Radiology and Imaging Sciences; Neuroimaging Core Leader, Indiana Alzheimer's Disease Research Center, Indiana University School of Medicine, Indianapolis, Indiana

Relationship Disclosure: Dr Risacher has received research support from the Alzheimer's Association, New Vision Award, and the National Institute on Aging (K01 AG049050, R01 AG061788, P30 AG010133, and P30 AG072976).

Unlabeled Use of Products/Investigational Use Disclosure: Dr Risacher reports no disclosure.

Julie G. Shulman, MD
Assistant Professor of Neurology, Boston Medical Center, Boston University School of Medicine, Boston, Massachusetts

Relationship Disclosure: Dr Shulman has received research support from the BU Spivack Neuroscience Pilot Award.

Unlabeled Use of Products/Investigational Use Disclosure: Dr Shulman reports no disclosure.

Jan-Mendelt Tillema, MD
Assistant Professor of Neurology, Mayo Clinic, Rochester, Minnesota

Relationship Disclosure: Dr Tillema reports no disclosure.

Unlabeled Use of Products/Investigational Use Disclosure: Dr Tillema reports no disclosure.

Robert E. Watson, MD, PhD
Professor of Radiology, Department of Radiology, Mayo Clinic, Rochester, Minnesota

Relationship Disclosure: Dr Watson has a noncompensated relationship as a Chair with the American Board of Magnetic Resonance Safety that is relevant to American Academy of Neurology interests or activities.

Unlabeled Use of Products/Investigational Use Disclosure: Dr Watson reports no disclosure.

Lifeng Yu, PhD
Professor of Medical Physics, Mayo Clinic, Rochester, Minnesota

Relationship Disclosure: Dr Yu reports no disclosure.

Unlabeled Use of Products/Investigational Use Disclosure: Dr Yu reports no disclosure.

Self-Assessment and CME Test Writers

Nuri Jacoby, MD
Associate Professor of Clinical Neurology, SUNY Downstate Health Sciences University; Attending Neurologist, Maimonides Medical Center, Brooklyn, New York

Relationship Disclosure: Dr Jacoby has received personal compensation in the range of $500 to $4999 for serving as a multiple-choice question writer for *Continuum* with the American Academy of Neurology and on a scientific advisory or data safety monitoring board for Alexion Pharmaceuticals, Inc and in the range of $5000 to $9999 for

Copyright © American Academy of Neurology. Unauthorized reproduction of this article is prohibited.

serving as an expert witness. The institution of Dr Jacoby has received research support from the American Board of Psychiatry and Neurology.

Unlabeled Use of Products/Investigational Use Disclosure: Dr Jacoby reports no disclosure.

Allison L. Weathers, MD, FAAN
Associate Chief Medical Information Officer, Cleveland Clinic; Assistant Professor, Cleveland Clinic Lerner College of Medicine, Cleveland, Ohio

Relationship Disclosure: Dr Weathers has a noncompensated relationship as chair of the adult neurosciences specialty steering board for Epic and as co-chair of the neurology leadership council for Cerner Corporation and has received personal compensation in the range of $0 to $499 for serving as a consultant for Dent Neurologic Institute and in the range of $500 to $4999 for serving as an associate editor and as a CME question writer and presenter with the American Academy of Neurology.

Unlabeled Use of Products/Investigational Use Disclosure: Dr Weathers reports no disclosure.

Copyright © American Academy of Neurology. Unauthorized reproduction of this article is prohibited.

Methods of Participation and Instructions for Use

Continuum: Lifelong Learning in Neurology® is designed to help practicing neurologists stay abreast of advances in the field while simultaneously developing lifelong self-directed learning skills. In *Continuum*, the process of absorbing, integrating, and applying the material presented is as important as, if not more important than, the material itself.

The goals of *Continuum* include disseminating up-to-date information to the practicing neurologist in a lively, interactive format; fostering self-assessment and lifelong study skills; encouraging critical thinking; and, in the final analysis, strengthening and improving patient care.

Each *Continuum* issue is prepared by distinguished authors who are acknowledged leaders in their respective fields. Six issues are published annually and are composed of review articles, case-based discussions on ethical and practice issues related to the issue topic, coding information, and comprehensive continuing medical education (CME) and self-assessment offerings. For detailed instructions regarding *Continuum* CME and self-assessment activities, visit *continpub.com/CME*.

The review articles emphasize clinical issues emerging in the field in recent years. Case reports and vignettes are used liberally, as are tables and illustrations. Audio interviews with the authors of *Continuum* articles are published alongside each article, and video material relating to the issue topic accompanies issues when applicable.

The text can be reviewed and digested most effectively by establishing a regular schedule of study in the office or at home, either alone or in an interactive group. If subscribers use such regular and perhaps new study habits, *Continuum*'s goal of establishing lifelong learning patterns can be met.

Copyright © American Academy of Neurology. Unauthorized reproduction of this article is prohibited.